# ACCURATE TREATMENT OF CEREBROVASCULAR DISEASES: FRONTIERS IN PATHOLOGY, DIAGNOSTIC METHODS AND TREATMENT TARGETS

EDITED BY: Shuo Wang, Zhao Jizong, Yuanli Zhao, Zeguang Ren and Shaohua Yang

PUBLISHED IN: Frontiers in Aging Neuroscience and Frontiers in Human Neuroscience

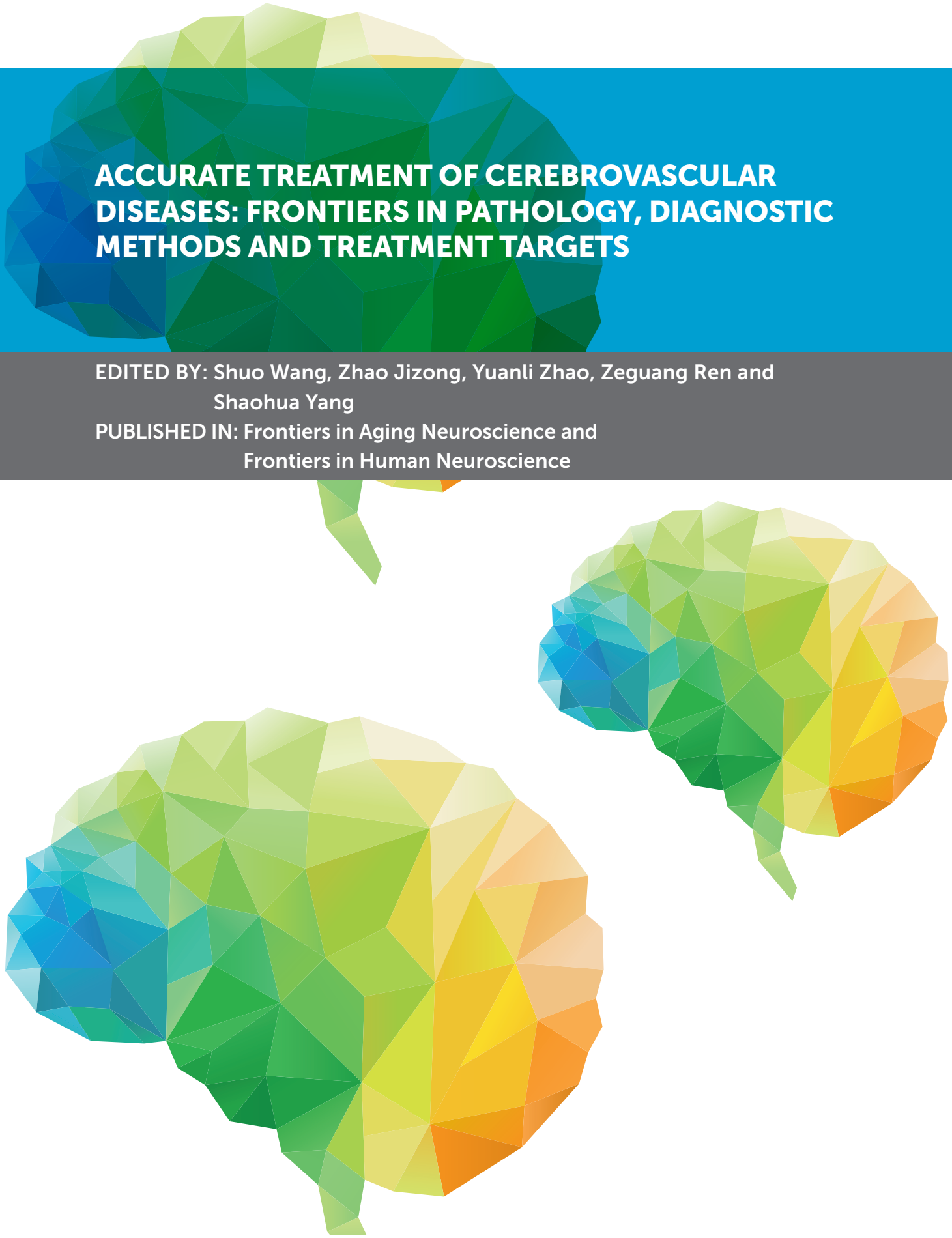

frontiers Research Topics

# frontiers



ISSN 1664-8714
ISBN 978-2-88976-005-3
DOI 10.3389/978-2-88976-005-3

## About Frontiers

Frontiers is more than just an open-access publisher of scholarly articles: it is a pioneering approach to the world of academia, radically improving the way scholarly research is managed. The grand vision of Frontiers is a world where all people have an equal opportunity to seek, share and generate knowledge. Frontiers provides immediate and permanent online open access to all its publications, but this alone is not enough to realize our grand goals.

## Frontiers Journal Series

The Frontiers Journal Series is a multi-tier and interdisciplinary set of open-access, online journals, promising a paradigm shift from the current review, selection and dissemination processes in academic publishing. All Frontiers journals are driven by researchers for researchers; therefore, they constitute a service to the scholarly community. At the same time, the Frontiers Journal Series operates on a revolutionary invention, the tiered publishing system, initially addressing specific communities of scholars, and gradually climbing up to broader public understanding, thus serving the interests of the lay society, too.

## Dedication to Quality

Each Frontiers article is a landmark of the highest quality, thanks to genuinely collaborative interactions between authors and review editors, who include some of the world's best academicians. Research must be certified by peers before entering a stream of knowledge that may eventually reach the public - and shape society; therefore, Frontiers only applies the most rigorous and unbiased reviews.
Frontiers revolutionizes research publishing by freely delivering the most outstanding research, evaluated with no bias from both the academic and social point of view. By applying the most advanced information technologies, Frontiers is catapulting scholarly publishing into a new generation.

## What are Frontiers Research Topics?

Frontiers Research Topics are very popular trademarks of the Frontiers Journals Series: they are collections of at least ten articles, all centered on a particular subject. With their unique mix of varied contributions from Original Research to Review Articles, Frontiers Research Topics unify the most influential researchers, the latest key findings and historical advances in a hot research area! Find out more on how to host your own Frontiers Research Topic or contribute to one as an author by contacting the Frontiers Editorial Office: frontiersin.org/about/contact

# ACCURATE TREATMENT OF CEREBROVASCULAR DISEASES: FRONTIERS IN PATHOLOGY, DIAGNOSTIC METHODS AND TREATMENT TARGETS

Topic Editors:
**Shuo Wang,** Capital Medical University, China
**Zhao Jizong,** Capital Medical University, China
**Yuanli Zhao,** Capital Medical University, China
**Zeguang Ren,** University of South Florida, United States
**Shaohua Yang,** University of North Texas Health Science Center, United States

**Citation:** Wang, S., Jizong, Z., Zhao, Y., Ren, Z., Yang, S., eds. (2022). Accurate Treatment of Cerebrovascular Diseases: Frontiers in Pathology, Diagnostic Methods and Treatment Targets. Lausanne: Frontiers Media SA. doi: 10.3389/978-2-88976-005-3

# Table of Contents

frontiers in Aging Neuroscience

ORIGINAL RESEARCH
published: 20 October 2020
doi: 10.3389/fnagi.2020.585218

# Detection of Cerebrovascular Loss in the Normal Aging C57BL/6 Mouse Brain Using *in vivo* Contrast-Enhanced Magnetic Resonance Angiography

*Lindsay K. Hill*[1,2,3,4†], *Dung Minh Hoang*[2,3†], *Luis A. Chiriboga*[5†], *Thomas Wisniewski*[5,6,7†], *Martin J. Sadowski*[6,7,8†] *and Youssef Z. Wadghiri*[2,3*†]

[1]*Department of Chemical and Biomolecular Engineering, NYU Tandon School of Engineering, Brooklyn, NY, United States,* [2]*Department of Radiology, Center for Advanced Imaging Innovation and Research (CAI2R), NYU Grossman School of Medicine, New York, NY, United States,* [3]*Department of Radiology, Bernard and Irene Schwartz Center for Biomedical Imaging, NYU Grossman School of Medicine, New York, NY, United States,* [4]*Department of Biomedical Engineering, SUNY Downstate Medical Center, Brooklyn, NY, United States,* [5]*Department of Pathology, NYU Grossman School of Medicine, New York, NY, United States,* [6]*Department of Neurology, NYU Grossman School of Medicine, New York, NY, United States,* [7]*Department of Psychiatry, NYU Grossman School of Medicine, New York, NY, United States,* [8]*Department of Biochemistry and Molecular Pharmacology, NYU Grossman School of Medicine, New York, NY, United States*

Microvascular rarefaction, or the decrease in vascular density, has been described in the cerebrovasculature of aging humans, rats, and, more recently, mice in the presence and absence of age-dependent diseases. Given the wide use of mice in modeling age-dependent human diseases of the cerebrovasculature, visualization, and quantification of the global murine cerebrovasculature is necessary for establishing the baseline changes that occur with aging. To provide *in vivo* whole-brain imaging of the cerebrovasculature in aging C57BL/6 mice longitudinally, contrast-enhanced magnetic resonance angiography (CE-MRA) was employed using a house-made gadolinium-bearing micellar blood pool agent. Enhancement in the vascular space permitted quantification of the detectable, or apparent, cerebral blood volume (aCBV), which was analyzed over 2 years of aging and compared to histological analysis of the cerebrovascular density. A significant loss in the aCBV was detected by CE-MRA over the aging period. Histological analysis *via* vessel-probing immunohistochemistry confirmed a significant loss in the cerebrovascular density over the same 2-year aging period, validating the CE-MRA findings. While these techniques use widely different methods of assessment and spatial resolutions, their comparable findings in detected vascular loss corroborate the growing body of literature describing vascular rarefaction aging. These findings suggest that such age-dependent changes can contribute to cerebrovascular and neurodegenerative diseases, which are modeled using wild-type and transgenic laboratory rodents.

**Keywords: magnetic resonance (MR) angiography, blood pool agent, mouse brain aging, cerebral blood volume (CBV), rarefaction, MRI**

OPEN ACCESS

***Edited by:***
*Shuo Wang,*
*Capital Medical University, China*

***Reviewed by:***
*Zoltan I. Ungvari,*
*University of Oklahoma Health Sciences Center, United States*
*Patrizia Giannoni,*
*University of Nîmes, France*

***Correspondence:**
*Youssef Z. Wadghiri*
*wadghiri@med.nyu.edu*

***†ORCID:***
*Lindsay K. Hill*
*orcid.org/0000-0002-1833-8574*
*Dung Minh Hoang*
*orcid.org/0000-0001-7613-7167*
*Luis A. Chiriboga*
*orcid.org/0000-0002-2028-6873*
*Thomas Wisniewski*
*orcid.org/0000-0002-3379-8966*
*Martin J. Sadowski*
*orcid.org/0000-0002-3830-1779*
*Youssef Z. Wadghiri*
*orcid.org/0000-0001-7175-9397*

***Received:*** *20 July 2020*
***Accepted:*** *11 September 2020*
***Published:*** *20 October 2020*

***Citation:***
*Hill LK, Hoang DM, Chiriboga LA, Wisniewski T, Sadowski MJ and Wadghiri YZ (2020) Detection of Cerebrovascular Loss in the Normal Aging C57BL/6 Mouse Brain Using in vivo Contrast-Enhanced Magnetic Resonance Angiography. Front. Aging Neurosci. 12:585218. doi: 10.3389/fnagi.2020.585218*

## INTRODUCTION

Pre-clinical mouse models continue to improve our understanding of clinically relevant biological and pathological processes and aid in our ability to diagnose and treat human diseases. The use of mice in biological research has led to substantial insight into their anatomy and, more recently, into murine cerebrovascular architecture. The cerebrovasculature is critical in supplying the brain with oxygen and nutrients to maintain normal brain function and cognition (Zlokovic, 2011; Hirsch et al., 2012; Ungvari and Sonntag, 2014). Alterations to the cerebrovasculature contribute to brain pathologies including brain tumors, stroke and transient ischemic attack, vascular dementia, Alzheimer's disease, and leukoaraiosis (de la Torre, 2004; Brown and Thore, 2011; Hirsch et al., 2012; Ni et al., 2019). Age-dependent reductions in the cerebrovascular density, or rarefaction (Bullitt et al., 2010), have been shown to contribute to reduced cerebral blood flow and perfusion, resulting in impaired clearance of misfolding-prone proteins and peptides that constitute the premise for several neurodegenerative diseases, including Alzheimer's disease (Martin et al., 1991; Klohs et al., 2014; Tarasoff-Conway et al., 2015; Yang et al., 2017). Notably, age is one of the most important independent risk factors in such vascular diseases (Brown and Thore, 2011; Hirsch et al., 2012; Xu et al., 2017). Therefore, our understanding of the murine cerebrovasculature and how it is impacted by normal aging is critical in studying age-dependent diseases of the brain.

In addition to well-characterized region-dependent changes in brain volume with age (Walhovd et al., 2005; Lockhart and DeCarli, 2014), aging studies of the cerebrovasculature, conducted primarily in humans and rats, have largely concluded that microvascular rarefaction occurs in the normal aging brain (Riddle et al., 2003; Brown and Thore, 2011). The extent of rarefaction is variable and region-dependent (Brown and Thore, 2011); for example, with capillary reductions reported in aged rats from 12% (Burns et al., 1981) to 43% (Amenta et al., 1995) in the cerebral cortex and from 20% (Jucker et al., 1990) to 49% (Amenta et al., 1995) in the hippocampus. Recently, *ex vivo* confocal microscopy of sectioned brains from aged C57BL/6 mice demonstrated region-dependent capillary density reductions from 19% to 34.5% over 2 years (Murugesan et al., 2012). While in agreement with prior human and rat studies, whole-brain quantifications are required to appreciate the impact of aging on the global murine cerebrovasculature.

Until recently, much of our understanding of the cerebrovasculature was contributed by *ex vivo* 2D histology (Hirsch et al., 2012; Wu et al., 2014), still considered the gold standard for visualizing tissue microvasculature (Moy et al., 2013). Recent advances have aimed to observe cerebrovasculature throughout the whole murine brain with high-resolution, including *via* micro-CT with or without vascular corrosion casting (Krucker et al., 2004, 2006; Heinzer et al., 2006, 2008; Dorr et al., 2007; Meyer et al., 2008; Chugh et al., 2009; Ghanavati et al., 2014a,b), scanning electron microscopy (Krucker et al., 2004, 2006), micro-optical sectioning tomography (MOST; Li et al., 2010; Wu et al., 2014; Xue et al., 2014; Xiong et al., 2017), and CLARITY (Chung et al., 2013; Zhang et al., 2018). While these techniques provide images with impressively high spatial resolution, they are only achievable *ex vivo* and are often destructive or otherwise induce tissue deformation or shrinkage (Wehrl et al., 2015). High-resolution *in vivo* techniques, such as two-photon microscopy, have also been used to quantify the cerebral blood volume (CBV), but the technique is largely limited to evaluating the cortical vasculature due to limited tissue penetrance (Serduc et al., 2006; Steinman et al., 2017). Still, such techniques have been employed to quantify the murine cerebrovasculature, which was found to range from 1% to 4.4% of the total brain volume (Boero et al., 1999; Heinzer et al., 2006, 2008; Serduc et al., 2006; Chugh et al., 2009; Tsai et al., 2009; Wu et al., 2014; Zhang et al., 2018). However, given the dynamic and often heterogeneous process of aging and age-dependent diseases, studies on changes in CBV or microvascular density would benefit from *in vivo* techniques, enabling individual subjects to be studied longitudinally.

Magnetic resonance angiography (MRA) is a non-destructive 3D imaging technique that can achieve repeatable *in vivo* neuroimaging of the cerebrovascular network (Nishimura et al., 1986; Beckmann, 2000; Krucker et al., 2004). Traditional time of flight (TOF)-MRA relies on fast laminar blood flow within the vascular space of proximal in-flowing arteries and, therefore, lacks signal in slow-flowing veins and tortuous and distal vessels (Axel, 1984; Nishimura, 1990). Contrast-enhanced MRA (CE-MRA), however, provides cerebrovascular signal indiscriminate of vessel size, flow, and location within the field of view due to the improved relaxation of water by an exogenous $T_1$-shortening contrast agent (Howles et al., 2009). Traditional small molecule $T_1$-agents, such as gadolinium-diethylenetriamine pentaacetic acid (Gd-DTPA, Magnevist), have long been used for clinical CE-MRA acquisition (Lohrke et al., 2016), but their small size allows for extravasation from the porous vasculature outside of the brain into the interstitial space, resulting in a lack of steady-state signal enhancement (Estelrich et al., 2015). This leakage is particularly deleterious for small animal imaging, which must not only consider the 4.5–6-fold shorter plasma half-lives for such agents in rodents (Aime and Caravan, 2009) but also requires considerably longer imaging times than clinical acquisitions for comparable anatomical resolution (Driehuys et al., 2008). To avoid vascular extravasation, blood pool contrast agents have been employed due to their larger size, a result of serum protein binding or multimeric macromolecular design (Caravan et al., 1999; Torchilin, 2000; Torchilin et al., 2000; Lee et al., 2012; Nielsen and Thomsen, 2012), thus slowing their rate of clearance and permitting the use of a longer imaging time (Estelrich et al., 2015) needed for higher spatial resolution (Nielsen and Thomsen, 2012).

In this study, we have employed Gd-micelle CE-MRA to quantify the cerebrovascular density in aged C57BL/6 mice, the most widely used inbred mouse strain (Bryant, 2011), throughout a 2-year aging period. Mice were imaged *via* CE-MRA at 2–4 months (young adulthood), 14–16 months, and 24–26 months (aged adulthood). A subset of mice was

studied longitudinally, allowing for the tracking of individuals throughout the 2-year study, while another subset was used for immunohistochemical (IHC) analysis of the cerebrovasculature. To achieve high signal intensity within the cerebrovascular space, we synthesized a lipid-based Gd-DTPA-bearing micelle, based on a modified version of the micellar design reported by Briley-Saebo et al. (2006, 2008). MRA datasets were aligned using automated registration (Friedel et al., 2014) allowing for virtual whole brain and regional segmentation (Dorr et al., 2008). The detected CBV within segmented regions, here dubbed the apparent CBV (aCBV), was quantified and compared between age groups along with the whole brain and ventricular volumetric assessment. The gold standard technique for microvascular visualization, IHC, was employed for comparative quantification of the microvascular density (McDonald and Choyke, 2003; Moy et al., 2013). While CE-MRA of the whole mouse head is limited in spatial resolution compared to IHC and other *ex vivo* techniques, it provides *in vivo* cerebrovascular information with whole brain coverage. Together, we have employed these techniques to quantify changes within the cerebrovascular density of normal aging wild-type C57BL/6 mice in an effort to elucidate vascular alterations due to aging that contribute to age-dependent diseases of the cerebrovasculature.

# MATERIALS AND METHODS

## Materials

Three lipids, 1,2-distearoyl-sn-glycero-3-phosphoethanolamine-N-[methoxy(polyethylene glycol)-2000] (ammonium salt) (PEG-2000-DPSE), DTPA-bis(stearylamide) (gadolinium salt) (Gd-DTPA-bis(stearylamide)), and 1,2-dipalmitoyl-sn-glycero-3-phosphoethanolamine-N-(lissamine rhodamine B sulfonyl) (ammonium salt) (Rhodamine-DPPE) were purchased from Avanti Polar Lipids. Chloroform, methanol, and [4-(2-hydroxyethyl)-1-piperazineethanesulfonic acid] (HEPES) were purchased from Sigma-Aldrich. Sodium chloride was from Thermo Fisher Scientific. Ethylenediaminetetraacetic acid was from Acros Organics. Acrodisc syringe filters, 0.2 μm, for micelle filtration were purchased from PALL. Magnevist (gadopentetate dimeglumine) was from Bayer Corporation. Intramedic™ Clay Adams™ brand polyethylene PE-10 tubing (inner diameter 0.28 mm, outer diameter 0.61 mm) was purchased from Becton Dickinson for cannulation and contrast agent injection. Vetbond™ was purchased from the 3M Company. Isoflurane was purchased from Piramal Enterprises and Ketathesia (ketamine HCl injection) was from Henry Schein Animal Health.

## Micelle Synthesis

Gd-micelles were synthesized using a thin-film protocol modified from Briley-Saebo et al. (2008). Three synthetic phospholipids, PEG2000-DSPE, DTPA-bis(stearyl amide), and Rhodamine-DPPE (Avanti Polar Lipids, Alabaster, AL, USA), were combined (molar ratio 450:500:1) and dissolved in a 100:2 chloroform:methanol solution. A thin lipid film was generated under heat, at 68°C, and vacuum on a rotary evaporator (RV10, IKA-Werke, Staufen im Breisgau, Germany). Gd-micelles were formed over 20 min on the evaporator by rehydrating the film in HEPES buffer, pH 7.0, under gentle agitation at 65°C in the absence of a vacuum. The hydrated product was filtered with a 0.2 μm syringe filter before characterization.

## Micelle Characterization

The micellar hydrodynamic diameter was measured using dynamic light scattering (DLS; Zetasizer Nano Series model Nano ZS90, Malvern Instruments, Malvern, UK) in a low volume disposable cuvette. A 50 μl aliquot of filtered micelles was added to 700 μl of HEPES and measurements were taken in triplicate, conducting 10 runs for each measurement (5 s per run). The Gd concentration within the micelles was determined *via* inductively coupled plasma-optical emission spectrometry (ICP-OES) by Galbraith Laboratories, Inc. (Knoxville, TN, USA). The longitudinal relaxivity, $r_1$, and the transverse relaxivity, $r_2$, of HEPES-diluted Magnevist (Gd-DTPA) and Gd-micelles were determined at 40°C on a 60 MHz (1.4-Tesla) Bruker minispec mq-one TD-NMR (Bruker Biospin, Billerica, MA, USA) using a previously described protocol (Briley-Saebo et al., 2006, 2008). Longitudinal and transverse relaxation times, $T_1$ and $T_2$, respectively, were acquired for six different concentrations of contrast agent diluted from a concentration of 3 mM Gd. $T_1$ values were determined using an inversion recovery sequence with 15 inversion times from 10 to 1,000 ms and $T_2$ values were acquired using a Car-Purcell-Meiboom-Gill (CPMG) spin-echo sequence where the inter-echo time varied between 0.1 and 2.0 ms. The inverse of the relaxation times $T_1$ and $T_2$ were calculated to obtain the corresponding relaxation rates, $R_1$ and $R_2$. Relaxivity values, $r_1$ and $r_2$, were separately calculated as the slopes of Gd concentration vs. relaxation rate, $R_1$ or $R_2$.

## Animals

All mouse care and experimental procedures were approved by the Institutional Animal Care and Use Committee of the New York University School of Medicine. All *in vivo* MRA experiments were performed on female C57BL/6 wild type mice. The C57BL/6 strain was chosen due to its popularity and importance in biomedical research (Bryant, 2011). Only female mice were studied to minimize effects and variability due to sex (Murugesan et al., 2012). Furthermore, the aging of male C57BL/6 mice often necessitates individual housing for each subject due to increased aggression with age (Svare et al., 1983; Eskola and Kaliste-Korhonen, 1999; An et al., 2011), which is considerably more costly than group-housing aging female mice. C57BL/6NTac mice purchased from Taconic Biosciences (Rensselaer, NY, USA) were used for micelle dosage studies at 2–4 months old and for longitudinal high-resolution MRA studies at 2–4 months ($N$ = 5), 14–16 months ($N$ = 5), and 24–26 months ($N$ = 3, as two subjects died before the final imaging session) following aging in-house. C57BL/6N mice at 2–4 months ($N$ = 9) were subsequently purchased from Charles River Laboratories (Wilmington, MA, USA) for additional MRA studies and histological analysis. Aged C57BL/6N mice were also acquired from National Institute on Aging, housed at Charles River Laboratories, at 14–16 months ($N$ = 7) and 24–26 months

($N$ = 5) for additional MRA studies and histological analysis at these age groups.

## Femoral Vein Cannulation and Animal Setup

Before each imaging session, mice were anesthetized *via* isoflurane inhalation at 1.5 L $min^{-1}$ oxygen using a vaporizer/anesthesia setup (VetEquip, Inc., Livermore, CA, USA). Up to 5% isoflurane in the air was used for anesthesia induction, followed by 1.0–1.5% isoflurane in the air *via* nose cone throughout the femoral vein cannulation procedure. Following anesthetic induction, mice were placed in the supine position on an electric heating blanket to maintain body temperature between 35 to 37°C. Fur over the femoral area of the hind limb was removed after the 30-s application of Nair® hair removal cream (Church and Dwight Company, Inc., Ewing Township, NJ, USA) using sterile cotton swabs. The area was rinsed with sterile water until all cream was removed. The surgical area was sterilized with Betadine and a 70% ethanol scrub. A 0.5 cm incision was made in the surgically prepared area over the femoral vein. If necessary, sterile blunt-tipped scissors were employed to gently remove connective tissue until the femoral vein was exposed. A 31-gauge needle was used to make a small incision in the vein. Contrast agent-primed PE-10 polyethylene tubing (Intramedic, Becton Dickinson, Franklin Lakes, NJ, USA), previously thinned using heat, was attached to a contrast agent-filled syringe and inserted approximately 0.3 cm into the femoral vein. The cannula was held in place with Vetbond™ (3M Company, Maplewood, MN, USA) and allowed to dry. Once dry, mice were placed in the prone position with their heads restrained on a house-made 3D-printed imaging holder equipped with a bite bar and ear bars to minimize motion. The mouse head was inserted into a custom-made radiofrequency (RF) coil built in-house for MRI acquisition, while the rest of the subject's body was covered with 3D-printed water-circulating warming pads to maintain a body temperature between 35 to 37°C. The whole mouse bed was inserted into the center of the bore magnet. Body temperature and breathing rate were monitored continuously throughout the image acquisition (SA Instruments Inc., Stony Brook, NY, USA) and maintained with 1.0–1.5% isoflurane in the air *via* a nose cone. Respiratory motion was monitored using a pneumatic pillow fixed to the subject's abdomen and the core body temperature was measured *via* a rectal probe. The length of PE-10 polyethylene cannula tubing used was long enough to enable remote contrast infusion using a PHD-2000 computer-controlled syringe pump (Harvard Apparatus, Holliston, MA, USA). With the mouse remaining in the magnet, the contrast agent was injected *via* a syringe pump at a 60 $\mu l\ min^{-1}$ infusion rate. The image acquisition began after a 1 min circulation period. The cannula was removed following image acquisition and the skin was sutured. Mice were allowed to recover in a heated cage.

## MRA Acquisition

All MRA experiments were performed on a 7-Tesla (7-T) micro-MRI system consisting of a 7-T 200 mm horizontal bore magnet (Magnex Scientific Limited, Yarnton, UK) interfaced to a Bruker Biospec Avance-2 console (Bruker Biospin, Billerica, MA, USA). The system was equipped with an actively shielded gradient coil (Resonance Research, Billerica, MA, USA: BGA-9S; ID 90 mm, 750 mT $m^{-1}$ gradient strength, 100 $\mu s$ rise time). A circularly polarized RF probe was developed in-house to resonate at a proton frequency of 300 MHz in both transmit and receive modes. Probe dimensions (length = 29 mm, outer diameter = 23.5 mm, and accessible diameter = 21.5 mm) ensured homogenous RF coverage of the whole adult mouse head. A modified three-dimensional (3D) $T_1$-weighted spoiled gradient recalled echo (SPGRE) sequence was employed to acquire an additional self-gated signal during the readout dephasing gradient within each repetition time (TR; Nieman et al., 2009). The gating signal was used retrospectively to correct for motion artifacts induced by respiration and generate artifact-free image reconstruction sets. Scan parameters were as follows: echo time, TE = 4.07 ms; TR = 50 ms; bandwidth, BW = 75 kHz; number of averages, NAV = 1; number of repetitions, NR = 3. The flip angle (FA) = 34° was chosen to provide the greatest $T_1$-enhancement contrast (Neelavalli and Haacke, 2007). Only the field of view (FOV), matrix size, and imaging time ($T_{IM}$) varied between low-resolution (150 $\mu m)^3$ scans (FOV = 19.2 mm × 19.2 mm × 19.2 mm, matrix size = 128 × 128 × 68, $T_{IM}$ = 30 min) and high-resolution (100 $\mu m)^3$ scans (FOV = 25.6 mm × 25.6 mm × 25.6 mm, matrix size = 256 × 256 × 136, $T_{IM}$ = 87 min). 3D imaging with isotropic resolution enables the image set to be reprocessed in any desired slice orientation, facilitating image comparison during co-registration between separately acquired subjects. The appropriate concentration of Gd-micelle administered for high-resolution (100 $\mu m)^3$ MRA studies was determined by a time course study comprised of serial (150 $\mu m)^3$ MRA acquisitions using varying Gd-micelle doses.

## Image Registration and Segmentation

Following (100 $\mu m)^3$ MRA acquisition of mice in all age groups, angiograms were compiled for automated anatomical registration using the mouse-build-model (MBM) pipeline within the Pydpiper toolkit, developed at the Hospital for Sick Children's Mouse Imaging Centre (Friedel et al., 2014). All images were compiled and aligned to a (100 $\mu m)^3$-resolution modified C57BL/6J mouse brain anatomical atlas developed by Dorr et al. (2008) using the MBM pipeline. The whole brain and brain regions (cerebral cortex, cerebellar cortex, entorhinal cortex, hippocampus, and striatum) were segmented for each aligned image using command-line tools from minc-stuffs, a suite of Medical Imaging NetCDF (MINC) tools, for image analysis (Vincent et al., 2004, 2016). The cerebral cortex, hippocampus, and entorhinal cortex were chosen for examination as these regions have previously demonstrated vascular and volumetric changes in diseases including Alzheimer's disease and vascular dementia (Schuff et al., 2001; Krucker et al., 2004; Kara et al., 2012), in addition to previously reported age-dependent microvascular rarefaction in the cortex and hippocampus (Riddle et al., 2003; Xu et al., 2017; Yang et al., 2017). The cerebellar cortex was assessed as it also demonstrates atrophy and vessel alterations with

age, including small vessel disease, micro-infarcts, and venous ischemia (Hoogendam et al., 2012; Cerchiai et al., 2017; De Cocker et al., 2017). Lastly, the striatum was included as vascular changes and reduced blood flow in the aging striatum may contribute to vascular parkinsonism and Parkinson's disease (Feekes and Cassell, 2006; Guan et al., 2013; Afonso-Oramas et al., 2014; Gray and Woulfe, 2015).

## Apparent Cerebral Blood Volume Quantification

Segmented brains and brain regions were imported into ImageJ software (National Institute of Health, Bethesda, MD, USA; Schneider et al., 2012), and the enhanced cerebrovasculature was assessed qualitatively by generating a Maximum Intensity Projection (MIP) using the 3D projection function. The MIP algorithm highlights voxels of the highest intensity from a 3D image set to be projected onto a 2D plane, aiding in the visualization of signal enhancing contrast agent distributed throughout the tissue. Quantitation of micelle-enhanced voxels corresponding to the aCBV was also performed in ImageJ *via* intensity-based segmentation using a thresholding function in which the aCBV was defined as the percentage of (100 $\mu$m)$^3$ voxels, within all voxels examined, demonstrating a signal intensity (SI) defined by the equation below. The threshold value of 2.5-fold the standard deviation above the mean SI of the region was chosen because it was the minimum value providing vascular segmentation while minimizing the inclusion of apparent background tissue:

$$SI_{CBV} \geq Mean\, SI_{ROI} + 2.5 \cdot ST\, Dev_{ROI}$$

## Deformation-Based Morphometry

RMINC, a package developed by the Mouse Imaging Center to read and write MINC volumes within the R environment, was used to perform statistical analyses on volumetric differences in mice of different age groups (Lerch et al., 2008). A deformation field was calculated between individual mice and a common space set by the Dorr et al. (2008) mouse brain atlas. The Jacobian determinant of the deformation field measured the expansion or contraction of volumes of interest on a voxel-wise basis (Chung et al., 2001) and significant volume changes were calculated per voxel with a false discovery rate, FDR, of <5% (Genovese et al., 2002). Volume differences in the segmented whole brain and ventricular system (the compiled lateral ventricles, third ventricle, cerebral aqueduct, and fourth ventricle) were also calculated and assessed for significance using one-way analysis of variance (ANOVA) test and Tukey's honestly significant difference (HSD) *post hoc* test for multiple pair-wise comparisons between the three age groups.

## Histological Preparation and Immunohistochemistry of the Cerebrovasculature

Following micelle clearance, i.e., approximately 24 h after image acquisition, five mice per age group (2–4, 14–16, and 24–26 months) were sacrificed for histological examination, which was conducted by the Experimental Pathology Research Laboratory at New York University School of Medicine. IHC against CD31 to detect vascular endothelium was performed on paraformaldehyde-fixed, paraffin-embedded, 5 $\mu$m murine brain sections. CD31, also known as a platelet-endothelial cell adhesion molecule (PECAM-1), is constitutively expressed by all endothelial cells and is, therefore, a widely used marker for vascular staining (Amtul and Hepburn, 2014). Immunofluorescence staining was performed on a Ventana Medical Systems Discovery XT instrument using Ventana's reagents and detection kits unless otherwise noted. Tissue sections were deparaffinized online and antigen retrieved using cell conditioner 1 for 36 min. Endogenous peroxidase activity was blocked with hydrogen peroxide. Unconjugated rabbit anti-mouse CD31 monoclonal antibody [Platelet Endothelial Cell Adhesion Molecule (clone D8V9E), CST #77699, Cell Signaling Technology, Danvers, MA, USA] was diluted 1:200 in Cell Signaling diluent and applied to the brain tissue for 2 h at room temperature. Following extensive washing in Ventana reaction buffer, the binding of the primary antibody to CD31 was detected with pre-diluted Ventana horseradish peroxidase-conjugated anti-rabbit secondary antibody, which was applied for 16 min and subsequently visualized with pre-diluted Ventana tyramide-conjugated rhodamine for 8 min. Slides were washed in distilled water and coverslipped with Prolong Gold anti-fade media (Molecular Probes, Eugene, OR, USA). A 1.0 mm tissue microarray composed of paraformaldehyde-fixed, paraffin-embedded murine tissues (skin, lung, liver, kidney, and brain) served as positive controls for optimization. The tissue microarray was also used as a negative control by using Cell Signaling diluent only for the primary antibody incubation. Stained brains were imaged on a NanoZoomer whole-slide scanner (Hamamatsu Photonics, Shizuoka, Japan) and analyzed in Visiopharm software (Hoersholm, Denmark).

Visiopharm's CD31-stained vessel quantification application was employed to detect vessels emitting fluorescence in the red channel (RGB-R) above a threshold that prevented the detection of background tissue. The density of vessels per brain section was counted and divided by the area of the section in mm$^2$ to acquire the number of vessels/mm$^2$ in 2–4, 14–16, and 24–26 months brains ($N$ = 5 sections per age). The same method for vascular analysis was applied to specific cortical and hippocampal regions of interest (ROIs) within the brain sections.

## Statistical Analysis

GraphPad Prism (GraphPad Software, San Diego, CA, USA) was utilized for all statistical analyses, except for that of deformation-based morphometry, which was built into the RMIC package. Specific statistical tests used are defined below for individual experiments. Differences were deemed statistically significant when demonstrating $p < 0.05$ (*), $p < 0.01$ (**), $p < 0.001$ (***), or $p < 0.0001$ (****).

For analysis of the aCBV obtained *via* MRA, aCBV values in the whole brain and brain regions were tested for normality using the D'Agostino-Pearson omnibus test (D'Agostino, 1986), the Shapiro–Wilk test (Shapiro and Wilk, 1965), and the Kolmogorov–Smirnov test with Dallal-Wilkinson-Lillie for *P*-value (Kolmogorov, 1933; Smirnov, 1939). Datasets were

considered of normal distribution if they passed two out of the three normality tests (Boutajangout et al., 2010). The aCBV results were subsequently compared and significance was assessed using a one-way ANOVA test and Tukey's HSD *post hoc* test for multiple pairwise comparisons between the three age groups for the entire female C57BL/6 cohort [2–4 ($N$ = 14), 14–16 ($N$ = 12), and 24–26 months ($N$ = 8)]. Additionally, the aCBV values of in-house longitudinally-aged and imaged female C57BL/6NTac mice [2–4 ($N$ = 5), 14–16 ($N$ = 5), and 24–26 months ($N$ = 3)] and the C57BL/6N mice imaged at single time points [2–4 ($N$ = 9), 14–16 ($N$ = 7), and 24–26 months ($N$ = 5)] were separately analyzed *via* one-way ANOVA and Tukey's HSD test between age groups. Separately, unpaired two-tailed Student's $t$-tests were conducted to determine if there was a significant difference in the aCBV values of the C57BL/6NTac and C57BL/6N sub-strain cohorts in each brain region studied.

For CD31-stained histological sections, the density of vessels in whole brain sections, as well as cortical and hippocampal ROIs, were compared for 2–4, 14–16, and 24–26 months brains *via* one-way ANOVA and Tukey's HSD *post hoc* test. CD31-stained vessels were also stratified by diameter, *via* minor axis length, using Visiopharm software with cut-offs of <50 μm, 50–100 μm, and >100 μm. All quantifications were subjected to two-way ANOVA and Tukey's HSD *post hoc* test to assess significance across age groups.

# RESULTS

## Gd-Micelle Characterization as a $T_1$-Shortening Blood Pool Agent

Following each batch synthesis, Gd-micelles (**Figure 1A**) were characterized for their hydrodynamic diameter, Gd concentration, and relaxation properties (**Table 1**, **Figures 1B,C**) to evaluate their capacity to serve as a blood pool agent with high relaxation properties. DLS confirmed an average hydrodynamic diameter of 15.63 ± 0.58 nm ($N$ = 5) for >99.0% of the micelle population by volume, within the 10–2,000 nm range typical for blood pool agents (Torchilin et al., 2000; **Table 1**, **Figure 1B**). The Gd concentration, assessed commercially *via* ICP-OES (Galbraith Laboratories, Knoxville, TN, USA), was 11.70 ± 0.85 mM ($N$ = 5; **Table 1**). The relaxation properties of Gd-micelles were compared to that of Magnevist at 60 MHz, corresponding to 1.4-Tesla, field strength (**Table 1**, **Figure 1C**). Specifically, the longitudinal and transverse relaxivity values, $r_1$ and $r_2$, were calculated as indicators of the MR signal enhancement or reduction potential, respectively (Burtea et al., 2008). The ratio $r_2/r_1$ was also calculated to assess of the agents' suitability for positive ($T_1$) or negative ($T_2$) contrast (Burtea et al., 2008). Magnevist demonstrated an $r_1$ of 3.29 $mM^{-1}$ $s^{-1}$ and $r_2$ of 3.37 $mM^{-1}$ $s^{-1}$ at a temperature of 37°C, comparable to values previously described (Rohrer et al., 2005; **Table 1**). Its $r_2/r_1$ ratio of 1.02 confirms its use as a $T_1$ agent, where 1.0 characterizes an optimal $T_1$ shortening agent (Hashemi et al., 2004). Gd-micelles demonstrated an $r_1$ of 12.90 ± 0.49 $mM^{-1}$ $s^{-1}$, 3.92-fold higher than the $r_1$ value of Magnevist, and $r_2$ of 17.80 ± 0.66 $mM^{-1}$ $s^{-1}$ ($N$ = 5; **Table 1**, **Figure 1C**). The resulting $r_2/r_1$ was 1.38 ± 0.01, remaining within the range of effective $T_1$-shortening contrast agents ($r_2/r_1$ = 1–2; Hagberg and Scheffler, 2013).

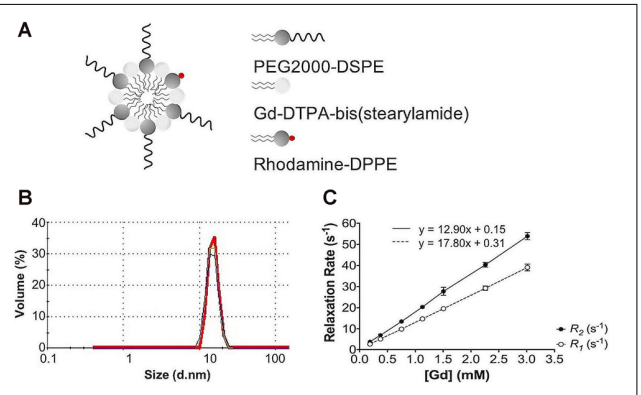


**FIGURE 1 |** Gd-micelle composition and characterization. **(A)** Schematic of the Gd-micelle construct composed of three phospholipids: PEG2000-DSPE, Gd-DTPA-bis(stearyl amide), and Rhodamine-DPPE. **(B)** Hydrodynamic diameter determined by dynamic light scattering. **(C)** Longitudinal and transverse relaxation properties of Gd-micelle agent with error bars indicating the standard deviation amongst $N$ = 5.

## *In vivo* 3D CE-MRA of Whole Murine Brains

Dosage studies compared the clinical equivalent dose of Magnevist by weight (3 μmol Gd/30 g) to varying doses of the Gd-micelle construct (from 0.38–1.875 μmol Gd/30 g) using 30 min (150 μm)$^3$ $T_1$-w angiograms in 2–4 months mice (**Figure 2**). Maximum intensity projections of the resulting angiograms demonstrated that Magnevist extravasated from the peripheral vasculature within 30 min, as determined by the enhanced signal intensity seen in the facial tissue of the mouse. As a result of this lack of steady-state recirculation, the signal enhancement in both the vasculature and the tissue returned to baseline within 2 h, suggesting that Magnevist would be inadequate as a steady-state $T_1$ agent for high-resolution (100 μm)$^3$ angiography. By contrast, Gd-micelles remained circulating within the vascular space as expected given the agent's blood pool agent size (Torchilin et al., 2000) and PEGylation (Croy and Kwon, 2006; Nishiyama and Kataoka, 2006; Qiu et al., 2007). The dose of 0.75 μmol Gd/30 g was chosen for subsequent high-resolution MRA studies as it provided steady-state signal enhancement within the vascular space throughout the 2 h time-course, yet was cleared from circulation by 24 h, returning to the pre-injection baseline.

A (100 μm)$^3$ $T_1$-w MRA sequence was employed to test the impact of 0.75 μmol Gd/30 g Gd-micelle administration on the signal-to-noise ratio (SNR) of the murine vascular space. The same 2–4 months C57BL/6 mouse was imaged without and with Gd-micelle enhancement and the images were aligned for direct comparison of vessel enhancement (**Figure 3**). In the absence of contrast enhancement, the detectable vascular space demonstrated an endogenous SNR, averaged over 10 regions of interest (ROIs), of 36.14 ± 13.89. Following Gd-micelle administration at 0.75 μmol Gd/30 g, the resulting angiogram revealed an intravascular SNR of 115.13 ± 20.46, a 3.19-

**TABLE 1** | Physicochemical properties of Gd-constructs.

| Construct | Hydrodynamic diameter (nm ± STDev) | Gadolinium concentration (mM ± STDev) | $r_1$ at 60 MHz in HEPES ($mM^{-1}$ $s^{-1}$ ± STDev) | $r_2$ at 60 MHz in HEPES ($mM^{-1}$ $s^{-1}$ ± STDev) | $r_2/r_1$ at 60 MHz |
|---|---|---|---|---|---|
| Gd-micelle | 15.63 ± 0.58 | 11.70 ± 0.85 | 12.90 ± 0.49 | 17.80 ± 0.66 | 1.38 ± 0.01 |
| Gd-DTPA (Magnevist) | *<1 nm | *500 | 3.29 | 3.37 | 1.02 |

*Characterization of the hydrodynamic diameter, Gd concentration, and relaxation properties at 60 MHz (1.4-Tesla) of Gd-micelle contrast agent compared to Magnevist. Gd-micelle data represent average values and standard deviations (N = 5). *Data determined by Bayer Corporation, Leverkusen, Germany.*

fold improvement. Notably, only vessels detectable in both angiograms, with and without contrast, were compared for signal enhancement, but many vessels were undetectable in the absence of Gd-micelle injection. As demonstrated by MIPs of the datasets pre- and post-virtual brain segmentation (**Figure 3**), in the absence of contrast, detectable vessels included large caudal arteries, while small rostral vessels and slow-flowing veins were not visible. Such enhancement is characteristic of the blood flow-dependent TOF-effect in which the magnetization of inflowing blood is refreshed, while slow-flowing blood and static background tissue remain saturated by the repeated radiofrequency (RF) pulse (Beckmann, 2000; Krucker et al., 2004). Gd-micelle CE-MRA, however, demonstrated global vascular enhancement indiscriminate of vessel type and location within the field of view (**Figure 3**). MIPs following virtual brain segmentation further confirmed that Gd-micelle enhancement provided significant vascular contrast throughout the brain not observed in the absence of contrast (**Figure 3**). These findings led us to perform the Gd-micelle-enhanced (100 μm)$^3$ MRA protocol on mice over 2 years of aging.

## Apparent Cerebral Blood Volumes of Aging Brains and Sub-brain Regions

Angiograms acquired at 2–4 ($N$ = 14), 14–16 ($N$ = 12), and 24–26 months ($N$ = 8) from both C57BL/6NTac mice (Taconic Biosciences, Rensselaer, NY, USA) studied longitudinally and C57BL/6N mice (Charles River Laboratories, Wilmington, MA, USA) were compiled and aligned using automated registration. The brains and brain ROIs were segmented using the Dorr et al. (2008) C57BL/6J mouse brain atlas. Following virtual segmentation, MIPs of the ROIs were used to visualize the cerebrovasculature, without obstruction from surrounding facial vessels. MIPs of each segmented ROI, as demonstrated by a representative brain from each age group, qualitatively demonstrated a decrease in the cerebrovasculature with increasing age, although the effect varied per anatomical region (**Figure 4**).

The CBV within each brain ROI detected by Gd micelle-enhanced MRA, the aCBV, was quantified following signal-based thresholding. MIPs of the thresholded aCBV in whole brains representative of each age group allowed for a qualitative appreciation of the decrease in the aCBV throughout the 2 years of aging (**Figure 5A**). The aCBV in each of

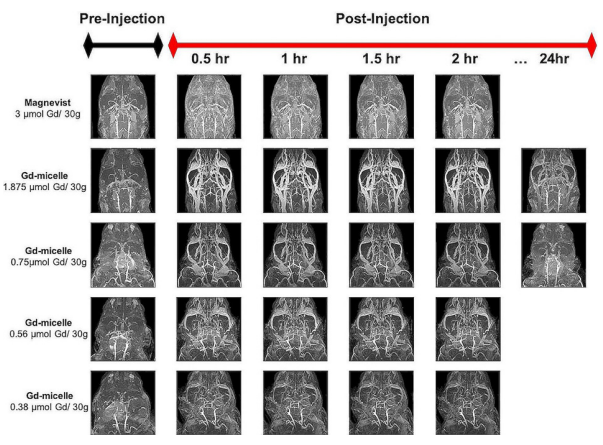


**FIGURE 2** | Time-course contrast-enhanced magnetic resonance angiography (CE-MRA) using Magnevist and Gd-micelle contrast. Time-course MRA study composed of a series of 30 min (150 μm)$^3$ acquisitions pre- and post-injection of Magnevist, at the clinical equivalent dose by weight, or decreasing doses of Gd-micelle. Datasets are displayed as Maximum Intensity Projections (MIPs) to illustrate cerebrovascular enhancement.

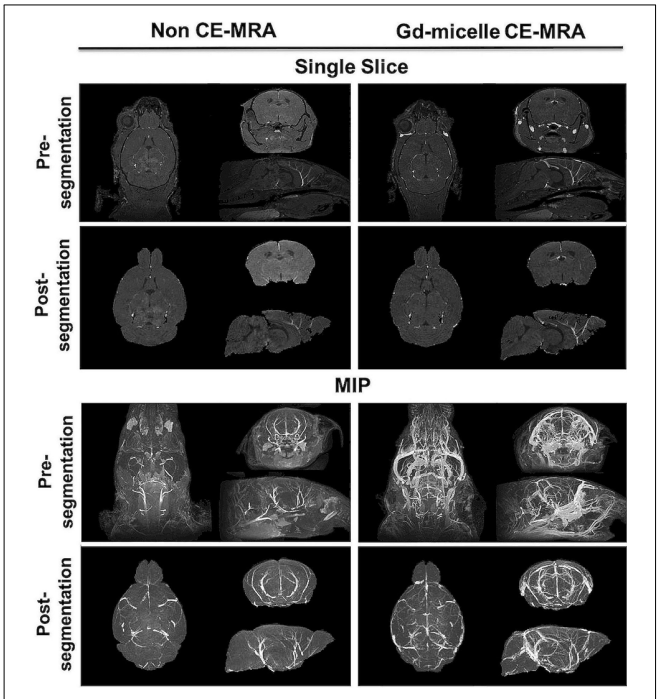


**FIGURE 3** | High-resolution MRA with and without Gd-micelle enhancement. 3D high-resolution MRA with and without Gd-micelle enhancement displayed as 2D single slices and MIPs pre- and post-virtual brain segmentation *via* registration to an anatomical brain atlas.

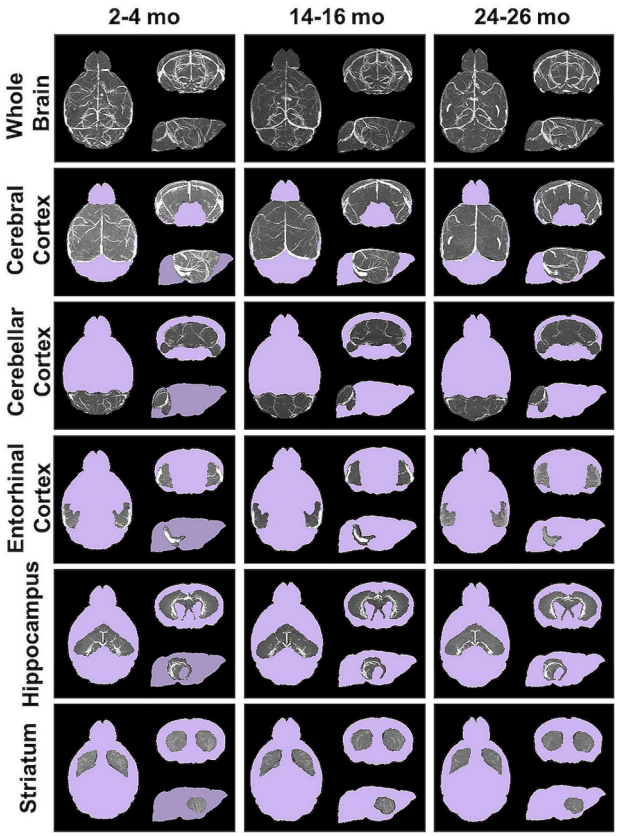


**FIGURE 4 |** Segmented brain regions of interest from Gd-micelle CE-MRA over aging. Illustrative examples of model brains from mice aged 2–4, 14–16, and 24–26 months demonstrating the virtually segmented whole brain and brain regions. Datasets are displayed as MIPs to illustrate cerebrovascular enhancement.

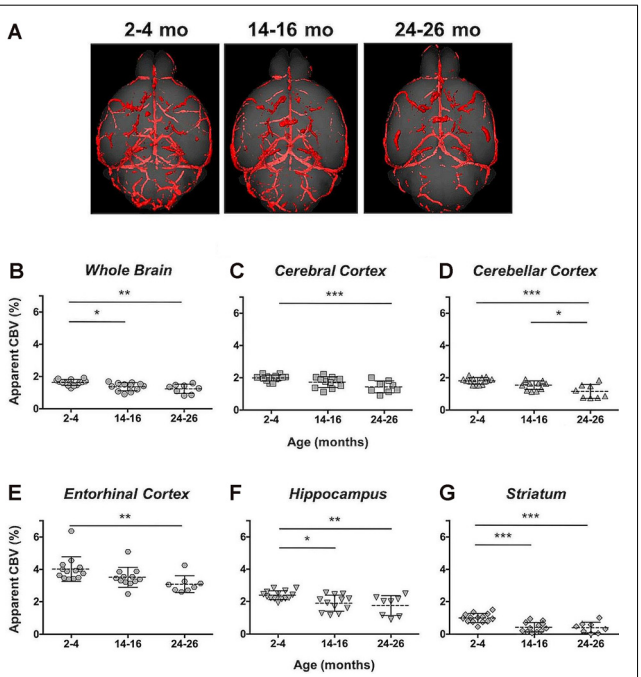


**FIGURE 5 |** Apparent cerebral blood volume of total C57BL/6 cohort assessed *via* CE-MRA. **(A)** Representative Gd-micelle CE-MR angiograms of murine brains at 2–4, 14–16, and 24–26 months displaying thresholded vessels, shown as MIPs, quantified as the apparent cerebral blood volume (aCBV). The aCBV of all mice studied *via* MRA was calculated and plotted for the **(B)** whole brain, **(C)** cerebral cortex, **(D)** cerebellar cortex, **(E)** entorhinal cortex, **(F)** hippocampus, and **(G)** striatum. Data represent average values and standard deviations. Tukey's honestly significant difference (HSD) tested was performed to assess the significance of differences between age groups, where $^{*}p < 0.05$, $^{**}p < 0.01$, and $^{***}p < 0.001$.

the six ROIs were quantified for all subjects together, as well as separated by cohorts of C57BL/6NTac subjects and C57BL/6N subjects, acknowledging that phenotypic and genetic differences have been observed among C57BL/6 substrains (Bryant, 2011). The aCBV values for the whole C57BL/6 cohort were determined to be normally distributed in the whole brain and all sub-brain regions. While aging produced region-specific differences, all ROIs examined from the total cohort (C57BL/6NTac and C57BL/6N mice) demonstrated an age-dependent significant decrease in the aCBV by one-way ANOVA (**Figures 5B–G**, **Table 2**, **Supplementary Table 1**) and specifically between 2–4 and 24–26 months brains by Tukey's HSD test (**Figures 5B–G**, **Table 2**). The percent of aCBV loss ranged from 19.95% in the entorhinal cortex to 58.59% in the striatum (**Table 2**).

The aCBV was also separately analyzed for the subset of five C57BL/6NTac mice studied longitudinally through repeat MRA acquisitions at the ages of interest over 2 years (**Figure 6**, **Table 3**). However, based on a one-way ANOVA, the hippocampus and striatum showed no significant change in aCBV with age (**Figure 6**, **Table 3**, **Supplementary Table 1**), and Tukey's HSD test found no significant difference between paired age groups for the whole brain, hippocampus, or striatum (**Figure 6**, **Table 3**), possibly in part due to the smaller cohort size and death of two animals before the final imaging session. Notably, the longitudinal investigation

**TABLE 2 |** Apparent cerebral blood volumes quantified in the total C57BL/6 cohort.

| | Apparent cerebral blood volume (%) | | | | | |
|---|---|---|---|---|---|---|
| **Age group months** | **Whole brain** | **Cerebral cortex** | **Cerebellar cortex** | **Entorhinal cortex** | **Hippocampus** | **Striatum** |
| 2–4 | 1.64 ± 0.18 | 1.99 ± 0.18 | 1.81 ± 0.20 | 4.02 ± 0.76 | 2.38 ± 0.27 | 0.99 ± 0.27 |
| 14–16 | 1.37 ± 0.25 | 1.73 ± 0.33 | 1.54 ± 0.27 | 3.52 ± 0.62 | 1.89 ± 0.50 | 0.44 ± 0.30 |
| 24–26 | 1.24 ± 0.29 | 1.43 ± 0.37 | 1.15 ± 0.43 | 3.09 ± 0.53 | 1.75 ± 0.61 | 0.41 ± 0.33 |

*Apparent CBV of brain and brain regions of interest from all mice studied via Gd-micelle CE-MRA. Values represent the average volume and standard deviation.*

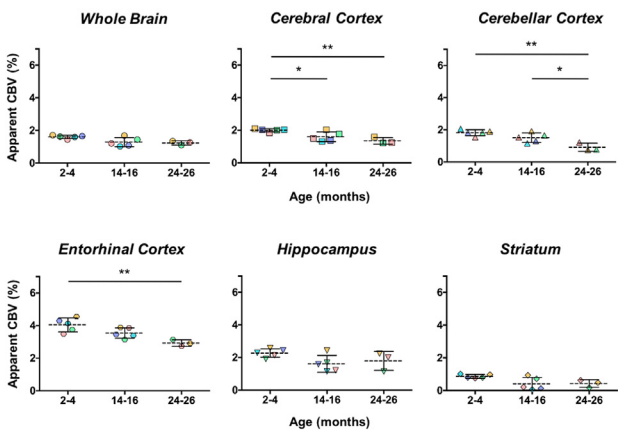


**FIGURE 6 |** Apparent CBV in C57BL/6NTac mice longitudinally assessed *via* CE-MRA. The apparent CBV was determined in the whole brain and brain regions of longitudinally studied mice. Colors indicate distinct mice aged in-house and imaged over their lifetime. Results of Tukey's HSD test for significance between age groups are shown, where $*p < 0.05$ and $**p < 0.01$.

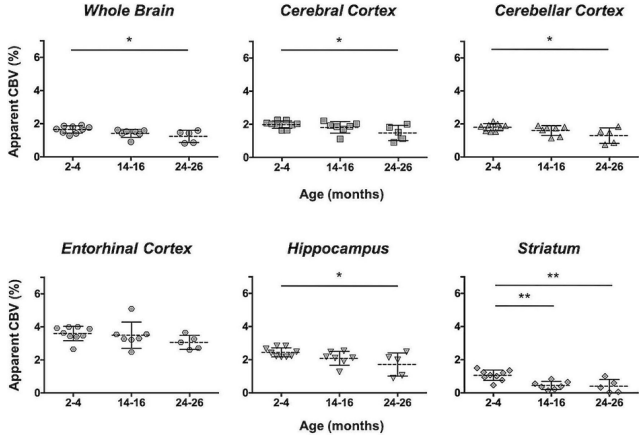


**FIGURE 7 |** Apparent CBV in C57BL/6N mice assessed *via* CE-MRA. The apparent CBV was determined in the whole brain and brain regions of C57BL/6N mice, excluding the longitudinally studied C57BL/6NTac cohort shown in **Figure 6**. Results of Tukey's HSD test for significance between age groups are shown, where $*p < 0.05$ and $**p < 0.01$.

highlights the heterogeneity typically described in the aging process (Lockhart and DeCarli, 2014), where specific mice demonstrate steeper declines in the aCBV (**Figure 6**, blue symbol) than others (**Figure 6**, yellow symbol; Hagberg and Scheffler, 2013).

Additionally, the cohort of C57BL/N mice was separately studied and revealed significant decreases in the aCBV with age by one-way ANOVA in all regions studied except for the entorhinal cortex (**Figure 7**, **Table 4**, **Supplementary Table 1**). Tukey's HSD test also found no significant difference between age groups for the entorhinal cortex (**Figure 7**, **Table 4**). Notably, based on unpaired two-tailed Student's *t*-tests performed between the C57BL/6NTac and C57BL/6N cohorts per brain region analyzed, there was no significant difference in the aCBV of C57BL/6NTac and C57BL/6N mice over the 2 years studied.

## Volumetric Changes With Aging

Automated CE-MRA registration also enabled volumetric comparisons of the brains *via* deformation-based morphometry. Voxel-wise global volumetric differences between the compiled and averaged 14–16 months datasets and 2–4 months datasets predominantly demonstrated significant growth (red-to-yellow) throughout the brain, while smaller regions of significant volumetric reduction (blue-to-cyan) were also observed (**Figure 8A**). A comparison of 24–26 months brains to 14–16 months brains revealed sporadic areas of brain growth and reduction (**Figure 8A**), but substantially fewer voxels showed significant differences in the second year of aging. In addition to voxel-wise global comparisons, volumetric differences between the three age groups were also assessed in the virtually segmented whole brain and ventricular system (**Figures 8B–D**, **Table 5**), both previously shown to increase in volume in aging C57BL/6 mice (Chen et al., 2011).

In agreement with the global voxel-wise assessment, a one-way ANOVA revealed a significant change in the whole brain volume with age over the 2-year-period ($***p < 0.001$), and Tukey's HSD test revealed statistically significant differences between each age group ($***p < 0.001$ for each age group comparison; **Figure 8B**, **Table 5**). The ventricular system, comprised of the lateral ventricles, the third ventricle, the cerebral aqueduct, and the fourth ventricle, also demonstrated statistically significant growth over 2 years by one-way ANOVA ($***p < 0.001$; **Figure 8C**, **Table 5**). Tukey's HSD test revealed significant differences between 2–4 and 14–16 months groups ($**p < 0.01$) and between 2–4 months and 24–26 months groups ($***p < 0.001$; **Figure 8C**, **Table 5**).

**TABLE 3 |** Apparent cerebral blood volumes quantified in C57BL/6NTac mice longitudinally assessed.

| | Apparent cerebral blood volume (%) | | | | | |
|---|---|---|---|---|---|---|
| **Age group months** | **Whole brain** | **Cerebral cortex** | **Cerebellar cortex** | **Entorhinal cortex** | **Hippocampus** | **Striatum** |
| 2–4 | 1.61 ± 0.10 | 2.00 ± 0.10 | 1.82 ± 0.19 | 4.04 ± 0.42 | 2.28 ± 0.26 | 0.87 ± 0.12 |
| 14–16 | 1.29 ± 0.28 | 1.60 ± 0.30 | 1.51 ± 0.30 | 3.54 ± 0.32 | 1.61 ± 0.51 | 0.42 ± 0.39 |
| 24–26 | 1.24 ± 0.13 | 1.35 ± 0.21 | 0.92 ± 0.26 | 2.93 ± 0.20 | 1.80 ± 0.58 | 0.43 ± 0.23 |

*Apparent CBV of brain and brain regions from mice studied longitudinally via Gd-micelle-enhanced MRA. Values represent the average volume and standard deviation.*

**TABLE 4** | Apparent cerebral blood volumes quantified in C57BL/6N mice.

| | Apparent cerebral blood volume (%) | | | | | |
|---|---|---|---|---|---|---|
| **Age group months** | **Whole brain** | **Cerebral cortex** | **Cerebellar cortex** | **Entorhinal cortex** | **Hippocampus** | **Striatum** |
| 2–4 | 1.65 ± 0.22 | 1.98 ± 0.22 | 1.80 ± 0.22 | 3.60 ± 0.43 | 2.44 ± 0.27 | 1.06 ± 0.31 |
| 14–16 | 1.42 ± 0.24 | 1.82 ± 0.35 | 1.60 ± 0.30 | 3.50 ± 0.79 | 2.08 ± 0.42 | 0.45 ± 0.24 |
| 24–26 | 1.23 ± 0.37 | 1.48 ± 0.46 | 1.29 ± 0.47 | 3.06 ± 0.43 | 1.71 ± 0.70 | 0.40 ± 0.41 |

*Apparent CBV of brain and brain regions from C57BL/6N mice studied via Gd-micelle-enhanced MRA. C57BL/6NTac mice studied longitudinally and described in **Table 3** are excluded. Values represent the average volume and standard deviation.*

**TABLE 5** | Volumetric changes over aging in the total C57BL/6 cohort.

| | Whole brain and ventricular volume ($mm^3$) | | |
|---|---|---|---|
| **Region** | **2–4 months** | **14–16 months** | **24–26 months** |
| Whole brain | 439.78 (426.76–451.32) | 452.86 (441.18–463.70) | 460.40 (451.26–469.53) |
| Ventricular system | 5.16 (4.96–5.36) | 6.43 (5.88–7.16) | 6.54 (5.97–7.30) |

*Volumetric changes in the whole brain and ventricular system from deformation-based morphometry of registered brains. Values represent the average volume and the minimum and maximum values with 95% confidence.*

## Immunohistochemical Analysis of the Cerebrovascular Density

Immunohistochemistry, the gold-standard technique for microvascular visualization (Moy et al., 2013), was employed to assess if a structural loss of vessels, or rarefaction, contributed to the reduction in aCBV detected by Gd-micelle CE-MRA. Brain sections probed for vascular CD31 from each age group ($N$ = 5 per age; **Figure 9A**) were quantified as the number of vessels/$mm^2$ throughout the section (**Figures 9B,C**, **Table 6**) as well as in the well-defined cerebral cortex and hippocampus (**Figures 9D–G**, **Table 6**). Quantification of whole sections demonstrated a reduction in vascular density with age from 458.18 ± 61.28 vessels/$mm^2$ at 2–4 months to 362.94 ± 49.34 vessels/$mm^2$ at 24–26 months, with $p = 0.05$ by one-way ANOVA and $p < 0.05$ by Tukey's HSD test between the 2–4 and 24–26 months groups (**Figure 9B**, **Table 6**). Additionally, the vessel composition was assessed by size and compared for each age group, with both age ($^*p < 0.05$) and vessel size ($^{****}p < 0.0001$) significantly contributing to changes in vascular density *via* two-way ANOVA (**Figure 9C**, **Supplementary Figure 1**). Furthermore, the density of vessels with diameters <50 μm, characteristic of most vessels detected by IHC, decreased from 456.92 ± 60.62 vessels/$mm^2$ at 2–4 months to 419.35 ± 57.91 vessels/$mm^2$ at 14–16 months and finally to 361.60 ± 49.03 vessels/$mm^2$ at 24–26 months. There was a significant difference between 14–16 and 24–26 months sections ($^*p < 0.05$) and between 2–4 and 24–26 months sections ($^{***}p < 0.001$) by Tukey's HSD *post hoc* test. By contrast, vessels with diameters between 50–100 and >100 μm were significantly less detected *via* IHC and showed no statistically significant difference amongst the age groups *via* Tukey's HSD test, suggesting that the majority of the decrease in density over 2 years was due to a reduction in vessels <50 μm in diameter. However, tissue deformation and shrinkage during histological preparation could affect these measurements (Wehrl et al., 2015).

The cerebrovascular densities in the cerebral cortex and hippocampus, well-defined within the histological sections, were also quantified in IHC sections. One-way ANOVA tests found statistically significant changes in cerebrovascular density with age across groups in both the cortex and hippocampus ($^*p < 0.05$). The cerebrovascular density of the cerebral cortex (**Figure 9D**) showed a minor decrease after 1-year aging, but, according to Tukey's HSD test, there was a significant decrease between 2–4 and 24–26 months age groups from 500.60 ± 81.91 to 377.02 ± 33.91 vessels/$mm^2$ ($^*p < 0.05$) and between 14–16 and 24–26 months sections ($^*p < 0.05$; **Figure 9F**, **Table 6**). According to Tukey's HSD test, the hippocampus (**Figure 9E**) demonstrated a significant decrease in the cerebrovascular density between 2–4 and 24–26 months age groups from 465.93 ± 83.71 to 341.89 ± 38.18 vessels/$mm^2$ ($^*p < 0.05$; **Figure 9G**, **Table 6**).

# DISCUSSION

The present study investigated the detectable aCBV of normal aging in wild type C57BL/6 mice using the non-destructive and minimally invasive CE-MRA approach throughout a 2-year aging period, accompanied by IHC analysis. To image the cerebrovasculature throughout the murine brain, indiscriminate of vessel type and location, CE-MRA was performed using a self-assembling Gd-micelle blood pool agent synthesized in-house to induce high and sustained $r_1$ relaxivity within the blood pool, resulting in $T_1$-weighted vessel contrast throughout the acquisition time needed for high-resolution MRA. This protocol enabled us to acquire MR angiograms for vascular quantification and the monitoring of volumetric changes compared to CD31-probed IHC.

In contrast to commercially available low molecular weight Gd-DTPA (Magnevist), which is extravasated from the vascular space within 30 min, the Gd-micelles remained circulating in the vasculature for at least 2 h, at a 4-fold lower Gd dose, and cleared by 24 h (**Figure 2**). The significant circulation

**TABLE 6** | Cerebrovascular density in aged brains by immunohistochemical analysis.

| Cerebrovascular density (vessels/mm$^2$) by CD31-stained immunohistochemistry | | | |
|---|---|---|---|
| **Age group months** | **Whole brain** | **Cerebral cortex** | **Hippocampus** |
| 2–4 | 458.18 ± 61.28 | 500.60 ± 81.91 | 465.93 ± 83.71 |
| 14–16 | 420.15 ± 57.96 | 476.97 ± 49.18 | 384.32 ± 68.26 |
| 24–26 | 362.94 ± 49.34 | 377.02 ± 33.91 | 341.89 ± 38.18 |

*Quantification of the cerebrovascular density analyzed via CD31-probed IHC. Values represent the average density and standard deviation (N = 5).*

time of the Gd-micelles is most likely due to both size (Torchilin et al., 2000) and PEGylation (Croy and Kwon, 2006; Nishiyama and Kataoka, 2006; Qiu et al., 2007). With an average 15.63 nm diameter (**Table 1**), extravasation of the blood pool agent is largely inhibited (Torchilin et al., 2000; Aime and Caravan, 2009) and PEG chains at the micellar surface, contributed by PEG2000-DSPE (**Figure 1A**), prevent serum protein adsorption and antibody opsonization to further extend circulation time (Croy and Kwon, 2006; Nishiyama and Kataoka, 2006; Qiu et al., 2007). The agent's large size also contributes to a slower tumbling rate, which effectively increased its relaxivity (Lauffer, 1987, 1991), providing a 3.92-fold increase in $r_1$ over that of Magnevist per mM Gd (**Table 1**). With improved relaxation properties, the Gd-micelles was able to

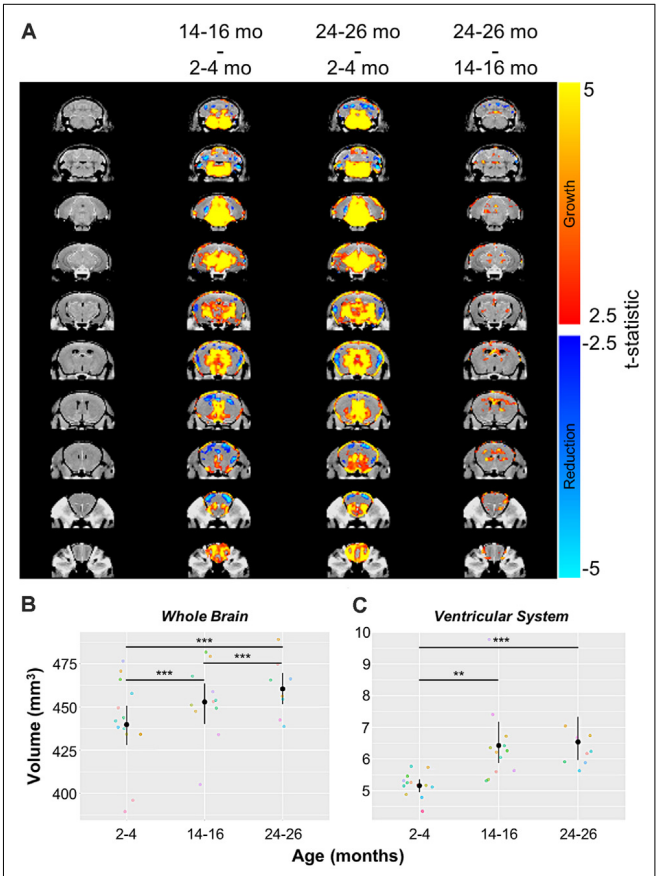


**FIGURE 8** | Volumetric changes in the whole brain and ventricular system over aging. **(A)** Deformation maps of global voxel-wise volumetric changes between 2–4 months, 14–16 months, and 24–26 months datasets with significance calculated per voxel with a false discovery rate <5%. Volumetric analyses of **(B)** the whole brain and **(C)** the ventricular system (the compiled lateral ventricles, third ventricle, cerebral aqueduct, and fourth ventricle). Symbol colors in **(B,C)** represent distinct mice and error bars represent the 95% confidence intervals. Separately, one-way analysis of variance (ANOVA) revealed a significant change in volume with age over the 2-year period for both the whole brain and ventricular system (***$p < 0.001$). Results of Tukey's HSD *post hoc* test between age groups are shown, where **$p < 0.01$, and ***$p < 0.001$.

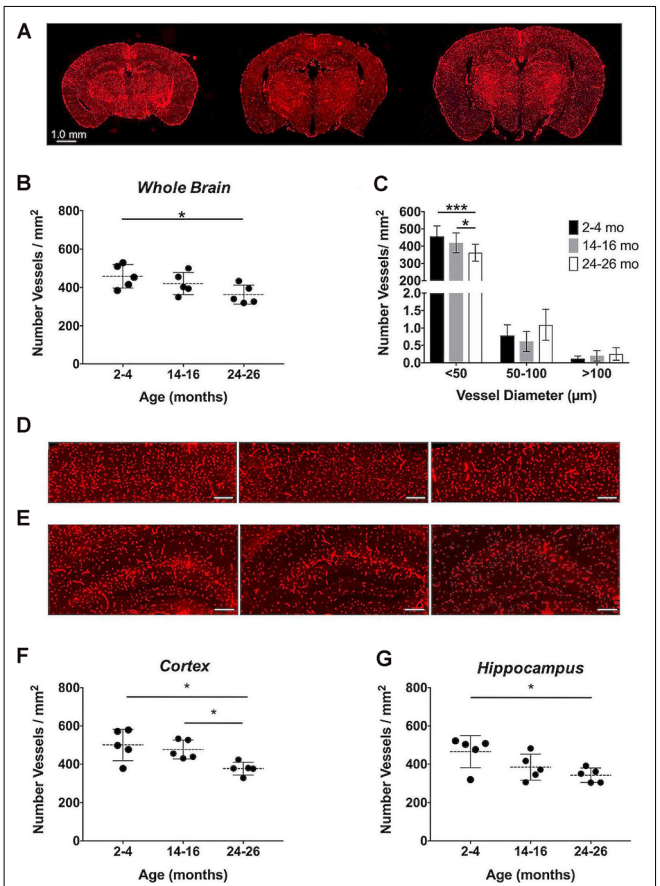


**FIGURE 9** | Immunohistochemical quantification of the cerebrovascular density over aging. **(A)** Representative CD31-stained histological sections of mouse brains at 2–4, 14–16, and 24–26 months (left-to-right). Quantification of the cerebrovascular density detected in the entire brain sections **(B)** overall and **(C)** separated by vessel size. Representative sections of the **(D)** cerebral cortex and **(E)** hippocampus at 2–4, 14–16, and 24–26 months (left-to-right), where scale bars indicate 200 μm. Quantifications of the cerebrovascular density in the **(F)** cerebral cortex and **(G)** hippocampus. All data represent the average density and standard deviation (*N* = 5 per age group). Results of Tukey's HSD test are shown, where *$p < 0.05$ and ***$p < 0.001$.

be injected at a 4-fold lower Gd dose than recommended for Magnevist (Lewis et al., 2012), reducing the potential risk of Gd-induced toxicity (Grobner and Prischl, 2007), while still providing adequate SNR, 3.19-fold higher than in the absence of contrast (**Figure 3**), for cerebrovascular detection. Together these results encouraged the use of Gd-micelles as a $T_1$-shortening blood pool agent for MRA studies of the cerebrovasculature in aging mice.

Automated registration (Friedel et al., 2014) of the MRA datasets to the previously developed C57BL/6J brain atlas (Dorr et al., 2008) compiled images acquired at 2–4, 14–16, and 24–26 mo within the same 3D space, allowing for virtual extraction of the whole brain as well as segmentation of major sub-brain ROIs. A visual assessment of the aligned brains and ROIs presented as MIPs revealed a loss of MRA-detectable vasculature, as demonstrated by model brains representative of each age group (**Figure 4**). Signal intensity-based thresholding of the cerebrovasculature that fit the criteria of aCBV in the whole brain volume (**Figure 5A**) revealed a 1.64% ± 0.18% aCBV at 2–4 months (**Figure 5B**, **Table 2**), within the 1–4.4% range previously described for the CBV in young adult murine brains (Boero et al., 1999; Heinzer et al., 2006, 2008; Serduc et al., 2006; Chugh et al., 2009; Tsai et al., 2009; Wu et al., 2014; Zhang et al., 2018), including those of the C57BL/6 strain (Chugh et al., 2009; Tsai et al., 2009; Wu et al., 2014; Zhang et al., 2018). Furthermore, the aCBV changes in the whole brain volume equated to an overall 24.39% loss of the aCBV over 2 years aging (**Figure 5B**, **Table 2**). While most aging studies focus on vascular quantification in specific regions of the brain, rather than the global cerebrovasculature, this loss is comparable to an *ex vivo* stereological examination of aged rats that demonstrated a 16% loss in global cerebrovasculature (Buchweitz-Milton and Weiss, 1987).

Specific sub-brain regions also demonstrated statistically significant decreases in the aCBV throughout aging (**Figures 5C–G**, **Table 2**). The cortex and hippocampus, two of the most widely examined regions for CBV loss in aging (Brown and Thore, 2011), demonstrated a 28.14 and 26.47% aCBV loss over 2 years, respectively (**Figures 5C,F**, **Table 2**). Both results are in agreement with previous studies of vascular reductions in the rat cortex (12–43% loss; Burns et al., 1981; Amenta et al., 1995) and hippocampus (20%–49%; Jucker et al., 1990; Amenta et al., 1995). While the smaller subset of mice studied longitudinally demonstrated similar losses in aCBV over aging, these reductions only demonstrated significance within the cerebral cortex, cerebellar cortex, and entorhinal cortex (**Figure 6**, **Table 3**), likely an effect of the smaller cohort size. Overall, Gd-micelle CE-MRA with 100 $(\mu m)^3$ resolution detected a decrease in the aCBV throughout the brain ROIs studied; however, improvements in sequence parameters, the use of cryoprobes, or increased Gd-micelle dose, may aid in achieving a higher spatial resolution to resolve vessels $<100$ μm in diameter, multiple of which may be contained within a single $(100\ \mu m)^3$ voxel in the current study.

Deformation-based morphometry revealed regions demonstrating both statistically significant growth and statistically significant reduction, with the majority of the brain showing growth from 2–4 to 14–16 months (**Figure 8A**). To a lesser extent, although still statistically significant, growth continued between 14–16 and 24–26 months (**Figure 8A**). Analysis of the whole brain and ventricular system both showed statistically significant increases in volume over the 2-year aging study with a 4.69% increase in whole brain volume and 26.74% increase in the volume of the ventricular system between mice aged 2–4 months and those aged 24–26 months, comparable to the percent enlargement demonstrated by Chen et al. (2011) in the whole brain and ventricles of similarly aged C57BL/6 mice. The percent volume occupied by the ventricles increased from 1.17% of the whole brain at 2–4 months to 1.42% at 14–16 months and 24–26 months (**Figures 8B,C**, **Table 5**). Previous aging studies have demonstrated statistically significant whole brain and ventricular growth in wild type mice over 14 months (Maheswaran et al., 2009) and nearly 2 years (Chen et al., 2011), with the relative brain volume occupied by the ventricles enlarging faster during early adulthood, before slowing at older ages. It is hypothesized that increases in ventricular volume beyond that demonstrated in normal aging could serve as a biomarker for Alzheimer's disease and its progression (Nestor et al., 2008; Chen et al., 2011). As demonstrated, CE-MRA is capable of simultaneously providing information on the volumetric changes of both the CBV and anatomical brain regions, supporting its use in exposing the differences in normal brain aging and disease.

IHC, probing for the endothelial cell marker CD31, demonstrated a statistically significant decrease in the cerebrovascular density over 2 years, with an overall 20.79% decrease (**Figures 9A,B**, **Table 6**). Although CE-MRA and IHC quantified the vasculature differently, percent volume ($mm^3/mm^3$) for CE-MRA and density ($vessels/mm^2$) for IHC, each with distinct limitations, the detected 20.79% percent decrease in cerebrovascular density by IHC was in good agreement with the 24.39% decrease in aCBV over 2 years. An evaluation of the vessel sizes detected that the major population of vessels, with diameters $<50$ μm, showed a significant reduction in density over 2 years (**Figure 9C**), supporting the well-described microvascular, particularly capillary, rarefaction detected in human and rat brains (Riddle et al., 2003; Brown and Thore, 2011). Cortical and hippocampal analyses by IHC also demonstrated significant decreases in vessel density over 2 years of aging (**Figures 9D–G**, **Table 6**). The 24.69% loss in vascular density that was detected in the cortex by IHC from 2–4 to 24–26 months (**Figures 9D,F**) was comparable to the 28.14% loss determined in the cortex by CE-MRA (**Figure 5C**, **Table 2**). Furthermore, these values are within the range of vascular loss described for rodent brains over aging (12–43%; Brown and Thore, 2011), but are moderately higher than the 19.26 ± 6.7% decrease recently described by Murugesan et al. (2012) in aging male C57BL/6J mice using *ex vivo* confocal microscopy between 6 and 24 months. IHC of the hippocampus demonstrated a 26.62% loss in vessel density over 2 years (**Figures 9E,G**, **Table 6**), compared to an overall 26.47% decrease detected in the hippocampus by CE-MRA (**Figure 5F**, **Table 2**).

Similarly, these values were within the range of vessel loss described in aging rats (20–49%; Brown and Thore, 2011) and were also in good agreement with the hippocampal loss detected by Murugesan et al. (2012) of 26.38 ± 5.63% in C57BL/6J mice.

While CE-MRA and IHC maintain vastly different capacities for resolving the cerebrovasculature, these techniques can be used in a complementary manner to monitor cerebrovascular alteration. Here, both methods have revealed a significant loss in vascularity in the aging C57BL/6 female mouse brain over a 2-year period. Differences between the two methods are contributed by MRA's lower resolution, whereby the current MRA protocol is capable of detecting, but not resolving, the <50 μm-diameter vessels largely identified *via* IHC. The IHC-determined loss in the number of vessels/mm$^2$ within whole brain sections, as well as in cortical and hippocampal regions, suggests that a structural loss in vascularity contributed significantly to the reduction in aCBV detected *via* CE-MRA.

Differences between the degree of cerebrovascular rarefaction described herein and that reported by Murugesan et al. (2012) may be due to the two studies' differing imaging modalities (MRA vs. confocal microscopy) and the nature of the tissue (*in vivo* vs. *ex vivo*). However, sex differences may also play a major role in brain aging. By limiting our study to aging female subjects, it is unknown if aging male C57BL/6 mice would have demonstrated a comparable loss of cerebrovasculature using our micelle-enhanced MRA methodology. Notably, previous studies of C57BL/6 mice have found that, compared to their aging male counterparts, aging female mice demonstrate a greater cognitive decline (Benice et al., 2006). An earlier onset for age-related hippocampal genetic alterations in the same mouse strain was also found in females that resulted in decreased bioenergetic metabolism and increased amyloid dyshomeostasis (Zhao et al., 2016). Considering these findings, the significant loss of cerebrovasculature in this female C57BL/6 cohort may serve as yet another characteristic of brain aging to which female mice may be more susceptible. Therefore, the use of an entirely female cohort could contribute to the greater vascular loss detected in the current study compared to that determined by Murugesan et al. (2012) for an all-male C57BL/6 cohort. Still, a single study of both sexes under identical conditions is needed to elucidate such differences. Furthermore, our results support previous research in demonstrating the profound impact that aging has on the brains of female C57BL/6 mice. How this translates to aging humans and predisposition to age-dependent conditions including Alzheimer's disease is still under investigation. Dementia and Alzheimer's disease have shown a higher prevalence in XX chromosome-harboring women over XY-harboring men (Beam et al., 2018). However, recent studies find that XX-women may have metabolically younger brains (Goyal et al., 2019) and demonstrate a slower rate of regional brain volume loss compared to age-matched XY-men (Armstrong et al., 2019). The evident complexity of brain aging and how it is impacted by variables including sex and co-morbidities is a further reason for conducting longitudinal studies in aging murine models as they may identify associated genetic, functional, and anatomic changes.

In addition to using this methodology to investigate age-matched sex differences, it can also be employed for qualitative and quantitative assessments of cerebrovascular alterations in neurovascular diseases and response to therapeutic interventions. The rapid recovery time following the femoral injection of the micellar contrast agent and clearance within 24 h allows our approach to be repeatable. Therefore, our MRA method is particularly well-suited for longitudinal studies aiming to track and localize the progression of regional vascular changes in angiopathies and neurodegenerative diseases. Additionally, this noninvasive and non-ionizing imaging technique can be equally valuable to monitor the response to therapy at a multitude of time points as well as to assess the variability amongst individual subjects. This technique is also applicable for single time point cross-sectional studies followed by IHC 24 h later.

In considering repeated studies, our choice of femoral cannulation was motivated by our need to control the precise dose and rate of infusion of the micellar blood pool agent to ensure reproducibility and prevent mis-administration typically associated with tail injection (Groman and Reinhardt, 2004). Hence, femoral cannulation would not be appropriate for daily examination. Instead, an indwelling catheter system such as those employed in repeat murine blood sampling (Park et al., 2018) could be considered. Alternatively, tail vein injection may be considered when performed by highly skilled researchers, enabling frequent injections. Animal exposure to anesthesia, such as isoflurane employed in our study, is another limiting factor. Repeated exposure to isoflurane, while generally considered a safe anesthetic option, has been reported to cause anxiety, motor deficits, altered white matter integrity (Bajwa et al., 2019), and oxidative stress (Berkowitz et al., 2020). The qualitative micelle pharmacokinetic characterization performed in **Figure 2** illustrates the tradeoff between effective vascular detection and complete micelle washout between imaging sessions. The reduced dose of 0.75 μmol Gd/30 g Gd-micelle enabled full clearance within 24 h and reduced the risk of Gd-induced toxicity (Grobner and Prischl, 2007) while providing remarkable vascular enhancement.

CE-MRA offers the advantage of indiscriminate whole head detection and visualization of both the arterial and venous blood volumes regardless of flow. In comparison, TOF-MRA typically limits the detection to arteries within a reduced FOV, which are governed by the inflowing strength of proximal blood. This in turn predominantly excludes the venous component (Axel, 1984; Nishimura, 1990). On the other hand, CE-MRA prevents an immediate understanding of whether cerebrovascular changes predominate in arteries or veins. In this case, the alignment of acquired images to cerebral vascular atlases, such as those described by Dorr et al. (2007) and Xiong et al. (2017), will help delineate the venous and arterial compartments and permit their respective quantification. This additional step may facilitate the examination of mouse models of cardiovascular diseases, including heart

failure associated with increased cerebral venous pressure, small vessel damage, and blood-brain barrier disruption (Fulop et al., 2019).

## CONCLUSION

We have observed a significant loss in cerebrovasculature over 2 years of aging in the C57BL/6 mouse strain using both *in vivo* whole head CE-MRA and IHC-probed histological analysis. While the majority of our knowledge regarding the cerebrovasculature is the result of *ex vivo* 2D studies, the use of *in vivo* whole-brain analyses, such as the CE-MRA technique described here, can improve our understanding of the global murine cerebrovasculature, its variability amongst subjects and strains, and its changes during aging. The $(100\ \mu m)^3$ resolution employed is significantly lower than that of histological examination. However, CE-MRA still provided minimally invasive *in vivo* assessment of the cerebrovascular morphology and detectable aCBV with coverage of the entire murine head. Due to its non-destructive and non-to-minimally invasive nature, this technique allowed for both single time point and longitudinal studies in aging subjects to illustrate significant, albeit variable, loss of CBV throughout the aging murine brain along with enlargement of the whole brain and ventricular volumes. Together, the changes detected by CE-MRA and IHC suggest that the vascular rarefaction widely-described in aging human and rat brains is also present in the most widely studied inbred mouse strain (Bryant, 2011). Age-dependent vascular rarefaction in wild type C57BL/6 mice should, therefore, be accounted for when using this popular strain for studies of age-dependent diseases of the cerebrovasculature.

## DATA AVAILABILITY STATEMENT

The raw data supporting the conclusions of this article will be made available by the authors, without undue reservation.

## ETHICS STATEMENT

The animal study was reviewed and approved by NYU Grossman School of Medicine's Institutional Animal Care and Use Committee (IACUC).

## AUTHOR CONTRIBUTIONS

LH: conceptualization, methodology, validation, formal analysis, investigation, data curation, writing—original draft, and visualization. DH: methodology, software, validation, and data curation. LC: methodology, validation, investigation, resources, data curation, and writing—review & editing. TW: methodology, and writing—review & editing. MS: methodology, resources, writing—review & editing, and funding acquisition. YW: conceptualization, methodology, software, resources, writing—review & editing, supervision, project administration, and funding acquisition. All authors contributed to the article and approved the submitted version.

## FUNDING

This work was initially supported in part by the Alzheimer Association IIRG-08-91618 and the American Health Assistance Foundation Alzheimer Disease Research Grant A2008-155 to YW and was subsequently partially funded by the NSF-DMREF under Award Number DMR 1728858 to YW, NSF-MRSEC Program under Award Number DMR 1420073, the NYU Shiffrin-Myers Breast Cancer Discovery Fund to YW and the NYU CTSA grant UL1 TR000038 from the National Center for Advancing Translational Sciences to YW and MS, National Institutes of Health. The majority of this work was performed at the NYU Langone Health Preclinical Imaging Laboratory, a shared resource partially supported by the NIH/SIG 1S10OD018337-01, the Laura and Isaac Perlmutter Cancer Center Support Grant, NIH/NCI 5P30CA016087, and the NIBIB Biomedical Technology Resource Center Grant NIH P41 EB017183. Acquisition of aged mice from the National Institute on Aging and their subsequent husbandry was supported through grants 1R01AG053990, K02AG034176-05S1, and 2R01AG031221 to MS, as well as P30AG066512 and P01AG060882 to TW. Micelles were characterized *via* ICP-OES by Galbraith Laboratories, Inc. Image registration and deformation were supported by The Mouse Imaging Centre and Compute Canada (www.computecanada.ca), with special thanks to Dr. Jason Lerch, Benjamin Darwin, and Matthijs van Eede. All *ex vivo* tissue processing and histology were performed by The NYU Experimental Pathology Immunohistochemistry Core Laboratory, which is supported in part by the Laura and Isaac Perlmutter Cancer Center Support Grant, NIH /NCI P30CA016087, and the NIH S10 Grants, NIH/ORIP S10OD01058, and S10OD018338.

## ACKNOWLEDGMENTS

We would like to thank Dr. Karen Briley for advisement on micelle synthesis and Drs. Zahi Fayad and Willem Mulder of the Icahn School of Medicine at Mount Sinai Hospital for access to their facilities, including the use of their Bruker Minispec MQ-one TD-NMR. We would also like to thank the laboratories of Drs. Daniel Turnbull, Sungheon Gene Kim, and Jiangyang Zhang for their critical advice, with special thanks to Dr. Harikrishna Rallapalli for his assistance in acquiring the deformation-based morphometry analysis, Willis Chen and Sebastian Mendoza for their assistance with brain extraction, Orlando Aristizábal for his assistance with Amira software, and Dr. César A. Berríos-Otero for his assistance with data processing.

## SUPPLEMENTARY MATERIAL

The Supplementary Material for this article can be found online at: https://www.frontiersin.org/articles/10.3389/fnagi.2020.585218/full#supplementary-material.

## REFERENCES


Afonso-Oramas, D., Cruz-Muros, I., Castro-Hernández, J., Salas-Hernández, J., Barroso-Chinea, P., García-Hernández, S., et al. (2014). Striatal vessels receive phosphorylated tyrosine hydroxylase-rich innervation from midbrain dopaminergic neurons. *Front. Neuroanat.* 8:84.doi: 10.3389/fnana.2014.00084

Aime, S., and Caravan, P. (2009). Biodistribution of gadolinium-based contrast agents, including gadolinium deposition. *J. Magn. Reson. Imaging* 30, 1259–1267. doi: 10.1002/jmri.21969

Amenta, F., Cavallotti, D., Del Valle, M., Mancini, M., Naves, F. J., Vega, J. A., et al. (1995). Age-related changes in brain microanatomy: sensitivity to treatment with the dihydropyridine calcium channel blocker darodipine (PY 108–068). *Brain Res. Bull.* 36, 453–460. doi: 10.1016/0361-9230(94)00210-r

Amtul, Z., and Hepburn, J. D. (2014). Protein markers of cerebrovascular disruption of neurovascular unit: immunohistochemical and imaging approaches. *Rev. Neurosci.* 25, 481–507. doi: 10.1515/revneuro-2013-0041

An, X.-L., Zou, J.-X., Wu, R.-Y., Yang, Y., Tai, F.-D., Zeng, S.-Y., et al. (2011). Strain and sex differences in anxiety-like and social behaviors in C57BL/6J and BALB/cJ mice. *Exp. Anim.* 60, 111–123. doi: 10.1538/expanim.60.111

Armstrong, N. M., An, Y., Beason-Held, L., Doshi, J., Erus, G., Ferrucci, L., et al. (2019). Sex differences in brain aging and predictors of neurodegeneration in cognitively healthy older adults. *Neurobiol. Aging* 81, 146–156. doi: 10.1016/j.neurobiolaging.2019.05.020

Axel, L. (1984). Blood flow effects in magnetic resonance imaging. *AJR Am. J. Roentgenol.* 143, 1157–1166.

Bajwa, N. M., Lee, J. B., Halavi, S., Hartman, R. E., and Obenaus, A. (2019). Repeated isoflurane in adult male mice leads to acute and persistent motor decrements with long-term modifications in corpus callosum microstructural integrity. *J. Neurosci. Res.* 97, 332–345. doi: 10.1002/jnr.24343

Beam, C. R., Kaneshiro, C., Jang, J. Y., Reynolds, C. A., Pedersen, N. L., and Gatz, M. (2018). Differences between women and men in incidence rates of dementia and alzheimer's disease. *J. Alzheimers Dis.* 64, 1077–1083. doi: 10.3233/JAD-180141

Beckmann, N. (2000). High resolution magnetic resonance angiography non-invasively reveals mouse strain differences in the cerebrovascular anatomy *in vivo*. *Magn. Reson. Med.* 44, 252–258. doi: 10.1002/1522-2594(200008)44:2<252::aid-mrm12>3.0.co;2-g

Benice, T. S., Rizk, A., Kohama, S., Pfankuch, T., and Raber, J. (2006). Sex-differences in age-related cognitive decline in C57BL/6J mice associated with increased brain microtubule-associated protein 2 and synaptophysin immunoreactivity. *Neuroscience* 137, 413–423. doi: 10.1016/j.neuroscience.2005.08.029

Berkowitz, B. A., Podolsky, R. H., Childers, K. L., Gow, A., Schneider, B. L., Lloyd, S. C., et al. (2020). Age-related murine hippocampal CA1 laminae oxidative stress measured *in vivo* by QUEnch-assiSTed (QUEST) MRI: impact of isoflurane anesthesia. *Geroscience* 42, 563–574. doi: 10.1007/s11357-020-00162-8

Boero, J. A., Ascher, J., Arregui, A., Rovainen, C., and Woolsey, T. A. (1999). Increased brain capillaries in chronic hypoxia. *J. Appl. Physiol.* 86, 1211–1219. doi: 10.1152/jappl.1999.86.4.1211

Boutajangout, A., Quartermain, D., and Sigurdsson, E. M. (2010). Immunotherapy targeting pathological tau prevents cognitive decline in a new tangle mouse model. *J. Neurosci.* 30, 16559–16566. doi: 10.1523/JNEUROSCI.4363-10.2010

Briley-Saebo, K. C., Amirbekian, V., Mani, V., Aguinaldo, J. G. S., Vucic, E., Carpenter, D., et al. (2006). Gadolinium mixed-micelles: effect of the amphiphile on *in vitro* and *in vivo* efficacy in apolipoprotein E knockout mouse models of atherosclerosis. *Magn. Reson. Med.* 56, 1336–1346. doi: 10.1002/mrm.21094

Briley-Saebo, K. C., Shaw, P. X., Mulder, W. J. M., Choi, S.-H., Vucic, E., Aguinaldo, J. G. S., et al. (2008). Targeted molecular probes for imaging atherosclerotic lesions with magnetic resonance using antibodies that recognize oxidation-specific epitopes. *Circulation* 117, 3206–3215. doi: 10.1161/CIRCULATIONAHA.107.757120

Brown, W. R., and Thore, C. R. (2011). Review: cerebral microvascular pathology in ageing and neurodegeneration. *Neuropathol. Appl. Neurobiol.* 37, 56–74. doi: 10.1111/j.1365-2990.2010.01139.x

Bryant, C. D. (2011). The blessings and curses of C57BL/6 substrains in mouse genetic studies. *Ann. N Y Acad. Sci.* 1245, 31–33. doi: 10.1111/j.1749-6632.2011.06325.x

Buchweitz-Milton, E., and Weiss, H. R. (1987). Perfused capillary morphometry in the senescent brain. *Neurobiol. Aging* 8, 271–276. doi: 10.1016/0197-4580(87)90012-1

Bullitt, E., Zeng, D., Mortamet, B., Ghosh, A., Aylward, S. R., Lin, W., et al. (2010). The effects of healthy aging on intracerebral blood vessels visualized by magnetic resonance angiography. *Neurobiol. Aging* 31, 290–300. doi: 10.1016/j.neurobiolaging.2008.03.022

Burns, E. M., Kruckeberg, T. W., and Gaetano, P. K. (1981). Changes with age in cerebral capillary morphology. *Neurobiol. Aging* 2, 283–291. doi: 10.1016/0197-4580(81)90037-3

Burtea, C., Laurent, S., Vander Elst, L., and Muller, R. N. (2008). Contrast agents: magnetic resonance. *Handb. Exp. Pharmacol.* 135–165. doi: 10.1007/978-3-540-72718-7_7

Caravan, P., Ellison, J. J., McMurry, T. J., and Lauffer, R. B. (1999). Gadolinium(III) chelates as MRI contrast agents: structure, dynamics and applications. *Chem. Rev.* 99, 2293–2352. doi: 10.1021/cr980440x

Cerchiai, N., Mancuso, M., Navari, E., Giannini, N., and Casani, A. P. (2017). Aging with cerebral small vessel disease and dizziness: the importance of undiagnosed peripheral vestibular disorders. *Front. Neurol.* 8:241.doi: 10.3389/fneur.2017.00241

Chen, C.-C. V., Tung, Y.-Y., and Chang, C. (2011). A lifespan MRI evaluation of ventricular enlargement in normal aging mice. *Neurobiol. Aging* 32, 2299–2307. doi: 10.1016/j.neurobiolaging.2010.01.013

Chugh, B. P., Lerch, J. P., Yu, L. X., Pienkowski, M., Harrison, R. V., Henkelman, R. M., et al. (2009). Measurement of cerebral blood volume in mouse brain regions using micro-computed tomography. *NeuroImage* 47, 1312–1318. doi: 10.1016/j.neuroimage.2009.03.083

Chung, K., Wallace, J., Kim, S.-Y., Kalyanasundaram, S., Andalman, A. S., Davidson, T. J., et al. (2013). Structural and molecular interrogation of intact biological systems. *Nature* 497, 332–337. doi: 10.1038/nature12107

Chung, M. K., Worsley, K. J., Paus, T., Cherif, C., Collins, D. L., Giedd, J. N., et al. (2001). A unified statistical approach to deformation-based morphometry. *NeuroImage* 14, 595–606. doi: 10.1006/nimg.2001.0862

Croy, S. R., and Kwon, G. S. (2006). Polymeric micelles for drug delivery. *Curr. Pharm. Des.* 12, 4669–4684. doi: 10.2174/138161206779026245

D'Agostino, R. B. (1986). *Goodness-of-Fit-Techniques (statistics: A Series Of Textbooks And Monographs, Vol. 68)*, 1st Edn. New York, NY: Dekker.

De Cocker, L. J. L., Lövblad, K.-O., and Hendrikse, J. (2017). MRI of cerebellar infarction. *Eur. Neurol.* 77, 137–146. doi: 10.1159/000455229

de la Torre, J. C. (2004). Is Alzheimer's disease a neurodegenerative or a vascular disorder? Data, dogma and dialectics. *Lancet Neurol.* 3, 184–190. doi: 10.1016/S1474-4422(04)00683-0

Dorr, A. E., Lerch, J. P., Spring, S., Kabani, N., and Henkelman, R. M. (2008). High resolution three-dimensional brain atlas using an average magnetic resonance image of 40 adult C57Bl/6J mice. *NeuroImage* 42, 60–69. doi: 10.1016/j.neuroimage.2008.03.037

Dorr, A., Sled, J. G., and Kabani, N. (2007). Three-dimensional cerebral vasculature of the CBA mouse brain: a magnetic resonance imaging and micro computed tomography study. *NeuroImage* 35, 1409–1423. doi: 10.1016/j.neuroimage.2006.12.040

Driehuys, B., Nouls, J., Badea, A., Bucholz, E., Ghaghada, K., Petiet, A., et al. (2008). Small animal imaging with magnetic resonance microscopy. *ILAR J.* 49, 35–53. doi: 10.1093/ilar.49.1.35

Eskola, S., and Kaliste-Korhonen, E. (1999). Aspen wood-wool is preferred as a resting place, but does not affect intracage fighting of male BALB/c and C57BL/6J mice. *Lab. Anim.* 33, 108–121. doi: 10.1258/002367799780578273

Estelrich, J., Sánchez-Martín, M. J., and Busquets, M. A. (2015). Nanoparticles in magnetic resonance imaging: from simple to dual contrast agents. *Int. J. Nanomedicine* 10, 1727–1741. doi: 10.2147/IJN.S76501

Feekes, J. A., and Cassell, M. D. (2006). The vascular supply of the functional compartments of the human striatum. *Brain* 129, 2189–2201. doi: 10.1093/brain/awl158

Friedel, M., van Eede, M. C., Pipitone, J., Chakravarty, M. M., and Lerch, J. P. (2014). Pydpiper: a flexible toolkit for constructing novel registration pipelines. *Front. Neuroinformatics* 8:67. doi: 10.3389/fninf.2014.00067

Fulop, G. A., Ahire, C., Csipo, T., Tarantini, S., Kiss, T., Balasubramanian, P., et al. (2019). Cerebral venous congestion promotes blood-brain barrier disruption and neuroinflammation, impairing cognitive function in mice. *Geroscience* 41, 575–589. doi: 10.1007/s11357-019-00110-1

Genovese, C. R., Lazar, N. A., and Nichols, T. (2002). Thresholding of statistical maps in functional neuroimaging using the false discovery rate. *NeuroImage* 15, 870–878. doi: 10.1006/nimg.2001.1037

Ghanavati, S., Lerch, J. P., and Sled, J. G. (2014a). Automatic anatomical labeling of the complete cerebral vasculature in mouse models. *NeuroImage* 95, 117–128. doi: 10.1016/j.neuroimage.2014.03.044

Ghanavati, S., Yu, L. X., Lerch, J. P., and Sled, J. G. (2014b). A perfusion procedure for imaging of the mouse cerebral vasculature by X-ray micro-CT. *J. Neurosci. Methods* 221, 70–77. doi: 10.1016/j.jneumeth.2013.09.002

Goyal, M. S., Blazey, T. M., Su, Y., Couture, L. E., Durbin, T. J., Bateman, R. J., et al. (2019). Persistent metabolic youth in the aging female brain. *Proc. Natl. Acad. Sci. U S A* 116, 3251–3255. doi: 10.1073/pnas.1815917116

Gray, M. T., and Woulfe, J. M. (2015). Striatal blood-brain barrier permeability in Parkinson's disease. *J. Cereb. Blood Flow Metab.* 35, 747–750. doi: 10.1038/jcbfm.2015.32

Grobner, T., and Prischl, F. C. (2007). Gadolinium and nephrogenic systemic fibrosis. *Kidney Int.* 72, 260–264. doi: 10.1038/sj.ki.5002338

Groman, E. V., and Reinhardt, C. P. (2004). Method to quantify tail vein injection technique in small animals. *Contemp. Top. Lab. Anim. Sci.* 43, 35–38.

Guan, J., Pavlovic, D., Dalkie, N., Waldvogel, H. J., O'Carroll, S. J., Green, C. R., et al. (2013). Vascular degeneration in Parkinson's disease. *Brain Pathol.* 23, 154–164. doi: 10.1111/j.1750-3639.2012.00628.x

Hagberg, G. E., and Scheffler, K. (2013). Effect of $r_1$ and $r_2$ relaxivity of gadolinium-based contrast agents on the $T_1$-weighted MR signal at increasing magnetic field strengths. *Contrast Media Mol. Imaging* 8, 456–465. doi: 10.1002/cmmi.1565

Hashemi, R. H., Bradley, W. G., and Lisanti, C. J. (2004). *MRI: The Basics.* Philadelphia, PA: Lippincott Williams and Wilkins.

Heinzer, S., Krucker, T., Stampanoni, M., Abela, R., Meyer, E. P., Schuler, A., et al. (2006). Hierarchical microimaging for multiscale analysis of large vascular networks. *NeuroImage* 32, 626–636. doi: 10.1016/j.neuroimage.2006.03.043

Heinzer, S., Kuhn, G., Krucker, T., Meyer, E., Ulmann-Schuler, A., Stampanoni, M., et al. (2008). Novel three-dimensional analysis tool for vascular trees indicates complete micro-networks, not single capillaries, as the angiogenic endpoint in mice overexpressing human VEGF(165) in the brain. *NeuroImage* 39, 1549–1558. doi: 10.1016/j.neuroimage.2007.10.054

Hirsch, S., Reichold, J., Schneider, M., Székely, G., and Weber, B. (2012). Topology and hemodynamics of the cortical cerebrovascular system. *J. Cereb. Blood Flow Metab.* 32, 952–967. doi: 10.1038/jcbfm.2012.39

Hoogendam, Y. Y., van der Geest, J. N., van der Lijn, F., van der Lugt, A., Niessen, W. J., Krestin, G. P., et al. (2012). Determinants of cerebellar and cerebral volume in the general elderly population. *Neurobiol. Aging* 33, 2774–2781. doi: 10.1016/j.neurobiolaging.2012.02.012

Howles, G. P., Ghaghada, K. B., Qi, Y., Mukundan, S., and Johnson, G. A. (2009). High-resolution magnetic resonance angiography in the mouse using a nanoparticle blood-pool contrast agent. *Magn. Reson. Med.* 62, 1447–1456. doi: 10.1002/mrm.22154

Jucker, M., Bättig, K., and Meier-Ruge, W. (1990). Effects of aging and vincamine derivatives on pericapillary microenvironment: stereological characterization of the cerebral capillary network. *Neurobiol. Aging* 11, 39–46. doi: 10.1016/0197-4580(90)90060-d

Kara, F., van Dongen, E. S., Schliebs, R., van Buchem, M. A., de Groot, H. J. M., and Alia, A. (2012). Monitoring blood flow alterations in the Tg2576 mouse model of Alzheimer's disease by *in vivo* magnetic resonance angiography at 17.6 T. *NeuroImage* 60, 958–966. doi: 10.1016/j.neuroimage.2011.12.055

Klohs, J., Rudin, M., Shimshek, D. R., and Beckmann, N. (2014). Imaging of cerebrovascular pathology in animal models of Alzheimer's disease. *Front. Aging Neurosci.* 6:32.doi: 10.3389/fnagi.2014.00032

Kolmogorov, A. (1933). Sulla determinazione empirica di una legge di distribuzione. *G. Inst. Ital. Attuari* 4, 83–91.

Krucker, T., Lang, A., and Meyer, E. P. (2006). New polyurethane-based material for vascular corrosion casting with improved physical and imaging characteristics. *Microsc. Res. Tech.* 69, 138–147. doi: 10.1002/jemt.20263

Krucker, T., Schuler, A., Meyer, E. P., Staufenbiel, M., and Beckmann, N. (2004). Magnetic resonance angiography and vascular corrosion casting as tools in biomedical research: application to transgenic mice modeling Alzheimer's disease. *Neurol. Res.* 26, 507–516. doi: 10.1179/016164104225016281

Lauffer, R. B. (1987). Paramagnetic metal complexes as water proton relaxation agents for NMR imaging: theory and design. *Chem. Rev.* 87, 901–927. doi: 10.1021/cr00081a003

Lauffer, R. B. (1991). Targeted relaxation enhancement agents for MRI. *Magn. Reson. Med.* 22, 339–342; discussion 343.doi: 10.1002/mrm.1910220237

Lee, G. H., Chang, Y., and Kim, T.-J. (2012). Blood-pool and targeting MRI contrast agents: from Gd-chelates to Gd-nanoparticles. *Eur. J. Inorg. Chem.* 2012, 1924–1933. doi: 10.1002/ejic.201101137

Lerch, J. P., Carroll, J. B., Spring, S., Bertram, L. N., Schwab, C., Hayden, M. R., et al. (2008). Automated deformation analysis in the YAC128 huntington disease mouse model. *NeuroImage* 39, 32–39. doi: 10.1016/j.neuroimage.2007.08.033

Lewis, M., Yanny, S., and Malcolm, P. N. (2012). Advantages of blood pool contrast agents in MR angiography: a pictorial review. *J. Med. Imaging Radiat. Oncol.* 56, 187–191. doi: 10.1111/j.1754-9485.2012.02347.x

Li, A., Gong, H., Zhang, B., Wang, Q., Yan, C., Wu, J., et al. (2010). Micro-optical sectioning tomography to obtain a high-resolution atlas of the mouse brain. *Science* 330, 1404–1408. doi: 10.1126/science.1191776

Lockhart, S. N., and DeCarli, C. (2014). Structural imaging measures of brain aging. *Neuropsychol. Rev.* 24, 271–289. doi: 10.1007/s11065-014-9268-3

Lohrke, J., Frenzel, T., Endrikat, J., Alves, F. C., Grist, T. M., Law, M., et al. (2016). 25 years of contrast-enhanced MRI: developments, current challenges and future perspectives. *Adv. Ther.* 33, 1–28. doi: 10.1007/s12325-015-0275-4

Maheswaran, S., Barjat, H., Rueckert, D., Bate, S. T., Howlett, D. R., Tilling, L., et al. (2009). Longitudinal regional brain volume changes quantified in normal aging and Alzheimer's APP × PS1 mice using MRI. *Brain Res.* 1270, 19–32. doi: 10.1016/j.brainres.2009.02.045

Martin, A. J., Friston, K. J., Colebatch, J. G., and Frackowiak, R. S. (1991). Decreases in regional cerebral blood flow with normal aging. *J. Cereb. Blood Flow Metab.* 11, 684–689. doi: 10.1038/jcbfm.1991.121

McDonald, D. M., and Choyke, P. L. (2003). Imaging of angiogenesis: from microscope to clinic. *Nat. Med.* 9, 713–725. doi: 10.1038/nm0603-713

Meyer, E. P., Ulmann-Schuler, A., Staufenbiel, M., and Krucker, T. (2008). Altered morphology and 3D architecture of brain vasculature in a mouse model for Alzheimer's disease. *Proc. Natl. Acad. Sci. U S A* 105, 3587–3592. doi: 10.1073/pnas.0709788105

Moy, A. J., Wiersma, M. P., and Choi, B. (2013). Optical histology: a method to visualize microvasculature in thick tissue sections of mouse brain. *PLoS One* 8:e53753.doi: 10.1371/journal.pone.0053753

Murugesan, N., Demarest, T. G., Madri, J. A., and Pachter, J. S. (2012). Brain regional angiogenic potential at the neurovascular unit during normal aging. *Neurobiol. Aging* 33, 1004.e1–1004.e16. doi: 10.1016/j.neurobiolaging.2011.09.022

Neelavalli, J., and Haacke, E. M. (2007). A simplified formula for T1 contrast optimization for short-TR steady-state incoherent (spoiled) gradient echo sequences. *Magn. Reson. Imaging* 25, 1397–1401. doi: 10.1016/j.mri.2007.03.026

Nestor, S. M., Rupsingh, R., Borrie, M., Smith, M., Accomazzi, V., Wells, J. L., et al. (2008). Ventricular enlargement as a possible measure of Alzheimer's disease progression validated using the Alzheimer's disease neuroimaging initiative database. *Brain* 131, 2443–2454. doi: 10.1093/brain/awn146

Ni, R., Kindler, D. R., Waag, R., Rouault, M., Ravikumar, P., Nitsch, R., et al. (2019). fMRI reveals mitigation of cerebrovascular dysfunction by bradykinin receptors 1 and 2 inhibitor noscapine in a mouse model of cerebral amyloidosis. *Front. Aging Neurosci.* 11:27.doi: 10.3389/fnagi.2019.00027

Nielsen, Y. W., and Thomsen, H. S. (2012). Contrast-enhanced peripheral MRA: technique and contrast agents. *Acta Radiol.* 53, 769–777. doi: 10.1258/ar.2012.120008

Nieman, B. J., Szulc, K. U., and Turnbull, D. H. (2009). Three-dimensional, *in vivo* MRI with self-gating and image coregistration in the mouse. *Magn. Reson. Med.* 61, 1148–1157. doi: 10.1002/mrm.21945

Nishimura, D. G. (1990). Time-of-flight MR angiography. *Magn. Reson. Med.* 14, 194–201. doi: 10.1002/mrm.1910140206

Nishimura, D. G., Macovski, A., and Pauly, J. M. (1986). Magnetic resonance angiography. *IEEE Trans. Med. Imaging* 5, 140–151. doi: 10.1109/TMI.1986.4307763

Nishiyama, N., and Kataoka, K. (2006). Current state, achievements and future prospects of polymeric micelles as nanocarriers for drug and gene delivery. *Pharmacol. Ther.* 112, 630–648. doi: 10.1016/j.pharmthera.2006.05.006

Park, A. Y., Plotsky, P. M., Pham, T. D., Pacak, K., Wynne, B. M., Wall, S. M., et al. (2018). Blood collection in unstressed, conscious, and freely moving mice through implantation of catheters in the jugular vein: a new simplified protocol. *Physiol. Rep.* 6:e13904.doi: 10.14814/phy2.13904

Qiu, L., Zheng, C., Jin, Y., and Zhu, K. (2007). Polymeric micelles as nanocarriers for drug delivery. *Expert Opin. Ther. Pat.* 17, 819–830. doi: 10.1517/13543776.17.7.819

Riddle, D. R., Sonntag, W. E., and Lichtenwalner, R. J. (2003). Microvascular plasticity in aging. *Ageing Res. Rev.* 2, 149–168. doi: 10.1016/s1568-1637(02)00064-8

Rohrer, M., Bauer, H., Mintorovitch, J., Requardt, M., and Weinmann, H.-J. (2005). Comparison of magnetic properties of MRI contrast media solutions at different magnetic field strengths. *Invest. Radiol.* 40, 715–724. doi: 10.1097/01.rli.0000184756.66360.d3

Schneider, C. A., Rasband, W. S., and Eliceiri, K. W. (2012). NIH Image to ImageJ: 25 years of image analysis. *Nat. Methods* 9, 671–675. doi: 10.1038/nmeth.2089

Schuff, N., Du, A. T., Amend, D., Hsu, Y. Y., Laakso, M. P., Jagust, W., et al. (2001). "MRI of Entorhinal cortex and hippocampus in Alzheimer's disease, subcortical ischemic vascular dementia and mixed dementia," in *Alzheimer's Disease: Advances in Etiology, Pathogenesis and Therapeutics*, eds K. Iqbal, S. S. Sisodia, and B. Winblad (Chichester, UK: John Wiley and Sons, Limited), 229–236.

Serduc, R., Vérant, P., Vial, J.-C., Farion, R., Rocas, L., Rémy, C., et al. (2006). *in vivo* two-photon microscopy study of short-term effects of microbeam irradiation on normal mouse brain microvasculature. *Int. J. Radiat. Oncol. Biol. Phys.* 64, 1519–1527. doi: 10.1016/j.ijrobp.2005.11.047

Shapiro, S. S., and Wilk, M. B. (1965). An analysis of variance test for normality (complete samples). *Biometrika* 52, 591–611. doi: 10.1093/biomet/52.3-4.591

Smirnov, N. V. (1939). *Estimate of Deviation Between Empirical Distribution Functions in Two Independent Samples.* Moscow, Russia: Bulletin Moscow University.

Steinman, J., Koletar, M. M., Stefanovic, B., and Sled, J. G. (2017). 3D morphological analysis of the mouse cerebral vasculature: comparison of *in vivo* and *ex vivo* methods. *PLoS One* 12:e0186676.doi: 10.1371/journal.pone.0186676

Svare, B., Mann, M., Broida, J., Kinsley, C., Ghiraldi, L., Miele, J., et al. (1983). Intermale aggression and infanticide in aged C57BL/6J male mice: behavioral deficits are not related to serum testosterone (T) levels and are not recovered by supplemental T. *Neurobiol. Aging* 4, 305–312. doi: 10.1016/0197-4580(83)90007-6

Tarasoff-Conway, J. M., Carare, R. O., Osorio, R. S., Glodzik, L., Butler, T., Fieremans, E., et al. (2015). Clearance systems in the brain-implications for Alzheimer disease. *Nat. Rev. Neurol.* 11, 457–470. doi: 10.1038/nrneurol.2015.119

Torchilin, V. P. (2000). Polymeric contrast agents for medical imaging. *Curr. Pharm. Biotechnol.* 1, 183–215. doi: 10.2174/1389201003378960

Torchilin, V., Babich, J., and Weissig, V. (2000). Liposomes and micelles to target the blood pool for imaging purposes. *J. Liposome Res.* 10, 483–499. doi: 10.3109/08982100009031113

Tsai, P. S., Kaufhold, J. P., Blinder, P., Friedman, B., Drew, P. J., Karten, H. J., et al. (2009). Correlations of neuronal and microvascular densities in murine cortex revealed by direct counting and colocalization of nuclei and vessels. *J. Neurosci.* 29, 14553–14570. doi: 10.1523/JNEUROSCI.3287-09.2009

Ungvari, Z., and Sonntag, W. E. (2014). Brain and cerebrovascular aging--new mechanisms and insights. *J. Gerontol. A Biol. Sci. Med. Sci.* 69, 1307–1310. doi: 10.1093/gerona/glu187

Vincent, R. D., Janke, A., Sled, J. G., and Baghdadi, L. (2004). "MINC 2.0: a modality independent format for multidimensional medical images," in *Proceedings of the 10th Annual Meeting of the Organization for Human Brain Mapping*, Vol. 22, Budapest.

Vincent, R. D., Neelin, P., Khalili-Mahani, N., Janke, A. L., Fonov, V. S., Robbins, S. M., et al. (2016). MINC 2.0: a flexible format for multi-modal images. *Front. Neuroinformatics* 10:35. doi: 10.3389/fninf.2016.00035

Walhovd, K. B., Fjell, A. M., Reinvang, I., Lundervold, A., Dale, A. M., Eilertsen, D. E., et al. (2005). Effects of age on volumes of cortex, white matter and subcortical structures. *Neurobiol. Aging* 26, 1261–1270; discussion 1275.doi: 10.1016/j.neurobiolaging.2005.05.020

Wehrl, H. F., Bezrukov, I., Wiehr, S., Lehnhoff, M., Fuchs, K., Mannheim, J. G., et al. (2015). Assessment of murine brain tissue shrinkage caused by different histological fixatives using magnetic resonance and computed tomography imaging. *Histol. Histopathol.* 30, 601–613. doi: 10.14670/HH-30.601

Wu, J., He, Y., Yang, Z., Guo, C., Luo, Q., Zhou, W., et al. (2014). 3D BrainCV: simultaneous visualization and analysis of cells and capillaries in a whole mouse brain with one-micron voxel resolution. *NeuroImage* 87, 199–208. doi: 10.1016/j.neuroimage.2013.10.036

Xiong, B., Li, A., Lou, Y., Chen, S., Long, B., Peng, J., et al. (2017). Precise cerebral vascular atlas in stereotaxic coordinates of whole mouse brain. *Front. Neuroanat.* 11:128.doi: 10.3389/fnana.2017.00128

Xu, X., Wang, B., Ren, C., Hu, J., Greenberg, D. A., Chen, T., et al. (2017). Age-related impairment of vascular structure and functions. *Aging Dis.* 8, 590–610. doi: 10.14336/AD.2017.0430

Xue, S., Gong, H., Jiang, T., Luo, W., Meng, Y., Liu, Q., et al. (2014). Indian-ink perfusion based method for reconstructing continuous vascular networks in whole mouse brain. *PLoS One* 9:e88067.doi: 10.1371/journal.pone.0088067

Yang, T., Sun, Y., Lu, Z., Leak, R. K., and Zhang, F. (2017). The impact of cerebrovascular aging on vascular cognitive impairment and dementia. *Ageing Res. Rev.* 34, 15–29. doi: 10.1016/j.arr.2016.09.007

Zhang, L.-Y., Lin, P., Pan, J., Ma, Y., Wei, Z., Jiang, L., et al. (2018). CLARITY for high-resolution imaging and quantification of vasculature in the whole mouse brain. *Aging Dis.* 9, 262–272. doi: 10.14336/AD.2017.0613

Zhao, L., Mao, Z., Woody, S. K., and Brinton, R. D. (2016). Sex differences in metabolic aging of the brain: insights into female susceptibility to Alzheimer's disease. *Neurobiol. Aging* 42, 69–79. doi: 10.1016/j.neurobiolaging.2016.02.011

Zlokovic, B. V. (2011). Neurovascular pathways to neurodegeneration in Alzheimer's disease and other disorders. *Nat. Rev. Neurosci.* 12, 723–738. doi: 10.1038/nrn3114

**Conflict of Interest**: The authors declare that the research was conducted in the absence of any commercial or financial relationships that could be construed as a potential conflict of interest.

frontiers in Aging Neuroscience

ORIGINAL RESEARCH
published: 19 November 2020
doi: 10.3389/fnagi.2020.603340

# Which Parameters of Beat-to-Beat Blood Pressure Best Predict Poor In-Hospital Outcome in Spontaneous Intracerebral Hemorrhage?

*Zhen-Ni Guo*[1,2,3†], *Yang Qu*[1,2,3†], *Hailili Reziya*[1,2,3†], *Jia Liu*[4], *Xiu-Li Yan*[1,2,3], *Peng Zhang*[1,2,3], *Pan-Deng Zhang*[4], *Shuang Qi*[1,2,3] *and Yi Yang*[1,2,3*]

[1] Department of Neurology, Stroke Center & Clinical Trial and Research Center for Stroke, The First Hospital of Jilin University, Changchun, China, [2] China National Comprehensive Stroke Center, Changchun, China, [3] Jilin Provincial Key Laboratory of Cerebrovascular Disease, Changchun, China, [4] Shenzhen Institutes of Advanced Technology, Chinese Academy of Sciences, Shenzhen, China

**Objective:** There is increasing evidence that high blood pressure (BP) levels and BP variability (BPV) over 24 h or longer are associated with poor clinical outcomes in patients with intracerebral hemorrhage (ICH). The objective of this study was to examine the association between different beat-to-beat BP parameters and in-hospital outcomes.

**Methods:** Patients with a diagnosis of acute spontaneous ICH were recruited consecutively and prospectively between September 2018 and January 2019. Beat-to-beat recordings were measured non-invasively for 5 min within the first 72 h after the onset of symptoms. BPV was analyzed by standard deviation (SD), coefficient of variation (CV), average real variability (ARV), and variation independent of mean (VIM). Outcome was assessed at discharge using the modified Rankin Scale (mRS) score. Multivariate logistic regression analysis was used to assess the association between BP levels, BPV, and clinical outcomes.

**Results:** A total of 66 patients were included, of whom 34 had poor outcomes (mRS score, 3–6). Patients with poor outcomes had significantly higher National Institute of Health Stroke Scale scores (4.5 vs. 9, $p < 0.001$), a larger ICH volume (8 vs. 14.5 mL, $p = 0.004$), and an increased systolic BP (SBP) -CV (3.2 vs. 4.8, $p < 0.001$) and diastolic BP (DBP) -CV (3.7 vs. 4.9, $p = 0.015$). After adjustment for major covariates, multivariate logistic regression analysis revealed that SBP-CV was independently associated with an increased risk of poor in-hospital outcomes [odds ratio (OR) 2.535; 95% confidence interval (CI), 1.211–5.305; $p = 0.014$]. The receiver operating characteristic area for SBP-CV in predicting poor in-hospital outcome was 0.827 (95% CI, 0.730–0.925; $p < 0.001$), and the best cutoff point was 3.551 (sensitivity, 82.35%; specificity, 68.75%).

**Conclusion:** A higher beat-to-beat BPV in the first 72 h of admission was associated with unfavorable in-hospital outcomes in patients with ICH. The stabilization of BPV during the acute phase may be a therapeutic target; this could be tested in future clinical trials.

**Keywords: intracerebral hemorrhage, blood pressure variability, blood pressure, outcome, stroke**

OPEN ACCESS

***Edited by:***
*Yuanli Zhao,*
*Capital Medical University, China*

***Reviewed by:***
*Elizabeth Margaret Sweeney,*
*Cornell University, United States*
*Anwen Shao,*
*Zhejiang University, China*

***Correspondence:**
*Yi Yang*
*doctoryangyi@163.com*

[†] *These authors have contributed equally to this work*

***Received:*** *06 September 2020*
***Accepted:*** *26 October 2020*
***Published:*** *19 November 2020*

***Citation:***
*Guo Z-N, Qu Y, Reziya H, Liu J, Yan X-L, Zhang P, Zhang P-D, Qi S and Yang Y (2020) Which Parameters of Beat-to-Beat Blood Pressure Best Predict Poor In-Hospital Outcome in Spontaneous Intracerebral Hemorrhage? Front. Aging Neurosci. 12:603340. doi: 10.3389/fnagi.2020.603340*

## INTRODUCTION

Spontaneous intracerebral hemorrhage (ICH) is a major cause of disability and mortality among patients with different types of stroke, and few effective treatment options are available (Flaherty et al., 2006). Elevated blood pressure (BP) is a risk factor for both ICH and worse clinical outcome (Qureshi et al., 2016). However, a meta-analysis of five randomized, controlled, single/double-blinded, parallel trials found no differences between aggressive and conservative BP-lowering strategies in the incidence rates of 3-months mortality and early neurological deterioration (Lattanzi et al., 2017). Post hoc analyses of the Field Administration of Stroke Therapy-Magnesium trial, Intensive Blood Pressure Reduction in Acute Cerebral Hemorrhage Trial, and Antihypertensive Treatment of Acute Cerebral Hemorrhage II trial showed that increased BP variability (BPV) was associated with a poor functional outcome (Manning et al., 2014; Chung et al., 2018; de Havenon et al., 2018). This indicated that, in addition to the absolute BP level, BPV might also be a significant risk factor for worse outcomes after ICH.

Beat-to-beat BPV is considered to be a very short-term BPV. In ischemic stroke, beat-to-beat BPV has been found to be associated with worse clinical outcomes, and might be associated with an increased risk of recurrent events (Dawson et al., 2000; Webb et al., 2018). Beat-to-beat BP parameters can be obtained continuously, non-invasively and have been correlated with baroreceptor sensitivity and autonomic nervous systematic function (Parati et al., 2013; Kishi, 2018). Previous studies have indicated that ICH is followed by an increase in sympathetic nervous system activity, as evidenced by increased plasma catecholamine and corticosteroid levels, and damage to the baroreceptor reflex arc (Meyer et al., 1973; Feibel et al., 1981). However, the characteristics of beat-to-beat BP parameters in acute ICH remain unclear. To date, no study has systematically evaluated the role of beat-to-beat systolic BP (SBP), diastolic BP (DBP), SBPV, and DBPV with clinical outcomes in acute ICH.

Hence, the main objective of this study was to identify any potential prognostic differences between the various parameters of beat-to-beat BP in outcome in patients with acute spontaneous supratentorial ICH.

## MATERIALS AND METHODS

### Participants

Patients with acute spontaneous supratentorial ICH who had been admitted to our stroke unit within the past 72 h were recruited consecutively and prospectively between September 2018 and January 2019. The diagnosis of ICH was based on computed tomography (CT, 64-slice, Somatom Definition; Siemens Healthcare, Germany) of the brain. Demographic data (age and sex), medical history, and vascular risk factors, including alcohol consumption, cigarette smoking, hypertension, diabetes mellitus, previous coronary heart disease, ischemic stroke, and ICH, were documented. Antihypertensive and diabetic medications were defined as taking any drugs intravenously or orally before or after admission. The initial stroke severity was assessed using the National Institute of Health Stroke Scale (NIHSS) upon admission to the stroke unit. The primary locations of ICH were classified into the basal ganglia, thalamic, or lobar areas. The presence of intraventricular hemorrhage was also recorded. The ICH volume was calculated from the first CT scan using the $(a \times b \times c)/2$ method, where $a$ is the greatest hemorrhage diameter by CT, $b$ is the diameter 90° to $a$, and $c$ is the approximate number of CT slices with hemorrhage multiplied by the slice thickness (Kothari et al., 1996; Huttner et al., 2006). Although hospitalized, 43 of 66 subjects underwent an additional 1 or 2 CT scans according to their clinical status, as determined by a neurologist at different time points. We did not use those data because of a potential selection bias. All patients received standard medical treatment according to the current guidelines from the American Heart Association/American Stroke Association in the comprehensive stroke center of our hospital (Hemphill et al., 2015).

The exclusion criteria of this study were as follows: age $<18$ or $>80$ years; premorbid modified Rankin Scale (mRS) $\geq 2$; patients who were unable to cooperate sufficiently to complete the beat-to-beat monitoring (for example, due to conditions such as atrial fibrillation during the recording).

This study was approved by the Ethics Review Committee of the First Hospital of Jilin University, and written informed consent was obtained from all participants or their direct relatives.

### BP Recording and Variability Measures

Admission BP was measured at the brachial artery using an automatic BP monitor (Omron 711, Japan). Beat-to-beat recordings of SBP (in mmHg) and DBP (in mmHg) were measured noninvasively for 5 min within the first 72 h after the onset of symptoms using a servo-controlled plethysmograph (Finometer model 1, FMS, Rotterdam, the Netherlands) on the middle finger in a specific, quiet examination room with a controlled temperature ranging from 20 to 24°C. Because BPV was heterogeneous according to different measuring time points, all beat-to-beat BP was recorded 9:00 to 10:00 AM. Before the examination, all participants were asked to relax in a supine position for 10 min in the room.

BPV on beat-to-beat monitoring was calculated for 5 min. Continuous recordings of beat-to-beat information were processed by MATLAB (R2017b, MathWorks, USA) using scripts developed by the research team. Ectopic beats and artifacts were automatically detected, visually reviewed, and removed by linear interpolation (Webb et al., 2018). Linear interpolation was conducted using the routine function "interp1" provided by MATLAB. Mean SBP and DBP were defined as the average BP measurements. Beat-to-beat BPV, including SBPV and DBPV, was evaluated using the standard deviation (SD), coefficient of variation (CV), average real variability (ARV), and variation independent of mean (VIM) of BP measurements. The SD and CV were the most frequently used measuring values in previous studies (Xia et al., 2017). However, the SD does not consider the time sequence of individual BP measurements, and CV might be correlated with the mean BP. On that basis, ARV and VIM were calculated (Mena et al., 2005; Rothwell et al., 2010; Xia et al.,

**TABLE 1 |** The formulas and characteristics of different blood pressure variability variables.

| Variables | Units | Formulas | Characteristics |
|---|---|---|---|
| Standard Deviation (SD) | mmHg | $SD = \sqrt{\frac{1}{n-1}\sum_{i=1}^{n}\left(X_i - X\right)^2}$ | Only reflecting the global fluctuation of BP measurements around the mean value; not taking the time sequence of measurements into account |
| Coefficient of Variation (CV) | nu. | $CV = 100\frac{SD}{X}$ | Correlating with the mean BP |
| Average Real Variability (ARV) | mmHg | $ARV = \frac{1}{n-1}\sum_{i=1}^{n}\lvert X_{i+1} - X_i\rvert$ | Taking the time series variability into account |
| Variation Independent of Mean (VIM) | nu. | $VIM = kSD/\overline{X}^m$ | Eliminating the effects of mean BP levels |

*n is the number of BP measurements of a subject; X1, X2, …, Xn denotes a set of BP measurements, $\overline{X}$ represents the mean value of the set of BP measurements, k and m were obtained from a fitting curve of the form $y = kx^m$ through a plot of SD BP (y-axis) against mean BP (x-axis), the parameter m is estimated from the data and k is a constant which can be chosen such that the values of VIM are on the same scale as values of SD.*
*BP, Blood Pressure.*

2017). The formulas and characteristics of these parameters were shown in **Table 1**.

## Outcome

The clinical outcome was assessed at discharge using the mRS, with mRS scores ranging from 0 (no symptoms) to 6 (death). We defined mRS scores ≥3 as a poor outcome and mRS scores ≤2 as a favorable outcome.

## Statistical Analysis

Statistical Program for Social Sciences version 22.0 (SPSS; IBM, West Grove, PA) was used for statistical analysis. The distribution of continuous variables was assessed using a one-sample Kolmogorov-Smirnov test. Normally distributed data are presented as the means and SD, and non-normally distributed data are presented as the median and interquartile range. The clinical characteristics and BPV parameters used in this study were dichotomized into favorable and poor outcome groups. Intergroup differences were compared using the Student's *t*-test or Mann–Whitney test for continuous variables, and the chi-squared test or Fisher's exact test for categorical variables. The variables with a univariate between-group comparison with a $p < 0.1$ were eligible for inclusion in the multivariate logistic regression models as the major covariates. Multivariate logistic analysis was conducted to explore the association between BPV and clinical outcome, and odds ratios (ORs) and 95% confidence intervals (CIs) were used to evaluate the risk of poor outcomes. A receiver operating characteristic (ROC) curve of the statistically significant variables associated with poor in-hospital outcome was drawn. All statistical tests were two-tailed, and $p < 0.05$ was considered statistically significant.

# RESULTS

Altogether, 66 patients with acute ICH were enrolled in the study, including 34 (51.5%) with poor outcomes (mRS score 3–6) and 32 (48.5%) with favorable outcomes (mRS score 0–2) at discharge. The overall characteristics of participants are shown in **Table 2**. The mean age of patients was 54.4 ± 10.1 years and 81.8% were men. The median NIHSS score at admission was 6 (interquartile range, 4–9), the median hemorrhage volume was 11.5 mL (interquartile range, 6–11.2 mL), and 18.2% had intraventricular hemorrhage. The average length ± SD of patient hospitalization was 12 days (interquartile range, 10.8–14.3 days).

A comparison of the patient characteristics between the favorable and poor groups are presented in **Table 2**. There were no differences in age, sex, vascular risk factors, or antihypertensive and diabetic medication between the poor outcome and favorable outcome groups. However, there was a significantly different NIHSS score at admission (4.5 vs. 9, $p < 0.001$) and ICH volume (8 vs. 14.5 mL, $p = 0.004$) between the two groups. As for BP magnitude, the poor outcome group had a tendency toward higher admission BP and mean BP than the good outcome group. For beat-to-beat BPV, poor outcome patients had an increased SBP-CV (3.2 vs. 4.8, $p < 0.001$) and DBP-CV (3.7 vs. 4.9, $p = 0.015$) and the other parameters also tended to be higher, although this was not significant.

Multivariate logistic regression analysis was performed to analyze the risk of poor in-hospital outcomes. The independent variables included in the analysis were admission NIHSS score, ICH volume, and beat-to-beat BPV (including SBP-CV and DBP-CV, respectively). The results showed that admission NIHSS score and SBP-CV were significant independent predictors of a poor in-hospital outcome in patients with spontaneous supratentorial ICH. The ORs, 95% CIs, and p-values are presented in **Figure 1**.

The ROC curve of the SBP-CV and DBP-CV is shown in **Figure 2**. The area under the ROC curve of SBP-CV for prediction of poor in-hospital outcome was 0.827 (95% CI, 0.730–0.925; $p < 0.001$), and the best cutoff point was 3.551 (sensitivity, 82.35%; specificity, 68.75%). The accuracy (Youden's index), positive predictive value and negative predictive value were 0.51, 73.68 and 78.57%, respectively. The area under the ROC curve of DBP-CV was 0.679 (95% CI, 0.551–0.808; $p = 0.012$), and the best cutoff point was 3.173 (sensitivity, 82.35%; specificity, 50%). The accuracy, positive predictive value and negative predictive value were 0.32, 63.63 and 72.73%, respectively.

# DISCUSSION

This study investigated the effect of various parameters of beat-to-beat BP on the clinical outcome in patients with acute spontaneous supratentorial ICH. We demonstrated that SBP-CV

**TABLE 2 |** Comparison of demographic and clinical characteristics between patients with favorable (mRS, 0–2) and poor (mRS, 3–6) outcomes.

| Variables | Total ($n = 66$) | Favorable outcome ($n = 32$) | Poor outcome ($n = 34$) | *P*-value |
|---|---|---|---|---|
| Age (year) | 54.4 ± 10.1 | 53.9 ± 11.1 | 54.9 ± 9.1 | 0.698 |
| Sex (male, *n* [%]) | 54 (81.8%) | 25 (80.6%) | 29 (82.9%) | 0.450 |
| Cigarette smoking, *n* (%) | 28 (42.4%) | 12 (38.8%) | 16 (45.7%) | 0.432 |
| Alcohol consumption, *n* (%) | 27 (40.9%) | 11 (35.5%) | 16 (45.7%) | 0.295 |
| Coronary heart disease, *n* (%) | 8 (12.1%) | 5 (16.1%) | 3 (8.6%) | 0.397 |
| Hypertension, *n* (%) | 63 (95.5%) | 30 (96.8%) | 33 (94.3%) | 0.519 |
| Diabetes mellitus, *n* (%) | 6 (9.1%) | 4 (12.9%) | 2 (5.7%) | 0.350 |
| Previous ischemic stroke, *n* (%) | 9 (13.6%) | 4 (12.9%) | 5 (14.3%) | 0.794 |
| Previous intracerebral hemorrhage, *n* (%) | 8 (12.1%) | 4 (12.9%) | 4 (11.4%) | 0.927 |
| Antihypertensive medication, *n* (%) | 52 (78.8%) | 26 (83.9%) | 26 (74.2%) | 0.281 |
| Diabetic medication, *n* (%) | 4 (6.1%) | 2 (6.5%) | 2 (5.7%) | 0.950 |
| Admission NIHSS score | 6 (4–9) | 4.5 (3–6) | 9 (6–11) | <0.001 |
| Hospitalization length | 12 (10.8–14.3) | 12 (10.3–14) | 13 (10.8–15) | 0.518 |
| **Location** | | | | |
| Basal ganglia, *n* (%) | 53 (80.3%) | 25 (80.6%) | 28 (80.0%) | 0.666 |
| Thalamus, *n* (%) | 10 (15.1%) | 6 (19.4%) | 4 (11.4%) | 0.629 |
| Lobar, *n* (%) | 3 (4.5%) | 1 (3.2%) | 2 (5.7%) | 0.591 |
| ICH volume (mL) | 11.5 (6–11.2) | 8 (4.3–14.3) | 14.5 (10–18) | 0.004 |
| Presence of IVH, *n* (%) | 12 (18.2%) | 4 (12.9%) | 8 (22.9%) | 0.246 |
| Admission SBP (mmHg) | 165.6 ± 19.4 | 164.1 ± 17.1 | 167.2 ± 21.9 | 0.526 |
| Admission DBP (mmHg) | 97.3 ± 14.3 | 94.3 ± 12.7 | 100.5 ± 15.3 | 0.180 |
| Mean SBP (mmHg) | 147.6 ± 21.4 | 144.1 ± 21.1 | 151.3 ± 21.5 | 0.175 |
| Mean DBP (mmHg) | 80.2 ± 16.6 | 78.7 ± 16.9 | 81.8 ± 16.3 | 0.439 |
| SBP-SD (mmHg) | 5.8 ± 2.5 | 5.6 ± 1.9 | 6.1 ± 2.9 | 0.388 |
| DBP-SD (mmHg) | 3.3 ± 1.5 | 3.2 ± 1.2 | 3.5 ± 1.6 | 0.378 |
| SBP-CV | 4.0 ± 1.6 | 3.2 ± 0.9 | 4.8 ± 1.7 | <0.001 |
| DBP-CV | 4.3 ± 2.1 | 3.7 ± 1.4 | 4.9 ± 2.4 | 0.015 |
| SBP-ARV (mmHg) | 2.5 ± 1.5 | 2.5 ± 1.3 | 2.5 ± 1.7 | 0.881 |
| DBP-ARV (mmHg) | 1.2 ± 0.5 | 1.2 ± 0.5 | 1.2 ± 0.5 | 0.909 |
| SBP-VIM | 5.9 ± 2.4 | 5.6 ± 1.9 | 6.2 ± 2.8 | 0.333 |
| DBP-VIM | 3.4 ± 1.5 | 3.2 ± 1.2 | 3.5 ± 1.7 | 0.322 |

*Data are expressed as mean ± standard deviation or n (%), except admission NIHSS score, hospitalization length, and ICH volume are median (interquartile range).*
*NIHSS, National Institutes of Health Stroke Scale; ICH, intracerebral hemorrhage; IVH, intraventricular hemorrhage; SBP, Systolic Blood Pressure; DBP, Diastolic Blood Pressure; SD, Standard Deviation; CV, Coefficient of Variation; ARV, Average Real Variability; VIM, Variation Independent of Mean.*

and DBP-CV were significantly increased in ICH patients with poor outcomes. SBP-CV was an independent risk factor for a poor in-hospital outcome; the greater the variability, the poorer the outcome, with this relationship holding true even when admission and mean beat-to-beat BP levels were taken into consideration.

To the best of our knowledge, this is the first study to evaluate the association between beat-to-beat BP parameters and in-hospital outcomes and to compare the potential prognostic differences between the various parameters of beat-to-beat BP in patients with acute spontaneous supratentorial ICH. BPV is primarily divided into the three following categories: long-term (days to months), short-term (minutes to hours), and very short-term (beat-to-beat) BPV (Parati et al., 2013). Most previous studies in patients with ICH have focused on the first two types of BPV and have reported that an increased BPV during both acute and subacute stages was independently associated with worse functional outcomes at 3 months (Manning et al., 2014; Tanaka et al., 2014; Lattanzi et al., 2015; Chung et al., 2018; de Havenon et al., 2018; Meeks et al., 2019). Tanaka et al. and Rodriguez-Luna et al. further revealed that SBPV was correlated with early neurological deterioration (Rodriguez-Luna et al., 2013; Tanaka et al., 2014). The prognostic values of beat-to-beat BP parameters have recently been demonstrated in patients with ischemic stroke, and were confirmed to be more strongly associated with recurrent stroke and cardiovascular events than long-term and short-term BPV (Dawson et al., 2000; Webb et al., 2018). This indicates that beat-to-beat BP parameters may be a useful additional marker of cardiovascular risk. To date, only two studies have explored the changes in beat-to-beat BPV in patients with acute ICH. Sykora et al. demonstrated that baroreflex sensitivity was decreased in patients with acute ICH and that this decrease was associated with an increased beat-to-beat BPV. The authors also found that the 72-h beat-to-beat mean arterial pressure variability was significantly correlated with relative edema and early neurologic deterioration; however, this was only significant in a univariate analysis and was not duplicated in a stepwise multivariate linear regression analysis (Sykora et al., 2008, 2009). The present study showed a 2.5-fold increase in the risk of poor in-hospital outcomes for every unit of beat-to-beat BPV increase, independent of admission and mean beat-to-beat BP level. The beat-to-beat BPV results presented here are comparable to those previously reported after ICH when longer recording periods are taken. Divani et al. explored the association between BPV in the first 24 h of admission and in-hospital outcomes, and found that a higher SBPV was associated with unfavorable outcomes at discharge (Divani et al., 2019).

The indices of beat-to-beat BPV are diverse (Xia et al., 2017); considering the influence of the time sequence of individual BP measurements and mean BP levels on BPV, we chose SD, CV, ARV, and VIM as BPV evaluators in the present study. In the univariate analysis, only SBP-CV and DBP-CV were significantly higher in patients with unfavorable outcomes, although a trend toward significance was seen in other parameters. These results may indicate that CV is the most sensitive parameter for predicting short-term clinical outcomes in patients with ICH. CV was defined as the ratio of the SD and mean BP levels, and was correlated with mean BP, which suggests that the total variability and mean BP levels may interact to influence ICH outcome. The insignificance of VIM further supports this conjecture. In addition, CV does not take the time series variability into

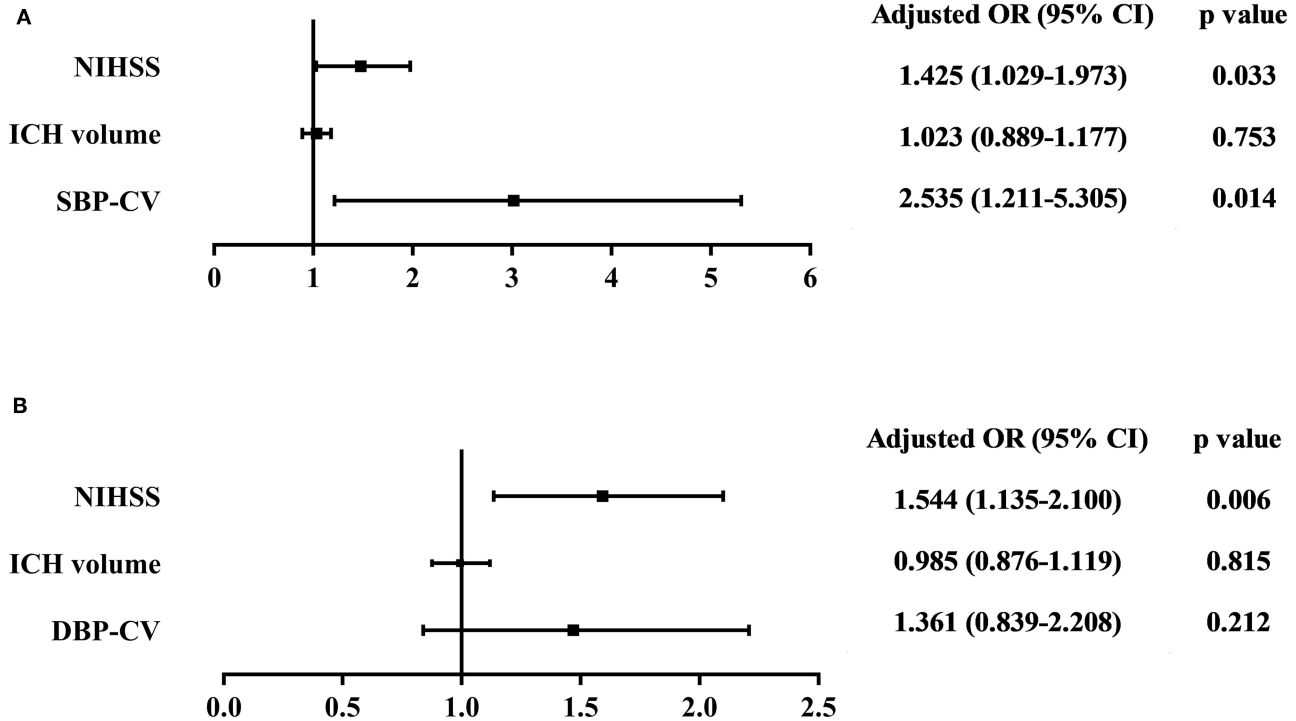


**FIGURE 1 |** Association between **(A)** SBP-CV, and **(B)** DBP-CV and poor in-hospital outcome. The independent variables included in the multivariate logistic regression analysis were admission NIHSS score, ICH volume, and beat-to-beat BPV (including SBP-CV and DBP-CV, respectively). The results showed that admission NIHSS score and SBP-CV were significant independent predictors of a poor in-hospital outcome in patients with spontaneous supratentorial ICH. SBP, Systolic Blood Pressure; DBP, Diastolic Blood Pressure; CV, Coefficient of Variation; NIHSS, National Institutes of Health Stroke Scale; ICH, intracerebral hemorrhage; BPV, Blood Pressure Variability.

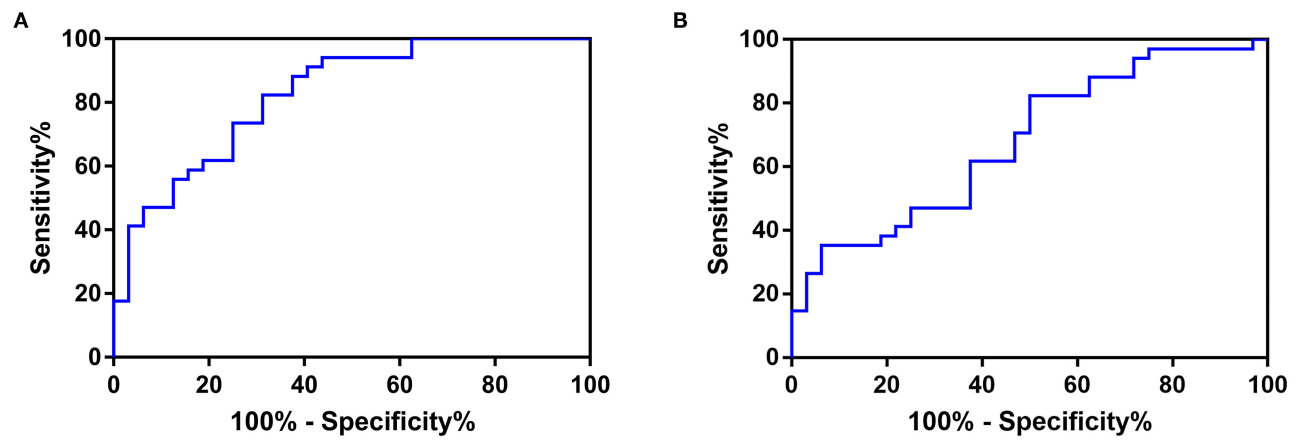


**FIGURE 2 |** The ROC curve of **(A)** SBP-CV, and **(B)** DBP-CV in predicting poor in-hospital outcome in patients with acute spontaneous supratentorial ICH. The area under the ROC curve of SBP-CV for prediction of poor in-hospital outcome was 0.827 (95% CI, 0.730–0.925; $p < 0.001$), and the best cutoff point was 3.551 (sensitivity, 82.35%; specificity, 68.75%). The accuracy (Youden's index), positive predictive value and negative predictive value were 0.51, 73.68 and 78.57%, respectively. The area under the ROC curve of DBP-CV was 0.679 (95% CI, 0.551–0.808; $p = 0.012$), and the best cutoff point was 3.173 (sensitivity, 82.35%; specificity, 50%). The accuracy, positive predictive value and negative predictive value were 0.32, 63.63 and 72.73%, respectively. ROC, Receiver Operating Characteristic; SBP, Systolic Blood Pressure; DBP, Diastolic Blood Pressure; CV, Coefficient of Variation; ICH, intracerebral hemorrhage.

consideration, and no difference was found in ARV. This may suggest that the relationship between ICH outcome and BPV is not associated with the time sequence of individual BP measurements within only several minutes. That said, this finding might also be due to the relatively small sample size; further prospective studies are needed to further investigate this.

Although DBP-CV was associated with outcome in the univariate analysis, this association disappeared after adjusting for admission NIHSS score and ICH volume. In contrast, SBP-CV remained strongly associated with outcome. Moreover, SBP-CV predicted poor outcome better than DBP-CV according to ROC curves. Several previous studies have demonstrated that there is a stronger predictive function of short-term and long-term SBPV than DBPV in patients with ischemic or hemorrhagic stroke (Rothwell et al., 2010; Geeganage et al., 2011; Endo et al., 2013; Rodriguez-Luna et al., 2013; Chung et al., 2018; Divani et al., 2019; Meeks et al., 2019). This finding suggests that SBPV is more critical than DBPV for ICH prognosis, not only in short-term and long-term recordings, but also in beat-to-beat measurements.

The mechanism by which beat-to-beat BPV affects the outcome in patients with ICH is not fully understood. Increased beat-to-beat BPV reflects central autonomic dysfunction with sympathetic predominance and baroreflex impairment, which is associated with pro-inflammatory cytokine production, hyperglycemia, and increased blood-brain-barrier permeability (Raichle et al., 1975; van der Poll and Lowry, 1997; Watanabe et al., 2008; Jafari and Damani, 2020), all of which may worsen the outcome of patients with ICH. Dynamic cerebral autoregulation has been reported to be bilaterally impaired in patients with acute ICH, which is suggestive of an impaired ability to maintain a constant cerebral blood flow (Ma et al., 2016); this might also contribute to the worse outcome in patients with ICH who have a higher BPV. Sudden rises and falls in BP may promote hematoma enlargement and perihematomal ischemia, respectively (Menon et al., 2012; Rodriguez-Luna et al., 2013). Therefore, one potential therapeutic target is the stabilization of BPV during this vulnerable period, and this should be investigated in future clinical trials (Moullaali et al., 2019).

Some limitations should be considered when interpreting the findings. First, this study had a relatively small sample size, and this limited sample size meant that classes of antihypertensive medications were not selected as major covariates. Second, ambulatory BP monitoring data were not obtained in this study; hence, the different prognostic functions of short-term, long-term, and beat-to-beat BPV could not be compared. Finally, only hospital discharge outcomes were considered, and further prospective studies are warranted to identify any cause–effect relationship between beat-to-beat BPV and functional outcomes.

## CONCLUSION

In conclusion, a higher beat-to-beat BPV (SBP-CV) in the first 72 h of admission was associated with unfavorable in-hospital outcomes in patients with acute spontaneous supratentorial ICH. A greater variability was associated with a worse outcome, and this relationship remained true even when admission and mean BP levels were taken into consideration. The stabilization of BPV during the acute phase may be a therapeutic target for future clinical trials.

## DATA AVAILABILITY STATEMENT

The raw data supporting the conclusions of this article will be made available by the authors, without undue reservation.

## ETHICS STATEMENT

The studies involving human participants were reviewed and approved by the Human and Research Ethics committees of the First Hospital of Jilin University. The patients/participants provided their written informed consent to participate in this study.

## AUTHOR CONTRIBUTIONS

YY and Z-NG devised the study design and supervised study procedures. YQ, Z-NG, JL, and P-DZ analyzed the data and wrote the manuscript. HR, X-LY, and SQ collected the data. PZ provided significant statistical support. All authors provided critical review, edits, and approval of the final manuscript.

## FUNDING

This work was supported by the National Natural Science Foundation of China (81771243), JLUSTIRT (2017TD-12), and Jilin Provincial Key Laboratory (20190901005JC) to YY and was funded in part by National Natural Science Foundation of China (81871447 and 81661168015) to JL.

## REFERENCES

Chung, P. W., Kim, J. T., Sanossian, N., Starkmann, S., Hamilton, S., Gornbein, J., et al. (2018). Association between hyperacute stage blood pressure variability and outcome in patients with spontaneous intracerebral hemorrhage. *Stroke* 49, 348–354. doi: 10.1161/STROKEAHA.117.017701

Dawson, S. L., Manktelow, B. N., Robinson, T. G., Panerai, R. B., and Potter, J. F. (2000). Which parameters of beat-to-beat blood pressure and variability best predict early outcome after acute ischemic stroke? *Stroke* 31, 463–468. doi: 10.1161/01.STR.31.2.463

de Havenon, A., Majersik, J. J., Stoddard, G., Wong, K. H., McNally, J. S., Smith, A. G., et al. (2018). Increased blood pressure variability contributes to worse outcome after intracerebral hemorrhage. *Stroke* 49, 1981–1984. doi: 10.1161/STROKEAHA.118.022133

Divani, A. A., Liu, X., Di Napoli, M., Lattanzi, S., Ziai, W., James, M. L., et al. (2019). Blood pressure variability predicts poor in-hospital outcome in spontaneous intracerebral hemorrhage. *Stroke* 50, 2023–2029. doi: 10.1161/STROKEAHA.119.025514

Endo, K., Kario, K., Koga, M., Nakagawara, J., Shiokawa, Y., Yamagami, H., et al. (2013). Impact of early blood pressure variability on stroke outcomes after thrombolysis: the SAMURAI rt-PA registry. *Stroke* 44, 816–818. doi: 10.1161/STROKEAHA.112.681007

Feibel, J. H., Baldwin, C. A., and Joynt, R. J. (1981). Catecholamine-associated refractory hypertension following acute intracranial hemorrhage: control with propranolol. *Ann. Neurol.* 9, 340–343. doi: 10.1002/ana.410090405

Flaherty, M. L., Haverbusch, M., Sekar, P., Kissela, B., Kleindorfer, D., Moomaw, C. J., et al. (2006). Long-term mortality after intracerebral hemorrhage. *Neurology* 66, 1182–1186. doi: 10.1212/01.wnl.0000208400.08722.7c

Geeganage, C., Tracy, M., England, T., Sare, G., Moulin, T., Woimant, F., et al. (2011). Relationship between baseline blood pressure parameters (including mean pressure, pulse pressure, and variability) and early outcome after stroke: data from the Tinzaparin in Acute Ischaemic Stroke Trial (TAIST). *Stroke* 42, 491–493. doi: 10.1161/STROKEAHA.110.596163

Hemphill, J. C. 3rd., Greenberg, S. M., Anderson, C. S., Becker, K., Bendok, B. R., Cushman, M., et al. (2015). Guidelines for the management of spontaneous intracerebral hemorrhage: a guideline for healthcare professionals from the American Heart Association/American Stroke Association. *Stroke* 46, 2032–2060. doi: 10.1161/STR.0000000000000069

Huttner, H. B., Steiner, T., Hartmann, M., Kohrmann, M., Juettler, E., Mueller, S., et al. (2006). Comparison of ABC/2 estimation technique to computer-assisted planimetric analysis in warfarin-related intracerebral parenchymal hemorrhage. *Stroke* 37, 404–408. doi: 10.1161/01.STR.0000198806.67472.5c

Jafari, M., and Damani, R. (2020). Blood pressure variability and outcome after acute intracerebral hemorrhage. *J. Neurol. Sci.* 413:116766. doi: 10.1016/j.jns.2020.116766

Kishi, T. (2018). Baroreflex failure and beat-to-beat blood pressure variation. *Hypertens. Res.* 41, 547–552. doi: 10.1038/s41440-018-0056-y

Kothari, R. U., Brott, T., Broderick, J. P., Barsan, W. G., Sauerbeck, L. R., Zuccarello, M., et al. (1996). The ABCs of measuring intracerebral hemorrhage volumes. *Stroke* 27, 1304–1305. doi: 10.1161/01.STR.27.8.1304

Lattanzi, S., Cagnetti, C., Provinciali, L., and Silvestrini, M. (2015). Blood pressure variability and clinical outcome in patients with acute intracerebral hemorrhage. *J. Stroke Cerebrovasc. Dis.* 24, 1493–1499. doi: 10.1016/j.jstrokecerebrovasdis.2015.03.014

Lattanzi, S., Cagnetti, C., Provinciali, L., and Silvestrini, M. (2017). How should we lower blood pressure after cerebral hemorrhage? A systematic review and meta-analysis. *Cerebrovasc. Dis.* 43, 207–213. doi: 10.1159/000462986

Ma, H., Guo, Z. N., Liu, J., Xing, Y., Zhao, R., and Yang, Y. (2016). Temporal course of dynamic cerebral autoregulation in patients with intracerebral hemorrhage. *Stroke* 47, 674–681. doi: 10.1161/STROKEAHA.115.011453

Manning, L., Hirakawa, Y., Arima, H., Wang, X., Chalmers, J., Wang, J., et al. (2014). Blood pressure variability and outcome after acute intracerebral haemorrhage: a *post-hoc* analysis of INTERACT2, a randomised controlled trial. *Lancet Neurol.* 13, 364–373. doi: 10.1016/S1474-4422(14)70018-3

Meeks, J. R., Bambhroliya, A. B., Meyer, E. G., Slaughter, K. B., Fraher, C. J., Sharrief, A. Z., et al. (2019). High in-hospital blood pressure variability and severe disability or death in primary intracerebral hemorrhage patients. *Int. J. Stroke* 14, 987–995. doi: 10.1177/1747493019827763

Mena, L., Pintos, S., Queipo, N. V., Aizpurua, J. A., Maestre, G., and Sulbaran, T. (2005). A reliable index for the prognostic significance of blood pressure variability. *J. Hypertens.* 23, 505–511. doi: 10.1097/01.hjh.0000160205.81652.5a

Menon, R. S., Burgess, R. E., Wing, J. J., Gibbons, M. C., Shara, N. M., Fernandez, S., et al. (2012). Predictors of highly prevalent brain ischemia in intracerebral hemorrhage. *Ann. Neurol.* 71, 199–205. doi: 10.1002/ana.22668

Meyer, J. S., Stoica, E., Pascu, I., Shimazu, K., and Hartmann, A. (1973). Catecholamine concentrations in CSF and plasma of patients with cerebral infarction and haemorrhage. *Brain* 96, 277–288. doi: 10.1093/brain/96.2.277

Moullaali, T. J., Wang, X., Martin, R. H., Shipes, V. B., Robinson, T. G., Chalmers, J., et al. (2019). Blood pressure control and clinical outcomes in acute intracerebral haemorrhage: a preplanned pooled analysis of individual participant data. *Lancet Neurol.* 18, 857–864. doi: 10.1016/S1474-4422(19)30196-6

Parati, G., Ochoa, J. E., Lombardi, C., and Bilo, G. (2013). Assessment and management of blood-pressure variability. *Nat. Rev. Cardiol.* 10, 143–155. doi: 10.1038/nrcardio.2013.1

Qureshi, A. I., Palesch, Y. Y., Barsan, W. G., Hanley, D. F., Hsu, C. Y., Martin, R. L., et al. (2016). Intensive blood-pressure lowering in patients with acute cerebral hemorrhage. *N. Engl. J. Med.* 375, 1033–1043. doi: 10.1056/NEJMoa1603460

Raichle, M. E., Hartman, B. K., Eichling, J. O., and Sharpe, L. G. (1975). Central noradrenergic regulation of cerebral blood flow and vascular permeability. *Proc. Natl. Acad. Sci. U. S. A.* 72, 3726–3730. doi: 10.1073/pnas.72.9.3726

Rodriguez-Luna, D., Pineiro, S., Rubiera, M., Ribo, M., Coscojuela, P., Pagola, J., et al. (2013). Impact of blood pressure changes and course on hematoma growth in acute intracerebral hemorrhage. *Eur. J. Neurol.* 20, 1277–1283. doi: 10.1111/ene.12180

Rothwell, P. M., Howard, S. C., Dolan, E., O'Brien, E., Dobson, J. E., Dahlof, B., et al. (2010). Prognostic significance of visit-to-visit variability, maximum systolic blood pressure, and episodic hypertension. *Lancet* 375, 895–905. doi: 10.1016/S0140-6736(10)60308-X

Sykora, M., Diedler, J., Rupp, A., Turcani, P., Rocco, A., and Steiner, T. (2008). Impaired baroreflex sensitivity predicts outcome of acute intracerebral hemorrhage. *Crit. Care Med.* 36, 3074–3079. doi: 10.1097/CCM.0b013e31818b306d

Sykora, M., Diedler, J., Turcani, P., Rupp, A., and Steiner, T. (2009). Subacute perihematomal edema in intracerebral hemorrhage is associated with impaired blood pressure regulation. *J. Neurol. Sci.* 284, 108–112. doi: 10.1016/j.jns.2009.04.028

Tanaka, E., Koga, M., Kobayashi, J., Kario, K., Kamiyama, K., Furui, E., et al. (2014). Blood pressure variability on antihypertensive therapy in acute intracerebral hemorrhage: the Stroke Acute Management with Urgent Risk-factor Assessment and Improvement-intracerebral hemorrhage study. *Stroke* 45, 2275–2279. doi: 10.1161/STROKEAHA.114.005420

van der Poll, T., and Lowry, S. F. (1997). Lipopolysaccharide-induced interleukin 8 production by human whole blood is enhanced by epinephrine and inhibited by hydrocortisone. *Infect. Immun.* 65, 2378–2381. doi: 10.1128/IAI.65.6.2378-2381.1997

Watanabe, M., Tomiyama-Miyaji, C., Kainuma, E., Inoue, M., Kuwano, Y., Ren, H., et al. (2008). Role of alpha-adrenergic stimulus in stress-induced modulation of body temperature, blood glucose and innate immunity. *Immunol. Lett.* 115, 43–49. doi: 10.1016/j.imlet.2007.09.010

Webb, A. J. S., Mazzucco, S., Li, L., and Rothwell, P. M. (2018). Prognostic significance of blood pressure variability on beat-to-beat monitoring after transient ischemic attack and stroke. *Stroke* 49, 62–67. doi: 10.1161/STROKEAHA.117.019107

Xia, Y., Wu, D., Gao, Z., Liu, X., Chen, Q., Ren, L., et al. (2017). Association between beat-to-beat blood pressure variability and vascular elasticity in normal young adults during the cold pressor test. *Medicine* 96:e6000. doi: 10.1097/MD.0000000000006000

**Conflict of Interest:** The authors declare that the research was conducted in the absence of any commercial or financial relationships that could be construed as a potential conflict of interest.

frontiers in Aging Neuroscience

ORIGINAL RESEARCH
published: 04 December 2020
doi: 10.3389/fnagi.2020.601471

# Effects of Early Changes in Blood Pressure During Intravenous Thrombolysis on the Prognosis of Acute Ischemic Stroke Patients

*Zhong-Xiu Wang*[1,2,3†], *Chao Wang*[1,2,3†], *Peng Zhang*[1,2,3], *Yang Qu*[1,2,3], *Zhen-Ni Guo*[1,2,3*] *and Yi Yang*[1,2,3*]

[1]*Department of Neurology, Stroke Center and Clinical Trial and Research Center for Stroke, The First Hospital of Jilin University, Changchun, China,* [2]*China National Comprehensive Stroke Center, Changchun, China,* [3]*Jilin Provincial Key Laboratory of Cerebrovascular Disease, Changchun, China*

**Background**: Intravenous thrombolysis (IVT) therapy is currently one of the best medical treatments available for patients with acute ischemic stroke. Studies have shown that blood pressure (BP) changes in patients treated with IVT are significantly correlated with prognosis.

**Objective**: Our study aimed to determine the relationship between BP changes during recombinant tissue plasminogen activator (rt-PA) infusion and the 3-month prognosis evaluated using the modified Rankin Scale (mRS) and determine the factors influencing BP changes during rt-PA infusion.

**Methods**: Consecutive patients who were treated with IVT and admitted to our stroke center between May 2015 and October 2017 were analyzed retrospectively. Patients were divided into two groups according to their 3-month prognosis status: patients with mRS $\leq$ 2 were defined as "favorable outcome group" and those with mRS $\geq$ 3 as "unfavorable outcome group". First, the factors affecting prognosis after thrombolysis were analyzed. Second, we analyzed the relationship between BP and the prognosis. BP was taken before and at regular intervals of 15 min during the rt-PA infusion (1 h). The average value of BP during thrombolysis was calculated and compared to the baseline BP. BP decrease was defined as the difference between the baseline BP and the average BP, provided it was greater than 0 mmHg. Third, univariate and multivariate analyses were performed to identify factors that may contribute to BP decrease.

**Results**: In total, 458 patients were included. Patients with a lower baseline National Institute of Health Stroke Scale (NIHSS) score (8.25 $\pm$ 5.57 vs. 13.51 $\pm$ 7.42, $P < 0.001$), a higher Alberta Stroke Program Early CT Score (ASPECTS; 8.65 $\pm$ 1.82 vs. 8.13 $\pm$ 2.00, $P = 0.005$), decreased BP during thrombolysis (69.4% vs. 59.8%, $P = 0.037$), and steady BP (SD $<$ 10 mmHg) were more likely to have a favorable outcome (73.9% vs. 60.6%, $P = 0.019$). High baseline BP (OR $>$ 1), hypertension history (OR $<$ 1), and baseline ASPECTS (OR $>$ 1) were independent factors of BP change during thrombolysis.

OPEN ACCESS

***Edited by:***
*Yuanli Zhao,*
*Capital Medical University, China*

***Reviewed by:***
*Shenqiang Yan,*
*Zhejiang University, China*
*Xinchun Jin,*
*Capital Medical University, China*

****Correspondence:***
*Zhen-Ni Guo,*
*zhen1ni2@jlu.edu.cn;*
*zhen1ni2@163.com*
*Yi Yang*
*yang_yi@jlu.edu.cn;*
*doctoryangyi@163.com*

*†These authors have contributed equally to this work and share first authorship*

***Received:*** *01 September 2020*
***Accepted:*** *11 November 2020*
***Published:*** *04 December 2020*

***Citation:***
*Wang Z-X, Wang C, Zhang P, Qu Y, Guo Z-N and Yang Y (2020) Effects of Early Changes in Blood Pressure During Intravenous Thrombolysis on the Prognosis of Acute Ischemic Stroke Patients. Front. Aging Neurosci. 12:601471. doi: 10.3389/fnagi.2020.601471*

**Conclusion**: Patients with decreased or steady BP during thrombolysis were more likely to have a favorable outcome. Baseline ASPECTS, baseline NIHSS score, and hypertension history influenced BP changes during thrombolysis.

**Keywords: acute cerebral infarction, blood pressure variability, intravenous thrombolysis, outcome, spontaneous blood pressure decrease**

## INTRODUCTION

Stroke is the leading cause of death in the Chinese population because of its high rate of morbidity, disability, mortality, and recurrence, and it negatively affects the national health and quality of life (Wang et al., 2017). Cerebral infarction is the most common type of stroke (Liesch, 2012). Intravenous thrombolysis (IVT) therapy is currently one of the best medical treatments available for patients with acute ischemic stroke. However, individual differences in the effects of IVT therapy are significant. Identifying relevant factors influencing IVT prognosis and conducting targeted interventions are important to improvement in IVT prognosis.

A sudden elevated blood pressure (BP) response to acute ischemic stroke has a high rate of incidence, certain self-limitations, and an effect on prognosis (Aslanyan et al., 2003). A study (Qureshi et al., 2007) of a nationally representative large dataset in the U.S. revealed that elevated BP was observed in about 60% of acute ischemic stroke patients admitted to the emergency department. Some studies (Kellert et al., 2012; Endo et al., 2013) showed that BP variability is relevant to poor outcomes. BP changes, including variability, are closely correlated with cerebral infarction prognosis (Miao et al., 2006; Tikhonoff et al., 2009). However, it is worth noting that the influence of BP fluctuation on stroke patients receiving IVT therapy is still controversial. One study (Aslanyan et al., 2003) has shown that high BP before thrombolysis and significant BP fluctuations after IVT therapy are risk factors for a poor prognosis, whereas another study (Liu et al., 2016) indicated that spontaneous BP decrease within a certain range is due to recanalization and reperfusion of the brain tissue, which is considered good prognostic factors. Thus, the relationship between BP changes and IVT therapy needs further research.

Our study aimed to investigate the relationship between BP changes during recombinant tissue plasminogen activator (rt-PA) infusion and 3-month prognosis evaluated using the modified Rankin Scale (mRS) and determine the factors influencing BP during the infusion to better understand this disease and improve its clinical management.

## MATERIALS AND METHODS

### Participants

Patients who were treated with IVT and admitted to the stroke center of the First Hospital of Jilin University from May 2015 to October 2017 were analyzed retrospectively. IVT was performed within 4.5 h from onset according to current guideline recommendations and the physician's decision (Jauch et al., 2013; Powers et al., 2018). After IVT, all patients received standard medical treatment and general care in the stroke center. Patients were excluded from this study if: (1) their laboratory data and/or follow-up data were unavailable; (2) they used intravenous antihypertensive drugs before or during thrombolysis; or (3) they accepted endovascular treatment.

We collected patient data including demographics, medical history, personal and family history, lab test results, imaging, treatment time point, and other related information. Medical history was defined as per the article (Wang et al., 2011) "The China National Stroke Registry for patients with acute cerebrovascular events: design, rationale, and baseline patient characteristics." Blood lipids were collected in the next morning after IVT.

Brachial BP was measured using an automatic cuff sphygmomanometer before and at regular intervals of 15 min during the infusion of rt-PA (1 h). Because several previous studies have demonstrated that there is a stronger predictive function of systolic BP (SBP) than diastolic BP in patients with ischemic stroke (Tikhonoff et al., 2009; Endo et al., 2013), we collected SBP to evaluate early BP changes. All the BP refers to SBP in the present study. The average value of BP during thrombolysis was calculated and compared to the baseline BP. BP decrease was defined as the difference between the baseline BP and the average BP, provided it was greater than 0 mmHg. BP fluctuation during thrombolysis was measured by the standard deviation (SD), which is the arithmetic square root of variance (Liu et al., 2015).

Baseline Alberta Stroke Program Early CT Score (ASPECTS) was evaluated using brain computed tomography (CT). CT examinations were repeated 24 h after thrombolysis. Hemorrhage transformation was evaluated using the 24 h CT scans, following the Second European Cooperative Acute Stroke Study (ECASS-II) classification.

mRS was evaluated at the 3-month double-blind follow-up after IVT. Doctors who had recorded the cases were not assigned to follow-up. Detailed addresses and phone numbers were documented on admission to the hospital. Patients with mRS $\leq$ 2 were included in the "favorable outcome group" and those with mRS $\geq$ 3 into the "unfavorable outcome group."

### Statistical Analysis

The statistical program for social sciences version 20.0 (SPSS, IBM, West Grove, PA, USA) was used to analyze all data. Continuous variables were expressed as mean ($\pm$ SD) and were analyzed using a *t*-test. Classified variables were analyzed using the Pearson chi-square test. $P < 0.05$ was considered statistically significant. A bivariate logistic regression model was used to verify independent 3-month prognostic factors of cerebral infarction and factors influencing BP. Variables with

$P < 0.1$ were included in the multivariate analysis model. Also, a history of atrial fibrillation, coronary heart disease, and hypertension may be potentially correlated with acute BP changes; thus, they were added to the above model.

# RESULTS

In total, 488 consecutive patients diagnosed with acute ischemic stroke who underwent IVT were screened. Thirty patients who did not meet BP standards or whose laboratory or follow-up data were unavailable were excluded from this study. Finally, 458 patients were included in the study.

## Relationship Between Baseline Data and Cerebral Infarction Prognosis

Baseline National Institute of Health Stroke Scale (NIHSS) score (8.25 ± 5.57 vs. 13.51 ± 7.42, $P < 0.001$) and HDL (1.24 ± 0.32 vs. 1.36 ± 0.41, $P = 0.012$) were significantly lower, whereas the CT ASPECTS (8.65 ± 1.82 vs. 8.13 ± 2.00, $P = 0.005$) was higher in the favorable outcomes group. Additionally, patients with favorable outcomes were more likely to have decreased BP during thrombolysis (69.4% vs. 59.8%, $P = 0.037$). The history of hypertension was significant (40% vs. 54%, $P = 0.011$) in the unfavorable outcome group. Rates of hemorrhage transformation after IVT were significantly different between the two groups (16% vs. 23.9%, $P = 0.034$). BP decrease developed less hemorrhage transformation (OR 0.459, 95% CI 0.276–0.761, $P < 0.001$). Other factors, such as sex, age, cerebral infarction/TIA history, diabetes mellitus, and other common risk factors, did not show a significant effect on prognosis (**Supplementary Table 1**).

## Relationship Between BP Changes and Prognosis

Patients were divided into decreasing and no decreasing groups (regardless of fluctuation extent) according to the features of BP during the rt-PA infusion process. There was no significant difference in baseline mRS score (3.62 ± 0.96 vs. 3.79 ± 0.82, $P = 0.08$) between the two groups. The 3-month mRS score was lower in the BP decreasing group (1.82 ± 1.79 vs. 2.62 ± 2.06, $P = 0.001$). Simultaneously, the improvement was more significant (1.79 ± 1.78 vs. 1.17 ± 2.03, $P = 0.01$) and the rate of favorable outcome (mRS ≤ 2) was higher (67.5% vs. 57.7%, $P = 0.037$) in the BP decreasing group. There was no significant difference in fatality rates between the two groups (7.3% vs. 11.5%, $P = 0.126$; **Table 1**). The number of patients with 3-month mRS ≤ 1 and mRS ≤ 2, which indicates a better prognosis, was significantly higher in the BP decreasing group (**Figure 1**).

## Relationship Between BP Fluctuation During Thrombolysis and Prognosis

There was a significant difference in the SD of BP between the BP decreasing group and the no decreasing group (74.8% vs. 62.8%, $P = 0.007$). For the BP decreasing group, the better prognosis was correlated with BP SD < 10 mmHg (73.9% vs. 60.6%, $P = 0.019$) but not with the range of decrease ($P = 0.235$ and $P = 0.705$). For the BP no decreasing group, poor prognosis was correlated with large fluctuations in BP (SD > 10 mmHg; *t*-test: SD: 7.24 ± 4.61 mmHg vs. 9.09 ± 5.97 mmHg, $P = 0.023$; Chi-square test: 76.9% vs. 66.2%, $P = 0.108$; **Table 2**).

**TABLE 1** | Relationship between blood pressure (BP) changes and prognosis.

| mRS score | | BP change | | *P* |
|---|---|---|---|---|
| | | Decreasing *n* = 302 | No decreasing *n* = 156 | |
| Baseline mRS | | 3.62 ± 0.96 | 3.79 ± 0.82 | 0.08 |
| 3 m mRS | | 1.82 ± 1.79 | 2.62 ± 2.06 | 0.001* |
| Variation of mRS** | | 1.79 | 1.17 | 0.01* |
| 3 m mRS ≤ 2 | *n* (%) | 203 (67.5) | 91 (57.7) | 0.037* |
| 3 m mRS = 6 (death) | *n* (%) | 22 (7.3) | 18 (11.5) | 0.126 |

**Denotes P < 0.05 for comparing between two groups; **denotes value calculated by baseline modified Rankin Scale (mRS) score minus 3 m mRS score.*

## Factors Influencing BP Decrease During Infusion of rt-PA

Univariate analysis of BP changes involved age, baseline BP, baseline NIHSS score, baseline ASPECTS, and medical history. Univariate analysis showed that patients with a higher baseline BP (154.65 ± 20.49 vs. 146.67 ± 19.57, $P < 0.001$) and a history of hypertension (32.8% vs. 42.3%, $P = 0.044$) were more likely to have a decrease in BP during thrombolysis. Baseline CT ASPECTS also significantly influenced BP (8.30 ± 1.70 vs. 7.88 ± 2.23, $P = 0.026$).

Variables of univariate analysis with statistical significance ($P < 0.1$) and diseases that may affect BP were included in the multivariate analysis. It was noted that baseline BP, history of hypertension, baseline ASPECTS were all independent factors associated with the changes in BP. Patients whose baseline BP (OR 1.02, 95% CI 1.01–1.031, $P < 0.001$) and baseline CT ASPECTS (OR 1.139, 95% CI 1.024–1.267, $P = 0.017$) were higher were more likely to have a decrease in BP during thrombolysis. Additionally, the presence of hypertension also increased the chances of BP decrease during thrombolysis (OR 0.602, 95% CI 0.38–0.952, $P = 0.030$; **Table 3**).

# DISCUSSION

In this study, we examined the effects of early changes in BP during IVT on the prognosis of acute ischemic stroke patients. Patients with a decreased and steady BP during thrombolysis were more likely to have a favorable outcome. Baseline BP, hypertension history, and baseline CT ASPECTS were found to be factors influencing the BP change.

The relationship between BP changes and cerebral infarction prognosis is important. Transient BP elevation is frequent in acute ischemic stroke and may increase perfusion of the ischemic penumbra (Miao et al., 2006). Hypoperfusion can lead to less perfusion and aggravate infarction (Olsen et al., 1983; Janardhan and Qureshi, 2004). Some of the hypertensive responses to acute ischemic stroke can result in a spontaneous BP decrease nearly to the former or normal level (Qureshi et al., 2007). Acute ischemic stroke may produce some stress

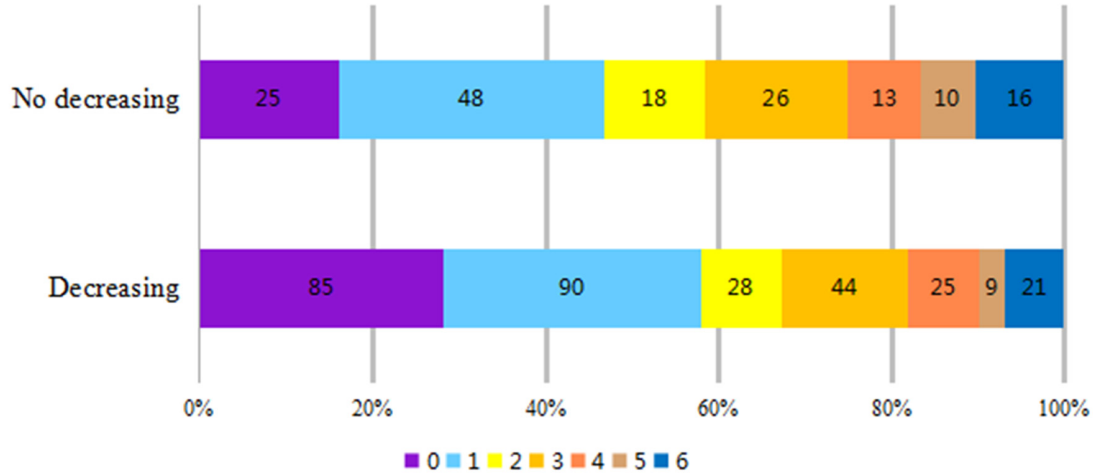


**FIGURE 1 |** Distribution of 3 m modified Rankin Scale (mRS) after thrombolysis.

**TABLE 2 |** Relationship between BP fluctuation during thrombolysis and 3 m favorable outcomes.

| BP fluctuation during IVT | | Prognosis (mRS) | | *P* |
|---|---|---|---|---|
| | | mRS ≤ 2 | mRS ≥ 3 | |
| **All patients** | | | | |
| BP standard deviation (SD) | mmHg | 8.42 ± 8.77 | 9.19 ± 6.78 | 0.325 |
| SD < 10 mmHg | *n* (%) | 220 (74.8) | 103 (62.8) | 0.007* |
| **BP decreasing** | | | | |
| BP standard deviation (SD) | mmHg | 8.95 ± 10.04 | 9.26 ± 7.29 | 0.822 |
| SD < 10 mmHg | *n* (%) | 150 (73.9) | 60 (60.6) | 0.019* |
| Decrease < 10 mmHg | *n* (%) | 98 (48.3) | 55 (55.6) | 0.235 |
| Decrease < 20 mmHg | *n* (%) | 156 (76.8) | 78 (78.8) | 0.705 |
| **BP no decreasing** | | | | |
| BP standard deviation (SD) | mmHg | 7.24 ± 4.61 | 9.09 ± 5.97 | 0.023* |
| SD < 10 mmHg | *n* (%) | 70 (76.9) | 43 (66.2) | 0.108 |
| Increase < 10 mmHg | *n* (%) | 62 (68.1) | 39 (60.0) | 0.252 |
| Increase < 20 mmHg | *n* (%) | 86 (94.5) | 52 (80.0) | 0.002* |

**Denotes P < 0.05 for comparing between two groups.*

factors that temporarily damage the BP regulation function (Murros et al., 1993). These factors can gradually diminish during vascular recanalization and reperfusion therapy with BP gradually decreasing to normal levels (Qureshi et al., 1999).

**TABLE 3 |** Multivariate analysis of BP decrease during recombinant tissue plasminogen activator (rt-PA) infusion.

| Factor | *P* | OR | 95% CI for OR | |
|---|---|---|---|---|
| | | | Lower bound | Upper bound |
| Baseline CT ASPECT score | 0.017* | 1.139 | 1.024 | 1.267 |
| Baseline BP | <0.001* | 1.02 | 1.01 | 1.031 |
| Coronary artery disease | 0.854 | 0.935 | 0.456 | 1.918 |
| Atrial fibrillation | 0.708 | 1.146 | 0.561 | 2.34 |
| History cerebral infarction/TIA history | 0.376 | 1.332 | 0.706 | 2.51 |
| Hypertension | 0.030* | 0.602 | 0.38 | 0.953 |
| Diabetes mellitus | 0.771 | 1.095 | 0.593 | 2.022 |

**Denotes P < 0.05 for comparing between two groups.*

Thus, a decrease in BP, to a certain extent, immediately after IVT may indicate vascular recanalization and brain tissue reperfusion, and these factors are relevant to good prognosis (Endo et al., 2013; Liu et al., 2016).

Liu et al. (2016) found that a sudden drop in SBP of 20 mmHg or greater between two continuous BP measurements within the first 2 h after IVT was associated with vascular recanalization and good outcomes. Most recanalizations induced by rt-PA occurred during the first hour after IVT and rarely presented after 2 h (Ribo et al., 2006). Our study showed that BP decrease within the first hour after IVT was associated with a favorable outcome, thus predicting prognosis faster. We did not find a significant association between outcomes and a BP decrease of over 20 mmHg, perhaps because we did not calculate the difference value between two continuous BP values. Nagaraja et al. (2014) observed that patients with a BP decrease of over 20 mmHg were associated with improved clinical symptoms and NIHSS scores. Mattle et al. (2005) also found that SBP within 24 h after IVT decreased significantly

faster in patients with good outcomes than in patients with failed recanalization. In our study, we did not perform vascular recanalization evaluation for all patients because of a lack of patient cooperation, but by evaluating changes in BP, we found that a BP decrease was relevant to a good prognosis, while a significant BP increase was associated with poor outcomes.

BP fluctuation (variability) also influences the prognosis of IVT (Aslanyan et al., 2003). In this study, we found that small BP fluctuations with SD <10 mmHg correlated with a good 3-month prognosis. The extent of BP decrease during IVT was not significantly related to prognosis; however, the extent of BP increase was relative to the outcome. In addition to large BP fluctuations, obvious BP increase (≥10 mmHg) also predicted a poor prognosis. An obvious decrease in BP is relevant to recanalization, while a large BP increase may be associated with hemorrhage transformation. Ko et al. (2010) found that SBP variability within 72 h after IVT was related to hemorrhage transformation. Endo et al. (2013) measured BP eight times within the first 25 h after IVT and found that patients with higher BP variability had a higher risk of hemorrhage transformation and mortality after thrombolysis. Our result that BP variability after IVT is related to the 3-month outcome is consistent with those of previous studies (Stead et al., 2006; Kellert et al., 2012; Endo et al., 2013; Chang et al., 2018). Liu et al. (2015) found that SBP variability during the first 24 h after IVT is negatively associated with cerebral reperfusion and the 3-month neurological outcome. Results of ECASS-I showed that low SBP/DBP and small BP fluctuation increased chances of a good 3-month prognosis for cerebral infarction. Mei Yong (Yong and Kaste, 2008) analyzed BP data of 793 patients in the ECASS-II trial and found that high variability of SBP was associated with 7-day hemorrhage transformation and predictive of a poor outcome.

High baseline BP and ASPECTS are more likely to cause BP to decrease, while hypertension history is less likely to cause BP to decrease. BP elevation may compensate for the reperfusion of the penumbra. When the average BP varies between 60 and 150 mmHg, capillary capacity can be regulated by constriction and dilation according to BP changes to maintain steady cerebral perfusion (Paulson et al., 1990). Local ischemic brain tissue at occlusive cerebral vessels loses cerebral autoregulation; thus, cerebral perfusion largely depends on BP. Excessively high or low BP are risk factors for poor prognosis (Symon et al., 1973). Kellert et al. (2011) found that the relationship between baseline BP and prognosis after IVT was S-shaped. When SBP elevated slightly to the 146–160 mmHg range, every 1 mm BP elevation was associated with a 10% higher good-prognosis. A similar outcome was observed when DBP was 80–90 mmHg, which suggested that proper BP elevation was beneficial to the penumbra. Thus, proper elevated baseline BP may increase blood flow and lead to recanalization, which tends to decrease BP after IVT. The ASPECTS evaluates the infarction condition and reflects collateral compensation. High ASPECTS is relevant to good perfusion. Patients with a history of hypertension have vascular hyaline degeneration; thus, their collateral compensation is poor (Tikhonoff et al., 2009), and consequently, they have poor recanalization and low baseline BP.

There are some limitations to our study. First, we excluded patients treated with antihypertensive agents before IVT; thus, we cannot use these findings to guide their BP control. Since we need guidance for BP control in all IVT patients, trials including patients treated with antihypertensive agents are warranted. Second, the study is based out of a single center, and the sample size is limited. Multi-center prospective trials are needed to obtain more reliable results.

## CONCLUSION

Patients with a decreased and steady BP during thrombolysis were more likely to have a favorable outcome. Baseline CT ASPECTS, baseline NIHSS score, and hypertension history were independent factors related to BP change. These findings could help predict the prognosis of patients treated with IVT and suggest that BP control during IVT might improve clinical outcomes.

## DATA AVAILABILITY STATEMENT

The raw data supporting the conclusions of this article will be made available by the authors, without undue reservation.

## ETHICS STATEMENT

The studies involving human participants were reviewed and approved by the Human Ethics and Research Ethic committees of the First Hospital of Jilin University. The patients/participants provided their written informed consent to participate in this study.

## AUTHOR CONTRIBUTIONS

ZW and CW conceived and designed the study, acquired the data, and drafted and revised the manuscript. All authors analyzed and interpreted the data and critically revised the manuscript for important intellectual content. All authors contributed to the article and approved the submitted version.

## FUNDING

This project was supported by the National Key R&D Program of China (2016YFC1301600), Program for Jilin University Science and Technology Innovative Research Team (JLUSTIRT; 2017TD-12), and Jilin Provincial Key Laboratory (20190901005JC) to YY.

## SUPPLEMENTARY MATERIAL

The Supplementary Material for this article can be found online at: https://www.frontiersin.org/articles/10.3389/fnagi.2020.601471/full#supplementary-material.

## REFERENCES


Aslanyan, S., Fazekas, F., Weir, C. J., Horner, S., Lees, K. R., and GAIN International Steering Committee and Investigators (2003). Effect of blood pressure during the acute period of ischemic stroke on stroke outcome: a tertiary analysis of the GAIN International Trial. *Stroke* 34, 2420–2425. doi: 10.1161/01.STR.0000091233.04524.0C

Chang, J. Y., Jeon, S. B., Lee, J. H., Kwon, O. K., and Han, M. K. (2018). The Relationship between blood pressure variability, recanalization degree and clinical outcome in large vessel occlusive stroke after an intra-arterial thrombectomy. *Cerebrovasc. Dis.* 46, 279–286. doi: 10.1159/000495300

Endo, K., Kario, K., Koga, M., Nakagawara, J., Shiokawa, Y., Yamagami, H., et al. (2013). Impact of early blood pressure variability on stroke outcomes after thrombolysis: the SAMURAI rt-PA Registry. *Stroke* 44, 816–818. doi: 10.1161/STROKEAHA.112.681007

Janardhan, V., and Qureshi, A. I. (2004). Mechanisms of ischemic brain injury. *Curr Cardiol Rep* 6, 117–123. doi: 10.1016/j.neuropharm.2008.01.005

Jauch, E. C., Saver, J. L., Adams, H. P., Jr., Bruno, A., Connors, J. J., Demaerschalk, B. M., et al. (2013). Guidelines for the early management of patients with acute ischemic stroke: a guideline for healthcare professionals from the American Heart Association/American Stroke Association. *Stroke* 44, 870–947. doi: 10.1161/STR.0b013e318284056a

Kellert, L., Rocco, A., Sykora, M., Hacke, W., and Ringleb, P. A. (2011). Frequency of increased blood pressure levels during systemic thrombolysis and risk of intracerebral hemorrhage. *Stroke* 42, 1702–1706. doi: 10.1161/STROKEAHA.110.604744.

Kellert, L., Sykora, M., Gumbinger, C., Herrmann, O., and Ringleb, P. A. (2012). Blood pressure variability after intravenous thrombolysis in acute stroke does not predict intracerebral hemorrhage but poor outcome. *Cerebrovasc. Dis.* 33, 135–140. doi: 10.1159/000334186

Ko, Y., Park, J. H., Yang, M. H., Ko, S. B., Han, M. K., Oh, C. W., et al. (2010). The significance of blood pressure variability for the development of hemorrhagic transformation in acute ischemic stroke. *Stroke* 41, 2512–2518. doi: 10.1161/STROKEAHA.110.595561

Liesch, M. (2012). Ischemic stroke and TIA. *Praxis (Bern 1994)* 101, 43–50. doi: 10.1024/1661-8157/a000809

Liu, K., Chen, Q., Yan, S., Zhang, S., and Lou, M. (2015). Relationship between early blood pressure variability and reperfusion in acute ischemic stroke patients with intravenous thrombolysis. *Zhejiang Da Xue Xue Bao Yi Xue Ban* 44, 603–610.

Liu, K., Yan, S., Zhang, S., Guo, Y., and Lou, M. (2016). Systolic blood pressure variability is associated with severe hemorrhagic transformation in the early stage after thrombolysis. *Transl. Stroke Res.* 7, 186–191. doi: 10.1007/s12975-016-0458-6

Mattle, H. P., Kappeler, L., Arnold, M., Fischer, U., Nedeltchev, K., Remonda, L., et al. (2005). Blood pressure and vessel recanalization in the first hours after ischemic stroke. *Stroke* 36, 264–268. doi: 10.1161/01.STR.0000153052.59113.89

Miao, C. Y., Xie, H. H., Zhan, L. S., and Su, D. F. (2006). Blood pressure variability is more important than blood pressure level in determination of end-organ damage in rats. *J. Hypertens.* 24, 1125–1135. doi: 10.1097/01.hjh.0000226203.57818.88

Murros, K., Fogelholm, R., Kettunen, S., and Vuorela, A. L. (1993). Serum cortisol and outcome of ischemic brain infarction. *J. Neurol. Sci.* 116, 12–17. doi: 10.1016/0022-510x(93)90083-b

Nagaraja, N., Warach, S., Hsia, A. W., Adams, H. P., Jr., Auh, S., Latour, L. L., et al. (2014). Association between neurologic improvement with decline in blood pressure and recanalization in stroke. *JAMA Neurol.* 71, 1555–1558. doi: 10.1001/jamaneurol.2014.2036

Olsen, T. S., Larsen, B., Herning, M., Skriver, E. B., and Lassen, N. A. (1983). Blood flow and vascular reactivity in collateral perfused brain tissue: Evidence of an ischemic penumbra. *Stroke* 14, 332–341. doi: 10.1161/01.str.14.3.332

Paulson, O. B., Strandgaard, S., and Edvinsson, L. (1990). Cerebral autoregulation. *Cerebrovasc. Brain Metab. Rev.* 2, 161–192.

Powers, W. J., Rabinstein, A. A., Ackerson, T., Adeoye, O. M., Bambakidis, N. C., Becker, K., et al. (2018). 2018 Guidelines for the early management of patients with acute ischemic stroke: a guideline for healthcare professionals from the american heart association/american stroke association. *Stroke* 49, e46–e110. doi: 10.1161/STR.0000000000000158

Qureshi, A. I., Ezzeddine, M. A., Nasar, A., Suri, M. F., Kirmani, J. F., Hussein, H. M., et al. (2007). Prevalence of elevated blood pressure in 563,704 adult patients with stroke presenting to the ED in the United States. *Am. J. Emerg. Med.* 25, 32–38. doi: 10.1016/j.ajem.2006.07.008

Qureshi, A. I., Luft, A. R., Sharma, M., Janardhan, V., Lopes, D. K., Khan, J., et al. (1999). Frequency and determinants of postprocedural hemodynamic instability after carotid angioplasty and stenting. *Stroke* 30, 2086–2093. doi: 10.1161/01.str.30.10.2086

Ribo, M., Alvarez-Sabin, J., Montaner, J., Romero, F., Delgado, P., Rubiera, M., et al. (2006). Temporal profile of recanalization after intravenous tissue plasminogen activator: selecting patients for rescue reperfusion techniques. *Stroke* 37, 1000–1004. doi: 10.1161/01.STR.0000206443.96112.d9

Stead, L. G., Gilmore, R. M., Vedula, K. C., Weaver, A. L., Decker, W. W., Brown, R. D., et al. (2006). Impact of acute blood pressure variability on ischemic stroke outcome. *Neurology* 66, 1878–1881. doi: 10.1212/01.wnl.0000219628.78513.b5

Symon, L., Held, K., and Dorsch, N. W. (1973). A study of regional autoregulation in the cerebral circulation to increased perfusion pressure in normocapnia and hypercapnia. *Stroke* 4, 139–147. doi: 10.1161/01.str.4.2.139

Tikhonoff, V., Zhang, H., Richart, T., and Staessen, J. A. (2009). Blood pressure as a prognostic factor after acute stroke. *Lancet Neurol.* 8, 938–948. doi: 10.1016/S1474-4422(09)70184-X

Wang, Y., Cui, L., Ji, X., Dong, Q., Zeng, J., Wang, Y., et al. (2011). The China national stroke registry for patients with acute cerebrovascular events: design, rationale and baseline patient characteristics. *Int. J. Stroke.* 6, 355–361. doi: 10.1111/j.1747-4949.2011.00584.x

Wang, W., Jiang, B., Sun, H., Ru, X., Sun, D., Wang, L., et al. (2017). Prevalence, incidence and mortality of stroke in chinaclinical perspective: results from a nationwide population-based survey of 480687 adults. *Circulation* 135, 759–771. doi: 10.1161/CIRCULATIONAHA.116.025250

Yong, M., and Kaste, M. (2008). Association of characteristics of blood pressure profiles and stroke outcomes in the ECASS-II trial. *Stroke* 39, 366–372. doi: 10.1161/STROKEAHA.107.492330


**Conflict of Interest**: The authors declare that the research was conducted in the absence of any commercial or financial relationships that could be construed as a potential conflict of interest.

frontiers in Aging Neuroscience

ORIGINAL RESEARCH
published: 07 December 2020
doi: 10.3389/fnagi.2020.584839

# Metabolic Disorder of Extracellular Matrix Mediated by Decorin Upregulation Is Associated With Brain Arteriovenous Malformation Diffuseness

*Maogui Li[1,2,3,4†], Qingyuan Liu[1,2,3,4†], Junhua Yang[1,2,3,4], Pengjun Jiang[1,2,3,4], Yi Yang[1,2,3,4], Yanan Zhang[5], Yong Cao[1,2,3,4], Jun Wu[1,2,3,4*] and Shuo Wang[1,2,3,4*]*

[1] Department of Neurosurgery, Beijing Tiantan Hospital, Capital Medical University, Beijing, China, [2] China National Clinical Research Center for Neurological Diseases, Beijing, China, [3] Center of Stroke, Beijing Institute for Brain Disorders, Beijing, China, [4] Beijing Key Laboratory of Translational Medicine for Cerebrovascular Diseases, Beijing, China, [5] Department of Blood Transfusion, Beijing Tiantan Hospital, Capital Medical University, Beijing, China

OPEN ACCESS

**Edited by:**
*Aurel Popa-Wagner, University Hospital Essen, Germany*

**Reviewed by:**
*Alan David Snow, Cognitive Clarity Inc., United States*
*Diego Sepulveda-Falla, University Medical Center Hamburg-Eppendorf, Germany*

***Correspondence:**
*Shuo Wang*
*captain9858@126.com*
*Jun Wu*
*wujunslf@126.com*

[†] *These authors have contributed equally to this work*

**Received:** *18 July 2020*
**Accepted:** *29 October 2020*
**Published:** *07 December 2020*

**Citation:**
*Li M, Liu Q, Yang J, Jiang P, Yang Y, Zhang Y, Cao Y, Wu J and Wang S (2020) Metabolic Disorder of Extracellular Matrix Mediated by Decorin Upregulation Is Associated With Brain Arteriovenous Malformation Diffuseness. Front. Aging Neurosci. 12:584839. doi: 10.3389/fnagi.2020.584839*

**Background and Objective:** Diffuse brain arteriovenous malformations (BAVMs) are mixed up with normal brain parenchyma and therefore increase the difficulty of surgical resection, leading to poor surgical prognosis. Since the mechanism underlying BAVM diffuseness remains unknown, a quantitative proteomic analysis was performed to investigate the altered expression of proteins in diffuse BAVMs compared to compact ones.

**Methods:** We performed proteomic analysis on five diffuse BAVMs and five compact BAVMs. Bioinformatics analysis was conducted to identify potential signals related to BAVM diffuseness. Candidate proteins were then investigated in BAVM specimens using immunofluorescence and Western blot analysis. Tube formation assays were used to investigate the effects of candidate proteins on the angiogenesis of human umbilical endothelial cells (HUVECs). Finally, Masson, Sirius red staining, and immunofluorescence were used to evaluate the characteristics of extracellular matrix (ECM) in BAVM tissues.

**Results:** A total of 58 proteins were found to be differentially expressed between diffuse and compact BAVMs via proteomic analysis. TGF-β (transforming growth factor-beta) signaling pathway, ECM–receptor pathway, relaxin signaling pathway, and several other pathways were associated with BAVM diffuseness. The TGF-β signaling pathway is associated with angiogenesis; the role of this pathway in the formation of diffuse BAVMs was investigated, and the decorin (DCN) upregulation played an important role in this process. Immunofluorescence showed that DCN was significantly upregulated within and around the malformed vessels of diffuse BAVMs. Functional assays showed that exogenous DCN could promote the tube formation ability of HUVECs through

inhibiting the TGF-β signaling pathway and overproducing ECM. Histological staining demonstrated the overproduction of ECM in diffuse BAVMs.

**Conclusion:** TGF-β signaling pathway inhibited by DCN in vascular endothelial cells is related to BAVM diffuseness. The metabolic disorder of ECM caused by DCN upregulation may significantly contribute to the formation of diffuse BAVMs.

**Keywords: brain arteriovenous malformation, diffuseness, extracellular matrix, DCN, TGF-beta pathway**

## INTRODUCTION

Brain arteriovenous malformations (BAVMs) are characterized by the nidus of dysplastic connections between feeding arteries and draining veins (Moftakhar et al., 2009; Rangel-Castilla et al., 2014; Derdeyn et al., 2017). Most BAVMs have a compact architecture with little brain tissue within the nidus (Spears et al., 2006; Du et al., 2007; Hashimoto et al., 2007). However, in some rare cases classified as diffuse BAVMs (dBAVMs), there can be massive brain tissues interspersed among the malformed vessels (Chin et al., 1992; Spears et al., 2006; Du et al., 2007; Hashimoto et al., 2007). Previously, the features of dBAVMs have been well discussed for predicting the difficulty of surgical resection and poor surgical outcomes (Al-Shahi et al., 2002; Du et al., 2005, 2007; Spears et al., 2006).

Chin et al. (1992) firstly investigated the relationship between the radiological appearance and the histopathological features of dBAVMs and demonstrated the existing normal brain parenchyma among the malformed vessels. In another study, Du et al. revealed that dBAVMs are usually fed by the thin-walled and fragile arteries (Du et al., 2007). It was suggested that immature vascular formation and abnormal interaction between brain tissue and the vessels exist in dBAVMs. In a recent study, the somatic KRAS mutation was found in sporadic BAVMs and was thought to be involved in BAVM genesis and relative manifestations (Nikolaev et al., 2018). As one of the KRAS family, KRAS5 is supposed to activate related pathways, leading to the immature vascular formation and abnormal extracellular matrix (ECM) metabolism in BAVMs (Cheng and Nussinov, 2018). However, because of lacking relative studies, the mechanism underlying formation of dBAVMs remains unknown.

To date only a few proteomic studies on BAVMs have been performed; moreover, only the altered proteins in BAVMs versus normal arteries have been researched (Bicer et al., 2010; Simonian et al., 2017; Wang et al., 2017). In this study, the differentially expressed proteins between dBAVMs and compact BAVMs (cBAVMs) were identified using isobaric tags for relative and absolute quantification (iTRAQ) method, with the aim to demonstrate the pathological mechanism of vascular development in dBAVMs at the protein level.

## MATERIALS AND METHODS

### Patients and Samples Preparation

Between January 2017 and April 2018, patients who underwent microsurgical resection of BAVMs in our institution were recruited. The exclusion criteria were (1) patients older than 60 years; (2) patients who have a history of non-surgical treatment such as radiosurgery and endovascular treatment; and (3) patients who have cerebral infarction or other cerebrovascular diseases such as arteriovenous fistula and cavernous hemangioma. The nidus types were divided into cBAVMs and dBAVMs. In this study, a dBAVM was defined as the nidus containing normal brain parenchyma interspersed among the malformed vessels (Chin et al., 1992; Du et al., 2007). Two experienced neurosurgeons (J.W. and P.J.) who were blind to the clinical data documented the type of the nidus according to T1-weighted, T2-weighted, and time-of-flight magnetic resonance angiography (MRA) images, and possible divergence was resolved by consulting with a senior researcher (S.W.). Clinical information including age, gender, and hemorrhage history were collected from the electronic medical record system. Radiological features including nidus size, location, deep venous drainage, and perforating artery supply were identified on MRA and digital subtraction angiography (DSA). The Spetzler–Martine (S-M) grade was calculated.

The BAVM samples were obtained during surgery after total resection. All visible brain tissue and blood clot were removed, and only the malformed vessels were collected. Besides, the superficial temporal arteries (STA) of some patients (cases 1, 2, 3, 5, 8, and 9) were collected. Subsequently, each tissue sample was washed with low-temperature phosphate-buffered saline (PBS) in order to remove the blood cells within the vessels.

### Isobaric Tags for Relative and Absolute Quantification (iTRAQ) Labeling and Nano-LC-MS/MS Analysis

Frozen tissue samples were homogenized with RIPA buffer (Sigma-Aldrich, United States) by hand. The lysis buffers were placed on ice for 30 min and then centrifuged for 20 min under 15,000 *g* to remove insoluble components. The concentration of the extracted protein was quantitatively analyzed using the Bicinchoninic acid method (BCA method). One hundred fifty micrograms from each sample was alkylated and digested in the centrifugal unit. Then, the protein of each pool was dissolved with 1 M DTT for 1 h at 37°C and kept in the dark with 1 M indole-3-acetic acid for 1 h at ambient temperature after precipitating with acetone. Samples were dissolved and centrifuged twice with 120 μl of UA (8 M urea in 0.1 M Tris–HCl, pH 8.5) and then re-dissolved and centrifuged three times with 100 mM lautyltrethylammonium bromide. The proteins were digested with trypsin (Sigma-Aldrich, United States) and

incubated at 37°C overnight. Subsequently, each peptide pool was passed through a 0.2-μm centrifugal filter for 20 min under 12,000 *g* at 20°C. Prepared peptide samples were labeled using a 4-Plex iTRAQ Reagent Kit from AB SCIEX. cBAVMs, dBAVMs, and STAs were labeled with iTRAQ tags, respectively. The labeled peptide mixtures were separated and then trapped on a PepMap100 C18, 5 μm, 100 μm × 2 cm column (Thermo Scientific, United States) using the EASY-nLC 1000 system (Thermo Scientific, United States). Subsequently, the peptides were separated on a PepMap100 RSLC C18, 2.4 μm, 75 μm × 15 cm analytic column by a 102-min mobile phase gradient (from 5 to 90%). Spectra were recorded by the Orbitrap Elite system (Thermo Scientific, United States). Full scan MS spectra were obtained in the $m/z$ range 400–1600 at a resolution of 60,000; the top precursors were selected for high-energy collision-induced dissociation with a collision energy of 35%; the product ions were detected at a resolution of 15,000 by Data Dependent Analysis.

## Bioinformatics Analysis

First, the raw data were searched and discovered using Proteome Discoverer 1.4 (Thermo Scientific, United States). Subsequently, we excluded the proteins with unique peptide as 0 or described as false-positive proteins in the Decoy database. Next, the altered proteins with $P$ value $< 0.05$ and fold value $\geq 2$ or $\leq 0.5$ between dBAVMs and cBAVMs were selected (selected proteins). Then, the proteins whose difference was not obvious between dBAVMs and STAs (fold value was between 0.5 and 2.0) were excluded from the selected proteins; meanwhile, the remaining proteins were summarized as a new altered protein database. Besides, CytoScape 3.6.1 (a free software) was used for further bioinformatics analysis. According to this database, pathway enrichment analysis was performed based on the Kyoto Encyclopedia of Genes and Genomes (KEGG) database using ClueGo (a free plug-in in CytoScape). Gene Ontology (GO) database was employed for the biological interpretation of the identified protein using ClueGo. The differentially expressed proteins of GO were stratified into two types, namely, molecular function and cellular component. The function interaction between different pathways was conducted based on the REACTOME database. The protein–protein interaction (PPI) analysis was conducted based on the STRING database.

## Western Blot Analysis

Besides the 10 BAVM samples for iTRAQ analysis, another 6 BAVM samples were also collected for further validation. Equal amounts of protein were separated by SDS-PAGE and then electro-transferred to PVDF membranes. Subsequently, membranes were blocked with the PBST containing 5% bovine serum album (Sigma-Aldrich, United States) for 1 h and then probed with primary antibodies at 4°C overnight, including rabbit anti-DCN antibody (Abcam, United Kingdom) at 1:1000, rabbit anti-Smad2/3 antibody (Abcam, United Kingdom) at 1:100, rabbit anti-Col I antibody (Abcam, United Kingdom) at 1:1000, and rabbit anti-GAPDH antibody (Abclonal Technology, Wuhan, China). After primary incubation and being washed with PBST, membranes were incubated with secondary antibodies at 1:5000 for 1 h at room temperature. Bands were visualized by an ECL detection system (GeneSys, Alcatel, France). The expression levels were quantified with ImageJ (version 1.8.0, a free software). The expression levels of target proteins were evaluated by performing densitometric analysis. Ratios of target protein densitometric measurements to GAPDH were used for further analysis.

## Histological Staining

We performed histological staining in all 16 BAVM samples. The samples with appropriate volume were taken before dehydration, fixation, and paraffin embedding. For histology, sections were stained with H-E (Hematoxylin–Eosin), Masson, and Sirius red kit (Solarbio, China). For immunofluorescence (IF), sections were blocked with Protein block (Abcam, United Kingdom) after antigen retrieval and permeabilization. Then, sections were incubated with primary antibodies at 4°C overnight, including rabbit anti-DCN (Abcam, United Kingdom) at 1:100, rabbit anti-Smad 2/3 (Abcam, United Kingdom) at 1:100, rabbit anti-Col I antibody (Abcam, United Kingdom) at 1:500, rabbit anti-Col III antibody (Abcam, United Kingdom) at 1:1000, and rabbit anti-Col VI antibody (Abcam, United Kingdom) at 1:500. After being washed with PBST, sections were incubated with secondary antibody (Alexa Fluor® 488 Goat anti-rabbit IgG, Abcam, United Kingdom, and Alexa Fluor® 647 Goat anti-rabbit IgG, Abcam, United Kingdom) at 1:500. Subsequently, sections were stained with DAPI (4′,6-diamidino-2-phenylindole, Solarbio, China) after being washed with PBST. Besides, a laser confocal microscopy workstation (LSM 710, ZEISS, Germany) was used to capture images. Identical conditions and set integration times were applied to facilitate comparisons between samples.

The Masson staining was used to detect fibrosis in BAVMs. Three random sections were measured by two investigators (Q.L. and J.Y.) using ImageJ blinded to the type of BAVMs. The fibers were stained blue, and the non-fibrotic area was stained red. We defined the fibrotic area as the blue area/(blue area + red area). As for IF, ImageJ was used to calculate the integrated optical density (IOD) and count the cell number based on the DAPI image. We used the IOD/cell for further analysis.

## Cell Culture and Decorin Treatment

The human umbilical vein endothelial cells (HUVECs) were purchased from ScienCell (Carlsbad, CA) and maintained in endothelial cell medium (ScienCell corporation) supplemented with 5% fetal bovine serum (Gibco), 100 U/ml penicillin, and 100 μg/ml streptomycin. We used Recombinant Human Decorin Protein (1 μg/ml, R&D Corporation) to treat HUVECs for 24 h. After appropriate treatment, the cells were used for further analysis.

## Tube Formation Assay

Tube formation assays were performed using Ibidi μ-Slide angiogenesis (Ibidi Corporation) according to the manufacturer's protocol. A total of $1.5 \times 10^4$ HUVECs in 50 μl of complete media were planted with Matrigel. The slides were subsequently incubated at 37°C for 24 h. The tube formation was observed

using the Fluorescence Inversion Microscope system, and ImageJ was used to calculate the number of meshes.

## Statistical Analysis

All statistical analyses were conducted using GraphPad Prism 5 (GraphPad Software, American). Variables were compared by the χ2 test, Fisher's exact test, independent Student's *t* test, or Mann–Whitney *U* test. $P < 0.05$ was considered to be statistically significant.

# RESULTS

## Demographic and Clinical Characteristics of the Study Population

A total of 10 patients with BAVMs were recruited in this study, including 5 dBAVMs and 5 cBAVMs (cases 1–10, see **Supplementary Figure 1**). The clinical information of all cases is listed in **Table 1**. Five patients were female and five were males, with ages ranging from 16 to 41 years. The average diameter of nidus was 4.81 cm (ranged from 3.71 to 5.69 cm). No significant difference was found in age, sex, hemorrhage history, nidus size, and S-M grade between the dBAVMs group and cBAVMs group. Three patients who suffered from acute BAVM rupture received early surgical treatment within 3 days after admission. The S-M grade of these BAVMs was only II or III, because of the limited chances of obtaining samples from grade I BAVMs and the rare surgical cases of grade IV or V.

## TGF-β Signaling Pathway Was Associated With BAVM Diffuseness

Proteomic changes among the samples of five dBAVMs, five cBAVMs, and six STAs were assessed using iTRAQ analysis. A total of 84 significantly altered proteins were identified (defined as fold value $\geq 2$ or $\leq 0.5$ and a $P$ value $< 0.05$) from 3080 proteins. Twenty-six proteins were then excluded for no significance between BAVMs and STAs (defined as fold value of 0.5 to 2.0). Of the 58 altered proteins (see **Figure 1A** and **Supplementary Table 1**), 33 proteins were upregulated, and 25 proteins were downregulated (the Top 10 upregulated and downregulated proteins are listed in **Tables 2**, **3**, respectively).

**TABLE 1 |** The demographic and clinical information of BAVM patients.

| Characteristics | cBAVMs *n* = 5 | dBAVMs *n* = 5 | *P* value |
|---|---|---|---|
| Age, years | 29.3 ± 11.0 | 24.5 ± 8.1 | 0.548 |
| Male, n (%) | 2 | 3 | 0.690 |
| Hemorrhage history, *n* (%) | 2 | 1 | 0.690 |
| Locations, *n* (%) | | | 0.548 |
| Temporal | 3 | 2 | |
| Frontal | 2 | 2 | |
| Occipital | 0 | 1 | |
| Size, cm | 5.2 ± 0.6 | 4.5 ± 0.8 | 0.841 |
| Deep venous drainage, *n* (%) | 3 | 3 | 1.000 |
| Perforating artery supply, *n* (%) | 2 | 3 | 0690 |
| Spetzler–Martin grade, *n* (%) | | | 1.000 |
| 2 | 1 | 1 | |
| 3 | 4 | 4 | |

*cBAVMs, compact brain arteriovenous malformations; dBAVMs, diffuse brain arteriovenous malformations.*

An enrichment analysis was performed to elucidate the functional implications of the altered proteins. Based on the GO database, most of the altered proteins were located in the ECM, presynapse, and axon part; moreover, the molecular function of altered proteins included glycosaminoglycan binding and ECM structural constituent conferring tensile strength (see **Figure 1B**). The analysis based on REACTOME database showed that altered proteins were mainly clustered in the degradation of the ECM, microtubule-dependent trafficking of connexons from Golgi to the plasma membrane, Serotonin Neurotransmitter Release cycle, and Ca2 + pathway (see **Supplementary Figure 2A**). Therefore, we supposed that the metabolism of ECM might play an important role in the formation of dBAVMs, which was determined to be the focus of our next analysis. The analysis based on KEGG database showed several clusters related to the TGF-β (transformation growth factor-beta) signaling pathway, ECM–receptor pathway, protein digest and absorption, relaxin signaling pathways, and gap junction (see **Table 4** and **Figure 1C**). The ECM proteins (CO6A6, CO3A1, and so on) mainly enriches in ECM–receptor pathway, relaxin signaling pathway, and protein digestion and absorption pathway. Our further analysis showed that the TGF-β signaling pathway could interact with the ECM–receptor pathway and relaxin signaling pathway (see **Supplementary Figure 2B**). TGF-β signaling pathway is associated with angiogenesis and metabolism of ECM and is related to the diffuseness of BAVMs. Although our analysis also confirmed the role of Relaxin signaling pathway, this pathway mainly regulates the process of post-injury healing, vasoconstriction, and inflammation (Dschietzig et al., 2012; Moon et al., 2014; Valle Raleigh et al., 2017), which is related to atherosclerosis, bone formation, and so on. During the process of angiogenesis, the TGF-β signaling pathway could regulate the endothelial cell and the metabolism of ECM. Among the protein enriched in the TGF-β signaling pathway, the decorin (DCN) was identified as the most strongly altered protein (see **Supplementary Figure 2C**). DCN interacts with some major component of ECM, which suggests that DCN may play an important role in metabolism of ECM in BAVMs (see **Figure 1D**). The expression of DCN in dBAVMs, cBAVMs, and STA was found to be significantly differential by Western blot (see **Figure 1E** and **Supplementary Figure 3**). The level of TGF-β was not significant between cBAVMs and dBAVMs (**Supplementary Figure 3**). These results suggested that inhibition of TGF-β signaling pathway was associated with BAVM diffuseness, and DCN might play an important role in this pathological process.

## DCN Was Upregulated in Malformed Vessels and Might Regulate the Expression of Smad 2/3

To further validate the differential expression of DCN between cBAVMs and dBAVMs, and to determine the distribution

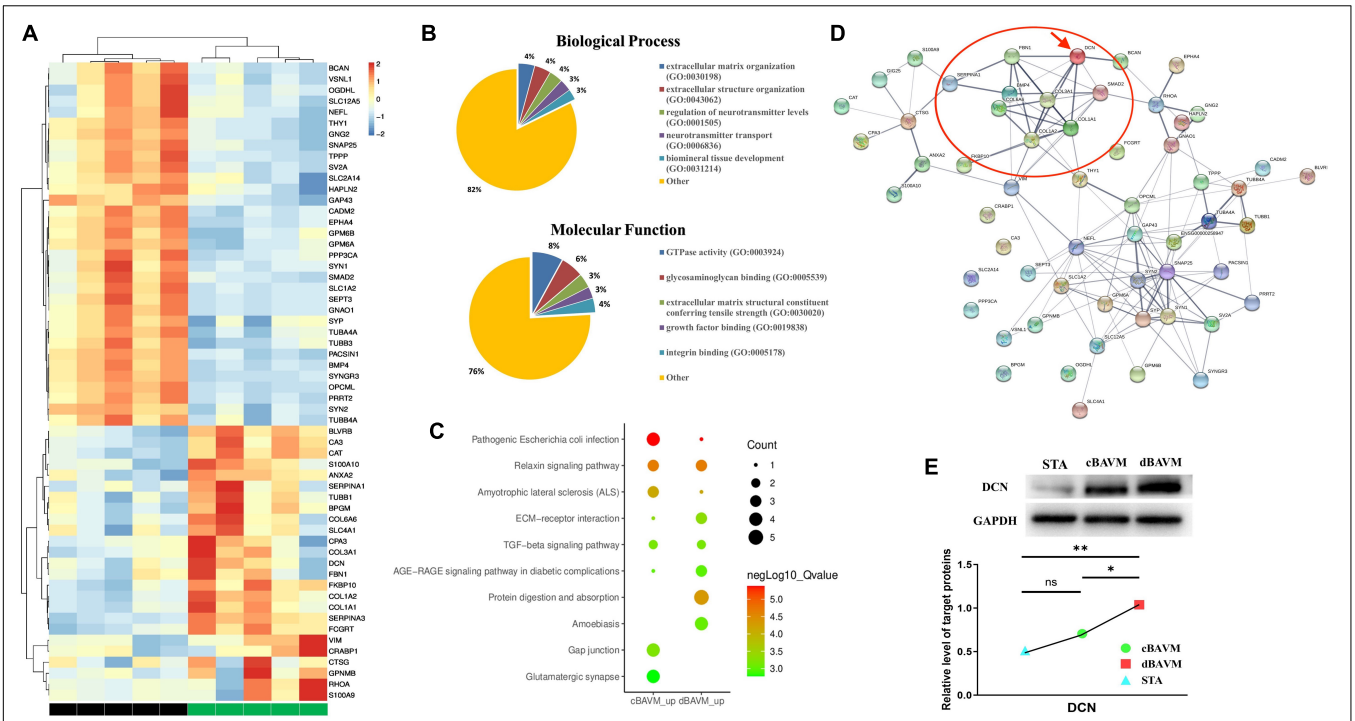


**FIGURE 1 |** Proteome profiles of diffuse and compact brain arteriovenous malformations (BAVMs). **(A)** Protein expression levels in diffuse and compact BAVMs ($P \leq 0.05$, fold change $\geq 2$ or $\leq 0.5$, and excluded the proteins with fold value of 0.5 to 2.0 between diffuse BAVMs and superficial temporal arteries). **(B)** The function and biological process enriched by altered protein by Gene Ontology (GO) analysis. **(C)** Top 10 pathways enriched by protein upregulation in diffuse and compact BAVMs by Kyoto Encyclopedia of Genes and Genomes (KEGG) analysis. **(D)** The protein–protein interaction network of altered proteins by STRING analysis; the decorin (DCN) was highlighted by a red arrow. The proteins interacted with DCN were highlighted by a red circle. **(E)** Validation of DCN expression among superficial temporal arteries, compact BAVMs, and diffuse BAVMs. A group of representative cases from each sample is shown; moreover, the level of DCN in each sample was given in **Supplementary Figure 3**. $^*P < 0.05$; $^{**}P < 0.01$; ns, $P > 0.05$. STA, superficial temporal arteries; cBAVMs, compact brain arteriovenous malformations; dBAVMs, diffuse brain arteriovenous malformations.

**TABLE 2 |** Top 10 proteins significantly upregulated in dBAVMs comparing with cBAVMs.

| No. | Protein | Accession no. | Gene name | Protein function | Fold change |
|---|---|---|---|---|---|
| 1 | Mast cell carboxypeptidase A | CBPA3 | CPA3 | Metallocarboxypeptidase activity | 2.43 |
| 2 | Alpha-1-antichymotrypsin | AACT | SERPINA3 | Serine-type endopeptidase inhibitor activity | 2.42 |
| 3 | Collagen alpha-2(I) chain | A0A087WTA8 | COL1A2 | ECM structural constituent | 2.38 |
| 4 | Collagen alpha-1(I) chain | CO1A1 | COL1A1 | ECM structural constituent | 2.36 |
| 5 | Protein S100-A10 | S10AA | S100A10 | Calcium ion binding | 2.31 |
| 6 | Collagen alpha-6(VI) chain | CO6A6 | COL6A6 | ECM structural constituent | 2.29 |
| 7 | Tubulin beta-1 chain | TBB1 | TUBB1 | Structural constituent of cytoskeleton | 2.28 |
| 8 | Collagen alpha-1(III) chain | CO3A1 | COL3A1 | ECM structural constituent | 2.26 |
| 9 | Decorin | DCN | PGS2 | ECM structural constituent | 2.20 |
| 10 | Rho-related GTP-binding protein | RHOA | RHOA | Protein binding | 2.20 |

*ECM, extracellular matrix.*

characteristics of DCN, we performed IF and Western blot. The information of another six patients was given in the **Supplementary Table 2**. For another six BAVMs, the Western blot showed that DCN was upregulated but Smad 2/3 were downregulated in dBAVMs (see **Figure 2A**). For all 16 BAVMs, the IF showed that DCN was mainly detected in and around malformed vessels and was upregulated in dBAVMs ($P < 0.001$); moreover, as was mainly expressed by vascular endothelial cells (which were marked by CD31), Smad 2/3 was downregulated as the DCN increased in dBAVMs (see **Figure 2B**).

## DCN Upregulation Promoted Endothelial Cell Tube Formation by Regulating the Production of ECM

As an extracellular protein, DCN can interact with transforming growth factor (TGF) to inhibit the TGF-β pathways. To

**TABLE 3 |** Top 10 proteins significantly downregulated in dBAVMs compared with cBAVMs.

| No. | Protein | Accession no. | Gene name | Protein function | Fold change |
|---|---|---|---|---|---|
| 1 | Proline-rich transmembrane protein 2 | PRRT2 | PRRT2 | Protein binding | 0.34 |
| 2 | Ephrin type-A receptor 4 | E9PG71 | EPHA4 | ATP binding | 0.37 |
| 3 | Cell adhesion molecule 2 | CADM2 | IGSF4D | Cell adhesion | 0.38 |
| 4 | Neuronal membrane glycoprotein M6-a | GPM6A | M6A | Calcium channel activity | 0.39 |
| 5 | Hyaluronan and proteoglycan link protein 2 | Q9GZV7 | HPLN2 | Hyaluronic acid binding | 0.39 |
| 6 | Guanine nucleotide-binding protein G subunit alpha | GNAO | GNAO1 | Protein binding | 0.41 |
| 7 | Tubulin beta-3 chain | TBB3 | TUBB4 | Structural constituent of cytoskeleton | 0.41 |
| 8 | Excitatory amino acid transporter 2 | EAA2 | EAAT2 | Glutamate: sodium symporter activity | 0.41 |
| 9 | Synaptic vesicle glycoprotein 2A | SV2A | KIAA0736 | Protein binding | 0.41 |
| 10 | Visinin-like protein 1 | VISL1 | VISL1 | Calcium ion binding | 0.43 |

investigate the effect of DCN on TGF-β pathway and the role of DCN in angiogenesis, we added exogenous DCN (1 μg/ml) to HUVEC. After stimulating the HUVEC by DCN, both IF and Western blot confirmed the downregulation of Smad 2/3 and upregulation of Col I (see **Figures 3A–C**). ECM includes collagen, laminin, fibronectin, and proteoglycans. In this study, we mainly detected the expression of Col I, which is the major component of collagen. Smad 2/3 is a cell-intrinsic regulator of TGF-β pathway and can affect the process of angiogenesis; also, Col I is associated with angiogenesis.

As DCN was upregulated in dBAVMs, we hypothesized that DCN could promote the angiogenesis by stimulating the overproduction of ECM. After DCN stimulation, phosphorylated Smad 2/3 was significantly downregulated in HUVECs compared to the HUVECs without DCN treatment. Moreover, further study showed that the tube formation of HUVECs was enhanced after treatment of DCN (see **Figure 3D**). Collectively, these results showed that DCN could promote the endothelial cell tube formation by inhibiting the TGF-β pathway and stimulating the overproduction of ECM.

## Metabolic Disorder of ECM Might Promote BAVM Diffuseness

To further investigate the composition and characteristics of ECM in cBAVMs and dBAVMs, we performed histological staining in all the 10 BAVMs. The results from the Masson staining showed an obvious vascular fibrosis in cBAVMs compared with dBAVMs; moreover, the Sirius red staining showed a larger area of collagen I and less area of other type of collagen (see **Figures 4A,B**). In proteomic analysis, the result showed that only collagen I, III, and VI might be significantly altered between the two groups. Subsequently, we performed IFs to detect the differential expression of collagen I, III, and VI between cBAVMs and dBAVMs. Our findings showed that collagen I and collagen VI were both significantly upregulated in dBAVMs (see **Figures 4C,D**). These results demonstrated the dysregulation of ECM in dBAVMs. The abnormal metabolism of collagen I and collagen VI may lead to BAVM diffuseness during the process of angiogenesis.

**TABLE 4 |** Top 10 enriched pathways identified by KEGG analysis.

| No. | Term | Count | ID | *P* value |
|---|---|---|---|---|
| 1 | Relaxin signaling pathway | 6 | hsa04926 | <0.001 |
| | Protein digestion and absorption | 5 | hsa04974 | <0.001 |
| 2 | Pathogenic *Escherichia coli* infection | 5 | hsa05130 | <0.001 |
| 3 | TGF-beta signaling pathway | 4 | hsa04724 | <0.001 |
| 4 | ECM–receptor interaction | 4 | hsa04512 | <0.001 |
| 5 | Gap junction | 4 | hsa04540 | <0.001 |
| 6 | AGE-RAGE signaling pathway in diabetic complication | 4 | hsa04933 | <0.001 |
| 7 | Amyotrophic lateral sclerosis (ALS) | 4 | hsa05014 | <0.001 |
| 8 | Amoebiasis | 4 | hsa05146 | <0.001 |
| 10 | Glutamatergic synapse | 4 | hsa04724 | <0.001 |

# DISCUSSION

Although previous studies revealed several mechanisms underlying BAVM genesis and rupture (Moftakhar et al., 2009; Rangel-Castilla et al., 2014; Wang et al., 2017), the forming mechanisms of dBAVMs remain unknown. Studying the altered molecular of dBAVMs contributes to understanding the vascular dysplasia in BAVMs and promoting the possibility of medical treatment. In this study, we performed a proteomics study using the iTRAQ method and revealed that metabolic disorder mediated by DCN might play an important role in the formation of dBAVMs.

In this study, after excluding similar proteins between BAVMs and normal STAs, we found that there were a total of 58 significantly altered proteins, including 33 upregulated and 25 downregulated in dBAVMs compared with cBAVMs. Interestingly, the altered proteins between dBAVMs and cBAVMs are mainly involved in the ECM structural constituent and metabolism of ECM, suggesting that the composition of ECM may be different between different types of BAVMs. Moreover, the majority of enriched pathways take part in regulating the metabolism of ECM and interact with the TGF-β signaling pathway. Previous studies found that TGF-β signaling pathway plays an important role in the formation and clinical features of BAVMs (Wang et al., 2018; Fu et al., 2020). According to the

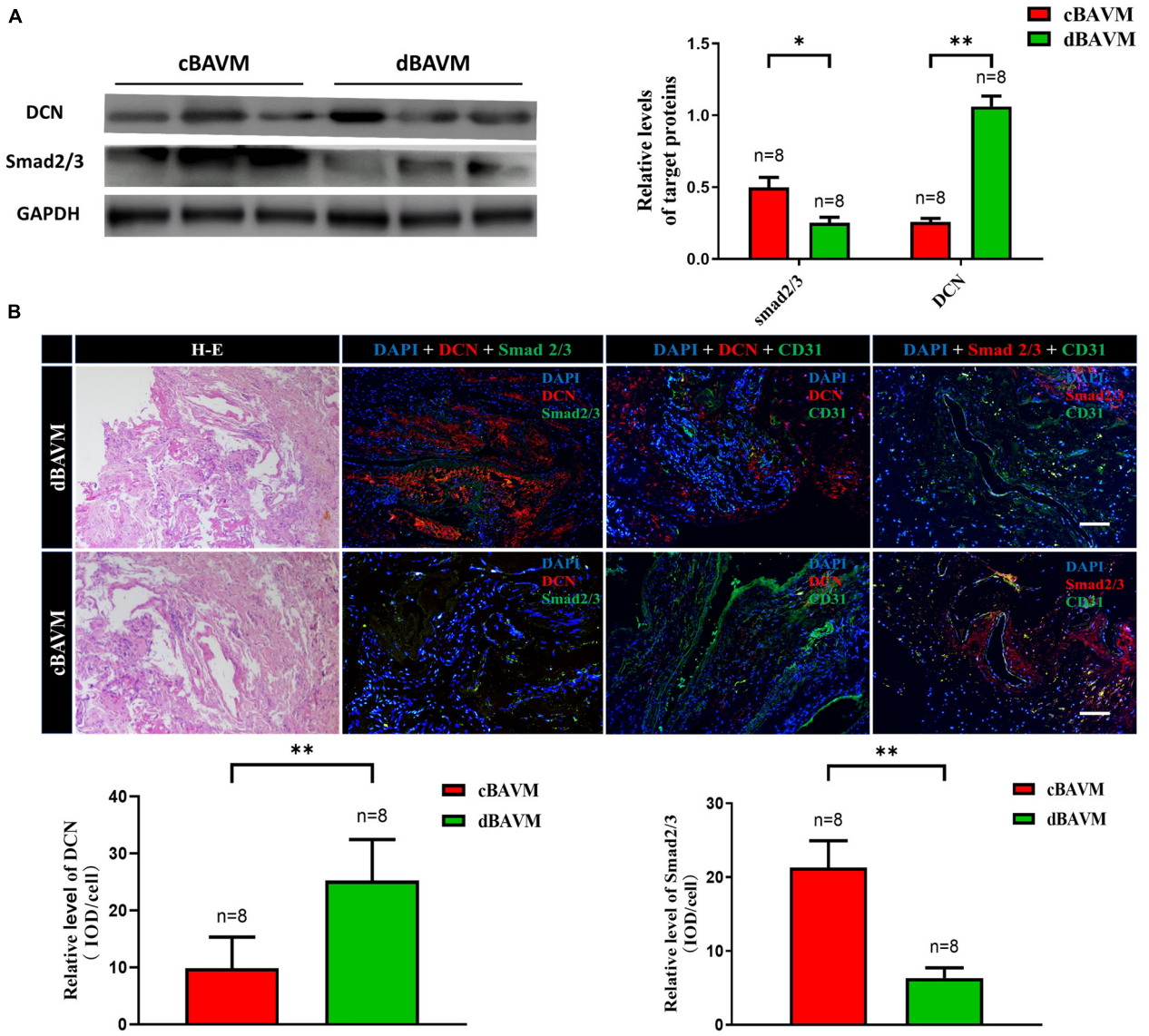


**FIGURE 2 |** The expression level of DCN and Smad 2/3 in BAVM tissues. **(A)** Western blot analysis further validated the upregulation of DCN and downregulation of Smad 2/3 (Smad family member 2 and 3) in another six BAVM tissues (three cBAVMs and three dBAVMs; the information of these six BAVM patients was given in **Supplementary Table 2**). $^{*}P < 0.05$; $^{**}P < 0.01$. **(B)** Histological staining was performed in all 16 BAVM samples. Two groups of representative images of hematoxylin–eosin (H-E) and immunofluorescence staining for DCN, Smad 2/3, and CD31 in BAVM tissues. The histograms showed the semiquantitative grading of DCN and Smad 2/3 expression levels in diffuse and compact BAVMs. The scale bar corresponds to 200 μm. $^{**}P < 0.01$.

classical theory of angiogenesis, the formation of blood vessels consists of two critical parts, vasculogenesis and angiogenesis, which are induced by the orchestra effect of vascular cells and ECM (Hanahan, 1997; Rangel-Castilla et al., 2014). Normal metabolism of ECM is important for guaranteeing the process of angiogenesis (Rangel-Castilla et al., 2014). Notably, in addition to TGF-β pathway, we found the high expression of collagen I, III, and VI (enriched in the ECM receptor pathway) in dBAVMs, suggesting an overproduction of ECM in dBAVMs compared to cBAVMs. Therefore, we supposed that the metabolic disorder of ECM, presenting as overproduction of and less degradation of ECM, inhibits the formation of connections between vascular trunks, leading to the malformed vessels to be immature, scattered, and mixed up with brain tissues in dBAVMs.

The analyses based on the REACTOME and KEGG database implied that the pathways related to metabolism of ECM might play important roles in formation of dBAVMs. Previous studies identified that the ECM–receptor interaction pathway was important for BAVM genesis and development (Seker et al., 2006; Wang et al., 2017). In another study, it was found that the overgrowth of vessels activated by angiogenic factors might cause an incomplete vascular structure containing massive collagen (Hashimoto et al., 2005). Interestingly, after analyzing the

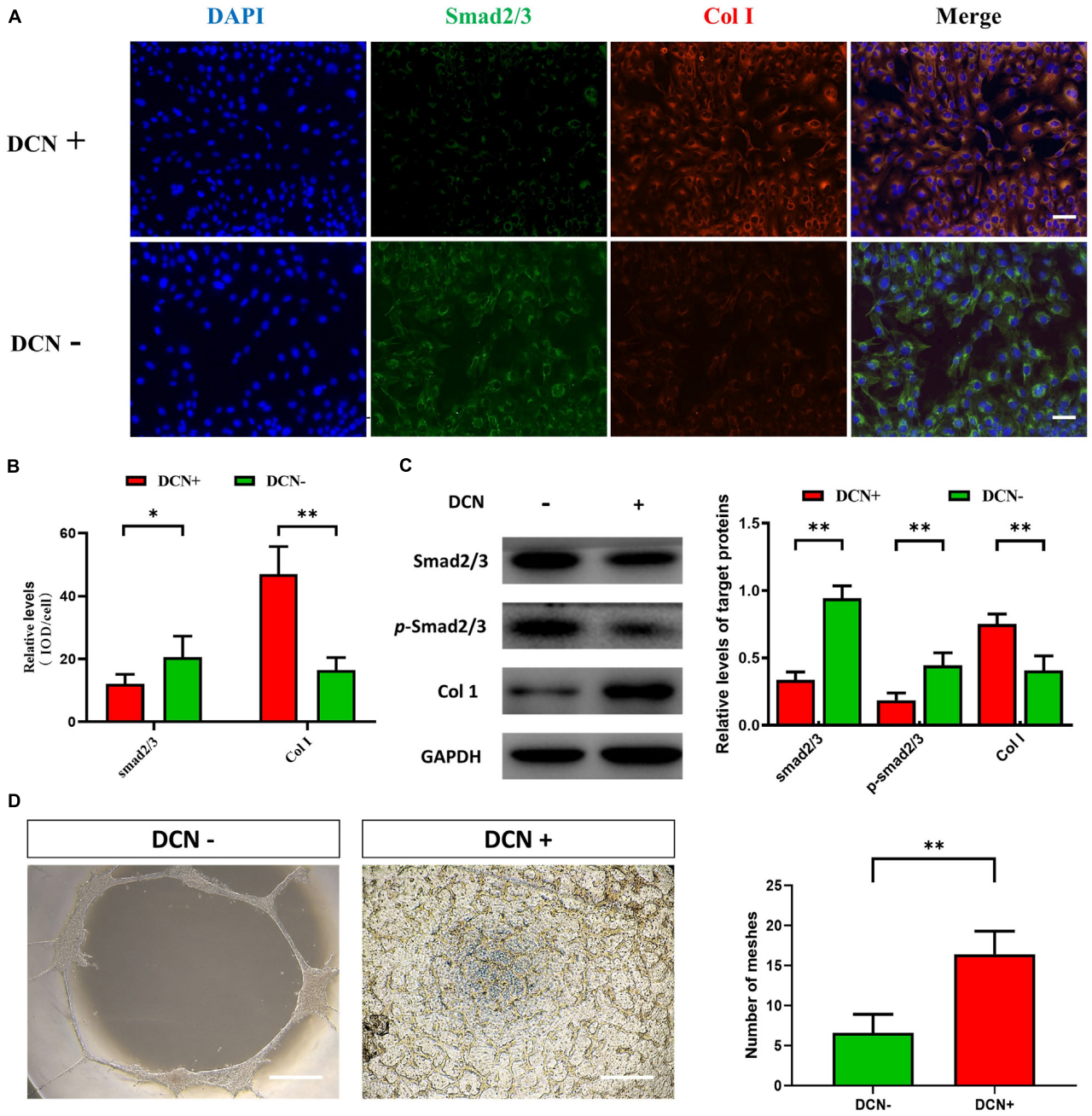


**FIGURE 3 |** The effect of DCN upregulation on angiogenesis for human umbilical vascular endothelial cells (HUVECs). **(A)** Immunofluorescence staining for HUVECs with and without DCN treatment. One representative experiment of 3 is shown. The scale bar corresponds to 50 μm. **(B)** The histograms showed the semiquantitative grading of DCN and Smad 2/3 expression levels by immunofluorescence staining in HUVECs with and without DCN treatment. $^{*}P < 0.05$; $^{**}P < 0.01$. **(C)** Western blot analysis of total Smad 2/3, phosphorylated Smad 2/3 (p-Smad 2/3), and Col I in HUVECs with and without DCN treatment. One representative experiment of 3 is shown. The histograms showed the semiquantitative grading of total Smad 2/3, p-Smad 2/3, and Col I expression levels in HUVECs with and without DCN treatment. $^{**}P < 0.01$. **(D)** Tube formation assays after different treatment. The scale bar corresponds to 50 μm. One representative experiment is shown. $^{**}P < 0.01$.

interaction among pathways, we found that the ECM–receptor pathway was interacted with the TGF-β pathway. Considering the TGF-β signaling pathway is associated with angiogenesis and metabolism of ECM, we suggest that the dysregulation of TGF-β signaling pathways can lead to metabolic disorder of ECM, which may cause excessive proliferation of vasculature and immature vascular development, resulting in tiny vessels scattered within normal brain tissues. Based on these findings, we further investigate the expression level of proteins in the TGF-β pathway and found that DCN was the most strongly

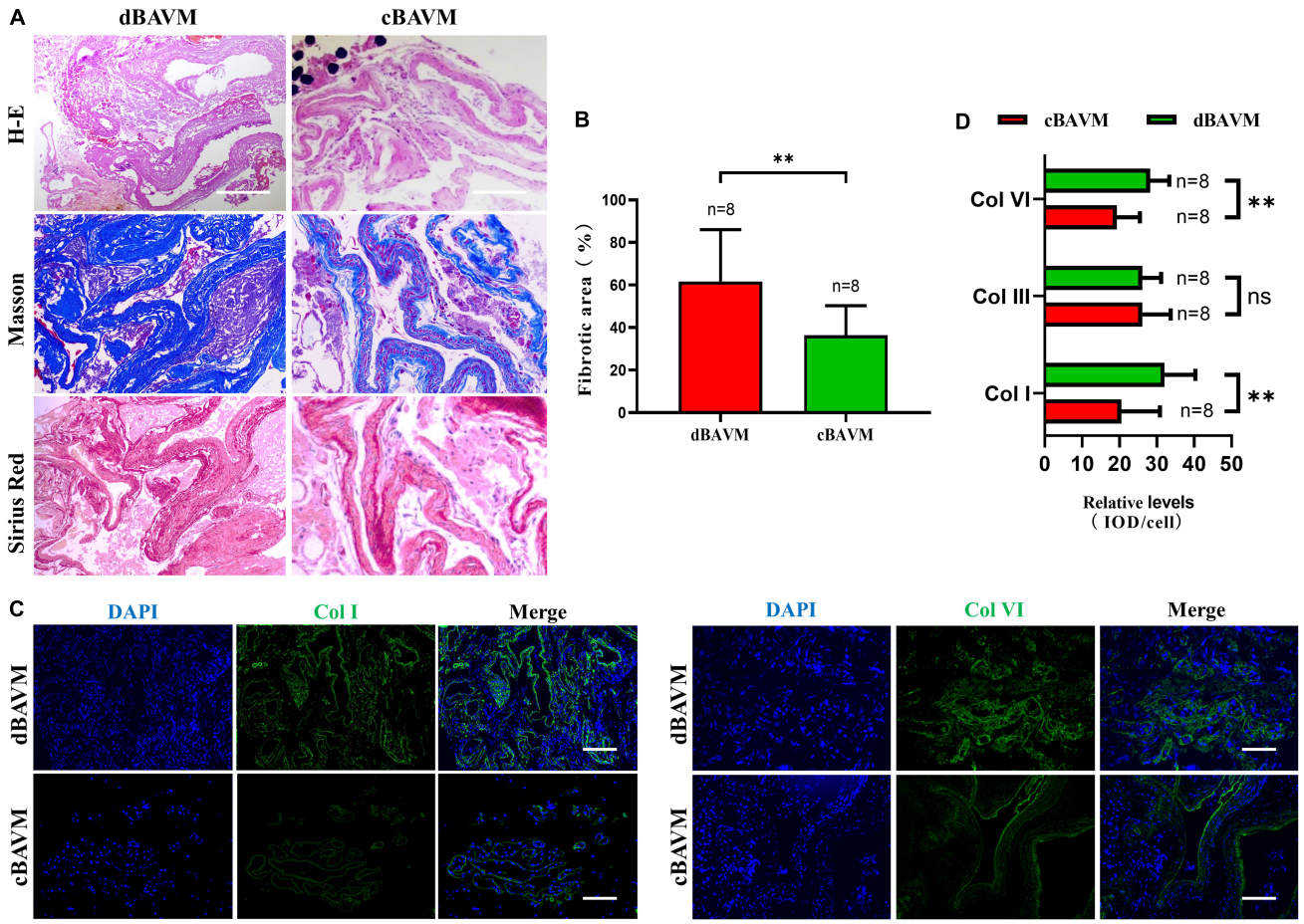


**FIGURE 4 |** Upregulation of DCN promotes the overproduction of extracellular matrix in diffuse BAVMs. **(A)** Masson and Sirius red staining for collagen deposition in BAVM tissues. Fibronectin and collagen area indicated as blue. The scale bar corresponds to 200 μm. $^{**}P < 0.01$. **(B)** The histograms showed the semiquantitative grading of fibrotic area in diffuse and compact BAVMs. **(C)** Immunofluorescence staining for Col I and Col VI in BAVM tissues. Several representative images of diffuse and compact BAVMs are shown. The scale bar corresponds to 200 μm. **(D)** The histograms showed the semiquantitative grading of Col I, Col III, and Col VI in diffuse and compact BAVMs. $^{**}P < 0.01$; ns, $P > 0.05$.

altered protein in dBAVMs compared to cBAVMs. Encoded by PGS2, DCN is a small dermatan sulfate proteoglycan that can interact with a variety of proteins associated with ECM assembly (Hocking et al., 1998). Several biological functions including cell migration, proliferation, and angiogenesis may be regulated by this molecule (Nash et al., 1999; Merle et al., 2015a,b). The biological effect of DCN is primarily suppressive for cell proliferation but promotive for ECM production, especially for collagen fibrils (Jarvelainen et al., 1991; Nili et al., 2003; Salomaki et al., 2008). Thus, we hypothesized that the metabolic disorder of ECM in dBAVMs might be mediated by DCN.

Based on this assumption, we further validated the expression level of DCN and Smad 2/3 (a cell-intrinsic regulator of TGF-β pathway) in BAVM tissues. It was shown that DCN was upregulated and Smad 2/3 was downregulated in dBAVMs; moreover, the DCN was found within and around the malformed vessels, and Smad 2/3 was mainly detected in vascular endothelial cells. In addition, the expression of COL I was upregulated in DCN treatment group. In further *vitro* study, we used exogenous DCN to treat HUVECs. The result showed that the expression of Smad 2/3 was inhibited after DCN treatment. Both Western-blot and IF suggested that DCN could inhibit TGF-β pathway and stimulate the expression of ECM, which was consistent with previous studies (Yan et al., 2009; Cabello-Verrugio et al., 2012). In a recent study, Jiang et al. found that DCN could interfere with the interaction of TGF-β and TGF receptor and promote ECM synthesis (Jiang et al., 2020). This pathological process could promote the angiogenesis of vascular endothelial cell, which was further verified by further functional assays where the ability of tube formation was enhanced after being treated by DCN. Subsequently, we determined the existing metabolic disorder in dBAVMs, presenting as overproduction of collagen, especially collagen I and VI. Collectively, the metabolic disorder of ECM mediated by DCN may play an important role in the formation of dBAVMs. The expression level of DCN is associated with the formation of dBAVMs, which suggests that the level of DCN in serum may be served as a non-invasive and quick biomarker

to identify development of BAVM diffuseness. We suppose that evaluating and correcting the expression level of DCN may contribute insights into the diagnosis and treatment of dBAVMs. Future *in vivo* experiments may help to verify our hypothesis.

## LIMITATIONS

There were several limitations in the present study. First, due to the difficulty of collecting BAVM samples, the proteomic analysis based on limited samples might compromise the power of the results. Meanwhile, selection bias may exist in the present study, since we could not collect the STA samples of every patient for the limited scope of surgery. Second, the confounding effects of blood clot could not be completely excluded because the molecules such as S100A10 were also involved in clot formation (Seker et al., 2006). Nevertheless, since most of these molecules were involved in the metabolism of ECM, we thought that these molecules largely contributed to the metabolism of ECM. Finally, the other proteins and pathways identified in this work still need to be studied by further studies, since there may be other potential mechanisms that were not discussed in this study.

## CONCLUSION

This study is the first to explore the molecular mechanisms of BAVM diffuseness at the protein level. In total, 58 significantly altered proteins were identified in dBAVMs compared to cBAVMs. These altered proteins were primarily enriched in pathways related to the metabolism of ECM. TGF-β signaling pathway inhibited by DCN in vascular endothelial cells is related to BAVM diffuseness. The metabolic disorder of ECM induced by DCN upregulation significantly contributed to the formation of diffuse BAVMs. The definite association between DCN and dBAVMs needs to be investigated by further *in vivo* experiments. Our findings provide extra insights into understanding the mechanisms and promoting the possibility of medical treatment of dBAVMs.

## DATA AVAILABILITY STATEMENT

The raw data supporting the conclusions of this article will be made available by the authors, without undue reservation.

## ETHICS STATEMENT

The studies involving human participants were reviewed and approved by the Institutional Review Board of Beijing Tiantan Hospital. The patients/participants provided their written informed consent to participate in this study.

## AUTHOR CONTRIBUTIONS

SW is the principal investigator of this study and obtained the research funding, approved publication of this final manuscript. ML and QL have developed this manuscript. QL and JY revised this manuscript. PJ, YY, YZ, and YC provided assistant in experiments and statistics. All authors contributed to the article and approved the submitted version.

## FUNDING

This study was supported by the Beijing Municipal Science and Technology Project (Grant No. D161100003816006, SW) and the National Key Research and Development Program of China (Grant No. 2016YFC1301800, SW).

## SUPPLEMENTARY MATERIAL

The Supplementary Material for this article can be found online at: https://www.frontiersin.org/articles/10.3389/fnagi.2020.584839/full#supplementary-material

## REFERENCES

Al-Shahi, R., Pal, N., Lewis, S. C., Bhattacharya, J. J., Sellar, R. J., Warlow, C. P., et al. (2002). Observer agreement in the angiographic assessment of arteriovenous malformations of the brain. *Stroke* 33, 1501–1508. doi: 10.1161/01.str.0000018318.83802.18

Bicer, A., Guclu, B., Ozkan, A., Kurtkaya, O., Koc, D. Y., Necmettin Pamir, M., et al. (2010). Expressions of angiogenesis associated matrix metalloproteinases and extracellular matrix proteins in cerebral vascular malformations. *J. Clin. Neurosci.* 17, 232–236. doi: 10.1016/j.jocn.2009.06.008

Cabello-Verrugio, C., Santander, C., Cofré, C., Acuña, M. J., Melo, F., and Brandan, E. (2012). The internal region leucine-rich repeat 6 of decorin interacts with low density lipoprotein receptor-related protein-1, modulates transforming growth factor (TGF)-β-dependent signaling, and inhibits TGF-β-dependent fibrotic response in skeletal muscles. *J. Biol. Chem.* 287, 6773–6787. doi: 10.1074/jbc.m111.312488

Cheng, F., and Nussinov, R. (2018). KRAS activating signaling triggers arteriovenous malformations. *Trends Biochem. Sci.* 43, 481–483. doi: 10.1016/j.tibs.2018.04.007

Chin, L. S., Raffel, C., Gonzalezgomez, I., Giannotta, S. L., and Mccomb, J. G. (1992). Diffuse arteriovenous malformations: a clinical, radiological, and pathological description. *Neurosurgery* 31, 863–868. doi: 10.1227/00006123-199211000-00006

Derdeyn, C. P., Zipfel, G. J., Albuquerque, F. C., Cooke, D. L., Feldmann, E., Sheehan, J. P., et al. (2017). Management of brain arteriovenous malformations: a scientific statement for healthcare professionals from the American Heart Association/American Stroke Association. *Stroke* 48, e200–e224.

Dschietzig, T., Brecht, A., Bartsch, C., Baumann, G., Stangl, K., and Alexiou, K. (2012). Relaxin improves TNF-alpha-induced endothelial dysfunction: the role of glucocorticoid receptor and phosphatidylinositol 3-kinase signalling. *Cardiovasc. Res.* 95, 97–107. doi: 10.1093/cvr/cvs149

Du, R., Dowd, C. F., Johnston, S. C., Young, W. L., and Lawton, M. T. (2005). Interobserver variability in grading of brain arteriovenous malformations using the Spetzler-Martin system. *Neurosurgery* 57, 668–675. doi: 10.1227/01.neu.0000175548.23140.12

Du, R., Keyoung, H. M., Dowd, C. F., Young, W. L., and Lawton, M. T. (2007). The effects of diffuseness and deep perforating artery supply on outcomes after microsurgical resection of brain arteriovenous malformations. *Neurosurgery* 60, 638–46; discussion 646–648.

Fu, W., Huo, R., Yan, Z., Xu, H., Li, H., Jiao, Y., et al. (2020). Mesenchymal behavior of the endothelium promoted by SMAD6 downregulation is associated with brain arteriovenous malformation microhemorrhage. *Stroke* 51, 2197–2207. doi: 10.1161/strokeaha.120.030046

Hanahan, D. (1997). Signaling vascular morphogenesis and maintenance. *Science* 277, 48–50. doi: 10.1126/science.277.5322.48

Hashimoto, N., Nozaki, K., Takagi, Y., Kikuta, K., and Mikuni, N. (2007). Surgery of cerebral arteriovenous malformations. *Neurosurgery* 61, 375–87; discussion 387–389.

Hashimoto, T., Wu, Y., Lawton, M. T., Yang, G. Y., Barbaro, N. M., and Young, W. L. (2005). Coexpression of angiogenic factors in brain arteriovenous malformations. *Neurosurgery* 56, 1058–65; discussion 1058–1065.

Hocking, A. M., Shinomura, T., and McQuillan, D. J. (1998). Leucine-rich repeat glycoproteins of the extracellular matrix. *Matrix Biol.* 17, 1–19. doi: 10.1016/s0945-053x(98)90121-4

Jarvelainen, H. T., Kinsella, M. G., Wight, T. N., and Sandell, L. J. (1991). Differential expression of small chondroitin/dermatan sulfate proteoglycans, PG-I/biglycan and PG-II/decorin, by vascular smooth muscle and endothelial cells in culture. *J. Biol. Chem.* 266, 23274–23281.

Jiang, N., Zhang, Q., Chau, M. K., Yip, M. S., Lui, S. L., Liu, S., et al. (2020). Anti-fibrotic effect of decorin in peritoneal dialysis and PD-associated peritonitis. *EBioMedicine* 52:102661. doi: 10.1016/j.ebiom.2020.102661

Merle, B., Durussel, L., Delmas, P. D., and Clézardin, P. (2015a). Decorin inhibits cell migration through a process requiring its glycosaminoglycan side chain. *J. Cell. Biochem.* 75, 538–546. doi: 10.1002/(sici)1097-4644(19991201)75:3<538::aid-jcb17>3.0.co;2-y

Merle, B., Malaval, L., Lawler, J., Delmas, P., and Clezardin, P. (2015b). Decorin inhibits cell attachment to thrombospondin-1 by binding to a KKTR-dependent cell adhesive site present within the N-terminal domain of thrombospondin-1. *J. Cell. Biochem.* 67, 75–83. doi: 10.1002/(sici)1097-4644(19971001)67:1<75::aid-jcb8>3.0.co;2-t

Moftakhar, P., Hauptman, J. S., Malkasian, D., and Martin, N. A. (2009). Cerebral arteriovenous malformations. *Part* 1: cellular and molecular biology. *Neurosurg. Focus* 26:E10.

Moon, J. S., Kim, S. H., Oh, S. H., Jeong, Y. W., Kang, J. H., Park, J. C., et al. (2014). Relaxin augments BMP-2-induced osteoblast differentiation and bone formation. *J. Bone Miner. Res.* 29, 1586–1596. doi: 10.1002/jbmr.2197

Nash, M. A., Loercher, A. E., and Freedman, R. S. (1999). In vitro growth inhibition of ovarian cancer cells by decorin: synergism of action between decorin and carboplatin. *Cancer Res.* 59, 6192–6196.

Nikolaev, S. I., Vetiska, S., Bonilla, X., Boudreau, E., Jauhiainen, S., Rezai Jahromi, B., et al. (2018). Somatic activating KRAS mutations in arteriovenous malformations of the brain. *N. Engl. J. Med.* 378, 250–261.

Nili, N., Cheema, A. N., Giordano, F. J., Barolet, A. W., Babaei, S., Hickey, R., et al. (2003). Decorin inhibition of PDGF-stimulated vascular smooth muscle cell function: potential mechanism for inhibition of intimal hyperplasia after balloon angioplasty. *Am. J. Pathol.* 163, 869–878. doi: 10.1016/s0002-9440(10)63447-5

Rangel-Castilla, L., Russin, J. J., Martinez-Del-Campo, E., Soriano-Baron, H., Spetzler, R. F., and Nakaji, P. (2014). Molecular and cellular biology of cerebral arteriovenous malformations: a review of current concepts and future trends in treatment. *Neurosurg. Focus* 37:E1.

Salomaki, H. H., Sainio, A. O., Soderstrom, M., Pakkanen, S., Laine, J., and Jarvelainen, H. T. (2008). Differential expression of decorin by human malignant and benign vascular tumors. *J. Histochem. Cytochem.* 56, 639–646. doi: 10.1369/jhc.2008.950287

Seker, A., Yildirim, O., Kurtkaya, O., Sav, A., Gunel, M., Pamir, M. N., et al. (2006). Expression of integrins in cerebral arteriovenous and cavernous malformations. *Neurosurgery* 58, 159–68; discussion 159–168.

Simonian, M., Loo, R. O., Rannulu, N., Loo, J. A., Molloy, M. P., and Stoodley, M. A. (2017). Identification of protein targets in cerebral endothelial cells for brain arteriovenous malformation (AVMs) molecular therapies. *Clin. Proteomics* 14:17.

Spears, J., Terbrugge, K. G., Moosavian, M., Montanera, W., Willinsky, R. A., Wallace, M. C., et al. (2006). A discriminative prediction model of neurological outcome for patients undergoing surgery of brain arteriovenous malformations. *Stroke* 37, 1457–1464. doi: 10.1161/01.str.0000222937.30216.13

Valle Raleigh, J., Mauro, A. G., Devarakonda, T., Marchetti, C., He, J., Kim, E., et al. (2017). Reperfusion therapy with recombinant human relaxin-2 (Serelaxin) attenuates myocardial infarct size and NLRP3 inflammasome following ischemia/reperfusion injury via eNOS-dependent mechanism. *Cardiovasc. Res.* 113, 609–619.

Wang, K., Zhao, S., Liu, B., Zhang, Q., Li, Y., Liu, J., et al. (2018). Perturbations of BMP/TGF-beta and VEGF/VEGFR signalling pathways in non-syndromic sporadic brain arteriovenous malformations (BAVM). *J. Med. Genet.* 55, 675–684. doi: 10.1136/jmedgenet-2017-105224

Wang, X., Hao, Q., Zhao, Y., Guo, Y., and Ge, W. (2017). Dysregulation of cell-cell interactions in brain arteriovenous malformations: a quantitative proteomic study. *Proteomics Clin Appl* 11, 5–6.

Yan, W., Wang, P., Zhao, C. X., Tang, J., Xiao, X., and Wang, D. W. (2009). Decorin gene delivery inhibits cardiac fibrosis in spontaneously hypertensive rats by modulation of transforming growth factor-beta/Smad and p38 mitogen-activated protein kinase signaling pathways. *Hum. Gene Ther.* 20, 1190–1200. doi: 10.1089/hum.2008.204

**Conflict of Interest:** The authors declare that the research was conducted in the absence of any commercial or financial relationships that could be construed as a potential conflict of interest.

frontiers in Human Neuroscience

CASE REPORT
published: 09 February 2021
doi: 10.3389/fnhum.2021.610945

# Massive Cerebral Infarction Following Facial Injection of Autologous Fat: A Case Report and Review of the Literature

*Huan Qian[1], Yuxiao Ling[2], Mengwen Zhang[1], Cameron Lenahan[3,4], Chen Wang[1], Zhe Zheng[5], Anwen Shao[5]* and Jianmin Zhang[5]*

[1] Department of Plastic Surgery, The Second Affiliated Hospital, School of Medicine, Zhejiang University, Hangzhou, China, [2] School of Public Health, Hangzhou Medical College, Hangzhou, China, [3] Center for Neuroscience Research, Loma Linda University School of Medicine, Loma Linda, CA, United States, [4] Burrell College of Osteopathic Medicine, Las Cruces, NM, United States, [5] Department of Neurosurgery, The Second Affiliated Hospital, School of Medicine, Zhejiang University, Hangzhou, China

Facial fat grafting techniques often offer impressive surgical results. However, fatal complications, such as irreversible cerebral ischemia, blindness, and hemiplegia are associated with them. We have presented a case report of a patient who presented with a massive cerebral infarction, a serious complication of facial autologous fat injection. The patient was a 28-year-old female who experienced motor dysfunction of the left extremities, which was accompanied with loss of consciousness immediately following fat grafting for facial augmentation. Imaging studies suggested that the patient had a large cerebral infarction on the right frontal, temporal, and parietal lobes due to complete occlusion of her right external carotid artery. Emergency decompressive craniectomy was completed in addition to multiple follow-up medical treatments. The patient recovered after 4 months with reduced motor function in her left upper extremity. This report further summarizes published cases of massive cerebral ischemia after facial injection of autologous fat, as well as lists high-risk facial areas and critical warnings.

**Keywords: autologous fat grafting, vascular embolization, massive cerebral ischemia, hemiparesis, carotid artery**

OPEN ACCESS

***Edited by:***
*Zhao Jizong,*
*Capital Medical University, China*

***Reviewed by:***
*Yujie Chen,*
*Army Medical University, China*
*Yorito Hattori,*
*Cornell University, United States*

***Correspondence:**
*Anwen Shao*
*21118116@zju.edu.cn;*
*anwenshao@sina.com*

***Specialty section:***
*This article was submitted to Brain Imaging and Stimulation, a section of the journal Frontiers in Human Neuroscience*

***Received:*** *07 October 2020*
***Accepted:*** *18 January 2021*
***Published:*** *09 February 2021*

***Citation:***
*Qian H, Ling Y, Zhang M, Lenahan C, Wang C, Zheng Z, Shao A and Zhang J (2021) Massive Cerebral Infarction Following Facial Injection of Autologous Fat: A Case Report and Review of the Literature. Front. Hum. Neurosci. 15:610945. doi: 10.3389/fnhum.2021.610945*

## INTRODUCTION

Massive cerebral infarction is a rare, but devastating complication that can occur after facial soft tissue augmentation. It can cause permanent blindness and hemiplegia (Egro and Coleman, 2020). We present a case of right massive cerebral infarction, which was secondary to autologous fat graft.

This report describes a 28-year-old female patient who presented with drowsiness and left limb motor weakness after a facial autologous fat graft. Neuroimaging studies revealed that the patient had a large cerebral infarction on the right frontal, temporal, and parietal lobes, as well as the basal ganglia. Computed tomographic angiography (CTA) of the neck suggested that the right external carotid artery was occluded.

Additionally, this report summarizes all similar published cases. The high-risk facial areas, initial clinical characteristics, treatment modalities, and prognosis of this serious complication after autologous fat facial injection were fully investigated.

## CASE PRESENTATION

A previously healthy 28-year-old woman underwent autologous fat grafting for facial augmentation by a plastic surgeon at a local clinic. A total volume of 77 ml of fat was grafted for the whole face under general anesthesia. Twenty ml fat was injected into each temple, 20 ml into the forehead, and 17 ml was injected in the cheeks. The patient experienced left limb movement disorder and drowsiness following the procedure. The patient was referred to the emergency room 24 h later with Glasgow Coma Scale (GCS) 14 points (Eye 4+Verbal 5+Motor 5). The left limb muscle strength was grade 2 (muscle can move only if the resistance of gravity is removed.), while the right limb muscle strength was grade 5 (muscle contracts normally against full resistance) at the time of admission. Emergency computed tomography (CT) suggested that the patient had a large cerebral infarction of the right frontal, temporal, and parietal lobes, as well as the basal ganglia, causing a midline shift to the left (**Figure 1A**). The neck CTA suggested that the right external carotid artery was occluded (**Figure 1B**). She underwent emergency decompressive craniectomy for decompression of right massive cerebral infarction. Because the arterial occlusion resulted from autologous fat embolization, it would not respond to traditional pharmacologic thrombolysis. The patient was transferred to the ICU after surgery, and was treated for dehydration, infection prophylaxis, gastric protection, and seizure prophylaxis treatment, etc.

The post-surgery CT scan revealed a large cerebral infarction on the right side, as well as hemorrhage and gas accumulation in the operative field (**Figure 1C**). Patient was treated for 10 days with intravenous mannitol injection. A subsequent CT examination, completed after 10 days of treatment mentioned above, confirmed a reduction in brain edema and hemorrhage (**Figures 1D,E**). Physical examination completed on day 11 revealed that the patient had a left limb muscle strength of 2, with numbness on the left limb, and no obvious abnormality on the right side. The patient was transferred to a rehabilitation hospital for further treatment.

The follow-up MRI-FLAIR (**Figure 1F**) showed attenuated brain edema, and MRA (**Figure 1G**) showed vascular recanalization of the intracranial area. An MRI-SWAN (**Figure 1H**) scan performed 2 months after onset showed that the hemorrhage was gradually decreased with no other obvious hemorrhage. The patient achieved better motor function of the left extremities (Her muscle strength recovered to grade 2+ on the left distal upper extremity, grade 4+ on the left proximal upper limb, and grade 5 on the left lower extremity) after 4 months of rehabilitation. Due to the outbreak of Corona Virus Disease-19 (COVID-19), the patient was discharged from the rehabilitation hospital in February. From that point forward, she

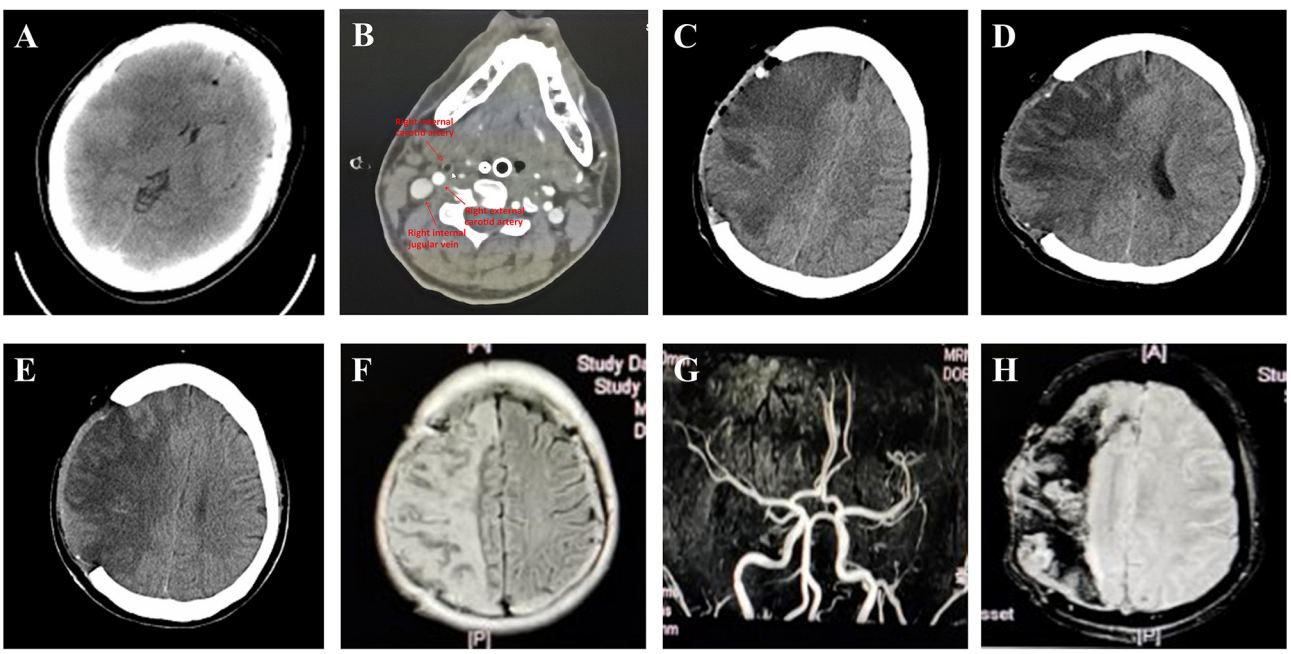


**FIGURE 1 |** Imaging in different stages after cerebral infarction of this case. **(A)** Brain CT imaging of the patient shows massive cerebral infarction on the right frontal, temporal, and parietal lobes, and basal ganglia. **(B)** The neck CTA suggested that the right external carotid artery was occluded. ICA, ECA, or jugular vein are pointed out with arrows. **(C)** Post-surgery brain CT imaging of the patient. **(D)** Post-surgery Brain CT imaging of the patient 1 week post-surgery (2019-11-11). **(E)** Post-surgery Brain CT imaging of the patient 12 days post-surgery (2019-11-16). Images show improvement of edema, emorrhage absorbed. **(F)** The follow-up MRI-FLAIR performed 1 month after onset showed attenuated brain edema, and **(G)** MRA performed 2 months after onset showed vascular recanalization of intracranial area. **(H)** MRI-SWAN performed 2 months after onset showed the hemorrhage was gradually decreased with no other obvious hemorrhage.

**TABLE 1 |** Summary of facial autologous fat injection-induced cerebral ischemia.

| References | Age | Gender | Onset | Location | Volume per side | Artery | Onset symptoms | Evolution |
|---|---|---|---|---|---|---|---|---|
| Huo et al. (2018) | 33 | F | 0 | Glabella | Not mentioned | LICA, LMCA | Right hemiparesis with loss of consciousness | Motor aphasia, reduce motor function on right limbs |
| | 25 | F | 0 | Glabella | Not mentioned | LMCA-M3, LACA | Right hemiparesis with loss of consciousness | Reduce motor function on right limbs |
| | 24 | F | 2 h | Periocular | Not mentioned | LACA, RCCA, RICA, RMCA-M1, M3, RPCA-P2 | Seizure, left hemiparesis and loss of consciousness | Died |
| | 19 | M | 1 h | Glabella | Not mentioned | LMCA | Right hemiparesis with loss of consciousness | Aphasia, reduce motor function on right limbs |
| | 28 | M | 5 h | Glabella | Not mentioned | Not examined | Seizure with loss of consciousness | Died |
| Wang et al. (2018) | 22 | F | 0 | Temporal | Not mentioned | RMCA | Left hemiparesis with loss of consciousness | Paralysis of the left limb, ageusia and vision loss in both eye |
| | 30 | F | 0 | Temporal | Not mentioned | Right brain hemisphere | Left limbs motor disturbance | Recovery of the left limb |
| Liu et al. (2018) | 29 | F | 0 | Left forehead | 15 ml | LOA, LMCA | Left visual disturbance with no light sensation and right motor disturbance, nausea and vomit | Left eye blindness |
| | 38 | F | 0 | Left forehead | 5 ml | LOA | Left visual disturbance and necrosis in the left forehead skin | Left eye blindness and skin scar |
| Kang et al. (2016) | 32 | F | 30 min | Glabella | Not mentioned | LACA, LMCA, LOA | Right hemiparesis with loss of consciousness | Left eye blindness and able to walk and raise her arm with minimal resistance |
| Shen et al. (2016) | 30 | F | 8 h | Temporal chin | Not mentioned | RECA, RICA | Left hemiparesis with loss of consciousness | Reduce motor function on right and left limbs |
| Thaunat et al. (2004) | 39 | M | 0 | Temporal Periocular glabella | 17 ml | LACA, RACA, AcoA | Confusion, hypertonia, high blood pressure | Aphasia and paraplegia |
| Lee et al. (2011) | 44 | F | 2 h | Periocular | Not mentioned | LOA, LMCA | Left visual loss, dysarthria and the skin necrosis | Left eye blindness and skin scar |
| Hong et al. (2014) | 31 | F | 0 | Glabella | Not mentioned | ROA, RMCA | Right visual disturbance and weakness in left arm | Decrease in visual acuity, the weakness in left arm improved to normal |
| Lee et al. (2012) | 26 | F | 13 h | Face | Not mentioned | Not examined | Right visual loss and left hemiparesis | Not mentioned |
| Hu et al. (2011) | 28 | F | 0 | Temporal | Not mentioned | LMCA-M1 | Drowsy, developed expressive aphasia, right hemiparesis | Considerable neurologic recovery (NIHSS score 6) |
| Yoon et al. (2003) | 39 | F | 1 min | Glabella | 5 ml | LICA | Drowsy, global aphasia, right hemiparesis | Died |
| Danesh-Meyer et al. (2001) | 43 | M | 10 min | Nose lip Nasolabial groove | 3 ml | LOA and MCA | Left visual loss and right hemiparesis | Left eye blindness |
| Wang et al. (2014) | 22 | F | 5 h | Temporal forehead | 25 ml/24 ml | LICA, LACA, LMCA | Right hemiparesis, aphasia, left visual loss | Left eye blindness, improvement in the aphasia and skin scar |
| Allali et al. (2006) | 49 | F | 24 h | Glabella | Not mentioned | Multiple strips in LOA | Left visual loss | Left eye blindness |
| Feinendegen et al. (1998) | 45 | M | 7 h | Nasolabial folds lower lip chin | Not mentioned | LMCA and ROA and choroidal arterioles | Aphasia and mild right sensorimotor hemiparesis | Not mentioned |
| Lee et al. (1996) | 42 | F | 0 | Nasolabial groove | 0.5 ml | LOA | Left visual disturbance and drowsy | Decrease in visual acuity |
| Dreizen and Framm (1989) | 44 | F | 0 | Glabella | Not mentioned | ROA | Right visual loss and right hemicranial | Right eye blindness |

*M, male; F, female; LMCA, left middle cerebral artery; LACA, left anterior cerebral artery; RMCA, right middle cerebral artery; RACA, right anterior cerebral artery; RCCA, right common carotid artery; RPCA, right posterior cerebral artery; RICA, right internal carotid artery; LICA, left internal carotid artery; RECA, right external carotid artery; LECA, left external carotid artery; LOA, left ophthalmic artery; ROA, right ophthalmic artery; AcoA, anterior communicating artery.*

continued her rehabilitation training from home. No imaging was performed on the patient at 4 months post-surgery. '

## DISCUSSION

Autologous fat grafting is a widely performed procedure in facial surgery for soft-tissue correction, and was first published by Coleman in 1995 (Egro and Coleman, 2020). Autologous fat is an ideal filler for augmenting facial volume (Yoshimura and Coleman, 2015), during transplantation, fat aliquots, within 0.1 ml each pass, should be injected when the microcannula is withdrawn (Egro and Coleman, 2020). Common complications of this aesthetic surgery include volume under- or overcorrection, contour irregularities, prolonged bruising and swelling, infection, granulomas, and inflammation. However, severe complications, such as ocular embolization with visual loss, cerebral arterial infarct, and death are extremely rare (Yoshimura and Coleman, 2015; Cuzalina and Guerrero, 2018). Some complications may occur due to improper operations, therefore, one purpose of our case report is to remind the plastic surgeons paying more attention to every procedures, especially the injection operation.

We present a rare case of a female patient who had a severe cerebral infarction after autologous fat grafting, which resulted from right external carotid artery occlusion. In this case, we highly suspect that the fat tissue was injected into the right superficial temporal artery, and was then forced retrograde into the right external carotid artery (ECA). Given the demonstrated occlusion of the ECA, the fat emboli managed to travel retrograde from the right ECA to the carotid bifurcation and then anterograde into the right internal carotid artery. Finally, it caused right cerebral infarction in the right frontal, temporal, and parietal lobes, as well as basal ganglia. We then compared all the studies describing a massive stroke (excluding simple ocular artery embolization) after fat grafting (**Table 1**).

### Demographic Information

General information of the patients included in the literature review is displayed, and of the 24 patients reported, 19 (79.17%) were women and 5 (20.83%) were men; the ages of the sample group ranged from 19 to 49 years (Mean = 32.9). Most of the patients were young and otherwise healthy women.

### Onset

In these cases, fat embolism after facial autologous fat injection developed either immediately after surgery or up to 3 days post-surgery. Patients who developed fat embolism experienced sudden headache, visual disturbance, cutaneous signs (e.g., pale skin), vomiting, and neurological symptoms (e.g., mental status changes, aphasia, or hemiparesis). Coma and death were also observed in some patients. As most cases of acute stroke with major artery embolisms occur within 24 h after plastic surgery, patients should be under professional medical observation for the first 24 h post-surgery.

### Location and Participating Arteries

The patient described in our case study had a very rare occurrence of fat embolism in the external carotid artery, which has not yet been reported. Embolic cerebral strokes after autologous fat injection are primarily seen in common carotid artery, internal carotid artery, anterior/middle/posterior cerebral artery, and the ophthalmic artery (**Table 1**). A retrograde intravascular fat emboli can be a significant contributor. In other cases, the intravascular fat travels retrograde through the communicating branches between the facial artery and the internal carotid artery, eventually leading to a fat embolism of major cerebral arteries or the ophthalmic artery. Potential blood routes include the dorsal, nasal, angular, supraorbital arteries, temporal superficial arteriovenous, or any anatomic variation. This leads to necrosis of the brain tissue and the optic nerve (Yoshimura and Coleman, 2015; Cuzalina and Guerrero, 2018; Sisti et al., 2019; Egro and Coleman, 2020).

The most dangerous injection areas (high-risk for fat embolism) were the glabella (angular and supraorbital arteries) (41.67%) and temporal area (temporal superficial arteriovenous) (29.17%). Areas with lower risk include the nose, lips, and chin. The artery deserving of special attention with a high risk of

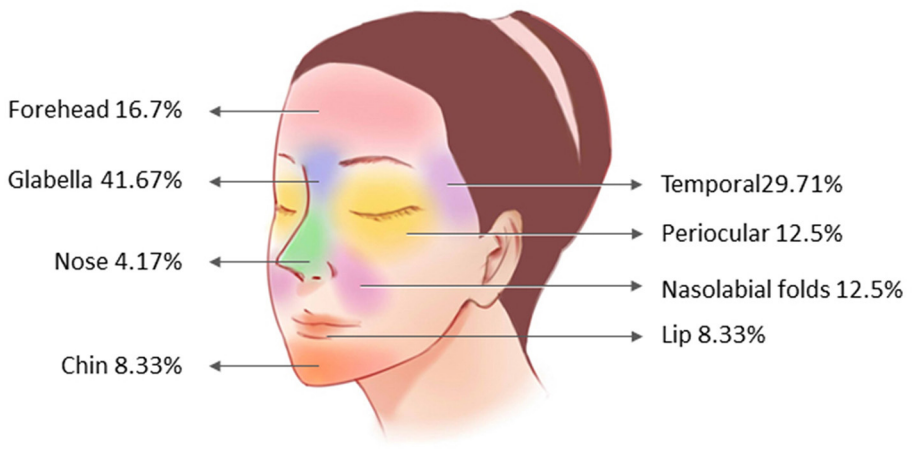


**FIGURE 2 |** Distribution of fat receiving areas in patients with cerebral infarction.

fat embolism is consistent with the corresponding area listed in **Figure 2**.

### Volume and Surgical Technique

Previous studies have demonstrated that injection of 0.5–30 ml in one area can lead to complications. Compared with breast or buttock augmentation, facial areas have a greater risk because small volumes of fat grafts can enter through the arteries, eventually flowing into the brain due to the rich vasculature. On the other hand, the physician may need to fill a moderate volume of fat in one area. Multiple dosages, number of injections, and massages may damage the local vascular network and increase the local pressure, which may increase the risk of arterial embolism.

A skilled surgical technique is essential to avoid post-surgical complications. Surgeons need to inject the fat slowly with low pressure, and they must ensure that there is no backflow of blood into the delivering syringe. Use of excessive force and velocity to administer injections may increase local pressure and the risk of retrograde travel of fat (Egro and Coleman, 2020). The cases described above provide evidence that minimal force should be exerted, and that a minimal dose should be used to seed the fat in tissue. Meanwhile, the use of a blunt cannula, withdrawn before injection, is also key in preventing intra-arterial injections.

### Outcome

Patients suffering from massive cerebral infarction in these cases received comprehensive treatment. The artery embolized with autologous fat particles did not respond to thrombolytic agents. However, there were several effective treatments, such as decompressive craniectomy paired with mannitol treatment, hyperbaric oxygen therapy, intravenous infusion of dextran glucose solution, hydrocortisone, anti-platelet agents, and systemic neurotrophic factor therapy. If detected early, vascular recanalization can be achieved via mechanical thrombectomy. However, currently, there are no published studies providing evidence of that. Partial recovery, aphasia, blindness, hemiparesis, and death were the prognoses seen in the patients analyzed in the literature review. Hence, the prevention of fat embolism is of utmost importance.

## CONCLUSIONS

To the best of our knowledge, this is the first paper summarizing the serious complications of fat transplantation in facial cosmetic surgery. Our understanding is that there might be a substantial number of unreported cases with similar complications of fat transplantation due to local legal issues. Therefore, it is of vital importance for surgeons to discern the causes of, as well as minimize, fatal complications.

## DATA AVAILABILITY STATEMENT

The raw data supporting the conclusions of this article will be made available by the authors, without undue reservation.

## ETHICS STATEMENT

The studies involving human participants were reviewed and approved by the Human and Research Ethics committees of the Second Hospital of Zhejiang University. The patients/participants provided their written informed consent to participate in this study. Written informed consent was obtained from the individual(s) for the publication of any potentially identifiable images or data included in this article.

## AUTHOR CONTRIBUTIONS

HQ, YL, and AS conceptualized the research project. HQ and YL drafted the manuscript. AS, ZZ, MZ, and CW reviewed and modified the manuscript. AS and JZ supervised the research and led the discussion. All authors approved the final version of the manuscript.

## FUNDING

This work was funded by National Natural Science Foundation of China (81701144) and Zhejiang Provincial Natural Science Foundation of China (LGD21H150001).

## REFERENCES

Allali, J., Bernard, A., Assaraf, E., Bourges, J. L., and Renard, G. (2006). Multiple embolizations of the branches of the ophthalmic artery: an unknown serious complication of facial surgeries. *J. Fr. Ophtalmol.* 29, 51–57. doi: 10.1016/S0181-5512(06)73748-2

Cuzalina, A., and Guerrero, A. V. (2018). Complications in fat grafting. *Atlas Oral Maxillofac Surg. Clin. North Am.* 26, 77–80. doi: 10.1016/j.cxom.2017.11.003

Danesh-Meyer, H. V., Savino, P. J., and Sergott, R. C. (2001). Case reports and small case series: ocular and cerebral ischemia following facial injection of autologous fat. *Arch. Ophthalmol.* 119, 777–778.

Dreizen, N. G., and Framm, L. (1989). Sudden unilateral visual loss after autologous fat injection into the glabellar area. *Am. J. Ophthalmol.* 107, 85–87. doi: 10.1016/0002-9394(89)90823-4

Egro, F. M., and Coleman, S. R. (2020). Facial fat grafting: the past, present, and future. *Clin. Plast. Surg.* 47, 1–6. doi: 10.1016/j.cps.2019.08.004

Feinendegen, D. L., Baumgartner, R. W., Schroth, G., Mattle, H. P., and Tschopp, H. (1998). Middle cerebral artery occlusion AND ocular fat embolism after autologous fat injection in the face. *J. Neurol.* 245, 53–54. doi: 10.1007/s004150050177

Hong, D. K., Seo, Y. J., Lee, J. H., and Im, M. (2014). Sudden visual loss and multiple cerebral infarction after autologous fat injection into the glabella. *Dermatol. Surg.* 40, 485–487. doi: 10.1111/dsu.12426

Hu, J., Chen, W., Wu, Y., Chen, K., Luo, C., Liang, Y., et al. (2011). Middle cerebral artery occlusion following autologous bitemporal fat injection. *Neurol. India* 59, 474–475. doi: 10.4103/0028-3886.82749

Huo, X., Liu, R., Wang, Y., Sun, J., Lin, M., Han, J., et al. (2018). Cerebral fat embolism as complication of facial fat graft: retrospective analysis of clinical characteristics, treatment, and prognosis. *World Neurosurg.* 120, 249–255. doi: 10.1016/j.wneu.2018.08.148

Kang, J. H., Park, K. H., and Park, J. S. (2016). Acute mental change and hemiplegia after autologous fat injection. *J. Cosmet. Laser Ther.* 18, 413–416. doi: 10.1080/14764172.2016.1197400

Lee, C. M., Hong, I. H., and Park, S. P. (2011). Ophthalmic artery obstruction and cerebral infarction following periocular injection of autologous fat. *Korean J. Ophthalmol.* 25, 358–361. doi: 10.3341/kjo.2011.25.5.358

Lee, D. H., Yang, H. N., Kim, J. C., and Shyn, K. H. (1996). Sudden unilateral visual loss and brain infarction after autologous fat injection into nasolabial groove. *Br. J. Ophthalmol.* 80, 1026–1027. doi: 10.1136/bjo.80.11.1026

Lee, K. M., Kim, E. J., Jahng, G. H., and Chang, D. I. (2012). Magnetic resonance findings in two episodes of repeated cerebral fat embolisms in a patient with autologous fat injection into the face. *J. Korean Neurosurg. Soc.* 51, 312–315. doi: 10.3340/jkns.2012.51.5.312

Liu, H., Chen, D., and Zhang, J. (2018). Ophthalmic artery occlusion after forehead autologous fat injection. *Retin. Cases Brief Rep.* 14, 271–274. doi: 10.1097/ICB.0000000000000694

Shen, X., Li, Q., and Zhang, H. (2016). Massive cerebral infarction following facial fat injection. *Aesthetic Plast. Surg.* 40 801–805. doi: 10.1007/s00266-016-0681-2

Sisti, A., Boczar, D., and Forte, A. J. (2019). Fat injection in facial artery. *JAMA Facial Plast. Surg.* 21:171. doi: 10.1001/jamafacial.2018.1320

Thaunat, O., Thaler, F., Loirat, P., Decroix, J. P., and Boulin, A. (2004). Cerebral fat embolism induced by facial fat injection. *Plast. Reconstr. Surg.* 113, 2235–2236. doi: 10.1097/01.PRS.0000123627.33690.9E

Wang, D. W., Yin, Y. M., and Yao, Y. M. (2014). Internal and external carotid artery embolism following facial injection of autologous fat. *Aesthet. Surg. J.* 34, NP83–NP87. doi: 10.1177/1090820X14539973

Wang, X., Wu, M., Zhou, X., Liu, H., Zhang, Y., and Wang, H. (2018). Autologous fat used for facial filling can lead to massive cerebral infarction through middle cerebral artery or facial intracranial branches. *J. Craniofac. Surg.* 29, 1341–1343. doi: 10.1097/SCS.0000000000004625

Yoon, S. S., Chang, D. I., and Chung, K. C. (2003). Acute fatal stroke immediately following autologous fat injection into the face. *Neurology* 61, 1151–1152. doi: 10.1212/WNL.61.8.1151

Yoshimura, K., and Coleman, S. R. (2015). Complications of fat grafting: how they occur and how to find, avoid, and treat them. *Clin. Plast. Surg.* 42, 383–388. doi: 10.1016/j.cps.2015.04.002

**Conflict of Interest:** The authors declare that the research was conducted in the absence of any commercial or financial relationships that could be construed as a potential conflict of interest.

frontiers in Aging Neuroscience

ORIGINAL RESEARCH
published: 18 February 2021
doi: 10.3389/fnagi.2021.609588

# Long-Term Outcomes of Elderly Brain Arteriovenous Malformations After Different Management Modalities: A Multicenter Retrospective Study

*Yu Chen[1], Debin Yan[1], Zhipeng Li[1], Li Ma[1], Yahui Zhao[1], Hao Wang[1], Xun Ye[1,2], Xiangyu Meng[3], Hengwei Jin[3], Youxiang Li[3], Dezhi Gao[4], Shibin Sun[4], Ali Liu[4], Shuo Wang[1], Xiaolin Chen[1]* and Yuanli Zhao[1,2]**

[1] Department of Neurosurgery, Beijing Tiantan Hospital, Capital Medical University, Beijing, China, [2] Department of Neurosurgery, Peking University International Hospital, Peking University, Beijing, China, [3] Department of Interventional Neuroradiology, Beijing Tiantan Hospital, Capital Medical University, Beijing, China, [4] Department of Gamma-Knife Center, Beijing Tiantan Hospital, Capital Medical University, Beijing, China

**Background:** More and more elderly patients are being diagnosed with arteriovenous malformation (AVM) in this global aging society, while the treatment strategy remains controversial among these aging population. This study aimed to clarify the long-term outcomes of elderly AVMs after different management modalities.

**Methods:** The authors retrospectively reviewed 71 elderly AVMs (>60 years) in two tertiary neurosurgery centers between 2011 and 2019. Patients were divided into four groups: conservation, microsurgery, embolization, and stereotactic radiosurgery (SRS). The perioperative complications, short-term and long-term neurological outcomes, obliteration rates, annualized rupture risk, and mortality rates were compared among different management modalities in the ruptured and unruptured subgroups. Kaplan-Meier survival analysis was employed to compare the death-free survival rates among different management modalities. Logistic regression analyses were conducted to calculate the odds ratios (ORs) and 95% confidence intervals (CI) for predictors of long-term unfavorable outcomes (mRS > 2).

**Results:** A total of 71 elderly AVMs were followed up for an average of 4.2 ± 2.3 years. Fifty-four (76.1%) presented with hemorrhage, and the preoperative annualized rupture risk was 9.4%. Among these patients, 21 cases (29.6%) received conservative treatment, 30 (42.3%) underwent microsurgical resection, 13 (18.3%) received embolization, and 7 (9.9%) underwent SRS. In the prognostic comparison, the short-term and long-term neurological outcomes were similar between conservation and intervention both in the ruptured and unruptured subgroups (ruptured: $p = 0.096$, $p = 0.904$, respectively; unruptured: $p = 0.568$, $p = 0.306$, respectively). In the ruptured subgroup, the intervention cannot reduce long-term mortality ($p = 0.654$) despite the significant reduction of subsequent hemorrhage than conservation ($p = 0.014$), and the main cause of death in the intervention group was treatment-related complications (five of seven, 71.4%).

OPEN ACCESS

**Edited by:**
*Mark Stecker,*
*Independent Practitioner, Fresno, CA, United States*

**Reviewed by:**
*Kun Xiong,*
*Independent Researcher, Changsha, China*
*Antti Lindgren,*
*Kuopio University Hospital, Finland*

***Correspondence:**
*Xiaolin Chen*
*xiaolinchen488@hotmail.com*
*Yuanli Zhao*
*zhaoyuanli@126.com*

**Received:** 23 September 2020
**Accepted:** 01 February 2021
**Published:** 18 February 2021

**Citation:**
*Chen Y, Yan D, Li Z, Ma L, Zhao Y, Wang H, Ye X, Meng X, Jin H, Li Y, Gao D, Sun S, Liu A, Wang S, Chen X and Zhao Y (2021) Long-Term Outcomes of Elderly Brain Arteriovenous Malformations After Different Management Modalities: A Multicenter Retrospective Study. Front. Aging Neurosci. 13:609588. doi: 10.3389/fnagi.2021.609588*

In the logistic regression analysis, higher admission mRS score (OR 3.070, 95% CI 1.559–6.043, $p = 0.001$) was the independent predictor of long-term unfavorable outcomes (mRS>2) in the intervention group, while complete obliteration (OR 0.146, 95% CI 0.026–0.828, $p = 0.030$) was the protective factor.

**Conclusions:** The long-term outcomes of elderly AVMs after different management modalities were similar. Intervention for unruptured elderly AVMs was not recommended. For those ruptured, we should carefully weigh the risk of subsequent hemorrhage and treatment-related complications. Besides, complete obliteration should be pursued once the intervention was initiated.

**Clinical Trial Registration:** http://www.clinicaltrials.gov. Unique identifier: NCT04136860

**Keywords: arteriovenous malformation, elderly, outcomes, conservation, intervention**

## INTRODUCTION

Brain arteriovenous malformations (AVMs) were described as cerebrovascular abnormalities with fistulous connections between arteries and veins without normal intervening capillary beds (Crawford et al., 1986; Solomon and Connolly, 2017; Goldberg et al., 2018). Most AVMs were diagnosed in the fourth and fifth decade of life (Perret and Nishioka, 1966), and elderly AVMs were relatively uncommon in clinical practice. Over the past three decades, neurosurgeons have not yet reached a consensus on whether or not to intervene in these patients. Initially, several studies suggested that the risk of rupture decreases as a person reaches middle age, and these lesions are relatively benign in elderly patients (Luessenhop and Rosa, 1984; Heros and Tu, 1987). However, Harbaugh et al. suggested the opposite (Harbaugh and Harbaugh, 1994). Several subsequent studies reported that 35.7–65.6% of elderly AVMs presented with hemorrhage, and they recommended microsurgical resection or stereotactic radiosurgical surgery (SRS) for carefully selected patients (Hashimoto et al., 2004; Nagata et al., 2006; Pabaney et al., 2016; Burkhardt et al., 2018; Chen et al., 2018). However, the previous studies only included a single treatment strategy for analysis and did not compare the long-term outcomes of different management modalities.

As life expectancy continues to increase in this global aging society, more elderly AVMs are being diagnosed. We must clarify the long-term outcomes of different management modalities for these patients. The present study retrospectively reviewed 71 elderly AVMs from our multi-center retrospective database of 2861 AVMs to specify the natural history and long-term outcomes after different management modalities.

## MATERIALS AND METHODS

### Study Design and Participants

We retrospectively reviewed all elderly brain AVM patients (>60 years) admitted to Beijing Tiantan Hospital and Peking University International Hospital between April 2011 and July 2019. The inclusion criteria were as follows: (1) Diagnosed with AVM by digital subtraction angiography (DSA) and/or magnetic resonance imaging; (2) The patient's age was 60 years or older on admission. Exclusion criteria were: (1) Patient's concomitant diagnosis of hereditary hemorrhagic telangiectasia; (2) Patients missing critical baseline information or those lost to follow-up; and (3) Patients who received intervention before admission. The study was carried out according to the Helsinki Declaration guideline and was approved by the ethics committees of these two hospitals.

A total of 88 elderly AVMs met the inclusion criteria from our multi-center retrospective database of 2861 AVMs, of which 17 patients were lost to follow-up. The baseline characteristics were consistent between patients who were lost to follow-up and patients who maintained followed up (**Supplementary Material 1**). Finally, the remaining 71 elderly AVM patients were included in the statistical analysis (**Figure 1**).

### Data Collection and Variable Definition

The baseline clinical characteristics included age on admission, sex, onset manifestation (hemorrhage, seizure, neurofunctional deficits, and others), and neurological status. The hemorrhagic presentation was defined as hemorrhage that could be ascribed to AVM rupture. The definition of eloquent area and deep venous drainage was consistent with the evaluation criteria in the Spetzler-Martin (SM) Grading system (Spetzler and Martin, 1986). Treatment modalities included conservation, microsurgical resection, embolization, and SRS. The rupture risk was represented by annualized rupture risk, and we defined the observational interval of natural history as the first diagnosis of AVM to admission (Chen et al., 2020). In-hospital complications were defined as intracranial hemorrhage, epilepsy, new-onset neurofunctional deficits, wound infection, intracranial infection, lung infection, major adverse cardiac events (MACEs, with the occurrence of an arrhythmia, myocardial infarction, acute heart failure, and cardiac arrest), deep venous thrombosis (DVT), and electrolyte disturbance. The neurofunctional status was evaluated by the modified Rankin Scale (mRS), and mRS > 2 was considered as neurological disabilities. Subsequent hemorrhage

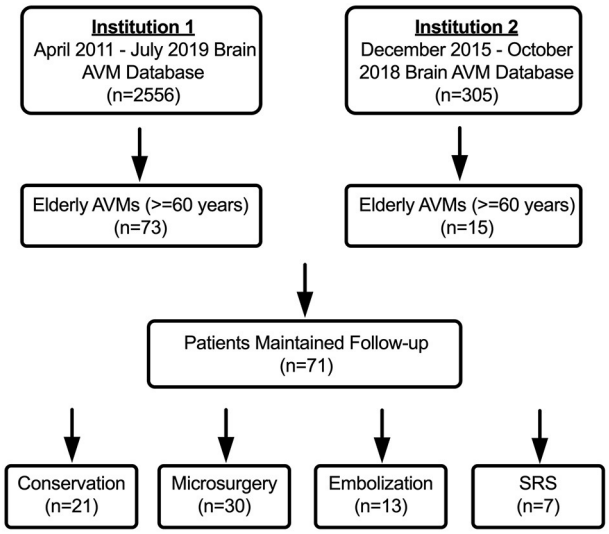


**FIGURE 1 |** The flow diagram of patient screening. Institution 1: Department of Neurosurgery, Beijing Tiantan Hospital, Beijing, China; Institution 2: Department of Neurosurgery, Peking University International Hospital, Beijing, China.

was defined as any hemorrhage attributable to AVM rupture during the follow-up.

Follow-up was conducted at the first 3–6 months and annually by clinical visits and telephone interviews. Two neurosurgeons with at least 5 years' experience in clinical practice evaluated all the clinical parameters. All the images were independently interpreted by at least two radiologists who worked more than 5 years in our institute's radiology center. Researchers who performed follow-up assessments were blinded to treatment modalities.

## Statistical Analysis

Categorical variables are presented as counts (with percentages); continuous variables are presented as the mean ± standard deviations (SD). Patients were divided into four groups based on different management modalities. In the comparison of the baseline characteristics, perioperative complications, short-term and long-term outcomes among different management modalities, the Pearson chi-square test, Fisher exact test, or Kruskal-Wallis ANOVA test were used to compare categorical variables as appropriate, and the two-tailed *t*-test or one-way ANOVA test were employed to compare continuous variables (normal distribution variables). Wilcoxon rank-sum test was applied to compare non-normal distribution continuous variables. Poisson rate test was used to compare the differences in annualized rupture risk. Bonferroni correction was adopted in the adjusted *post-hoc* analysis to avoid Type I errors in subgroup analyses. The subgroup analyses were conducted to compare the outcomes of different management modalities in the ruptured and unruptured elderly AVMs. Kaplan-Meier survival analysis was employed to compare the death-free survival rates (all causes, AVM and treatment-related) among different management modalities (only included patients in the first three-quarters of the follow-up duration). Univariate and multivariate logistic regression analyses were used to calculated odds ratios (ORs) and 95% confidence intervals (CI) for predictors of long-term neurological disabilities or death (mRS > 2). A forward stepwise regression procedure was adopted in the multivariable model. *P*-value < 0.05 was considered to be statistically significant. Statistical analysis was performed using SPSS (version 25.0, IBM, New York, USA).

# RESULTS

## Baseline Characteristics

A total of 71 elderly AVMs were included according to the inclusion and exclusion criteria. Among them, 21 patients (29.6%) took conservative management and 50 patients (70.4%) received intervention, including 30 patients (42.3%) undergoing microsurgery, 13 patients (18.3%) embolization, and seven patients (9.9%) SRS. The average age was 64.7 ± 3.5 years (range, 60.0–75.2 years), and 34 patients (47.9%) were older than 65 years (**Table 1**). There were 54 patients (76.1%) presenting with hemorrhage. The presentation, SM grade, and imaging features between any two treatment strategies showed no significant difference after adjusted *post-hoc* Bonferroni correction analysis. From the first diagnosis to admission, 11 patients occurred 14 rupture events during the cumulative observational duration of 148.9 patient-years, translating to the natural annualized rupture risk of 9.4%. The mean admission mRS score was 1.4 ± 1.3, and the microsurgery group had a significant higher mRS score than conservation and SRS groups after adjusted *post-hoc* Bonferroni correction analysis ($p = 0.021$, $p = 0.013$, respectively), which may be caused by the fact that emergency patients (with higher mRS scores) were more likely to receive microsurgical resection.

Most of the elderly patients were classified as SM grade I-III (61 cases, 85.9%). There was no significant difference in the SM grade among different management modalities after adjusted *post-hoc* Bonferroni correction analysis. Of the 53 DSA-available elderly AVMs, the angiographic characteristics were similar among these four management modalities.

## Clinical Outcomes

The incidence of perioperative complications of microsurgical resection was significantly higher than that of embolization and SRS ($p = 0.007$, $p < 0.001$, respectively) (**Table 2**). In the microsurgery group, 13.3% patients occurred intracranial hemorrhage, 23.3% intracranial infection, 6.7% MACEs, and 20.0% DVT. In the embolization group, two patients (15.4%) experienced intraoperative hemorrhage, which led to serious perioperative complications, such as new-onset neurofunctional deficits, lung infection, DVT, and electrolyte disturbance. The discharge mRS scores were similar between different management modalities after adjusting the *post-hoc* Bonferroni correction analysis ($p > 0.05$).

All the 71 elderly AVMs were followed up clinically and angiographically for an average of 4.2 ± 2.3 years (**Table 2**). The microsurgery group had a significantly higher obliteration

**TABLE 1 |** Baseline characteristics of the included elderly bAVMs.

| Characteristics | Total ($n = 71$) | Conservation ($n = 21$) | Microsurgery ($n = 30$) | Embolization ($n = 13$) | SRS ($n = 7$) | $p$-value |
|---|---|---|---|---|---|---|
| Sex (male) | 52 (73.2) | 13 (61.9) | 20 (66.7) | 11 (84.6) | 6 (85.7) | 0.412 |
| Age (years) | 64.7 ± 3.5 | 64.5 ± 4.0 | 65.8 ± 3.5 | 64.1 ± 2.2 | 62.2 ± 1.9 | 0.060 |
| Age (>65 years) | 34 (47.9) | 9 (42.9) | 19 (63.3) | 5 (38.5) | 1 (14.3) | 0.068 |
| Onset manifestation (primary) | | | | | | |
| Hemorrhage | 54 (76.1) | 13 (61.9) | 28 (93.3) | 9 (69.2) | 4 (57.1) | 0.019* |
| Seizure | 4 (5.6) | 0 (0.0) | 2 (6.7) | 1 (7.7) | 1 (14.3) | 0.349 |
| Neurofunctional deficit | 4 (5.6) | 2 (9.5) | 0 (0.0) | 1 (7.7) | 1 (14.3) | 0.189 |
| Others | 9 (12.7) | 6 (28.6) | 0 (0.0) | 2 (15.4) | 1 (14.3) | 0.008* |
| No. of hemorrhagic events between diagnosis and treatment | 14 | 2 | 6 | 4 | 2 | |
| Annualized rupture risk | 9.4% | 6.3% | 13.6% | 8.4% | 7.9% | |
| Admission mRS score | 1.4 ± 1.3 | 1.1 ± 0.9 | 2.0 ± 1.4 | 1.1 ± 0.6 | 0.6 ± 0.5 | 0.002* |
| Size (cm) | 2.9 ± 1.5 | 3.0 ± 1.5 | 3.2 ± 1.4 | 2.8 ± 1.8 | 1.7 ± 0.5 | 0.021* |
| Eloquent area | 41 (57.7) | 13 (61.9) | 14 (46.7) | 10 (76.9) | 4 (57.1) | 0.290 |
| Supratentorial location | 51 (71.8) | 15 (71.4) | 24 (80.0) | 8 (61.5) | 4 (57.1) | 0.496 |
| Deep venous drainage | 31 (43.7) | 11 (52.3) | 10 (33.3) | 7 (53.8) | 3 (42.9) | 0.471 |
| SM grade | | | | | | 0.620 |
| I | 15 (21.1) | 3 (14.3) | 8 (26.7) | 2 (15.4) | 2 (28.6) | |
| II | 22 (31.0) | 6 (28.6) | 10 (33.3) | 3 (23.1) | 3 (42.9) | |
| III | 24 (33.8) | 8 (38.1) | 7 (23.3) | 7 (53.8) | 2 (28.6) | |
| IV | 7 (9.9) | 3 (14.3) | 4 (13.3) | 0 (0.0) | 0 (0.0) | |
| V | 3 (4.2) | 1 (4.8) | 1 (3.3) | 1 (7.7) | 0 (0.0) | |
| Follow-up duration (years) | 4.2 ± 2.3 | 4.3 ± 2.3 | 4.3 ± 2.6 | 3.5 ± 1.9 | 4.5 ± 1.3 | 0.695 |
| Angioarchitecture characteristics (DSA available, $n = 53$) | $n = 53$ | $n = 20$ | $n = 20$ | $n = 12$ | $n = 1$ | |
| Drainage venous stenosis | 27 (50.9) | 10 (50.0) | 13 (65.0) | 4 (33.3) | 0 (0.0) | 0.207 |
| Long venous drainage | 32 (60.4) | 12 (60.0) | 16 (80.0) | 4 (33.3) | 0 (0.0) | 0.346 |
| Deep perforating arteries | 17 (32.1) | 8 (40.0) | 3 (15.0) | 5 (41.7) | 1 (0.0) | 0.053 |
| Diffuse nidus | 21 (39.6) | 7 (35.0) | 7 (35.0) | 6 (50.0) | 1 (100.0) | 0.360 |
| Aneurysms (flow-related) | 11 (20.8) | 2 (10.0) | 7 (35.0) | 2 (16.7) | 0 (0.0) | 0.235 |

*AVM, Arteriovenous Malformation; DSA, Digital Subtraction Angiography; mRS, modified Rankin Scale; SM grade, Spetzler-Martin grade; SRS, Stereotactic Radiosurgery. Values are expressed as number of cases (%) or mean ± standard deviation, unless otherwise indicated.*
**Statistical significance ($p < 0.05$).*

rate than embolization and SRS groups ($p < 0.001$, $p = 0.007$, respectively). In terms of long-term mRS score, neurological disabilities (mRS > 2), and worsened mRS, there were no significant differences among the four management modalities ($p = 0.721$, $p = 0.431$, $p = 0.648$, respectively). We showed that 68.0% cases in the intervention group and 81.0% in the conservation group could achieve favorable outcomes (mRS ≤ 2). However, the Poisson rate test of annualized rupture risk for conservation and intervention during follow-up was significant (4.4 vs. 0.5%, $p = 0.040$). Twelve patients (16.9%) died during 295.1 patient-years clinical follow-up. The main cause of death in the conservation group was subsequent hemorrhage (3 of 4, 75.0%), while the main cause of death in the intervention group was treatment-related complications (5 of 7, 71.4%). One patient in the conservation group and one in the embolization group died of MACEs. The Kaplan-Meier analysis (**Figure 2**) showed no significant difference in the death-free survival among different management modalities (all causes, $p = 0.924$; AVM and treatment-related, $p = 0.970$).

In the subgroup analysis, all prognostic parameters were similar among different management modalities in the unruptured subgroup, except for the obliteration rates. In the ruptured group, the discharge mRS and long-term mRS were similar among these four management modalities after adjusted *post-hoc* Bonferroni correction analysis ($p = 0.096$, $p = 0.904$, respectively) (**Table 3**). The same was true for >65 years old ruptured AVMs (conservation vs. intervention: $p = 0.095$, $p = 0.892$, respectively; conservation vs. microsurgery: $p = 0.106$, $p = 0.765$, respectively) (**Supplementary Material 2**). The Poisson rate test of annualized rupture risk for conservation and intervention during follow-up in the ruptured subgroup was significant ($p = 0.014$). However, the Kaplan-Meier analysis (**Figure 3**) showed no significant difference in the death-free survival

**TABLE 2 |** Perioperative complications and long-term outcomes among different treatment modalities in the elderly AVMs.

| Characteristics | Conservation ($n = 21$) | Microsurgery ($n = 30$) | Embolization ($n = 13$) | SRS ($n = 7$) | $p$-value |
|---|---|---|---|---|---|
| Perioperative complications | NA | 18 (60.0) | 2 (15.4) | 0 (0.0) | <0.001* |
| Intracranial hemorrhage | NA | 4 (13.3) | 2 (15.4) | 0 (0.0) | 0.374 |
| Epilepsy | NA | 1 (3.3) | 1 (7.7) | 0 (0.0) | 0.614 |
| New-onset neurofunctional deficit | NA | 6 (20.0) | 2 (15.4) | 0 (0.0) | 0.249 |
| Wound infection | NA | 2 (6.7) | 1 (7.7) | 0 (0.0) | 0.622 |
| Intracranial infection | NA | 7 (23.3) | 0 (0.0) | 0 (0.0) | 0.019* |
| Lung infection | NA | 5 (16.7) | 2 (15.4) | 0 (0.0) | 0.317 |
| MACEs | NA | 2 (6.7) | 1 (7.7) | 0 (0.0) | 0.622 |
| DVT | NA | 6 (20.0) | 2 (15.4) | 0 (0.0) | 0.249 |
| Electrolyte disturbance | NA | 7 (23.3) | 2 (15.4) | 0 (0.0) | 0.184 |
| Discharge mRS | 0.9 ± 0.7 | 1.7 ± 1.4 | 1.7 ± 1.7 | 0.6 ± 0.5 | 0.031* |
| Follow-up duration (years) | 4.3 ± 2.3 | 4.3 ± 2.6 | 3.5 ± 1.9 | 4.5 ± 1.3 | 0.695 |
| Obliteration | 0 (0.0) | 28 (93.3) | 1 (7.7) | 3 (42.9) | <0.001* |
| Long-term mRS score | 1.7 ± 2.3 | 2.1 ± 2.2 | 2.2 ± 2.3 | 1.1 ± 2.3 | 0.721 |
| Neurological disability (mRS > 2) | 4 (19.0) | 11 (36.7) | 4 (30.8) | 1 (14.3) | 0.431 |
| Worsened mRS | 4 (19.0) | 7 (23.3) | 5 (38.5) | 2 (28.6) | 0.648 |
| No. of subsequent hemorrhage | 4 | 1 | 0 | 0 | 0.073 |
| Annualized rupture risk[a] | 4.4% | 0.8% | 0.0% | 0.0% | |
| Death | 4 (19.0) | 4 (13.3) | 3 (23.1) | 1 (14.3) | 0.870 |
| Annualized mortality (all causes) | 4.4% | 3.1% | 6.6% | 3.2% | |
| Annualized mortality (AVM-related) | 3.3% | 0.8% | 0.0% | 3.2% | |
| Annualized mortality (treatment-related) | NA | 2.3% | 4.4% | 0.0% | |
| Annualized mortality (other causes) | 1.1% | 0.0% | 2.2% | 0.0% | |

*AVM, Arteriovenous Malformation; DVT, Deep Vein Thrombosis; MACE, Major Adverse Cardiac Events; mRS, modified Rankin Scale; SM grade, Spetzler-Martin grade; SRS, Stereotactic Radiosurgery.*

*Values are expressed as number of cases (%) or mean ± standard deviation, unless otherwise indicated.*

[a]*Poisson rate test of annualized rupture risk for conservation and intervention during follow-up is significant ($p = 0.040$).*

**Statistical significance ($p < 0.05$).*

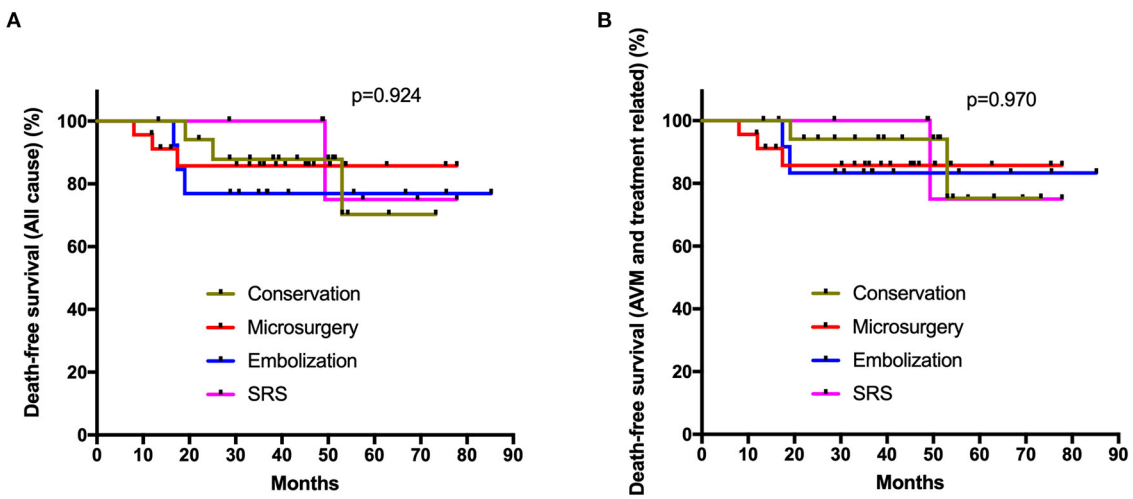


**FIGURE 2 |** Kaplan-Meier plot. The Kaplan-Meier analysis showed no significant difference in the death-free survival among different management modalities (**A**: all causes, $p = 0.924$; **B**: AVM and treatment related, $p = 0.970$; log-rank test).

**TABLE 3 |** Perioperative complications and long-term outcomes among different treatment modalities in the ruptured and unruptured elderly AVMs.

| Characteristics (Ruptured) | Conservation ($n = 13$) | Microsurgery ($n = 28$) | Embolization ($n = 9$) | SRS ($n = 4$) | *p*-value |
|---|---|---|---|---|---|
| Age (years) | 63.7 ± 4.2 | 65.8 ± 3.6 | 64.2 ± 1.8 | 62.3 ± 2.2 | 0.122 |
| Age (>65 years) | 5 (38.5) | 18 (64.3) | 3 (33.3) | 1 (25.0) | 0.166 |
| Admission mRS score | 1.1 ± 0.9 | 2.1 ± 1.4 | 1.0 ± 0.5 | 0.8 ± 0.5 | 0.010* |
| SM grade (IV-V) | 3 (23.1) | 5 (17.9) | 0 (0.0) | 0 (0.0) | 0.173 |
| Perioperative complications | NA | 18 (64.3) | 2 (22.2) | 0 (0.0) | 0.005* |
| Intracranial hemorrhage | NA | 4 (14.3) | 1 (11.1) | 0 (0.0) | 0.560 |
| Epilepsy | NA | 1 (3.6) | 0 (0.0) | 0 (0.0) | 0.679 |
| New-onset neurofunctional deficit | NA | 6 (21.4) | 2 (22.2) | 0 (0.0) | 0.398 |
| Wound infection | NA | 2 (7.1) | 0 (0.0) | 0 (0.0) | 0.456 |
| Intracranial infection | NA | 7 (25.0) | 0 (0.0) | 0 (0.0) | 0.050 |
| Lung infection | NA | 5 (17.9) | 2 (22.2) | 0 (0.0) | 0.435 |
| MACEs | NA | 2 (7.1) | 1 (11.1) | 0 (0.0) | 0.678 |
| DVT | NA | 6 (21.4) | 2 (22.2) | 0 (0.0) | 0.398 |
| Electrolyte disturbance | NA | 7 (25.0) | 2 (22.2) | 0 (0.0) | 0.345 |
| Discharge mRS | 0.8 ± 0.7 | 1.8 ± 1.5 | 1.9 ± 1.8 | 0.8 ± 0.5 | 0.096 |
| Follow-up duration (years) | 4.0 ± 2.1 | 4.3 ± 2.7 | 3.1 ± 1.8 | 4.1 ± 1.4 | 0.660 |
| Obliteration | 0 (0.0) | 25 (89.3) | 1 (11.1) | 2 (50.0) | <0.001* |
| Long-term mRS score | 1.9 ± 2.4 | 2.2 ± 2.2 | 2.4 ± 2.7 | 1.5 ± 3.0 | 0.904 |
| Neurological disability (mRS > 2) | 3 (23.1) | 11 (39.3) | 3 (33.3) | 1 (25.0) | 0.748 |
| Worsened mRS | 4 (30.8) | 7 (25.0) | 3 (33.3) | 1 (25.0) | 0.957 |
| No. of subsequent hemorrhage | 4 | 1 | 0 | 0 | 0.034* |
| Annualized rupture risk[a] | 7.8% | 0.8% | 0.0% | 0.0% | |
| Death | 3 (23.1) | 4 (14.3) | 3 (33.3) | 1 (25.0) | 0.654 |
| Annualized mortality (all causes) | 5.8% | 3.3% | 10.6% | 6.1% | |
| Annualized mortality (AVM-related) | 5.8% | 0.8% | 0.0% | 6.1% | |
| Annualized mortality (treatment-related) | NA | 2.5% | 7.1% | 0.0% | |
| Annualized mortality (other causes) | 0.0% | 0.0% | 3.5% | 0.0% | |
| **Characteristics (Unruptured)** | **Conservation ($n = 8$)** | **Microsurgery ($n = 2$)** | **Embolization ($n = 4$)** | **SRS ($n = 3$)** | ***p*-value** |
| Age (years) | 65.7 ± 3.5 | 65.8 ± 1.0 | 64.0 ± 3.4 | 62.0 ± 2.0 | 0.380 |
| Age (>65 years) | 4 (50.0) | 1 (50.0) | 2 (50.0) | 0 (0.0) | 0.305 |
| Admission mRS score | 1.1 ± 1.0 | 1.0 ± 0.0 | 1.3 ± 1.0 | 0.3 ± 0.6 | 0.558 |
| SM grade (IV-V) | 0 (0.0) | 0 (0.0) | 1 (25.0) | 0(0.0) | 0.375 |
| Perioperative complications | NA | 0 (0.0) | 1 (25.0) | 0 (0.0) | 0.411 |
| Intracranial hemorrhage | NA | 0 (0.0) | 1 (25.0) | 0 (0.0) | 0.411 |
| Epilepsy | NA | 0 (0.0) | 0 (0.0) | 0 (0.0) | >0.999 |
| New-onset neurofunctional deficit | NA | 0 (0.0) | 1 (25.0) | 0 (0.0) | 0.411 |
| Wound infection | NA | 0 (0.0) | 0 (0.0) | 0 (0.0) | >0.999 |
| Intracranial infection | NA | 0 (0.0) | 0 (0.0) | 0 (0.0) | >0.999 |
| Lung infection | NA | 0 (0.0) | 0 (0.0) | 0 (0.0) | >0.999 |
| MACEs | NA | 0 (0.0) | 0 (0.0) | 0 (0.0) | >0.999 |
| DVT | NA | 0 (0.0) | 0 (0.0) | 0 (0.0) | >0.999 |
| Electrolyte disturbance | NA | 0 (0.0) | 0 (0.0) | 0 (0.0) | >0.999 |
| Discharge mRS | 1.0 ± 0.8 | 1.0 ± 0.0 | 1.3 ± 1.3 | 0.3 ± 0.6 | 0.568 |
| Follow-up duration (years) | 4.8 ± 2.5 | 4.4 ± 2.7 | 4.3 ± 1.9 | 5.1 ± 1.2 | 0.960 |
| Obliteration | 0 (0.0) | 2 (100.0) | 0 (0.0) | 2 (66.7) | 0.002* |
| Long-term mRS score | 1.3 ± 2.1 | 0.0 ± 0.0 | 1.5 ± 1.0 | 0.7 ± 1.2 | 0.728 |
| Neurological disability (mRS > 2) | 1 (12.5) | 0 (0.0) | 1 (25.0) | 0 (0.0) | 0.618 |

*(Continued)*

**TABLE 3** | Continued

| Characteristics (Unruptured) | Conservation ($n = 8$) | Microsurgery ($n = 2$) | Embolization ($n = 4$) | SRS ($n = 3$) | *p*-value |
|---|---|---|---|---|---|
| Worsened mRS | 0 (0.0) | 0 (0.0) | 2 (50.0) | 1 (33.3) | 0.090 |
| No. of subsequent hemorrhage | 0 | 0 | 0 | 0 | >0.999 |
| Annualized rupture risk | 0.0% | 0.0% | 0.0% | 0.0% | |
| Death | 1 (12.5) | 0 (0.0) | 0 (0.0) | 0 (0.0) | 0.664 |
| Annualized mortality (all causes) | 2.6% | 0.0% | 0.0% | 0.0% | |
| Annualized mortality (AVM-related) | 0.0% | 0.0% | 0.0% | 0.0% | |
| Annualized mortality (treatment-related) | NA | 0.0% | 0.0% | 0.0% | |
| Annualized mortality (other causes) | 2.6% | 0.0% | 0.0% | 0.0% | |

*AVM, Arteriovenous Malformation; DVT, Deep Vein Thrombosis; MACE, Major Adverse Cardiac Events; mRS, modified Rankin Scale; SM grade, Spetzler-Martin grade; SRS, Stereotactic Radiosurgery.*

*Values are expressed as number of cases (%) or mean ± standard deviation, unless otherwise indicated.*

[a]*Poisson rate test of annualized rupture risk for conservation and intervention during follow-up in the ruptured subgroup is significant ($p = 0.014$).*

**Statistical significance ($p < 0.05$).*

among different management modalities in the ruptured subgroup (all causes, $p = 0.751$; AVM and treatment-related, $p = 0.964$).

## Predictors of Long-Term Unfavorable Outcomes (mRS > 2)

During the clinical follow-up, 20 patients experienced long-term unfavorable outcomes (mRS > 2), including four (20.0%) in the conservation group, 11 (55.0%) in the microsurgery group, four (20.0%) in the embolization group, and one (5.0%) in the SRS group (**Table 4**). In the univariable regression analysis, age (>65 years) (75.0 vs. 37.3%, $p = 0.006$), higher admission mRS score (2.2 ± 1.4 vs. 1.2 ± 1.0, $p = 0.003$), and SM grade IV-V (30.0 vs. 7.8%, $p = 0.024$) were associated with long-term unfavorable outcomes (mRS > 2). In the multivariate logistic regression analysis, age (>65 years) (OR 4.276, 95% CI 1.155–15.839, $p = 0.030$), higher admission mRS score (OR 1.749, 95% CI 1.048–2.920, $p = 0.033$), and SM grade IV-V (OR 6.079, 95% CI 1.182–31.258, $p = 0.031$) were significantly associated with long-term unfavorable outcomes (mRS > 2) in the whole cohort. The management modalities and complete obliteration rate had no significant correlation with long-term unfavorable outcomes (mRS > 2) ($p = 0.431$, $p = 0.951$, respectively). In the intervention group, higher admission mRS score (OR 3.070, 95% CI 1.559–6.043, $p = 0.001$) and complete obliteration (OR 0.146, 95% CI 0.026–0.828, $p = 0.030$) were the independent predictors of long-term unfavorable outcomes (mRS > 2). In the microsurgical resection group, higher admission mRS score (OR 4.010, 95% CI 1.321–12.175, $p = 0.014$) and SM grade IV-V (OR 39.048, 95% CI 1.016–1500.618, $p = 0.049$) were the independent predictors of long-term unfavorable outcomes (mRS > 2).

# DISCUSSION

As the life expectancy of the overall population continues to increase in this global aging society, whether radical interventions for elderly AVMs can achieve longer survival time and better neurological functional state than conservative management is an urgent problem to be solved (Harbaugh and Harbaugh, 1994; Lanzino et al., 1997; Hashimoto et al., 2004; Nagata et al., 2006; Tong et al., 2015; Burkhardt et al., 2018; Chen et al., 2018). We conducted a multicenter retrospective study involving multiple management modalities (conservation, microsurgery, embolization, SRS) for elderly AVMs. Our study found that elderly AVMs demonstrated an aggressive natural history, with an annualized natural rupture rate of 9.4%. The long-term outcomes and mortality in elderly AVMs were similar among different management modalities in the ruptured and unruptured groups. Although the intervention (microsurgery, embolization, SRS) could significantly reduce the risk of subsequent hemorrhage than conservation in the ruptured subgroup, it should be noted that the main cause of death in the intervention group was treatment-related complications. Therefore, we do not recommend intervention for unruptured elderly AVMs, and for those ruptured, we should carefully weigh the risk of subsequent hemorrhage and treatment-related complications. Besides, uncomplete obliteration was found to be significantly associated with unfavorable outcomes (mRS > 2) in the intervention group. Therefore, complete obliteration should be a must if the intervention strategy were chosen.

## Natural History

About 30 years ago, the elderly AVMs were considered relatively benign, and the risk of bleeding would decrease as the patient reached middle age (Luessenhop and Rosa, 1984; Heros and Tu, 1987; Goldberg et al., 2018). However, in recent decades, this view was challenged by the increased sample size of elderly AVMs due to the aging of population and the refinement of neuroimaging modalities (Crawford et al., 1986; Brown et al., 1996; Hetts et al., 2014; Pabaney et al., 2016; Burkhardt et al., 2018). Kim et al. conducted a multicenter, individual patient-level meta-analysis, and showed that increasing age is an independent predictor of hemorrhage during follow-up (Kim et al., 2014). However, no

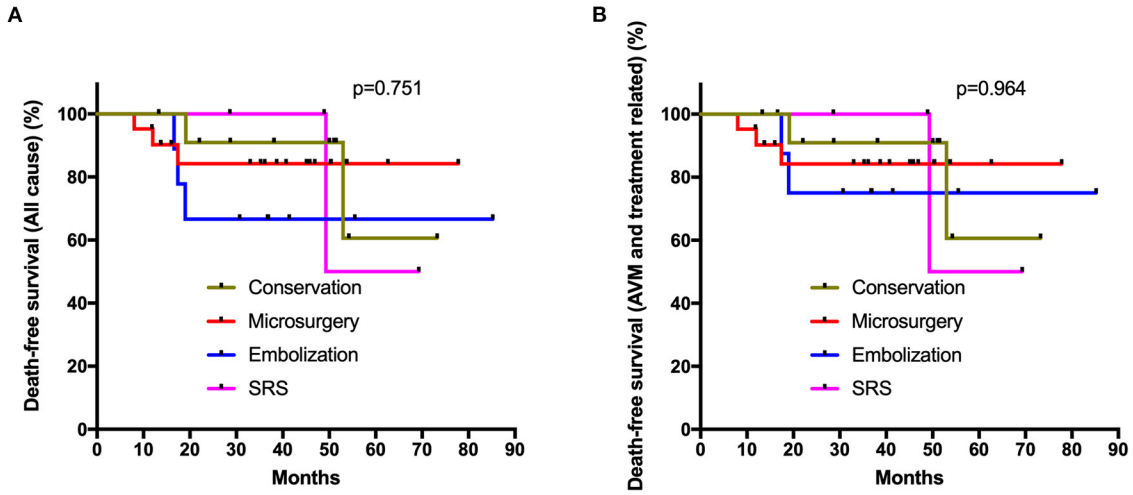


**FIGURE 3 |** Kaplan-Meier plot. The Kaplan-Meier analysis showed no significant difference in the death-free survival among different management modalities in the ruptured subgroup (**A**: all causes, $p = 0.751$; **B**: AVM and treatment related, $p = 0.964$; log-rank test).

previous study calculated the annualized rupture rate in elderly AVMs. This study defined the observational duration of natural history as the interval from the first diagnosis to admission. Finally, we calculated an annualized rupture risk of 9.4% in the elderly AVM cohort, which was higher than that in the overall AVM cohort (2–4% per year) published in previous studies (Itoyama et al., 1989; Goldberg et al., 2018). We demonstrated that the elderly AVMs may be even more aggressive than young AVMs, rather than benign lesions as reported.

## Conservation or Intervention

Generally, SM grade I/II/III are amenable to intervention (SM grade I/II: microsurgical resection, endovascular embolization, SRS; SM grade III: multimodal approach), and SM grade IV/V are recommended to be monitored unless ruptured (Derdeyn et al., 2017). In reviewing the previous literature on elderly AVMs, we found no subgroup analysis was performed in terms of rupture and unruptured presentation. In 2014, a randomized trial of unruptured brain AVMs (ARUBA) concluded that medical therapy was superior in preventing stroke and death over a follow-up period of 33 months (Mohr et al., 2014). In this study, the long-term outcomes were similar (long-term mRS score and mortality) among different management modalities in the unruptured subgroup. No patients in the conservation group occurred hemorrhage event during clinical follow-up. Therefore, it may not be advisable to intervene for unruptured elderly AVMs because of the low rupture risk and the relatively shorter life expectancy.

In the ruptured elderly AVMs, the risk of severe complications after intervention must be weighed against the natural re-rupture risk of lesions. Previous studies have drawn ambiguous attitudes about whether to intervene with elderly AVMs. Although the rupture risk is positively correlated with age progression, advanced age is also significantly correlated with a higher risk of neurological disabilities and mortality after the intervention (Ding and Liu, 2013). Hashimoto et al. reported that 69.6% of the elderly AVMs could achieve satisfactory outcomes after microsurgery, so they recommended microsurgical resection for SM grade I-II AVMs (Hashimoto et al., 2004). One recent study conducted by Burkhardt et al. proposed that 71% of elderly AVMs could achieve favorable outcomes after microsurgical resection, and they recommended microsurgical resection for carefully selected patients (Burkhardt et al., 2018). However, in Burkhardt's study, it should be noted that 84% could achieve favorable outcomes after conservation (higher than intervention). Besides, several studies recommended SRS for elderly AVMs because the advanced age does not reduce the obliteration rate or increase the incidence of complications (Ding et al., 2015; Chen et al., 2018; Hasegawa et al., 2018). In this study, the long-term outcomes were similar (long-term mRS score and mortality) among different management modalities in the ruptured subgroup. On the one hand, intervention could significantly reduce the risk of subsequent hemorrhage compared with conservation in the ruptured elderly AVMs. Nevertheless, on the other hand, we also found that the main cause of death in the microsurgery and embolization group was treatment-related complications. Therefore, the management modality selection for ruptured elderly AVMs should be determined after carefully weighing the risk of subsequent hemorrhage and treatment-related complications.

## Predictors of Unfavorable Outcomes (mRS > 2)

Spetzler and Martin proposed the SM grading system to predict the morbidity and mortality of the operative treatment (Spetzler and Martin, 1986). Several previous studies indicated that the SM grading system was also applicable to elderly AVMs (Tong et al., 2015; Burkhardt et al., 2018). In this

**TABLE 4 |** Univariate and multivariate logistic regression analysis for long-term unfavorable outcomes (mRS > 2).

| **Characteristics (Total)** | **Univariate** | | | ***p*-value** | **Multivariate** | ***p*-value** |
|---|---|---|---|---|---|---|
| | **Present (*n* = 20)** | **Absent (*n* = 51)** | **OR (95% CI)** | | **OR (95% CI)** | |
| Sex (male) | 15 (75.0) | 37 (72.5) | 0.881 (0.270–2.879) | 0.834 | | |
| Age (>65 years) | 15 (75.0) | 19 (37.3) | 5.053 (1.583–16.125) | 0.006* | 4.276 (1.155–15.839) | 0.030* |
| Hemorrhagic presentation | 18 (90.0) | 36 (70.6) | 3.750 (0.772–18.209) | 0.085 | | |
| Admission mRS score | 2.2 ± 1.4 | 1.2 ± 1.0 | 2.001 (1.260–3.179) | 0.003* | 1.749 (1.048–2.920) | 0.033* |
| Supratentorial location | 14 (70.0) | 37 (72.5) | 0.883 (0.283–2.752) | 0.830 | | |
| Size (cm) | 3.3 ± 1.7 | 2.8 ± 1.4 | 1.024 (0.990–1.059) | 0.168 | | |
| SM grade (IV–V) | 6 (30.0) | 4 (7.8) | 5.036 (1.243–20.397) | 0.024* | 6.079 (1.182–31.258) | 0.031* |
| Management modalities | | | | 0.468 | | |
| Conservation | 4 (20.0) | 17 (33.3) | Ref. | | | |
| Microsurgery | 11 (55.0) | 19 (37.3) | 0.768 (0.191–3.089) | 0.710 | | |
| Embolization | 4 (20.0) | 9 (17.6) | 0.288 (0.031–2.714) | 0.277 | | |
| SRS | 1 (5.0) | 6 (11.8) | 0.406 (0.109–1.519) | 0.181 | | |
| Complete obliteration | 8 (40.0) | 20 (39.2) | 1.033 (0.359–2.972) | 0.951 | | |
| **Characteristics (intervention)** | **Univariate** | | | ***p*-value** | **Multivariate** | ***p*-value** |
| | **Present (*n* = 16)** | **Absent (*n* = 34)** | **OR (95% CI)** | | **OR (95% CI)** | |
| Sex (male) | 12 (75.0) | 27 (79.4) | 1.286 (0.316–5.235) | 0.726 | | |
| Age (>65 years) | 12 (75.0) | 13 (38.2) | 4.846 (1.287–18.255) | 0.020* | | |
| Hemorrhagic presentation | 15 (93.8) | 26 (76.5) | 4.615 (0.525–40.577) | 0.168 | | |
| Admission mRS score | 2.4 ± 1.5 | 1.2 ± 1.0 | 2.279 (1.319–3.939) | 0.003* | 3.070 (1.559–6.043) | 0.001* |
| Supratentorial location | 11 (68.8) | 25 (73.5) | 0.792 (0.215–2.915) | 0.726 | | |
| Size (cm) | 3.3 ± 1.7 | 2.7 ± 1.4 | 1.024 (0.985–1.064) | 0.232 | | |
| SM grade (IV-V) | 4 (25.0) | 2 (5.9) | 5.333 (0.862–32.997) | 0.072 | | |
| Management modalities | | | | 0.544 | | |
| Microsurgery | 11 (68.8) | 19 (55.9) | Ref. | | | |
| Embolization | 4 (25.0) | 9 (26.5) | 0.768 (0.191–3.089) | 0.710 | | |
| SRS | 1 (6.3) | 6 (17.6) | 0.288 (0.031–2.714) | 0.277 | | |
| Complete obliteration | 8 (50.0) | 20 (58.8) | 0.578 (0.177–1.882) | 0.363 | 0.146 (0.026–0.828) | 0.030* |
| **Characteristics (Microsurgery)** | **Univariate** | | | ***p*-value** | **Multivariate** | ***p*-value** |
| | **Present (*n* = 11)** | **Absent (*n* = 19)** | **OR (95% CI)** | | **OR (95% CI)** | |
| Sex (male) | 8 (72.7) | 14 (73.7) | 1.050 (0.197–5.602) | 0.954 | | |
| Age (>65 years) | 9 (81.8) | 10 (52.6) | 4.050 (0.685–23.949) | 0.123 | | |
| Hemorrhagic presentation | 11 (100) | 17 (89.5) | $1.0*10^9$ (0.000-) | >0.999 | | |
| Admission mRS score | 3.1 ± 1.3 | 1.4 ± 1.1 | 2.775 (1.377–5.595) | 0.004* | 4.010 (1.321–12.175) | 0.014* |
| Supratentorial location | 9 (81.8) | 15 (78.9) | 1.200 (0.182–7.926) | 0.850 | | |
| Size (cm) | 3.7 ± 1.7 | 3.0 ± 1.2 | 1.041 (0.985–1.099) | 0.156 | | |
| SM grade (IV-V) | 4 (36.4) | 1 (5.3) | 15.000 (1.449–155.313) | 0.023* | 39.048 (1.016–1500.618) | 0.049* |
| Complete obliteration | 8 (72.7) | 19 (100.0) | 0.000 (0.000-) | >0.999 | | |

*CI, Confidence Intervals; mRS, modified Rankin Scale; OR, Odds Ratio; SM grade, Spetzler-Martin grade; SRS, Stereotactic Radiosurgery.*
*Values are expressed as number of cases (%) or mean ± standard deviation, unless otherwise indicated.*
**Statistical significance ($p < 0.05$).*

study, SM grade IV-V and higher admission mRS score were found to be significantly associated with long-term unfavorable outcomes (mRS > 2) both in the whole cohort and microsurgery group, which was consistent with previous studies (Tong et al., 2015). Burkhardt et al. and Nagata et al. suggested that age >65 years was an independent predictor of unfavorable outcomes after microsurgical resection (Nagata et al., 2006; Burkhardt et al., 2018). In our study, we only found a significant correlation between age >65 years and unfavorable outcomes in the whole elderly AVM

cohort. In the intervention group, higher admission mRS scores and uncomplete obliteration were correlated with unfavorable outcomes, which means that we must obliterate the lesions completely as we operated.

We acknowledge that our study has several limitations. First, the selection bias exists due to the retrospective nature of our study design. Many elderly AVMs with lower rupture risk may be recommended for conservative treatment without hospitalization, which would increase the number of ruptured patients in the study cohort, and thus render an overestimation of the aggressiveness of their natural history. Second, the sample size was small, especially in the embolization group and SRS group, impeding us from conducting in-depth analysis in each management modality. Third, it may not be appropriate to define the elderly as >60 years old in today's aging population. However, the retirement age is 60 years old in China, and we thought it is reasonable for us to define it as such in this study. Fourth, the follow-up duration is relatively short (4.2 ± 2.3 years). Previous studies have confirmed that 5–10 years after the first rupture may be the peak period of rebleeding. Therefore, the similarity in long-term outcomes may be due to the absence of rebleeding events in the conservation group during our follow-up. Our study shows consistencies and discrepancies compared with previous studies, and further multicenter studies with larger sample sizes are needed to verify our findings.

## CONCLUSIONS

The natural history of elderly AVMs is not benign, with an annualized natural rupture rate of 9.4%. The long-term neurological outcomes and mortality of different management modalities for elderly AVMs were similar both in the ruptured and unruptured subgroup. Although intervention could significantly reduce the risk of subsequent hemorrhage than conservation in the ruptured subgroup, the treatment-related complications were the main cause of death in the intervention group. All in all, intervention for unruptured elderly AVMs was not recommended. For the ruptured elderly AVMs, we should carefully weigh the risk of subsequent hemorrhage and treatment-related complications before formulating individualized treatment strategies. Besides, complete obliteration is required if we chose to intervene.

## DATA AVAILABILITY STATEMENT

The raw data supporting the conclusions of this article will be made available by the authors, without undue reservation.

## ETHICS STATEMENT

The studies involving human participants were reviewed and approved by the ethics committee of Beijing Tiantan Hospital and Peking University International Hospital. The patients/participants provided their written informed consent to participate in this study.

## AUTHOR CONTRIBUTIONS

YC conceived the idea, designed the paper, and wrote the manuscript. YC, DY, and LM performed the statistical analysis. ZL, YC, DY, LM, and YaZ collected the data. LM, XC, HW, and YuZ funded the study. HW, XY, HJ, YL, DG, SS, AL, SW, XC, and YuZ critically revised the manuscript and approved the final manuscript as submitted. All authors agreed to be accountable for all aspects of the work in ensuring that questions related to the accuracy or integrity of any part of the work are appropriately investigated and resolved.

## FUNDING

This study was supported by Natural Science Foundation of China (81571110 and 81771234 to YuZ; 81500995 to XC; 81801140 to LM), Bai Qian Wan Talent Plan (2017A07 to YuZ), National Key R&D Program (2020YFC2004701 to XC), and Beijing Municipal Administration of Hospital Incubating Program (PX2016034 to HW).

## ACKNOWLEDGMENTS

We thank the Cerebrovascular Surgery Study Project of Beijing Tiantan Hospital and the Neurosurgery Center of Perking University International Hospital.

## SUPPLEMENTARY MATERIAL

The Supplementary Material for this article can be found online at: https://www.frontiersin.org/articles/10.3389/fnagi.2021.609588/full#supplementary-material

## REFERENCES

Brown, R. D. Jr., Wiebers, D. O., Torner, J. C., and O'Fallon, W. M. (1996). Frequency of intracranial hemorrhage as a presenting symptom and subtype analysis: a population-based study of intracranial vascular malformations in Olmsted Country, Minnesota. *J. Neurosurg.* 85, 29–32. doi: 10.3171/jns.1996.85.1.0029

Burkhardt, J. K., Lasker, G. F., Winkler, E. A., Kim, H., and Lawton, M. T. (2018). Microsurgical resection of brain arteriovenous malformations in the elderly: outcomes analysis and risk stratification. *J. Neurosurg.* 129, 1107–1113. doi: 10.3171/2017.6.JNS17392

Chen, C. J., Ding, D., Kano, H., Mathieu, D., Kondziolka, D., Feliciano, C., et al. (2018). Effect of advanced age on stereotactic radiosurgery outcomes for brain arteriovenous malformations: a multicenter matched cohort study. *World Neurosurg.* 119, e429–e440. doi: 10.1016/j.wneu.2018.07.178

Chen, Y., Li, R., Ma, L., Meng, X., Yan, D., Wang, H., et al. (2020). Long-term outcomes of brainstem arteriovenous malformations after different management modalities: a single-centre experience. *Stroke Vasc. Neurol.* doi: 10.1136/svn-2020-000407. [Epub ahead of print].

Crawford, P. M., West, C. R., Chadwick, D. W., and Shaw, M. D. (1986). Arteriovenous malformations of the brain: natural history in unoperated patients. *J. Neurol. Neurosurg. Psychiatry* 49, 1–10. doi: 10.1136/jnnp.49.1.1

Derdeyn, C. P., Zipfel, G. J., Albuquerque, F. C., Cooke, D. L., Feldmann, E., Sheehan, J. P., et al. (2017). Management of brain arteriovenous malformations: a scientific statement for healthcare professionals from the American Heart Association/American Stroke Association. *Stroke* 48, e200–e224. doi: 10.1161/STR.0000000000000134

Ding, D., and Liu, K. C. (2013). Predictive capability of the spetzler-martin vs. supplementary grading scale for microsurgical outcomes of cerebellar arteriovenous malformations. *J. Cerebrovasc. Endovasc. Neurosurg.* 15, 307–310. doi: 10.7461/jcen.2013.15.4.307

Ding, D., Xu, Z., Yen, C. P., Starke, R. M., and Sheehan, J. P. (2015). Radiosurgery for cerebral arteriovenous malformations in elderly patients: effect of advanced age on outcomes after intervention. *World Neurosurg.* 84, 795–804. doi: 10.1016/j.wneu.2015.05.012

Goldberg, J., Raabe, A., and Bervini, D. (2018). Natural history of brain arteriovenous malformations: systematic review. *J. Neurosurg. Sci.* 62, 437–443. doi: 10.23736/S0390-5616.18.04452-1

Harbaugh, K. S., and Harbaugh, R. E. (1994). Arteriovenous malformations in elderly patients. *Neurosurgery* 35, 579–584. doi: 10.1227/00006123-199410000-00001

Hasegawa, H., Hanakita, S., Shin, M., Sugiyama, T., Kawashima, M., Takahashi, W., et al. (2018). Does advanced age affect the outcomes of stereotactic radiosurgery for cerebral arteriovenous malformation? *World Neurosurg.* 109, e715–e723. doi: 10.1016/j.wneu.2017.10.071

Hashimoto, H., Iida, J., Kawaguchi, S., and Sakaki, T. (2004). Clinical features and management of brain arteriovenous malformations in elderly patients. *Acta Neurochir. (Wien)* 146, 1091–1098. discussion: 1098. doi: 10.1007/s00701-004-0346-9

Heros, R. C., and Tu, Y. K. (1987). Is surgical therapy needed for unruptured arteriovenous malformations? *Neurology* 37, 279–286. doi: 10.1212/WNL.37.2.279

Hetts, S. W., Cooke, D. L., Nelson, J., Gupta, N., Fullerton, H., Amans, M. R., et al. (2014). Influence of patient age on angioarchitecture of brain arteriovenous malformations. *AJNR Am. J. Neuroradiol.* 35, 1376–1380. doi: 10.3174/ajnr.A3886

Itoyama, Y., Uemura, S., Ushio, Y., Kuratsu, J., Nonaka, N., Wada, H., et al. (1989). Natural course of unoperated intracranial arteriovenous malformations: study of 50 cases. *J. Neurosurg.* 71, 805–809. doi: 10.3171/jns.1989.71.6.0805

Kim, H., Al-Shahi Salman, R., McCulloch, C. E., Stapf, C., Young, W. L., and Coinvestigators, M. (2014). Untreated brain arteriovenous malformation: patient-level meta-analysis of hemorrhage predictors. *Neurology* 83, 590–597. doi: 10.1212/WNL.0000000000000688

Lanzino, G., Fergus, A. H., Jensen, M. E., Kongable, G. L., and Kassell, N. F. (1997). Long-term outcome aftersurgical excision of parenchymal arteriovenous malformations in patients over 60 years of age. *Surg. Neurol.* 47, 258–263. discussion 263–254. doi: 10.1016/S0090-3019(96)00391-6

Luessenhop, A. J., and Rosa, L. (1984). Cerebral arteriovenous malformations. Indications for and results of surgery, and the role of intravascular techniques. *J. Neurosurg.* 60, 14–22. doi: 10.3171/jns.1984.60.1.0014

Mohr, J. P., Parides, M. K., Stapf, C., Moquete, E., Moy, C. S., Overbey, J. R., et al. (2014). Medical management with or without interventional therapy for unruptured brain arteriovenous malformations (ARUBA): a multicentre, non-blinded, randomised trial. *Lancet* 383, 614–621. doi: 10.1016/S0140-6736(13)62302-8

Nagata, S., Matsukado, K., Natori, Y., Sasaki, T., and Fukui, M. (2006). Surgical indications for arteriovenous malformations in patients over the age of 60 years: retrospective analysis of 33 patients. *Br. J. Neurosurg.* 20, 146–149. doi: 10.1080/02688690600776895

Pabaney, A. H., Reinard, K. A., Kole, M. K., Seyfried, D. M., and Malik, G. M. (2016). Management of arteriovenous malformations in the elderly: a single-center case series and analysis of outcomes. *J. Neurosurg.* 125, 145–151. doi: 10.3171/2015.6.JNS15293

Perret, G., and Nishioka, H. (1966). Report on the cooperative study of intracranial aneurysms and subarachnoid hemorrhage. Section VI. Arteriovenous malformations. An analysis of 545 cases of cranio-cerebral arteriovenous malformations and fistulae reported to the cooperative study. *J. Neurosurg.* 25, 467–490. doi: 10.3171/jns.1966.25.4.0467

Solomon, R. A., and Connolly, E. S. Jr. (2017). Arteriovenous malformations of the brain. *N. Engl. J. Med.* 376, 1859–1866. doi: 10.1056/NEJMra1607407

Spetzler, R. F., and Martin, N. A. (1986). A proposed grading system for arteriovenous malformations. *J. Neurosurg.* 65, 476–483. doi: 10.3171/jns.1986.65.4.0476

Tong, X., Wu, J., Lin, F., Cao, Y., Zhao, Y., Ning, B., et al. (2015). Brain arteriovenous malformations in elderly patients: clinical features and treatment outcome. *Acta Neurochir. (Wien)* 157, 1645–1653. discussion 1653–1644. doi: 10.1007/s00701-015-2521-6

**Conflict of Interest:** The authors declare that the research was conducted in the absence of any commercial or financial relationships that could be construed as a potential conflict of interest.

frontiers in Aging Neuroscience

ORIGINAL RESEARCH
published: 19 February 2021
doi: 10.3389/fnagi.2021.631738

# Plasma Neurofilament Light Chain as a Predictive Biomarker for Post-stroke Cognitive Impairment: A Prospective Cohort Study

*Zhiqiang Wang[1,2], Rongyu Wang[1,2], Yuxia Li[3], Mao Li[1,2], Yaodan Zhang[1,2], Lianyan Jiang[1,2], Jin Fan[2], Qingsong Wang[3]* and Dongdong Yang[1]**

[1] Department of Neurology, Hospital of Chengdu University of Traditional Chinese Medicine, Chengdu, China, [2] School of Clinical Medicine, Chengdu University of TCM, Chengdu, China, [3] Department of Neurology, The General Hospital of Western Theater Command, Chengdu, China

**Background:** Plasma neurofilaments light chain (pNfL) is a marker of axonal injury. The purpose of this study was to examine the role of pNfL as a predictive biomarker for post-stroke cognitive impairment (PSCI).

**Methods:** A prospective single-center observational cohort study was conducted at the General Hospital of Western Theater Command between July 1, 2017 and December 31, 2019. Consecutive patients ≥18 years with first-ever acute ischemic stroke (AIS) of anterior circulation within 24 h of symptom onset were included. PSCI was defined by the Montreal Cognitive Assessment (MOCA) (MOCA < 26) at 90 days after stroke onset.

**Results:** A total of 1,694 patients [male, 893 (52.70%); median age, 64 (16) years] were enrolled in the cohort analysis, and 1,029 (60.70%) were diagnosed with PSCI. Patients with PSCI had significantly higher pNfL [median (IQR), 55.96 (36.13) vs. 35.73 (17.57) pg/ml; $P < 0.001$] than Non-PSCI. pNfL was valuable for the prediction of PSCI (OR 1.044, 95% CI 1.038–1.049, $P < 0.001$) after a logistic regression analysis, even after adjusting for conventional risk factors including age, sex, education level, NIHSS, TOAST classification, and infarction volume (OR 1.041, 95% CI 1.034–1.047, $P < 0.001$). The optimal cutoff value of the pNfL concentration was 46.12 pg/ml, which yielded a sensitivity of 71.0% and a specificity of 81.5%, with the area under the curve (AUC) at 0.785 (95% CI 0.762–0.808, $P < 0.001$).

**Conclusion:** This prospective cohort study showed that the pNfL concentration within 48 h of onset was an independent risk factor for PSCI 90 days after an anterior circulation stroke, even after being adjusted for potential influencing factors regarded as clinically relevant.

**Clinical Trial Registration:** www.chictr.org.cn, identifier ChiCTR1800020330.

**Keywords: stroke, neurofilament light, biomarkers, post-stroke cognitive impairment, odds ratio, dementia**

OPEN ACCESS

***Edited by:***
*Shuo Wang,*
*Capital Medical University, China*

***Reviewed by:***
*Steffen Tiedt,*
*LMU Munich University Hospital, Germany*
*Jaime Ramos-Cejudo,*
*New York University, United States*

****Correspondence:***
*Qingsong Wang*
*wqscdgh@sina.com*
*Dongdong Yang*
*1241668186@qq.com*

***Received:*** *20 November 2020*
***Accepted:*** *22 January 2021*
***Published:*** *19 February 2021*

***Citation:***
*Wang Z, Wang R, Li Y, Li M, Zhang Y, Jiang L, Fan J, Wang Q and Yang D (2021) Plasma Neurofilament Light Chain as a Predictive Biomarker for Post-stroke Cognitive Impairment: A Prospective Cohort Study. Front. Aging Neurosci. 13:631738. doi: 10.3389/fnagi.2021.631738*

# INTRODUCTION

Stroke survivors are at increased risk for cognitive impairment. Studies have shown that even mild strokes can increase the risk of cognitive impairment in survivors and affect their quality of life (Fride et al., 2015). Epidemiological studies have shown that stroke causes cognitive dysfunction in approximately one-third of patients, but it is unknown which stroke patients will suffer from cognitive impairment. Thus, the diagnosis and prediction of post-stroke cognitive impairment (PSCI) functional recovery by biomarkers has become a hot research topic. Previous studies have indicated that inflammatory biomarkers, growth factors, oxidative damage biomarkers, genetic biomarkers, and metabolic biomarkers in the circulating blood of patients may be the key determinants for the diagnosis and prediction of cognitive impairment (Zhang and Bi, 2020). However, these markers cannot reflect the mechanism of cognitive impairment caused by a stroke. The direct pathological cause of PSCI is neuronal damage in key brain regions, so looking for markers related to neuronal damage may predict and reflect a decline in the cognitive level.

Neurofilament light chain (NfL) is a neuron-specific structural protein (Zetterberg, 2016) that has recently been suggested as a marker of axonal injury and neurodegeneration with potential applications for both patient monitoring and for observational and interventional studies (Tiedt et al., 2018). In recent years, with the development of the quantitative detection technology of plasma NfL (pNfL), studies regarding the role of pNfL in neurodegenerative diseases and brain injury have been increasing (Gattringer et al., 2017; Guedes et al., 2020; Quiroz et al., 2020). Recent studies have observed a significant correlation among pNfL and the National Institutes of Health Stroke Scale (NIHSS) upon admission (Traenka et al., 2015; Al-Khaled, 2018), age-related white matter changes, infarct volume (Gattringer et al., 2017; Tiedt et al., 2018; Onatsu et al., 2019) and clinical outcome 90 days after stroke (Uphaus et al., 2019). A meta-analysis showed that the pNfL was a promising predictive biomarker for ischemic stroke outcome (Liu et al., 2020). The pNfL concentration had also been considered to be related to cognitive deterioration (Zetterberg et al., 2016; Mattsson et al., 2017; Olsson et al., 2019). To date and to our knowledge, the usefulness of pNfL for understanding PSCI is unclear. To address this, a prospective single-center observational cohort study was conducted to determine the association between pNfL and PSCI.

# MATERIALS AND METHODS

## Study Design and Participants

This was a prospective single-center observational cohort study that included consecutive patients ≥18 years with first ever AIS of the anterior circulation within 24 h of symptom onset who were admitted to the General Hospital of Western Theater Command between July 1, 2017 and December 31, 2019. AIS was diagnosed according to the World Health Organization criteria and confirmed using brain computed tomography (CT) or magnetic resonance imaging (MRI). Patients were excluded if they (1) had a pre-existing cognitive impairment (clinical diagnosis or previous treatment or if the subject/caregiver reported progressive forgetfulness), mental illness or were unable to complete the cognitive assessments; (2) had issues combined with other non-vascular causes of neural function defects (brain injury, Alzheimer's disease, Parkinson's disease, and other neurological diseases);(3) were accompanied by serious medical diseases, tumor, hepatitis or an autoimmune disease; or (4) had survived less than 3 months.

Stroke severity was assessed using the National Institutes of Health Stroke Scale Score (NIHSS) and infarct volume (calculated using the MRI-DWI). The DWI lesion volumes were determined by the consensus of two experienced raters unaware of the clinical and laboratory results. The lesion size was calculated using the commonly used semiquantitative method (Broderick et al., 1993). All of the cases were invited for a 90-day follow-up visit. A physician blinded to the clinical data assessed changes in cognition. Post-stroke cognitive impairment (PSCI) was defined by the Montreal Cognitive Assessment (MOCA) (MOCA $< 26$) at 90 ( $\pm$ 5) days (Lees et al., 2014) after stroke onset via in-person interview.

## Blood Sampling and Biomarker Measurements

Venous blood samples were drawn upon admission or the next morning (within 48 h of stroke onset), and the time from stroke onset to blood collected was recorded. After centrifugation for 20 min at 3,000 g at room temperature, plasma (from the ethylene diamino tetraacetic acid (EDTA) tube) was aliquoted. The tubes were frozen locally at −80°C within 40 min after collection. The pNfL was measured using a single-molecule assay (SiMoA) platform (Quanterix, Lexington, MA, United States) as described (Weston et al., 2017; Tiedt et al., 2018). An in-house pool was used as an internal control and included in each assay for evaluating the assay performance. Samples were analyzed in duplicates, and the coefficient of variation (CV) was <11%.

## Statistical Analysis

Discrete variables were expressed as counts (percentages) and continuous variables as medians (interquartile range [IQR]). For the univariate analysis, the Mann-Whitney *U* test or chi-squared test was used to compare the demographic and clinical characteristics of patients with and without PSCI, as appropriate. The pNfL, MOCA, infarct volume, and NIHSS scores were log transformed (based 10) to closely normal distributions. In order to test for significant correlations between the clinical characteristics of patients and the plasma data, the Pearson correlational was used. The association of the pNfL levels upon admission with cognitive impairment was analyzed using a multiple logistic regression and adjusted for the established predictors. Variables that were identified as significant in univariate analyses ($P < 0.1$) were entered into the regression analyses together with other clinically significant variables. The optimal cutoff levels for the dichotomizing values were selected as the situation maximizing the Youden index. The receiver operating characteristic (ROC) analysis was performed

**TABLE 1 |** Baseline characteristics of the participants.

| Factors | Total | PSCI | Non-PSCI | *P* |
|---|---|---|---|---|
| Overall rate, *n* (%) | 1, 694 (100) | 1, 029 (60.74) | 665 (39.26) | |
| Sex, male, *n* (%) | 893 (52.72) | 538 (52.28) | 355 (53.38) | 0.658 |
| Age (y), median (IQR) | 64.00 (16.00) | 66.00 (18.50) | 62.00 (13.00) | **<0.001** |
| Education level, <6 years, *n* (%) | 900 (53.13) | 561 (64.52) | 339 (50.98) | 0.154 |
| BMI (kg/m$^2$) | 24.09 (1.53) | 24.22 (1.59) | 23.92 (1.43) | **<0.001** |
| **Vascular risk factors, *n* (%)** | | | | |
| Hypertension | 1, 015 (59.92) | 630 (61.22) | 385 (57.89) | 0.172 |
| Diabetes mellitus | 566 (33.41) | 346 (33.62) | 220 (33.08) | 0.817 |
| Hyperlipidemia | 385 (22.73) | 249 (24.20) | 136 (20.45) | 0.072 |
| Atrial fibrillation | 371 (21.90) | 267 (25.95) | 104 (15.64) | **<0.001** |
| Smoking | 478 (28.22) | 276 (26.82) | 202 (30.38) | 0.113 |
| Drinking | 318 (18.77) | 194 (18.85) | 124 (18.65) | 0.915 |
| NIHSS, median (IQR) | 4 (7) | 6 (8) | 3 (3) | **<0.001** |
| Infarct volume (ml), median (IQR) | 15.83 (11.33) | 15.99 (13.00) | 15.10 (11.01) | **<0.001** |
| **TOAST classification, *n* (%)** | | | | **<0.001** |
| Large-artery atherosclerosis | 928 (54.78) | 548 (53.26) | 380 (57.14) | |
| Cardioembolism | 239 (14.11) | 175 (17.01) | 64 (9.62) | |
| Small vessel occlusion | 154 (9.09) | 83 (8.07) | 71 (10.68) | |
| Other cause | 68 (4.01) | 45 (4.37) | 23 (3.46) | |
| Undetermined | 305 (18.01) | 178 (17.30) | 127 (19.10) | |
| Blood sampling time (h), median (IQR) | 19.00 (19.00) | 20.00 (19.25) | 17.00 (19.00) | 0.471 |
| pNfL (pg/mL), median (IQR) | 46.41 (36.26) | 55.96 (36.13) | 35.73 (17.57) | **<0.001** |
| HbA1c (%), median (IQR) | 5.9 (1.10) | 5.9 (1.20) | 5.9 (0.80) | 0.901 |
| HsCRP (mg/L), median (IQR) | 3.58 (2.75) | 3.51 (2.71) | 3.61 (2.87) | 0.332 |
| HCY (μmol/L), median (IQR) | 14.64 (9.45) | 15.18 (9.24) | 14.03 (10.15) | **<0.001** |
| MOCA, median (IQR) | 24 (7) | 21 (8) | 27 (2) | **<0.001** |

*PSCI, post-stroke cognitive impairment; IQR, interquartile range; BMI, Body Mass Index; pNfL, plasma neurofilament light chain concentration; NIHSS, National Institutes of Health Stroke Scale; and TOAST, Trial of ORG 10172 in Acute Stroke Treatment; HsCRP, high sensitivity C-reactive protein; HCY, homocysteine; MOCA, Montreal Cognitive Assessment. Bold text indicates a statistically less than 0.05.*

to determine the sensitivity, specificity, and area-under-the ROC curve of the pNfL for detection of PSCI. In order to validate the model, 5-fold cross-validation was employed using the RMS package available on R statistical software. Other analyses were performed using SPSS 22 (IBM, Chicago, IL). All of the tests were 2-sided, and a $P < 0.05$ was considered to be significant.

## RESULTS

A comparison of the demographic and clinical variables in the final dataset, including the pNfL data, is shown in **Table 1**. Of the 1,896 patients who were initially screened for eligibility, 202 (10.65%) were excluded for reasons that included: 68 (3.59%) death within 3 months, 45 (2.37%) combined with other central nervous system diseases, 43 (2.27%) unable to complete the cognitive assessments, 12 (0.63%) no plasma available, and 34 (1.79%) withdrew consent or were lost to follow-up. Finally, a total of 1,694 patients [male, 893 (52.72%); median age, 64 (IQR, 16) years] were enrolled in the cohort analysis, the median MOCA was 24 (IQR, 7), the median NIHSS was 4 (IQR, 7), the median blood sampling time was 19 h (IQR, 19; range 2–48), and the median pNfL was 46.41 (IQR, 36.26) pg/ml. A total of 1,029 (60.74%) were diagnosed with PSCI.

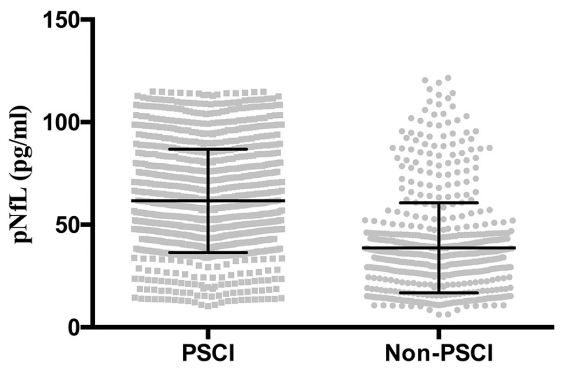


**FIGURE 1 |** Plasma neurofilament light chain (pNfL) concentration in the diagnostic groups are shown as scatterplots. The pNfL concentration was higher in the post-stroke cognitive impairment (PSCI) group compared with the non-PSCI group ($P < 0.001$).

The PSCI and non-PSCI patients were well matched for sex, education level, history of hypertension, hyperlipidemia, diabetes, smoking, alcohol (all $P > 0.05$). However, the participants with atrial fibrillation, of older age, more clinical severity on the NIHSS, a larger infarction volume (ml), or a

higher body mass index (BMI) were more common in the PSCI group ($P < 0.05$). No significant difference was observed between the two groups in terms of time to blood sampling (h), plasma high sensitivity C-reactive protein (HsCRP) level, and HbA1c levels (all $P > 0.05$). Compared with the non-PSCI group, the PSCI group exhibited significantly higher levels of pNFL and homocysteine (HCY) (both $P < 0.05$) (**Table 1** and **Figure 1**).

Correlation analysis showed that the $\log_{10}$ pNfL levels correlated with age ($r = 0.130$, $P < 0.001$), $\log_{10}$ cerebral infarction volumes ($r = 0.509$, $P < 0.001$; **Figure 2A**), the $\log_{10}$ NIHSS score ($r = 0.510$, $P < 0.001$; **Figure 2B**), and the $\log_{10}$ time to blood sampling ($r = 0.261$, $P < 0.001$; **Figure 2C**). The $\log_{10}$ pNfL levels were negatively correlated with cognitive impairment defined by $\log_{10}$ MOCA ($r = -0.523$, $P < 0.001$; **Figure 2D**).

A multivariable logistic regression revealed that patients with higher pNfL had a significantly higher risk of PSCI, even after adjusting for conventional risk factors including age, sex, education level, NIHSS score, TOAST classification and infarction volume ($P < 0.05$). This result indicated that the pNfL could be an independent risk factor for PSCI (**Table 2**).

The optimal cutoff value of the pNfL concentration as an indicator for auxiliary diagnosis of PSCI was assessed using the ROC curve. The optimal threshold was 46.12 pg/ml, which yielded a sensitivity of 71.0% and a specificity of 81.5%, with the AUC at 0.785 (95% CI, 0.762–0.808; $P < 0.001$; **Figure 3**). After 5-fold cross-validation, the c-statistic of the model was still 0.785. The calibration curve was very close to the actual curve, which showed that the model fits well.

## DISCUSSION

This prospective cohort study showed that the pNfL concentration within 48 h of onset was an independent risk factor for PSCI within 90 days after an anterior circulation stroke, even after adjustment for potential influencing factors regarded as clinically relevant. In the present study, it was found that PSCI patients exhibited higher pNfL and Hcy levels than non-PSCI patients. Ages, BMI, atrial fibrillation, clinical severity on the NIHSS, and the infarction volume were also associated with cognitive function in post-stroke patients. The pNfL was positively correlated with the NIHSS score, infarct volume and the time to blood sampling time, negatively correlated with the MOCA. The levels of pNfL showed significant diagnostic accuracy in discriminating patients with PSCI from those without PSCI. This is the first study that has investigated the pNfL levels in patients with PSCI.

NfL, a neuron-specific structural protein (Zetterberg, 2016), has recently been suggested as a marker of neuroaxonal injury after ischemic stroke with potential application prospects for patient monitoring, observation, and intervention studies (Tiedt et al., 2018). Cerebrospinal fluid (CSF) NfL concentrations can

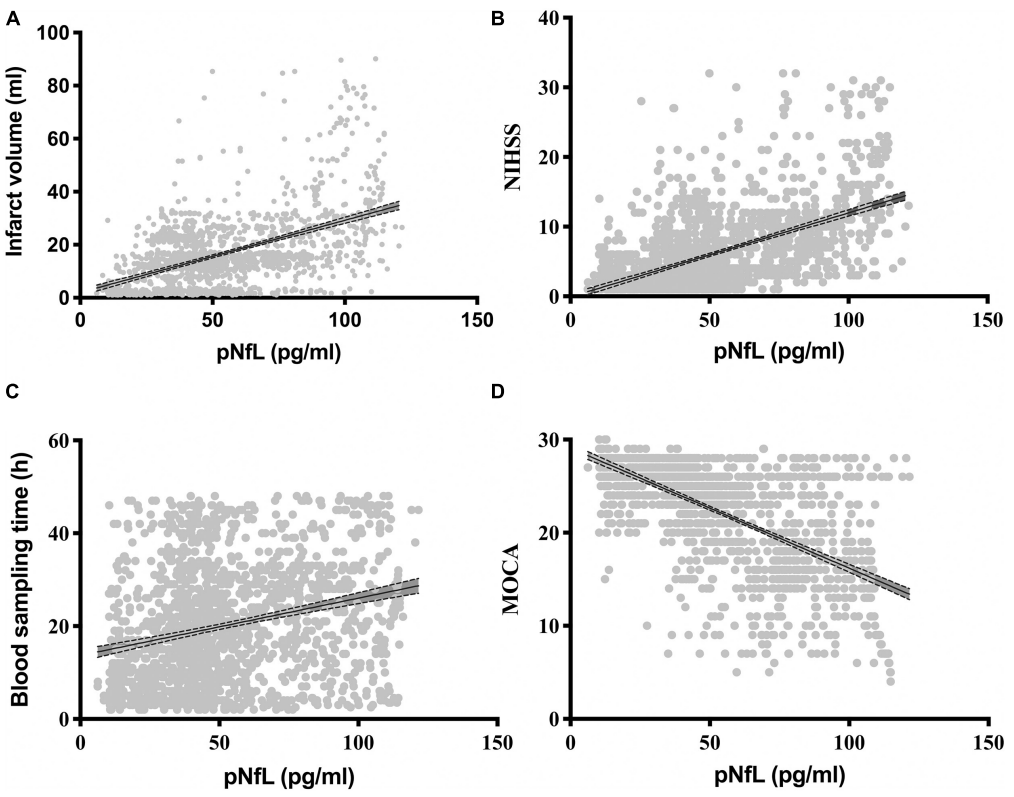


**FIGURE 2 |** Correlations of the plasma neurofilament light chain (pNfL) concentration with **(A)** the infarction volume (ml), **(B)** the National Institutes of Health Stroke Scale (NIHSS), **(C)** the blood sampling time (h), and **(D)** the Montreal Cognitive Assessment (MOCA).

**TABLE 2 |** Logistic regression analysis for the association of pNfL with PSCI at 90-days.

| Variables | OR | 95%CI | *P* |
|---|---|---|---|
| Unadjusted pNfL | 1.044 | 1.038–1.049 | **<0.001** |
| Model 1 pNfL | 1.044 | 1.038–1.050 | **<0.001** |
| Model 2 pNfL | 1.041 | 1.034–1.047 | **<0.001** |

*pNfL, plasma neurofilament light chain. Model 1 adjusted for age, sex, and education status. Model 2 adjusted for Model 1 and infarct volume, NIHSS and TOAST. Bold text indicates a statistical significance of less than 0.05.*

be used as markers of axonal damage in white matter and other subcortical brain structures (Lycke et al., 1998; Zetterberg et al., 2006). Previous studies have shown that NfL expression was associated with dementia (Rosengren et al., 1999; de Jong et al., 2007; Howell et al., 2017; Zhao et al., 2019), small vessel disease (Gattringer et al., 2017), and other neurodegenerative diseases (Ge et al., 2018; Khalil et al., 2018; Bridel et al., 2019; Gagliardi et al., 2019; Gao et al., 2020). In addition, an increasing number of studies have demonstrated that pNfL levels were associated with clinical characteristics and outcome in stroke patients (Tiedt et al., 2018; Uphaus et al., 2019; Nielsen et al., 2020), and the CSF NfL increased months before the first dementia symptoms appeared, suggesting it might serve as a preclinical marker (Bacioglu et al., 2016). However, whether NfL expression is related to the occurrence of PSCI is still unknown. This study is the first to show that pNfL concentration was a blood marker of PSCI and has significant diagnostic accuracy in discriminating patients with PSCI from those without PSCI. The exclusion criteria of this study were not harsh; for example, patients with cortical infarction, large infarct size, or specific causes of stroke were not excluded. Hence, these findings could be considered representative of the spectrum of PSCI.

This study was the first to reveal the correlation between the NfL expression in plasma and the occurrence of PSCI. Previous studies have shown that the expression of NfL in the cerebral spinal fluid (CSF) was correlated with cognitive function, including Alzheimer's disease (AD) (Weston et al., 2017), and frontotemporal dementia (FTD) (Rohrer et al., 2016), even in a small sample of vascular dementia (VaD) studies (Rosengren et al., 1999; Skillbäck et al., 2014). A network meta-analysis further demonstrated a significant increase in the CSF NfL expression level in dementias that engage the subcortical brain regions, such as VaD, than other types of dementia (Skillbäck et al., 2014; Zhao et al., 2019). Because the CSF collection is relatively complex, especially for stroke patients, the development of blood biomarkers (such as exosomes) is particularly important, and it is an important target for the future study of PSCI markers. The recent development of methods to quantify NfL in plasma had demonstrated that the pNfL concentration was closely correlated with cerebrospinal fluid NfL and directly reflected neurodegeneration within the central nervous system (Palermo et al., 2020). Consistent with what would be expected of a marker of neuronal damage, results from these studies showed a higher pNfL in patients with PSCI and correlations between pNfL and PSCI were observed (Gattringer et al., 2017; Tiedt et al., 2018). In agreement with earlier studies, it was found in this study that the severity of cognitive impairment increased with increasing pNfL levels (Gendron et al., 2020), making pNfL an easily accessible biomarker of the progression of neurodegenerative dementia diseases (Mattsson et al., 2017; Weston et al., 2017; Olsson et al., 2019).

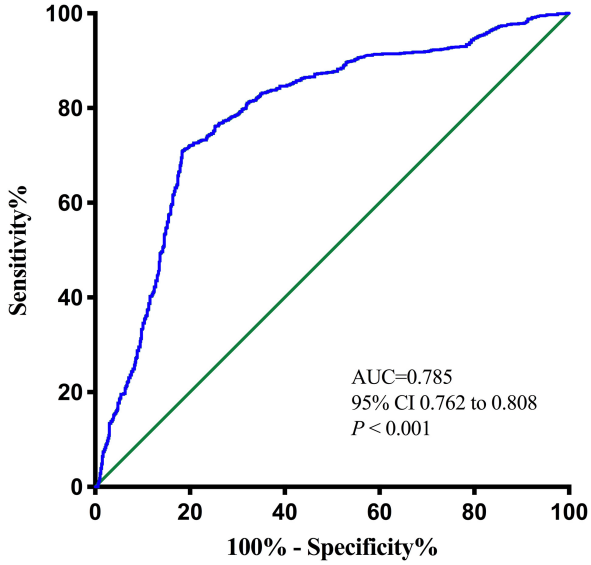


**FIGURE 3 |** Receiver operating characteristic (ROC) curve for the plasma neurofilament light chain. AUC, area under curve.

In this study, a prospective cohort study was designed to show that pNfL was an independent risk factor for PSCI. Previous small-sample case-control studies only observed increased NfL expression in CSF of VaD patients (Sjögren et al., 2001; Wallin and Sjögren, 2001; Skillbäck et al., 2014; Zhao et al., 2019). In this study, by using a prospective cohort design, the regression analysis showed that pNfL expression was an independent risk factor for PSCI. The risks of PSCI were associated with age and vascular risk factors, such as atrial fibrillation, which was consistent with a previous study (Pendlebury et al., 2019). Also, stroke severity and infarction volume should be considered (Tiedt et al., 2018). In this study, all parameters were included when assessing the correlation of PSCI and pNfL. Nevertheless, after controlling for the confounders, the pNfL level displayed as an independent predictor of PSCI. The role of NfL in the pathophysiology of PSCI might be through some possible signaling pathways. pNfL is related to stroke severity (NIHSS score and lesion volume) and clinical outcomes (Onatsu et al., 2019; Pedersen et al., 2019), which are independent predictors of PSCI. However, pNfL still was a predictor for PSCI after adjusting for the NIHSS score and lesion volume, which was consistent

with the results of a recent study (Gendron et al., 2020). The potential reasons behind why pNfL adds an additional predictive value apart from stroke severity should be considered. Acute infarcts further induce secondary neurodegeneration outside the infarct area, such as white matter tracts connected to the infarct. That secondary damage could contribute to poor cognitive and blocked neurotransmitter synthesis that leads to PSCI.

This study identified the correlation between pNfL and PSCI within 48 h of onset. There is evidence that pNfL increases with the time from symptom onset to blood-draw (Traenka et al., 2015; Gattringer et al., 2017; Tiedt et al., 2018), illustrating that the time point of measurement is of great importance when evaluating pNfL (Al-Khaled, 2018; Tiedt et al., 2018). To control the influence of blood collection time on the results, blood was collected within 48 h after the onset of the disease. It should be noted that patients within 24 h after stroke symptoms onset were included in this study. However, as some patients had their blood collected the next morning, the overall blood collection time was 48 h. This study showed that there was weak correlation between the concentration of pNfL and the blood collection time, and there was no difference in the blood collection time between groups. In contrast to a previous study that showed an association among functional outcomes 90 days after ischemic stroke and pNfL measured 7 days after symptom onset (Al-Khaled, 2018; Tiedt et al., 2018), as well as NfL that was independently correlated with the Mini-Mental State Examination at 0–8 days (Gendron et al., 2020), it was possible to already show a predictive effect of the NfL measured in plasma collected within 48 h after symptom onset. This was consistent with recent studies (Pedersen et al., 2019; Uphaus et al., 2019). This is especially important, as biomarker-based decision-making might be mandatory before the 7-day time point (Uphaus et al., 2019).

This study had several limitations. First, single-center cohorts, the exclusion of patients with aphasia or other severe conditions and patients in whom measurement of the pNfL levels failed may have led to an underestimation of the actual incidence of PSCI. Second, pNfL was measured only once. It may be essential to conduct a longitudinal study that measures at multiple time points after stroke to provide better prognostic information. Third, the centrifugal operation process was slightly different from the current standard guidelines (Tiedt et al., 2018), and the results should be further validated in future studies. Finally, single biomarkers may not be sufficient, and multiple biomarkers combined with a machine-learning algorithm should be used to automatically diagnose and predict PSCI.

## CONCLUSION

In conclusion, in this study, it was demonstrated that high pNfL levels within 48 h after first-ever anterior circulation stroke were associated with the development of PSCI 90 days after an acute ischemic stroke (AIS). In addition, this study showed significant diagnostic accuracy for discriminating patients with PSCI from patients without cognitive impairment. Further studies are needed to verify this association.

## DATA AVAILABILITY STATEMENT

The raw data supporting the conclusions of this article will be made available by the authors, without undue reservation.

## ETHICS STATEMENT

The studies involving human participants were reviewed and approved by the Ethics Committee of General Hospital of Western Theater Command. The patients/participants provided their written informed consent to participate in this study.

## AUTHOR CONTRIBUTIONS

DY: conceptualization, methodology, and software. QW: conceptualization, methodology, supervision, and investigation. ZW: data curation, writing the original draft, reviewing, and editing. RW: data curation and writing the original draft. ML and LJ: data curation. YL: data curation and investigation. YZ: software and validation. JF: supervision. All the authors reviewed the manuscript and approved the submitted version.

## FUNDING

This study was supported by the Scientific Research Project of Health and Family Planning Commission of Sichuan Province (No. 16PJ014).

## ACKNOWLEDGMENTS

We thank all of the patients and their families for their participation in the study and the investigators.

## REFERENCES

Al-Khaled, M. (2018). Serum neurofilament light as diagnostic biomarker for acute cerebral ischemia: a promising tool. *Eur. J. Neurol.* 25:609. doi: 10.1111/ene.13588

Bacioglu, M., Maia, L. F., Preische, O., Schelle, J., Apel, A., Kaeser, S. A., et al. (2016). Neurofilament light chain in blood and CSF as marker of disease progression in mouse models and in Neurodegenerative Diseases. *Neuron* 91, 56–66. doi: 10.1016/j.neuron.2016.05.018

Bridel, C., Van Wieringen, W. N., Zetterberg, H., Tijms, B. M., Teunissen, C. E., and Alvarez-Cermeño, J. C. (2019). Diagnostic value of cerebrospinal fluid neurofilament light protein in neurology: a systematic review and meta-analysis. *JAMA Neurol.* 76, 1035–1048.

Broderick, J. P., Brott, T. G., Duldner, J. E., Tomsick, T., and Huster, G. (1993). Volume of intracerebral hemorrhage. A powerful and easy-to-use predictor of 30-day mortality. *Stroke* 24, 987–993. doi: 10.1161/01.str.24.7.987

de Jong, D., Jansen, R. W., Pijnenburg, Y. A., Van Geel, W. J., Borm, G. F., Kremer, H. P., et al. (2007). CSF neurofilament proteins in the differential diagnosis of

dementia. *J. Neurol. Neurosurg. Psychiatry* 78, 936–938. doi: 10.1136/jnnp.2006.107326

Fride, Y., Adamit, T., Maeir, A., Ben Assayag, E., Bornstein, N. M., Korczyn, A. D., et al. (2015). What are the correlates of cognition and participation to return to work after first ever mild stroke? *Top. Stroke Rehabil.* 22, 317–325. doi: 10.1179/1074935714z.0000000013

Gagliardi, D., Meneri, M., Saccomanno, D., Bresolin, N., Comi, G. P., and Corti, S. (2019). Diagnostic and prognostic role of blood and cerebrospinal fluid and blood neurofilaments in amyotrophic lateral sclerosis: a review of the literature. *Int. J. Mol. Sci.* 20:4152. doi: 10.3390/ijms20174152

Gao, W., Zhang, Z., Lv, X., Wu, Q., Yan, J., Mao, G., et al. (2020). Neurofilament light chain level in traumatic brain injury: a system review and meta-analysis. *Medicine* 99:e22363. doi: 10.1097/md.0000000000022363

Gattringer, T., Pinter, D., Enzinger, C., Seifert-Held, T., Kneihsl, M., Fandler, S., et al. (2017). Serum neurofilament light is sensitive to active cerebral small vessel disease. *Neurology* 89, 2108–2114. doi: 10.1212/wnl.0000000000004645

Ge, F., Ding, J., Liu, Y., Lin, H., and Chang, T. (2018). Cerebrospinal fluid NFL in the differential diagnosis of parkinsonian disorders: a meta-analysis. *Neurosci. Lett.* 685, 35–41. doi: 10.1016/j.neulet.2018.07.030

Gendron, T. F., Badi, M. K., Heckman, M. G., Jansen-West, K. R., Vilanilam, G. K., and Johnson, P. W. (2020). Plasma neurofilament light predicts mortality in patients with stroke. *Sci. Transl. Med.* 12:eaay1913.

Guedes, V. A., Kenney, K., Shahim, P., Qu, B. X., Lai, C., Devoto, C., et al. (2020). Exosomal neurofilament light: a prognostic biomarker for remote symptoms after mild traumatic brain injury? *Neurology* 94, e2412–e2423.

Howell, J. C., Watts, K. D., Parker, M. W., Wu, J., Kollhoff, A., Wingo, T. S., et al. (2017). Race modifies the relationship between cognition and Alzheimer's disease cerebrospinal fluid biomarkers. *Alzheimers Res. Ther.* 9:88.

Khalil, M., Teunissen, C. E., Otto, M., Piehl, F., Sormani, M. P., Gattringer, T., et al. (2018). Neurofilaments as biomarkers in neurological disorders. *Nat. Rev. Neurol.* 14, 577–589.

Lees, R., Selvarajah, J., Fenton, C., Pendlebury, S. T., Langhorne, P., Stott, D. J., et al. (2014). Test accuracy of cognitive screening tests for diagnosis of dementia and multidomain cognitive impairment in stroke. *Stroke* 45, 3008–3018. doi: 10.1161/strokeaha.114.005842

Liu, D., Chen, J., Wang, X., Xin, J., Cao, R., and Liu, Z. (2020). Serum neurofilament light chain as a predictive biomarker for ischemic stroke outcome: a systematic review and meta-analysis. *J. Stroke Cerebrovasc. Dis.* 29:104813. doi: 10.1016/j.jstrokecerebrovasdis.2020.104813

Lycke, J. N., Karlsson, J. E., Andersen, O., and Rosengren, L. E. (1998). Neurofilament protein in cerebrospinal fluid: a potential marker of activity in multiple sclerosis. *J. Neurol. Neurosurg. Psychiatry* 64, 402–404. doi: 10.1136/jnnp.64.3.402

Mattsson, N., Andreasson, U., Zetterberg, H., and Blennow, K. (2017). Association of plasma neurofilament light with neurodegeneration in patients with alzheimer disease. *JAMA Neurol.* 74, 557–566. doi: 10.1001/jamaneurol.2016.6117

Nielsen, H. H., Soares, C. B., Høgedal, S. S., Madsen, J. S., Hansen, R. B., and Christensen, A. A. (2020). Acute neurofilament light chain plasma levels correlate with stroke severity and clinical outcome in ischemic stroke patients. *Front. Neurol.* 11:448. doi: 10.3389/fneur.2020.00448

Olsson, B., Portelius, E., Cullen, N. C., Sandelius, Å, Zetterberg, H., Andreasson, U., et al. (2019). Association of cerebrospinal fluid neurofilament light protein levels with cognition in patients with dementia, motor neuron disease, and movement disorders. *JAMA Neurol.* 76, 318–325. doi: 10.1001/jamaneurol.2018.3746

Onatsu, J., Vanninen, R., Jäkälä, P., Mustonen, P., Pulkki, K., Korhonen, M., et al. (2019). Serum neurofilament light chain concentration correlates with infarct volume but not prognosis in acute ischemic stroke. *J. Stroke Cerebrovasc. Dis.* 28, 2242–2249. doi: 10.1016/j.jstrokecerebrovasdis.2019.05.008

Palermo, G., Mazzucchi, S., Della Vecchia, A., Siciliano, G., Bonuccelli, U., Azuar, C., et al. (2020). Different clinical contexts of use of blood neurofilament light chain protein in the spectrum of Neurodegenerative Diseases. *Mol. Neurobiol.* 57, 4667–4691. doi: 10.1007/s12035-020-02035-9

Pedersen, A., Stanne, T. M., Nilsson, S., Klasson, S., Rosengren, L., Holmegaard, L., et al. (2019). Circulating neurofilament light in ischemic stroke: temporal profile and outcome prediction. *J. Neurol.* 266, 2796–2806. doi: 10.1007/s00415-019-09477-9

Pendlebury, S. T., Rothwell, P. M., and Oxford Vascular, S. (2019). Incidence and prevalence of dementia associated with transient ischaemic attack and stroke: analysis of the population-based Oxford Vascular Study. *Lancet Neurol.* 18, 248–258. doi: 10.1016/s1474-4422(18)30442-3

Quiroz, Y. T., Zetterberg, H., Reiman, E. M., Chen, Y., Su, Y., Fox-Fuller, J. T., et al. (2020). Plasma neurofilament light chain in the presenilin 1 E280A autosomal dominant Alzheimer's disease kindred: a cross-sectional and longitudinal cohort study. *Lancet Neurol.* 19, 513–521. doi: 10.1016/s1474-4422(20)30137-x

Rohrer, J. D., Woollacott, I. O., Dick, K. M., Brotherhood, E., Gordon, E., Fellows, A., et al. (2016). Serum neurofilament light chain protein is a measure of disease intensity in frontotemporal dementia. *Neurology* 87, 1329–1336. doi: 10.1212/wnl.0000000000003154

Rosengren, L. E., Karlsson, J. E., Sjögren, M., Blennow, K., and Wallin, A. (1999). Neurofilament protein levels in CSF are increased in dementia. *Neurology* 52, 1090–1093. doi: 10.1212/wnl.52.5.1090

Sjögren, M., Blomberg, M., Jonsson, M., Wahlund, L. O., Edman, A., Lind, K., et al. (2001). Neurofilament protein in cerebrospinal fluid: a marker of white matter changes. *J. Neurosci. Res.* 66, 510–516. doi: 10.1002/jnr.1242

Skillbäck, T., Farahmand, B., Bartlett, J. W., Rosén, C., Mattsson, N., Nägga, K., et al. (2014). CSF neurofilament light differs in neurodegenerative diseases and predicts severity and survival. *Neurology* 83, 1945–1953. doi: 10.1212/wnl.0000000000001015

Tiedt, S., Duering, M., Barro, C., Kaya, A. G., Boeck, J., Bode, F. J., et al. (2018). Serum neurofilament light: a biomarker of neuroaxonal injury after ischemic stroke. *Neurology* 91, e1338–e1347.

Traenka, C., Disanto, G., Seiffge, D. J., Gensicke, H., Hert, L., Grond-Ginsbach, C., et al. (2015). Serum neurofilament light chain levels are associated with clinical characteristics and outcome in patients with cervical artery dissection. *Cerebrovasc. Dis.* 40, 222–227. doi: 10.1159/000440774

Uphaus, T., Bittner, S., Gröschel, S., Steffen, F., Muthuraman, M., Wasser, K., et al. (2019). NfL (Neurofilament Light Chain) levels as a predictive marker for long-term outcome after ischemic stroke. *Stroke* 50, 3077–3084.

Wallin, A., and Sjögren, M. (2001). Cerebrospinal fluid cytoskeleton proteins in patients with subcortical white-matter dementia. *Mech. Ageing Dev.* 122, 1937–1949. doi: 10.1016/s0047-6374(01)00306-2

Weston, P. S. J., Poole, T., Ryan, N. S., Nair, A., Liang, Y., Macpherson, K., et al. (2017). Serum neurofilament light in familial Alzheimer disease: a marker of early neurodegeneration. *Neurology* 89, 2167–2175. doi: 10.1212/wnl.0000000000004667

Zetterberg, H. (2016). Neurofilament light: a dynamic cross-disease fluid biomarker for neurodegeneration. *Neuron* 91, 1–3. doi: 10.1016/j.neuron.2016.06.030

Zetterberg, H., Hietala, M. A., Jonsson, M., Andreasen, N., Styrud, E., Karlsson, I., et al. (2006). Neurochemical aftermath of amateur boxing. *Arch. Neurol.* 63, 1277–1280. doi: 10.1001/archneur.63.9.1277

Zetterberg, H., Skillbäck, T., Mattsson, N., Trojanowski, J. Q., Portelius, E., Shaw, L. M., et al. (2016). Association of cerebrospinal fluid neurofilament light concentration With Alzheimer Disease progression. *JAMA Neurol.* 73, 60–67. doi: 10.1001/jamaneurol.2015.3037

Zhang, X., and Bi, X. (2020). Post-stroke cognitive impairment: a review focusing on molecular biomarkers. *J. Mol. Neurosci.* 70, 1244–1254. doi: 10.1007/s12031-020-01533-8

Zhao, Y., Xin, Y., Meng, S., He, Z., and Hu, W. (2019). Neurofilament light chain protein in neurodegenerative dementia: a systematic review and network meta-analysis. *Neurosci. Biobehav. Rev.* 102, 123–138. doi: 10.1016/j.neubiorev.2019.04.014

**Conflict of Interest:** The authors declare that the research was conducted in the absence of any commercial or financial relationships that could be construed as a potential conflict of interest.

frontiers in Aging Neuroscience

ORIGINAL RESEARCH
published: 08 March 2021
doi: 10.3389/fnagi.2021.632374

# DI-3-n-Butylphthalide Alleviates Demyelination and Improves Cognitive Function by Promoting Mitochondrial Dynamics in White Matter Lesions

*Yiwei Feng[1†], Min Guo[1†], Hongchen Zhao[1], Sida Han[1], Yining Hao[1], Yiwen Yuan[1], Weiwei Shen[1], Jian Sun[1], Qiang Dong[2*] and Mei Cui[1*]*

[1] Department of Neurology, Huashan Hospital, Fudan University, Shanghai, China, [2] Department of Neurology, Huashan Hospital, State Key Laboratory of Medical Neurobiology and Ministry of Education Frontiers Center for Brain Science, Fudan University, Shanghai, China

White matter lesions (WMLs) are a type of cerebrovascular disorder accompanied by demyelination and cognitive decline. DI-3-n-butylphthalide (D1-NBP) is a neuroprotective drug used for the treatment of ischemic cerebrovascular diseases, although the function of DI-NBP on WML is still not clear. This study aims to investigate whether DI-NBP affects cognitive function and ameliorates demyelination in a model of WML. The bilateral carotid artery stenosis (BCAS) mouse model and *in vitro* brain slice cultures with low glucose and low oxygen (LGLO) treatment were adopted. The DI-NBP was administered intragastrically for 28 days after BCAS or added at a dose of 50 μm for 48 h after LGLO. Spatial learning and memory were evaluated by an eight-arm radial maze. Demyelination was detected using a TEM. Mitochondrial dynamics were assessed by time-lapse imaging in the cultured brain slices. The function of the synapse was evaluated by the patch clamp technique. In BCAS mice, obvious demyelination and cognitive decline were observed, while both were significantly relieved by a high-dose D1-NBP treatment (100 mg/kg). Along with demyelination, mitochondrial accumulation in the axons was significantly increased in the BCAS mice model, but with the treatment of a high-dose D1-NBP, mitochondrial accumulation was mitigated, and the anterograde/retrograde transport of mitochondria was increased. Following the improved anterograde/retrograde transport of mitochondria, the synapse activity was significantly upregulated while the reactive oxygen species (ROS) generation was remarkably decreased in the cultured brain slices. In addition, we identified syntaphilin (SNPH) as the downstream target of D1-NBP. The overexpression of SNPH mediated the effects of D1-NBP in mitigating axonal mitochondrial accumulation. In conclusion, the D1-NBP treatment significantly relieved demyelination and improved spatial learning and memory in the WML model by promoting mitochondrial dynamics. These neuroprotective effects of D1-NBP were mediated by inhibiting the mitochondrial arching protein, SNPH, which provided a potential therapeutic target for WML.

**Keywords: DI-3-n-butylphthalide, white matter lesions, mitochondria dynamics, demyelination, cognitive impairment**

OPEN ACCESS

***Edited by:***
*Shuo Wang,*
*Capital Medical University, China*

***Reviewed by:***
*Beita Zhao,*
*Northwest a and f University, China*
*Chen Ding,*
*Yale University, United States*

***Correspondence:**
*Qiang Dong*
*dong_qiang@fudan.edu.cn*
*Mei Cui*
*cuimei@fudan.edu.cn*

*[†]These authors have contributed equally to this work*

***Received:*** *23 November 2020*
***Accepted:*** *02 February 2021*
***Published:*** *08 March 2021*

***Citation:***
*Feng Y, Guo M, Zhao H, Han S, Hao Y, Yuan Y, Shen W, Sun J, Dong Q and Cui M (2021) DI-3-n-Butylphthalide Alleviates Demyelination and Improves Cognitive Function by Promoting Mitochondrial Dynamics in White Matter Lesions. Front. Aging Neurosci. 13:632374. doi: 10.3389/fnagi.2021.632374*

## INTRODUCTION

White matter lesions (WMLs) are one of the major contributors that lead to cognitive decline and vascular dementia (VaD), especially among the elderly (Alber et al., 2019). The WML is usually caused by a modest, but chronic, reduction of blood flow, accompanied by a shortage of oxygen supply through small vessels (Ben-Ari et al., 2019). Demyelination is a characteristic of the pathological changes in WML, which accounts for the worse clinical outcomes and impaired cognitive function in patients (Datta et al., 2017). It is, therefore, urgent to figure out how to alleviate the demyelination damage and mitigate the impaired brain function.

In 2002, the FDA of China approved the use of Dl-3-n-butylphthalide (Dl-NBP), a compound extracted from the seeds of celery in treating ischemic stroke (Wang et al., 2018; Chen et al., 2019; Yang et al., 2019). It is also undergoing a Phase II trial for the treatment of ischemic stroke in the USA (Cui et al., 2013; Xue et al., 2016). Previously, more attention was given to the acute phase of stroke, and the neuroprotective effects of Dl-NBP on stroke are supported widely by both clinical and basic research (Chen et al., 2020). Mechanically, studies have shown that the Dl-NBP could inhibit the apoptosis of neurons, endoplasmic reticulum stress, and oxidative stress and improve hemodynamics as well as neurogenesis (Sun et al., 2017; Wang et al., 2018, 2019). However, as a promising molecular compound in treating ischemic injuries of the brain, the function of Dl-NBP in WML and demyelination is neither clear nor has it been confirmed.

From the limited studies on WML, evidence shows that the Dl-NBP could promote the cognitive function in VaD models caused by chronic hypoperfusion (Li et al., 2019). The normal cognitive function requires a relatively normal electronic signal and a synaptic signal, which rely on intact myelin, as well as cholinergic neurotransmission (Feng et al., 2020b). The beneficial effects of Dl-NBP on VaD were demonstrated by improving remyelination and enhancing the function of the cholinergic system (Tian et al., 2020). Yet, remyelination happens at the late stage of WML injury and the function of the cholinergic system is closely related to the electronic signal from the axons (Lema et al., 2017). Whether the Dl-NBP can benefit the electronic function of synapse or alleviate myelin breakdown at the early stage remains to be determined.

Under hypoperfusion, mitochondria are the most sensitive organisms in neurons that sense ischemia/hypoxia and quickly change their dynamics and metabolism (Bargiela et al., 2018). Axons suffer ischemic damage and display abnormal mitochondrial dynamics, showing disturbed fission–fusion transport in axons (Chen et al., 2018; Thomas and Ashcroft, 2019). The reduced retrograde transport of dysfunctional mitochondria can block mitophagy and cause unfavorable reactive oxygen species (ROS), which is harmful to myelin (Palikaras et al., 2015). The anterograde of mitochondria is vital for the supply of energy to the synapse for neurotransmitter release (Zheng et al., 2019). Therefore, we speculated that the Dl-NBP might relive demyelination in WMLs by regulating mitochondrial dynamics. In the present study, we investigated the effects of Dl-NBP on mitochondrial dynamics and demyelination using a WML model.

**Abbreviations:** WMLs, white matter lesions; APs, action potentials; BCAS, bilateral common carotid artery stenosis; LGLO, low glucose and low oxygen; mEPSC, miniature excitatory postsynaptic current; MS, multiple sclerosis; SNPH, syntaphilin; TEM, transmission electron microscopy; VaD, vascular dementia.

## MATERIALS AND METHODS

### Animals

C57BL/6J male mice (9–12 weeks, 25–30 g) were purchased from Charles River Laboratories and housed in the Experimental Animal Center of Fudan University, Shanghai, China in a temperature- and humidity-controlled specific-pathogen-free laboratory with a 12/12 h light/dark cycle. All procedures were performed in accordance with the Guide for the National Science Council of the People's Republic of China, and the study was approved by the Ethics Committee of Fudan University (IRB approval number 20190972A259). This manuscript was written in accordance with the Animal Research: Reporting of *in vivo* Experiments (ARRIVE) guidelines.

### The BCAS Model and Dl-NBP Treatment

The bilateral carotid artery stenosis (BCAS) model was performed as described previously (Feng et al., 2020b). Briefly, the mice were anesthetized using 4% isoflurane in 28% $O_2$ and 68% $N_2$ and maintained on 2% isoflurane in 29% $O_2$ and 69% $N_2$ by a mask. After making a midline skin incision on the neck, the bilateral common carotid arteries were isolated and subsequently stenosed using 0.18 mm steel micro coils (Wuxi Samini/Sawane Spring Co., Ltd., Hamamatsu City, Japan). For sham-operated mice, a similar procedure was followed, whereas micro-coils were not used for the induction of BCAS. For the D1-NBP treatment, a low-dose treatment of DI-NBP (L-NBP, 50 mg/kg/day) and a high-dose treatment of D1-NBP (H-NBP, 100 mg/kg/day) were intragastrically administrated 1 day after the BCAS surgery for 28 days.

All experimental groups were randomized, and all outcome analyses were carried out by independent investigators blinded to the treatment conditions and mouse types. Randomization of each experimental group was performed before the surgical procedure by using the random number generator in GraphPad. The preliminary data from the TEM and the eight-arm maze experiments indicated that 6 and 12 animals per group, respectively, would be sufficient to obtain 80% power at a significance level of $< 0.05$ with a two-sided test.

### The Cerebellum Slice Culture and the D1-NBP Treatment

For cerebellar organotypic slice culture, the postnatal day 8–9 (P8-9) mice were used. About 400 μm P8-9 mouse cerebellum parasagittal slices were obtained using a vibratome (ZQP-86, Zhixin Co., Ltd., Shanghai, China). The slices were placed on cell culture inserts (Millipore, Bedford, MA, USA) and were cultured in 50% Dulbecco's modified eagle's medium (DMEM) with 25% Hanks' balanced salt solution (HBSS), 25% horse serum, and 5

mg/ml glucose (Invitrogen, Carlsbad, CA, USA) in cell culture chambers at 37°C.

The low glucose and low oxygen (LGLO) (2% $O_2$ and 1 mg/ml glucose) treatment was used to give a chronic hypoperfusion environment to the slices for 48 h. The D1-NBP, at a dose of 50 μm, was added to the cultured slices before the LGLO treatment, which is a relatively high dose consistently used with previous studies (Li et al., 2019). Experiments and data analyses were performed in a double-blinded manner.

## The Overexpression of Syntaphilin

The overexpression (OE) of syntaphilin (SNPH) plasmid and adeno-associated virus (AAV) 2/9 or lentivirus was constructed by Genomeditech (Genomeditech, Shanghai, China). For culturing cerebellum slices, lentivirus was added to the medium of the slice at $1*10^{10}$ gene copies, 5 days before the LGLO treatment.

For mice, AAV 2/9 SNPH-OE plasmid or AAV empty vector was stereoscopically injected into lateral ventricles. The mice were anesthetized using 4% isoflurane in 30% $O_2$ and 70% $N_2$ and maintained on 2% isoflurane in 30% $O_2$ and 70% $N_2$ by a mask. The AAV vectors were infused into the left lateral ventricle (coordinates from bregma: AP, −0.2 mm; ML, +1.0 mm; DV, −2.3 mm). The genome copies of size $5 \times 10^{11}$ were infused at a rate of 1 μl/min. After injection, the needle was left in place for 2 min to prevent backflow before the withdrawl.

## Time-Lapse Imaging Using Confocal Microscopy

As described previously (Lin et al., 2017), the mitochondria were labeled with MitoTracker Red CMXRos, M7512 (Thermofisher Scientific, USA) for 3 h after the brain slices were treated with LGLO. After an extensive wash, the slices were placed in an airstream incubator at 37°C and imaged by an Olympus inverted confocal microscope using a 60 × 1.3 NA oil immersion objective with 512 × 512-pixel resolution (FV1200, Olympus).

Upon imaging, a total of 5 min with 15 s intervals were imaged for each experiment. The total live imaging time was restricted to 20 min to minimize phototoxic damage. The length, area, and diameter of the axonal mitochondria were measured by the ImageJ program (NIH, USA). The number and mean velocity of motile mitochondria were analyzed by kymographs. Stationary sites in this study were defined as CMXRos-positive profiles that were stationary during a 5-min period. To measure the size of the stationary mitochondria, a pair of image stacks, including all CMXRos-positive profiles of each axon, were obtained at the time periods 0 and 5 min.

## Immunofluorescence

Brain slices were fixed overnight in 4% paraformaldehyde (PFA) and then in 30% sucrose for 2 days at 4°C. Subsequently, the slices were blocked with 5% bovine serum albumin (BSA) for 1 h and permeabilized with 0.1% Triton X-100 in phosphate buffered saline (PBS) for 15 min. Primary antibodies, diluted in a blocking buffer, were added to the slices and were incubated overnight at 4°C. The primary antibodies used in this experiment were anti-NF (1:50, ab8135, Abcam, USA) and anti-maltose binding protein (MBP) (1:200, ab40390, Abcam, USA). The slices were washed three times with PBS and labeled with a fluorescence-conjugated secondary antibody for 1 h at room temperature (Alexa Fluor 488 and 594, 1:1,000, Life Technologies). Nuclei were visualized by mounting with DAPI (28718-90-3; Sigma Aldrich, USA).

For ROS staining in mitochondria, the MitoSOX™ Red mitochondrial superoxide indicator (M36008, ThermoFisher, USA) was used to label ROS in mitochondria. The MitoSOX was diluted according to the manufacturer's instruction and incubated with the slices for 3 h. After an extensive wash with PBS, the slices were replenished with the indicated culture medium.

## Western Blot

Brain slices were collected and lysed in the radioimmunoprecipitation assay (RIPA) buffer [50 mm Tris-HCl, pH 7.5, 150 mm NaCl, 1% Triton X-100, 0.1% sodium dodecyl sulfate (SDS), 0.5% deoxycholate] with a protease inhibitor. Equal amounts of proteins, measured by the BCA method, were loaded on 15% Bris-Tris NuPAGE, electrophoresed, and transferred into 0.22 μm nitrocellulose membranes. After blocking with 5% BSA in TBST for 1 h, the membranes were incubated overnight at 4°C with the following primary antibodies: anti-SNPH (ab69992, Abcam, USA), anti-Miro1 (ab188029, Abcam, USA), anti-Trak1 (ab28751, Abcam, USA), anti-HSP60 (ab190828, Abcam, USA), and anti-β-actin (ab115777, Abcam, USA) at a dilution of 1:1,000 (Tris-buffered saline with 0.1% Tween® 20 detergent).

## Transmission Electron Microscope

The TEM was performed as described previously (Guo et al., 2019). In short, the brain samples were perfused with PBS and 4% paraformaldehyde (PFA). Dissected tissues (1 mm in thickness) were postfixed in buffered $OsO_4$, dehydrated in graded alcohol solutions and propylene, embedded in Epon, and examined by light microscopy after staining with toluidine blue. Thin sections cut on using formvar-coated slot grids and stained with uranyl acetate and lead citrate were examined using a JEOL 1200 electron microscope. G-ratios were determined as the inner to outer axonal circumference ratio using the ImageJ program.

## The Eight-Arm Radial Maze Test

The eight-arm radial maze test was performed as described previously (Xu et al., 2019). The maze consisted of a central platform (24 cm in diameter) with eight arms that extended radially. The mouse was allowed to visit each arm to eat eight pellets in food cups placed near the end of each arm. Each test animal was trained once per day to memorize the apparatus. The performance of the test animals in each trial was assessed using the two parameters, namely the number of correct choices in the initial eight chosen arms and the number of errors (defined as choosing arms that had already been visited). When the test animals had made seven or eight correct choices with no more than one error in three successive sessions, they were deemed to have memorized the maze.

## Whole-Cell Patch-Clamp Electrophysiology

As described previously (Feng et al., 2020a), the cultured brain slices were transferred to the patch-clamp bath solution for 1 h prior to recording. The bath solution contained 126 mm NaCl, 2.5 mm KCl, 26 mm $NaHCO_3$, 1.25 mm $NaH_2PO_4$, 2 mm $CaCl_2$, 2 mm $MgCl_2$, and 11 mm glucose bubbled with 95% $O_2$ + 5% $CO_2$. The temperature of the bath solution was maintained at 32°C. For miniature excitatory postsynaptic current (mEPSC) recordings, patch pipettes containing 126 mm K-gluconate, 4 mm KCl, 4 mm ATP-Mg, 0.3 mm GTP-$Na_2$, 10 mm PO creatine, 10 mm HEPES, and 0.2–0.5% biocytin (pH 7.3 adjusted using KOH, 300 mOsm maintained using sucrose) with a tip resistance of 6–8 MΩ were used. During mEPSC recording, tetrodotoxin (TTX) (0.5 μm) was administered to silence the network activity through the inhibition of voltage-sensitive sodium channels, and bicuculline (10 μm) was given to block the GABA-A-mediated inhibitory signaling.

For the recording of action potentials (APs), patch pipettes containing 140 mm K-gluconate, 5 mm ethylene glycol-bis(β-aminoethyl ether) (EGTA), 0.5 mm $CaCl_2$, 2 mm ATP-Mg, 0.3 mm guanosine-5′-triphosphate (GTP)-$Na_2$, 10 mm sucrose, 10 mm HEPES, and 0.2–0.5% biocytin (pH 7.3 adjusted using KOH, 300 mOsm maintained using sucrose) with a tip resistance of 6–8 MΩ were used.

Series resistance was monitored at an interval of 2 min, and recordings were excluded if the series resistance and leak current changed significantly and/or exceeded 40 MΩ or 200 pA, respectively.

## Golgi Silver Staining

Golgi silver staining was performed as described previously (Du, 2019). The mice were sacrificed and perfused with 4% PFA. The brain was dissected, cut into half at the junction between the cortex and midbrain, and further incubated in the PFA solution for a further 10 min, followed by the immersion in the Golgi solution (FD Neurotechnologies, Rapid Golgi Kit). The Golgi solution was changed after 6 h, and the brain was kept immersed as such for 2 weeks before development as per the instructions of the manufacturer.

## Statistical Analysis

Data were analyzed using SPSS Statistics 22 and graphed with GraphPad Prism 8.0. The sample size was calculated

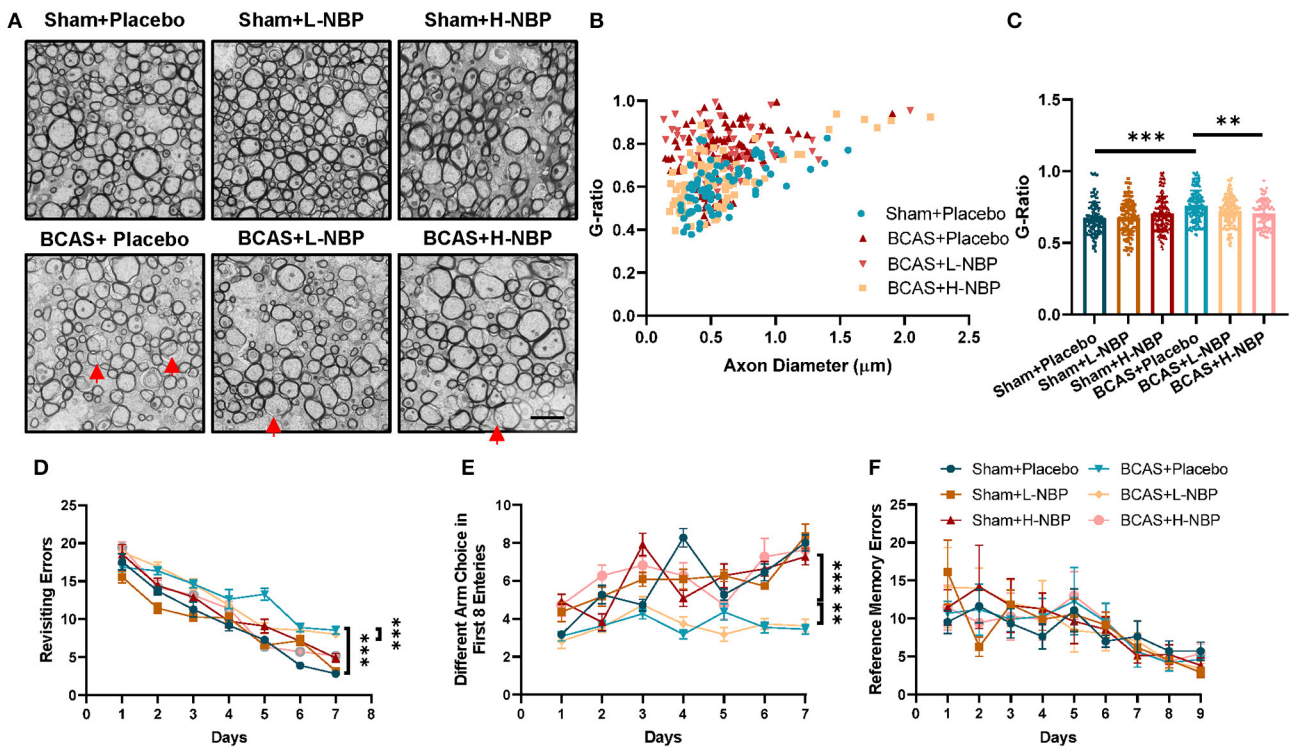


**FIGURE 1 | (A)** High-dose treatment of DI-3-n-butylphthalide (D1-NBP) mitigated demyelination and improved the cognitive impairment in the bilateral carotid artery stenosis (BCAS) model. **(A–C)** Representative TEM images **(A)** and quantitative analysis of the G-ratio **(B,C)** in Sham+Placebo, Sham+L-NBP, Sham+H-NBP, BCAS+Placebo, BCAS+L-NBP, and BCAS+H-NBP groups. Scale bar, 2 μm. A one-way ANOVA with Tukey's correction. $n = 80$ myelinated axons (20 axons per mouse, 4 mice per group). **(D–F)** Working and reference memory were assessed by the eight-arm radial maze. Impaired working memory in the BCAS mice was remitted by a high-dose administration of DI-NBP, as evidenced by the less revisiting errors **(D)** and more different choices **(E)** in the BCAS+H-NBP group. There is no significant difference in the spatial reference memory between different groups **(F)**. A two-way ANOVA with the Dunnett's *post-hoc* test, $n = 11$ mice in each group. Data are represented as means ± SD (**$p < 0.01$; ***$p < 0.001$; ns: non-significant differences). L-NBP, low dose of DI-NBP; H-NBP, high dose of D1-NBP.

based on the power as 0.95 and α as 0.05. All data from the mice are represented as the mean ± SD and the data from the brain slices are represented as mean ± SEM. Different treatment groups were evaluated using a one-way ANOVA with the Tukey's test for multiple comparisons. The null hypothesis was rejected when *p*-value was <0.05.

# RESULTS

## DI-NBP Mitigates Demyelination and Improved Cognitive Impairment in the BCAS Model

To study the therapeutic potential of D1-NBP in mitigating demyelination and cognitive impairment caused by whole-brain

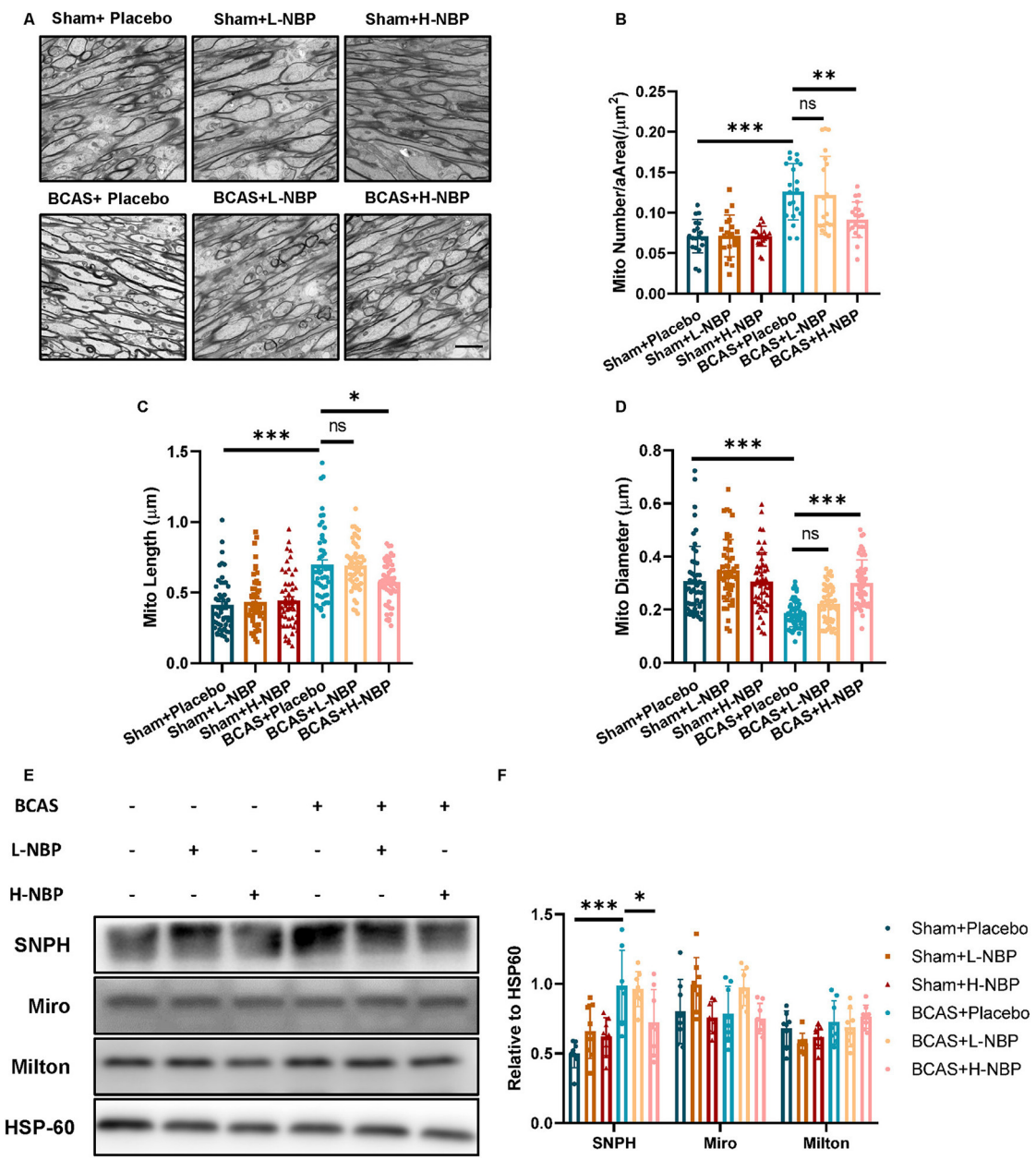


**FIGURE 2 |** Alleviated demyelination and cognitive impairment by a high-dose treatment of D1-NBP was accompanied by decreased mitochondrial accumulation among the axons. **(A–D)** Representative TEM images of mitochondrial load in axons **(A)** and quantitative analysis of mitochondrial number per area (/$\mu m^2$) **(B)**, mitochondrial length **(C)** and mitochondrial diameter **(D)** in Sham+Placebo, Sham+L-NBP, Sham+H-NBP, BCAS+Placebo, BCAS+L-NBP, BCAS+H-NBP groups. Scale bar, 2 μm. A one-way ANOVA with Tukey's correction. For mitochondrial load per area analysis, $n = 20$ visual fields (4 visual fields per mouse, 5 mice per group). For mitochondrial length analysis, $n = 50$ (10 mitochondria per mouse, 5 mice per group). For mitochondrial diameter analysis, $n = 50$ (10 mitochondria per mouse, 5 mice per group). **(E,F)** Immunoblot **(E)** and quantitative analysis **(F)** of syntaphilin (SNPH), Miro1, and Milton in different groups. A one-way ANOVA with Tukey's correction, $n = 8$ mice per group. Data are represented as means ± SD (*$p < 0.05$; **$p < 0.01$; ***$p < 0.001$; ns, non-significant differences).

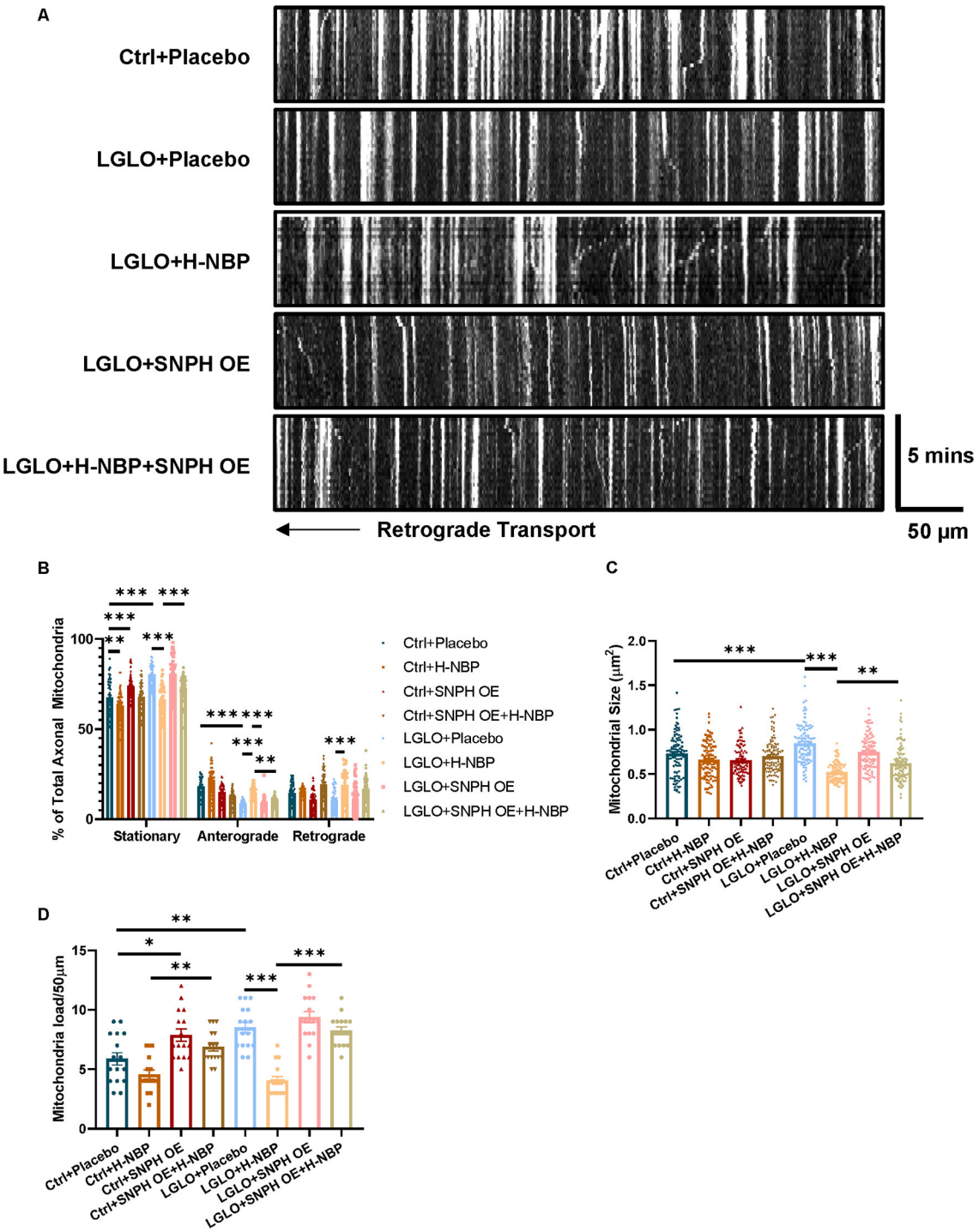


**FIGURE 3 | (A)** High-dose treatment of D1-NBP alleviates mitochondrial accumulation by promoting mitochondrial dynamics. **(A–D)** Representative kymograph **(A)** and quantitative analysis of the percentage of stationary, anterograde, and retrograde mitochondria in the axons **(B)**, mitochondrial load per 50 μm **(C)**, and mitochondrial size **(D)** in cerebellum slices subjected to Ctrl+ phosphate buffered saline (PBS), Ctrl+NBP, Ctrl+SNPH OE, Ctrl+SNPH OE+H-NBP, low glucose and low oxygen (LGLO)+PBS, LGLO+NBP, LGLO+SNPH OE, LGLO+SNPH OE+H-NBP. The high-dose treatment of D1-NBP alleviated the LGLO-induced impairment of retrograde and anterograde mitochondrial transport. A one-way ANOVA with Tukey's correction. For the percentage stationary, anterograde, and retrograde mitochondria analysis, $n = 60$ mitochondria per group. For mitochondrial load per 50 μm analysis, $n = 20$ axons per group. For mitochondrial size analysis, $n = 400$ per group. Scale bar, 50 μm and 5 min, respectively. Data are represented as means ± SEM (*$p < 0.05$; **$p < 0.01$; ***$p < 0.001$; ns, non-significant differences).

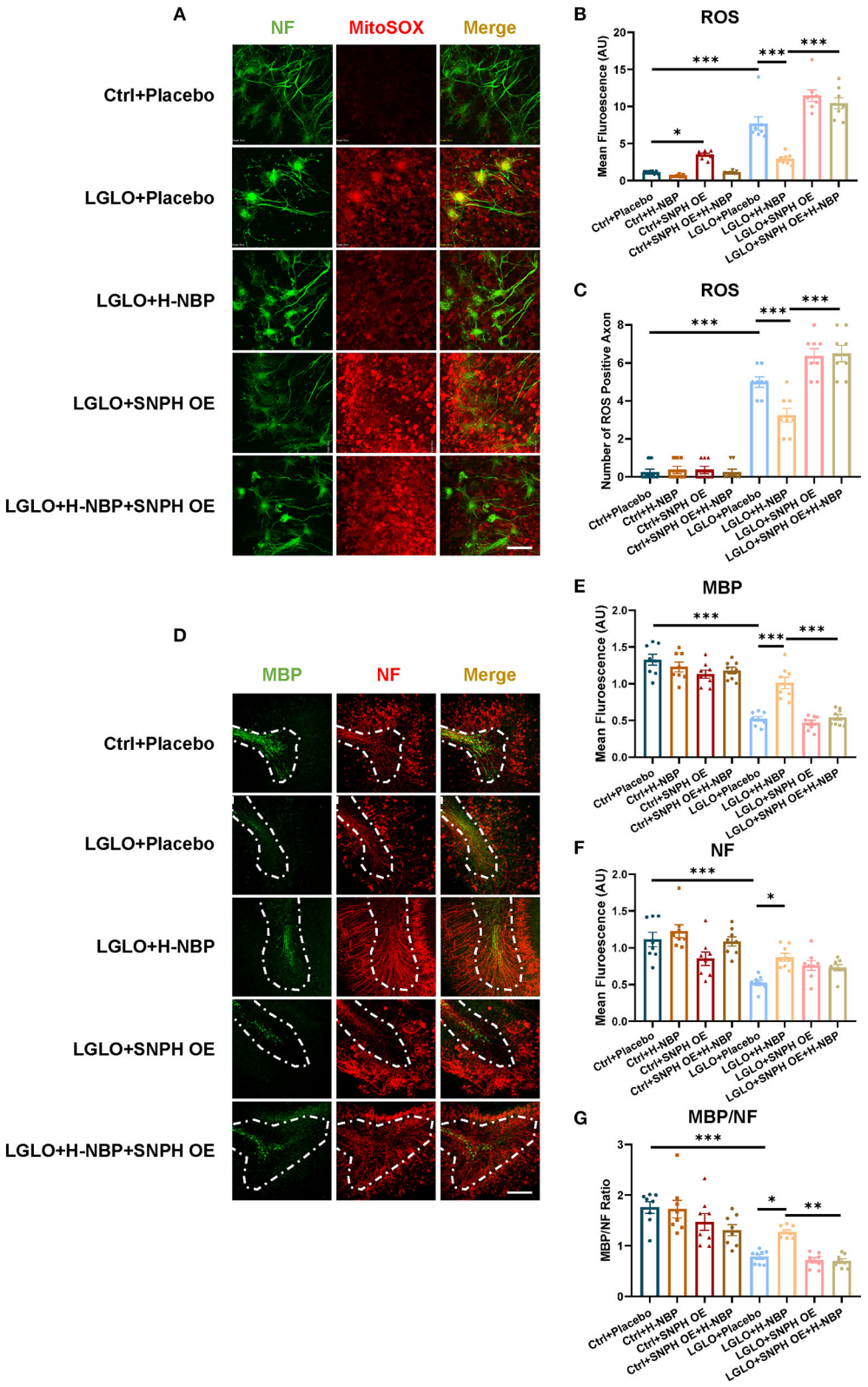


**FIGURE 4 |** Enhanced retrograde transport of mitochondria by a high-dose treatment of D1-NBP alleviated demyelination by decreasing the ROS production among the axons. **(A–C)** Representative confocal images **(A)** and quantitative analysis of the ROS expression **(B)** and the number of ROS positive axons **(C)**. Scale bar,

*(Continued)*

**FIGURE 4 |** 100 μm. The high-dose treatment of D1-NBP mitigated LGLO-induced ROS generation. A one-way ANOVA with Tukey's correction, $n = 8$ slices per group. **(D–G)** Representative confocal images **(D)** and quantitative analysis of maltose binding protein (MBP) (green) expression **(E)**, NF (red) expression **(F)**, and the MBP/NF ratio **(G)**. High dose of DI-NBP treatment alleviated LGLO-induced demyelination. Scale bar, 50 μm. A one-way ANOVA with Tukey's correction. $n = 8$ slices per group. Data are represented as means ± SEM (*$p < 0.05$; **$p < 0.01$; ***$p < 0.001$; ns, non-significant differences).

hypoperfusion, we used the BCAS mouse model in which coils were placed around the bilateral common carotid arteries. After BCAS modeling, demyelination and cognitive impairment were significant at day 28 after BCAS, indicating the successful modeling of hypoperfusion-induced VaD (**Figures 1A–F**). For the D1-NBP treatment group, the mice were given daily intragastric administration of Dl-NBP or Placebo 1 day after BCAS until sacrifice. The status of myelination of the different treatment groups was evaluated by TEM. It could be observed that the whole-brain hypoperfusion by BCAS changed the overall axonal G-ratio distribution to a higher G-ratio rate, which is accompanied by a significant increase of G-ratio in the BCAS group. Although a low-dose treatment of D1-NBP (L-NBP, 50 mg/kg/day) did not retrieve demyelination, an increased dose of D1-NBP treatment (H-NBP) to a 100 mg/kg/day robustly alleviated the BCAS-induced demyelination (**Figures 1A–C**).

We further evaluated the therapeutic effect of D1-NBP on BCAS-induced cognitive impairment, which is tested by the eight-arm radial maze. In the BCAS treatment group, the mice exhibited higher revisiting errors and a lower different arm choice in the first eight entries, indicating a significant impairment of working memory in the BCAS mice. Reference memory errors showed that reference memory was not influenced by BCAS. Consistent with the previous results, the high dose DI-NBP treatment significantly mitigated the impaired working memory by BCAS (**Figures 1D–F**). Altogether, we found that a high-dose treatment of DI-NBP enabled the retrieval of demyelination and cognitive impairment induced by whole-brain hypoperfusion.

## Alleviated Demyelination and Cognitive Impairment by DI-NBP Treatment Is Accompanied With Decreased Mitochondrial Accumulation Among the Axons

Compared to myelin, the axons are more vulnerable to the hypoxic-ischemic environment (Cui et al., 2020). Since mitochondria and its related mitochondrial dynamics are the major therapeutic targets of D1-NBP in various models of diseases, we reasoned that the therapeutic targets of D1-NBP on hypoxic-ischemic demyelination are done by regulating the axonal mitochondrial dynamics in the BCAS mice. By detecting the mitochondrial load among the axons using TEM, we found that the mitochondrial load among the axons was significantly increased in the BCAS group, which was accompanied with abnormal mitochondrial morphology. However, a high-dose treatment of DI-NBP significantly mitigated the mitochondrial load and alleviated the abnormal mitochondrial morphology in the BCAS mice (**Figures 2A–D**).

Mitochondrial load among the axons was further determined by mitochondrial dynamics and motor proteins that underlie the changes in the mitochondrial dynamics. We probed the protein changes related to mitochondrial dynamics. Although motor proteins, such as Miro and Milton, did not show significant changes after BCAS, SNPH, which anchored the mitochondria to the microtube, showed significant elevation after BCAS. Interestingly, a high-dose treatment of D1-NBP significantly mitigated the SNPH expression, indicating that a high-dose treatment of DI-NBP mitigated mitochondrial accumulation probably by inhibiting the expression of SNPH (**Figures 2E,F**).

## DI-NBP Alleviates Mitochondrial Accumulation by Promoting Mitochondrial Dynamics

To further clarify the mechanisms underlying the mitigated mitochondrial accumulation by D1-NBP, we established an *in vitro* model of hypoperfusion by supplying chronic LGLO conditions in the culture containing slices of cerebellum. We used lentivirus to overexpress SNPH, and the slices of cerebellum were transfected 72 h before the LGLO treatment. Right after the LGLO treatment, D1-NBP, at a dose of 50 μm, was added to the culture medium and the mitochondrial dynamics were assessed 48 h later.

We found that the LGLO treatment significantly increased the mitochondrial load, which was accompanied with decreased mitochondrial dynamics, as evidenced by increased stationary mitochondria after LGLO. Interestingly, the DI-NBP treatment rescued the dynamic drop by LGLO and alleviated the mitochondrial load among the axons. Since we found that a high-dose treatment of DI-NBP mitigates mitochondrial load by inhibiting the expression of SNPH *in vivo*, we further overexpressed the SNPH on the cultured slices and found that the alleviated mitochondrial load by a high dose of DI-NBP was abolished by the SNPH OE (**Figures 3A–D**).

## Enhanced Mitochondrial Dynamics by DI-NBP Alleviates Demyelination by Decreasing ROS Production Among the Axons

Functional mitochondrial dynamics plays a critical role in maintaining mitochondrial homeostasis. Impaired transportation of mitochondria and mitochondrial overload in the axons are harmful to neurons, especially in terms of disrupted clearance of malfunctioning mitochondria through retrograde transport (López-Doménech et al., 2018). Increased ROS production has also been reported to damage myelination in the model of multiple sclerosis (MS) (Su et al., 2013). We, therefore, detected mitochondrial ROS production after LGLO. We found that the production of ROS was elevated after LGLO, but the D1-NBP treatment significantly decreased the ROS among axons and mitigated the overall ROS production

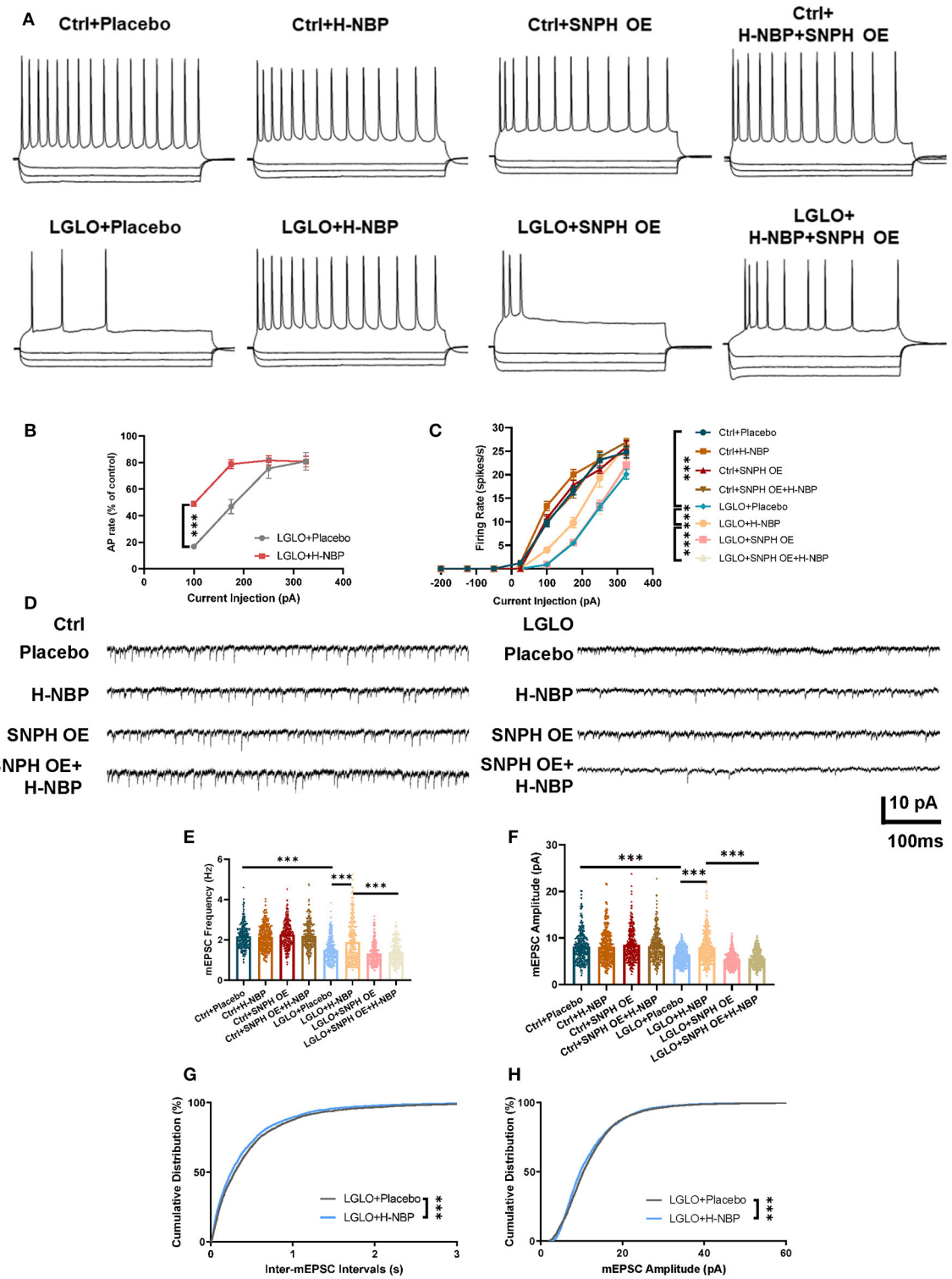


**FIGURE 5 |** Enhanced anterograde transport of mitochondria by a high-dose treatment of D1-NBP retrieved impaired neuronal synapse signaling. **(A–C)** Representative firing responses **(A)** to depolarizing (175 pA) and hyperpolarizing (−50, −135, and −200 pA) current injections and quantitative analysis percentage of control firing rates and **(B)** firing rate responses to a series of linear current injections (−200 to −50 pA) **(C)** in different treated cerebellum slices. A two-way ANOVA with the Dunnett's *post-hoc* test. For the percentage of the control firing rate analysis, $n = 9$ neurons per group (3 neurons per slices). For firing rate responses to a series of linear current injection analysis, $n = 9$ neurons per group (3 neurons per slices). **(D–H)** Representative mEPSC traces **(D)** and quantitative analysis of

*(Continued)*

**FIGURE 5 |** miniature excitatory postsynaptic current (mEPSC) frequency **(E)**, amplitude **(F)**, and cumulative distribution of inter-mEPSC interval **(G)** and mEPSCamplitude **(H)**. Under LGLO conditions, impaired intrinsic neuronal excitability and synapse function showed remarkable improvement by H-NBP treatment. For mEPSC frequency and amplitude, one-way ANOVA with Tukey's correction. For cumulative distribution of inter-mEPSC interval and mEPSC amplitude, the Mann–Whitney test. For mEPSC frequency, $n = 30$ per group. For mEPSC amplitude, $n = 30$ per group. For cumulative distribution of inter-mEPSC interval, $n =$ 4,291 per group. For cumulative distribution of mEPSC amplitude, $n = 4{,}319$ per group. Scale bar, 10 pA and 100 ms, respectively. Data are represented as means ± SEM (***$p < 0.001$; ns, non-significant differences).

(**Figures 4A–C**). Thus, the impaired mitochondrial dynamics were responsible for the mitochondrial accumulation and it significantly increased the production of ROS among the axons. This is harmful for myelination, as evidenced by the significantly decreased MBP expression, NF expression, and MBP/NF ratio in the LGLO group. The DI-NBP mitigated myelination, which is dependent on SNPH (**Figures 4D–G**).

Together, the DI-NBP treatment decreased the ROS production among axons and rescued myelination, which is related to the improved mitochondria retrograde transport of mitochondria.

## Enhanced Dynamics of Mitochondria by DI-NBP Retrieves Impaired Neuronal Synapse Signaling

Anterograde transport of mitochondria replenishes fresh mitochondria necessary for synaptic function (Hollenbeck and Saxton, 2005; Lovas and Wang, 2013). Since we detected an increased anterograde mitochondrial transport, we then tested the changes in the synapse signaling after DI-NBP treatment and under LGLO by patch-clamp. The LGLO treatment resulted in a remarkable drop in firing rate at all injection amplitudes and the most significant drop in firing rate was observed in relatively small current injections. However, the DI-NBP treatment rescued the neuronal intrinsic excitability and SNPH OE abolished the therapeutic effect of D1-NBP to some extent (**Figures 5A–C**). We further tested the changes in the synaptic signaling after LGLO. Both mEPSC amplitude and frequency decreased dramatically after the LGLO treatment, whereas a high dose of DI-NBP retrieved the drop of mEPSC amplitude and frequency, and SNPH OE abolished these therapeutic effects (**Figures 5D–F**). A cumulative mEPSC distribution curve analysis showed that the D1-NBP treatment built up a significantly more abundant mEPSC amplitude and smaller inter-mEPSC intervals (**Figures 5G,H**). These results indicated that D1-NBP promoted the neuronal intrinsic excitability and synapse function, which is related to mitochondrial anterograde transportation.

## DI-NBP Mitigates Demyelination and Cognitive Impairment by Inhibiting SNPH *in vivo*

Based on our *in vitro* findings that SNPH OE abolished the effects of DI-NBP in promoting mitochondrial dynamics, we further validated whether SNPH underlies the effects of DI-NBP in mitigating demyelination and cognitive impairment in the BCAS model. An AAV 2/9 overexpressing SNPH was stereoscopically injected into lateral ventricles in neonatal mice. A BCAS surgery was performed at 2 months of age. We found that SNPH OE significantly abolished the therapeutic effect of D1-NBP on mitigating demyelination, as indicated by the elevated G-ratio after SNPH OE in the high-dose DI-NBP treatment group (**Figures 6A,B**). Meanwhile, decreased mitochondrial load and recovered mitochondrial morphology in the high-dose DI-NBP treatment group were also diminished by SNPH OE (**Figures 6C–E**). Moreover, increased synapse through a high-dose treatment of D1-NBP was lost in the DI-NBP+SNPH OE group, which was accompanied by fewer mushroom-shaped synapses (**Figures 6F–H**). Improved working memory by DI-NBP was abandoned by SNPH OE (**Figures 6I–K**).

From the above results, we could draw the conclusion that the therapeutic potential of D1-NBP on mitigating demyelination and cognitive impairment in hypoxic–ischemic demyelination was done by abolishing SNPH elevation among the axons, which retrieved the malfunctioned mitochondrial dynamics and promoted the anterograde mitochondrial transport for synapse signaling and retrograde mitochondrial transport for ROS alleviation by mitophagy.

# DISCUSSION

The results of the present study have demonstrated the effects of Dl-NBP on mitigating demyelination as well as the effects of Dl-NBP in promoting axonal mitochondrial dynamics in WMLs using a BCAS mice model as well as an *in vitro* brain slice culture treated with LGLO. Our results demonstrated that the mitochondrial dynamics were suppressed while the static mitochondria accumulated in the axons after an injury to ischemia/hypoxia, which was mediated by the elevated expression of SNPH, an axonal specific arching protein. A high-dose treatment of Dl-NBP improved the anterograde and retrograde transport of mitochondria and reduced mitochondrial accumulation in axons, thus arresting myelin disruption and improving the electrical function of the synapse. The high-dose treatment of Dl-NBP also improved the number of synapses and cognitive function. In addition, we investigated the mechanism of Dl-NBP and revealed that a high-dose treatment of Dl-NBP suppressed the expression of SNPH. SNPH OE abolished the protective function of Dl-NBP in reducing demyelination and improving the cognitive function.

White matter lesions, also termed leukoaraiosis, are very common and are considered as an important contributor to cognitive decline, especially in the elderly (Alber et al., 2019). The primary cerebrovascular pathologies that cause WMLs include multi-arteriolosclerosis, carotid stenosis, or occlusion, which lead to cerebral hypoperfusion in deep white matter regions (van Norden et al., 2011). White matter, composed of bundles of

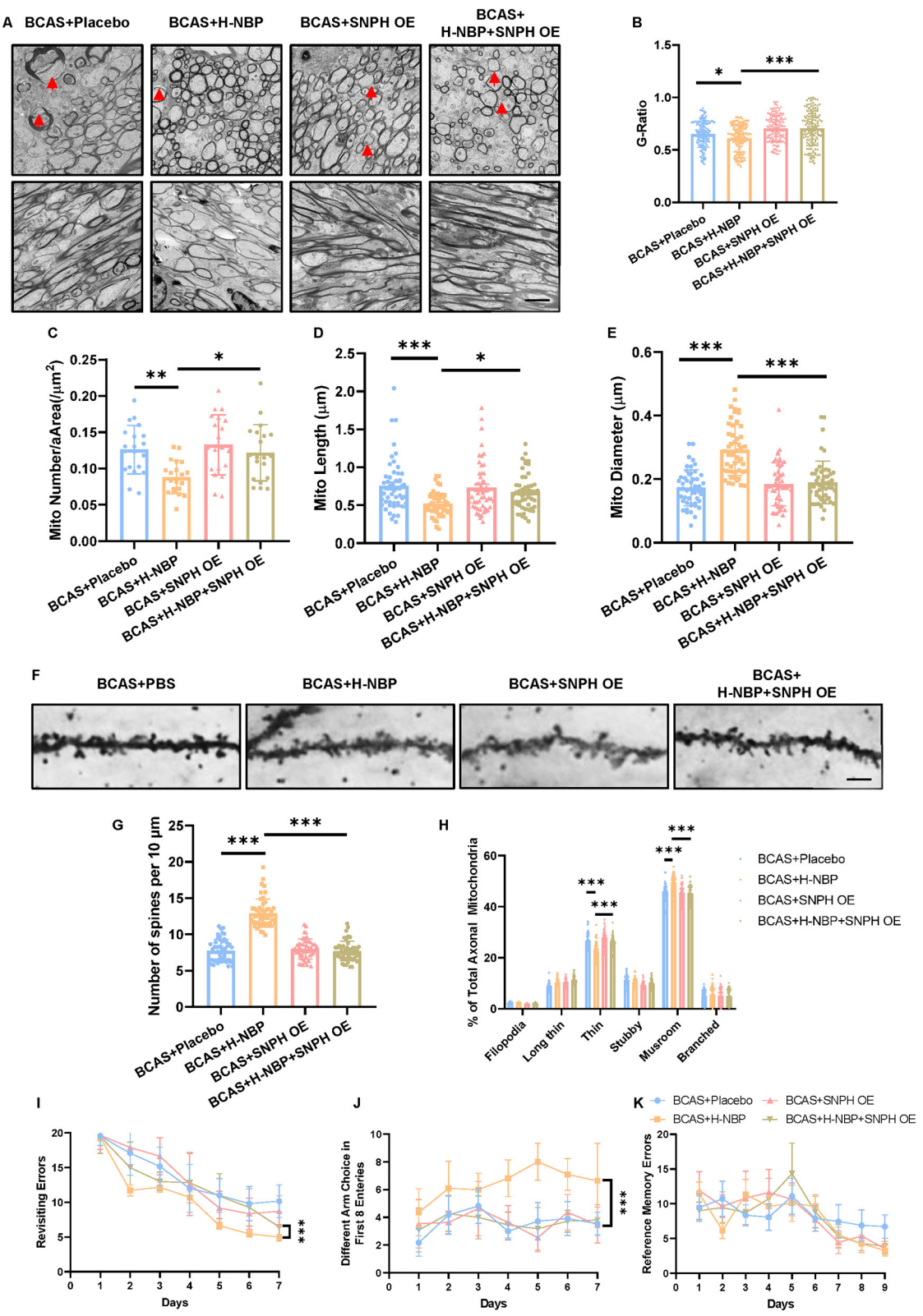


**FIGURE 6 | (A)** High-dose treatment of D1-NBP mitigated demyelination and cognitive impairment by rescuing mitochondrial dynamic *in vivo*. **(A–E)** Representative TEM images depicting myelination status (Upper panel) and mitochondrial load in the axons **(A)** and quantitative analysis of the G-ratio **(B)**, mitochondrial load per

*(Continued)*

**FIGURE 6 |** area **(C)**, mitochondrial length **(D)**, and mitochondrial diameter **(E)** in BCAS+Placebo, BCAS+H-NBP, BCAS+SNPH OE, and BCAS+SNPH OE+H-NBP groups. The therapeutic effects of H-NBP on mitigating demyelination and cognitive impairment were dependent on mitochondrial dynamics. Scale bar, 2 μm. A one-way ANOVA with Tukey's correction. For G-ratio, $n = 80$ myelinated axons. For mitochondrial load per area analysis, $n = 20$ visual fields (4 visual fields per mouse, 5 mice per group). For mitochondrial length analysis, $n = 50$ (10 mitochondria per mouse, 5 mice per group). For mitochondrial diameter analysis, $n = 50$ (10 mitochondria per mouse, 5 mice per group). **(F–H)** Representative silver staining images. **(F)** Quantitative analysis of the number of spines per 10 μm. **(G)** Different kinds of spine morphology in different groups **(H)**. A one-way ANOVA with Tukey's correction. For the number of spines per 10 μm analysis, $n = 10$ axons per mouse, 5 mice per group. For different kinds of spine morphology analysis, $n = 10$ axons per mouse, 5 mice per group. Scale bar, 10 μm. **(I–K)** Working and reference memory were assessed by the eight-arm radial maze. The improvement of working memory by H-NBP in BCAS mice was abolished by SNPH OE, as evidenced by the increased revisiting errors. **(I)** Less different choices **(J)** in the BCAS+H-NBP+SNPH OE group. There is no significant difference in the spatial reference memory between different groups **(K)**. A two-way ANOVA with the Dunnett's *post-hoc* test, $n = 11$ mice in each group. Data are represented as means ± SD (*$p < 0.05$; **$p < 0.01$; ***$p < 0.001$; ns, non-significant differences).

myelinated axons, plays a vital role in signal transmission. It has been reported that the Dl-NBP treatment improved the learning and memory deficits induced by chronic cerebral hypoperfusion in the animal model (Li et al., 2019). We speculate that Dl-NBP improves cognitive function in hypoperfusion partly by preventing the disruption of myelin and increasing the signal transmission. In the present study, we also observed that the Dl-NBP treatment improved the cognitive impairment in the BCAS model. Next, we examined the effects of Dl-NBP on demyelination because the intact and functional myelin is the structural foundation of the electrical signal traveling from the body of the cell down the synapse of the axon. Results showed that a high-dose treatment of Dl-NBP significantly mitigated demyelination compared with the BCAS model group. Further, we evaluated the synapse signaling, which is related to the activity of the central cholinergic system. Results indicated that a high dose of Dl-NBP promoted neuronal intrinsic excitability and synapse function compared with the BCAS model group. These two neuroprotective aspects of Dl-NBP eventually benefited the cognitive function recovery after BCAS.

White matter is more susceptible to chronic cerebral hypoperfusion than gray matter, which involves both axonal and myelin components (Wakita et al., 2002). Myelin is produced by oligodendrocytes, which are attached to the axons and, therefore, could interact with the axons in the central nervous system. During the process of demyelination caused by hypoperfusion, the axonal changes are non-ignorable. It was reported recently that the degradation of axons was accompanied by mitochondrial shortening in the *in vitro* model of WML (Cui et al., 2020). While in our study, we observed abnormal-shaped mitochondria in the BCAS mice showed an increased length and a reduced diameter. After a high-dose treatment of Dl-NBP, the morphological changes of mitochondria recovered significantly. Mitochondria are the most sensitive organisms to hypoxia and respond quickly upon ischemial insult. Normally, mitochondria undergo massive fusion and fission events, as well as transportation along the axons, to continuously maintain their function and maintain the energy supply to cells (Youle and van der Bliek, 2012; Lee and Yoon, 2016; Meyer et al., 2017). An impaired balance of mitochondrial dynamics occurs under hypoperfusion. Meanwhile, we observed an increased number of abnormal mitochondria accumulated in the axons of BCAS mice, but a high-dose treatment of Dl-NBP reduced their accumulation. These results indicated that Dl-NBP targets axonal mitochondria in alleviating demyelination damage.

Syntaphilin is a major mitochondrial anchoring protein targeting the axons (Joshi et al., 2019). The SNPH deletion produces striking benefits in the MS demyelination model by prolonging survival, reducing cerebellar damage, suppressing oxidative stress, and improving mitochondrial health (Joshi et al., 2015). Later, we examined the SNPH levels and found a high expression of SNPH in BCAS mice, accompanied with increased stationary mitochondria in the axons. A high-dose treatment of Dl-NBP inhibited the SNPH levels, which then promoted both the anterograde and retrograde transport of mitochondria. Through SNPH OE, the protective effects of Dl-NBP on mitigating demyelination disappeared. Further, the protection of cognitive function was abolished as well. Thus, we found SNPH to be a novel target of Dl-NBP in hypoperfusion-induced WML.

One of the primary roles of mitochondria is to produce ATP. The anterograde transport of mitochondria will increase mitochondrial respiration and ATP production (Roger et al., 2017; Rangaraju et al., 2019). The increased anterograde transport of mitochondria might help the axons to maintain energy stability, and this is likely to underlie the improved synapse signaling function in a high-dose Dl-NBP treated group. The retrograde transport of mitochondria causes mitophagy of dysfunctional mitochondria, which alleviated the ROS production. Since myelin is sensitive to ROS, the reduced ROS production in Dl-NBP treated mice may explain the protection of myelin and keep the structure of the synapses intact.

In conclusion, our results indicate that a high dose of Dl-NBP inhibited the expression of SNPH, which is an axonal specific mitochondrial arching protein. The SNPH inhibition by Dl-NBP alleviates mitochondrial load among the axons and promotes the anterograde and retrograde mitochondrial transport, which then rescued demyelination and cognitive function in the WML model. These findings of our study suggest that Dl-NBP is a promising treatment for alleviating the cognitive dysfunction and alleviating demyelination in WML.

## DATA AVAILABILITY STATEMENT

The original contributions presented in the study are included in the article/supplementary material, further inquiries can be directed to the corresponding authors.

## ETHICS STATEMENT

The animal study was reviewed and approved by the Ethics Committee of Fudan University, Shanghai, China. Written informed consent was obtained from the owners for the participation of their animals in this study.

## AUTHOR CONTRIBUTIONS

YWF and MG drafted the manuscript. YWF and SH carried out the experiment. YWF and HZ helped with the statistics and the preparation of figures. MC and QD designed the experiment. All authors read and approved the final manuscript.

## FUNDING

This study was supported by the National Natural Science Foundation of China (81971013 to MC; 81870915 and 81571109 to QD) and from a Grant from the Science and Technology Commission of Shanghai Municipality (16411970200).

## REFERENCES

Alber, J., Alladi, S., Bae, H. J., Barton, D. A., Beckett, L. A., Bell, J. M., et al. (2019). White matter hyperintensities in vascular contributions to cognitive impairment and dementia (VCID): knowledge gaps and opportunities. *Alzheimers Dement* 5, 107–117. doi: 10.1016/j.trci.2019.02.001

Bargiela, D., Burr, S. P., and Chinnery, P. F. (2018). Mitochondria and hypoxia: metabolic crosstalk in cell-fate decisions. *Trends Endocrinol. Metab.* 29, 249–259. doi: 10.1016/j.tem.2018.02.002

Ben-Ari, H., Lifschytz, T., Wolf, G., Rigbi, A., Blumenfeld-Katzir, T., Merzel, T. K., et al. (2019). White matter lesions, cerebral inflammation and cognitive function in a mouse model of cerebral hypoperfusion. *Brain Res.* 1711, 193–201. doi: 10.1016/j.brainres.2019.01.017

Chen, D., Yin, Y., Shi, J., Yang, F., Wang, K., Zhao, F., et al. (2020). DL-3-n-butylphthalide improves cerebral hypoperfusion in patients with large cerebral atherosclerotic stenosis: a single-center, randomized, double-blind, placebo-controlled study. *BMC Neurol.* 20:212. doi: 10.1186/s12883-020-01801-5

Chen, J., Liu, N., Wang, X., Zhao, Y., He, J., Yang, L., et al. (2019). Dl-3-n-butylphthalide inhibits phenytoin-induced neuronal apoptosis in rat hippocampus and cerebellum. *J. Integr. Neurosci.* 18, 277–283. doi: 10.31083/j.jin.2019.03.174

Chen, N., Zhou, Z., Li, J., Li, B., Feng, J., He, D., et al. (2018). 3-n-butylphthalide exerts neuroprotective effects by enhancing anti-oxidation and attenuating mitochondrial dysfunction in an *in vitro* model of ischemic stroke. *Drug Des. Devel. Ther.* 12, 4261–4271. doi: 10.2147/DDDT.S189472

Cui, L. Y., Zhu, Y. C., Gao, S., Wang, J. M., Peng, B., Ni, J., et al. (2013). Ninety-day administration of dl-3-n-butylphthalide for acute ischemic stroke: a randomized, double-blind trial. *Chin. Med. J.* 126, 3405–3410. doi: 10.3760/cma.j.issn.0366-6999.20123240

Cui, Y., Jin, X., Choi, D. J., Choi, J. Y., Kim, H. S., Hwang, D. H., et al. (2020). Axonal degeneration in an *in vitro* model of ischemic white matter injury. *Neurobiol. Dis.* 134:104672. doi: 10.1016/j.nbd.2019.104672

Datta, G., Colasanti, A., Rabiner, E. A., Gunn, R. N., Malik, O., Ciccarelli, O., et al. (2017). Neuroinflammation and its relationship to changes in brain volume and white matter lesions in multiple sclerosis. *Brain* 140, 2927–2938. doi: 10.1093/brain/awx228

Du, F. (2019). Golgi-cox staining of neuronal dendrites and dendritic spines with FD Rapid GolgiStain$^{TM}$ Kit. *Curr. Protoc. Neurosci.* 88:e69. doi: 10.1002/cpns.69

Feng, Y. W., Huang, Y. Q., Yan, Y., Li, G., He, X. F., Liang, F. Y., et al. (2020a). Phasic GABA signaling mediates the protective effects of cTBS against cerebral ischemia in mice. *Neurosci. Lett.* 715:134611. doi: 10.1016/j.neulet.2019.134611

Feng, Y. W., Wu, C., Liang, F. Y., Lin, T., Li, W. Q., Jing, Y. H., et al. (2020b). hUCMSCs mitigate LPS-induced trained immunity in ischemic stroke. *Front. Immunol.* 11:1746. doi: 10.3389/fimmu.2020.01746

Guo, M., Ma, X., Feng, Y., Han, S., Dong, Q., Cui, M., et al. (2019). In chronic hypoxia, glucose availability and hypoxic severity dictate the balance between HIF-1 and HIF-2 in astrocytes. *FASEB J.* 33, 11123–11136. doi: 10.1096/fj.201900402RR

Hollenbeck, P. J., and Saxton, W. M. (2005). The axonal transport of mitochondria. *J. Cell Sci.* 118(Pt 23), 5411–5419. doi: 10.1242/jcs.02745

Joshi, D. C., Zhang, C. L., Babujee, L., Vevea, J. D., August, B. K., Sheng, Z. H., et al. (2019). Inappropriate intrusion of an axonal mitochondrial anchor into dendrites causes neurodegeneration. *Cell Rep.* 29, 685–696.e5. doi: 10.1016/j.celrep.2019.09.012

Joshi, D. C., Zhang, C. L., Lin, T. M., Gusain, A., Harris, M. G., Tree, E., et al. (2015). Deletion of mitochondrial anchoring protects dysmyelinating shiverer: implications for progressive MS. *J. Neurosci.* 35, 5293–5306. doi: 10.1523/JNEUROSCI.3859-14.2015

Lee, H., and Yoon, Y. (2016). Mitochondrial fission and fusion. *Biochem. Soc. Trans.* 44, 1725–1735. doi: 10.1042/BST20160129

Lema, A., Bishop, C., Malik, O., Mattoscio, M., Ali, R., Nicholas, R., et al. (2017). A comparison of magnetization transfer methods to assess brain and cervical cord microstructure in multiple sclerosis. *J. Neuroimaging* 27, 221–226. doi: 10.1111/jon.12377

Li, W., Wei, D., Lin, J., Liang, J., Xie, X., Song, K., et al. (2019). Dl-3-n-butylphthalide reduces cognitive impairment induced by chronic cerebral hypoperfusion through GDNF/GFRα1/Ret signaling preventing hippocampal neuron apoptosis. *Front. Cell. Neurosci.* 13:351. doi: 10.3389/fncel.2019.00351

Lin, M. Y., Cheng, X. T., Tammineni, P., Xie, Y., Zhou, B., Cai, Q., et al. (2017). Releasing syntaphilin removes stressed mitochondria from axons independent of mitophagy under pathophysiological conditions. *Neuron.* 94, 595–610.e6. doi: 10.1016/j.neuron.2017.04.004

López-Doménech, G., Covill-Cooke, C., Ivankovic, D., Halff, E. F., Sheehan, D. F., Norkett, R., et al. (2018). Miro proteins coordinate microtubule- and actin-dependent mitochondrial transport and distribution. *EMBO J.* 37, 321–336. doi: 10.15252/embj.201696380

Lovas, J. R., and Wang, X. (2013). The meaning of mitochondrial movement to a neuron's life. *Biochim. Biophys. Acta* 1833, 184–194. doi: 10.1016/j.bbamcr.2012.04.007

Meyer, J. N., Leuthner, T. C., and Luz, A. L. (2017). Mitochondrial fusion, fission, and mitochondrial toxicity. *Toxicology* 391, 42–53. doi: 10.1016/j.tox.2017.07.019

Palikaras, K., Lionaki, E., and Tavernarakis, N. (2015). Coordination of mitophagy and mitochondrial biogenesis during ageing in *C. elegans*. *Nature* 521, 525–528. doi: 10.1038/nature14300

Rangaraju, V., Lewis, T. L. Jr., Hirabayashi, Y., Bergami, M., Motori, E., Cartoni, R., et al. (2019). Pleiotropic mitochondria: the influence of mitochondria on neuronal development and disease. *J. Neurosci.* 39, 8200–8208. doi: 10.1523/JNEUROSCI.1157-19.2019

Roger, A. J., Muñoz-Gómez, S. A., and Kamikawa, R. (2017). The origin and diversification of mitochondria. *Curr. Biol.* 27, r1177–r1192. doi: 10.1016/j.cub.2017.09.015

Su, K., Bourdette, D., and Forte, M. (2013). Mitochondrial dysfunction and neurodegeneration in multiple sclerosis. *Front. Physiol.* 4:169. doi: 10.3389/fphys.2013.00169

Sun, Y., Cheng, X., Wang, H., Mu, X., Liang, Y., Luo, Y., et al. (2017). dl-3-n-butylphthalide promotes neuroplasticity and motor recovery in stroke rats. *Behav. Brain Res.* 329, 67–74. doi: 10.1016/j.bbr.2017.04.039

Thomas, L. W., and Ashcroft, M. (2019). Exploring the molecular interface between hypoxia-inducible factor signalling and mitochondria. *Cell. Mol. Life Sci.* 76, 1759–1777. doi: 10.1007/s00018-019-03039-y

Tian, A., Li, W., Zai, Q., Li, H., and Zhang, R. W. (2020). 3-N-Butyphthalide improves learning and memory in rats with vascular cognitive impairment by activating the SIRT1/BDNF pathway. *Mol. Med. Rep*. 22, 525–533. doi: 10.3892/mmr.2020.11106

van Norden, A. G., de Laat, K. F., Gons, R. A., van Uden, I. W., van Dijk, E. J., van Oudheusden, L. J., et al. (2011). Causes and consequences of cerebral small vessel disease. The RUN DMC study: a prospective cohort study. Study rationale and protocol. *BMC Neurol*. 11:29. doi: 10.1186/1471-2377-11-29

Wakita, H., Tomimoto, H., Akiguchi, I., Matsuo, A., Lin, J. X., Ihara, M., et al. (2002). Axonal damage and demyelination in the white matter after chronic cerebral hypoperfusion in the rat. *Brain Res*. 924, 63–70. doi: 10.1016/S0006-8993(01)03223-1

Wang, C. Y., Xu, Y., Wang, X., Guo, C., Wang, T., and Wang, Z. Y. (2019). Dl-3-n-butylphthalide inhibits NLRP3 inflammasome and mitigates Alzheimer's-like pathology via Nrf2-TXNIP-TrX axis. *Antioxid. Redox Signal*. 30, 1411–1431. doi: 10.1089/ars.2017.7440

Wang, S., Ma, F., Huang, L., Zhang, Y., Peng, Y., Xing, C., et al. (2018). Dl-3-n-butylphthalide (NBP): a promising therapeutic agent for ischemic stroke. *CNS Neurol. Disord. Drug Targets* 17, 338–347. doi: 10.2174/1871527317666180612125843

Xu, H., Baracskay, P., O'Neill, J., and Csicsvari, J. (2019). Assembly responses of hippocampal CA1 place cells predict learned behavior in goal-directed spatial tasks on the radial eight-arm maze. *Neuron* 101, 119–132.e4. doi: 10.1016/j.neuron.2018.11.015

Xue, L.-X., Zhang, T., Zhao, Y.-W., Geng, Z., Chen, J.-J., and Chen, H. (2016). Efficacy and safety comparison of DL-3-n-butylphthalide and Cerebrolysin: Effects on neurological and behavioral outcomes in acute ischemic stroke. *Exp. Ther. Med*. 11, 2015–2020. doi: 10.3892/etm.2016.3139

Yang, C. S., Guo, A., Li, Y., Shi, K., Shi, F. D., and Li, M. (2019). Dl-3-n-butylphthalide reduces neurovascular inflammation and ischemic brain injury in mice. *Aging Dis*. 10, 964–976. doi: 10.14336/AD.2019.0608

Youle, R. J., and van der Bliek, A. M. (2012). Mitochondrial fission, fusion, and stress. *Science* 337, 1062–1065. doi: 10.1126/science.1219855

Zheng, Y., Wu, X., Chen, Z., and Zhang, X. (2019). Come and eat: mitochondrial transport guides mitophagy in ischemic neuronal axons. *Autophagy* 15, 1483–1484. doi: 10.1080/15548627.2019.1618099

**Conflict of Interest:** The authors declare that the research was conducted in the absence of any commercial or financial relationships that could be construed as a potential conflict of interest.

frontiers in Aging Neuroscience

ORIGINAL RESEARCH
published: 15 March 2021
doi: 10.3389/fnagi.2021.596829

# A New Classification of Anterior Choroidal Artery Aneurysms and Its Clinical Application

*Yu Duan*[1], *Xuanfeng Qin*[2], *Qinqzhu An*[2], *Yikui Liu*[1], *Jian Li*[1] *and Gong Chen*[2]*

[1] Department of Neurosurgery, Huadong Hospital, Fudan University, Shanghai, China, [2] Department of Neurosurgery, Huashan Hospital, Fudan University, Shanghai, China

**Background and Purpose:** The aim of this study was to compare the different subtypes of anterior choroidal artery (AChoA) aneurysm based on a new classification and to analyze the risk factors according to individual endovascular treatment (EVT).

**Methods:** In the new classification, AChoA aneurysms are classified into independent type (I type) and dependent type (II type) based on the relationship between the AChoA and the aneurysm. II type aneurysms have three subtypes, IIa (neck), IIb (body), and IIc (direct). We retrospectively analyzed 52 cases of AChoA aneurysm treated in our center between 2015 to 2019. There were 13 (25.0%) I type aneurysms, 24 (46.2%) IIa aneurysms, 15 (28.8%) IIb aneurysms, and no IIc type; 28 cases had a subarachnoid hemorrhage. According to our preoperative EVT plan for the different subtypes: II type should achieve Raymond-Roy Occlusion Class 1 (RROC 1) where possible. To protect the AChoA, it is best to preserve the neck of the IIa type aneurysms (RROC 2), and RROC 3 is enough for IIb type.

**Results:** Ten asymptomatic cases with minimal aneurysms were treated conservatively. Of the other cases, 42 were treated with individualized EVT (26 with a simple coil, 6 with balloon-assisted coiling, 7 with stent-assisted coiling, and 3 by flow diverter. Different subtypes had different RROC ($Z = 14.026$, $P = 0.001$). IIb type aneurysms ($\chi^2 = 7.54$, $P = 0.023$) were one of the factors related to temporary or permanent AChoA injury during surgery. Overall, two patients (IIa = 1, IIb = 1) developed contralateral hemiparesis.

**Conclusions:** The new classification diagram clearly shows the features of all types of AChoA aneurysm and makes EVT planning more explicit. The II type (particularly IIb) was a potential risk factor for AChoA injury.

**Keywords: anterior choroidal artery aneurysm, classification, endovascular intervention therapy, risk, embolization**

OPEN ACCESS

***Edited by:***
*Yuanli Zhao,*
*Capital Medical University, China*

***Reviewed by:***
*Henning U. Voss,*
*Cornell University, United States*
*Steve M. Cordina,*
*University of South Alabama, United States*
*Alberto Maud,*
*Texas Tech University Health Sciences Center El Paso, United States*

***Correspondence:**
*Gong Chen*
*onlycg1000@sina.com*

***Received:*** *20 August 2020*
***Accepted:*** *18 February 2021*
***Published:*** *15 March 2021*

***Citation:***
*Duan Y, Qin X, An Q, Liu Y, Li J and Chen G (2021) A New Classification of Anterior Choroidal Artery Aneurysms and Its Clinical Application. Front. Aging Neurosci. 13:596829. doi: 10.3389/fnagi.2021.596829*

## INTRODUCTION

Anterior choroidal artery (AChoA) aneurysms are rare, accounting for approximately 2–5% of all intracranial aneurysms (Locksley et al., 1966; Kim et al., 2009; Aoki et al., 2016). Compared with clipping, endovascular treatment (EVT) is an established treatment option for intracranial aneurysms with shorter hospital stays and better recovery specially in the elderly people (Sadamasa et al., 2014). When dealing with such aneurysms, it is important to pack the aneurysm more densely to maintain AChoA patency, however, the delicate AChoA can be easily injured, resulting in serious

complications (Friedman et al., 2001; Kim et al., 2008; Kang et al., 2009; Andre et al., 2018).

Over the last few decades, several different classifications for AChoA aneurysms have been suggested; however, they have usually been based on the surgeon's subjective feeling. Some are used for clipping (Friedman et al., 2001; Heros, 2010; Li et al., 2012) and some only for EVT (Kim et al., 2008; Kang et al., 2009; Senturk et al., 2009). No unified standard has been established and the treatment of these aneurysms is still challenging. In this study, we propose a new classification of AChoA aneurysms and provide a comprehensive analysis of clinical efficacy and the risk factors for EVT based on the new classification.

# METHODS

## Clinical Data

From January 2015 to October 2019, 52 patients with a diagnosis of AChoA aneurysm were recruited in our single center. The patients' mean age was 53.8 ± 9.4 years, and there were 21 males and 31 females. Twenty-eight cases (53.8%) presented as subarachnoid hemorrhage (SAH). Of these, 15 cases were Hunt-Hess grade I, 10 cases were grade II, and 3 were grade III.

## The New Classification of AChoA Aneurysms

The definitive diagnosis was made by digital subtraction angiography (DSA) and 3D-DSA in all patients. The aneurysms were divided into two types according to the relationship between the aneurysm and AChoA. The independent type (I type) and dependent type (II type) in the new classification are shown in **Figure 1**. In the I type, the aneurysm is located independently at the AChoA section of the internal carotid artery (ICA). In the II type, the aneurysm has a common trunk with the AChoA. In the IIa subtype the neck of the aneurysm is the origin of the AChoA (neck type), while in the IIb type the AChoA originates from the body of aneurysm (body type). The IIc type aneurysm is located directly at the AChoA (direct type). Of the 52 cases, 13 aneurysms (25.0%) were I type, 24 (46.2%) were IIa, 15 (28.8%) were IIb and there were no IIc type aneurysms (0%).

## Interventional Methods

First, having identified the subtype of aneurysm, the EVT target was determined. For I type aneurysms, as with other side-wall aneurysms, the aim was to reach Raymond-Ray Occlusion Class (RROC) 1 where possible. For II type aneurysms, however, it is more important to maintain AChoA patency; the neck must be preserved (RROC 2) for IIa, and RROC 3 is enough for IIb. For ruptured aneurysms, simple coiling and balloon-assisted coiling (BAC) would be the chosen method. Other features of the aneurysm, such as shape, neck width, height (neck-dome), height/width ratio, for example, were considerations for personalized EVT.

## Assessment and Follow Up

The degree of embolism, by RROC, was evaluated by DSA and CTA/MRA (Mascitelli et al., 2015). The clinical score was assessed by the modified Rankin Scale (mRS).

## Statistical Analysis

All data was analyzed by Social Science Version 25.0 for Windows (SPSS, Chicago, Illinois, USA) and presented as mean and SD for continuous variables or as number and percentage for categorical variables. Univariate analysis was performed using Pearson's $\chi^2$ (categorical variables) or one-way analysis of variance for three groups and independent samples $T$ test for two groups (continuous variables, normal distribution), Mann–Whitney $U$ test (abnormal distribution). $P < 0.05$ was taken as statistical significance.

# RESULTS

## Operational Results

The ten asymptomatic cases (9.5%) with minor aneurysms (≤ 2.0 mm) were followed up without intervention. Of the 42 cases treated with EVT, the maximum aneurysm height varied from 1.5 mm to 5.5 (mean 3.51 ± 1.26 mm), the maximum neck width ranged from 1.5 to 5.3 mm (mean 3.26 ± 1.09 mm). Concerning shape, 81% (34/42) of aneurysms were regular and saccular, eight were irregular (fusiform, Gaussian-like shape, or biphasic shape). Multiple aneurysms occurred in 17 cases (40.5%, 17/42), while 13 (31%, 13/42) had a posterior communicating artery (PCA) aneurysm, 2 had an ophthalmic artery aneurysm, and 2 had a middle cerebral artery aneurysm. Thirty cases (71.4%, 30/42) were treated with simple coiling, 3 cases (7.9%, 3/42) with a flow diverter (FD-Tubridge, MicroPort Medical Company, Shanghai, China) and 9 cases (71.4%, 9/42) with stent-assisted coiling (SAC). States), and the other three cases, with Enterprise (Cordis Neurovascular, Miami Six of these were treated with Low-profile Visualized Intraluminal Support (MicroVention, Tustin, CA, United Lakes, FL, United States).

Based on the new classification, the different aneurysm types had different RROCs ($Z = 14.046$, $P = 0.001$, shown in **Table 1**). In addition, compared with unruptured aneurysms treated with SAC, ruptured aneurysms were embolized by coiling or BAC ($Z = -2.833$, $P = 0.005$, shown in **Table 2**). Five patients (four IIb type, one IIa type) suffered AChoA flow reduction or occlusion during the procedure and four were improved by adjusting the coils. The IIb type had the highest risk of AChoA injury ($\chi^2 = 7.54$, $P = 0.023$). After EVT, two patients (all II type) presented with focal infarction of the AChoA area confirmed by CT or MRI, after showing AChoA-related symptoms and none of the AChoA aneurysm treated with flow diversion complicated with AChoA infarct.

## Follow Up

All cases were followed up (from 7 to 62 months, mean 25 months) with assessment by MRA, CTA, or DSA. Three aneurysms (2 IIa, and 1 IIb) had degradation (two at the neck growth, and one at coil extrusion).

By the third postoperative month, two patients presented with progressive neurological improvement, with reductions in their mRS score from 5 to 3 and 3 to 1. During follow up, there were no recurrences of SAH, and no patients got worse or died. The AChoA aneurysms managed without EVT remained stable during follow up.

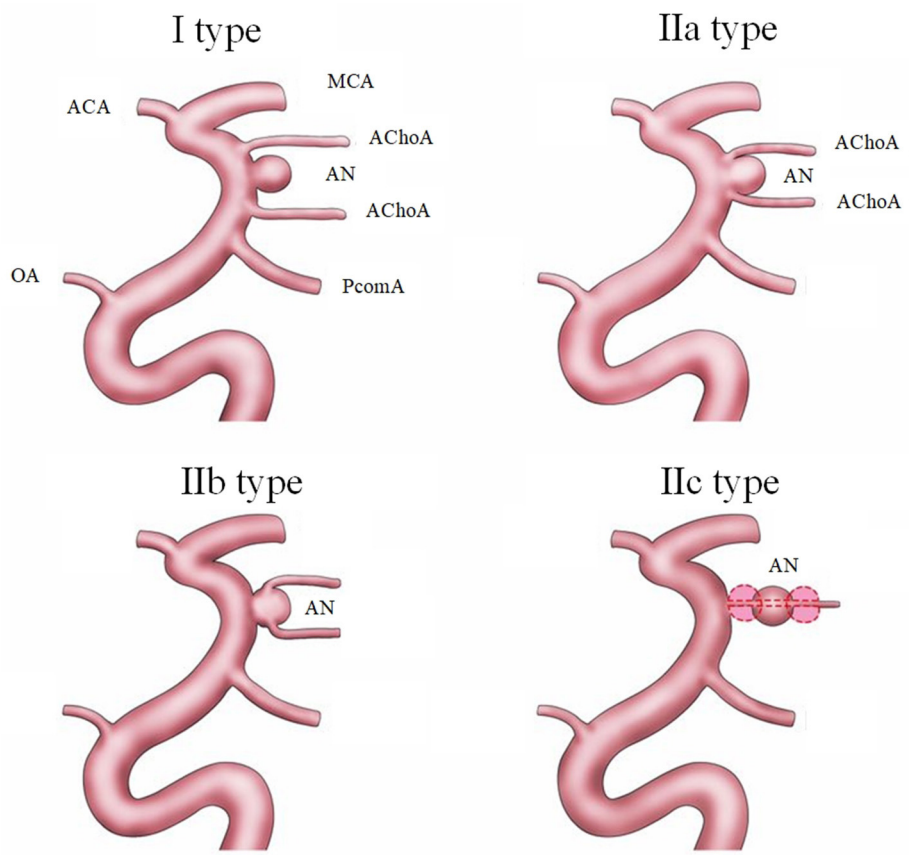


**FIGURE 1 |** The new classification of AChoA aneurysms includes I type (dependent type) and II type (independent type). The II type is further divided into three subtypes: IIa type, (neck), where the AChoA originates from the neck of the aneurysm; the IIb type (body), where the AChoA originates from the body of the aneurysm; and the IIc type (direct), where the aneurysm originates directly from the AChoA.

## DISCUSSION

The terminal fields of supply of the AChoA are the posterior limb of the internal capsule, the beginning of the optic radiation, the lateral geniculate body, medial globus pallidus, and middle third of the crus cerebri (Rhoton et al., 1979; Champeaux et al., 2016; Ghali et al., 2018). If the AChoA is acutely occluded, it can lead to severe complications such as hemiplegia, hemianesthesia, homologous hemianopsia, and dysarthria, (called AChoA-syndromes), because of weak collateral circulation (Friedman et al., 2001). In 1968 and 1978, Drake and Yasargil, respectively, described the relationship between aneurysms and the AChoA according to their experience of a few cases treated by clipping (Drake et al., 1968; Yasargil et al., 1978). Because of technical limitations, the surgery treatment had not raised markedly at that period. In 2001, Friedman delineated three common anatomical variations of AChoA aneurysm according to the origins of AChoA and its spatial position in relation to the aneurysm (Friedman et al., 2001). In 2010, Heros classified the aneurysms into four types based on the spatial position of the aneurysm dome; these were the anterolateral, superolateral, posterolateral, and direct types (Heros, 2010). In 2012, Jin Li et al., summarized two groups based on the relationship between the AChoA and the aneurysm neck. In Group 1, the aneurysm originates from the ICA or the junction of the ICA and AChoA origin. In Group 2, the aneurysm originates entirely or in part from the AChoA itself. They found that Group 2 aneurysms had a higher risk of complications (Li et al., 2012). All the above classifications had significant differences and were based on the surgeons' subjective view. However, classifications based on spatial location does not assist EVT based on 3D-DSA.

Over the last decade, the use of EVT has gradually increased. The most common classification of aneurysms has two types (the independent type, and dependent type) (Kim et al., 2008; Kang et al., 2009; Senturk et al., 2009). In 2008, Cho added one more type, the direct type, in which the aneurysm originates entirely from the AChoA (Cho et al., 2008). In 2016, Aoki designated four types. In type A, the AChoA arises directly from the ICA, in type B, the AChoA arises from the aneurysmal neck, in type C, it arises from the aneurysmal dome, and in type D (truncal type) the aneurysms originate in a part of the AChoA itself. There are also several subtypes of B and C groups, according to the number of AChoA, which are too complicated for general classification criteria (Aoki et al., 2016). In our new classification, referring

**TABLE 1 |** The characteristics of the different types.

| | I-type ($n = 13$) | IIa-type ($n = 24$) | IIb-type ($n = 15$) | Test value | *P* value |
|---|---|---|---|---|---|
| Female (*n*) | 6 | 11 | 9 | 1.255* | 0.534 |
| SAH (*n*) | 6 | 13 | 9 | 1.129* | 0.569 |
| Multiple (*n*) | 4 | 8 | 5 | 1.105* | 0.949 |
| **EVT methods** | | | | | |
| Coiling | 6 | 13 | 7 | 4.028$^{\Delta}$ | 0.379 |
| SAC | 2 | 3 | 2 | | |
| BAC | 1 | 1 | 1 | | |
| FD | 1 | 1 | 1 | | |
| **RROC** | | | | 14.026$^{\Delta}$ | 0.001 |
| 1 | 8 | 0 | 0 | | |
| 2 | 3 | 17 | 0 | | |
| 3a | 0 | 2 | 10 | | |
| 3b | 0 | 0 | 2 | | |
| **Complications** | | | | | |
| AChoAOcclusion | 0 | 1 | 4 | 7.54* | 0.023 |
| Infarction | 0 | 1 | 1 | 0.898* | 0.638 |
| **DSA follow up** | | | | | |
| Improve | 1 | 7 | 6 | | |
| Stable | 9 | 10 | 5 | 1.54$^{\Delta}$ | 0.215 |
| Worsen | 0 | 2 | 1 | | |

**Pearson's $\chi^2$, $^{\Delta}$one-way analysis of variance.*

to the above classifications, we thought the first hierarchy must include the independent type (I type) and the dependent (II type). In the dependent type, it is important to differentiate the neck type (IIa), body type (IIb), and direct types (IIc). The new classification is clear and simple and could be applied for surgical clipping and EVT. We believe it will help to further establish a common, extensive, enforceable guideline.

According to the characteristics of the different subtypes, we redesigned the individual EVT plans. For I type, like the other side-wall aneurysms (Patel et al., 2014), 72.7% achieved complete obliteration without AChoA injury (shown in **Figures 2A–D**) and had a good clinical outcome (Andre et al., 2018). Based on protecting the AChoA, reaching RROC 2 in IIa type (shown in **Figures 2E–H**), and RROC 3a or 3b in IIb type were the goals (shown in **Figure 3**). To achieve the target, techniques such as double microcatheter, BAC, SAC or a combination of the above could be employed (Kim et al., 2010; Gimonet et al., 2016; Sheen and Suh, 2017). Even so, in this study, five II type (4 IIb, and 1 IIa) AChoA aneurysm cases suffered temporary or permanent injury, and two II type cases (4.8%, 2/42) developed the AChoA-syndrome. We found that II type, in particular IIb, had the highest risk ($\chi^2 = 7.54$, $P = 0.023$).

The IIc type aneurysms are extremely rare. We did not find this subtype in our study, which was a different result than Cho, who reported 24.5% (13/53) (Cho et al., 2008). We speculate that most of the IIc type aneurysms may be dissecting, fusiform, or dolichoectatic (Rutledge et al., 2019). The FD device may be a good choice for these, if there is no SAH.

It has been proven that the FD device is effective for aneurysm occlusion and the protection of perforated vessels in intracranial aneurysms. A multicenter experience showed that 83.3% of AChoA aneurysms achieved major occlusion and all AChoA were protected at follow up with the Pipeline embolization device (PED) (Srinivasan et al., 2018). Bhogal reported 30 cases of AChoA aneurysm treated by PED. Complete occlusion was reached in 50% of aneurysms immediately, and during follow up, 76.6% had also achieved it. All AChoAs were retained (Bhogal et al., 2019). In this study, three cases with a Turbridge stent in the ICA also achieved good results. The experience with FD devices in our center are as follows: the small II type aneurysms which were difficult to treat by conventional techniques (particularly the IIb and IIc type); those coexisting with adjacent multiple aneurysms (shown in **Figure 4**), and dissecting or fusiform aneurysms, and those without SAH.

At craniotomy, the AChoA may be more difficult to identify under the microscope, especially after SAH (Cho et al., 2008; Winkler et al., 2019), even with microvascular Doppler sonography (Shibata et al., 2000), intraoperative indocyanine green (Spiotta et al., 2011), or an intraoperative angiography device (Torne et al., 2019). SAH could lead to serious vasospasm and cerebral ischemia (Lee et al., 2018). In this cohort, four patients with SAH had AChoA injury, although this was not a statistically significant difference, SAH cannot be excluded as a risk factor. Based on the new classification, the long-term clinical effect of all treatment plans and relative risks need to be further researched.

Referring to the related literature (Senturk et al., 2009) and our 52 cases, the AChoA aneurysms have the following

**TABLE 2 |** The characteristics of ruptured and unruptured aneurysms.

| | Ruptured ($n = 28$) | Unruptured ($n = 14$) | Test value | *P* value |
|---|---|---|---|---|
| Female (*n*) | 16 | 10 | 0.808* | 0.368 |
| Age (year) | 55.39 + 10.48 | 50.79 + 7.60 | 1.46$^{\Delta}$ | 0.152 |
| Maximum height (mm) | 3.61 + 1.26 | 3.31 + 0.65 | 0.853$^{\Delta}$ | 0.399 |
| Maximum height (mm) | 3.20 + 0.99 | 3.38 + 0.56 | −0.613$^{\Delta}$ | 0.543 |
| Multiple (*n*) | 14 | 3 | 0.791* | 0.374 |
| **EVT methods** | | | −3.951$^{\#}$ | 0.00 |
| Coiling | 24 | 2 | | |
| SAC | 0 | 7 | | |
| BAC | 4 | 2 | | |
| FD | 0 | 3 | | |
| **RROC** | | | −1.017$^{\#}$ | 0.309 |
| 1 | 4 | 4 | | |
| 2 | 13 | 7 | | |
| 3a | 10 | 2 | | |
| 3b | 1 | 1 | | |
| **Complications** | | | | |
| AChoA occlusion | 4 | 1 | 0.875* | 0.352 |
| Infarction | 1 | 1 | 0.263* | 0.608 |
| **DSA follow up** | | | −0.485* | 0.628 |
| Improve | 9 | 6 | | |
| Stable | 18 | 6 | | |
| Worsen | 3 | 2 | | |

**Pearson's $\chi^2$, $^{\Delta}$T test, $^{\#}$Mann–Whitney U test.*

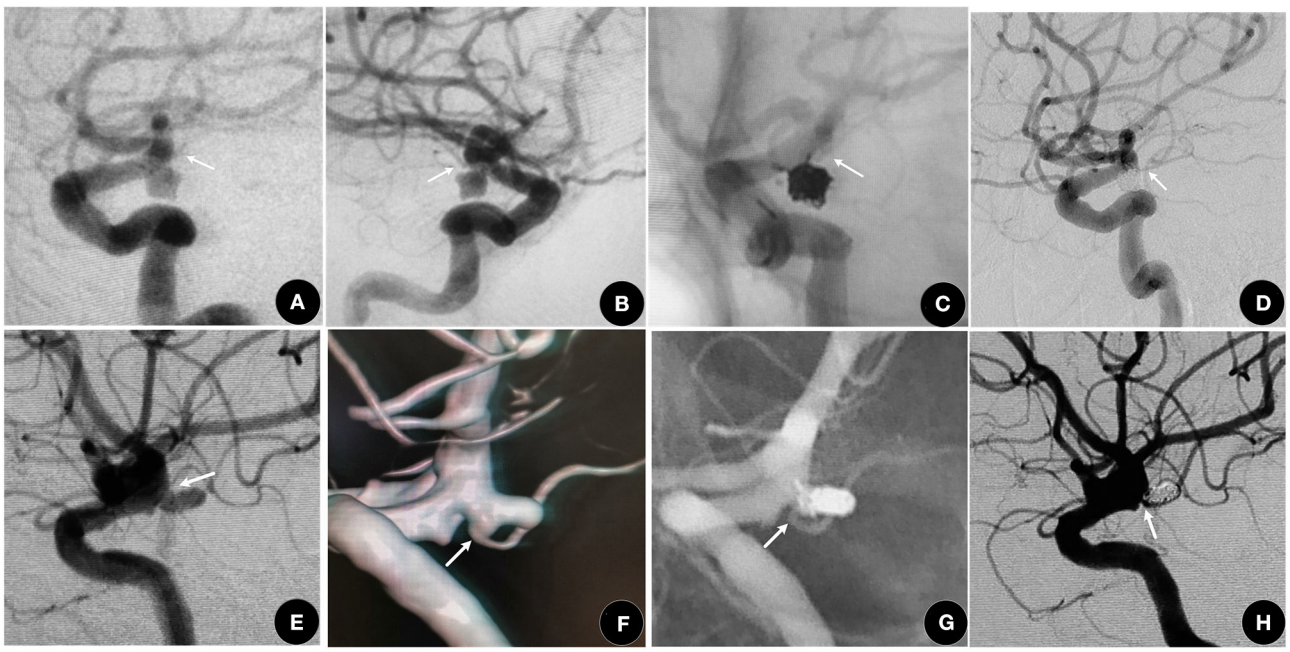


**FIGURE 2 | (A–D)** A 63-year-old female who suffered with an SAH for 2 days. **(A,B)** showing a I type aneurysm. **(C)** RROC 1 was achieved using the double microcatheter technique and the AChoA (arrow) was well-protected. **(D)** One year later, the aneurysm was still at RROC 1 with a normal AChoA (arrow). **(E–H)** A 61-year-old female, suffered with SAH for 4 days. **(E,F)** showing a IIa type aneurysm (arrow). **(G,H)** The aneurysm was packed with the double microcatheter technique, reaching RROC 2. The AChoA (arrow) was well-protected.

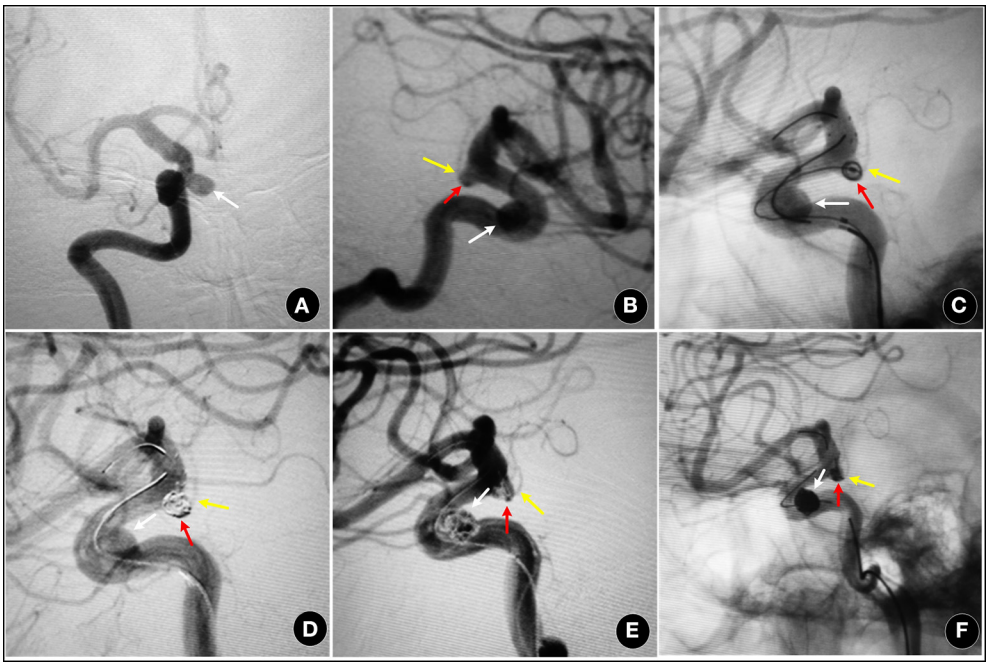


**FIGURE 3 |** A 55-year-old female, with an aneurysm found on routine examination. **(A,B)** showing a IIb type aneurysm (red arrow) and an ipsilateral ophthalmic artery aneurysm (white arrow). **(C–F)** two aneurysms were treated by SAC (Enterprise stent), and partially packed (RROC 3a). The AChoA was well-preserved (yellow arrow).

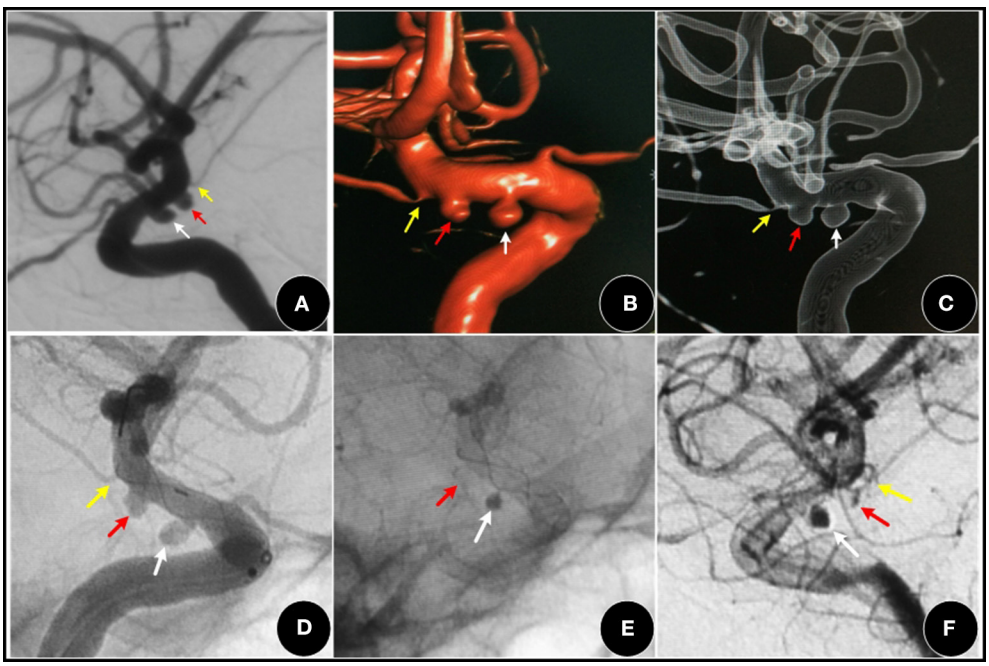


**FIGURE 4 |** A 52-year-old female, with a three-month history of dizziness. **(A–C)** showing a I type aneurysm (red arrow) and an adjacent PCA aneurysm (white arrow). **(D–F)** two aneurysms were covered by an FD (Tubridge stent), the AChoA aneurysm was barely visible (red arrow). The PCA aneurysm (white arrow) showed obvious retention of contrast media, while the AChoA (yellow arrow) was patent.

characteristics: more female patients (61.9%); a younger age (mean 53.9 years); a lower degree of SAH (84.6%, 25/28, Hunt-Hess I or II); a more regular shape (78.6%) and smaller size (41 cases $\leq$ 4 mm, 78.8%); more often associated with multiple aneurysms (32.7%, 17/52) (Senturk et al., 2009), especially with ipsilateral PCA aneurysm (76.5%, 13/17). As the number of cases and the length of follow up have increased, the features and outcomes of AChoA aneurysms will become clearer. There is another kind of AChoA aneurysm, the distal AChoA aneurysm. This is located at the distal part of the choroid point of the AChoA, and is rarely seen, except in conditions such as moyamoya disease (Choulakian et al., 2010). Because of its different pathogenic mechanism, lower risk, and treatment methods (Tanriover et al., 2014; Rutledge et al., 2019), this aneurysm is not included in the new classification. The new classification can also be called "AChoA originating aneurysms."

### Study Limitations

The sample size here was small and follow-up was not long. In the future, these results based on new classification should be confirmed with a larger sample size and longitudinal follow up.

## CONCLUSIONS

The new classification diagram was simple and clear. We firstly and systematically differentiated the dependent type of AChoA aneurysm into IIa, IIb, and IIc type and summarized their features. The II type (specially IIb) was one of potential risk factors for AChoA injured during operation.

## DATA AVAILABILITY STATEMENT

The raw data supporting the conclusions of this article will be made available by the authors, without undue reservation.

## ETHICS STATEMENT

The studies involving human participants were reviewed and approved by the ethics committee of Huashan hospital, Fudan university, Shanghai, China. The patients provided their written informed consent to participate in the study.

## AUTHOR CONTRIBUTIONS

YD and GC: conceptualization, GC, XQ, QA, JL, and YD: surgery, YL and YD: data analysis, YD and GC: writing. All authors contributed to the article and approved the submitted version.

## FUNDING

This study was provided by Shanghai Science and Technology Committee (No. 18411962400), Shanghai, China.

## ACKNOWLEDGMENTS

Thanks for Dr. Qinzhu An' help in AChoA aneurysm schematic drawing.

## REFERENCES

Andre, A., Boch, A. L., Di Maria, F., Nouet, A., Sourour, N., Clemenceau, S., et al. (2018). Complication risk factors in anterior choroidal artery aneurysm treatment. *Clin. Neuroradiol.* 28, 345–356. doi: 10.1007/s00062-017-0575-y

Aoki, T., Hirohata, M., Noguchi, K., Komaki, S., Orito, K., and Morioka, M. (2016). Comparative outcome analysis of anterior choroidal artery aneurysms treated with endovascular coiling or surgical clipping. *Surg. Neurol. Int.* 7, S504–509. doi: 10.4103/2152-7806.187492

Bhogal, P., Ganslandt, O., Bazner, H., Henkes, H., and Aguilar Perez, M. (2019). Treatment of unruptured, saccular, anterior choroidal artery aneurysms with flow diversion: a single centre experience. *Clin. Neuroradiol.* 29, 459–465. doi: 10.1007/s00062-018-0677-1

Champeaux, C., Jecko, V., Eimer, S., and Penchet, G. (2016). Usefulness of motor-evoked potentials monitoring for neurosurgical treatment of an unusual distal anterior choroidal artery aneurysm. *J. Korean Neurosurg. Soc.* 59, 414–419. doi: 10.3340/jkns.2016.59.4.414

Cho, M. S., Kim, M. S., Chang, C. H., Kim, S. W., Kim, S. H., and Choi, B. Y. (2008). Analysis of clip-induced Ischemic complication of anterior choroidal artery aneurysms. *J. Korean Neurosurg. Soc.* 43, 131–134. doi: 10.3340/jkns.2008.43.3.131

Choulakian, A., Drazin, D., and Alexander, M. J. (2010). NBCA embolization of a ruptured intraventricular distal anterior choroidal artery aneurysm in a patient with moyamoya disease. *J. Neurointerv. Surg.* 2, 368–370. doi: 10.1136/jnis.2010.002253

Drake, C. G., Vanderlinden, R. G., and Amacher, A. L. (1968). Carotid-choroidal aneurysms. *J. Neurosurg.* 29, 32–36. doi: 10.3171/jns.1968.29.1.0032

Friedman, J. A., Pichelmann, M. A., Piepgras, D. G., Atkinson, J. L., Maher, C. O., Meyer, F. B., et al. (2001). Ischemic complications of surgery for anterior choroidal artery aneurysms. *J. Neurosurg.* 94, 565–572. doi: 10.3171/jns.2001.94.4.0565

Ghali, M. G. Z., Srinivasan, V. M., Wagner, K. M., Lam, S., Johnson, J. N., and Kan, P. (2018). Anterior choroidal artery aneurysms: influence of regional microsurgical anatomy on safety of endovascular treatment. *J. Cerebrovasc. Endovasc. Neurosurg.* 20, 47–52. doi: 10.7461/jcen.2018.20.1.47

Gimonet, H., Desal, H. A., Mosimann, P. J., Stracke, P., Daumas-Duport, B., Lintia-Gaultier, A., et al. (2016). A new endovascular technique for small anterior choroidal artery aneurysms. A consecutive series using the 3-catheter-protective technique. *J. Neuroradiol.* 43, 223–226. doi: 10.1016/j.neurad.2016.02.004

Heros, R. C. (2010). Microneurosurgical management of anterior choroidal artery aneurysms. *World Neurosurg.* 73, 459–460. doi: 10.1016/j.wneu.2010.03.013

Kang, H. S., Kwon, B. J., Kwon, O. K., Jung, C., Kim, J. E., Oh, C. W., et al. (2009). Endovascular coil embolization of anterior choroidal artery aneurysms. *Clin. Article. J. Neurosurg.* 111, 963–969. doi: 10.3171/2009.4.JNS08934

Kim, B. M., Kim, D. I., Chung, E. C., Kim, S. Y., Shin, Y. S., Park, S. I., et al. (2008). Endovascular coil embolization for anterior choroidal artery aneurysms. *Neuroradiology* 50, 251–257. doi: 10.1007/s00234-007-0331-0

Kim, B. M., Park, S. I., Kim, D. J., Kim, D. I., Suh, S. H., Kwon, T. H., et al. (2010). Endovascular coil embolization of aneurysms with a branch incorporated into the sac. *AJNR Am. J. Neuroradiol.* 31, 145–151. doi: 10.3174/ajnr.A1785

Kim, S. H., Kwon, O. K., Jung, C. K., Kang, H. S., Oh, C. W., Han, M. H., et al. (2009). Endovascular treatment of ruptured aneurysms or pseudoaneurysms on the collateral vessels in patients with moyamoya disease. *Neurosurgery* 65, 1000–1004; discussion 1004. doi: 10.1227/01.NEU.0000345648.46096.CE

Lee, H., Perry, J. J., English, S. W., Alkherayf, F., Joseph, J., Nobile, S., et al. (2018). Clinical prediction of delayed cerebral ischemia in aneurysmal subarachnoid hemorrhage. *J. Neurosurg.* 130:1–8.

Li, J., Mukherjee, R., Lan, Z., Liu, Y., and He, M. (2012). Microneurosurgical management of anterior choroidal artery aneurysms: a 16-year institutional experience of 102 patients. *Neurol. Res.* 34, 272–280. doi: 10.1179/1743132812Y.0000000008

Locksley, H. B., Sahs, A. L., and Sandler, R. (1966). Report on the cooperative study of intracranial aneurysms and subarachnoid hemorrhage. 3. Subarachnoid hemorrhage unrelated to intracranial aneurysm and A-V malformation. A study of associated diseases and prognosis. *J. Neurosurg.* 24, 1034–1056. doi: 10.3171/jns.1966.24.6.1034

Mascitelli, J. R., Moyle, H., Oermann, E. K., Polykarpou, M. F., Patel, A. A., Doshi, A. H., et al. (2015). An update to the Raymond-Roy occlusion classification of intracranial aneurysms treated with coil embolization. *J. Neurointerv. Surg.* 7, 496–502. doi: 10.1136/neurintsurg-2014-011258

Patel, B. M., Ahmed, A., and Niemann, D. (2014). Endovascular treatment of supraclinoid internal carotid artery aneurysms. *Neurosurg. Clin. N. Am.* 25, 425–435. doi: 10.1016/j.nec.2014.04.003

Rhoton, A. L. Jr., Fujii, K., and Fradd, B. (1979). Microsurgical anatomy of the anterior choroidal artery. *Surg. Neurol.* 12, 171–187.

Rutledge, C., Jonzzon, S., Winkler, E. A., Hetts, S. W., and Abla, A. A. (2019). Transcortical transventricular transchoroidal-fissure approach to distal fusiform hyperplastic anterior choroidal artery aneurysms. *Br. J. Neurosurg.* 1–5. doi: 10.1080/02688697.2019.1594691

Sadamasa, N., Koyanagi, M., Fukuda, H., Chin, M., Handa, A., and Yamagata, S. (2014). Is aneurysm repair justified for the patients aged 80 or older after aneurysmal subarachnoid hemorrhage? *J. Neurointerv. Surg.* 6, 664–666. doi: 10.1136/neurintsurg-2013-010951

Senturk, C., Bandeira, A., Bruneau, M., Dewindt, A., Baleriaux, D., De Witte, O., et al. (2009). Endovascular treatment of anterior choroidal artery aneurysms. *J. Neuroradiol.* 36, 228–232. doi: 10.1016/j.neurad.2008.12.002

Sheen, J. J., and Suh, D. C. (2017). Low-angled microcatheter approach for coil embolization of the anterior choroidal artery aneurysm. *Neuroradiology* 59, 1053–1056. doi: 10.1007/s00234-017-1879-y

Shibata, Y., Fujita, S., Kawaguchi, T., Hosoda, K., Komatsu, H., and Tamaki, N. (2000). Use of microvascular Doppler sonography in aneurysm surgery on the anterior choroidal artery. *Neurol. Med. Chir. (Tokyo)* 40, 30–35; discussion 35-37. doi: 10.2176/nmc.40.30

Spiotta, A. M., Schuette, A., Hui, F., Gupta, R., Cawley, C. M., and Moskowitz, S. I. (2011). Experience with coil embolization of previously clipped aneurysms presenting with rupture. *J. Neurointerv. Surg.* 3, 331–334. doi: 10.1136/jnis.2010.004143

Srinivasan, V. M., Ghali, M. G. Z., Cherian, J., Mokin, M., Puri, A. S., Grandhi, R., et al. (2018). Flow diversion for anterior choroidal artery (AChA) aneurysms: a multi-institutional experience. *J. Neurointerv. Surg.* 10, 634–637. doi: 10.1136/neurintsurg-2017-013466

Tanriover, N., Kucukyuruk, B., Ulu, M. O., Isler, C., Sam, B., Abuzayed, B., et al. (2014). Microsurgical anatomy of the cisternal anterior choroidal artery with special emphasis on the preoptic and postoptic subdivisions. *J. Neurosurg.* 120, 1217–1228. doi: 10.3171/2014.1.JNS131325

Torne, R., Garcia, S., Sanroman, L., Rodriguez-Hernandez, A., Reyes, L., Tercero, J., et al. (2019). Safety and feasibility assessment of the O-arm as an intraoperative angiography device in aneurysm surgery. *World Neurosurg.* 127, e1159–e1165. doi: 10.1016/j.wneu.2019.04.076

Winkler, E. A., Lu, A., Burkhardt, J. K., Rutledge, W. C., Yue, J. K., Birk, H. S., et al. (2019). Microsurgical clipping of anterior choroidal artery aneurysms: a systematic approach to reducing ischemic complications in an experience with 146 patients. *Oper. Neurosurg. (Hagerstown)* 17, 413–423. doi: 10.1093/ons/opz007

Yasargil, M. G., Yonas, H., and Gasser, J. C. (1978). Anterior choroidal artery aneurysms: their anatomy and surgical significance. *Surg. Neurol.* 9, 129–138.

**Conflict of Interest:** The authors declare that the research was conducted in the absence of any commercial or financial relationships that could be construed as a potential conflict of interest.

frontiers in Aging Neuroscience

ORIGINAL RESEARCH
published: 16 March 2021
doi: 10.3389/fnagi.2021.625874

# Fixel-Based Analysis of White Matter Degeneration in Patients With Progressive Supranuclear Palsy or Multiple System Atrophy, as Compared to Parkinson's Disease

*Thanh-Thao Nguyen*[1†], *Jur-Shan Cheng*[2,3,4†], *Yao-Liang Chen*[5,6†], *Yu-Chun Lin*[6,7], *Chih-Chien Tsai*[8], *Chin-Song Lu*[9,10,11], *Yi-Hsin Weng*[10,11,12], *Yi-Ming Wu*[6,7], *Ngoc-Thanh Hoang*[1] *and Jiun-Jie Wang*[5,7,8,13*]

[1] Department of Radiology, Hue University of Medicine and Pharmacy, Hue University, Hue, Vietnam, [2] Clinical Informatics and Medical Statistics Research Center, College of Medicine, Chang Gung University, Taoyuan, Taiwan, [3] Department of Biomedical Sciences, College of Medicine, Chang Gung University, Taoyuan, Taiwan, [4] Department of Emergency Medicine, Chang Gung Memorial Hospital, Keelung, Taiwan, [5] Department of Diagnostic Radiology, Chang Gung Memorial Hospital, Keelung, Taiwan, [6] Department of Medical Imaging and Intervention, Chang Gung Memorial Hospital, Linkou, Taiwan, [7] Department of Medical Imaging and Radiological Sciences, Chang Gung University, Taoyuan, Taiwan, [8] Healthy Aging Research Center, Chang Gung University, Taoyuan, Taiwan, [9] Professor Lu Neurological Clinic, Taoyuan, Taiwan, [10] Division of Movement Disorders, Department of Neurology, Chang Gung Memorial Hospital, Linkou, Taiwan, [11] Neuroscience Research Center, Chang Gung Memorial Hospital, Linkou, Taiwan, [12] School of Medicine, Chang Gung University, Taoyuan, Taiwan, [13] Medical Imaging Research Center, Institute for Radiological Research, Chang Gung University/Chang Gung Memorial Hospital, Linkou, Taiwan

OPEN ACCESS

**Edited by:**
*Yuanli Zhao,*
*Capital Medical University, China*

**Reviewed by:**
*Jong-Min Kim,*
*Seoul National University Bundang Hospital, South Korea*
*Agenor Limon,*
*University of Texas Medical Branch at Galveston, United States*

***Correspondence:**
*Jiun-Jie Wang*
*jwang@mail.cgu.edu.tw*

[†] *These authors have contributed equally to this work*

**Received:** *04 November 2020*
**Accepted:** *18 February 2021*
**Published:** *16 March 2021*

**Citation:**
*Nguyen T-T, Cheng J-S, Chen Y-L, Lin Y-C, Tsai C-C, Lu C-S, Weng Y-H, Wu Y-M, Hoang N-T and Wang J-J (2021) Fixel-Based Analysis of White Matter Degeneration in Patients With Progressive Supranuclear Palsy or Multiple System Atrophy, as Compared to Parkinson's Disease. Front. Aging Neurosci. 13:625874. doi: 10.3389/fnagi.2021.625874*

**Introduction:** White matter degeneration may contribute to clinical symptoms of parkinsonism.

**Objective:** We used fixel-based analysis (FBA) to compare the extent and patterns of white matter degeneration in different parkinsonian syndromes—including idiopathic Parkinson's disease (PD), multiple system atrophy (MSA), and progressive supranuclear palsy (PSP).

**Methods:** This is a retrospective interpretation of prospectively acquired data of patients recruited in previous studies during 2008 and 2019. Diffusion-weighted images were acquired on a 3-Tesla scanner (diffusion weighting b = 1000 s/mm$^2$–applied along either 64 or 30 non-collinear directions) from 53 patients with PD (men/women: 29/24; mean age: 65.06 ± 5.51 years), 47 with MSA (men/women: 20/27; mean age: 63.00 ± 7.19 years), and 50 with PSP men/women: 20/30; mean age: 65.96 ± 3.14 years). Non-parametric permutation tests were used to detect intergroup differences in fixel-related indices—including fiber density, fiber cross-section, and their combination.

**Results:** Patterns of white matter degeneration were significantly different between PD and atypical parkinsonisms (MSA and PSP). Compared with patients with PD, those with MSA and PSP showed a more extensive white matter involvement—noticeably descending tracts from primary motor cortex to corona radiata and cerebral peduncle. Lesions of corpus callosum were specific to PSP and absent in both MSA and PD.

**Discussion:** FBA identified specific patterns of white matter changes in MSA and PSP patients compared to PD. Our results proved the utility of FBA in evaluation of implied biological processes of white matter changes in parkinsonism. Our study set the stage for future applications of this technique in patients with parkinsonian syndromes.

**Keywords: fixel-based analysis, white matter, Parkinson's disease, multiple system atrophy, progressive supranuclear palsy, diffusion weighted Imaging**

## INTRODUCTION

Parkinsonism is a progressive neurodegenerative disorder characterized by resting tremor, rigidity, bradykinesia/akinesia, and postural instability (McFarland, 2016). Although idiopathic Parkinson's disease (PD) is the most common form of parkinsonism, this condition also comprises multiple system atrophy (MSA) and progressive supranuclear palsy (PSP)—two atypical parkinsonian syndromes that tend to have a more rapid functional deterioration compared with idiopathic PD (McFarland and Hess, 2017). Apart from the pathogenetic changes in basal ganglia, neuroimaging studies in PD have shown various extents of atrophy affecting different brain regions—including a reduced gray matter volume in the frontal (Burton et al., 2004), and pre-frontal lobes (Biundo et al., 2011). Atrophy in the cortical and subcortical areas and noticeably in the cerebellum has been reported in patients with PSP (Giordano et al., 2013), whereas cerebellar white matter atrophy has been described in MSA(Matsusue et al., 2009). Extensive involvement of different brain regions is accompanied by white matter degeneration, which may result in a clinically relevant functional decline (Whitwell et al., 2011).

Although diffusion tensor imaging (DTI) has been previously applied to investigate white matter changes in patients with parkinsonism, this technique suffers from several shortcomings. Erroneous interpretations in DTI may result from oversimplification of the underlying anatomical structures (Mori and Zhang, 2006; Chen et al., 2019), especially in regions with crossing fibers (Jbabdi et al., 2010). In this scenario, fixel-based analysis (FBA) has emerged as a novel approach based on a higher-order diffusion model to compute fiber orientation density function (Raffelt et al., 2017). FBA allows investigating the micro- and macrostructural properties of individual fiber populations within each voxel—with a single fiber population within a voxel termed fixel (Pecheva et al., 2019). Three fixel-based indices can be derived, which are fiber density (FD)—the volume of intra-axonal space of particular fixel; fiber cross-section (FC)—the cross-sectional area of particular fixel; and the combination of fiber density and cross-section (FDC) (Pecheva et al., 2019).

Previous studies supported the clinical usefulness of FBA in investigating white matter degeneration in patients with neurodegenerative diseases (Mito et al., 2018; Rau et al., 2019). Understandings of white matter changes in parkinsonism may provide new insights into the pathogenesis of motor and non-motor symptoms in these clinical entities, which may eventually lead to more personalized care in terms of diagnosis and treatment. The study is original by using FBA, which is a novel development and could provide new interpretation of the underlying changes in the brain as measured by diffusion. We therefore designed this retrospective analysis of prospectively collected data. We used fixel-based analysis to compare the extent and patterns of white matter degeneration in different parkinsonian syndromes—including idiopathic Parkinson's disease, multiple system atrophy, and progressive supranuclear palsy.

## MATERIALS AND METHODS

This is a retrospective interpretation of prospectively acquired data of diffusion MRI. Both diffusion tensor imaging and structural images (as acquired from T1 weighted MPRAGE sequence) were extracted during the period of 2008 and 2019 from medical records. The study protocol complied with the tenets of the Helsinki declaration, and ethical approval was granted by the Chang Gung Medical Foundation Institutional Review Board. Owing to the retrospective nature of the study, the need for informed consent was waived.

### Patients

Images were obtained from 53 patients with PD (29 men and 24 women; mean age: 65.06 ± 5.51 years), 47 with MSA (20

**TABLE 1 |** Demographic and clinical variables.

| | PD | MSA | PSP | *p*-value |
|---|---|---|---|---|
| Number of subject | 53 | 47 | 50 | |
| Sex (M/F) | 29/24 | 20/27 | 20/30 | 0.277 |
| Age (years) | 65.1 ± 5.5 | 63.0 ± 7.2 | 66.0 ± 3.1 | 0.069 |
| Duration (months) | 77.9 ± 52.5[a] | 49.3 ± 31.4 | 62.9 ± 37.7 | 0.004 |
| MHY | | | | <0.001 |
| 1 | 15 | 0 | 0 | |
| 1.5 | 4 | 0 | 1 | |
| 2 | 8 | 1 | 1 | |
| 2.5 | 10 | 2 | 2 | |
| ≥3 | 12 | 29 | 46 | |
| UPDRS III | 22.8 ± 15.2[b,c] | 37.2 ± 17.2 | 37.3 ± 17.8 | <0.001 |
| N/A* | 4 | 15 | 0 | |

*Data was not available in both MHY and UPDRS III. PD, Idiopathic Parkinson's disease; MSA, Multiple system atrophy; PSP, Progressive supranuclear palsy; MHY, Modified Hoehns and Yahr staging scale; UPDRS III, Motor subscale of Unified Parkinson's Disease Rating Scale.*

[a] *PD vs. MSA, $p = 0.001$.*

[b] *PD vs. MSA, $p < 0.001$.*

[c] *PD vs. PSP, $p < 0.001$.*

men and 27 women; mean age: 63.00 ± 7.19 years), and 50 with PSP (20 men and 30 women, mean age: 65.96 ± 3.14 years). Eighty-five participants were involved in prior publications, which focused on the analysis of diffusion tensor imaging and its application in the diagnosis and prognosis of patients with Parkinsonism, as well as longitudinal FBA analysis in patients with PD (Wang et al., 2010, 2011; Wai et al., 2012; Lu et al., 2016; Rau et al., 2019b; Chen et al., 2020; Tsai et al., 2020). The current submission employed patients with PD, MSA, and PSP, which investigated white matter difference by FBA analysis. A list of references was added in the **Supplementary Table 1**. Patients were clinically diagnosed made by two senior neurologists (CSL and YHW, 28 and 21 years of experience, respectively) according to commonly accepted criteria for PD (Hughes et al., 1992), MSA (Gilman et al., 1999), and PSP (Litvan et al., 1996), respectively. The acquisition should be consisted of both diffusion tensor imaging and high-resolution T1-weighted anatomical images. 99mTc-TRODAT-1, which binds to the dopamine transporter, was used to image the dopaminergic system in all participants. Exclusion criteria were as follows: (1) moderate-to-severe dementia; (2) severe dyskinesia; (3) major systemic medical conditions; (4) documented brain abnormalities based on MRI or $^{18}$FDG PET findings; (5) history of intracranial surgery; (6) significant neuropsychiatric disorders established by the corresponding diagnostic criteria, including stroke, brain tumor, demyelinating diseases of central nervous system (CNS), major depression, schizophrenia, and Alzheimer's disease; and (7) pharmacotherapy lasting for >10 years or treatment with drugs capable of crossing the blood-brain-barrier (the only exception being medications for parkinsonian syndromes). The Modified Hoehn and Yahr Staging (Goetz et al., 2004) and the motor subscale of Unified Parkinson Disease Rating Scale (UPDRS III) (Martinez-Martin et al., 1994) were used to assess clinical severity.

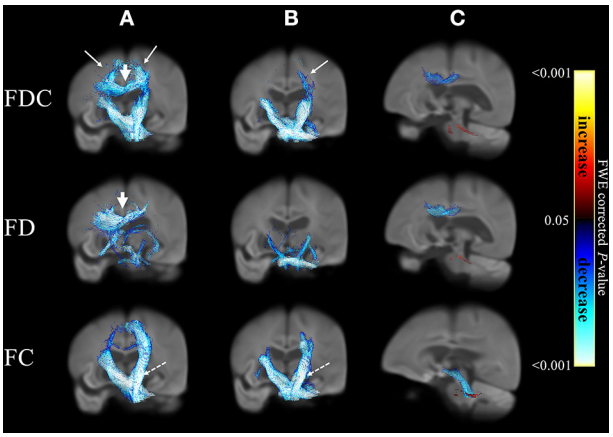


**FIGURE 1 |** Differences in fixel-related indices in PSP compared to PD (column a), MSA compared to PD (column b) and PSP compared to MSA (column c). The involved regions included corona radiata (white arrows in column a and column b) and cerebral peduncle (dashed arrows in columns a, b). Corpus callosum is specifically involved when compared PSP to PD (arrowhead in column a). In PSP group when compared to MSA (column c), the regions with reduced FDC and FD were mainly located in corpus callosum and regions with reduced FC can be found in midbrain and cerebral peduncles (blue). In MSA group when compared to PSP (column c), the regions with reduced FDC, FD and FC were located in middle cerebellar peduncles (red). The streamline showed *p*-values (family-wise error corrected $p < 0.05$, indicated by the colorbar).

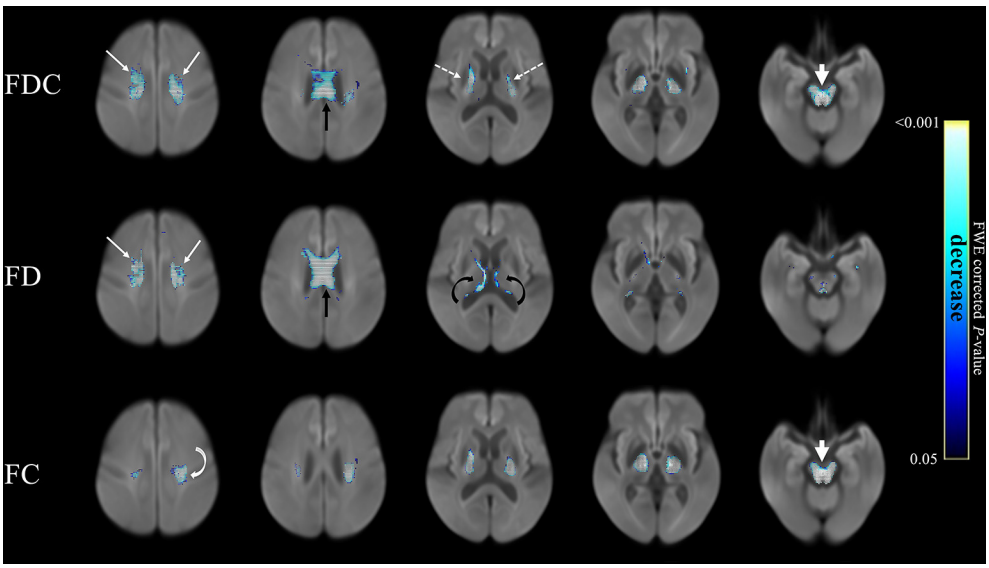


**FIGURE 2 |** Fixel-related indices in patients with PSP compared to that with PD. Reduction of FDC in the main white matter tracts, from superior region of corona radiata (upper row, white arrows), corpus callosum (upper row, black arrow) to posterior limbs of internal capsules (upper row, dashed arrows) and cerebral peduncles (upper row, arrowhead). Reduced FD was identified in corona radiata (middle row, white arrows), corpus callosum (middle row, black arrow) and the fornix (middle row, black curved arrows), which were symmetrical in the supratentorial compartment. Reduced FC was noticed in corona radiata to posterior limbs of internal capsules (bottom row, white curved arrow) and cerebral peduncles (bottom row, white arrowhead). The streamline showed *p*-values (family-wise error corrected $p < 0.05$, indicated by the colorbar).

**TABLE 2 |** Comparison of fiber tracts between patients with PSP and PD.

| Fixel-related indices | Name of tracts | Cluster size | Peak *p*-value |
|---|---|---|---|
| FDC | Body of corpus callosum | 2532 | 0.00020 |
| | Posterior limb of internal capsule L | 1025 | 0.00020 |
| | Superior corona radiata L | 992 | 0.00040 |
| | Posterior limb of internal capsule R | 896 | 0.00020 |
| | Superior corona radiata R | 743 | 0.00040 |
| | Cerebral peduncle R | 658 | 0.00020 |
| | Cerebral peduncle L | 643 | 0.00020 |
| | Anterior limb of internal capsule R | 259 | 0.00040 |
| | Superior cerebellar peduncle L | 251 | 0.00020 |
| | Superior cerebellar peduncle R | 246 | 0.00020 |
| | Corticospinal tract L | 204 | 0.00180 |
| | Pontine crossing tract | 190 | 0.00020 |
| | Corticospinal tract R | 137 | 0.00180 |
| | Medial lemniscus L | 86 | 0.00020 |
| | Medial lemniscus R | 63 | 0.00040 |
| | Anterior limb of internal capsule L | 54 | 0.01440 |
| | External capsule R | 39 | 0.02460 |
| | Crura of fornix R | 31 | 0.02620 |
| FD | Body of corpus callosum | 3130 | 0.00020 |
| | Superior corona radiata R | 489 | 0.00080 |
| | Superior corona radiata L | 271 | 0.00100 |
| | Crura of fornix R | 171 | 0.00160 |
| | Superior cerebellar peduncle R | 162 | 0.00200 |
| | Crura of fornix L | 152 | 0.00720 |
| | Superior cerebellar peduncle L | 88 | 0.00300 |
| | Cerebral peduncle L | 82 | 0.01700 |
| | Cerebral peduncle R | 78 | 0.02600 |
| | Anterior limb of internal capsule R | 63 | 0.00500 |
| | Posterior limb of internal capsule L | 55 | 0.02100 |
| | Genu of corpus callosum | 33 | 0.02920 |
| | Posterior limb of internal capsule R | 27 | 0.02400 |
| | Medial lemniscus R | 21 | 0.01200 |
| | Corticospinal tract R | 14 | 0.03300 |
| | Corticospinal tract L | 14 | 0.02100 |
| | Medial lemniscus L | 11 | 0.02800 |
| FC | Superior corona radiata L | 1549 | 0.00020 |
| | Posterior limb of internal capsule L | 1194 | 0.00020 |
| | Posterior limb of internal capsule R | 1086 | 0.00820 |
| | Cerebral peduncle L | 611 | 0.00020 |
| | Cerebral peduncle R | 564 | 0.00020 |
| | Superior corona radiata R | 552 | 0.00020 |
| | Superior cerebellar peduncle L | 261 | 0.00020 |
| | Body of corpus callosum | 258 | 0.00040 |
| | Pontine crossing tract | 235 | 0.00080 |
| | Corticospinal tract L | 234 | 0.00500 |
| | superior cerebellar peduncle R | 231 | 0.00020 |
| | posterior corona radiata L | 131 | 0.00340 |
| | anterior limb of internal capsule R | 127 | 0.00020 |
| | corticospinal tract R | 109 | 0.00500 |
| | middle cerebellar peduncle | 103 | 0.00220 |
| | medial lemniscus L | 82 | 0.00020 |
| | medial lemniscus R | 58 | 0.00060 |
| | inferior cerebellar peduncle L | 23 | 0.00200 |
| | anterior limb of internal capsule L | 11 | 0.00140 |
| | inferior cerebellar peduncle R | 10 | 0.00020 |

Two neuro-radiologists (YLC and YMW, 21 and 11 years of experience, respectively), who were blinded to the diagnosis, read the structural MR images independently.

## Data Acquisition

All images were acquired on a 3.0-Tesla scanner (Trio Magnetom; Siemens, Erlangen, Germany) using a 12-channel head coil. Diffusion-weighted imaging was performed using two protocols characterized by a different diffusion-sensitive spin-echo EPI sequence. In brief, images with a diffusion weighting $b = 1000$ s/mm$^2$ were acquired along 64 or 30 non-collinear directions. The voxel size was either $2 \times 2 \times 2$ mm$^3$ or $2 \times 2 \times 3$ mm$^3$. High-resolution T1-weighted anatomical images were obtained using magnetization-prepared rapid gradient-echo (MPRAGE) sequences with the following parameters: TR, 2000 ms; inversion time (TI), 900 ms; TE, 2.63 ms; voxel size, $1 \times 1 \times 1$ mm$^3$.

## Image Processing

FBA was carried out on diffusion MRI using MRtrix 3.0 following the recommendations of Raffelt et al. (2017). Pre-processing included denoising by principal component analysis (Veraart et al., 2016), removal of Gibbs ringing (Kellner et al., 2016), as well as correction for motion, distortion, and bias field (Tustison et al., 2010; Andersson and Sotiropoulos, 2015, 2016). Multi-tissue constrained spherical deconvolution was used to estimate fiber orientations distribution in each voxel (Jeurissen et al., 2014). A study-specific template was created by spatial normalization in all of the study patients using symmetric non-linear transformation fiber orientations distribution-based registration. Fiber density and fiber bundle cross-section were calculated within each voxel. A combined measure of fiber density and cross-section (FDC) was computed by multiplying FD by FC (10). For comparison, both Fractional Anisotropy (FA) and Mean Diffusivity (MD) from diffusion tensor imaging were analyzed by using Tract Based Spatial Statistics (TBSS) (Smith et al., 2006) following the recommended procedure.

## Statistical Analysis

Differences in fixel-related indices between the three study groups were assessed using non-parametric permutation testing and connectivity-based fixel enhancement as implemented in MRtrix 3.0. Age, sex, and different imaging protocol was used as potential confounding factors. A family-wise error corrected *p*-value $< 0.05$ was considered statistically significant (Nichols and Holmes, 2002).

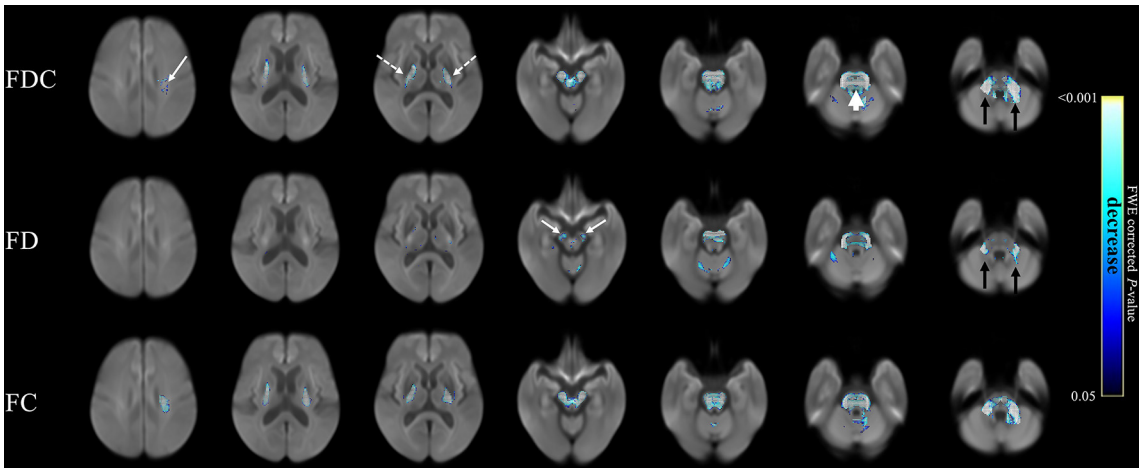


**FIGURE 3 |** Fixel-related indices in patients with MSA compared to that with PD. Reduced FDC were identified in the main descending white matter pathways, from left corona radiata (upper row, white arrow) to bilateral posterior limbs of internal capsule (upper row, white dashed arrows), cerebral peduncles, transvers pontine fibers (upper row, white arrowhead), and bilateral middle cerebellar peduncles (upper row, black arrows). Reduce FD was found in bilateral cerebral peduncles (middle row, white arrows) and middle cerebellar peduncles (middle row, black arrows). Left corona radiate and middle cerebellar peduncle are more affected than the right side. The streamline showed *p*-values (family-wise error corrected $p < 0.05$, indicated by the colorbar).

# RESULTS

## Demographic and Clinical Variables

**Table 1** depicts the general characteristics of the study patients. Age and sex did not differ significantly among the three study groups. Disease duration was longer in patients with PD than in those with MSA ($p = 0.001$). UPDRS III scores were significantly higher in the two atypical parkinsonian syndromes than in patients with PD ($p < 0.001$).

## Fixel-Related Indices in the Three Study Groups

**Figure 1** displays the changes in fixel-related indices in patients with atypical parkinsonian syndromes (column a: PSP; column b: MSA) compared with PD. All indices were consistently reduced. A 3D visualization of the affected regions with the color encoded the direction of the major fiber bundles are shown in **Supplementary Figure 1** (PSP) and **2** (MSA), respectively. With respect to PD, atypical parkinsonian syndromes were characterized by a significant involvement of white matter tract from corona radiata (white arrows in columns a and b) to cerebral peduncle (dashed arrows in columns a and b). Body of corpus callosum was found to be affected when PSP was compared with PD (arrow head in column a).

A comparison of PSP and MSA revealed a differential involvement of various brain areas (column c). **Supplementary Figure 3** showed the 3D visualization of the affected regions (color blue: reduction in PSP; color red: reduction in MSA). Regions characterized by reduced FDC (upper row) and FD (middle row) in patients with PSP were chiefly located in the body of corpus callosum, whereas midbrain and cerebral peduncles showed a reduction in FC (blue, bottom row). Regions displaying reduced FDC, FD, and FC values in patients with MSA were localized in the superior cerebellar peduncles (red).

## Comparison of Patients With PSP and PD

**Figure 2** compares fixel-related indices of patients with PSP and PD. Reductions of FDC (upper row) were evident in the main descending white matter tracts from the superior region of corona radiata (from motor cortex) (white arrows) through body of corpus callosum (black arrow) to posterior limbs of internal capsules (dashed arrows) and into the cerebral peduncles (arrow head). The regions with changes are consistent with that of reduced FD (middle row), noticeably in corona radiata (white arrows), and corpus callosum (black arrow). There was involvement of the medial thalamus (black curved arrow)—with a symmetrical involvement of the supratentorial compartment. Similar regions of reductions in FC (bottom row) were evident from corona radiata to the posterior limbs of internal capsules and cerebral peduncles (arrow head). Regions with a concomitant reduction of both FD and FC were generally overlapping to those with a reduced FDC. However, an isolated decreased of FD was evident in the thalamus. The names of tracts with significant difference, together with the cluster sizes and the peak *p*-values were summarized in **Table 2**.

## Comparison of Patients With MSA and PD

**Figure 3** compares fixel-related indices of patients with MSA and PD. Reductions of FDC (top row) were evident in the main descending white matter pathways from the left corona radiata (white arrows) to bilateral posterior limbs of internal capsule (white dashed arrows), cerebral peduncles, transverse pontine fibers (white arrow head), and bilateral middle cerebellar peduncles (black arrows). FD was found to be significantly reduced (middle row) in bilateral cerebral peduncles (white arrows) and middle cerebellar peduncles (black arrows).

**TABLE 3 |** Comparison of fiber tracts between patients with MSA and PD.

| Fixel-related indices | Name of tracts | Cluster size | Peak *p*-value |
|---|---|---|---|
| FDC | Posterior limb of internal capsule L | 1027 | 0.00020 |
| | Posterior limb of internal capsule R | 931 | 0.00020 |
| | Middle cerebellar peduncle | 800 | 0.00020 |
| | Cerebral peduncle R | 768 | 0.00020 |
| | Cerebral peduncle L | 701 | 0.00020 |
| | Superior corona radiata L | 378 | 0.00760 |
| | Corticospinal tract L | 321 | 0.00020 |
| | Corticospinal tract R | 305 | 0.00020 |
| | Pontine crossing tract | 293 | 0.00020 |
| | Superior cerebellar peduncle R | 178 | 0.00180 |
| | Superior cerebellar peduncle L | 149 | 0.00680 |
| | Anterior limb of internal capsule R | 125 | 0.00060 |
| | Medial lemniscus L | 83 | 0.00320 |
| | Medial lemniscus R | 58 | 0.00200 |
| | Retrolenticular part of internal capsule L | 52 | 0.00080 |
| | Posterior corona radiata L | 52 | 0.02280 |
| | Inferior cerebellar peduncle L | 49 | 0.00120 |
| | Retrolenticular part of internal capsule R | 49 | 0.00180 |
| | Anterior limb of internal capsule L | 29 | 0.01380 |
| | Superior corona radiata R | 14 | 0.01500 |
| FD | Middle cerebellar peduncle | 411 | 0.00020 |
| | Cerebral peduncle R | 368 | 0.00020 |
| | Cerebral peduncle L | 273 | 0.00040 |
| | Posterior limb of internal capsule R | 192 | 0.00660 |
| | Corticospinal tract L | 171 | 0.00040 |
| | Posterior limb of internal capsule L | 135 | 0.00620 |
| | Corticospinal tract R | 132 | 0.00140 |
| | Pontine crossing tract | 67 | 0.00640 |
| | Retrolenticular part of internal capsule R | 29 | 0.00600 |
| | Superior_part_cingulum_R | 27 | 0.02400 |
| | Superior cerebellar peduncle R | 24 | 0.02000 |
| | Crura of fornix L | 17 | 0.03800 |
| | Crura of fornix R | 14 | 0.02900 |
| FC | Posterior limb of internal capsule L | 1139 | 0.00020 |
| | Posterior limb of internal capsule R | 1024 | 0.00020 |
| | Superior corona radiata L | 991 | 0.00100 |
| | Middle cerebellar peduncle | 792 | 0.00020 |
| | Cerebral peduncle R | 662 | 0.00020 |
| | Cerebral peduncle L | 633 | 0.00020 |
| | Corticospinal tract L | 334 | 0.00020 |
| | Corticospinal tract R | 326 | 0.00020 |
| | Pontine crossing tract | 269 | 0.00020 |
| | Superior cerebellar peduncle L | 124 | 0.00460 |
| | Posterior corona radiata L | 117 | 0.00700 |
| | Superior corona radiata R | 96 | 0.01180 |
| | Anterior limb of internal capsule R | 71 | 0.00340 |
| | Superior cerebellar peduncle R | 66 | 0.00480 |
| | Inferior cerebellar peduncle L | 56 | 0.00440 |
| | Medial lemniscus L | 21 | 0.00700 |
| | Anterior limb of internal capsule L | 18 | 0.00700 |

Interestingly, regions with reduced FC (bottom row) almost invariably overlap with those showing a reduction in FDC. The names of tracts with significant difference, together with the cluster sizes and the peak *p*-values were summarized in **Table 3**.

## Comparison of Patients With PSP and MSA

**Figure 4** compares fixel-related indices of patients with PSP and MSA. Reductions of FDC and FD in patients with PSP were evident in body of corpus callosum (white arrows), whereas FC was found to be lowered in the midbrain (white dashed arrows). All fixel-related indices (FDC, FD, and FC) of patients with MSA were reduced in middle cerebellar peduncles (**Figure 4**, black arrows). The names of tracts with significant difference, together with the cluster sizes and the peak *p*-values were summarized in **Table 4**.

## Tract-Based Spatial Statistics in Patients With PSP or MSA, as Compared to PD

For comparison to conventional diffusion tensor imaging, **Figure 5** shows the result from tract-based spatial statistics relative to patients with PD. In patients with PSP, reduced FA (panel a) and increased MD (panel b) can be found in bilateral corona radiata, internal capsules, superior longitudinal fasciculi, posterior thalamic radiation, as well as genu and splenium of the corpus callosum. In patients with MSA, only increased MD (panel c) was found, which was located in the bilateral cerebellar peduncle.

# DISCUSSION

## Main Findings

FBA was used to assess the patterns of white matter changes in three different forms of parkinsonism. Our findings revealed profound differences in terms of white matter involvement among groups—with affected regions being more extensive in MSA and PSP than in PD. These results are consistent with the notion that both PSP and MSA portend a higher burden of clinical disability. Further, brain regions affected by white matter changes were in accordance with the current models of disease pathogenesis (Boxer et al., 2017; Meissner et al., 2019). Our analysis method might provide an interesting insight into the pathophysiology of various parkinsonisms. Taken together, our data indicate that the distribution and severity of white matter involvement in patients with PSP and MSA are characteristically different.

The identified regions can be overlapped between FBA and conventional DTI analysis using TBSS. Both techniques might provide complementary information regarding to the underlying microstructural changes. However, because different post-processing procedures may lead to either false-positive or false-negative results (Kuchling et al., 2018), the choice of the analysis approach might depend on the research question of interest. Our study demonstrated the use of fixel-related indices as potential biomarkers of disease progression. It may set the stage for future applications of this technique in patients with parkinsonian syndromes.

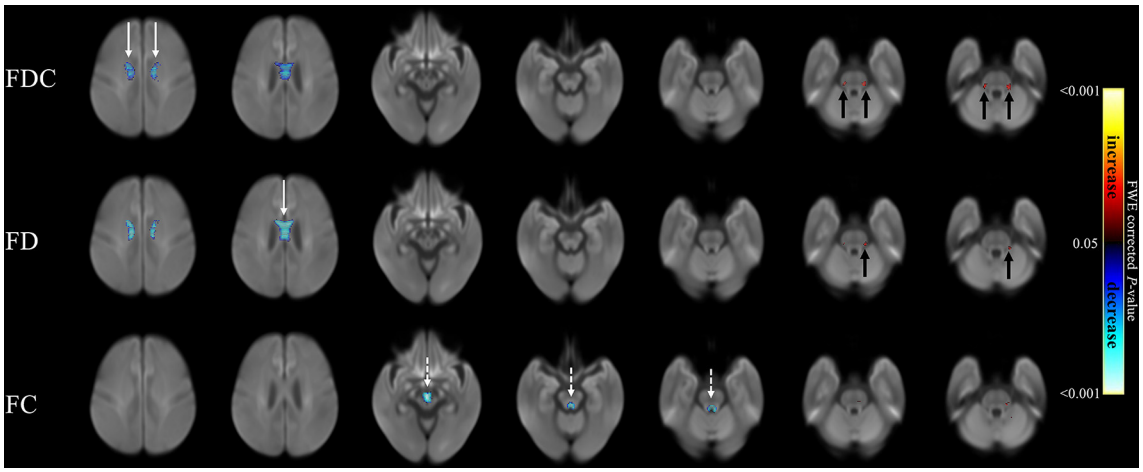


**FIGURE 4 |** Fixel-related indices in patients with PSP and MSA. Reduced FDC and FD were noticeable in corpus callosum (white arrows), while reduced FC were found in midbrain (white dashed arrows) in patients with PSP. On the other hand, the regions with reduced FDC, FD and FC were found in middle cerebellar peduncles (black arrows) in patients with MSA. The streamline showed *p*-values (family-wise error corrected $p < 0.05$, indicated by the colorbar).

**TABLE 4 |** Comparison of fiber tracts between patients with PSP and MSA.

| Fixel-related indices | Name of tract | Cluster size | Peak *p*-value |
|---|---|---|---|
| FDC | Body of corpus callosum | 1048 | 0.01360 |
| | Middle cerebellar peduncle | 118 | 0.03000 |
| | Superior corona radiata R | 110 | 0.01340 |
| | Corticospinal tract L | 40 | 0.02140 |
| | Superior corona radiata L | 35 | 0.01700 |
| | Corticospinal tract R | 25 | 0.02740 |
| | Cerebral peduncle L | 11 | 0.02400 |
| FD | Body of corpus callosum | 1196 | 0.00640 |
| | Superior corona radiata R | 55 | 0.01040 |
| | Superior corona radiata L | 22 | 0.02940 |
| | Corticospinal tract L | 18 | 0.02680 |
| | Cerebral peduncle L | 17 | 0.02000 |
| | Middle cerebellar peduncle | 13 | 0.03260 |
| | Corticospinal tract R | 10 | 0.03080 |
| FC | Middle cerebellar peduncle | 58 | 0.03160 |
| | Superior cerebellar peduncle R | 48 | 0.01680 |
| | Superior cerebellar peduncle L | 45 | 0.01340 |
| | Medial lemniscus L | 38 | 0.01080 |
| | Medial lemniscus R | 32 | 0.01680 |

## PSP: From Corpus Callosum, Internal Capsules, Thalamic Radiation to Midbrain

The corpus callosum consists of white matter fibers that interconnect the motor areas of the two hemispheres. When compared to patients with PD, reductions of FDC in the corpus callosum of PSP overlapped considerably with FD declines. Similarly, when compared to patients with MSA, a reduced FDC in the corpus callosum can be noticed, a change which was chiefly driven by a decline in FD rather than in FC. Reductions of FD may be related to a lowered intra-axonal volume as a result of axonal degeneration (Raffelt et al., 2017). In this scenario, our findings might reflect the occurrence of Wallerian degeneration in the affected descending pathways–possibly secondary to cortical gray matter atrophy (Worker et al., 2014). Our findings support the early-stage white matter involvement in corpus callosum in PSP, which may aid in our understanding of the difference in pathogenesis between PSP and MSA.

Previous studies have reported that patients with PSP display abnormal diffusion metrics in the main white matter tract in addition to corpus callosum—for example, the internal capsule (Padovani et al., 2006; Agosta et al., 2012). Our findings of altered fixel-related indices in these regions suggest that the previously reported abnormalities are likely the results of microstructural white matter injury. Patients with PSP have a reduced FDC in both the corona radiata and internal capsules. Such alterations are in line with the higher severity of motor deficits observed in patients with PSP than in those with PD (Alster et al., 2020).

Notably, regions with reduced FDC in the corona radiata, internal capsules, and midbrain had broad overlaps with those showing diminished FC. The latter alteration can be attributed to a narrowing of extra-axonal space followed by axonal loss and disruption of myelin sheaths as a result of white matter atrophy (Raffelt et al., 2017). Interestingly, regions with reduced FD was found in bilateral medial thalami. These fibers are parts of thalamic radiation which connect the thalami with the cortex via internal capsule (Sun et al., 2018). Reduced FD, rather than FC, might imply early changes within these fibers. Similar regions have been reported in a quantitative study of histology, which showed vacuolation and glial inclusion in descending white matter tract from frontal cortex through the internal capsules and midbrain (Armstrong, 2013). Our findings suggest the involvement of the thalamic radiation in PSP, which may help distinguishing this disease from PD and MSA.

Taken together, these results suggest that the severity of white matter damage in internal capsules, thalamic radiation and

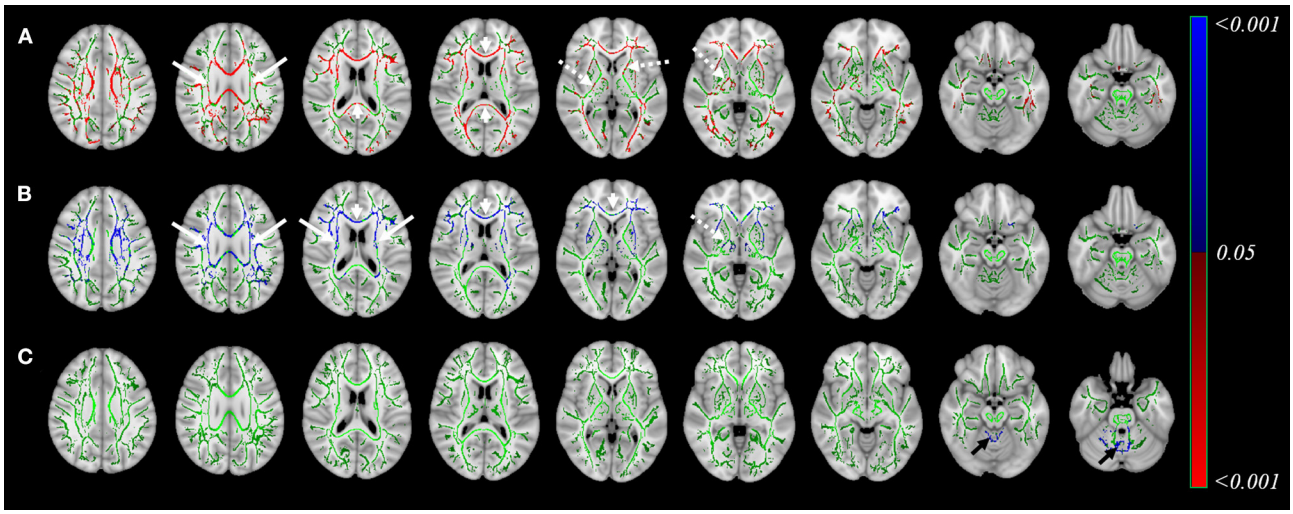


**FIGURE 5 |** Result of Tract-Based Spatial Statistics in patients with PSP or MSA as compared to PD. This figure shows the analysis from tract-based spatial statistics in patients with PSP or MSA, when compared to PD. Reduced fractional anisotropy (FA, Result of Tract-Based Spatial Statistics in patients with PSP or MSA as compared to PD. This figure shows the analysis from tract-based spatial statistics in patients with PSP or MSA, when compared to PD. Reduced fractional anisotropy (FA, A) and increased mean diffusivity (MD, B) in patients with PSP was found in bilateral corona radiate (arrows), internal capsules (dashed arrow), superior longitudinal fasciculi, posterior thalamic radiation, as well as genu and splenium of the corpus callosum (arrowhead). Increased MD in patients with MSA (C) was found in in bilateral cerebellar peduncle (black arrows). Color indicated the *p*-value, with color code included. Color Green: the identified white matter skeleton.) and increased mean diffusivity (MD, **B**) in patients with PSP was found in bilateral corona radiate (arrows), internal capsules (dashed arrow), superior longitudinal fasciculi, posterior thalamic radiation, as well as genu and splenium of the corpus callosum (arrowhead). Increased MD in patients with MSA **(C)** was found in in bilateral cerebellar peduncle (black arrows). Color indicated the *p*-value, with color code included. Color Green: the identified white matter skeleton.

midbrain in PSP is more pronounced than in PD. Our findings suggest that the previously reported abnormalities are likely the results of microstructural white matter injury.

## MSA: Corona Radiata, Internal Capsule, and Middle Cerebellar Peduncles

MSA is specifically characterized by an involvement of the middle cerebellar peduncles (Poewe and Wenning, 2002). When patients with MSA were compared to those with PD, we found significant reductions of both FDC and FC in the main descending white matter pathways. A previous DTI study identified large areas characterized by reduced FA and increased MD in white matter tracts—especially in the supratentorial and infratentorial compartments (Tha et al., 2010). Here, we provide evidence of a substantial axonal loss in the white matter located in these areas.

When compared with those with PD as well as PSP, we found significant reductions of FDC in the middle cerebellar peduncles—which was accompanied by parallel declines in both FD and FC. Increased diffusivity has been previously reported in this region (Tsukamoto et al., 2012). Our results indicate that these regions, characterized by a reduced FDC, were driven by a concomitant decline in both FD and FC suggesting that axonal degeneration is likely the main contributor to microstructural damage. MSA can be associated with a more severe axonal neurodegeneration and white matter atrophy in these areas compared with either PD or PSP. Previous postmortem pathology study showed that the white matter atrophy of the cerebellum in patients with MSA can be attributed to the loss of myelinated fibers and gliosis (Matsusue et al., 2009b). Our observation of reduced FD and FC, as explained by the simultaneous presence of axonal loss and white matter atrophy, might ultimately reflect more severe derangements as related to the motor deficits in patients with MSA than in those with PD.

Significant reductions of both FDC and FC were also found in the main descending white matter pathways, namely the left corona radiata, bilateral posterior limbs of internal capsule, cerebral peduncles, and ventral and dorsal transverse pontine fibers. Concomitant reduction of all three fixel-related indices in these regions implies severe white matter damages. This is in line with the more severe morbidity of MSA in comparison to PSP and PD. Here, we provide image-based evidence of a substantial axonal loss in the white matter located in these areas.

## Limitation

Our findings should be interpreted in the context of some limitations. In this study, patients with PD was used as a "parkinsonian control" group with which both the patients with MSA or PSP were compared to. In the future study when using a prospective design, we will recruit the healthy control in our study for a comprehensive understanding of the white matter involvement in Parkinsonism. Secondly, it may be argued that the study groups were different in terms of imaging protocols. However, the effect from this variable, together with age and sex, has been considered and controlled in the statistical analysis. Provided the acquisition and the analysis pipeline are the same, these measures can be quantifiable to allow for assessment of disease severity within study. However,

it would be necessary to perform advanced statistical analysis to determine the sensitivity and specificity before its potential application in early-stage therapeutic trials, or to monitor disease progression. More radiologic—pathologic correlation studies are necessary to scrutinize the biologic mechanisms of these fixel-related indices' alteration. These caveats notwithstanding, we successfully applied FBA and identified specific patterns of white matter degeneration that distinguished PD from atypical parkinsonisms (MSA and PSP).

## DATA AVAILABILITY STATEMENT

The data that support the findings of this study are available from the corresponding author upon reasonable request.

## ETHICS STATEMENT

The studies involving human participants were reviewed and approved by the study protocol complied with the tenets of the Helsinki declaration, and ethical approval was granted by the Chang Gung Medical Foundation Institutional Review Board. Owing to the retrospective nature of the study, the need for informed consent was waived. Written informed consent for participation was not required for this study in accordance with the national legislation and the institutional requirements.

## AUTHOR CONTRIBUTIONS

T-TN: conception and design of study, acquisition of clinical data, and writing and revision of the manuscript. J-SC: conception and design of study, statistical analysis, and writing the first draft. Y-LC, Y-CL, C-SL, Y-HW, and Y-MW: acquisition of clinical data and revision the manuscript. C-CT: statistical analysis and revision the manuscript. N-TH: revision the manuscript. J-JW: conception and design of study, writing and revision the manuscript, study supervision, and obtaining funding. All authors contributed to the article and approved the submitted version.

## FUNDING

This work was supported by the Ministry of Science and Technology Taiwan (grants MOST 106-2314-B-182-018-MY3, MOST 109-2221-E-182-009-MY3, MOST 109-2314-B-182-021-MY3); the Healthy Aging Research Center (grants EMRPD1I0501, EMRPD1I0471, EMRPD1K0451, EMRPD1K0481); and the Chang Gung Memorial Hospital (grants CMRPD1G0561-2, CMRPG2B0251, and CMRPG2J0141).

## ACKNOWLEDGMENTS

The imaging facility was supported by the Imaging Core Laboratory of the Institute for Radiological Research and the Center for Advanced Molecular Imaging and Translation. The authors thank the Neuroscience Research Center (Chang Gung Memorial Hospital) and the Healthy Aging Research Center (Chang Gung University) for their invaluable support.

## SUPPLEMENTARY MATERIAL

The Supplementary Material for this article can be found online at: https://www.frontiersin.org/articles/10.3389/fnagi.2021.625874/full#supplementary-material

## REFERENCES

Agosta, F., Pievani, M., Svetel, M., Jecmenica Lukic, M., Copetti, M., Tomic, A., et al. (2012). Diffusion tensor MRI contributes to differentiate Richardson's syndrome from PSP-parkinsonism. *Neurobiol. Aging* 33, 2817–2826. doi: 10.1016/j.neurobiolaging.2012.02.002

Alster, P., Madetko, N., Koziorowski, D., and Friedman, A. (2020). Progressive Supranuclear Palsy-Parkinsonism Predominant (PSP-P)-a clinical challenge at the boundaries of PSP and Parkinson's Disease (PD). *Front. Neurol.* 11:180. doi: 10.3389/fneur.2020.00180

Andersson, J. L., and Sotiropoulos, S. N. (2015). Non-parametric representation and prediction of single- and multi-shell diffusion-weighted MRI data using Gaussian processes. *Neuroimage* 122, 166–176. doi: 10.1016/j.neuroimage,.2015.07.067

Andersson, J. L. R., and Sotiropoulos, S. N. (2016). An integrated approach to correction for off-resonance effects and subject movement in diffusion MR imaging. *Neuroimage* 125, 1063–1078. doi: 10.1016/j.neuroimage.2015.10.019

Armstrong, R. A. (2013). White matter pathology in progressive supranuclear palsy (PSP): a quantitative study of 8 cases. *Clin. Neuropathol.* 32, 399–405. doi: 10.5414/NP300608

Biundo, R., Formento-Dojot, P., Facchini, S., Vallelunga, A., Ghezzo, L., Foscolo, L., et al. (2011). Brain volume changes in Parkinson's disease and their relationship with cognitive and behavioural abnormalities. *J. Neurol. Sci.* 310, 64–69. doi: 10.1016/j.jns.2011.08.001

Boxer, A. L., Yu, J. T., Golbe, L. I., Litvan, I., Lang, A. E., and Hoglinger, G. U. (2017). Advances in progressive supranuclear palsy: new diagnostic criteria, biomarkers, and therapeutic approaches. *Lancet Neurol.* 16, 552–563. doi: 10.1016/S1474-4422(17)30157-6

Burton, E. J., McKeith, I. G., Burn, D. J., Williams, E. D., and O'Brien, J. T. (2004). Cerebral atrophy in Parkinson's disease with and without dementia: a comparison with Alzheimer's disease, dementia with Lewy bodies and controls. *Brain* 127, 791–800. doi: 10.1093/brain/awh088

Chen, Y.-L., Zhao, X.-A., Ng, S.-H., Lu, C.-S., Lin, Y.-C., Cheng, J.-S., et al. (2020). Prediction of the clinical severity of progressive supranuclear palsy by diffusion tensor imaging. *J. Clin. Med.* 9:40. doi: 10.3390/jcm9010040

Chen, Y. L., Lin, Y. J., Lin, S. H., Tsai, C. C., Lin, Y. C., Cheng, J. S., et al. (2019). The effect of spatial resolution on the reproducibility of diffusion imaging when controlled signal to noise ratio. *Biomed. J.* 42, 268–276. doi: 10.1016/j.bj.2019.03.002

Gilman, S., Low, P. A., Quinn, N., Albanese, A., Ben-Shlomo, Y., Fowler, C. J., et al. (1999). Consensus statement on the diagnosis of multiple system atrophy. *J. Neurol. Sci.* 163, 94–98. doi: 10.1016/S0022-510X(98)00304-9

Giordano, A., Tessitore, A., Corbo, D., Cirillo, G., de Micco, R., Russo, A., et al. (2013). Clinical and cognitive correlations of regional gray matter atrophy in progressive supranuclear palsy. *Parkinsonism Relat. Disord.* 19, 590–594. doi: 10.1016/j.parkreldis.2013.02.005

Goetz, C. G., Poewe, W., Rascol, O., Sampaio, C., Stebbins, G. T., Counsell, C., et al. (2004). Movement Disorder society task force report on the Hoehn and Yahr staging scale: status and recommendations. *Mov. Disord.* 19, 1020–1028. doi: 10.1002/mds.20213

Hughes, A. J., Ben-Shlomo, Y., Daniel, S. E., and Lees, A. J. (1992). What features improve the accuracy of clinical diagnosis in Parkinson's disease:

a clinicopathologic study. *Neurology* 42, 1142–1146. doi: 10.1212/WNL.42.6.1142

Jbabdi, S., Behrens, T. E., and Smith, S. M. (2010). Crossing fibres in tract-based spatial statistics. *Neuroimage* 49, 249–256. doi: 10.1016/j.neuroimage.2009.08.039

Jeurissen, B., Tournier, J. D., Dhollander, T., Connelly, A., and Sijbers, J. (2014). Multi-tissue constrained spherical deconvolution for improved analysis of multi-shell diffusion MRI data. *Neuroimage* 103, 411–426. doi: 10.1016/j.neuroimage.2014.07.061

Kellner, E., Dhital, B., Kiselev, V. G., and Reisert, M. (2016). Gibbs-ringing artifact removal based on local subvoxel-shifts. *Magn. Reson. Med*. 76, 1574–1581. doi: 10.1002/mrm.26054

Kuchling, J., Backner, Y., Oertel, F. C., Raz, N., Bellmann-Strobl, J., Ruprecht, K., et al. (2018). Comparison of probabilistic tractography and tract-based spatial statistics for assessing optic radiation damage in patients with autoimmune inflammatory disorders of the central nervous system. *Neuroimage Clin*. 19, 538–550. doi: 10.1016/j.nicl.2018.05.004

Litvan, I., Agid, Y., Calne, D., Campbell, G., Dubois, B., Duvoisin, R. C., et al. (1996). Clinical research criteria for the diagnosis of progressive supranuclear palsy (Steele-Richardson-Olszewski syndrome): report of the NINDS-SPSP international workshop. *Neurology* 47, 1–9. doi: 10.1212/WNL.47.1.1

Lu, C.-S., Ng, S.-H., Weng, Y.-H., Cheng, J.-S., Lin, W.-Y., Wai, Y.-Y., et al. (2016). Alterations of diffusion tensor MRI parameters in the brains of patients with Parkinson's disease compared with normal brains: possible diagnostic use. *Eur. Radiol.* 26, 3978–3988. doi: 10.1007/s00330-016-4232-7

Martinez-Martin, P., Gil-Nagel, A., Gracia, L. M., Gomez, J. B., Martinez-Sarries, J., and Bermejo, F. (1994). Unified Parkinson's disease rating scale characteristics and structure. The cooperative multicentric group. *Mov. Disord*. 9, 76–83. doi: 10.1002/mds.870090112

Matsusue, E., Fujii, S., Kanasaki, Y., Kaminou, T., Ohama, E., and Ogawa, T. (2009). Cerebellar lesions in multiple system atrophy: postmortem MR imaging-pathologic correlations. *AJNR Am. J. Neuroradiol.* 30, 1725–1730. doi: 10.3174/ajnr.A1662

McFarland, N. R. (2016). Diagnostic approach to atypical Parkinsonian syndromes. *Continuum (Minneap. Minn)*. 22, 1117–1142. doi: 10.1212/CON.0000000000000348

McFarland, N. R., and Hess, C. W. (2017). Recognizing atypical Parkinsonisms: "Red Flags" and therapeutic approaches. *Semin. Neurol.* 37, 215–227. doi: 10.1055/s-0037-1602422

Meissner, W. G., Fernagut, P. O., Dehay, B., Peran, P., Traon, A. P., Foubert-Samier, A., et al. (2019). Multiple system atrophy: recent developments and future perspectives. *Mov. Disord.* 34, 1629–1642. doi: 10.1002/mds.27894

Mito, R., Raffelt, D., Dhollander, T., Vaughan, D. N., Tournier, J. D., Salvado, O., et al. (2018). Fibre-specific white matter reductions in Alzheimer's disease and mild cognitive impairment. *Brain* 141, 888–902. doi: 10.1093/brain/awx355

Mori, S., and Zhang, J. (2006). Principles of diffusion tensor imaging and its applications to basic neuroscience research. *Neuron* 51, 527–539. doi: 10.1016/j.neuron.2006.08.012

Nichols, T. E., and Holmes, A. P. (2002). Nonparametric permutation tests for functional neuroimaging: a primer with examples. *Hum. Brain Mapp*. 15, 1–25. doi: 10.1002/hbm.1058

Padovani, A., Borroni, B., Brambati, S. M., Agosti, C., Broli, M., Alonso, R., et al. (2006). Diffusion tensor imaging and voxel based morphometry study in early progressive supranuclear palsy. *J. Neurol. Neurosurg. Psychiatry* 77, 457–463. doi: 10.1136/jnnp.2005.075713

Pecheva, D., Tournier, J. D., Pietsch, M., Christiaens, D., Batalle, D., Alexander, D. C., et al. (2019). Fixel-based analysis of the preterm brain: disentangling bundle-specific white matter microstructural and macrostructural changes in relation to clinical risk factors. *Neuroimage Clin.* 23:101820. doi: 10.1016/j.nicl.2019.101820

Poewe, W., and Wenning, G. (2002). The differential diagnosis of Parkinson's disease. *Eur. J. Neurol.* 9, 23–30. doi: 10.1046/j.1468-1331.9.s3.3.x

Raffelt, D. A., Tournier, J. D., Smith, R. E., Vaughan, D. N., Jackson, G., Ridgway, G. R., et al. (2017). Investigating white matter fibre density and morphology using fixel-based analysis. *Neuroimage* 144, 58–73. doi: 10.1016/j.neuroimage.2016.09.029

Rau, Y. A., Wang, S. M., Tournier, J. D., Lin, S. H., Lu, C. S., Weng, Y. H., et al. (2019). A longitudinal fixel-based analysis of white matter alterations in patients with Parkinson's disease. *Neuroimage Clin.* 24:102098. doi: 10.1016/j.nicl.2019.102098

Smith, S. M., Jenkinson, M., Johansen-Berg, H., Rueckert, D., Nichols, T. E., Mackay, C. E., et al. (2006). Tract-based spatial statistics: voxelwise analysis of multi-subject diffusion data. *Neuroimage* 31, 1487–1505. doi: 10.1016/j.neuroimage.2006.02.024

Sun, C., Wang, Y., Cui, R., Wu, C., Li, X., Bao, Y., et al. (2018). Human thalamic-prefrontal peduncle connectivity revealed by diffusion spectrum imaging fiber tracking. *Front. Neuroanat*. 12:24. doi: 10.3389/fnana.2018.00024

Tha, K. K., Terae, S., Yabe, I., Miyamoto, T., Soma, H., Zaitsu, Y., et al. (2010). Microstructural white matter abnormalities of multiple system atrophy: *in vivo* topographic illustration by using diffusion-tensor MR imaging. *Radiology* 255, 563–569. doi: 10.1148/radiol.10090988

Tsai, C.-C., Weng, Y.-H., Lin, S.-H., Chen, P.-Y., and Wu, Y.-M. (2020). A method for the prediction of clinical outcome using diffusion magnetic resonance imaging: application on Parkinson's disease. *J. Clin. Med.* 9:647. doi: 10.3390/jcm,9030647

Tsukamoto, K., Matsusue, E., Kanasaki, Y., Kakite, S., Fujii, S., Kaminou, T., et al. (2012). Significance of apparent diffusion coefficient measurement for the differential diagnosis of multiple system atrophy, progressive supranuclear palsy, and Parkinson's disease: evaluation by 3.0-T MR imaging. *Neuroradiology* 54, 947–955. doi: 10.1007/s00234-012-1009-9

Tustison, N. J., Avants, B. B., Cook, P. A., Zheng, Y., Egan, A., Yushkevich, P. A., et al. (2010). N4ITK: improved N3 bias correction. *IEEE Trans. Med. Imaging* 29, 1310–1320. doi: 10.1109/TMI.2010.2046908

Veraart, J., Novikov, D. S., Christiaens, D., Ades-Aron, B., Sijbers, J., and Fieremans, E. (2016). Denoising of diffusion MRI using random matrix theory. *Neuroimage* 142, 394–406. doi: 10.1016/j.neuroimage.2016.08.016

Wai, Y.-Y., Wang, J.-J., Weng, Y.-H., Lin, W.-Y., Ma, H.-K., Ng, S.-H., et al. (2012). Cortical involvement in a gait-related imagery task: comparison between Parkinson's disease and normal aging. *Parkinsonism Relat. Disord.* 18, 537–542. doi: 10.1016/j.parkreldis.2012.02.004

Wang, J., Wai, Y., Lin, W. Y., Ng, S., Wang, C. H., Hsieh, R., et al. (2010). Microstructural changes in patients with progressive supranuclear palsy: a diffusion tensor imaging study. *J. Magn. Reson. Imaging* 32, 69–75. doi: 10.1002/jmri.22229

Wang, J.-J., Lin, W.-Y., Lu, C.-S., Weng, Y.-H., Ng, S.-H., Wang, C.-H., et al. (2011). Parkinson disease: diagnostic utility of diffusion kurtosis imaging. *Radiology* 261, 210–217. doi: 10.1148/radiol.11102277

Whitwell, J. L., Master, A. V., Avula, R., Kantarci, K., Eggers, S. D., Edmonson, H. A., et al. (2011). Clinical correlates of white matter tract degeneration in progressive supranuclear palsy. *Arch. Neurol.* 68, 753–760. doi: 10.1001/archneurol.2011.107

Worker, A., Blain, C., Jarosz, J., Chaudhuri, K. R., Barker, G. J., Williams, S. C., et al. (2014). Diffusion tensor imaging of Parkinson's disease, multiple system atrophy and progressive supranuclear palsy: a tract-based spatial statistics study. *PLoS ONE* 9:e112638. doi: 10.1371/journal.pone.0112638

**Conflict of Interest:** The authors declare that the research was conducted in the absence of any commercial or financial relationships that could be construed as a potential conflict of interest.

frontiers in Aging Neuroscience

REVIEW
published: 13 April 2021
doi: 10.3389/fnagi.2021.632054

# Mechanism of White Matter Injury and Promising Therapeutic Strategies of MSCs After Intracerebral Hemorrhage

*Jing Li[1], Linglong Xiao[1], Dian He[1], Yunhao Luo[2] and Haitao Sun[1,2,3]**

*[1] Neurosurgery Center, The National Key Clinical Specialty, The Engineering Technology Research Center of Education Ministry of China on Diagnosis and Treatment of Cerebrovascular Disease, Guangdong Provincial Key Laboratory on Brain Function Repair and Regeneration, The Neurosurgery Institute of Guangdong Province, Zhujiang Hospital, Southern Medical University, Guangzhou, China, [2] Division of Laboratory Medicine, Clinical Biobank Center, Microbiome Medicine Center, Zhujiang Hospital, Southern Medical University, Guangzhou, China, [3] Key Laboratory of Mental Health of The Ministry of Education, Guangdong-Hong Kong-Macao Greater Bay Area Center for Brain Science and Brain-Inspired Intelligence, Southern Medical University, Guangzhou, China*

Intracerebral hemorrhage (ICH) is the most fatal subtype of stroke with high disability and high mortality rates, and there is no effective treatment. The predilection site of ICH is in the area of the basal ganglia and internal capsule (IC), where exist abundant white matter (WM) fiber tracts, such as the corticospinal tract (CST) in the IC. Proximal or distal white matter injury (WMI) caused by intracerebral parenchymal hemorrhage is closely associated with poor prognosis after ICH, especially motor and sensory dysfunction. The pathophysiological mechanisms involved in WMI are quite complex and still far from clear. In recent years, the neuroprotection and repairment capacity of mesenchymal stem cells (MSCs) has been widely investigated after ICH. MSCs exert many unique biological effects, including self-recovery by producing growth factors and cytokines, regenerative repair, immunomodulation, and neuroprotection against oxidative stress, providing a promising cellular therapeutic approach for the treatment of WMI. Taken together, our goal is to discuss the characteristics of WMI following ICH, including the mechanism and potential promising therapeutic targets of MSCs, aiming at providing new clues for future therapeutic strategies.

**Keywords: intracerebral hemorrhage, white matter injury, mesenchymal stem cells, corticospinal tract, cell therapy**

OPEN ACCESS

***Edited by:***
*Yuanli Zhao,*
*Capital Medical University, China*

***Reviewed by:***
*Gang Chen,*
*First Affiliated Hospital of Soochow University, China*
*Julien Rossignol,*
*Central Michigan University, United States*

***Correspondence:**
*Haitao Sun*
*2009sht@smu.edu.cn*

***Received:*** *22 November 2020*
***Accepted:*** *18 March 2021*
***Published:*** *13 April 2021*

***Citation:***
*Li J, Xiao L, He D, Luo Y and Sun H (2021) Mechanism of White Matter Injury and Promising Therapeutic Strategies of MSCs After Intracerebral Hemorrhage. Front. Aging Neurosci. 13:632054. doi: 10.3389/fnagi.2021.632054*

## INTRODUCTION

Intracerebral hemorrhage (ICH) is triggered by the spontaneous rupture of blood vessels, wherein the blood constituents penetrate the brain parenchyma following a path of least resistance and thus destroy both gray and white matter (GM and WM) structures (Qureshi et al., 2009). ICH is the most lethal form of stroke characterized by high morbidity, high disability, and high mortality with no

effective treatment. It was demonstrated that more than 77% of ICH patients suffered WM injury (WMI), and a better understanding of WMI and remyelination may shed new light on the treatment of ICH (Smith et al., 2004).

Damage to WM fibers which establish connections among different regions impairs brain connectivity, leading to functional deficits. Dysfunction following cerebral parenchymal hemorrhage derives not only from neuron or synapse losses, but also from primary damage to the WM axons. The area of the basal ganglia where abundant WM fiber tracts cross is the predominant location of hematoma in human ICH. The internal capsule (IC), which lies between the putamen (embraced in the basal ganglia) and the thalamus, contains both descending and ascending fiber bundles conducting sensory, motor, and visual information. Once bleeding occurs in this region, the physiological structure and function of the WM are interrupted to varying degrees, leading to various complications and dysfunctions, such as hemiplegia, hemianopia, hemidysesthesia, and aphasia (Kusano et al., 2009; Balami and Buchan, 2012; Keep et al., 2012; Wu et al., 2017). The corticospinal tracts (CSTs) and corticonuclear tracts' damage can cause contralateral hemiplegia. Destruction of the optic radiation following deep basal ganglia ICH leads to hemianopia, while hemidysesthesia is caused due to lesions of the central thalamic radiations. It is worth mentioning that IC injury can present all these three clinical manifestations resulting in serious sensorimotor dysfunction in human ICH. WMI is considered the major cause of motor-sensory disorders commonly seen in ICH patients. Therefore, reducing WMI or repairing WM after ICH is critical for reducing long-term neurological deficits, especially for motor function recovery.

In the past few decades, stem cell therapy has been actively explored for the treatment of stroke. Mesenchymal stem cells (MSCs) are pivotal to tissue homeostasis, repair, and regeneration for their self-renewing and multipotent characteristics, which are emerging as the most promising means of allogeneic cell therapy. Basic and clinical research clarify that MSCs are not antigen-presenting cells and would not cause activation of the host's immune system (Tse et al., 2003). These cells can be harvested and expanded from a variety of adult and perinatal tissues, such as bone marrow, adipose tissue, peripheral blood, fetal tissues, umbilical cord tissues, and placental tissues. The neuroprotection and repairment capacity of MSCs has been widely investigated after ICH. MSCs exert many unique biological effects in tissue replacement, neurotrophy, neurogenesis, angiogenesis, anti-apoptosis, and immunomodulation (Caplan and Dennis, 2006; Mine et al., 2013; Galipeau and Sensebe, 2018; Song et al., 2020), which provides a promising therapeutic strategy in the treatment of WMI. MSCs participate in both innate immunity and adaptive immunity. Their immunomodulatory functions are exerted mainly via the release of bioactive factors and interactions with immune cells, which then change the damaged microenvironment by shifting the balance from toxic to protective regenerative events.

Herein, this review is primarily focused on the pathophysiology and onset mechanism of post-ICH WMI and potential therapy methods of MSCs, in hopes that it can benefit clinical treatment.

## COMPOSITION AND THE MAIN FUNCTION OF BRAIN WM

White matter comprises over 40% of the total volume of adult brain tissue and takes an indispensable part in distributed neural networks that are responsible for neurobehavioral management (Bedell and Narayana, 1998; Herndon et al., 1998). The two main parts- myelinated axon tracts and supporting glial cells including oligodendrocytes (OLs), astrocytes, and microglia- are embraced in WM. The axons (nerve fibers) are surrounded by multiple dense myelin membranes produced by mature OLs (Kang and Yao, 2019), the molecular structure integrity of which makes axons insulated from each other, thus promising the quick and efficient conduction of electrical nerve impulses (transmitting the action potentials) and protecting the nerve fibers from injury (Roncagliolo et al., 2006).

Specifically, three parts constitute WM fiber bundles: projection tracts, commissural tracts, and association tracts (Gerrish et al., 2014). Projection tracts transmit nerve signals from the cortex to other regions of the central nervous system (CNS) (Ge et al., 2002). For instance, CST is the dominant pathway responsible for conveying descending information from the cerebral cortex to the spinal cord. The commissural tracts allow the communication between the left and right cerebral hemispheres (Ge et al., 2002). The association tracts build up connections among cortical lobes within the ipsilateral hemisphere. All these tracts form networks between different regions and serve diverse functions (Ge et al., 2002). Up to now, a large amount of research has clarified the brain functions associated with WM, such as cognitive function, motor function, reading, and practicing abilities (Schmahmann et al., 2008; Carreiras et al., 2009).

## PATHOPHYSIOLOGY OF WMI AFTER ICH

The pathophysiology change of WMI after ICH is mainly characterized by demyelination, axonal injury, and death of OLs. OLs are the sole source of myelin in the adult CNS, and generally form insulating myelin sheaths marked by myelin basic protein (MBP), enhancing the propagation of action potentials and supporting neuronal and axonal integrity through metabolic coupling under physical circumstances (Bacmeister et al., 2020). OLs contain a high level of iron and are especially sensitive to iron overload, which makes them quite vulnerable to hemorrhagic insults; meanwhile, missed OLs leave axons susceptible to degeneration (Windrem et al., 2020). With the degradation of hemoglobin released from dead erythrocytes, there is a sharp increase in intracellular $Fe^{2+}$ destroying OLs, and iron chelator can inhibit this oxidative toxicity in OLs. Both apoptosis and necrosis are involved in the mechanism of OLs loss. With the onset of ICH, OLs' expression of caspase-3 in the lesion increases and most of the damaged cells undergo necrosis. Mitochondrial dysfunction is also attributed to OLs apoptosis. Fortunately, OLs maintain the capacity of regeneration and repair after damage to the CNS. OLs death is accompanied by oligodendrocyte progenitor cells (OPCs) proliferation during

the acute period in the perihematomal WMI, which is responsible for generating new OLs to remyelinate denuded axons and reconstruct neuronal function.

Dramatical demyelination and axonal damage were first observed at the perihematomal site within three days after ICH, and the axonal damage gradually extended to the adjacent parenchyma over time (Wasserman and Schlichter, 2008). These pathologic changes are highly related to brain edema and neurologic dysfunction, indicating that WMI plays a critical role in neurologic impairment. Hijioka et al. (2016) has investigated the exact relationship between axon pathology and impaired sensorimotor functions; the former mainly referred to axonal transport deficits and structural destruction. The axonal dysfunction in the IC was confirmed to be strongly linked with early motion disturbance after ICH in mice (Hijioka et al., 2016). Remyelination and axonal regeneration are considered valid repair forms in WMI (Joseph et al., 2016). Remyelination is defined as adult OPCs differentiating into new myelin-forming OLs in a regenerative process after CNS demyelination (Gensert and Goldman, 1997; Fancy et al., 2004; Kang and Yao, 2019). To successfully regenerate, damaged axons must reseal denuded stumps, rebuild the cytoskeleton, colligate and transport building substrates, package axon modules, and form growth cones, which is a highly energy-demanding process (Bradke et al., 2012; Lu et al., 2014; He and Jin, 2016). Based on this, Han et al. (2020) raised the "energy deficit" definition and proved that enhancing mitochondrial transport and energetic metabolism can dramatically stimulate axonal regeneration, promoting functional restoration in a spinal cord injury (SCI) animal model. Ultrastructural features of collagenase-induced ICH have been systematically examined in mice over time (Li et al., 2018). Obvious axonal demyelination and degeneration, and the presence of dystrophic neurites in the axons, were demonstrated but OLs proliferation was also observed, which is responsible for the myelination of axons (Li et al., 2018). They first showed a robust inflammatory response of erythrophagocytosis by microglia and macrophages after ICH by transmission electronic microscope (TEM) (Li et al., 2018). Myelination could also be regulated by the growth factor neuregulin (NRG) through binding to the transmembrane tyrosine kinase receptors (ErbB) on unsheathing OLs. Collectively, severe changes of myelin destruction and swelling axons are clear in the ICH animal models, but the exact mechanisms contributing to the loss of motor function are uncertain.

# PATHOPHYSIOLOGY MECHANISM OF WMI AFTER ICH

The influx of blood from vessels into the brain destroys GM and WM. Increasing studies have focused on the implicated pathophysiology of WMI after ICH (Wasserman and Schlichter, 2008; Gerrish et al., 2014; Chen W. et al., 2019; Chen Z. et al., 2019). It is demonstrated that the mass effect and barotrauma during hematoma formation present immediate compression of adjacent brain tissue the moment of ICH onset, which is defined as the primary brain injury. Soon afterward, secondary brain injury- excitotoxicity, oxidative stress, and neuroinflammation- aggravate the WMI leading to neurological deterioration (Aronowski and Zhao, 2011; Babu et al., 2012; Duan et al., 2016; Lan et al., 2017b), accompanied by a succession of pathologic changes which contain hemodynamic changes resulted from ischemia, increased cerebral edema, disruption of the blood–brain barrier (BBB) function, effects of erythrocytes decomposition products, and apoptosis (Aronowski and Zhao, 2011; Keep et al., 2012; Zhou et al., 2014; Chen S. et al., 2015). And it was shown that intracerebral hematoma extended via perivascular spaces and the perineurium (Yin et al., 2013). All these pathologic changes make the nerve fibers within the hematoma lesion distend, distort, and finally disrupt to a point at which they cannot be rescued (**Figure 1**). Those located in the perihematomal, meanwhile, exert varying degrees of impairment, exactly where researchers continuously focus on and try to intervene.

## Immune Inflammatory Response

Complex immune and inflammatory cascades characterized by the mobilization and activation of inflammatory molecules are triggered at the moment the blood composition is released into the substance, which plays a pivotal role in ICH-induced brain injury (Lan et al., 2017b), especially during the secondary WMI. The primary and secondary damage usually mutually affect the whole developing process. The leakage of BBB after ICH is mainly derived from endothelial cell activation and vascular $ONOO^-$ formation, leading to the reduction of key tight junction proteins which generally promise the BBB permeability such as claudin-5, occludin, and zonula occludens (ZO)-1 (Abbott et al., 2010). There is increasing evidence that an inflammatory response can promote the formation of edema by increasing the BBB permeability near the hematoma, thereby aggravating the mass effect, enhancing the process of cell death through secondary ischemia, and further causing inflammatory damage to the surrounding brain tissue (Chu et al., 2014; Wang T. et al., 2015). Many inflammatory cells have been demonstrated to be involved and work in concert to modulate the inflammatory response both in ischemic stroke and ICH. Herein, we introduce several immune cells involved in inflammation in detail as follows.

### Microglia

Microglia, the resident myeloid phagocytes in the brain parenchyma, constantly and rapidly monitor the brain microenvironment for threats and damage and play a critical role in maintaining homeostasis in the brain by removing pathogens and injured brain tissue debris, and reconstructing the extracellular matrix and synapses, just like a "cop." When encountered with ICH, they can be activated within minutes and migrate to the lesion together with peripheral macrophages (Lan et al., 2017b), and become highly phagocytic to respond to factors secreted by necrotic neurons or astrocytes, like adenosine triphosphate (ATP), galactin-3, or high mobility group box 1 (HMGB1), which are all embraced in damage-associated molecular pattern molecules (DAMPs, also known as alarmins) (Kong and Le, 2011; Ohnishi et al., 2011; Fang et al., 2013; Zhou et al., 2014; Xiao et al., 2020). Meanwhile,

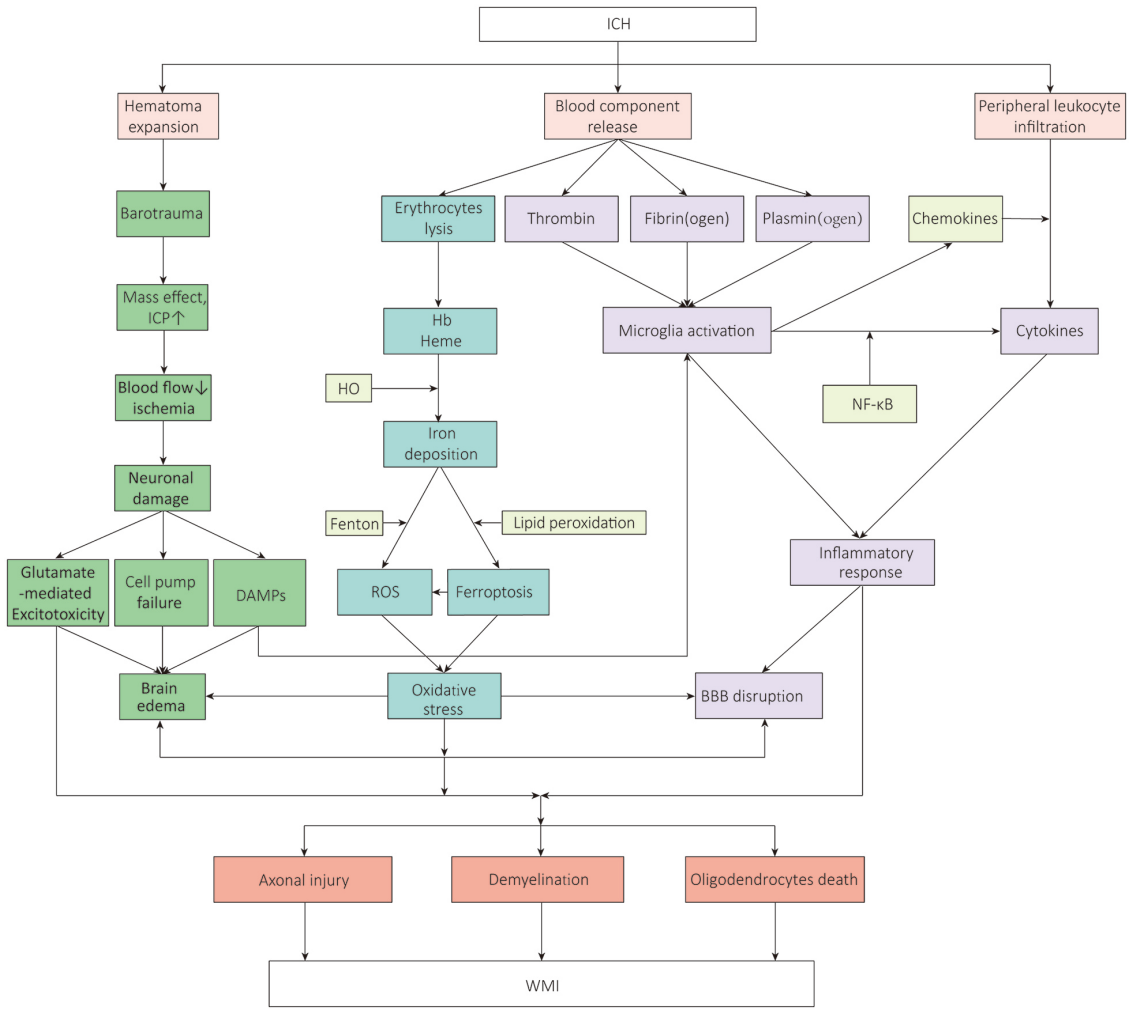


**FIGURE 1 |** The mechanisms and signal pathways of white matter injury after intracerebral hemorrhage. WMI, white matter injury; ICH, intracerebral hemorrhage; ICP, intracranial pressure; DAMPs, damage-associated molecular pattern molecules; HO, hemeoxygenase; BBB, blood-brain barrier; NF-κB, nuclear factor-κB; ROS, reactive oxygen species.

microglia cells secrete multiple cytokines and chemokines associated with the axon-glial injury via the transcription factor nuclear factor-κB (NF-κB), and show enhanced phagocytosis, thereby aggravating structural WMI. DAMPs can initiate the activation of microglia via several toll-like receptors (TLRs) in the neuroinflammatory processes after ICH. The TLR4 on microglia cell surfaces generally interacts with TRIF and MyD88, and then the information is passed through downstream NF-κB, like phosphorylated P65, and several other secreted proinflammatory factors, causing inflammation (Zhou et al., 2014; Lan et al., 2017a). It was proven that traumatic brain injury (TBI) could induce a rapid and persistent up-regulation of Myd88, NF-κB, and proinflammatory cytokines (Ling et al., 2013). Microglial activation can also be induced by thrombin and complement factors via protease-activated receptors (PARs). A newly found adenosine diphosphate (ADP)/ATP-responsive G-protein coupled receptor, P2Y12, helps microglia migrate to the site of injury (Suzuki et al., 2020). Subsequently, microglia cells in an activated state and the toxic molecules secreted further destroy the BBB, leading to peripheral immune cells' infiltration, thus propagating inflammatory damage.

According to the surface markers and intracellular cytokines expressed, microglia can be polarized into classically activated (M1, pro-inflammatory, and neurotoxic) and alternatively activated (M2, anti-inflammatory, and neuroprotective) phenotypes (Zhang et al., 2017). That the microglia can dynamically and temporally change their phenotypes in response to acute brain injury is exactly the pointcut of brain damage intervention researchers pay attention to. M1 microglia could release high levels of proinflammatory cytokines, that, in turn, hinder axonal regeneration and OLs maturation (Lampron et al., 2015; Chen et al., 2017; Qin et al., 2017). In contrast, polarized M2 microglia typically secrete restorative cytokines and growth factors, remove tissue debris through phagocytosis, and promote

remyelination (Olah et al., 2012; Zhao et al., 2015). It was proven that activated microglia act as a double-edged sword and the transfer of M1 to M2 can dramatically alleviate the brain injury caused by inflammation (Zhao et al., 2019).

### Astrocytes

Astrocytes are recognized as active elements of the brain circuitry, and play key roles in maintaining homeostasis of the extracellular environment, including neurotrophic and structural supporting functions, stabilization of cell–cell communications, and anti-oxidative stress functions (Ransom and Ransom, 2012). Activated astrocytes usually respond to CNS disorders through reactive astrogliosis which represent a series of successive processes including changes of gene and protein expression, proliferation and migration of cells, cellular hypertrophy, and formation of glial scars. Some research demonstrated that reactive astrocytes generate neurotrophic factors (NTFs), isolate injured sites, and prevent harmful inflammation. Whereas it was shown that astrocytes could restrain axonal regeneration and hamper other repair processes in the brain by expressing a wide range of molecules as demonstrated in an earlier study (McKeon et al., 1991). Moreover, axonal regeneration and the reconnection among neurons are further inhibited by the resulting glial scar, inhibiting the formation of which does not always alleviate tissue damage in animal experiments (Wanner et al., 2013; Cregg et al., 2014).

### T Lymphocytes

Lymphocytes play a vital role in immune surveillance and homeostasis maintenance in the peripheral system, among which T cells mainly participate in adaptive cellular immunity. $CD4^+$ T cells dominate the lymphocyte population whether in autoblood- or collagenase-induced ICH models, while $CD8^+$ T cells constitute an extremely small infiltrating leukocyte population. Undisputedly, $FoxP3^+CD4^+$ regulatory T cells (Tregs) are the major immunosuppressive lineage of the $CD4^+$ T cell compartment. It is generally supposed that T cells rarely enter the brain parenchyma except when pathologic changes occur, and only when the stroke onset, T cells would migrate largely and infiltrate into the lesion site following the activation of microglia (Ito et al., 2019).

Recent research demonstrated that it was the regulatory T cells inside the brain that exerted robust neuronal protection in ischemic stroke by suppressing neurotoxic astrogliosis through producing epidermal growth factor receptor (EGFR) ligand (Ito et al., 2019). This finding suggests that, in the repair of the ICH process, the function of brain T cells should also be highly focused on. Apart from sustaining immune tolerance (Sakaguchi et al., 2010; Lowther and Hafler, 2012), Tregs perform specialized functions in tissue homeostasis and remodeling mainly through restraining the activation and release of cytokines (Liesz et al., 2009; Ito et al., 2019). IL-10 originating from Tregs can trigger hemoglobin-activated microglia/macrophages toward the M2 phenotype. Similarly, it was indicated that Tregs protected against ICH-induced inflammatory injury by modulating microglia/macrophages polarization through the IL-10/GSK3β/PTEN axis which might exert importance in Treg-induced microglia polarization (Zhou et al., 2017). When co-cultured *in vitro*, Tregs also changed the polarization of microglia, decreased the expression of MHC-II, IL-6, and TNF-α, and increased expression of CD206.

CCR5 participates in the regulation of T cells and monocytes/macrophage lines' migration, mainly expressed on the T cells at rest, monocytes, and immature dendritic cells (Joy et al., 2019). Also, accumulating evidence highlighted a central role for mTOR as a fundamental determinant of cell fate in antigen-activated $CD4^+$ T cells. It was shown that suppression of activity in the Akt/mTOR pathway impaired Th17 and Th1 differentiation and promoted the development of Tregs. Fingolimod is recognized as an inhibitor of peripheral immune cell infiltration and can reduce inflammatory injury after ICH (Wei et al., 2011; Fu et al., 2014). These results demonstrated that the number of protective Tregs in the CNS was reduced when the infiltrating inflammatory cells were non-specifically inhibited. It was proven that the transfer of protective Tregs attenuated neurological deficit after ICH.

## Oxidative Stress

Oxidative stress initiated by the blood breakdown component or factors of the plasma plays a central role in the pathogenesis of WMI. Hemolysis after ICH is not that rapid. Rather, the main component of hematoma-erythrocytes starts to lyse 1 day after ICH and continues over days to weeks, followed by the release of decomposition products, including hemoglobin (Hb), heme, and iron, which exert neurotoxic effects on the lesion site and perihematomal regions (Cao et al., 2016). These metabolites, on the one hand, cause consecutive oxidative reactions; on the other hand, they can trigger inflammatory reaction via TLRs. Iron is derived from the collapse of heme by hemeoxygenase (HO)-1 and HO-2. Iron mediates neuronal ferroptosis, generating reactive oxygen species (ROS) and turning $Fe^{2+}$ into $Fe^{3+}$ via the Fenton reaction (Hu et al., 2016). ROS also mediates the inflammatory cascade, giving rise to cell death and perihematomal swelling, which finally leads to WMI.

## Neurotoxicity Mediated by Glutamate

In addition to increased ROS and oxidative stress, the levels of extracellular glutamate can also be augmented after ICH. It was confirmed followed by an increase of oxidative stress leading to sustained neuronal loss that ICH-induced striatal lesion produces distinct changes of EAAT1 and EAAT2 glutamate transporters expression and glutamate uptake activity. Besides, the level of perihematomal glutamate is highly related to the outcome in clinical ICH patients (Wu et al., 2013). It was demonstrated that in hemiplegic patients with basal ganglia bleeding affecting the IC, the earlier mini surgery was conducted, the less glutamate existing in peri-hematoma and the better prognosis, which means the level of glutamate is highly correlated with the outcome of ICH (Wu et al., 2013). Several pieces of research showed blood glutamate grabbing was effective at lessening the excitotoxicity of extracellular glutamate released during ischemic brain injury, although this did seemingly occur

in ICH (Castillo et al., 2016; da Silva-Candal et al., 2018). It was indicated that blood glutamate grabbing cannot reduce the hematoma but still can serve as a safe excitotoxic treatment modality following ICH.

## FUNCTIONS AND POSSIBLE MECHANISMS OF MSCs TRANSPLANTATION TARGETING WMI AFTER ICH

Ongoing research efforts are confirming our acknowledgment of the robust potential applications in regenerative medicine of stem cells (Chen et al., 2008), the therapeutic effectiveness of which has been reported in numerous previous experiments conducted in animal models of ICH. Among various stem cells, the multipotency and self-renewal capacity make MSCs a promising candidate for WMI treatment (Ramos-Cabrer et al., 2010; Huang et al., 2013; Mine et al., 2013), which can be expatiated as many unique biological effects including self-recovery by producing growth factors and cytokines, regenerative repair, inherent immunomodulation, and neuroprotection against oxidative stress, and can be further engineered to enhance immunomodulatory functions (Caplan and Dennis, 2006; Lee et al., 2014; Galipeau and Sensebe, 2018; Song et al., 2020), etc.

### Application of MSCs in ICH

There are various sources of MSCs including adult tissues (e.g., bone marrow, adipose tissue, inner organs, and peripheral blood) and neonatal tissues (e.g., umbilical cord, placenta, amniotic fluid, and amniotic membrane). MSCs can be administered either via intracerebral injection into a specific brain region or by intravenous/intraarterial injection (**Table 1**). In an earlier study on the rat ICH model, intracerebral administration of MSCs enhanced motor coordination and balance, which was attributed to nerve fiber remyelination and axonal regeneration (Liu et al., 2010). Allogeneic and syngeneic BMSCs treatment after stroke in rats improved neurological recovery and enhanced reactive oligodendrocyte and astrocyte-related axonal remodeling with no indication of immunologic sensitization in the adult rat brain (Li et al., 2006). Furthermore, the safety and efficiency of MSCs therapy have also been proven in many clinical trials for stroke, and some of these trials proved the significant neuroprotective effects of MSCs (**Table 2**). These stem cells are mostly derived from umbilical cord blood, bone marrow, and adipose tissues. Human umbilical cord-derived MSCs (UCMSCs) have been used in clinical trials as a treatment for some neurological diseases since 2011. While the clinical evidence showing the regenerative and immunomodulatory potential of the MSCs on ischemic stroke continues to expand rapidly, the clinical studies on ICH are still scarce. Besides, the proliferation and functions of MSCs are known to decline during the process of senescence. The immunomodulatory functions of MSCs can be compromised due to increased reactive oxygen species and oxidative stress in aged cells. Therefore, early passage MSCs or strategies to prevent senescence must be considered to yield better therapeutic function (Li et al., 2017; Fafián-Labora et al., 2019). And freshly thawed MSCs seem to have an impaired immunomodulatory capacity compared to continuously cultured MSCs (Moll et al., 2016).

### Promoting Self-Recovery and Regenerative Repair

The organism itself possesses a few endogenous mechanisms, such as migration of endogenous stem cells and hematoma clearance, which benefit the repair of injured WM structures. Transplanting exogenous stem cells also exerts significant neuroprotection on ICH although the difficulty in obtainment limits their clinical applications. Other sources of stem cells are required for replacement therapy and MSCs rise in response to the proper time and conditions. MSCs can secrete many trophic molecules when transferred into the body generally by two approaches-orthotopic transplantation and caudal vein transplantation (Smith and Gavins, 2012; Shichinohe et al., 2015)- thus promoting endogenous repair mechanism, which eventually accelerates functional recovery after stroke.

Mesenchymal stem cells transplantation is promising in terms of angiogenesis. Pfeiffer et al. (2019) found human amnion–derived MSCs (hAMSCs), well-known for their favorable angiogenic potential, enhanced human placental endothelial cells (hPEC) viability, and network formation of endothelial cells by paracrine factors *in vitro* (Konig et al., 2015) and promoted angiogenesis *in vivo* (Kinzer et al., 2014; Tuca et al., 2016; Ertl et al., 2018). Brain-derived neurotrophic factor (BDNF), as the most abundant neurotrophin in the CNS, can promote neurogenesis, oligodendrocyte genesis, myelination, and synaptic plasticity through interaction with protein tropomyosin receptor kinase B (TrkB), which is also a receptor of neurotrophin-4 (NT4) (Tolar et al., 2010; Lim et al., 2011). Recently, given the fact that TrkB usually can't be expressed by the MSCs in an undifferentiated state and the capacity of EA in promoting neurofunctional recovery through specific NTFs, such as VEGF, BDNF, and NT4 (Ahn et al., 2016), investigators combined the electroacupuncture (EA) with genetically modified TrkB gene-transfected MSCs (TrkB-MSCs) in a mouse model of ischemic stroke (Ahn et al., 2019). Consistent with the original assumption, the results showed the combination facilitated further neural survival and differentiation via stimulating the BDNF/NT4-TrkB signaling pathway rather than simply the administration of MSCs (Ahn et al., 2019). EA could directly stimulate the proliferation and differentiation of endogenous neural NSC in a rat model of ischemic stroke (Tan et al., 2018). BDNF can also exert neurotrophic effects on neuronal survival and neurite outgrowth, particularly the CST axons (Gupta et al., 2009). This procedure can be mediated by growth-associated protein-43 (GAP-43) which is highly distributed in the presynaptic membrane associated with neurite extension and long-term synaptic enhancement (Ramakers et al., 2000; Gupta et al., 2009; Morita and Miyata, 2013). Cui et al. (2017) elaborated that MSC graft increased GAP-43 expression via the ERK1/2 and pro-survival phosphatidylinositol 3-kinase (PI3K)/Akt signaling pathways after transplanting BMSC into a rat model of

**TABLE 1 |** An overview of the administration of MSCs involved in animal models.

| Diseases model | Model animals | Origin of MSCs | Treatment route | Dose | Functions | Mechanisms | References |
|---|---|---|---|---|---|---|---|
| ICH (collagenase I) | Wistar rats (270–320 g) | BMSCs, passage 3 | Intracerebral injection (right striatum) | $5.0 \times 10^5$ cells | Improved functional deficits and reduced lesion volume | BMSCs decreased apoptotic cells | Yang et al. (2011) |
| MCAO | Male Balb/c mice (8 W) | BMSCs, passage 3 | Intracerebral injection | $2.0 \times 10^5$ cells | Promoted regeneration of the infarcted brain | BMSCs triggered endogenous signaling pathways of survival and repair in neurons by secreting soluble neurotrophic factors | Shichinohe et al. (2015) |
| MCAO | Male C57BL/6J mice (5 and 8 W) | BMSCs, passage 3 | Intracerebral injection (peri-infarct site) | $1.0 \times 10^6$ cells | Improved stroke-associated motor and cognitive dysfunction | EA combined with grafted TrkB-MSCs stimulated the BDNF/NT4-TrkB signaling pathway | Ahn et al. (2019) |
| ICH (autologous arterial blood) | Adult male SD rats (250–280 g) | BMSCs (femurs of 21-day-old male SD rats), passage 4 | Intravenous injection (retro-orbital) | NA | Neuroprotective effects: attenuated neurological deficits and activated axonal regeneration | BMSCs increases of GAP-43 expression through ERK1/2 and PI3K/Akt activation | Cui et al. (2017) |
| ICH (collagenase IV) | Adult male SD rats (250–350 g) | hPD-MSCs | Intravenous injection (tail vein) | $1.0 \times 10^6$ cells | Improve neurological recovery; prevent hematoma expansion in the hyperacute stage of ICH and decrease acute mortality | MSCs increased the expression of tight junction proteins associated with the enhancement of cerebrovascular integrity | Choi et al. (2018) |
| MCAO | Adult male Wistar rats (270–300 g) | HP-BMSCs (femurs and tibias of 2-week-old Wistar rats) | Intravenous injection (tail vein) | $1.0 \times 10^6$ cells | Promoted locomotion recovery; enhanced angiogenesis and neurogenesis | Hypoxic preconditioning enhanced BMSCs survival and regenerative properties: downregulated inflammatory genes and reduced expression of inflammatory factors, enhanced expression, and release of trophic/growth factors | Wei et al. (2012) |
| ICH (collagenase IV) | Adult male C57BL/6 mice (8–10 W, 25–28 g) | HP-BMSCs (tibias of post-natal day 21 Wistar rats), passage 5 | Intranasal injection | $1.0 \times 10^6$ cells | Promoted behavioral recovery | HP-BMSCs increased the expression of neurotrophic factors and enhances endogenous neurogenesis | Sun et al. (2015) |
| ICH (collagenase AOF type A) | Male C57BL/6J mice (7–9 W) | hAD-MSCs, passage 4 | Intravenous injection | $1.0 \times 10^6$ cells | Improved neurological deficits: ameliorates motor and cognitive function | hADSCs suppressed acute inflammation mediated by $CD11^+CD45^+$ subpopulations | Kuramoto et al. (2019) |
| MCAO | Female SD rats (14–16 W, 225–275 g) | aMSCγ (femurs and tibias of SD rats < 4W) | Intravenous injection (retro-orbital sinus) | $5.0 \times 10^6$ cells/kg | Minimized the infarct and penumbra; improved functional recovery | aMSCγ reversed the proinflammatory phenotype of microglia and reduce inflammatory signaling; induced OLs differentiation and myelination | Tobin et al. (2020) |

*(Continued)*

**TABLE 1 |** Continued

| Diseases model | Model animals | Origin of MSCs | Treatment route | Dose | Functions | Mechanisms | References |
|---|---|---|---|---|---|---|---|
| MCAO | Male CX3CR1$^{eGFP/+}$ CCR2$^{RFP/+}$mice (11–13 W, 22–26 g) | IL13-MSCs | Intracerebral injection | 5.0 × $10^4$ cells | No obvious differences were observed | IL13-MSCs polarized both microglia and macrophages to a neuroprotective M2 phenotype during the pro-inflammatory status | Hamzei Taj et al. (2018) |
| ICH (collagenase VII) | Adult male SD rats (270–300 g) | MSCs, passage 10 | Intracerebral/ intravenous injection (CA/CV/LV) | 2.0 × $10^6$ cells | Improved the motor function | MSCs differentiate into neurons, astrocytes and OLs | Zhang et al. (2006) |
| HI brain injury | C57BL/6 mouse pups (P9) | hMSCs, passage 3 | Intranasal injection | 1.0/2.0 × $10^6$ cells | Improved sensorimotor function, promoted neuroregeneration, decreased lesion volume, reduced scar formation | hMSCs decreased microglia and astrocytes activity by secreting anti-inflammatory cytokines | Donega et al. (2014) |
| ICH (collagenase IV) | Adult male C57BL/6 mice (6–8 W, 22–25 g) | BMSCs (femurs and tibias of SD rats), passage 2–5 | Intracerebral injection (the ipsilateral lesion area) | 2.0 × $10^6$ cells | Attenuated brain water content, reduced hematoma volume, and improved neurological behavior impairment | BMSCs improve the anti-apoptotic ability of reactive astrocytes, trigger GFAP/VIM switch, and inhibit the final formation of the glial scar | Chen et al. (2020) |
| TBI | Adult male SD rats (220–250 g) | BMSCs (from SD rats), passage 3–8 | Intravenous injection (jugular vein) | 4.0 × $10^6$ cells | Improved neurological recovery; reduced brain water content | MSCs enhanced expression of TSG-6, and modulate inflammation-associated immune cells and cytokines | Zhang (2013) |
| ICH (collagenase IV) | Adult male SD rats (250–300 g) | BMSCs (femurs and tibias of 5-week-old SD rats), passage 3 | Intravenous injection (jugular vein) | 5.0 × $10^6$ cells | Improved neurological deficits; reduced brain water content | TSG-6 produced by MSCs suppressed activation of the NF-κB signaling pathway and the degree of BBB leakage was decreased | Chen M. et al. (2015) |
| ICH (collagenase) | Adult male SD rats (12 W, 220 g) | HGF transduced hUC-MSCs, passage 4–6 | Intracerebral injection | 6.0 × $10^5$ cells | Improved motor recovery (motor coordination and balance) | HGF-transduced MSCs enhance nerve fiber remyelination and axonal regeneration | Liu et al. (2010) |
| ICH (collagenase VII) | Adult male SD rats (190–210 g) | Flk-1$^+$ hBMSCs, passage 5 | Intracerebral injection (ipsilateral brain parenchyma) | 2.0 × $10^5$ cells | Reduced brain edema; improved neurological function | Flk-1$^+$ hBMSCs reduced inflammatory infiltration, decreased cell apoptosis, and promoted angiogenesis | Bao et al. (2013) |
| ICH (collagenase VII) | Male SD rats (230–260 g) | hUC-MSCs | Intracerebral injection | 2.0 × $10^5$ cells | Reduced injured lesion; accelerated functional recovery | hUC-MSCs inhibited inflammation and promoted angiogenesis | Liao et al. (2009) |
| ICH (autologous arterial blood) | Male *Macaca fascicularis* monkeys (4–6 years old, 4.0–4.4 kg) | hBMSCs, passage 6 | Intracerebral injection | 1.0–5.0 × $10^6$ cells | Improved the recovery from ICH in a primate model | No mention | Feng et al. (2010) |
| ICH (collagenase IV) | Male SD rats (7 W, 240–280 g) | WJ-MSCs | Intracerebral injection (ipsilateral striatum) | 2.0 × $10^5$ cells | Improved behavioral recovery | WJ-MSCs upregulated GDNF and increased differentiation into neuron-like cells | Lee et al. (2015) |

*(Continued)*

**TABLE 1 |** Continued

| Diseases model | Model animals | Origin of MSCs | Treatment route | Dose | Functions | Mechanisms | References |
|---|---|---|---|---|---|---|---|
| ICH (collagenase VII) | Adult male SD rats (250–300 g) | hUCB-MSCs | Intracerebral injection (left lateral ventricle) | $5.0 \times 10^5$ cells | Improve neurological recovery | hUCB-MSCs modulated the inflammatory environment, promoting neurogenesis and angiogenesis | Kim et al. (2015) |
| ICH (autologous blood) | Male SHR and WKY rats | BMSCs (femurs and tibias of 8-week-old SHR), passage 3 | Intravenous injection (tail vein) | $2.0 \times 10^7$ cells | Enhanced neurological function recovery | BMSCs improved the integrity of the BBB | Wang C. et al. (2015) |
| ICH (collagenase VII) | Male SD rats (230–260 g) | hUC-MSCs, passage 3–6 | Intravenous/ intracerebral injection | $2.0 \times 10^6$ cells | Improved neurological function and decreased injury volume | hUC-MSCs promoted angiogenesis | Xie et al. (2016) |
| ICH (collagenase IV) | Female adult Wistar rats (200–250 g) | BMSCs (femurs and tibias of Wistar rats) | Intracerebral injection (lesion zone) | $5.0 \times 10^6$ cells | Improved neurological function | Platelet-rich plasma-derived scaffolds increased the viability and biologic activity of BMSCs and optimize functional recovery | Vaquero et al. (2013) |
| subcortical IS with WMI | Male SD rats (200–250 g) | AD-MSCs (adipose tissue of SD rats) | Intravenous injection (tail vein) | $2.0 \times 10^6$ cells | Improved functional recovery | AD-MSCs reduced cell death, increased cell proliferation, and upregulated levels of white matter-associated markers (NF, MBP, and Olig-2) leading to the restoration of white tract connectivity | Otero-Ortega et al. (2015) |
| MCAO | Adult male SD rats (270–300 g) | BMSCs (SD rats), passage 3 | Intracerebral injection (left lateral ventricle) | $3.0 \times 10^3$ cells | Alleviated the WMI | BMSCs alleviated neuronal/axonal injury and promote the proliferation of OPCs and formation of the myelin sheath | Yu et al. (2018) |
| MCAO | Rat pups (P10) | MSCs | Intranasal injection | $1.0 \times 10^6$ cells | Improved long-term motor functional outcome | MSC enhanced white matter integrity | van Velthoven et al. (2017) |
| ICH (autologous blood) | Adult male Wistar rats (270–320 g) | hBMSCs | Intraarterial (internal carotid artery)/intravenous (tail vein) injection | $1.0 \times 10^6$ cells | Improved neurological functional outcome | hBMSCs improved histochemical parameters of neural regeneration and reduced the anatomical and pathological consequences of ICH | Seyfried et al. (2008) |
| ICH (collagenase VII) | Male ICR mice (7 W, 20–30 g) | hBMSCs, passage 4–11 | Intracerebral injection (ipsilateral striatum) | $2.0 \times 10^5$ cells | Improved motor functional recovery | hBMSCs could be induced to differentiate mostly into neurons and a smaller number of astrocytes *in vitro* and *in vivo* and produce many neuroprotective factors | Nagai et al. (2007) |

*(Continued)*

**TABLE 1** | Continued

| Diseases model | Model animals | Origin of MSCs | Treatment route | Dose | Functions | Mechanisms | References |
|---|---|---|---|---|---|---|---|
| ICH (collagenase IV) | Adult male Wistar rats (393.1–450.9 g) | hAD-MSCs | Intravenous injection | $3.0 \times 10^6$ cells | Improved the functional outcome | hAD-MSCs activated the neuronal endogenous progenitor cells | Fatar et al. (2008) |
| Preterm WMI | Wistar rat pups | hWJ-MSCs | Intranasal injection | $1.4 \times 10^4$ cells | Improved neurological recovery | hWJ-MSC prevented hypomyelination and microgliosis in a model of WMI in the premature rat brain | Oppliger et al. (2016) |

*W, weeks; g, gram; ICH, intracerebral hemorrhage; WMI, white matter injury; MCAO, middle cerebral artery occlusion; IS, ischemic stroke; HI, hypoxic-ischemic; TBI, traumatic brain injury; MSCs, mesenchymal stem cells; BMSCs, bone marrow mesenchymal stem cells; hMSCs, human MSCs; hBMSCs, human BMSCs; HP-BMSCs, hypoxic preconditioned BMSCs; hUC-MSCs, human umbilical cord-derived MSCs; hADSCs, human adipose-derived stem cells; hAD-MSCs, human adipose-derived MSCs; hPD-MSCs, human placenta-derived MSCs; aMSCγ, interferon-γ–activated MSCs; WJ-MSCs, Wharton's jelly-derived MSCs; hUCB-MSCs, human umbilical cord blood-derived MSCs; Flk-1, fetal liver kinase 1; TrkB, tropomyosin receptor kinase B; EA, electroacupuncture; BDNF, brain-derived neurotrophic factor; NT4, neurotrophin-4/5; GAP-43, growth-associated protein-43; SD, Sprague-Dawley; OLs, oligodendrocytes; IL13, interleukin 13; CA, carotid artery; CV, cervical vein; LV, lateral ventricle; GFAP, glial fibrillary acidic protein; VIM, vimentin; TSG-6, tumor necrosis factor (TNF-α) stimulated gene/protein 6; NF-κB, nuclear factor-κB; BBB, blood–brain barrier; HGF, hepatocyte growth factor; GDNF, glial cell line-derived neurotrophic factor; WKY rat, Wistar-Kyoto rat; SHR, spontaneously hypertensive rat; OPCs, oligodendrocyte progenitor cells.*

autologous blood injection. It means that MSC transplantation alleviated axonal damage and enhanced synaptic plasticity to some extent. GAP-43 may be considered a potential therapeutic target for MSCs in the treatment of axonal injury following ICH.

The CST is the only descending conduction pathway, in which some axons directly take shape synapses with spinal motoneurons, evolved in the major system for skilled voluntary movement in human and motor functions in rodents. Motor deficits in a stroke critically lie in an interruption of CST integrity, i.e., the motor fibers descending from the cortex to the spinal cord (Hijioka et al., 2016; Jang et al., 2018; Chen W. et al., 2019). Our previous research detected WM degeneration which lasted for at least 5 weeks after ICH, i.e., even during the chronic phase following stroke (Ng et al., 2020). And the longitudinal pathological alternations of the CST in the cervical portion of the spinal cord after unilateral striatal hemorrhage in adult mice were first illustrated, implying that the structural integrity of the CST was compromised extensively after ICH (Ng et al., 2020). In general, the establishment of compensatory re-innervation in the bilateral hemispheres after brain injury is mainly achieved through axonal sprouting of surviving neurons, new synapse formation, and factors produced by the brain. MSCs have been reported to promote neurogenesis and to alleviate side effects in injured brain regions, where both differentiation and secretion of MSCs involve axonal plasticity. In addition to the neuroprotective and neurotrophic effects, Choi et al. (2018) proved that MSCs may also prevent hematoma expansion in the hyperacute stage of ICH by enhancing endothelial integrity of cerebral vasculature by uplifting the expression of tight junction proteins (ZO-1, occludin).

## Immunomodulating Properties of MSCs

The scientific fact that neuroinflammation makes a principal contribution to the progress of ICH-induced brain damage is well acknowledged. Thus, modulating the immune response could help improve brain injury outcomes following ICH. The highly anti-inflammatory and immunomodulatory properties make MSCs suitable therapeutic candidates in inflammatory diseases, through regulating infiltration of microglia and neutrophils and increasing anti-inflammatory cytokines levels, while also downregulating the expression of proinflammatory cytokines.

Emerging knowledge in targeting neuroinflammation argues MSCs are effective modifiers of microglial phenotype by maintaining a resting, pro-regenerative microglial phenotype, or by controlling the microglial activation following stroke (Wei et al., 2012; Yan et al., 2013). Neurological deficits of collagenase-induced ICH-bearing mice during the subacute phase were improved by human adipose-derived stem cells (hADSCs) which suppressed the acute inflammation mediated by $CD11^+CD45^+$ cells subpopulations (Kuramoto et al., 2019). In a middle cerebral artery occlusion (MCAO) model of rats, microglia activation and inflammatory signaling were dramatically reduced by transplanted MSCs activated by interferon (INF)-γ, along with oligodendrogenesis and the minimization of the infarct and penumbra (Tobin et al., 2020). The activation of microglia is largely determined by CX3CR1, and MSCs are known to shift activated inflammatory M1 macrophages to an M2 macrophage-like phenotype through prostaglandin E2 (PGE2). In a global cerebral ischemia (GCI) mice model conducted by Du et al. (2020), CX3CR1 downregulation markedly reduced activation of microglia and inflammatory responses and promoted the generation of mature OLs from OPCs, and thus protected myelin from ischemia-induced damage. Similarly, Hamzei Taj et al. (2018) transplanted the BMSCs line which was genetically engineered to express the anti-inflammatory cytokine IL-13 (further named as IL13-MSCs) to $CX3CR1^{eGFP/+}$ $CCR2^{RFP/+}$ knock-in fluorescent protein reporter mice to distinguish brain-resident microglia from infiltrated macrophages after ischemic stroke. They found the transplantation of IL13-MSCs shifted microglia and macrophages toward an anti-inflammatory, neuroprotective phenotype at 14 days after ischemia (Hamzei Taj et al., 2018). Compared with MSCs, IL13-MSCs were proven to

**TABLE 2 |** An overview of the administration of MSCs involved in clinical trials.

| Diseases | Clinical trials | Time from onset | Trial design | Origin of MSCs | Application | Dose | Safety analysis | Efficacy analysis | Functional results | Side effects | Limitation | References |
|---|---|---|---|---|---|---|---|---|---|---|---|---|
| IS | Prospective, randomized, open-label, blinded-endpoint | Acute and chronic phase | Treatment, $n$ = 40; control, $n$ = 20. Follow-up, 3 months | Autologous MSCs preconditioned with early-phase stroke serum | Intravenous infusion | $1.0 \times 10^6$ cells/kg | Screening tests monitored vascular occlusion | Multimodal MRI and detailed functional assessments | Safe and feasible | Not mentioned | Short duration of the follow-up evaluation | Kim et al. (2013) |
| IS | Phase IIa, prospective, randomized, double-blind, placebo-controlled, single-center, pilot | Acute phase (the first 2 weeks) | Treatment, $n$ = 10; control (placebo or vehicle), $n$ = 10. Follow-up, 2 years | Allogeneic MSCs from adipose tissue | Single intravenous infusion | $1.0 \times 10^6$ units/kg | AEs, SAEs, neurologic and systemic complications, tumor development | mRS; NIHSS; infarct size; biomarkers | (1) Safe and feasible; (2) significantly improved recovery in the early stages of stroke by repairing ischemic brain tissue | Not mentioned | Small sample size | Díez-Tejedor et al. (2014) |
| IS | Phase II, prospective, randomized, controlled, observer-blinded | Subacute phase (30–90 days) | Treatment, $n$ = 59; control, $n$ = 59. Follow-up, 360 days | Allogenic BMSCs | Four intrathecal infusions once a week | $1.0 \times 10^6$ cells/kg | AEs, Neurological worsening tumor formation or abnormal cell growth, routine tests | NIHSS; mRS; mBI; FMA, ARAT, and MWS; MoCA; infarction volume; tissue metabolism; fiber tract of the injured brain; the level of biomarkers | Safe and feasible | Not mentioned | Not mentioned | Deng et al. (2019) |
| IS | Phase I/II, multi-center, open-label | Chronic phase (>6 months) | Phase 1, $N$ = 15; phase 2, $N$ = 21. Follow-up, 1 year | Allogeneic ischemia-tolerant MSCs | Single intravenous infusion | Phase 1: $0.5/1.0/1.5 \times 10^6$ cells/kg; phase 2: $1.5 \times 10^6$ cells/kg | AEs | NIHSS, BI, Mini-Mental Status Exam, Geriatric Depression Scale scores | (1) Safe and feasible; (2) behavioral gains | Infections, vascular disorders, and pain syndromes, unrelated or unlikely related to the investigational product; urinary tract infection and intravenous site irritation | Uncontrolled design; Mechanism of action was not studied; no appropriate training | Levy et al. (2019) |

*(Continued)*

**TABLE 2 |** Continued

| Diseases | Clinical trials | Time from onset | Trial design | Origin of MSCs | Application | Dose | Safety analysis | Efficacy analysis | Functional results | Side effects | Limitation | References |
|---|---|---|---|---|---|---|---|---|---|---|---|---|
| IVH | Phase I, open-label, single-arm, single-center | 23–34 weeks | No control. Premature infants, *N* = 9 | Allogeneic hUCB-MSCs | Single intraventricular infusion | 3 received $5.0 \times 10^6$ cells/kg, 6 received $1.0 \times 10^7$ cells/kg | SAEs, DLT, MRI, death after transplantation, anaphylactic shock | Cranial ultrasono graphy, biomarkers | Safe and feasible | Inguinal hernia, late-onset sepsis, and meningitis. These SAEs are not directly related to MSCs | Small sample size; uncontrolled design | Ahn et al. (2018) |
| Stroke | Phase 1/2a small-scale, open-label, dose-escalation | Chronic phase | No control. Treatment, *N* = 18. Follow-up, 1 year | Modified BMSCs (SB623) | Stereotactic implantation | 3 cohorts: $2.5/5.0/10.0 \times 10^6$ cells | TEAEs | NIHSS, MRI, FM total score, and FM motor function total score | (1) Safe and well-tolerated; (2) significant improvement in neurological function | All patients experienced at least 1 TEAE. None were related to cell treatment | Small sample size; non-randomized, uncontrolled design | Steinberg et al. (2016) |
| IS | Prospective, single-center, open-label, blinded-endpoint randomized controlled | Subacute phase, <2 weeks following moderate-severe ischemic carotid stroke | Treatment, *n* = 16; control, *n* = 15. Follow-up, 2 years | Autologous BMSCs | Single intravenous infusion | $1.0/3.0 \times 10^8$ cells/kg | AEs | NIHSS, mRS, BI, ITT, LMM, motor FM score, task-related fMRI | (1) Safe and feasible; (2) improve motor recovery through sensorimotor neuroplasticity | 10 and 16 AEs in treated patients, and 12 and 24 in controls at 6-month and 2-year follow-up, respectively | Use of autologous MSCs; no sample size justification for the primary endpoint; small sample size | Jaillard et al. (2020) |
| IS | Phase I, open-label, uncontrolled, dose–response, pilot | Acute phase | No control. Treatment, *N* = 6. Follow-up, 1 year | Novel Bone marrOW stem cell (RAINBOW): autologous BMSC product HUNS001–01 | Intraparen chymal infusion | 3 received $2.0 \times 10^7$cells; 3 received $5.0 \times 10^7$ cells | AEs | NIHSS, mRS, FIM, BI, FM, MRI, FDG-PET, IMZ-SPECT | Safe and feasible | No AE | Small sample size; uncertain time point of cell administration | Shichinohe et al. (2017) |
| ICH | Prospective | 5–7 days | Treatment, *n* = 60; control, *n* = 40. Follow-up, 6 months | BMSCs | Intracerebral injection (perihemor rhage area in the base ganglia) | Median number of MSCs: $9.47 \times 10^5$/L (range, $7.25 \times 10^5$ to $1.35 \times 10^6$/L), 3.5 mL/patient | Cell viability, re-bleeding or infection, blood pressure control | NIHSS; BI | Reduced neurological impairment and improved activities of daily living | Low grade fever; continuous dull chest pain 4 months after the implantation | Uncertain functional cell types; unclear effectiveness of mononuclear cell therapy in all ICH patients; experimental nature of the stem cell treatment | Li et al. (2013) |

*(Continued)*

**TABLE 2 |** Continued

| Diseases | Clinical trials | Time from onset | Trial design | Origin of MSCs | Application | Dose | Safety analysis | Efficacy analysis | Functional results | Side effects | Limitation | References |
|---|---|---|---|---|---|---|---|---|---|---|---|---|
| IS | Pilot | Acute (<1 week); subacute (1 week to 1 month); stroke sequelae (0.5–2 years) | No control. **Treatment 1:** *N* = 2, 1 dead; **Treatment 2:** *N* = 4. Follow-up, 2 years | Transplantation of NSPCs and UC-MSCs | Intravenous and intrathecal infusions | **Treatment 1:** $0.5 \times 10^6$/kg, 4 times; **Treatment 2:** 1 with MSCs ($0.5 \times 10^6$/kg) + 3 with MSCs ($5.0 \times 10^6$/patient) and NSPCs ($6.0 \times 10^6$/patient) | Neurological deterioration or infection, tumorigenesis | NIHSS, mRS, BI, | (1) Safe and feasible; (2) improved the neurological functions, disability levels, and daily living abilities | Low-grade fever; minor dizziness | Small sample size; short duration of the follow-up evaluation; uncontrolled design | Qiao et al. (2014) |
| ICH/IS | Pilot | Within 3 months | No control. Treatment, *N* = 4, 3 with IS, 1 with ICH. Follow-up, 6 months | UC-MSCs | Single intra-artery infusion | $2.0 \times 10^7$ cells | Angiography, MRI | mRS | (1) Safe and feasible; (2) improve the neurological function of IS patients with the MCA territory infarcts, but not ICH | No obvious AEs | Limited number of enrolled patients; short duration of the follow-up evaluation | Jiang et al. (2013) |
| IS | Randomized open-labeled, observer-blinded | Acute phase | Treatment, *n* = 16, 4 dead; control, *n* = 36, 21 dead. Follow-up, 5 years | Autologous *ex vivo* cultured MSCs | Intravenous infusion | $5.0 \times 10^7$ cells | Mortality, SAEs; immediate reaction | mRS, biomarkers, degree of involvement of the subventricular region of the lateral ventricle | (1) Long-term safe and feasible; (2) MSCs may improve recovery after stroke | No obvious AEs | Small sample size; not double-blinded; no exclusion of placebo effects | Lee et al. (2010) |
| IS | Phase I, unblinded | Subacute or chronic phase | No control. Treatment, *N* = 12, patients with ischemic gray matter, white matter, and mixed lesions. Follow-up, 1 year | Auto serum-expanded autologous human MSCs | Single intravenous infusion | $0.6–1.6 \times 10^8$ cells | AEs, MRI-tumorigenesis and abnormal cell growth | NIHSS; mRS; MRI; MRA; brain 3D CT angiography | Safe and feasible | Slight itching at the injection site; mild fever and nausea; slight appetite loss; no other obvious adverse events | Unblinded; No overall function or relative functional importance of different types of deficits; No mention of placebo effects or a contribution of recovery of the natural history of stroke | Honmou et al. (2011) |

*(Continued)*

**TABLE 2 |** Continued

| Diseases | Clinical trials | Time from onset | Trial design | Origin of MSCs | Application | Dose | Safety analysis | Efficacy analysis | Functional results | Side effects | Limitation | References |
|---|---|---|---|---|---|---|---|---|---|---|---|---|
| ICH/IS | Pilot | Chronic | No control. Treatment, *N* = 10, 6 with IS, and 4 with ICH. Follow-up, 6 months to 2 years | UC-MSCs, OECs, NPCs, Schwann cell | Intracranial /intravascular infusion | Mixed cells: UC-MSCs, $1.0/2.3 \times 10^7$ cells; | Clinic Neurologic Impairment Scale; BI | Clinic Neurologic Impairment Scale; BI | (1) Relatively clinically safe; (2) neurological function amelioration | No AE | Small sample size; methodological limitations; incomplete outcome data; absence of environmental enrichment or cell-only treatment groups | Chen et al. (2013) |
| Stroke | Unblinded non-randomized experimental controlled | Chronic | Treatment, *n* = 20; control, *n* = 20. Follow-up, 24 weeks | Autologous BMSCs | Intravenous infusion | $5.0–6.0 \times 10^7$ cells | Routine laboratory tests | Strength, Tone (modified Ashworth), FM, Edinburgh handedness inventory, mBI, functional MRI scanning | (1) Safe and feasible. (2) Stem cells act as "scaffolds" for neural transplantation and may aid in repair mechanisms in stroke | No AE | Small sample size; non-randomized design | Bhasin et al. (2013) |
| Stroke | Non-randomized experimental controlled | Chronic | Treatment, *n* = 6; control, *n* = 6. Follow-up, 24 weeks | Autologous BMSCs | Intravenous infusion | $5.0–6.0 \times 10^7$ cells | Routine laboratory tests, tumorigenesis, ectopic tissue formation, behavioral abnormality | FM, mBI, MRC, Ashworth tone grade scale scores, Functional imaging scans | Safe and feasible | No AE | Small sample size; non-randomized design; limitation of dose of cells, site, and mode of transplantation | Bhasin et al. (2011) |
| TBI | Randomized, single-blind controlled | Sequelae of TBI | Treatment, *n* = 20; control, *n* = 20. Follow-up, 6 months | UC-MSCs | Lumbar puncture infusion | $1.0 \times 10^7$ cells | FM; FIM | FM; FIM | (1) Safe and feasible; (2) UC-MSCs improved the neurological function and self-care in patients with TBI sequels | Low intracranial pressure reactions (mild dizziness and headache) | Small sample size, a multicenter, and large sample size prospective randomized clinical trial is needed | Wang et al. (2013) |

*ICH, intracerebral hemorrhage; IS, ischemic stroke; IVH, intraventricular hemorrhage; TBI, traumatic brain injury; MCA, middle cerebral artery; NSPCs, neural stem/progenitor cells; MSCs, mesenchymal stromal cells; BMSCs, bone marrow MSCs; UC-MSCs, umbilical cord-derived MSCs; hUCB-MSCs, human umbilical cord blood-derived MSCs; OEC, olfactory ensheathing cell; NPC, neural progenitor cell; NIHSS, National Institute of Health Stroke Scale; mRS, modified Rankin Scale; FM, Fugl Meyer assessment; BI, Barthel Index; mBI, modified Barthel Index; FIM, Functional Independence Measure; ITT, intent to treat analyses; LMM, linear mixed models analyses; MRI, magnetic resonance imaging; SPECT, single-photon emission computed tomography; FDG-PET, $^{18}$F-fluorodeoxyglucose positron emission tomography; IMZSPECT, $^{123}$I–iomazenil single-photon emission computed tomography; AEs, adverse events; SAEs, serious AEs; TEAEs, treatment-emergent AEs; DLT, dose-limiting toxicity; MRA, magnetic resonance angiography; FIM, functional independence measures.*

better limit oligodendrocyte loss and demyelination in a model for neuroinflammation and demyelination of cuprizone-treated mice, and promote histopathological and functional recovery in SCI of mice (Hamzei Taj et al., 2018). Engineered MSCs were also applied in malignant glioma tumor models (Sun et al., 2011).

As one of the main components of glial cells, astrocytes' regulation is also a promising target in WMI treatment (Zhang et al., 2006), although there is not adequate research recorded. Donega et al. (2014) reported that intranasal administration of human-MSC successfully reduced the expression of GFAP (a biomarker of astrocytes) and the formation of glial scars. Interestingly, in experiments conducted by Chen et al. (2020), transplanting BMSCs led to an elevation of GFAP level of expression; this difference might lie in the inherent double-edged features of activated astrocytes. Fortunately, the transplantation of MSCs into the CNS of ICH mice significantly improved cognitive and motor function and decreased hemorrhagic volume, which is consistent with previous research (Bedini et al., 2018). The key challenge in the treatment of ICH is to therefore understand how to magnify the advantages and minify the disadvantage of reactive astrocytes. Another factor that presents a double-edged sword function due to producing both pro-inflammatory and anti-inflammatory cytokines is IL-33; it was proven that IL-33 improved wound healing through enhanced M2 macrophage polarization in diabetic mice (He et al., 2017). It is a member of the IL-1 family mainly expressed in astrocytes, microglia, and OLs in CNS (Schmitz et al., 2005). Besides, a late research voted for IL-33 as a neuroprotective target which shifted microglia polarization from M1 to M2 and thus promoted OLs differentiation and WM repair banding with its ligand ST2 after ICH (Chen Z. et al., 2019).

The immunomodulatory functions of MSCs can also be exerted by secreting multifunctional paracrine signaling factors (Zhang, 2013; Zhao et al., 2013; Liu et al., 2014; Zhou et al., 2019), including cytokines, growth factors, and chemokines, which combine to regulate the immune cells' function. Systemically delivered MSCs can pass through the BBB while very few of these cells are detected homing to and survive in the lesion site of the brain (Chen et al., 2001). Functional activities are still improved by transplantation therapy. It has been commonly accepted that the functional benefits of MSCs' transplantation are due to increased trophic support from these cells that reduce overall inflammation, thereby eliminating the potentially toxic environment (Caplan and Dennis, 2006; Hess and Borlongan, 2008). Some studies described the bystander mechanism of MSCs that MSCs is related to some soluble factors such as IL-10, indoleamine 2,3-dioxygenase (IDO), PGE2, transforming growth factor-β1 (TGF-β1), tumor necrosis factor-α (TNF-α), and TNF-α stimulated gene/protein 6 (TSG-6) (Nemeth et al., 2009). These molecules are encapsulated in cell-secreted extracellular vesicles (EVs), which are usually divided into exosomes, microvesicles (MVs), and apoptotic bodies according to the size and cell of origin. TSG-6 is an anti-inflammatory factor that can suppress neutrophil migration into the inflammation region, interact through the CD44 receptor on resident macrophages, and inhibit the NF-κB signaling pathway (Chen M. et al., 2015). The BMSCs, injected from the jugular vein of ICH-bearing rats, attenuated the inflammatory response and decreased BBB disruption by secreting TSG-6 after being trapped in the lung (Chen M. et al., 2015). Most recently, researchers have verified the MSC-derived EVs (MSC-EVs), which mediate cell-to-cell inflammation and trophic signaling, to be feasible therapeutic targets for functional recovery after cortical injury in a monkey model (Medalla et al., 2020). Besides, MSC-EVs can also trigger macrophage polarization by increasing the formation of anti-inflammatory M2 phenotype over M1-like pro-inflammatory phenotype via downregulation of level of IL-23 and IL-22.

An *in vitro* experiment was performed which preclinically investigated the potential effect of MSCs on Treg and showed that MSCs induced the generation of Treg via epigenetic conversion of human conventional CD4 T cells, possibly partly through TGF-β and/or PD-1/PD-L1 pathway (Azevedo et al., 2020). PD-L1 was found to result in generating more Th2 and Treg cells but fewer Th1 and Th17 cells from naive $CD4^+$ T cells via inhibiting the mTOR pathway *in vitro* experiment. Administrating PD-L1 could promote the development of Treg cells and inhibit the differentiation of Th17 cells and thus significantly alleviate symptoms and suppress disease progression in several murine models (Fujiwara et al., 2014; Ding et al., 2016; Han et al., 2017). Besides, PD-L1 usually promotes the phosphorylation of immune-receptor tyrosine and conveys negative modulation signals, leading to cell inactivation via STAT or Janus kinase (JAK). When the STAT1 phosphorylation was hampered, overexpressing PD-1/PD-L1 could decrease the M1 microglia, indicating a potential approach of transferring to the anti-inflammatory phenotype via inhibiting STAT1. The findings mentioned above may attract researchers to conduct further investigation on the specific mechanism and therapeutic effect of MSCs transplantation based on PD-1/PD-L1 after ICH.

### Reducing Oxidative Stress

The antioxidative stress properties of MSCs have been validated in many previous studies (Shalaby et al., 2014), as diminishing ROS via the Nrf2 signaling pathway and protecting the body from oxidative stress was proven in many diseases such as acute lung injury (ALI), acute respiratory distress syndrome (ARDS), acute myocardial infarction (AMI), and acute liver failure (ALF). Various preconditioning strategies have been used to enhance the therapeutic efficacy of MSCs. Hypoxia preconditioning is thought to enhance MSCs' survival and the expression of various trophic factors of MSCs, and even to strengthen the engraftment and paracrine properties (Hu and Li, 2018).

## CONCLUSION AND PERSPECTIVES

For the past two decades, great progress in understanding the mechanisms of ICH-induced brain injury has been made (Balami and Buchan, 2012; Fang et al., 2013; Chen S. et al., 2015; Duan et al., 2016; Bobinger et al., 2018). But not until recently has the importance of WM damage in ICH, which exerts a high correlation with functional outcomes, been acknowledged. The

WM is involved in the transmission of motor and sensory information between the cerebral cortex and spinal cord. Therefore, whether in hemorrhagic or ischemic stroke, WMI can cause serious cognitive dysfunction, emotional disorders, and motor disturbance. Without the parallel protection of WM, true lasting neurorestoration cannot be achieved.

Mesenchymal stem cells have proven to be an extremely promising therapy for WMI due to their multipotency and self-renewal capacity. Furthermore, they exert reduced immunogenicity because of a low MHC class I expression and the absence of MHC class II molecules and co-stimulatory factors. Most importantly, MSCs can produce many immunomodulatory, neurotrophic, and angiogenic factors and have a potential immunomodulatory effect on immune cells (Caplan and Dennis, 2006; Chen et al., 2008; Bedini et al., 2018; Galipeau and Sensebe, 2018). And the neuroprotective effects have been well recognized in numerous pieces of research. To enhance the therapeutic effects of MSC transplantation by boosting the immunomodulatory properties of MSCs, investigators can also make some improvements to the MSC and the results show enhanced therapeutic effect, especially for the inflammatory modulation.

It is true that numerous signaling molecular pathways are involved in inflammatory responses and further exacerbate secondary brain damage (Zhou et al., 2014; Zhu et al., 2019). Although the modulation of immunological response after ICH showed promising results in a small proof-of-concept study, larger trials need to be done to further verify this. There are still several questions that remain to be addressed. First, studies in WMI are insufficient, whether effective drug targets of MSCs in the diseases mentioned above are equally effective in WM damage after ICH requires further verification. Second, human ICH pathomechanisms cannot be entirely mimicked by experimental models. The proportion of WM in rodent animals, especially in rats and mice, is much smaller than that of humans. It is essential to apply animals whose brain structures fit better with humans in future studies. Third, a majority of studies on post-ICH WMI after ICH concentrate on single−factor intervention; agents with multiple targets or combined drug therapy strategies remain to be designed and tested in further research. Last but not least, cell resources, invasive extraction procedures, and cell quantity make future research of this therapy challenging. An improvement on MSCs calls for further investigation so that it can be better applied in ICH treatment.

## AUTHOR CONTRIBUTIONS

The work presented here was carried out in collaboration with all authors. HS conceived and designed the review. JL wrote the manuscript. LX, DH, and YL helped with literature searching and summarizing. All authors read, commented on, and approved this manuscript.

## FUNDING

This research was funded by the National Natural Science Foundation of China (81701243), Guangdong Basic and Applied Basic Research Foundation (2020A1515010038), the Pearl River S&T Nova Program of Guangzhou (201710010047), and the Presidential Foundation of Zhujiang Hospital of Southern Medical University (No. yzjj2018rc03).

## ACKNOWLEDGMENTS

The support from the National Natural Science Foundation of China is gratefully acknowledged.

## REFERENCES

Abbott, N. J., Patabendige, A. A., Dolman, D. E., Yusof, S. R., and Begley, D. J. (2010). Structure and function of the blood-brain barrier. *Neurobiol. Dis.* 37, 13–25. doi: 10.1016/j.nbd.2009.07.030

Ahn, S. M., Kim, Y. R., Kim, H. N., Shin, Y. I., Shin, H. K., and Choi, B. T. (2016). Electroacupuncture ameliorates memory impairments by enhancing oligodendrocyte regeneration in a mouse model of prolonged cerebral hypoperfusion. *Sci. Rep.* 6:28646. doi: 10.1038/srep28646

Ahn, S. M., Kim, Y. R., Shin, Y. I., Ha, K. T., Lee, S. Y., Shin, H. K., et al. (2019). Therapeutic potential of a combination of electroacupuncture and TrkB-Expressing mesenchymal stem cells for ischemic stroke. *Mol. Neurobiol.* 56, 157–173. doi: 10.1007/s12035-018-1067-z

Ahn, S. Y., Chang, Y. S., Sung, S. I., and Park, W. S. (2018). Mesenchymal stem cells for severe intraventricular hemorrhage in preterm infants: phase I dose-escalation clinical trial. *Stem Cells Transl. Med.* 7, 847–856. doi: 10.1002/sctm.17-0219

Aronowski, J., and Zhao, X. (2011). Molecular pathophysiology of cerebral hemorrhage: secondary brain injury. *Stroke* 42, 1781–1786. doi: 10.1161/strokeaha.110.596718

Azevedo, R. I., Minskaia, E., Fernandes-Platzgummer, A., Vieira, A. I. S., da Silva, C. L., Cabral, J. M. S., et al. (2020). Mesenchymal stromal cells induce regulatory T cells via epigenetic conversion of human conventional CD4 T cells in vitro. *Stem Cells* 38, 1007–1019. doi: 10.1002/stem.3185

Babu, R., Bagley, J. H., Di, C., Friedman, A. H., and Adamson, C. (2012). Thrombin and hemin as central factors in the mechanisms of intracerebral hemorrhage-induced secondary brain injury and as potential targets for intervention. *Neurosurg. Focus* 32:E8. doi: 10.3171/2012.1.Focus11366

Bacmeister, C. M., Barr, H. J., McClain, C. R., Thornton, M. A., Nettles, D., Welle, C. G., et al. (2020). Motor learning promotes remyelination via new and surviving oligodendrocytes. *Nat. Neurosci.* 23, 819–831. doi: 10.1038/s41593-020-0637-3

Balami, J. S., and Buchan, A. M. (2012). Complications of intracerebral haemorrhage. *Lancet Neurol.* 11, 101–118. doi: 10.1016/s1474-4422(11)70264-2

Bao, X. J., Liu, F. Y., Lu, S., Han, Q., Feng, M., Wei, J. J., et al. (2013). Transplantation of Flk-1+ human bone marrow-derived mesenchymal stem cells promotes behavioral recovery and anti-inflammatory and angiogenesis effects in an intracerebral hemorrhage rat model. *Int. J, Mol. Med.* 31, 1087–1096. doi: 10.3892/ijmm.2013.1290

Bedell, B. J., and Narayana, P. A. (1998). Volumetric analysis of white matter, gray matter, and CSF using fractional volume analysis. *Magn. Reson. Med.* 39, 961–969. doi: 10.1002/mrm.1910390614

Bedini, G., Bersano, A., Zanier, E. R., Pischiutta, F., and Parati, E. A. (2018). Mesenchymal stem cell therapy in intracerebral haemorrhagic stroke. *Curr. Med. Chem.* 25, 2176–2197. doi: 10.2174/0929867325666180111101410

Bhasin, A., Srivastava, M. V., Kumaran, S. S., Mohanty, S., Bhatia, R., Bose, S., et al. (2011). Autologous mesenchymal stem cells in chronic stroke. *Cerebrovasc. Dis. Extra* 1, 93–104. doi: 10.1159/000333381

Bhasin, A., Srivastava, M. V., Mohanty, S., Bhatia, R., Kumaran, S. S., and Bose, S. (2013). Stem cell therapy: a clinical trial of stroke. *Clin. Neurol. Neurosurg.* 115, 1003–1008. doi: 10.1016/j.clineuro.2012.10.015

Bobinger, T., Burkardt, P., Huttner, H. B., and Manaenko, A. (2018). programmed cell death after intracerebral hemorrhage. *Curr. Neuropharmacol.* 16, 1267–1281. doi: 10.2174/1570159X15666170602112851

Bradke, F., Fawcett, J. W., and Spira, M. E. (2012). Assembly of a new growth cone after axotomy: the precursor to axon regeneration. *Nat. Rev. Neurosci.* 13, 183–193. doi: 10.1038/nrn3176

Cao, S., Zheng, M., Hua, Y., Chen, G., Keep, R. F., and Xi, G. (2016). Hematoma changes during clot resolution after experimental intracerebral hemorrhage. *Stroke* 47, 1626–1631. doi: 10.1161/strokeaha.116.013146

Caplan, A. I., and Dennis, J. E. (2006). Mesenchymal stem cells as trophic mediators. *J. Cell Biochem.* 98, 1076–1084. doi: 10.1002/jcb.20886

Carreiras, M., Seghier, M. L., Baquero, S., Estévez, A., Lozano, A., Devlin, J. T., et al. (2009). An anatomical signature for literacy. *Nature* 461, 983–986. doi: 10.1038/nature08461

Castillo, J., Loza, M. I., Mirelman, D., Brea, J., Blanco, M., Sobrino, T., et al. (2016). A novel mechanism of neuroprotection: blood glutamate grabber. *J. Cereb. Blood Flow Metab.* 36, 292–301. doi: 10.1177/0271678x15606721

Chen, J., Li, Y., Wang, L., Zhang, Z., Lu, D., Lu, M., et al. (2001). Therapeutic benefit of intravenous administration of bone marrow stromal cells after cerebral ischemia in rats. *Stroke* 32, 1005–1011. doi: 10.1161/01.str.32.4.1005

Chen, L., Xi, H., Huang, H., Zhang, F., Liu, Y., Chen, D., et al. (2013). Multiple cell transplantation based on an intraparenchymal approach for patients with chronic phase stroke. *Cell Transplant.* 22(Suppl. 1), S83–S91. doi: 10.3727/096368913x672154

Chen, M., Li, X., Zhang, X., He, X., Lai, L., Liu, Y., et al. (2015). The inhibitory effect of mesenchymal stem cell on blood-brain barrier disruption following intracerebral hemorrhage in rats: contribution of TSG-6. *J. Neuroinflammation* 12:61. doi: 10.1186/s12974-015-0284-x

Chen, S., Yang, Q., Chen, G., and Zhang, J. H. (2015). An update on inflammation in the acute phase of intracerebral hemorrhage. *Transl. Stroke Res.* 6, 4–8. doi: 10.1007/s12975-014-0384-4

Chen, W., Xia, M., Guo, C., Jia, Z., Wang, J., Li, C., et al. (2019). Modified behavioural tests to detect white matter injury- induced motor deficits after intracerebral haemorrhage in mice. *Sci. Rep.* 9:16958. doi: 10.1038/s41598-019-53263-6

Chen, X., Liang, H., Xi, Z., Yang, Y., Shan, H., Wang, B., et al. (2020). BM-MSC transplantation alleviates intracerebral hemorrhage-induced brain injury, promotes astrocytes vimentin expression, and enhances astrocytes antioxidation via the Cx43/Nrf2/HO-1 Axis. *Front. Cell Dev. Biol.* 8:302. doi: 10.3389/fcell.2020.00302

Chen, Y., Shao, J.-Z., Xiang, L.-X., Dong, X.-J., and Zhang, G.-R. (2008). Mesenchymal stem cells: a promising candidate in regenerative medicine. *Int. J. Biochem. Cell Biol.* 40, 815–820. doi: 10.1016/j.biocel.2008.01.007

Chen, Y., Tian, H., Yao, E., Tian, Y., Zhang, H., Xu, L., et al. (2017). Soluble epoxide hydrolase inhibition promotes white matter integrity and long-term functional recovery after chronic hypoperfusion in mice. *Sci. Rep.* 7:7758. doi: 10.1038/s41598-017-08227-z

Chen, Z., Xu, N., Dai, X., Zhao, C., Wu, X., Shankar, S., et al. (2019). Interleukin-33 reduces neuronal damage and white matter injury via selective microglia M2 polarization after intracerebral hemorrhage in rats. *Brain Res. Bull.* 150, 127–135. doi: 10.1016/j.brainresbull.2019.05.016

Choi, B. Y., Kim, O. J., Min, S. H., Jeong, J. H., Suh, S. W., and Chung, T. N. (2018). Human placenta-derived mesenchymal stem cells reduce mortality and hematoma size in a rat intracerebral hemorrhage model in an acute phase. *Stem Cells Int.* 2018:1658195. doi: 10.1155/2018/1658195

Chu, H., Ding, H., Tang, Y., and Dong, Q. (2014). Erythropoietin protects against hemorrhagic blood-brain barrier disruption through the effects of aquaporin-4. *Lab Invest.* 94, 1042–1053. doi: 10.1038/labinvest.2014.84

Cregg, J. M., DePaul, M. A., Filous, A. R., Lang, B. T., Tran, A., and Silver, J. (2014). Functional regeneration beyond the glial scar. *Exp. Neurol.* 253, 197–207. doi: 10.1016/j.expneurol.2013.12.024

Cui, J., Cui, C., Cui, Y., Li, R., Sheng, H., Jiang, X., et al. (2017). Bone marrow mesenchymal stem cell transplantation increases GAP-43 Expression via ERK1/2 and PI3K/Akt pathways in intracerebral hemorrhage. *Cell Physiol. Biochem.* 42, 137–144. doi: 10.1159/000477122

da Silva-Candal, A., Pérez-Díaz, A., Santamaría, M., Correa-Paz, C., Rodríguez-Yáñez, M., Ardá, A., et al. (2018). Clinical validation of blood/brain glutamate grabbing in acute ischemic stroke. *Ann. Neurol.* 84, 260–273. doi: 10.1002/ana.25286

Deng, L., Peng, Q., Wang, H., Pan, J., Zhou, Y., Pan, K., et al. (2019). Intrathecal injection of allogenic bone marrow-derived mesenchymal stromal cells in treatment of patients with severe ischemic stroke: study protocol for a randomized controlled observer-blinded trial. *Transl Stroke Res.* 10, 170–177. doi: 10.1007/s12975-018-0634-y

Díez-Tejedor, E., Gutiérrez-Fernández, M., Martínez-Sánchez, P., Rodríguez-Frutos, B., Ruiz-Ares, G., Lara, M. L., et al. (2014). Reparative therapy for acute ischemic stroke with allogeneic mesenchymal stem cells from adipose tissue: a safety assessment: a phase II randomized, double-blind, placebo-controlled, single-center, pilot clinical trial. *J. Stroke Cerebrovasc. Dis.* 23, 2694–2700. doi: 10.1016/j.jstrokecerebrovasdis.2014.06.011

Ding, Y., Han, R., Jiang, W., Xiao, J., Liu, H., Chen, X., et al. (2016). Programmed death ligand 1 plays a neuroprotective role in experimental autoimmune neuritis by controlling peripheral nervous system inflammation of rats. *J. Immunol.* 197, 3831–3840. doi: 10.4049/jimmunol.1601083

Donega, V., Nijboer, C. H., Braccioli, L., Slaper-Cortenbach, I., Kavelaars, A., van Bel, F., et al. (2014). Intranasal administration of human MSC for ischemic brain injury in the mouse: in vitro and in vivo neuroregenerative functions. *PLoS One* 9:e112339. doi: 10.1371/journal.pone.0112339

Du, B., Liang, M., Zheng, H., Fan, C., Zhang, H., Lu, X., et al. (2020). Anti-mouse CX3CR1 antibody alleviates cognitive impairment, neuronal loss and myelin deficits in an animal model of brain ischemia. *Neuroscience* 438, 169–181. doi: 10.1016/j.neuroscience.2020.05.011

Duan, X., Wen, Z., Shen, H., Shen, M., and Chen, G. (2016). Intracerebral hemorrhage, oxidative stress, and antioxidant therapy. *Oxid. Med. Cell Longev.* 2016:1203285. doi: 10.1155/2016/1203285

Ertl, J., Pichlsberger, M., Tuca, A. C., Wurzer, P., Fuchs, J., Geyer, S. H., et al. (2018). Comparative study of regenerative effects of mesenchymal stem cells derived from placental amnion, chorion and umbilical cord on dermal wounds. *Placenta* 65, 37–46. doi: 10.1016/j.placenta.2018.04.004

Fafián-Labora, J. A., Morente-López, M., and Arufe, M. C. (2019). Effect of aging on behaviour of mesenchymal stem cells. *World J. Stem Cells* 11, 337–346. doi: 10.4252/wjsc.v11.i6.337

Fancy, S. P., Zhao, C., and Franklin, R. J. (2004). Increased expression of Nkx2.2 and Olig2 identifies reactive oligodendrocyte progenitor cells responding to demyelination in the adult CNS. *Mol. Cell Neurosci.* 27, 247–254. doi: 10.1016/j.mcn.2004.06.015

Fang, H., Wang, P. F., Zhou, Y., Wang, Y. C., and Yang, Q. W. (2013). Toll-like receptor 4 signaling in intracerebral hemorrhage-induced inflammation and injury. *J. Neuroinflammation* 10:27. doi: 10.1186/1742-2094-10-27

Fatar, M., Stroick, M., Griebe, M., Marwedel, I., Kern, S., Bieback, K., et al. (2008). Lipoaspirate-derived adult mesenchymal stem cells improve functional outcome during intracerebral hemorrhage by proliferation of endogenous progenitor cells stem cells in intracerebral hemorrhages. *Neurosci. Lett.* 443, 174–178. doi: 10.1016/j.neulet.2008.07.077

Feng, M., Zhu, H., Zhu, Z., Wei, J., Lu, S., Li, Q., et al. (2010). Serial 18F-FDG PET demonstrates benefit of human mesenchymal stem cells in treatment of intracerebral hematoma: a translational study in a primate model. *J. Nucl. Med.* 52, 90–97. doi: 10.2967/jnumed.110.080325

Fu, Y., Hao, J., Zhang, N., Ren, L., Sun, N., Li, Y. J., et al. (2014). Fingolimod for the treatment of intracerebral hemorrhage: a 2-arm proof-of-concept study. *JAMA Neurol.* 71, 1092–1101. doi: 10.1001/jamaneurol.2014.1065

Fujiwara, H., Maeda, Y., Kobayashi, K., Nishimori, H., Matsuoka, K., Fujii, N., et al. (2014). Programmed death-1 pathway in host tissues ameliorates Th17/Th1-mediated experimental chronic graft-versus-host disease. *J. Immunol.* 193, 2565–2573. doi: 10.4049/jimmunol.1400954

Galipeau, J., and Sensebe, L. (2018). Mesenchymal stromal cells: clinical challenges and therapeutic opportunities. *Cell Stem Cell* 22, 824–833. doi: 10.1016/j.stem.2018.05.004

Ge, Y., Grossman, R. I., Babb, J. S., Rabin, M. L., Mannon, L. J., and Kolson, D. L. (2002). Age-related total gray matter and white matter changes in normal adult brain. Part II: quantitative magnetization transfer ratio histogram analysis. *AJNR Am. J. Neuroradiol.* 23, 1334–1341.

Gensert, J. M., and Goldman, J. E. (1997). Endogenous progenitors remyelinate demyelinated axons in the adult CNS. *Neuron* 19, 197–203. doi: 10.1016/s0896-6273(00)80359-1

Gerrish, A. C., Thomas, A. G., and Dineen, R. A. (2014). Brain white matter tracts: functional anatomy and clinical relevance. *Semin. Ultrasound. CT MR* 35, 432–444. doi: 10.1053/j.sult.2014.06.003

Gupta, S. K., Mishra, R., Kusum, S., Spedding, M., Meiri, K. F., Gressens, P., et al. (2009). GAP-43 is essential for the neurotrophic effects of BDNF and positive AMPA receptor modulator S18986. *Cell Death Differ.* 16, 624–637. doi: 10.1038/cdd.2008.188

Hamzei Taj, S., Le Blon, D., Hoornaert, C., Daans, J., Quarta, A., Praet, J., et al. (2018). Targeted intracerebral delivery of the anti-inflammatory cytokine IL13 promotes alternative activation of both microglia and macrophages after stroke. *J. Neuroinflammation* 15:174. doi: 10.1186/s12974-018-1212-7

Han, Q., Xie, Y., Ordaz, J. D., Huh, A. J., Huang, N., Wu, W., et al. (2020). Restoring cellular energetics promotes axonal regeneration and functional recovery after spinal cord injury. *Cell Metab.* 31, 623.e8–641.e8. doi: 10.1016/j.cmet.2020.02.002

Han, R., Luo, J., Shi, Y., Yao, Y., and Hao, J. (2017). PD-L1 (Programmed Death Ligand 1) protects against experimental intracerebral hemorrhage-induced brain injury. *Stroke* 48, 2255–2262. doi: 10.1161/strokeaha.117.016705

He, R., Yin, H., Yuan, B., Liu, T., Luo, L., Huang, P., et al. (2017). IL-33 improves wound healing through enhanced M2 macrophage polarization in diabetic mice. *Mol. Immunol.* 90, 42–49. doi: 10.1016/j.molimm.2017.06.249

He, Z., and Jin, Y. (2016). Intrinsic control of axon regeneration. *Neuron* 90, 437–451. doi: 10.1016/j.neuron.2016.04.022

Herndon, R. C., Lancaster, J. L., Giedd, J. N., and Fox, P. T. (1998). Quantification of white matter and gray matter volumes from three-dimensional magnetic resonance volume studies using fuzzy classifiers. *J. Magn. Reson. Imaging* 8, 1097–1105. doi: 10.1002/jmri.1880080515

Hess, D. C., and Borlongan, C. V. (2008). Stem cells and neurological diseases. *Cell Prolif.* 41(Suppl. 1), 94–114. doi: 10.1111/j.1365-2184.2008.00486.x

Hijioka, M., Anan, J., Matsushita, H., Ishibashi, H., Kurauchi, Y., Hisatsune, A., et al. (2016). Axonal dysfunction in internal capsule is closely associated with early motor deficits after intracerebral hemorrhage in mice. *Neurosci. Res.* 106, 38–46. doi: 10.1016/j.neures.2015.10.006

Honmou, O., Houkin, K., Matsunaga, T., Niitsu, Y., Ishiai, S., Onodera, R., et al. (2011). Intravenous administration of auto serum-expanded autologous mesenchymal stem cells in stroke. *Brain* 134(Pt 6), 1790–1807. doi: 10.1093/brain/awr063

Hu, C., and Li, L. (2018). Preconditioning influences mesenchymal stem cell properties in vitro and in vivo. *J. Cell Mol. Med.* 22, 1428–1442. doi: 10.1111/jcmm.13492

Hu, X., Tao, C., Gan, Q., Zheng, J., Li, H., and You, C. (2016). Oxidative stress in intracerebral hemorrhage: sources. mechanisms, and therapeutic targets. *Oxid. Med. Cell Longev.* 2016:3215391. doi: 10.1155/2016/3215391

Huang, W., Mo, X., Qin, C., Zheng, J., Liang, Z., and Zhang, C. (2013). Transplantation of differentiated bone marrow stromal cells promotes motor functional recovery in rats with stroke. *Neurol. Res.* 35, 320–328. doi: 10.1179/1743132812y.0000000151

Ito, M., Komai, K., Mise-Omata, S., Iizuka-Koga, M., Noguchi, Y., Kondo, T., et al. (2019). Brain regulatory T cells suppress astrogliosis and potentiate neurological recovery. *Nature* 565, 246–250. doi: 10.1038/s41586-018-0824-5

Jaillard, A., Hommel, M., Moisan, A., Zeffiro, T. A., Favre-Wiki, I. M., Barbieux-Guillot, M., et al. (2020). Autologous mesenchymal stem cells improve motor recovery in subacute ischemic stroke: a randomized clinical trial. *Transl. Stroke Res.* 11, 910–923. doi: 10.1007/s12975-020-00787-z

Jang, S., Kwon, Y., and Kwak, S. (2018). Change of an injured corticospinal tract during 3 weeks' rehabilitation after putaminal hemorrhage. *Am. J. Phys. Med. Rehabil.* 97, e29–e30. doi: 10.1097/phm.0000000000000787

Jiang, Y., Zhu, W., Zhu, J., Wu, L., Xu, G., and Liu, X. (2013). Feasibility of delivering mesenchymal stem cells via catheter to the proximal end of the lesion artery in patients with stroke in the territory of the middle cerebral artery. *Cell Transplant* 22, 2291–2298. doi: 10.3727/096368912x658818

Joseph, M. J. E., Caliaperumal, J., and Schlichter, L. C. (2016). After intracerebral hemorrhage, oligodendrocyte precursors proliferate and differentiate inside white-matter tracts in the rat striatum. *Transl. Stroke Res.* 7, 192–208. doi: 10.1007/s12975-015-0445-3

Joy, M. T., Ben Assayag, E., Shabashov-Stone, D., Liraz-Zaltsman, S., Mazzitelli, J., Arenas, M., et al. (2019). CCR5 is a therapeutic target for recovery after stroke and traumatic brain injury. *Cell* 176, 1143.e13–1157.e13. doi: 10.1016/j.cell.2019.01.044

Kang, M., and Yao, Y. (2019). Oligodendrocytes in intracerebral hemorrhage. *CNS Neurosc. Ther.* 25, 1075–1084. doi: 10.1111/cns.13193

Keep, R. F., Hua, Y., and Xi, G. (2012). Intracerebral haemorrhage: mechanisms of injury and therapeutic targets. *Lancet Neurol.* 11, 720–731. doi: 10.1016/s1474-4422(12)70104-7

Kim, K., Park, H. W., Moon, H. E., Kim, J. W., Bae, S., Chang, J. W., et al. (2015). The effect of human umbilical cord blood-derived mesenchymal stem cells in a collagenase-induced intracerebral hemorrhage rat model. *Exp. Neurobiol.* 24, 146–155. doi: 10.5607/en.2015.24.2.146

Kim, S. J., Moon, G. J., Chang, W. H., Kim, Y. H., and Bang, O. Y. (2013). Intravenous transplantation of mesenchymal stem cells preconditioned with early phase stroke serum: current evidence and study protocol for a randomized trial. *Trials* 14:317. doi: 10.1186/1745-6215-14-317

Kinzer, M., Hingerl, K., Konig, J., Reinisch, A., Strunk, D., Huppertz, B., et al. (2014). Mesenchymal stromal cells from the human placenta promote neovascularization in a mouse model in vivo. *Placenta* 35, 517–519. doi: 10.1016/j.placenta.2014.04.004

Kong, Y., and Le, Y. (2011). Toll-like receptors in inflammation of the central nervous system. *Int/ Immunopharmacol.* 11, 1407–1414. doi: 10.1016/j.intimp.2011.04.025

Konig, J., Weiss, G., Rossi, D., Wankhammer, K., Reinisch, A., Kinzer, M., et al. (2015). Placental mesenchymal stromal cells derived from blood vessels or avascular tissues: what is the better choice to support endothelial cell function? *Stem Cells Dev.* 24, 115–131. doi: 10.1089/scd.2014.0115

Kuramoto, Y., Takagi, T., Tatebayashi, K., Beppu, M., Doe, N., Fujita, M., et al. (2019). Intravenous administration of human adipose-derived stem cells ameliorates motor and cognitive function for intracerebral hemorrhage mouse model. *Brain Res.* 1711, 58–67. doi: 10.1016/j.brainres.2018.12.042

Kusano, Y., Seguchi, T., Horiuchi, T., Kakizawa, Y., Kobayashi, T., Tanaka, Y., et al. (2009). Prediction of functional outcome in acute cerebral hemorrhage using diffusion tensor imaging at 3T: a prospective study. *AJNR Am. J. Neuroradiol.* 30, 1561–1565. doi: 10.3174/ajnr.A1639

Lampron, A., Larochelle, A., Laflamme, N., Préfontaine, P., Plante, M. M., Sánchez, M. G., et al. (2015). Inefficient clearance of myelin debris by microglia impairs remyelinating processes. *J. Exp. Med.* 212, 481–495. doi: 10.1084/jem.20141656

Lan, X., Han, X., Li, Q., Li, Q., Gao, Y., Cheng, T., et al. (2017a). Pinocembrin protects hemorrhagic brain primarily by inhibiting toll-like receptor 4 and reducing M1 phenotype microglia. *Brain Behav. Immun.* 61, 326–339. doi: 10.1016/j.bbi.2016.12.012

Lan, X., Han, X., Li, Q., Yang, Q. W., and Wang, J. (2017b). Modulators of microglial activation and polarization after intracerebral haemorrhage. *Nat. Rev. Neurol.* 13, 420–433. doi: 10.1038/nrneurol.2017.69

Lee, H. K., Finniss, S., Cazacu, S., Xiang, C., and Brodie, C. (2014). Mesenchymal stem cells deliver exogenous miRNAs to neural cells and induce their differentiation and glutamate transporter expression. *Stem Cells Dev.* 23, 2851–2861. doi: 10.1089/scd.2014.0146

Lee, H. S., Kim, K. S., Lim, H. S., Choi, M., Kim, H. K., Ahn, H. Y., et al. (2015). Priming Wharton's jelly-derived mesenchymal stromal/stem cells with ROCK inhibitor improves recovery in an intracerebral hemorrhage model. *J. Cell Biochem.* 116, 310–319. doi: 10.1002/jcb.24969

Lee, J. S., Hong, J. M., Moon, G. J., Lee, P. H., Ahn, Y. H., and Bang, O. Y. (2010). A long-term follow-up study of intravenous autologous mesenchymal stem cell transplantation in patients with ischemic stroke. *Stem Cells* 28, 1099–1106. doi: 10.1002/stem.430

Levy, M. L., Crawford, J. R., Dib, N., Verkh, L., Tankovich, N., and Cramer, S. C. (2019). Phase I/II study of safety and preliminary efficacy of intravenous allogeneic mesenchymal stem cells in chronic stroke. *Stroke* 50, 2835–2841. doi: 10.1161/strokeaha.119.026318

Li, Q., Weiland, A., Chen, X., Lan, X., Han, X., Durham, F., et al. (2018). Ultrastructural characteristics of neuronal death and white matter injury in

mouse brain tissues after intracerebral hemorrhage: coexistence of ferroptosis. Autophagy, and Necrosis. *Front. Neurol.* 9:581. doi: 10.3389/fneur.2018.00581

Li, Y., McIntosh, K., Chen, J., Zhang, C., Gao, Q., Borneman, J., et al. (2006). Allogeneic bone marrow stromal cells promote glial-axonal remodeling without immunologic sensitization after stroke in rats. *Exp. Neurol.* 198, 313–325. doi: 10.1016/j.expneurol.2005.11.029

Li, Y., Wu, Q., Wang, Y., Li, L., Bu, H., and Bao, J. (2017). Senescence of mesenchymal stem cells (Review). *Int. J. Mol. Med.* 39, 775–782. doi: 10.3892/ijmm.2017.2912

Li, Z. M., Zhang, Z. T., Guo, C. J., Geng, F. Y., Qiang, F., and Wang, L. X. (2013). Autologous bone marrow mononuclear cell implantation for intracerebral hemorrhage-a prospective clinical observation. *Clin. Neurol. Neurosurg.* 115, 72–76. doi: 10.1016/j.clineuro.2012.04.030

Liao, W., Zhong, J., Yu, J., Xie, J., Liu, Y., Du, L., et al. (2009). Therapeutic benefit of human umbilical cord derived mesenchymal stromal cells in intracerebral hemorrhage rat: implications of anti-inflammation and angiogenesis. *Cell Physiol. Biochem.* 24, 307–316. doi: 10.1159/000233255

Liesz, A., Suri-Payer, E., Veltkamp, C., Doerr, H., Sommer, C., Rivest, S., et al. (2009). Regulatory T cells are key cerebroprotective immunomodulators in acute experimental stroke. *Nat. Med.* 15, 192–199. doi: 10.1038/nm.1927

Lim, J. Y., Park, S. I., Kim, S. M., Jun, J. A., Oh, J. H., Ryu, C. H., et al. (2011). Neural differentiation of brain-derived neurotrophic factor-expressing human umbilical cord blood-derived mesenchymal stem cells in culture via TrkB-mediated ERK and β-catenin phosphorylation and following transplantation into the developing brain. *Cell Transplant* 20, 1855–1866. doi: 10.3727/096368910x557236

Ling, H. P., Li, W., Zhou, M. L., Tang, Y., Chen, Z. R., and Hang, C. H. (2013). Expression of intestinal myeloid differentiation primary response protein 88 (Myd88) following experimental traumatic brain injury in a mouse model. *J. Surg. Res.* 179, e227–e234. doi: 10.1016/j.jss.2012.03.030

Liu, A. M., Lu, G., Tsang, K. S., Li, G., Wu, Y., Huang, Z. S., et al. (2010). Umbilical cord-derived mesenchymal stem cells with forced expression of hepatocyte growth factor enhance remyelination and functional recovery in a rat intracerebral hemorrhage model. *Neurosurgery* 67, 357–365. doi: 10.1227/01.NEU.0000371983.06278.B3 discussion 365-6,

Liu, L., Yu, Y., Hou, Y., Chai, J., Duan, H., Chu, W., et al. (2014). Human umbilical cord mesenchymal stem cells transplantation promotes cutaneous wound healing of severe burned rats. *PLoS One* 9:e88348. doi: 10.1371/journal.pone.0088348

Lowther, D. E., and Hafler, D. A. (2012). Regulatory T cells in the central nervous system. *Immunol. Rev.* 248, 156–169. doi: 10.1111/j.1600-065X.2012.01130.x

Lu, P., Woodruff, G., Wang, Y., Graham, L., Hunt, M., Wu, D., et al. (2014). Long-distance axonal growth from human induced pluripotent stem cells after spinal cord injury. *Neuron* 83, 789–796. doi: 10.1016/j.neuron.2014.07.014

McKeon, R. J., Schreiber, R. C., Rudge, J. S., and Silver, J. (1991). Reduction of neurite outgrowth in a model of glial scarring following CNS injury is correlated with the expression of inhibitory molecules on reactive astrocytes. *J. Neurosci.* 11, 3398–3411. doi: 10.1523/jneurosci.11-11-03398.1991

Medalla, M., Chang, W., Calderazzo, S. M., Go, V., Tsolias, A., Goodliffe, J. W., et al. (2020). Treatment with mesenchymal-derived extracellular vesicles reduces injury-related pathology in pyramidal neurons of monkey perilesional ventral premotor cortex. *J. Neurosci.* 40, 3385–3407. doi: 10.1523/JNEUROSCI.2226-19.2020

Mine, Y., Tatarishvili, J., Oki, K., Monni, E., Kokaia, Z., and Lindvall, O. (2013). Grafted human neural stem cells enhance several steps of endogenous neurogenesis and improve behavioral recovery after middle cerebral artery occlusion in rats. *Neurobiol. Dis.* 52, 191–203. doi: 10.1016/j.nbd.2012.12.006

Moll, G., Geißler, S., Catar, R., Ignatowicz, L., Hoogduijn, M. J., Strunk, D., et al. (2016). Cryopreserved or fresh mesenchymal stromal cells: only a matter of taste or key to unleash the full clinical potential of MSC therapy? *Adv. Exp. Med. Biol.* 951, 77–98. doi: 10.1007/978-3-319-45457-3_7

Morita, S., and Miyata, S. (2013). Synaptic localization of growth-associated protein 43 in cultured hippocampal neurons during synaptogenesis. *Cell Biochem. Funct.* 31, 400–411. doi: 10.1002/cbf.2914

Nagai, A., Kim, W. K., Lee, H. J., Jeong, H. S., Kim, K. S., Hong, S. H., et al. (2007). Multilineage potential of stable human mesenchymal stem cell line derived from fetal marrow. *PLoS One* 2:e1272. doi: 10.1371/journal.pone.0001272

Nemeth, K., Leelahavanichkul, A., Yuen, P. S., Mayer, B., Parmelee, A., Doi, K., et al. (2009). Bone marrow stromal cells attenuate sepsis via prostaglandin E(2)-dependent reprogramming of host macrophages to increase their interleukin-10 production. *Nat. Med.* 15, 42–49. doi: 10.1038/nm.1905

Ng, A. C. K., Yao, M., Cheng, S. Y., Li, J., Huang, J. D., Wu, W., et al. (2020). Protracted morphological changes in the corticospinal tract within the cervical spinal cord after intracerebral hemorrhage in the right striatum of mice. *Front. Neurosci.* 14:506. doi: 10.3389/fnins.2020.00506

Ohnishi, M., Katsuki, H., Fukutomi, C., Takahashi, M., Motomura, M., Fukunaga, M., et al. (2011). HMGB1 inhibitor glycyrrhizin attenuates intracerebral hemorrhage-induced injury in rats. *Neuropharmacology* 61, 975–980. doi: 10.1016/j.neuropharm.2011.06.026

Olah, M., Amor, S., Brouwer, N., Vinet, J., Eggen, B., Biber, K., et al. (2012). Identification of a microglia phenotype supportive of remyelination. *Glia* 60, 306–321. doi: 10.1002/glia.21266

Oppliger, B., Joerger-Messerli, M., Mueller, M., Reinhart, U., Schneider, P., Surbek, D. V., et al. (2016). Intranasal delivery of umbilical cord-derived mesenchymal stem cells preserves myelination in perinatal brain damage. *Stem Cells Dev.* 25, 1234–1242. doi: 10.1089/scd.2016.0027

Otero-Ortega, L., Gutierrez-Fernandez, M., Ramos-Cejudo, J., Rodriguez-Frutos, B., Fuentes, B., Sobrino, T., et al. (2015). White matter injury restoration after stem cell administration in subcortical ischemic stroke. *Stem Cell Res. Ther.* 6:121. doi: 10.1186/s13287-015-0111-4

Pfeiffer, D., Wankhammer, K., Stefanitsch, C., Hingerl, K., Huppertz, B., Dohr, G., et al. (2019). Amnion-derived mesenchymal stem cells improve viability of endothelial cells exposed to shear stress in ePTFE grafts. *Int. J. Artif. Organs.* 42, 80–87. doi: 10.1177/0391398818815470

Qiao, L. Y., Huang, F. J., Zhao, M., Xie, J. H., Shi, J., Wang, J., et al. (2014). A two-year follow-up study of cotransplantation with neural stem/progenitor cells and mesenchymal stromal cells in ischemic stroke patients. *Cell Transplant* 23(Suppl. 1), S65–S72. doi: 10.3727/096368914x684961

Qin, C., Fan, W. H., Liu, Q., Shang, K., Murugan, M., Wu, L. J., et al. (2017). Fingolimod protects against ischemic white matter damage by modulating microglia toward M2 polarization via STAT3 pathway. *Stroke* 48, 3336–3346. doi: 10.1161/strokeaha.117.018505

Qureshi, A. I., Mendelow, A. D., and Hanley, D. F. (2009). Intracerebral haemorrhage. *Lancet* 373, 1632–1644. doi: 10.1016/s0140-6736(09)60371-8

Ramakers, G. M., Heinen, K., Gispen, W. H., and de Graan, P. N. (2000). Long term depression in the CA1 field is associated with a transient decrease in pre- and postsynaptic PKC substrate phosphorylation. *J. Biol. Chem.* 275, 28682–28687. doi: 10.1074/jbc.M003068200

Ramos-Cabrer, P., Justicia, C., Wiedermann, D., and Hoehn, M. (2010). Stem cell mediation of functional recovery after stroke in the rat. *PLoS One* 5:e12779. doi: 10.1371/journal.pone.0012779

Ransom, B. R., and Ransom, C. B. (2012). Astrocytes: multitalented stars of the central nervous system. *Methods Mol. Biol.* 814, 3–7. doi: 10.1007/978-1-61779-452-0_1

Roncagliolo, M., Schlageter, C., León, C., Couve, E., Bonansco, C., and Eguibar, J. R. (2006). Developmental impairment of compound action potential in the optic nerve of myelin mutant taiep rats. *Brain Res.* 1067, 78–84. doi: 10.1016/j.brainres.2005.10.010

Sakaguchi, S., Miyara, M., Costantino, C. M., and Hafler, D. A. (2010). FOXP3+ regulatory T cells in the human immune system. *Nat. Rev. Immunol.* 10, 490–500. doi: 10.1038/nri2785

Schmahmann, J. D., Smith, E. E., Eichler, F. S., and Filley, C. M. (2008). Cerebral white matter: neuroanatomy, clinical neurology, and neurobehavioral correlates. *Ann. N. Y. Acad. Sci.* 1142, 266–309. doi: 10.1196/annals.1444.017

Schmitz, J., Owyang, A., Oldham, E., Song, Y., Murphy, E., McClanahan, T. K., et al. (2005). IL-33, an interleukin-1-like cytokine that signals via the IL-1 receptor-related protein ST2 and induces T helper type 2-associated cytokines. *Immunity* 23, 479–490. doi: 10.1016/j.immuni.2005.09.015

Seyfried, D. M., Han, Y., Yang, D., Ding, J., Savant-Bhonsale, S., Shukairy, M. S., et al. (2008). Mannitol enhances delivery of marrow stromal cells to the brain after experimental intracerebral hemorrhage. *Brain Res.* 1224, 12–19. doi: 10.1016/j.brainres.2008.05.080

Shalaby, S. M., El-Shal, A. S., Abd-Allah, S. H., Selim, A. O., Selim, S. A., Gouda, Z. A., et al. (2014). Mesenchymal stromal cell injection protects

against oxidative stress in *Escherichia coli*-induced acute lung injury in mice. *Cytotherapy* 16, 764–775. doi: 10.1016/j.jcyt.2013.12.006

Shichinohe, H., Ishihara, T., Takahashi, K., Tanaka, Y., Miyamoto, M., Yamauchi, T., et al. (2015). Bone marrow stromal cells rescue ischemic brain by trophic effects and phenotypic change toward neural cells. *Neurorehabil. Neural. Repair.* 29, 80–89. doi: 10.1177/1545968314525856

Shichinohe, H., Kawabori, M., Iijima, H., Teramoto, T., Abumiya, T., Nakayama, N., et al. (2017). Research on advanced intervention using novel bone marrOW stem cell (RAINBOW): a study protocol for a phase I, open-label, uncontrolled, dose-response trial of autologous bone marrow stromal cell transplantation in patients with acute ischemic stroke. *BMC Neurol.* 17:179. doi: 10.1186/s12883-017-0955-6

Smith, E. E., Gurol, M. E., Eng, J. A., Engel, C. R., Nguyen, T. N., Rosand, J., et al. (2004). White matter lesions, cognition, and recurrent hemorrhage in lobar intracerebral hemorrhage. *Neurology* 63, 1606–1612. doi: 10.1212/01.wnl.0000142966.22886.20

Smith, H. K., and Gavins, F. N. (2012). The potential of stem cell therapy for stroke: is PISCES the sign? *Faseb J.* 26, 2239–2252. doi: 10.1096/fj.11-195719

Song, N., Scholtemeijer, M., and Shah, K. (2020). Mesenchymal stem cell immunomodulation: mechanisms and therapeutic potential. *Trends Pharmacol. Sci.* 41, 653–664. doi: 10.1016/j.tips.2020.06.009

Steinberg, G. K., Kondziolka, D., Wechsler, L. R., Lunsford, L. D., Coburn, M. L., Billigen, J. B., et al. (2016). Clinical outcomes of transplanted modified bone marrow-derived mesenchymal stem cells in stroke: a phase 1/2a study. *Stroke* 47, 1817–1824. doi: 10.1161/strokeaha.116.012995

Sun, J., Wei, Z. Z., Gu, X., Zhang, J. Y., Zhang, Y., Li, J., et al. (2015). Intranasal delivery of hypoxia-preconditioned bone marrow-derived mesenchymal stem cells enhanced regenerative effects after intracerebral hemorrhagic stroke in mice. *Exp. Neurol.* 272, 78–87. doi: 10.1016/j.expneurol.2015.03.011

Sun, X. L., Xu, Z. M., Ke, Y. Q., Hu, C. C., Wang, S. Y., Ling, G. Q., et al. (2011). Molecular targeting of malignant glioma cells with an EphA2-specific immunotoxin delivered by human bone marrow-derived mesenchymal stem cells. *Cancer Lett.* 312, 168–177. doi: 10.1016/j.canlet.2011.07.035

Suzuki, T., Kohyama, K., Moriyama, K., Ozaki, M., Hasegawa, S., Ueno, T., et al. (2020). Extracellular ADP augments microglial inflammasome and NF-κB activation via the P2Y12 receptor. *Eur. J. Immunol.* 50, 205–219. doi: 10.1002/eji.201848013

Tan, F., Wang, J., Liu, J. X., Wang, C., Li, M. D., and Gu, Y. (2018). Electroacupuncture stimulates the proliferation and differentiation of endogenous neural stem cells in a rat model of ischemic stroke. *Exp. Ther. Med.* 16, 4943–4950. doi: 10.3892/etm.2018.6848

Tobin, M. K., Stephen, T. K. L., Lopez, K. L., Pergande, M. R., Bartholomew, A. M., Cologna, S. M., et al. (2020). Activated mesenchymal stem cells induce recovery following stroke via regulation of inflammation and oligodendrogenesis. *J. Am. Heart Assoc.* 9:e013583. doi: 10.1161/jaha.119.013583

Tolar, J., Le Blanc, K., Keating, A., and Blazar, B. R. (2010). Concise review: hitting the right spot with mesenchymal stromal cells. *Stem Cells* 28, 1446–1455. doi: 10.1002/stem.459

Tse, W. T., Pendleton, J. D., Beyer, W. M., Egalka, M. C., and Guinan, E. C. (2003). Suppression of allogeneic T-cell proliferation by human marrow stromal cells: implications in transplantation. *Transplantation* 75, 389–397. doi: 10.1097/01.TP.0000045055.63901.A9

Tuca, A. C., Ertl, J., Hingerl, K., Pichlsberger, M., Fuchs, J., Wurzer, P., et al. (2016). Comparison of matrigel and matriderm as a carrier for human amnion-derived mesenchymal stem cells in wound healing. *Placenta* 48, 99–103. doi: 10.1016/j.placenta.2016.10.015

van Velthoven, C. T., Dzietko, M., Wendland, M. F., Derugin, N., Faustino, J., Heijnen, C. J., et al. (2017). Mesenchymal stem cells attenuate MRI-identifiable injury, protect white matter, and improve long-term functional outcomes after neonatal focal stroke in rats. *J. Neurosci. Res.* 95, 1225–1236. doi: 10.1002/jnr.23954

Vaquero, J., Otero, L., Bonilla, C., Aguayo, C., Rico, M. A., Rodriguez, A., et al. (2013). Cell therapy with bone marrow stromal cells after intracerebral hemorrhage: impact of platelet-rich plasma scaffolds. *Cytotherapy* 15, 33–43. doi: 10.1016/j.jcyt.2012.10.005

Wang, C., Fei, Y., Xu, C., Zhao, Y., and Pan, Y. (2015). Bone marrow mesenchymal stem cells ameliorate neurological deficits and blood-brain barrier dysfunction after intracerebral hemorrhage in spontaneously hypertensive rats. *Int. J. Clin. Exp. Pathol.* 8, 4715–4724.

Wang, S., Cheng, H., Dai, G., Wang, X., Hua, R., Liu, X., et al. (2013). Umbilical cord mesenchymal stem cell transplantation significantly improves neurological function in patients with sequelae of traumatic brain injury. *Brain Res.* 1532, 76–84. doi: 10.1016/j.brainres.2013.08.001

Wang, T., Chen, X., Wang, Z., Zhang, M., Meng, H., Gao, Y., et al. (2015). Poloxamer-188 can attenuate blood-brain barrier damage to exert neuroprotective effect in mice intracerebral hemorrhage model. *J. Mol. Neurosci.* 55, 240–250. doi: 10.1007/s12031-014-0313-8

Wanner, I. B., Anderson, M. A., Song, B., Levine, J., Fernandez, A., Gray-Thompson, Z., et al. (2013). Glial scar borders are formed by newly proliferated, elongated astrocytes that interact to corral inflammatory and fibrotic cells via STAT3-dependent mechanisms after spinal cord injury. *J. Neurosci.* 33, 12870–12886. doi: 10.1523/jneurosci.2121-13.2013

Wasserman, J. K., and Schlichter, L. C. (2008). White matter injury in young and aged rats after intracerebral hemorrhage. *Exp. Neurol.* 214, 266–275. doi: 10.1016/j.expneurol.2008.08.010

Wei, L., Fraser, J. L., Lu, Z. Y., Hu, X., and Yu, S. P. (2012). Transplantation of hypoxia preconditioned bone marrow mesenchymal stem cells enhances angiogenesis and neurogenesis after cerebral ischemia in rats. *Neurobiol. Dis.* 46, 635–645. doi: 10.1016/j.nbd.2012.03.002

Wei, Y., Yemisci, M., Kim, H. H., Yung, L. M., Shin, H. K., Hwang, S. K., et al. (2011). Fingolimod provides long-term protection in rodent models of cerebral ischemia. *Ann. Neurol.* 69, 119–129. doi: 10.1002/ana.22186

Windrem, M. S., Schanz, S. J., Zou, L., Chandler-Militello, D., Kuypers, N. J., and Nedergaard, M. (2020). Human glial progenitor cells effectively remyelinate the demyelinated adult brain. *Cell Rep.* 31:107658. doi: 10.1016/j.celrep.2020.107658

Wu, G., Li, S., Wang, L., and Mao, Y. (2013). The perihematomal glutamate level is associated with the outcome of patients with basal ganglia hematomas treated by minimally invasive procedures. *Neurol. Res.* 35, 829–836. doi: 10.1179/1743132813y.0000000220

Wu, W., Xiong, W., Zhang, P., Chen, L., Fang, J., Shields, C., et al. (2017). Increased threshold of short-latency motor evoked potentials in transgenic mice expressing Channelrhodopsin-2. *PLoS One* 12:e0178803. doi: 10.1371/journal.pone.0178803

Xiao, L., Zheng, H., Li, J., Wang, Q., and Sun, H. (2020). Neuroinflammation mediated by NLRP3 inflammasome after intracerebral hemorrhage and potential therapeutic targets. *Mol. Neurobiol.* 57, 5130–5149. doi: 10.1007/s12035-020-02082-2

Xie, J., Wang, B., Wang, L., Dong, F., Bai, G., and Liu, Y. (2016). Intracerebral and intravenous transplantation represents a favorable approach for application of human umbilical cord mesenchymal stromal cells in intracerebral hemorrhage rats. *Med. Sci. Monit.* 22, 3552–3561. doi: 10.12659/msm.900512

Yan, K., Zhang, R., Sun, C., Chen, L., Li, P., Liu, Y., et al. (2013). Bone marrow-derived mesenchymal stem cells maintain the resting phenotype of microglia and inhibit microglial activation. *PLoS One* 8:e84116. doi: 10.1371/journal.pone.0084116

Yang, C., Zhou, L., Gao, X., Chen, B., Tu, J., Sun, H., et al. (2011). Neuroprotective effects of bone marrow stem cells overexpressing glial cell line-derived neurotrophic factor on rats with intracerebral hemorrhage and neurons exposed to hypoxia/reoxygenation. *Neurosurgery* 68, 691–704. doi: 10.1227/NEU.0b013e3182098a8a

Yin, J., Lü, T. M., Qiu, G., Huang, R. Y., Fang, M., Wang, Y. Y., et al. (2013). Intracerebral hematoma extends via perivascular spaces and perineurium. *Tohoku J. Exp. Med.* 230, 133–139. doi: 10.1620/tjem.230.133

Yu, X., Wu, H., Zhao, Y., Guo, Y., Chen, Y., Dong, P., et al. (2018). Bone marrow mesenchymal stromal cells alleviate brain white matter injury via the enhanced proliferation of oligodendrocyte progenitor cells in focal cerebral ischemic rats. *Brain Res.* 1680, 127–136. doi: 10.1016/j.brainres.2017.12.019

Zhang, H., Huang, Z., Xu, Y., and Zhang, S. (2006). Differentiation and neurological benefit of the mesenchymal stem cells transplanted into the rat brain following intracerebral hemorrhage. *Neurol,. Res.* 28, 104–112. doi: 10.1179/016164106x91960

Zhang, R. (2013). Anti-inflammatory and immunomodulatory mechanisms of mesenchymal stem cell transplantation in experimental traumatic brain injury. *J. Neuroinflammation* 10:106.

Zhang, Z., Zhang, Z., Lu, H., Yang, Q., Wu, H., and Wang, J. (2017). Microglial polarization and inflammatory mediators after intracerebral hemorrhage. *Mol. Neurobiol.* 54, 1874–1886. doi: 10.1007/s12035-016-9785-6

Zhao, X., Li, J., and Sun, H. (2019). CD200-CD200R interaction: an important regulator after stroke. *Front. Neurosci.* 13:840. doi: 10.3389/fnins.2019.00840

Zhao, X., Wang, H., Sun, G., Zhang, J., Edwards, N. J., and Aronowski, J. (2015). Neuronal Interleukin-4 as a modulator of microglial pathways and ischemic brain damage. *J. Neurosci.* 35, 11281–11291. doi: 10.1523/jneurosci.1685-15.2015

Zhao, Y., Gao, J., and Lu, F. (2013). Human adipose-derived stem cell adipogenesis induces paracrine regulation of the invasive ability of MCF-7 human breast cancer cells in vitro. *Exp. Ther. Med.* 6, 937–942. doi: 10.3892/etm.2013.1237

Zhou, K., Zhong, Q., Wang, Y. C., Xiong, X. Y., Meng, Z. Y., Zhao, T., et al. (2017). Regulatory T cells ameliorate intracerebral hemorrhage-induced inflammatory injury by modulating microglia/macrophage polarization through the IL-10/GSK3beta/PTEN axis. *J. Cereb. Blood Flow Metab.* 37, 967–979. doi: 10.1177/0271678X16648712

Zhou, Y., Wang, Y., Wang, J., Anne Stetler, R., and Yang, Q. W. (2014). Inflammation in intracerebral hemorrhage: from mechanisms to clinical translation. *Prog. Neurobiol.* 115, 25–44. doi: 10.1016/j.pneurobio.2013.11.003

Zhou, Y., Yamamoto, Y., Xiao, Z., and Ochiya, T. (2019). The immunomodulatory functions of mesenchymal stromal/stem cells mediated via paracrine activity. *J. Clin. Med.* 8:1025. doi: 10.3390/jcm8071025

Zhu, H., Wang, Z., Yu, J., Yang, X., He, F., Liu, Z., et al. (2019). Role and mechanisms of cytokines in the secondary brain injury after intracerebral hemorrhage. *Prog. Neurobiol.* 178:101610. doi: 10.1016/j.pneurobio.2019.03.003

**Conflict of Interest:** The authors declare that the research was conducted in the absence of any commercial or financial relationships that could be construed as a potential conflict of interest.

frontiers in Aging Neuroscience

ORIGINAL RESEARCH
published: 19 May 2021
doi: 10.3389/fnagi.2021.632448

# Circular RNA circDUS2 Is a Potential Biomarker for Intracranial Aneurysm

*Xin Chen*[1,2,3,4], *Shuzhe Yang*[1,2,3,4], *Junhua Yang*[1,2,3,4], *Qingyuan Liu*[1,2,3,4], *Maogui Li*[1,2,3,4], *Jun Wu*[1,2,3,4], *Hao Wang*[1,2,3,4]* and *Shuo Wang*[1,2,3,4]*

[1] Department of Neurosurgery, Beijing Tiantan Hospital, Capital Medical University, Beijing, China, [2] China National Clinical Research Center for Neurological Diseases, Beijing, China, [3] Center of Stroke, Beijing Institute for Brain Disorders, Beijing, China, [4] Beijing Key Laboratory of Translational Medicine for Cerebrovascular Diseases, Beijing, China

**Background:** CircRNAs have been found to play a crucial role in the pathological process of various kinds of diseases. However, the role of circRNAs in the formation and rupture of intracranial aneurysm is still unknown.

**Methods:** Differentially expressed circRNAs profiles between superficial temporal arteries ($n = 5$) and intracranial aneurysms ($n = 5$) were analyzed using the Arraystar human circRNAs microarray. Quantitative real-time PCR was utilized to validate the differential expression of circDUS2. Fluorescence *in situ* hybridization (FISH) was meant for the location of circDUS2 in human brain vascular smooth muscle cell (HBVSMC). Structural analysis was used to speculate on the function of circDUS2.

**Results:** Five hundred forty-three upregulated and 397 downregulated significantly in intracranial aneurysm as compared to superficial temporal arteries. Quantitative real-time PCR verified the elevated expression of the upregulated circDUS2. The FISH test revealed that circDUS2 is located in the cytoplasm of brain vascular smooth muscle cells.

**Conclusion:** This study showed differential expression data of circRNAs between superficial temporal artery and intracranial aneurysm and revealed that circDUS2 is a potential molecular marker for intracranial aneurysm.

**Keywords: circular RNA, intracranial aneurysm, circDUS2, circRNA microarray, smad**

OPEN ACCESS

***Edited by:***
*Guo-Yuan Yang,*
*Shanghai Jiao Tong University, China*

***Reviewed by:***
*Julien Rossignol,*
*Central Michigan University, United States*
*Zhijun Zhang,*
*Shanghai Jiao Tong University, China*

***Correspondence:**
*Hao Wang*
*cmu990103@163.com*
*Shuo Wang*
*captain9858@126.com*

***Received:*** *23 November 2020*
***Accepted:*** *11 March 2021*
***Published:*** *19 May 2021*

***Citation:***
*Chen X, Yang S, Yang J, Liu Q, Li M, Wu J, Wang H and Wang S (2021) Circular RNA circDUS2 Is a Potential Biomarker for Intracranial Aneurysm. Front. Aging Neurosci. 13:632448. doi: 10.3389/fnagi.2021.632448*

## INTRODUCTION

Intracranial aneurysm (IA) is abnormal bulging brought about by structural damage to intracranial artery walls because of multiple factors. Depending on the latest epidemiological research, the morbidity of IA is 8% (Vlak et al., 2011). The rupture of IA can pose a serious threat to human life and health. The mortality of IA rupture within 30 days is nearly 50% and 30% of survivors suffered moderate to severe disabilities (Lawton and Vates, 2017). The assessment of the possibility of rupture is essential to the therapy of IA. Existing research speculated that inflammation, family heredity, geometrical morphology of IA, and hemodynamics are related to the reconstruction of the aneurysm wall, but the details are far from clear. In recent years, the molecular mechanism of aneurysm occurrence and rupture has been studied deeply; inflammation, apoptosis, phenotypic changes of vascular smooth muscle cells, cell adhesion, atherosclerosis, and abnormal extracellular matrix metabolism may be involved in the rupture mechanism of IA (Jiang et al., 2018; Jabbarli et al., 2020). Therefore, the exploration of the mechanism of IA rupture and the search for reliable molecular targets are of great significance for the prediction and diagnosis of IA rupture in advance, guiding the selection of treatment strategies for unruptured aneurysms, directing primary and

secondary prevention, and reducing mortality and disability rates. Circular RNA (CircRNA) is one of a specific type of non-coding RNA. It used to think to be a low abundance RNA due to the incorrect splicing of the exon transcript. In recent years, as the use of the RNA sequencing technique became widespread, it has been found that many exon transcripts can accept non-linear reverse splicing or gene rearrangement to form circRNA (Chen and Yang, 2015). Research on the biological function of circRNA and the effect of human diseases has just started (Chen et al., 2017). Some characteristics of circRNA have been disclosed. It is broadly expressed in human cells (Salzman et al., 2012) and is hard to degrade by exonuclease (Memczak et al., 2013); most of them are located in the cytoplasm instead of the cell nucleus (Zhang et al., 2013). Functions of circRNAs also have been explored, such as microRNA sponges (Hansen et al., 2013), which interact with different proteins (Du et al., 2017) and even encode functional peptides or proteins (Pamudurti et al., 2017; Yang et al., 2017). It is becoming increasingly clear that circRNAs play a crucial role in the pathological process of many kinds of cancers, such as colorectal cancer (Zeng et al., 2018), breast cancer (Pamudurti et al., 2017), and hepatocellular carcinoma (Yang et al., 2017). However, research about the role of circRNAs in the formation and rupture of intracranial aneurysm is rare, and the overall pathophysiological contributions of circRNAs to intracranial aneurysm remain largely unknown. In the present study, we used the circRNA microarray to acquire circRNA profiles in human IA tissues as compared to superficial temporal artery tissues. Subsequently, we performed bioinformatical analysis to explore the potential functions of circRNA in IA. Thus, these data would lay a foundation for future investigations on the molecular functions of circRNAs in IA.

# MATERIALS AND METHODS

## Patients and Specimens

This study was approved by the Medical Ethics Committee of Beijing Tiantan Hospital, Capital Medical University. Every patient admitted in this research has written informed consent. IA specimens were obtained from 15 IA patients undergoing aneurysm clipping. Superficial temporal artery specimens were collected from 15 matched patients without IAs. Among them, five pairs of STA and IA samples were used to conduct a circRNA microarray analysis. Other samples were used to perform qRT-PCR. All these specimens were suspended in liquid nitrogen immediately.

## Total RNA Isolation and Quality Control

Total RNA was extracted from five paired STA tissues and IAs with the use of a Trizol Reagent (Invitrogen). The NanoDrop ND-1000 (Thermo Fisher Scientific, Wilmington, DE, USA) was utilized to test the purity and concentration of RNA (**Supplementary Table 1**). We excluded the contamination of DNA. The integrity of the total RNA was achieved by electrophoresis on a denatured agarose gel.

## RNA Labeling and Hybridization

Sample labeling and array hybridization were performed according to the manufacturer's protocol (Arraystar Inc.). Briefly, total RNAs were digested with Rnase R (Epicenter, Inc.) to remove linear RNAs and rich circular RNAs. Then, the enriched circular RNAs were amplified and transcribed into fluorescent cRNA utilizing a random priming method (Arraystar Super RNA Labeling Kit; Arraystar). The labeled cRNAs were purified by an RNeasy Mini Kit (Qiagen). The concentration and specific activity of the labeled cRNAs (pmol Cy3/μg cRNA) was measured by NanoDrop ND-1000. One microgram of each labeled cRNA was fragmented by adding a 5 μl 10× blocking agent and 1 μl of a 25 × fragmentation buffer, then the mixture was heated at 60°C for 30 min, and finally a 25 μl 2 × hybridization buffer was added to dilute the labeled cRNA. Fifty microliters of hybridization solution was dispensed into the gasket slide and assembled to the circRNA expression microarray slide. The slides were incubated for 17 h at 65°C in an Agilent Hybridization Oven. Hybridized arrays were washed, fixed, and scanned using the Agilent Scanner G2505C.

## circRNA Microarray Analysis

Agilent Feature Extraction software (version 11.0.1.1) was used to analyze the acquired array images. Quantile normalization and subsequent data processing were performed using the R software limma package. Differentially expressed circRNAs with statistical significance between two groups were identified through Volcano Plot filtering. Differentially expressed circRNAs between two samples were determined through Fold Change filtering. Hierarchical Clustering was performed to show the distinguishable circRNAs expression pattern among samples.

## Quantitative Real-Time PCR

Five upregulated circRNAs were selected for further investigation. Quantitative real-time PCR was utilized to verify these differential expressions. We have achieved total RNA of IAs and STA tissues. RNase R (Lucigen, 20U, 37°C, 3 h) was used to purify the circRNAs again. The relevant cDNAs were composed (M-MLV, Promega) and stored in −20°C. QuantStudio5 Real-Time PCR System (Applied Biosystems) was used to perform qRT-PCR. The sequence of circRNA results was obtained from the database "circBase" (http://circrna.org). Primers were obtained by RiboBio (Guangzhou, China) (**Supplementary Table 3**). Owing to the influence of concentration quantitative error and reverse transcription efficiency error, the cDNA content of every sample was different. In order to correct these errors, we regarded housekeeping gene β-actin as an internal reference; as a result, we accepted the ratio of genes to be tested and the internal reference, in other words, the relative content of the gene to be tested.

## GO and KEGG Pathway Analysis

The GO enrichment analysis divides gene functions into three aspects: cellular components (CCs), molecular functions (MFs), and biological processes (BPs). After we find out our target circRNAs, miRNAs binding on our target circRNAs also can be found. We perform GO analysis on parental genes of these

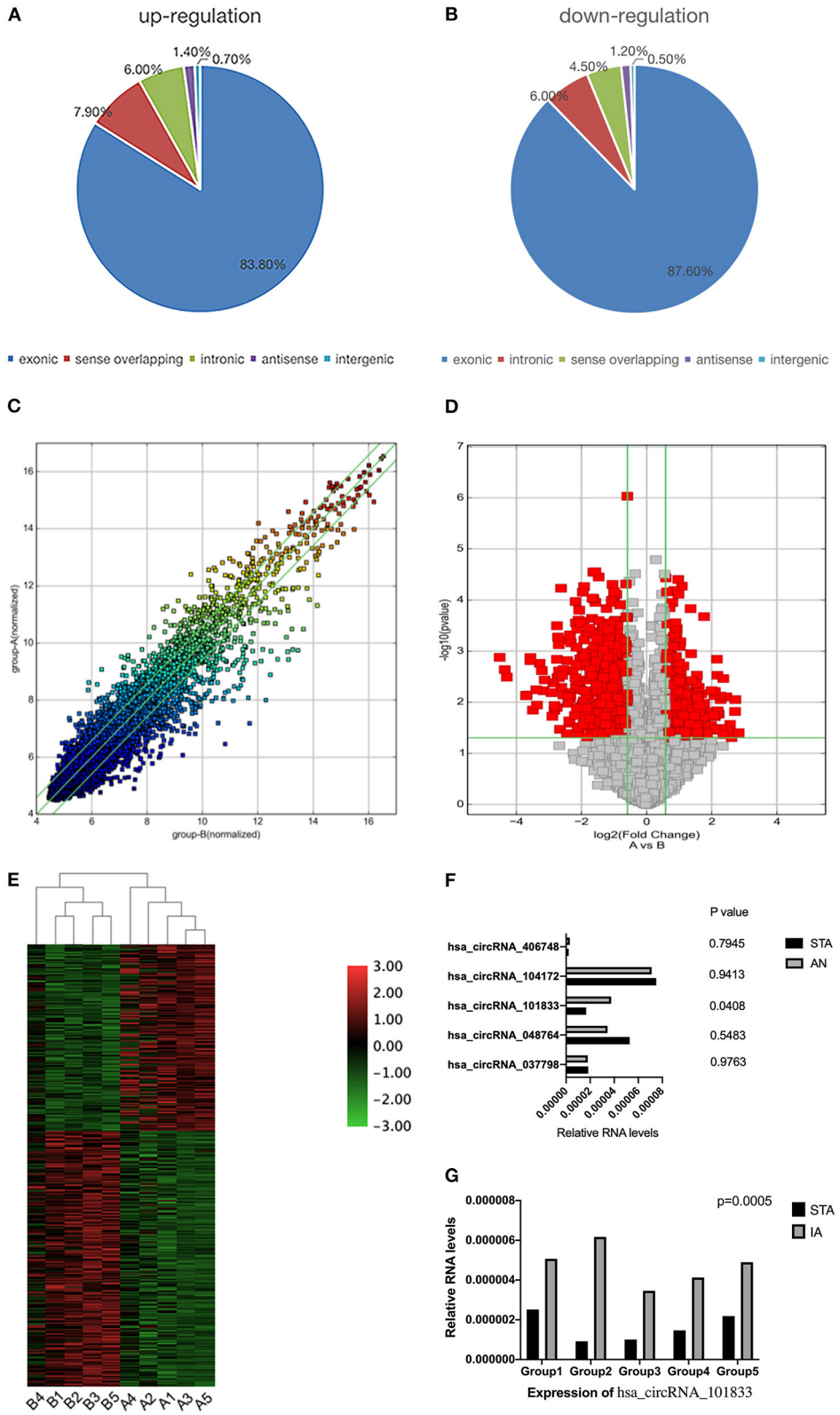


**FIGURE 1 |** Differential expression of circRNAs in IA tissues. **(A)** The constituent of upregulated circRNAs. **(B)** The constituent of downregulated circRNAs. **(C)** The scatterplot is used for assessing the circRNA expression variation between the two compared samples or two compared groups of samples. The values of X and Y

*(Continued)*

**FIGURE 1 |** axes in the scatterplot are the normalized signal values of the samples ($log_2$ scaled) or the averaged normalized signal values of groups of samples ($log_2$ scaled). The green lines are Fold Change Lines. The circRNAs above the top green line and below the bottom green line indicate more than 1.5-fold change of circRNAs between the two compared samples. **(D)** Volcano Plots are used for visualizing differential expression between two different conditions. The vertical lines correspond to 1.5-fold up and down, respectively, and the horizontal line represents a *p*-value of 0.05. So the red point in the plot represents the differentially expressed circRNAs with statistical significance. Group A represented STA samples; group B represented IA samples. **(E)** The hierarchical clustering of differentially expressed circRNAs. "Red" indicates high relative expression, and "green" indicates low relative expression. Group A represented STA samples; group B represented IA samples. **(F)** Validation of the differential expression of five upregulated circRNAs. **(G)** Validation of the differential expression of hsa_circRNA_101833 in another five coupled groups. STA, superficial temporal arteries; IA, IA.

miRNAs with R. The *P*-value after adjustment represents the significance of GO terms. We also perform a KEGG pathway analysis of parental genes of circRNA-binding miRNAs in order to reveal the biological or pathological processes in which circRNAs participate. The *P*-value after adjustment represents the significance of pathway correlations as well.

## Statistical Analysis

The fold changes were estimated by unpaired Student's *t*-test and used to identify the differentially expressed circRNAs in the sample of IAs. CircRNA was selected as differentially expressed with a $P < 0.05$ and a fold change $>1.5$, which means they were statistically significant. The significance of qRT-PCR was evaluated by Student's *t*-test, and $P < 0.05$ was considered statistically significant; it was analyzed by GraphPad Prism 8.4.0 (GraphPad Software, La Jolla, CA, USA). Other statistical methods such as chi-squared test, Wilcoxon signed-rank test, and Mann–Whitney *U*-test were also performed. All statistical analyses were done by SPSS 19.0 (SPSS, Inc., Chicago, IL).

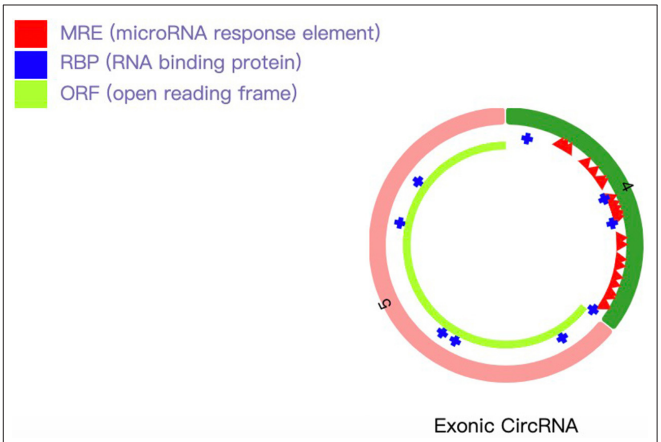


**FIGURE 2 |** Schematic diagram of hsa_circRNA_101833. The light green bar represents the open reading frame, the blue bar represents proteins binding with hsa_circRNA_101833, and the red bar represents the microRNA binding sites.

# RESULTS

## Identification of circRNA Microarray in Human IA and STA Samples

We detected a total of 13,174 circRNAs using the Arraystar human circRNA Microarray (**Supplementary Table 4**). Among them, 942 circRNAs dysregulated between STA and IA tissues (fold change $> 1.5$; $P < 0.05$), and 750 of them have been identified in circBase by other studies. Furthermore, comparing IA with superficial temporal artery, 544 circRNAs upregulated while 398 of them downregulated (**Supplementary Table 5**). All circRNAs were classified into five types: "exonic," "intronic," "antisense," "sense overlapping," and "intergenic." Among the upregulated circRNAs, 456 (83.82%) circRNAs consist of exons, 43 (7.9%) circRNAs transcribed from the same gene locus as the linear transcript but not classified into "exonic" and "intronic" were classified as sense overlapping, 33 (6.07%) were intronic, 8 (1.47%) were antisense, and 4 (0.74%) were intergenic (**Figure 1A**). For downregulated circRNAs, there were 349 (87.69%) exonic, 24 (6.03%) intronic, 18 (4.52%) sense overlapping, 5 (1.26%) antisense, and 2 (0.5%) intergenic (**Figure 1B**). CircRNA expression variations between the two compared groups of samples were assessed (**Figure 1C**). The Volcano Plot was constructed through fold change values and *p*-values and used for visualizing the differential expression between the STA and IA samples (**Figure 1D**). Hierarchical clustering revealed the circRNA expression in IAs and the superficial temporal artery (**Figure 1E**). For further investigation, we selected five circRNAs upregulated in aneurysm samples (hsa_circRNA_104172, hsa_circRNA_048764, hsa_circRNA_037798, hsa_circRNA_406748, and hsa_circRNA_101833). Besides fold change $> 1.5$ and $P < 0.05$, their raw intensities in both the IA and STA groups were more than 200, and their parental genes were well-investigated by other researchers in order to reveal these circRNAs' functions better. We perform qRT-PCR in another five paired STA and IA samples to verify the circRNA microarray profiling expression results. The results showed that two of the five circRNAs that we have selected upregulated in IA, but only the overexpression of hsa_circRNA_101833 was significant ($P < 0.05$; **Figure 1F**). Then, five more paired samples were used to verify the differential expression of hsa_circRNA_101833 in two groups, and the result was identical to the microarray analysis and the qRT-PCR performed for the first time (**Figure 1G**).

## Characteristics and Functions of circDUS2

hsa_circRNA_101833 is derived from exon 4 and exon 5 of the DUS2 gene, and its CircBase ID is hsa_circ_0039908. hsa_circRNA_101833 contains an open reading frame (ORF). MicroRNA binding sites also have the ability of binding protein (**Figure 2**). To determine whether this ORF is functional, we have achieved the nucleotide sequence of hsa_circRNA_101833 from CircBase, and then three ORFs were detected by ORFfinder

**TABLE 1 |** Open reading frames detected from hsa_circRNA_101833.

| Label | Strand | Frame | Start | Stop | Length (nt\|aa) | Nucleotide sequence |
|---|---|---|---|---|---|---|
| ORF1 | + | 3 | 99 | >224 | 126\|41 | MILNSLSLCYHNKLILAPMVRVGTLPMRLLALDYGADIVYCE |
| ORF2 | – | 1 | 131 | 45 | 87\|28 | MVTQREAIQNHFLLCYSLLFCSDTSGLL |
| ORF3 | – | 3 | 177 | 64 | 114\|37 | MEESLPEPLGPGLAYYGNTERGYSKSFPPLLQPIILF |

*ORF, open reading frame.*

(https://www.ncbi.nlm.nih.gov/orffinde) (**Table 1**). Among the three ORFs, only the longest one has the capacity to encode protein. The results of the Conserved Domains (https://www.ncbi.nlm.nih.gov/Structure/cdd/wrpsb.cgi) showed that. The ORF may encode the triose phosphate isomerase (TIM) superfamily (Bit Score = 56.73, *E*-value = 4.13e-12). According to previous researches, TIM is a dimeric, non-allosteric enzyme of the glycolytic pathway and catalyzes the interconversion of the three-carbon sugars dihydroxyacetone phosphate (DHAP) and D-glyceraldehyde 3-phosphate (GAP) (Wierenga et al., 2010). Another function of circRNA is as microRNA sponges, which means to control gene transcription by binding with microRNAs. To elucidate the function of microRNA sponges, miRNAs connected with hsa_circRNA_101833 were found (CSCD, http://gb.whu.edu.cn/CSCD/) and listed in **Table 2**. Furthermore, we recognized proteins binding with hsa_circRNA_101833 from CSCD, and the result is listed in **Table 3**.

**TABLE 2 |** miRNAs that connected with hsa_circRNA_101833.

| ID | microRNA | MSA start | MSA end | Site type |
|---|---|---|---|---|
| 1 | let-7a-2-3p/7g-3p | 72 | 79 | 8mer-1a |
| 2 | let-7c-3p | 73 | 79 | 7mer-1a |
| 3 | miR-101-3p.1 | 42 | 47 | 6mer |
| 4 | miR-128-3p/216-3p/3681-3p | 43 | 49 | 7mer-1a |
| 5 | miR-136-5p | 25 | 30 | 6mer |
| 6 | miR-144-3p | 42 | 47 | 6mer |
| 7 | miR-144-5p | 51 | 57 | 7mer-1a |
| 8 | miR-149-5p | 80 | 86 | 7mer-1a |
| 9 | miR-27-3p | 43 | 49 | 7mer-m8 |
| 10 | miR-30-5p | 38 | 44 | 7mer-m8 |
| 11 | miR-3064-5p/6504-5p | 80 | 86 | 7mer-1a |
| 12 | miR-3119 | 78 | 84 | 7mer-1a |
| 13 | miR-340-5p | 66 | 71 | 6mer |
| 14 | miR-342-3p | 45 | 50 | 6mer |
| 15 | miR-375 | 58 | 63 | 6mer |
| 16 | miR-3918 | 15 | 20 | 6mer |
| 17 | miR-4273/7156-5p | 84 | 89 | 6mer |
| 18 | miR-4677-5p | 84 | 89 | 6mer |
| 19 | miR-4685-5p/6837-5p | 15 | 22 | 8mer-1a |
| 20 | miR-4797-5p | 69 | 76 | 8mer-1a |
| 21 | miR-493-5p | 73 | 79 | 7mer-1a |
| 22 | miR-5011-5p | 91 | 96 | 6mer |
| 23 | miR-511-3p | 87 | 93 | 7mer-1a |
| 24 | miR-513-3p | 33 | 38 | 6mer |
| 25 | miR-513a-5p | 44 | 49 | 6mer |
| 26 | miR-545-5p | 40 | 46 | 7mer-m8 |
| 27 | miR-5571-5p | 63 | 69 | 7mer-1a |
| 28 | miR-5586-5p | 18 | 23 | 6mer |
| 29 | miR-572 | 28 | 34 | 7mer-m8 |
| 30 | miR-599 | 53 | 59 | 7mer-1a |
| 31 | miR-599 | 94 | 100 | 7mer-1a |
| 32 | miR-664-5p/4794 | 80 | 86 | 7mer-1a |
| 33 | miR-6834-3p | 32 | 37 | 6mer |
| 34 | miR-6844 | 59 | 66 | 8mer-1a |
| 35 | miR-7113-5p | 16 | 22 | 7mer-1a |
| 36 | miR-759 | 69 | 74 | 6mer |

*MSA, Multiple sequence alignment.*

## GO and KEGG Pathway Analysis

After microRNAs binding on hsa_circRNA_101833 have been found, we searched the target genes of these microRNAs through TargetScan, miRDB, and miRTarBase (**Supplementary Table 6**). We finally enriched 19 GO terms, and all these terms were significantly different. The results revealed that the target genes of these microRNAs favored SMAD binding and histone deacetylase binding (**Figure 3A**). Among them, SMAD binding may be more likely to progress in which hsa_circRNA_101833 participates in the formation of IAs. According to several studies, the SMAD family is related to the formation of thoracic aortic aneurysm (Regalado et al., 2011; Mao et al., 2012; Wang et al., 2016), and animal experiments have proven that the deficiency of SMAD3 would promote the formation of thoracic aortic aneurysm (Dai et al., 2015). Also, KEGG pathway analysis has been performed. Depending on our annotation, the target genes of these microRNAs are associated with signaling pathways regulating the pluripotency of stem cells, insulin resistance, FoxO signaling pathway, Prolactin signaling pathway, AMPK signaling pathway, breast cancer, and aldosterone-regulated sodium reabsorption (**Figure 3B**). Among them, the signaling pathways regulating the pluripotency of stem cells and the FoxO signaling pathway contain the TGF-β signaling pathway and the MAPK signaling pathway (**Figure 3C**), and both of them are well-studied pathways related to the pathological processes of IAs (Weinsheimer et al., 2007; Yamashita et al., 2008).

## DISCUSSION

In our study, we revealed hundreds of differentially expressed circRNAs between human IA tissues and STA tissues. Based on their expressive intensity and other criteria as mentioned before, five upregulated circRNAs were selected; finally, only hsa_circRNA_101833 overexpressed significantly after being verified by qRT-PCR. With GO analysis of the target genes of microRNAs binding on hsa_circRNA_101833,

**TABLE 3 |** Proteins that bind with hsa_circRNA_101833.

| ID | RBP | Details |
|---|---|---|
| 1 | eIF4AIII_Human_GSE40778_HITS-CLIP | HHLE2_439259_eIF4AIII_rep2_439259_2 |
| 2 | hnRNPC_Human_E-MTAB-1371_iCLIP | HIUHC_160199_HNRNPC_160199 |
| 3 | hnRNPC_Human_E-MTAB-1371_iCLIP | HIUHC_160202_HNRNPC_160202 |
| 4 | UPF1_Human_GSE47976_iCLIP | HIMP2_139591_UPF1_rep2_puromycoin_139591 |
| 5 | eIF4AIII_Human_GSE40778_HITS-CLIP | HHLE2_439262_eIF4AIII_rep2_439262_17 |
| 6 | AGO2_Human_GSE42701_HITS-CLIP | HHFKP_56722_cluster-8685_1_12 |
| 7 | FUS_Human_GSE43308_HITS-CLIP | HHMF2_146682_FUS_rep2_1 |
| 8 | UPF1_Human_GSE47976_iCLIP | HIMU2_172057_UPF1_rep2_untreated_172057 |
| 9 | eIF4AIII_Human_GSE40778_HITS-CLIP | HHLE2_439261_eIF4AIII_rep2_439261_1 |
| 10 | U2AF65_Human_E-MTAB-1371_iCLIP | HIUUC_189306_U2AF65_ctrl_189306 |
| 11 | eIF4AIII_Human_GSE40778_HITS-CLIP | HHLE1_131383_eIF4AIII_rep1_131383_13 |
| 12 | AGO2_Human_GSE42701_HITS-CLIP | HHFKP_56723_cluster-8685_2_12 |
| 13 | eIF4AIII_Human_GSE40778_HITS-CLIP | HHLE1_131378_eIF4AIII_rep1_131378_1 |
| 14 | U2AF65_Human_E-MTAB-1371_iCLIP | HIUUS_407000_U2AF65_ctrl_plus_HNRNPC_kd_407000 |
| 15 | UPF1_Human_GSE47976_iCLIP | HIMP2_139590_UPF1_rep2_puromycoin_139590 |
| 16 | PTB_Human_GSE42701_HITS-CLIP | HHFPT_109417_PTB_cluster-8685_7_9 |
| 17 | AGO2_Human_GSE32109_PAR-CLIP | HPCB1_15634_G19662.1_68071959 |
| 18 | hnRNPC_Human_E-MTAB-1371_iCLIP | HIUHC_160200_HNRNPC_160200 |
| 19 | U2AF65_Human_E-MTAB-1371_iCLIP | HIUUS_406996_U2AF65_ctrl_plus_HNRNPC_kd_406996 |
| 20 | hnRNPC_Human_E-MTAB-1371_iCLIP | HIUHC_160206_HNRNPC_160206 |
| 21 | UPF1_Human_GSE47976_iCLIP | HIMU2_172058_UPF1_rep2_untreated_172058 |
| 22 | U2AF65_Human_E-MTAB-1371_iCLIP | HIUUS_406993_U2AF65_ctrl_plus_HNRNPC_kd_406993 |
| 23 | FUS_Human_GSE43308_HITS-CLIP | HHMF1_114226_FUS_rep1_6 |
| 24 | hnRNPC_Human_E-MTAB-1371_iCLIP | HIUHC_160207_HNRNPC_160207 |
| 25 | eIF4AIII_Human_GSE40778_HITS-CLIP | HHLE1_131379_eIF4AIII_rep1_131379_4 |
| 26 | U2AF65_Human_E-MTAB-1371_iCLIP | HIUUS_406999_U2AF65_ctrl_plus_HNRNPC_kd_406999 |
| 27 | U2AF65_Human_E-MTAB-1371_iCLIP | HIUUS_406998_U2AF65_ctrl_plus_HNRNPC_kd_406998 |
| 28 | eIF4AIII_Human_GSE40778_HITS-CLIP | HHLE1_131380_eIF4AIII_rep1_131380_1 |
| 29 | eIF4AIII_Human_GSE40778_HITS-CLIP | HHLE1_131382_eIF4AIII_rep1_131382_1 |
| 30 | hnRNPC_Human_E-MTAB-1371_iCLIP | HIUHC_160204_HNRNPC_160204 |
| 31 | hnRNPC_Human_E-MTAB-1371_iCLIP | HIUHC_160205_HNRNPC_160205 |
| 32 | U2AF65_Human_E-MTAB-1371_iCLIP | HIUUS_406991_U2AF65_ctrl_plus_HNRNPC_kd_406991 |
| 33 | PTB_Human_GSE42701_HITS-CLIP | HHFPT_109418_PTB_cluster-8685_8_10 |
| 34 | U2AF65_Human_E-MTAB-1371_iCLIP | HIUUS_407001_U2AF65_ctrl_plus_HNRNPC_kd_407001 |
| 35 | eIF4AIII_Human_GSE40778_HITS-CLIP | HHLE2_439260_eIF4AIII_rep2_439260_1 |
| 36 | eIF4AIII_Human_GSE40778_HITS-CLIP | HHLE2_439258_eIF4AIII_rep2_439258_3 |
| 37 | U2AF65_Human_E-MTAB-1371_iCLIP | HIUUC_189305_U2AF65_ctrl_189305 |
| 38 | U2AF65_Human_E-MTAB-1371_iCLIP | HIUUS_406994_U2AF65_ctrl_plus_HNRNPC_kd_406994 |
| 39 | UPF1_Human_GSE47976_iCLIP | HIMP2_139588_UPF1_rep2_puromycoin_139588 |
| 40 | eIF4AIII_Human_GSE40778_HITS-CLIP | HHLE1_131381_eIF4AIII_rep1_131381_1 |
| 41 | hnRNPC_Human_E-MTAB-1371_iCLIP | HIUHC_160201_HNRNPC_160201 |
| 42 | U2AF65_Human_E-MTAB-1371_iCLIP | HIUUC_189304_U2AF65_ctrl_189304 |
| 43 | eIF4AIII_Human_GSE40778_HITS-CLIP | HHLE2_439257_eIF4AIII_rep2_439257_18 |
| 44 | UPF1_Human_GSE47976_iCLIP | HIMP2_139589_UPF1_rep2_puromycoin_139589 |
| 45 | U2AF65_Human_E-MTAB-1371_iCLIP | HIUUC_189303_U2AF65_ctrl_189303 |
| 46 | U2AF65_Human_E-MTAB-1371_iCLIP | HIUUS_406995_U2AF65_ctrl_plus_HNRNPC_kd_406995 |
| 47 | U2AF65_Human_E-MTAB-1371_iCLIP | HIUUS_406992_U2AF65_ctrl_plus_HNRNPC_kd_406992 |
| 48 | UPF1_Human_GSE47976_iCLIP | HIMP2_139592_UPF1_rep2_puromycoin_139592 |
| 49 | ZC3H7B_Human_GSE38201_PAR-CLIP | HPLZC_25397_ZC3H7B_CID_009358_68059398 |
| 50 | hnRNPC_Human_E-MTAB-1371_iCLIP | HIUHC_160203_HNRNPC_160203 |
| 51 | UPF1_Human_GSE47976_iCLIP | HIMP2_139593_UPF1_rep2_puromycoin_139593 |
| 52 | U2AF65_Human_E-MTAB-1371_iCLIP | HIUUS_406997_U2AF65_ctrl_plus_HNRNPC_kd_406997 |

*RBP, RNA binding protein.*

hsa_circRNA_101833 might participate in the pathological processes of IAs, especially through the way of SMAD binding.

The SMAD family contains three subfamilies: the five receptor-activated SMADs (R-SMADs), the one common mediator SMAD (Co-SMAD), and the two inhibitory SMADs (I-SMADs) (Moustakas et al., 2001; Derynck and Zhang, 2003; Shi and Massague, 2003). Smad2 and 3 are signals for TGF-β (transforming growth factor-β) (Flanders, 2004). TGF-β has a

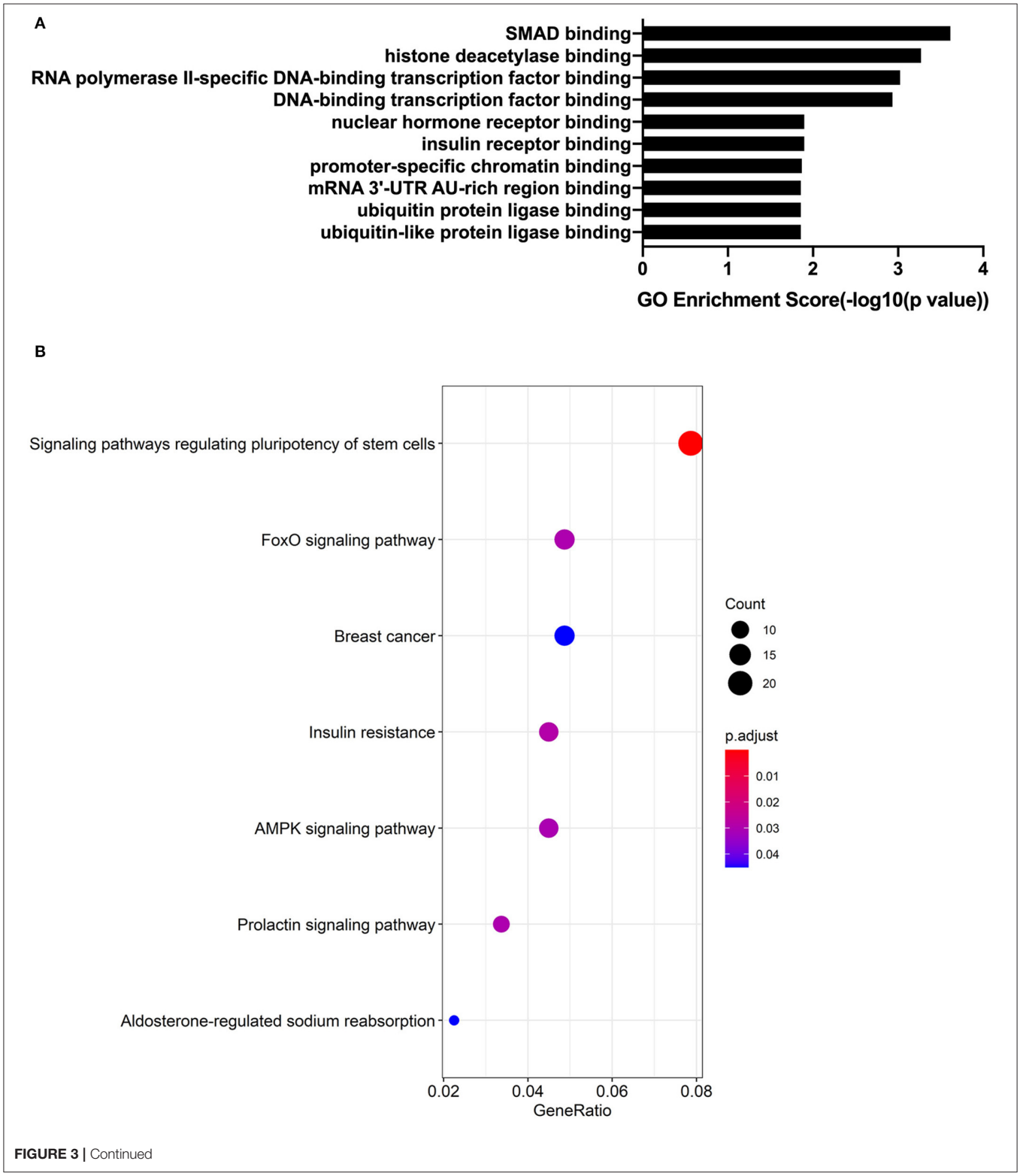


**FIGURE 3 |** Continued

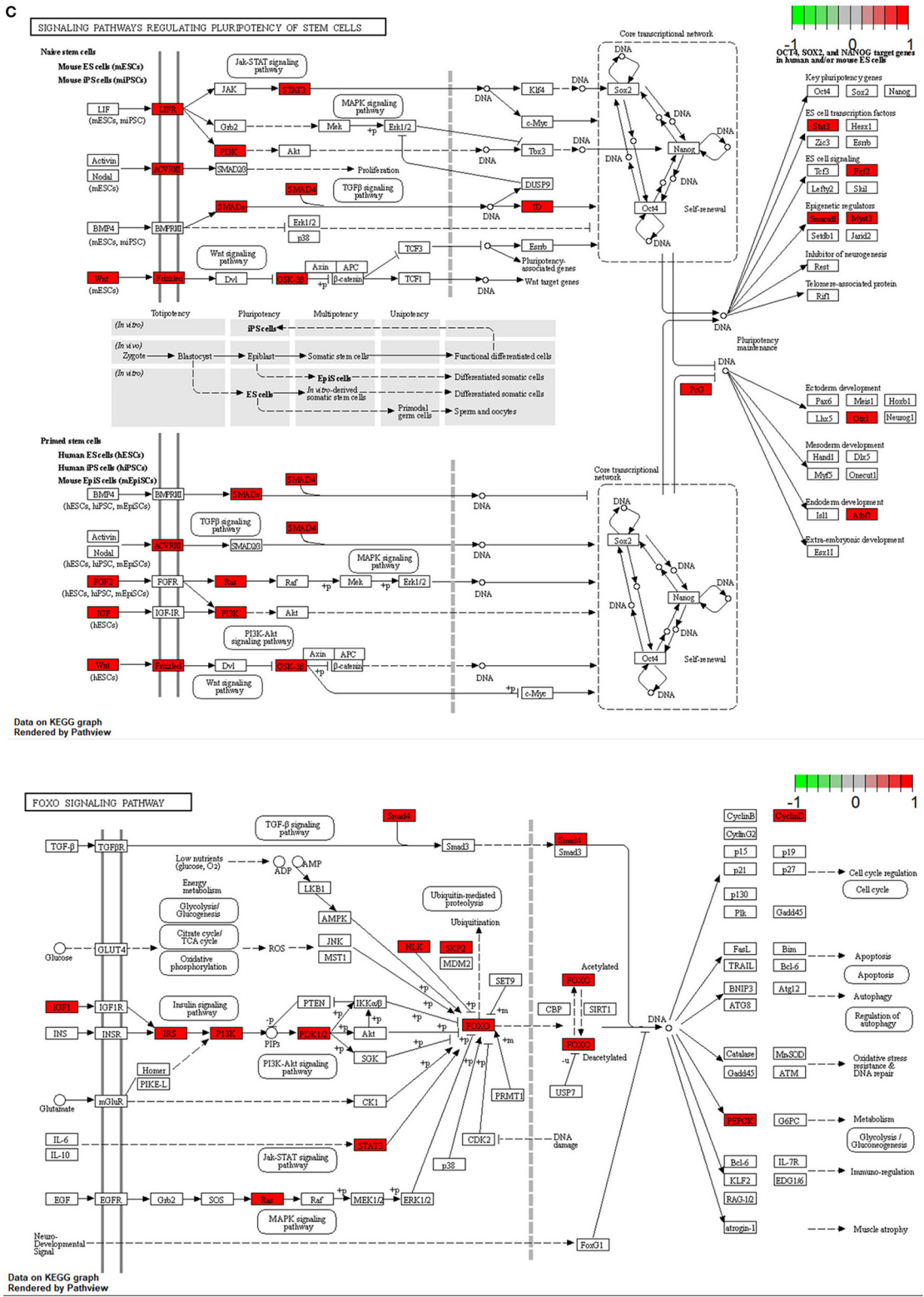


**FIGURE 3 |** GO and KEGG analysis results. **(A)** GO annotations of target genes of microRNAs binding on hsa_circRNA_101833 with top 10 enrichment score encompassing the domains of physiological processes. **(B)** Dotplot of KEGG pathway analysis; the size of the circle represents the count of genes, and the color represents the *p*-values of pathways. **(C)** The visualization of signaling pathways regulating the pluripotency of stem cells and the FoxO signaling pathway conducted by Pathview.

lot of functions, acts on a variety of different cells, and regulates many distinctive complex intracellular functions. And several studies suggest that TGF-β plays a critical role in the pathological processes of IAs (Yamashita et al., 2008; Carta et al., 2009), and the interactions between R-SMAD (SMAD2 and SMAD3) and Co-SMAD (SMAD4) regulate the canonical pathway that TGF-β attends (Akhurst, 2012). Numerous studies have proven the relationship between SMAD and aneurysm. Regalado et al. (2011) showed that SMAD3 mutations are responsible for 2% of familial thoracic aortic aneurysms and dissections, and aneurysms resulting from the SMAD3 mutation involve different arteries, including intracranial arteries. What is more, a study about the association between SMAD3 gene and IA (Liao et al., 2018) demonstrates that SMAD3 gene polymorphisms were significantly related to IAs. Apart from SMAD3, the relationship between SMAD4 and aneurysms also has been studied. Mao et al. (2012) found that silencing SMAD4 of the vascular smooth muscle cell (VSMC) would result in vascular defects by decreasing VSMC differentiation, proliferation, migration, as well as cell attachment and spreading. And the differentiation and migration of VSMC may be one of the mechanisms that contribute to the formation of aneurysm. Furthermore, we performed a KEGG pathway analysis to annotate the target genes of microRNAs binding on hsa_circRNA_101833. Our results showed that these genes associated with the signaling pathways regulating the pluripotency of stem cells and the FoxO signaling pathway that are involved in the formation of IA. Both GO enrichment and KEGG analysis suggested that upregulation of hsa_circRNA_101833 may promote the formation of IA.

We detected hundreds of differentially expressed circRNAs using the Arraystar human circRNA Microarray; 456 (83.82%) of the upregulated circRNAs and 349 (87.69%) of the downregulated circRNAs belong to the exonic type. This constitution of circRNAs is in common with previous studies (Cordes et al., 2009; Merk et al., 2012; Zhang et al., 2013). We also found that circRNAs can adsorb microRNAs and interact with different proteins. These findings are all in accordance with previous studies (Hansen et al., 2013; Du et al., 2017). Besides, the function of hsa_circRNA_101833 has been analyzed in human IA tissues for the first time. We revealed that the ORF of hsa_circRNA_101833 may encode the TIM superfamily, but the relationship between TIM and aneurysm is still unknown, so we cannot determine whether hsa_circRNA_101833 influences the pathological process through its expression product. Inevitably, there are several limitations in this study. First of all, our tissue sample size is small. Our results need a larger number of IA samples to testify. Secondly, because aneurysm samples are rare, some of our samples were stored in liquid nitrogen for several weeks; perhaps this would affect the amount of circRNAs. Thirdly, this study is mainly a bioinformatic analysis. Further studies should be done to prove the function of hsa_circRNA_101833 in the aneurysm pathological process. Lastly, due to the lack of studies about circRNAs in aneurysm, we cannot compare our results with others in order to enhance our methods.

In general, hundreds of differentially expressed circRNAs using the Arraystar human circRNA Microarray were detected in IAs as compared to the STA tissue. The up-regulation of hsa_circRNA_101833 was associated with the formation of IAs through the impact on the SMAD family or participating the TGF-β sigaling pathway and MAPK signaling pathway

## DATA AVAILABILITY STATEMENT

The datasets presented in this study can be found in online repositories. The names of the repository/repositories and accession number(s) can be found in the article/**Supplementary Material**.

## ETHICS STATEMENT

The studies involving human participants were reviewed and approved by Institutional review board of the Beijing Tiantan hospital. The patients/participants provided their written informed consent to participate in this study.

## AUTHOR CONTRIBUTIONS

SW and HW were in charge of supervising the whole study. XC contributed to the conception or design of the work. XC and SY were responsible for drafting and revising. QL, ML, JW, and JY were responsible for analysis and interpretation of data. All authors contributed to manuscript revision, read, and approved the submission.

## FUNDING

This work was supported by the National Key Research and Development Program of China (Grant No. 2016YFC1301800, SW) and the National Natural Science Foundation of China (Grant No. 81671129, SW).

## SUPPLEMENTARY MATERIAL

The Supplementary Material for this article can be found online at: https://www.frontiersin.org/articles/10.3389/fnagi.2021.632448/full#supplementary-material

## REFERENCES

Akhurst, R. J. (2012). The paradoxical TGF-beta vasculopathies. *Nat. Genet.* 44, 838–839. doi: 10.1038/ng.2366

Carta, L., Smaldone, S., Zilberberg, L., Loch, D., Dietz, H. C., Rifkin, D. B., et al. (2009). p38 MAPK is an early determinant of promiscuous Smad2/3 signaling in the aortas of fifibrillin-1 (Fbn1)-null mice. *J. Biol. Chem.* 284, 5630–5636. doi: 10.1074/jbc.M806962200

Chen, L. L., and Yang, L. (2015). Regulation of circRNA biogenesis. *RNA Biol*. 12, 381–388. doi: 10.1080/15476286.2015.1020271

Chen, Y., Li, C., Tan, C., and Liu, X. (2017). Circular RNAs: a new frontier in the study of human diseases. *J. Med. Genet*. 53, 359–365. doi: 10.1136/jmedgenet-2016-103758

Cordes, K. R., Sheehy, N. T., White, M. P., Berry, E. C., Morton, S. U., Muth, A. N., et al. (2009). miR-145 and miR-143 regulate smooth muscle cell fate and plasticity. *Nature* 460, 705–710. doi: 10.1038/nature08195

Dai, X., Shen, J., Annam, N. P., Jiang, H., Levi, E., Schworer, C. M., et al. (2015). SMAD3 deficiency promotes vessel wall remodeling, collagen fiber reorganization and leukocyte infiltration in an inflammatory abdominal aortic aneurysm mouse model. *Sci Rep*. 5:10180. doi: 10.1038/srep10180

Derynck, R., and Zhang, Y. E. (2003). Smad-dependent and Smadindependent pathways in TGF-beta family signalling. *Nature* 425, 577–584. doi: 10.1038/nature02006

Du, W. W., Zhang, C., Yang, W., Yong, T., Awan, F. M., Yang, B. B., et al. (2017). Identifying and characterizing circRNA-protein interaction. *Theranostics* 7, 4183–4191. doi: 10.7150/thno.21299

Flanders, K. C. (2004). Smad3 as a mediator of the fibrotic response. *Int. J. Exp. Pathol.* 85, 47–64. doi: 10.1111/j.0959-9673.2004.00377.x

Hansen, T. B., Jensen, T. I., Clausen, B. H., Bramsen, J. B., Finsen, B., Damgaard, C. K., et al. (2013). Natural RNA circles function as efficient microRNA sponges. *Nature* 495, 384–388. doi: 10.1038/nature11993

Jabbarli, R., Rauschenbach, L., Dinger, T. F., Oppong, M. D., Rodemerk, J., Pierscianek, D., et al. (2020). In the wall lies the truth: a systematic review of diagnostic markers in IAs. *Brain Pathol.* 30, 437–445. doi: 10.1111/bpa.12828

Jiang, P., Wu, J., Chen, X., Ning, B., Liu, Q. Y., Li, Z. S., et al. (2018). Quantitative proteomics analysis of differentially expressed proteins in ruptured and unruptured cerebral aneurysms by iTRAQ. *J. Proteomics* 182, 45–52. doi: 10.1016/j.jprot.2018.05.001

Lawton, M. T., and Vates, G. E. (2017). Subarachnoid hemorrhage. *N. Engl. J. Med*. 377, 257–266. doi: 10.1056/NEJMcp1605827

Liao, M. F., Gong, Q. W., Liu, L., Xiong, X. Y., Zhang, Q., Gong, C. X., et al. (2018). Association between polymorphism of SMAD3 gene and risk of sporadic intracranial arterial aneurysms in the Chinese Han population. *J. Clin. Neurosci.* 47, 269–272. doi: 10.1016/j.jocn.2017.09.006

Mao, X., Debenedittis, P., Sun, Y., Chen, J., Yuan, K., Jiao, K., et al. (2012). Vascular smooth muscle cell Smad4 gene is important for mouse vascular development. *Arterioscler. Thromb. Vasc. Biol*. 32, 2171–2177. doi: 10.1161/ATVBAHA.112.253872

Memczak, S., Jens, M., Elefsinioti, A., Torti, F., Krueger, J., Rybak, A., et al. (2013). Circular RNAs are a large class of animal RNAs with regulatory potency. *Nature* 495, 333–338. doi: 10.1038/nature11928

Merk, D. R., Chin, J. T., Dake, B. A., Maegdefessel, L., Miller, M. O., Kimura, N., et al. (2012). miR- 29b participates in early aneurysm development in Marfan syndrome. *Circ Res*. 110, 312–324. doi: 10.1161/CIRCRESAHA.111.253740

Moustakas, A., Souchelnytskyi, S., and Heldin, C. H. (2001). Smad regulation in TGF-beta signal transduction. *J. Cell Sci.* 114 (Pt. 24), 4359–4369.

Pamudurti, N. R., Bartok, O., Jens, M., Fluss, R. A., Stottmeister, C., Ruhe, L., et al. (2017). Translation of circRNAs. *Mol. Cell* 66, 9–21. doi: 10.1016/j.molcel.2017.02.021

Regalado, E. S., Guo, D. C., Villamizar, C., Avidan, N., Gilchrist, D., McGillivray, B., et al. (2011). Exome sequencing identifies SMAD3 mutations as a cause of familial thoracic aortic aneurysm and dissection with intracranial and other arterial aneurysms. *Circ. Res.* 109, 680–686. doi: 10.1161/CIRCRESAHA.111.248161

Salzman, J., Gawad, C., Wang, P. L., Lacayo, N., and Brown, P. O. (2012). Circular RNAs are the predominant transcript isoform from hundreds of human genes in diverse cell types. *PLoS ONE* 7:e30733. doi: 10.1371/journal.pone.0030733

Shi, Y., and Massague, J. (2003). Mechanisms of TGF-beta signaling from cell membrane to the nucleus. *Cell* 113, 685–700. doi: 10.1016/S0092-8674(03)00432-X

Vlak, M. H., Algra, A., Brandenburg, R., and Rinkel, G. J. (2011). Prevalence of unruptured IAs, withemphasis on sex, age, comorbidity, country, and time period: a systematic review and meta-analysis. *Lancet Neurol*. 10, 626–636. doi: 10.1016/S1474-4422(11)70109-0

Wang, Y., Huang, H. Y., Bian, G. L., Yu, Y. S., Ye, W. X., Hua, F., et al. (2016). A functional variant of SMAD4 enhances thoracic aortic aneurysm and dissection risk through promoting smooth muscle cells apoptosis and proteoglycans degradation. *EBioMedicine* 21, 197–205. doi: 10.1016/j.ebiom.2017.06.022

Weinsheimer, S., Lenk, G. M., van der Voet, M., Land, S., Ronkainen, A., Alafuzoff, I., et al. (2007). Integration of expression profiles and genetic mapping data to identify candidate genes in IA. *Physiol. Genomics* 32, 45–57. doi: 10.1152/physiolgenomics.00015.2007

Wierenga, R. K., Kapetaniou, E. G., and Venkatesan, R. (2010). Triosephosphate isomerase: a highly evolved biocatalyst. *Cell. Mol. Life Sci.* 67, 3961–3982. doi: 10.1007/s00018-010-0473-9

Yamashita, M., Fatyol, K., Jin, C., Wang, X., Liu, Z., and Zhang, Y. E. (2008). TRAF6 mediates smadindependent activation of JNK and p38 by TGF-beta. *Mol. Cell*. 31, 918–924. doi: 10.1016/j.molcel.2008.09.002

Yang, Y., Fan, X., Mao, M., Song, X., Wu, P., Zhang, Y., et al. (2017). Extensive translation of circular RNAs driven by N6-methyladenosine. *Cell Res*. 27, 626–641. doi: 10.1038/cr.2017.31

Zeng, K., Chen, X., Xu, M., Liu, X., Hu, X., Xu, T., et al. (2018). Circhipk3 promotes colorectal cancer growth and metastasis by sponging mir-7. *Cell Death Dis*. 9:417. doi: 10.1038/s41419-018-0454-8

Zhang, Y., Zhang, X. O., Chen, T., Xiang, J. F., Yin, Q. F., Xing, Y. H., et al. (2013). Circular intronic long noncoding RNAs. *Mol Cell* 51, 792–806. doi: 10.1016/j.molcel.2013.08.017

**Conflict of Interest:** The authors declare that the research was conducted in the absence of any commercial or financial relationships that could be construed as a potential conflict of interest.

frontiers in Aging Neuroscience

ORIGINAL RESEARCH
published: 19 May 2021
doi: 10.3389/fnagi.2021.636184

# Repetitive Transcranial Magnetic Stimulation on the Affected Hemisphere Enhances Hand Functional Recovery in Subacute Adult Stroke Patients: A Randomized Trial

*Yawen Yang[1†], Huijuan Pan[2†], Wenxiu Pan[1], Yang Liu[1], Xiaohui Song[1], Chuanxin M. Niu[1], Wuwei Feng[3], Jixian Wang[1*] and Qing Xie[1,2*]*

[1] Department of Rehabilitation Medicine, Ruijin Hospital, Shanghai Jiao Tong University School of Medicine, Shanghai, China, [2] Department of Rehabilitation Medicine, Shanghai Ruijin Rehabilitation Hospital, Shanghai, China, [3] Department of Neurology, Duke University School of Medicine, Durham, NC, United States

OPEN ACCESS

**Edited by:**
Yuanli Zhao,
Capital Medical University, China

**Reviewed by:**
Laura Mordillo-Mateos,
National Paraplegic Hospital, Spain
Henri Leinonen,
University of California, Irvine,
United States

***Correspondence:**
Jixian Wang
wangjixian6@163.com
Qing Xie
ruijin_xq@163.com

[†] These authors have contributed equally to this work and share first authorship

**Received:** 01 December 2020
**Accepted:** 09 March 2021
**Published:** 19 May 2021

**Citation:**
Yang Y, Pan H, Pan W, Liu Y, Song X, Niu CM, Feng W, Wang J and Xie Q (2021) Repetitive Transcranial Magnetic Stimulation on the Affected Hemisphere Enhances Hand Functional Recovery in Subacute Adult Stroke Patients: A Randomized Trial. Front. Aging Neurosci. 13:636184. doi: 10.3389/fnagi.2021.636184

**Objectives:** Either motor training or repetitive transcranial magnetic stimulation (rTMS) could modulate the neural plasticity after stroke. Therefore, synchronizing the two interventions may optimize the efficiency of recovery. In the present study, we aim to investigate the effect of rTMS along with hand grip training on the neurobehavioral and hand functional recovery in one cohort of subacute stroke patients.

**Methods:** Thirty-nine stroke patients were enrolled in a single-center, single-blinded, randomized clinical trial. We tested different intervention effects of rTMS and hand grip training (group A), rTMS alone (group B), and hand grip training alone (group C). For the rTMS-treated groups, patients received 10 consecutive sessions of 5-Hz stimulation over the affected hemisphere with 750 pulses. Jebsen–Taylor Hand Function Test (JTHFT), Fugl-Meyer assessment of upper extremity (FMA-UE), grip strength, modified Barthel index (mBI), and ipsilesional motor evoked potential (iMEP) latency were assessed and compared across the groups.

**Results:** We found that only rTMS along with hand grip training group all improved in JTHFT, FMA-UE, grip strength, and mBI ($p \leq 0.01$) compared with the baseline among the three groups. Furthermore, this study demonstrated that rTMS plus hand grip training had much better results in improvement of neurobehavioral outcomes compared to the rTMS alone- and hand grip training alone-treated patients ($p < 0.05$). However, no significant differences were detected in neurophysiologic outcome between intra-groups and inter-groups ($p > 0.05$).

**Conclusion:** These proof-of-concept results suggested that rTMS alone with hand grip training was a unique approach to promote hand functional recovery in stroke patients. It provided important information to design a large-scale multi-center clinical trial to further demonstrate the efficiency of the combination of central and peripheral stimulation.

**Clinical Trial Registration:** http://www.chictr.org.cn (#ChiCTR1900023443).

**Keywords: hand function, neuro-modulation, stroke, transcranial magnetic stimulation, rehabilitation**

## INTRODUCTION

Despite intensive neurorehabilitation efforts, hand- and finger-related functional abilities remain unsatisfactory following a neurological event. Studies demonstrated that 27% of stroke patients lose integral hand function due to hemiplegia (Fischer et al., 2007). It was no surprise that one of the most commonly expressed goals of individuals who sustained stroke was to engage in neurorehabilitation interventions that could enhance hand function. For stroke survivors, therefore, improving related hand functional abilities and promoting the hand function become crucial for optimal social participation and daily life (Higgins et al., 2013). Previous studies demonstrated that the establishment of neural plasticity after stroke is essential for the motor recovery (Hermann and Chopp, 2012). Furthermore, motor training is capable of promoting neuroplasticity to attenuate the motor dysfunction in stroke patients (Kleim et al., 2003; Adkins et al., 2006). For instance, hand grip training could be beneficial for the finger flexor and extensor tendon to recruit more motor units and improve the innervation and functional neuroplasticity, which played an important role in the motor recovery of stroke survivors (Murphy and Corbett, 2009). From the view of previous trials, hand functional training could regulate the neuronal excitatory input in the nerve reflex circuits and accelerate the process of reorganization of brain connectivity and neuroplasticity (Wolf et al., 2006; Buma et al., 2010).

Repetitive transcranial magnetic stimulation (rTMS) could re-balance inter-hemisphere inhibition (IHI) by either up-regulating or down-regulating cortical excitability (Nowak et al., 2009). The influence of stroke is mainly restricted to the affected hemisphere, and facilitating affected M1 directly might produce more enhancement of motor recovery than suppressing the unaffected M1 excitability (McDonnell and Stinear, 2017). Despite rTMS representing an ideal approach to promote neural plasticity (Fregni et al., 2006; Bolognini et al., 2009), whether the combination of rTMS and motor training could enhance the therapeutic effect and prolong the effective period was largely unknown. The application of motor training combined with rTMS over targeted motor cortex in healthy subjects and chronic stroke patients showed strong support both in the concept (Morris, 1999) and initial experimental evidence (Bütefisch et al., 2004; Izumi et al., 2008; Massie et al., 2013a). However, the brain tissue repair process was more complicated especially in the subacute phase. Providing corresponding proof was necessary and timely.

We aim to investigate the combined effect of high-frequency rTMS (HF-rTMS) and hand grip training on the impaired hand functional recovery in stroke survivors. We hypothesized that HF-rTMS, along with hand grip training, induces significant hand functional recovery in subacute stroke patients as compared to the controls, which was related to the establishment of functional neuroplasticity.

## MATERIALS AND METHODS

### General Information

The study protocol was approved by the Institutional Ethics Review Board, Shanghai Ruijin Rehabilitation Hospital, Shanghai, China. The clinical trial was registered in the Chinese Clinical Trial Registry (ChiCTR) with the registration number ChiCTR1900023443. All enrolled patients signed the informed consent prior to the enrollment to this study.

Thirty-nine hemiparetic stroke patients were enrolled at Shanghai Ruijin Rehabilitation Hospital from March 2019 to December 2019. The criteria of enrollment were as follows: (1) confirmed clinical stroke diagnosis, which was based on the Fourth National Conference on Cerebrovascular Diseases in 1995; (2) the first ischemic or hemorrhagic stroke confirmed by CT or MRI scans; (3) 1 to 6 months from stroke onset; (4) age from 40 to 75 years old; (5) Brunnstrom of hemiplegic upper limb and hand staging from 4 to 5; (6) Mini Mental State Examination (MMSE) $>$ 20/30; and (7) informed consent to the study and signed the consent of rTMS. The exclusion criteria were as follows: (1) uncontrolled hypertension; (2) history of seizure or using epileptic drugs either before or after stroke; (3) heart, lung, liver, kidney, or other essential organ functional decline or failure; (4) aphasia, ipsilateral neglect, hemianopia, or affective disorder that affects participant's ability to comply with study procedure; and (5) known risk factors for TMS such as having a pacemaker, intracranially implanted metal, skull defects, etc.

This study was a randomized, well-designed and controlled, prospective clinical trial conducted at a single center, which included four phases: (1) baseline evaluation, (2) randomization, (3) intervention, and (4) post-intervention evaluation. Thirty-nine stroke patients were randomly assigned by a number generated from a computer randomization table. All of the participants who met the criteria were assigned to three groups (groups A, B, and C) on the basis of the random numbers. Thirty-nine stroke patients with mild motor dysfunction recruited from inpatients and outpatients were randomized into rTMS with hand grip training (group A), rTMS alone (group B), and hand grip training alone (group C). The clinical demographic characteristics of participants are listed in **Table 1**.

**TABLE 1 |** Demographic and clinical characteristics.

| | Group A | Group B | Group C | *p* |
|---|---|---|---|---|
| | *n* = 12 | *n* = 14 | *n* = 13 | |
| Gender—m/f | 10/2 | 10/4 | 8/5 | 0.481[a] |
| Age (years) | 64±8 | 61±10 | 64±8 | 0.724[b] |
| Stroke Onset (days) | 64±23 | 79±43 | 75±49 | 0.820[b] |
| Stroke—i/h | 10/2 | 11/3 | 10/3 | 0.919[a] |
| Lesion location | | | | 0.176[a] |
| Cortex | 0 | 0 | 2 | |
| Subcortex | 9 | 13 | 10 | |
| Both | 3 | 1 | 1 | |
| FMA-UE | 47±6 | 47±8 | 47±7 | 0.990[c] |

*Group A, high-frequency rTMS during hand grip training; Group B, high-frequency rTMS alone; Group C, hand grip training alone; rTMS, repetitive transcranial magnetic stimulation.*
*m, male; f, female; i, ischemic; h, hemorrhagic; FMA-UE, Fugl–Meyer assessment of upper extremity; rTMS, repetitive transcranial magnetic stimulation.*
*Data are mean ± SD. p[a], chi-squared test; p[b], nonparametric Kruskal–Wallis H test; p,: one-way ANOVA.*

## Intervention

Intervention lasted 10 days with two interventions: (1) 5 min of real/sham 5-Hz rTMS. Each session consisted of 5-Hz rTMS for 1 s, which was both preceded and followed by a resting period of 1 s (total time = 150 s); and (2) 5 min of hand grip training. The hand grip training is composed of a repeated 1-Hz rhythmic voluntary grip by holding a ball. Apart from these, all of the participants received the conventional rehabilitation, which involved physical therapy and occupational therapy for 120 min daily for 10 sessions (5 days/week for 2 weeks). The interventions were required to be steadily implemented after conventional rehabilitation. It was worth mentioning that the practice of standardized conventional rehabilitation was requested to avoid involving evaluation projects.

During each intervention, patients seated in a comfortable and adjustable chair with headrest and armrests and took a comfortable supine position, maintaining the head and neck without displacement. Patients were instructed not to move their heads during the treatment period. The upper limb of the unaffected side was naturally placed on the armrest of the seat, and the upper limb of the affected side was placed on the side of the body.

A TMS device code with CCY-IV (Yi Ruide Company, Wuhan, China) with a 90-mm figure-of-eight coil was utilized for rTMS. rTMS intervention and evaluation were conducted in a quiet room and implemented by a trained research staff member. Motor evoked potential (MEP) signals were recorded by an electromyography (EMG) instrument that was connected to the stimulator. Ag-AgCl surface electrodes were firstly placed over the abductor pollicis brevis (APB) muscle of the unaffected hand. rTMS was applied over M1 of the unaffected hemisphere according to electroencephalogram (EEG) 10/20, where the MEP was elicited. The resting motor threshold (RMT) of APB of the unaffected upper extremity was determined by decreasing or increasing the intensity from 50% in a stepwise manner. Plus, the RMT was defined as the minimal stimulus intensity that produced a MEP response of at least 50 μV amplitude with the APB muscle at rest in at least 5 of 10 subsequent stimulations (Rossini et al., 2015). We selected the optimal stimulation site ("hot spot") in the unaffected hemisphere where the largest MEP could be consistently evoked, with the APB muscle at rest. Following that, the electrodes were placed on APB muscle of the affected hand when detecting the MEP signal of the injured hemisphere. If no MEP could be detected when stimulating over the affected M1, the optimal stimulation site was defined as the symmetric location to the "hot spot" of the unaffected hemisphere according to EEG 10/20. The MEP latency and amplitude of the targeted muscle were measured as the period (ms) between stimulus onset and the start of the largest MEP and their peak-to-peak (mV). The parameters of stimulation were 5 Hz, 100% RMT, and 750 pulses, for a total of 10 sessions (5 days/week for 2 weeks). The sham stimulation was conducted with the coil placed rotated 90°away from the scalp resulting in no current generated in the brain.

## Evaluation

Measurements of Jebsen–Taylor Hand Function Test (JTHFT), Fugl-Meyer assessment of upper extremity (FMA-UE), grip strength, modified Barthel Index (mBI), and ipsilesional motor evoked potential (iMEP) latency were assessed at baseline and post-intervention. Primary outcome was administered by a skilled clinician to evaluate the total time of accomplishing the tasks of JTHFT. Secondary outcomes included arm and hand function, force, daily living ability, and cortical excitability that were recorded by the same evaluator.

### Jebsen–Taylor Hand Function Test

The JTHFT assesses hand dexterity and consists of seven different subtasks: (1) writing a sentence, (2) turning cards, (3) moving small common objects, (4) simulating feeding, (5) stacking checkers, (6) picking up large light cans, and (7) moving heavy cans (Jebsen et al., 1969). The participants performed each task with the affected limbs and the duration of each task from onset (lifting hand from table) to the completion using a stopwatch to record in seconds (the maximal duration is 120 s per task) and summated as the total score (Radder et al., 2019). The result of JTHFT could explain three factors in relation to basic fine motor skills: motor coordination, speed of movement, and grip force scaling. Motor coordination includes tasks 1, 4, and 5. The speed of movement consists of tasks 2, 3, and 6. Task 7 reflects grip force scaling (Allgower and Hermsdorfer, 2017).

### Fugl-Meyer Assessment of Upper Extremity

The FMA-UE included 33 items, and the score range was 0–66. Among them, the hand function part accounted for 24 points. Each item was recorded in an ordinal scale (0 represents severe impairment and 2 represents no impairment) (Gladstone et al., 2002).

### Grip Strength

Grip strength was measured by a hand dynamometer (Mathiowetz et al., 1985). The subjects were requested to squeeze the handgrip of the dynamometer maximally for 5 s.

Each participant had three attempts, and the interval between the attempts was at least 60 s rest. The highest grip strength was recorded for analysis in kilograms.

### Modified Barthel Index

The mBI was recorded, which included personal hygiene, self-bathing, feeding, using the toilet, stair climbing, getting dressed, bowel control, bladder control, chair/bed transfer, and ambulation (Shah et al., 1989). The total score is 100 points.

### iMEP Latency

The MEP latency reflected the conduction time for neural impulses from the cortex to peripheral muscles and suggested cortical excitability (Bestmann and Krakauer, 2015). The target peripheral muscle in this study was APB. The MEP latency of the targeted muscle was measured as the period (ms) between stimulus onset and the start of the largest MEP. We selected five MEPs per subject with stable waveforms and calculated the mean of the iMEP latency as the measurement of cortical excitability.

## Statistical Analysis

According to the previous HF-rTMS studies, they suggested the sample size of $n = 8$ for each group to be adequate (Gladstone et al., 2002; Guo et al., 2016). Based on our research sample, we calculated the power of test statistic and the value was 0.84 ($\beta = 0.16$). Statistical analysis was performed in SPSS version 23.0. Shapiro-Wilk test was used to evaluate whether the assessment scores were normally distributed. Chi-squared test was used for categorical variables while one-way ANOVA or the nonparametric Kruskal–Wallis *H* test was utilized for continuous variables to compare among the three groups. A paired *t* test or Wilcoxon rank-sum test was performed to compare the values between baseline and post-intervention within each group. The change of FMA-UE and grip strength were analyzed by one-way ANOVA, while JTHFT, mBI, and iMEP latency changes were compared by nonparametric Kruskal–Wallis H test to determine the between-group differences. Data were presented as means ± standard deviation. $p < 0.05$ was considered statistically significant.

# RESULTS

Forty-four patients were assigned randomly to group A, B, or C. Five patients dropped out of the trial due to personal problems. Finally, thirty-nine patients completed the interventions without incident, severe side effects, or discomfort, indicating that the procedure was well tolerated (**Figure 1**). No significant differences in clinic–demographic characteristics and FMA-UE score were presented among the groups (**Table 1**).

## Behavioral Measures

### Jebsen–Taylor Hand Function Test

The change of JTHFT total score between baseline and post-intervention of the three groups (all $p \leq 0.01$) were statistically significant (**Table 2**). Group A and group B also showed significant differences in JTHFT without writing, motor coordination, speed of movement, and grip force scaling ($p < 0.05$). Unfortunately, group C only showed significant difference in JTHFT without writing and motor coordination ($p < 0.05$), which, as mentioned above, indicated that both rTMS only and rTMS with hand grip training were effective in improving hand function in stroke patients. In addition, compared to group C, group A showed better enhancement in the JTHFT score ($p < 0.05$) (**Table 3** and **Figures 2A,B**), suggesting that HF-rTMS combined with hand grip training was significantly greater than hand grip training only in hand function recovery among the stroke survivors.

### Fugl-Meyer Assessment of Upper Extremity

Evaluation of FMA-UE and FMA-UE (hand) between baseline and post-intervention among the groups was significantly different (**Table 2**). The data showed that FMA-UE scores were greatly improved in all groups ($p \leq 0.01$). Additionally, compared to group B ($p < 0.05$) and group C ($p < 0.01$), group A showed better potential in enhancing the score of FMA-UE and FMA-UE (hand) (**Table 3** and **Figure 2C**), further suggesting that HF-rTMS with hand grip training was particularly effective in promoting hand and upper limb motor function in stroke patients with mild impairment.

### Grip Strength

Significant improvement of grip strength was only found in group A after intervention ($p \leq 0.001$), which indicated that HF-rTMS with hand grip training was capable of increasing power-grip force in stroke patients (**Table 2**). However, there were no significant differences found between groups in grip strength improvements ($p > 0.05$) (**Table 3** and **Figure 2D**).

### Modified Barthel Index

In the three groups, assessment of mBI revealed a significant increase at post- relative to pre-intervention ($p < 0.05$) in **Table 2**. However, no significant difference was detected between groups ($p > 0.05$) (**Table 3** and **Figure 2E**).

## Neurophysiological Measures

### iMEP Latency

The number of iMEP latency detected in these three groups is displayed in the **Supplementary Material 1**. Both group A and group C increased one patient in the detected number of iMEP. Notably, the iMEP latency shortened in all groups with no significant difference ($p > 0.05$) (**Supplementary Material 2**). In addition, there was similarly no statistical difference presented between groups ($p > 0.05$) (**Figure 2F** and **Supplementary Table 3**).

# DISCUSSION

In this trial, we conducted a randomized and sham-controlled clinical research to detect the differential effects of HF-rTMS with hand grip training, HF-rTMS alone over the affected hemisphere, and hand grip training alone on the recovery of hand function in adult stroke patients suffering from mild impairment. From

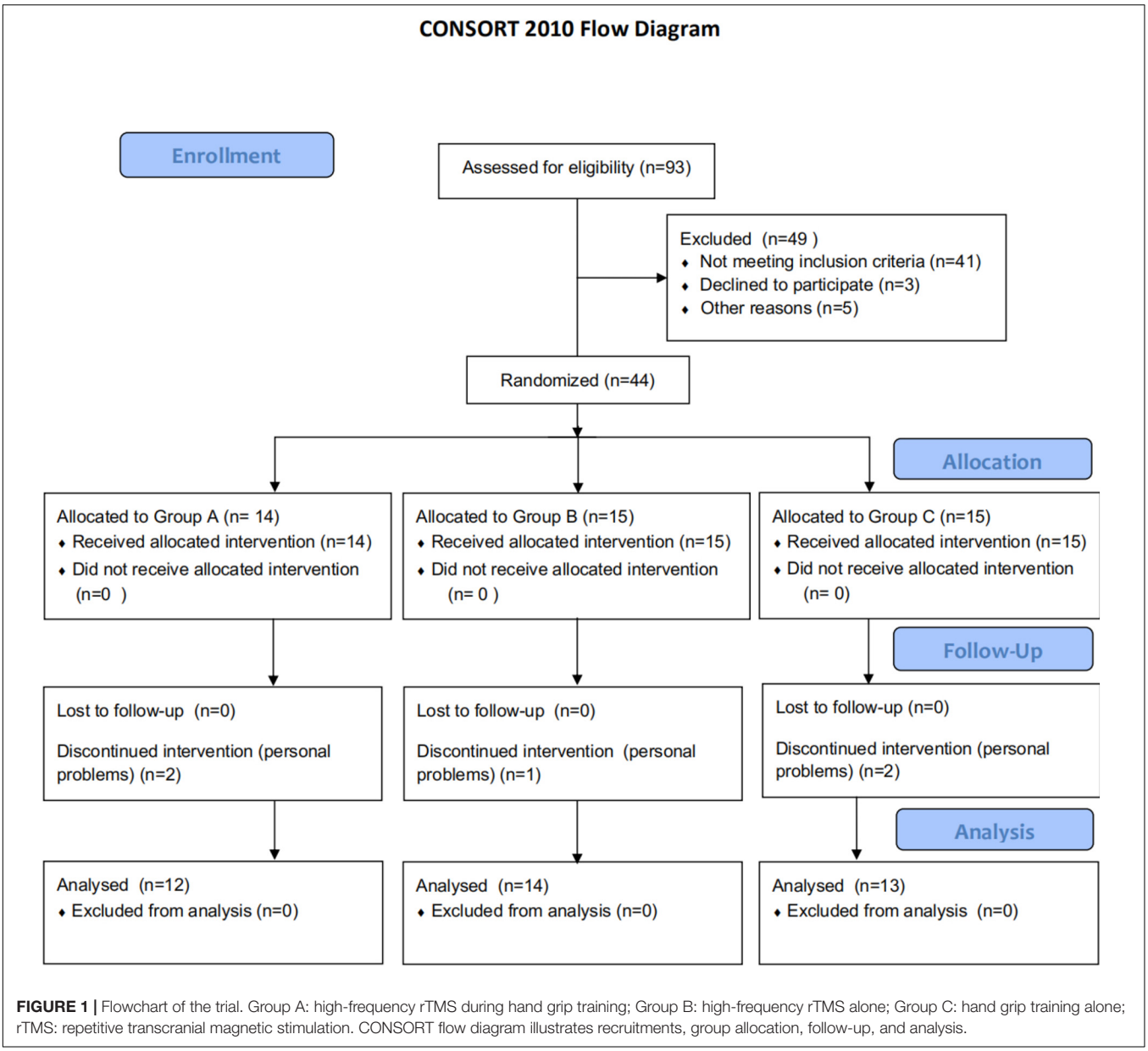


**FIGURE 1 |** Flowchart of the trial. Group A: high-frequency rTMS during hand grip training; Group B: high-frequency rTMS alone; Group C: hand grip training alone; rTMS: repetitive transcranial magnetic stimulation. CONSORT flow diagram illustrates recruitments, group allocation, follow-up, and analysis.

a clinical perspective, we found that all the three methods were beneficial to improve hand function and daily living ability in subacute adult stroke patients. Besides, we also detected that HF-rTMS with hand grip training method was superior to HF-rTMS alone and hand grip training alone. The results suggested that both central and peripheral stimulation were capable of enhancing hand functional recovery. Furthermore, our study provides evidence that the combination of central and peripheral stimulation could be the optimal approach for post-stroke rehabilitation and could increase the efficacy of rTMS.

Over the past decade, peripheral stimulation such as motor training was found favorable to promote injured cortical repair and remodeling *via* stimulating angiogenesis, neurogenesis, synaptogenesis, and dendritic plasticity (Zhang and Chopp, 2009). In recent years, numerous researches have been conducted to develop methods of improving the neurorehabilitation efficacy in stroke patients *via* non-invasive brain stimulation (Hummel and Cohen, 2006). rTMS, based on the principle of electromagnetic induction, induced the current generated by the coil placed over the surface of the skull to activate neurons in the cortical and subcortical regions, yielding neuronal depolarization (Kobayashi and Pascual-Leone, 2003). A single TMS stimulus could act on inhibitory or excitatory axons to depolarize them and deliver them backward. TMS induced changes in cell excitability and permeability (Ridding and Rothwell, 2007), which could influence cortical plasticity (Muller-Dahlhaus and Ziemann, 2015). Either rTMS or motor training could modulate neural plasticity and played a role in remodeling brain networks. In consequence, the hypothesis that the bond of rTMS and motor training might maximize their respective

**TABLE 2 |** Behavioral outcome scores at baseline and post-intervention (mean± SD).

| | Group A | | Group B | | Group C | |
|---|---|---|---|---|---|---|
| | **Pre** | **Post** | **Pre** | **Post** | **Pre** | **Post** |
| **JTHFT (s)** | | | | | | |
| JTHFT (total) | 399 ± 256 | 259 ± 200** | 323 ± 254 | 270 ± 235** | 373 ± 238 | 344 ± 229** |
| JTHFT (without writing) | 307 ± 235 | 183 ± 179** | 256 ± 228 | 204 ± 216*** | 301 ± 215 | 271 ± 198*** |
| Motor coordination | 190 ± 103 | 123 ± 59** | 146 ± 106 | 126 ± 89* | 170 ± 100 | 155 ± 100* |
| Speed of movement | 150 ± 111 | 103 ± 111** | 132 ± 114 | 108 ± 117** | 144 ± 109 | 133 ± 99 |
| Grip force scaling | 58 ± 47 | 33 ± 37** | 45 ± 43 | 37 ± 40* | 58 ± 45 | 56 ± 47 |
| FMA-UE | 47 ± 6 | 57 ± 5*** | 47 ± 8 | 53 ± 8*** | 47 ± 7 | 51 ± 7*** |
| FMA-UE (hand) | 16 ± 4 | 21 ± 3** | 16 ± 5 | 19 ± 4** | 15 ± 3 | 17 ± 4*** |
| Grip strength (kg) | 10 ± 5 | 1 ± 25*** | 11 ± 8 | 12 ± 28 | 11 ± 8 | 13 ± 9 |
| mBI | 89 ± 8 | 96 ± 26** | 87 ± 213 | 93 ± 21** | 78 ± 17 | 84 ± 15* |

*Group A, high-frequency rTMS during hand grip training; Group B, high-frequency rTMS alone; Group C, hand grip training alone; rTMS, repetitive transcranial magnetic stimulation.*
*JTHFT, Jebsen–Taylor Hand Function Test; FMA-UE, Fugl-Meyer assessment of upper extremity; mBI, modified Barthel index; rTMS, repetitive transcranial magnetic stimulation.*
*A paired t test or Wilcoxon rank-sum test was used to compare the values between baseline and post-intervention within each group.*
****$p \leq 0.001$ (compared to baseline). **$p \leq 0.01$ (compared to baseline). *$p < 0.05$ (compared to baseline).*

**TABLE 3 |** Behavioral changes among three groups (mean ± SD).

| | Group A | Group B | Group C | *p* | *p* (A vs B) | *p* (A vs C) | *p* (B vs C) |
|---|---|---|---|---|---|---|---|
| **ΔJTHFT(s)** | | | | | | | |
| ΔJTHFT (Total) | −140±153** | −53±75 | −28±23 | $0.006^b$ | $0.056^b$ | $0.006^b$ | $1.000^b$ |
| ΔJTHFT (without writing) | −124±140* | −52±65 | −29±29 | $0.013^b$ | $0.113^b$ | $0.012^b$ | $1.000^b$ |
| ΔMotor coordination | −55±49* | −35±71 | −15±20 | $0.029^b$ | $0.085^b$ | $0.041^b$ | $1.000^b$ |
| **Δ**Speed of movement | −47±62* | −24±29 | −11±22 | $0.035^b$ | $0.852^b$ | $0.031^b$ | $0.348^b$ |
| **Δ**Grip force scaling | −25±36* | −8±12 | −2±6 | $0.035^b$ | $0.469^b$ | $0.029^b$ | $0.647^b$ |
| ΔFMA-UE | 10±4**# | 6±4 | 4±2 | $0.002^c$ | $0.035^c$ | $0.001^c$ | $0.095^c$ |
| ΔFMA-UE (hand) | 5±3** | 3±2 | 2±2 | $0.021^c$ | $0.062^c$ | $0.006^c$ | $0.302^c$ |
| ΔGrip strength (kg) | 2±1 | 1±2 | 2±3 | $0.640^c$ | $0.406^c$ | $0.946^c$ | $0.436^c$ |
| ΔmBI | 7±4 | 6±8 | 6±8 | $0.211^b$ | $>0.05^b$ | $>0.05^b$ | $>0.05^b$ |

*Group A, high-frequency rTMS during hand grip training; Group B, high-frequency rTMS alone; Group C, hand grip training alone; rTMS, repetitive transcranial magnetic stimulation.*
*A vs B, Group A compared with Group B; A vs C, Group A compared with Group C; B vs C, Group B compared with Group C; JTHFT, Jebsen–Taylor Hand Function Test; FMA-UE, Fugl-Meyer assessment of upper extremity; mBI, modified Barthel index; rTMS, repetitive transcranial magnetic stimulation.*
*$p^b$: nonparametric Kruskal–Wallis H test; $p^c$: one-way ANOVA.*
***$p < 0.01$ (compared with Group C); *$p < 0.05$ (compared with Group C); #$p < 0.05$ (compared with Group B).*

therapeutic effect had been proposed. Previous studies aiming to investigate the effect of combined rTMS and motor training were mainly time-locked, which referred to rTMS generally preceded or followed by motor training (Higgins et al., 2013; Kakuda et al., 2016). In recent several years, TMS was implemented during the procedure of motor training to further improve the efficacy of stroke motor function rehabilitation. These studies showed that coupling rTMS with motor training could have a synergic impact on motor recovery after stroke (Buetefisch et al., 2011; Massie et al., 2013a). The synergic effect could be explained by the rTMS-induced modulation of neural plasticity and the consolidation with motor training-induced (Buetefisch et al., 2011). Previous researches demonstrated that TMS plus motor training significantly improved the longevity of motor memory (Bütefisch et al., 2004) and hand function after stroke (Izumi et al., 2008). Another study revealed that functional rTMS (EMG-triggered rTMS) promoted greater excitatory changes and selectively modulated agonistic muscle activity (Massie et al., 2013a). Furthermore, consecutive multi-session functional rTMS could equally enhance cortical excitability and improve stabilities of motor skills (Massie et al., 2013b). However, the participants mainly included healthy subjects and chronic stroke patients, and the therapeutic frequency and intensity of rTMS were variable. Considering that the effect of rTMS on the cortical excitability is subject to intra-individual and inter-individual variability (Bestmann et al., 2010; Cohen et al., 2010), and that the optimal rTMS protocol is undetermined, developing more efficient clinical protocol that fits stroke patients with mild motor dysfunction is desirable and necessary. Our results provided a highly efficient approach to subacute stroke patients with mild dysfunction to promote hand function and useful experimental data for further larger-scale clinical trial.

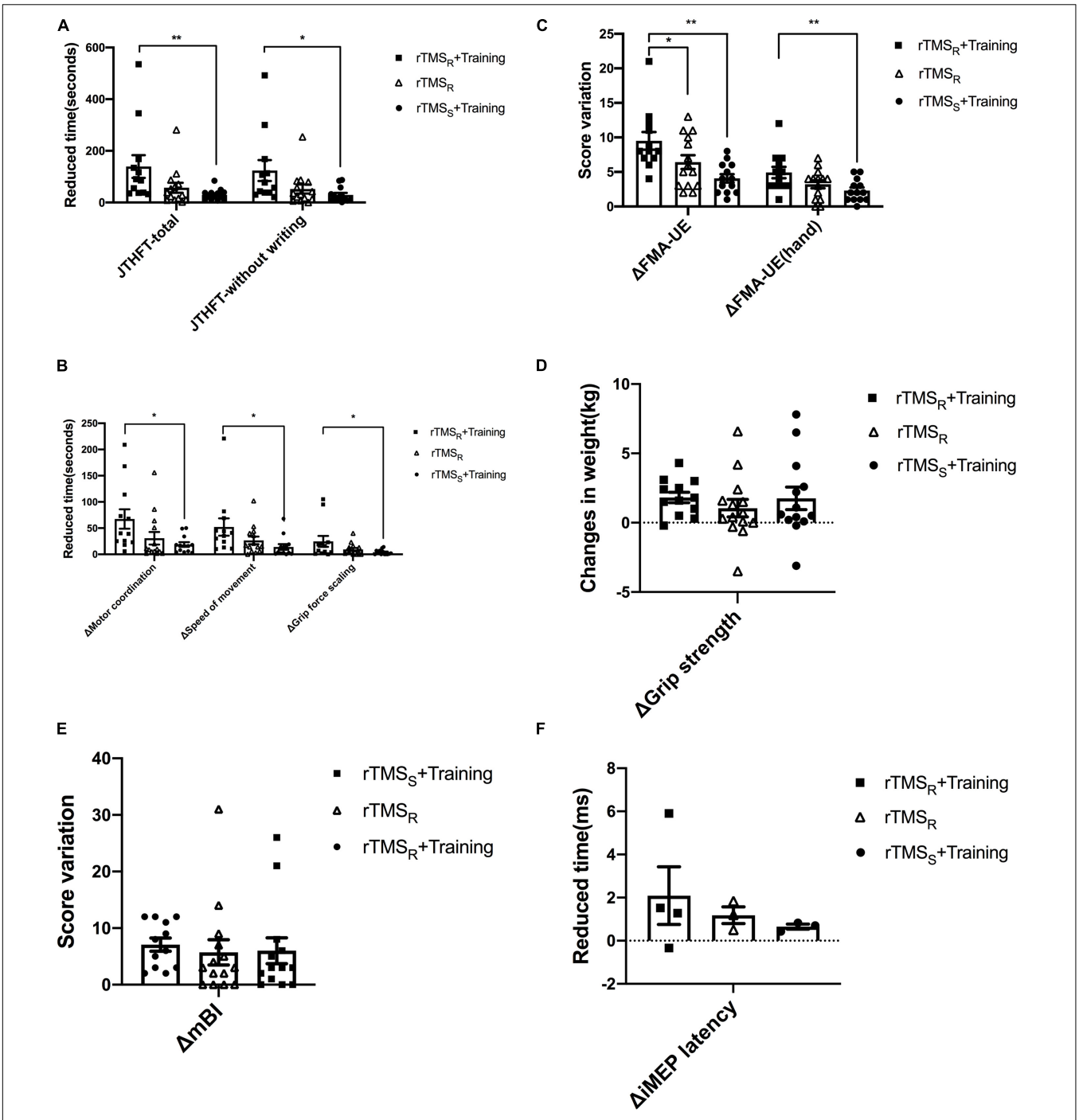


**FIGURE 2 |** Behavioral and neurophysiological changes among the three groups (mean±SEM). rTMS$_R$+Training: rTMS and hand grip training (Group A); rTMS$_R$: rTMS alone (Group B); rTMS$_S$+Training: hand grip training alone (Group C). rTMS: repetitive transcranial magnetic stimulation. One-way ANOVA or nonparametric Kruskal–Wallis *H* test was used to compare the behavioral and neurophysiological changes among the three groups, and multiple comparisons with the whole pairwise comparation. $^*p < 0.05$, $^{**}p < 0.01$.

Neuroplasticity presumably occurred in the connection between motor cortex neurons, which was naturally triggered during the period of muscle contraction, and simultaneously motivated over the motor cortex by rTMS (Edwardson et al., 2013). Considering our results from this standpoint, the rTMS plus hand grip training group was supposed to gain stronger excitability in the affected hemisphere. Unfortunately, the changes in the cortical excitability after HF-rTMS during hand grip training were not found. The following reasons may account for this result: the factors contributing to functional

impairment included loss of white matter projection, diaschisis, and interhemispheric imbalance (Auriat et al., 2015). The detection method of recording iMEP latency was not able to find structural changes; other methods such as functional magnetic resonance imaging should be evaluated in future studies. According to the IHI model, which is based on interhemispheric imbalance, suppressing the unaffected hemisphere excitability or facilitating the affected hemisphere excitability could promote motor function recovery in stroke patients (Nowak et al., 2009). However, a novel model for neurorehabilitation named bimodal balance-recovery model suggested that the IHI model was oversimplified or even incorrect. The new model links interhemispheric balancing and functional recovery to the structural reserve spared by the lesion; it could be utilized to tailor treatment for individual patients (di Pino et al., 2014). Similarly, the small sample size could be unfavorable and has limited our study.

This trial was conducted safely with no seizures and other specific discomfort, and no incident happened. Thus, our results also provided additional evidence of the safety of implementing HF-rTMS during hand grip training and HF-rTMS alone in the clinical setting. Meanwhile, we concluded that HF-rTMS was an effective way to promote hand function in subacute adult stroke patients with mild impairment. In recent years, HF-rTMS has been reported to have a more effective impact when compared to low-frequency rTMS (LF-rTMS) in animal and human studies (Sasaki et al., 2013; Caglayan et al., 2019). An animal study detected that intervening 20-Hz HF-rTMS on acute and subacute ischemic injury models in mice induced excellent outcomes compared to the 1-Hz LF-rTMS. They simultaneously demonstrated that HF-rTMS decreased apoptosis and infarct volume; activated neurogenesis, neuronal survival, and neuronal plasticity; and increased regional cerebral blood flow. It has a strong support for the rationale of using HF-rTMS in post-stroke patients aiming at improving motor functional recovery (Caglayan et al., 2019). Besides, a clinical study targeted at stroke patients detected that 10-Hz HF-rTMS applied over the affected hemisphere induced significant improvement on motor functional recovery compared to the 1-Hz LF-rTMS (Sasaki et al., 2013). A meta-analysis revealed that facilitating affected M1 excitability could be directly beneficial compared to the suppressing unaffected M1 excitability in improving post-stroke recovery (McDonnell and Stinear, 2017). Future studies can focus on investigating the differential effect of LF-rTMS or HF-TMS plus hand grip training on hand functional recovery.

Though there was no significant difference detected between rTMS alone and hand grip training alone groups in FMA-UE score, the rTMS alone group showed enhancement in FMA-UE and the change had a minimal clinically important difference (Page et al., 2012). The short intervention period (10 sessions lasting 2 weeks) could explain the reason of no significant difference in grip strength among the groups (Stock et al., 2019). However, focusing on post-stroke patients with mild motor impairments, having no significant difference among these groups in mBI might be due to the sensitivity of the measurement.

The limitations of our study are as follows: (1) this study was a single-center trial and lacked sufficient subjects to administer subgroup analysis according to the lesion, stroke volume, the course of disease, and the severity of stroke; (2) we collected data to evaluate the short-term benefit from the proposed interventions, but we did not collect long-term data to assess the sustained benefits; and (3) the proportion of patients with positive MEP was lower than prior reported studies, and it limited our understanding of the mechanism of motor improvement by rTMS. Further larger-scale clinical trials are necessary to confirm our data and to promote this novel rehabilitation therapy.

## CONCLUSION

Our study demonstrated the short-term benefit of combined 10 sessions of 5-Hz rTMS over the affected hemisphere with concurrent hand grip training protocol. It provided important preliminary data to plan a large-sample, multi-center study to systematically evaluate the benefit of rTMS in a stroke population.

## DATA AVAILABILITY STATEMENT

The original contributions presented in the study are included in the article/**Supplementary Material**, further inquiries can be directed to the corresponding author/s.

## ETHICS STATEMENT

The studies involving human participants were reviewed and approved by Institutional Ethics Review Board, Shanghai Ruijin Rehabilitation Hospital, Shanghai, China. The patients/participants provided their written informed consent to participate in this study.

## AUTHOR CONTRIBUTIONS

JW and QX: conception and design of the study and data confirmation. YY: data collection, analysis of data, statistical analysis, and drafting the manuscript. HP: data segmentation and analysis of data. WP and YL: evaluating the patients and statistical analysis. XS and CN: acquisition of data. WF: analysis and interpretation of data. All authors contributed to the study and article and approved the submitted version. All authors contributed to the article and approved the submitted version.

## FUNDING

This work was supported by Shanghai Municipal Key Clinical Specialty (Grant No. SHSLCZDZK02701, QX), Shanghai Jiao Tong University School of Medicine—Institute of Neuroscience, Chinese Academy of Sciences, Leading Startup Project of Brain Diseases Clinical Research Center (Grant No. 2017NKX002, QX), Shanghai Science and Technology Commission (Grant No. 18511108203, QX), Shanghai Municipal Health Commission (Grant No. 2019SY004, QX), and the National Natural Science Foundation of China (Grant No. 81802232, JW).

## ACKNOWLEDGMENTS

We thank our colleagues at the Department of Rehabilitation Medicine of Ruijin Hospital and Shanghai Ruijin Rehabilitation Hospital.

## SUPPLEMENTARY MATERIAL

The Supplementary Material for this article can be found online at: https://www.frontiersin.org/articles/10.3389/fnagi.2021.636184/full#supplementary-material

## REFERENCES

Adkins, D. L., Boychuk, J., Remple, M. S., and Kleim, J. A. (2006). Motor training induces experience-specific patterns of plasticity across motor cortex and spinal cord. *J. Appl. Physiol.* 101, 1776–1782. doi: 10.1152/japplphysiol.00515.2006

Allgower, K., and Hermsdorfer, J. (2017). Fine motor skills predict performance in the Jebsen Taylor Hand Function Test after stroke. *Clin. Neurophysiol.* 128, 1858–1871. doi: 10.1016/j.clinph.2017.07.408

Auriat, A. M., Neva, J. L., Peters, S., Ferris, J. K., and Boyd, L. A. (2015). A review of transcranial magnetic stimulation and multimodal neuroimaging to characterize post-stroke neuroplasticity. *Front. Neurol.* 6:226. doi: 10.3389/fneur.2015.00226

Bestmann, S., and Krakauer, J. W. (2015). The uses and interpretations of the motor-evoked potential for understanding behaviour. *Exp. Brain Res.* 233, 679–689. doi: 10.1007/s00221-014-4183-7

Bestmann, S., Swayne, O., Blankenburg, F., Ruff, C. C., Teo, J., Weiskopf, N., et al. (2010). The role of contralesional dorsal premotor cortex after stroke as studied with concurrent TMS-fMRI. *J. Neurosci.* 30, 11926–11937. doi: 10.1523/JNEUROSCI.5642-09.2010

Bolognini, N., Pascual-Leone, A., and Fregni, F. (2009). Using non-invasive brain stimulation to augment motor training-induced plasticity. *J. Neuroeng. Rehabil.* 6:8. doi: 10.1186/1743-0003-6-8

Buetefisch, C., Heger, R., Schicks, W., Seitz, R., and Netz, J. (2011). Hebbian-type stimulation during robot-assisted training in patients with stroke. *Neurorehabil. Neural Repair* 25, 645–655. doi: 10.1177/1545968311402507

Buma, F. E., Lindeman, E., Ramsey, N. F., and Kwakkel, G. (2010). Review: functional neuroimaging studies of early upper limb recovery after stroke: a systematic review of the literature. *Neurorehabil. Neural Repair* 24, 589–608. doi: 10.1177/1545968310364058

Bütefisch, C. M., Khurana, V., Kopylev, L., and Cohen, L. G. (2004). Enhancing encoding of a motor memory in the primary motor cortex by cortical stimulation. *J. Neurophysiol.* 91, 2110–2116. doi: 10.1152/jn.01038.2003

Caglayan, A. B., Beker, M. C., Caglayan, B., Yalcin, E., Caglayan, A., Yulug, B., et al. (2019). Acute and post-acute neuromodulation induces stroke recovery by promoting survival signaling, neurogenesis, and pyramidal tract plasticity. *Front. Cell. Neurosci.* 13:144. doi: 10.3389/fncel.2019.00144

Cohen, D. A., Freitas, C., Tormos, J. M., Oberman, L., Eldaief, M., and Pascual-Leone, A. (2010). Enhancing plasticity through repeated rTMS sessions: the benefits of a night of sleep. *Clin. Neurophysiol.* 121, 2159–2164. doi: 10.1016/j.clinph.2010.05.019

di Pino, G., Pellegrino, G., Assenza, G., Capone, F., Ferreri, F., Formica, D., et al. (2014). Modulation of brain plasticity in stroke: a novel model for neurorehabilitation. *Nat. Rev. Neurol.* 10, 597–608. doi: 10.1038/nrneurol.2014.162

Edwardson, M. A., Lucas, T. H., Carey, J. R., and Fetz, E. E. (2013). New modalities of brain stimulation for stroke rehabilitation. *Exp. Brain Res.* 224, 335–358. doi: 10.1007/s00221-012-3315-1

Fischer, H. C., Stubblefield, K., Kline, T., Luo, X., Kenyon, R. V., and Kamper, D. G. (2007). Hand rehabilitation following stroke: a pilot study of assisted finger extension training in a virtual environment. *Top. Stroke Rehabil.* 14, 1–12. doi: 10.1310/tsr1401-1

Fregni, F., Boggio, P. S., Valle, A. C., Rocha, R. R., Duarte, J., Ferreira, M. J. L., et al. (2006). A sham-controlled trial of a 5-day course of repetitive transcranial magnetic stimulation of the unaffected hemisphere in stroke patients. *Stroke* 37, 2115–2122. doi: 10.1161/01.STR.0000231390.58967.6b

Gladstone, D. J., Danells, C. J., and Black, S. E. (2002). The fugl-meyer assessment of motor recovery after stroke: a critical review of its measurement properties. *Neurorehabil. Neural Repair* 16, 232–240. doi: 10.1177/154596802401105171

Guo, Z., Jin, Y., Peng, H., Xing, G., Liao, X., Wang, Y., et al. (2016). Ipsilesional high frequency repetitive transcranial magnetic stimulation add-on therapy improved diffusion parameters of stroke patients with motor dysfunction: a preliminary DTI study. *Neural Plast.* 2016:6238575. doi: 10.1155/2016/6238575

Hermann, D. M., and Chopp, M. (2012). Promoting brain remodelling and plasticity for stroke recovery: therapeutic promise and potential pitfalls of clinical translation. *Lancet Neurol.* 11, 369–380. doi: 10.1016/S1474-4422(12)70039-X

Higgins, J., Koski, L., and Xie, H. (2013). Combining rTMS and task-oriented training in the rehabilitation of the arm after stroke: a pilot randomized controlled trial. *Stroke Res. Treat.* 2013:539146. doi: 10.1155/2013/539146

Hummel, F. C., and Cohen, L. G. (2006). Non-invasive brain stimulation: a new strategy to improve neurorehabilitation after stroke? *Lancet Neurol.* 5, 708–712. doi: 10.1016/S1474-4422(06)70525-7

Izumi, S.-I., Kondo, T., and Shindo, K. (2008). Transcranial magnetic stimulation synchronized with maximal movement effort of the hemiplegic hand after stroke: a double-blinded controlled pilot study. *J. Rehabil. Med.* 40, 49–54. doi: 10.2340/16501977-0133

Jebsen, R. H., Taylor, N., Trieschmann, R. B., Trotter, M. J., and Howard, L. A. (1969). An objective and standardized test of hand function. *Arch. Phys. Med. Rehabil.* 50, 311–319.

Kakuda, W., Abo, M., Sasanuma, J., Shimizu, M., Okamoto, T., Kimura, C., et al. (2016). Combination protocol of low-frequency rTMS and intensive occupational therapy for post-stroke upper limb hemiparesis: a 6-year experience of more than 1700 Japanese patients. *Transl. Stroke Res.* 7, 172–179. doi: 10.1007/s12975-016-0456-8

Kleim, J. A., Jones, T. A., and Schallert, T. (2003). Motor enrichment and the induction of plasticity before or after brain injury. *Neurochem. Res.* 28, 1757–1769. doi: 10.1023/a:1026025408742

Kobayashi, M., and Pascual-Leone, A. (2003). Transcranial magnetic stimulation in neurology. *Lancet Neurol.* 2, 145–156. doi: 10.1016/S1474-4422(03)00321-1

Massie, C. L., Tracy, B. L., and Malcolm, M. P. (2013a). Functional repetitive transcranial magnetic stimulation increases motor cortex excitability in survivors of stroke. *Clin. Neurophysiol.* 124, 371–378. doi: 10.1016/j.clinph.2012.07.026

Massie, C. L., Tracy, B. L., Paxton, R. J., and Malcolm, M. P. (2013b). Repeated sessions of functional repetitive transcranial magnetic stimulation increases motor cortex excitability and motor control in survivors of stroke. *NeuroRehabilitation* 33, 185–193. doi: 10.3233/NRE-130944

Mathiowetz, V., Kashman, N., Volland, G., Weber, K., Dowe, M., and Rogers, S. (1985). Grip and pinch strength: normative data for adults. *Arch. Phys. Med. Rehabil.* 66, 69–74.

McDonnell, M. N., and Stinear, C. M. (2017). TMS measures of motor cortex function after stroke: a meta-analysis. *Brain Stimul.* 10, 721–734. doi: 10.1016/j.brs.2017.03.008

Morris, R. G. M. (1999). D.O. Hebb: the organization of behavior, Wiley: New York; 1949. *Brain Res. Bull.* 50:437. doi: 10.1016/S0361-9230(99)00182-3

Muller-Dahlhaus, F., and Ziemann, U. (2015). Metaplasticity in human cortex. *Neuroscientist* 21, 185–202. doi: 10.1177/1073858414526645

Murphy, T. H., and Corbett, D. (2009). Plasticity during stroke recovery: from synapse to behaviour. *Nat. Rev. Neurosci.* 10, 861–872. doi: 10.1038/nrn2735

Nowak, D. A., Grefkes, C., Ameli, M., and Fink, G. R. (2009). Interhemispheric competition after stroke: brain stimulation to enhance recovery of function of the affected hand. *Neurorehabil. Neural Repair* 23, 641–656. doi: 10.1177/1545968309336661

Page, S. J., Fulk, G. D., and Boyne, P. (2012). Clinically important differences for the upper-extremity Fugl-Meyer Scale in people with minimal to moderate impairment due to chronic stroke. *Phys. Ther.* 92, 791–798. doi: 10.2522/ptj.20110009

Radder, B., Prange-Lasonder, G. B., Kottink, A. I. R., Holmberg, J., Sletta, K., van Dijk, M., et al. (2019). Home rehabilitation supported by a wearable soft-robotic device for improving hand function in older adults: a pilot randomized controlled trial. *PLoS One* 14:e0220544. doi: 10.1371/journal.pone.0220544

Ridding, M. C., and Rothwell, J. C. (2007). Is there a future for therapeutic use of transcranial magnetic stimulation? *Nat. Rev. Neurosci.* 8, 559–567. doi: 10.1038/nrn2169

Rossini, P. M., Burke, D., Chen, R., Cohen, L. G., Daskalakis, Z., Di Iorio, R., et al. (2015). Non-invasive electrical and magnetic stimulation of the brain, spinal cord, roots and peripheral nerves: basic principles and procedures for routine clinical and research application. An updated report from an I.F.C.N. Committee. *Clin. Neurophysiol.* 126, 1071–1107. doi: 10.1016/j.clinph.2015.02.001

Sasaki, N., Mizutani, S., Kakuda, W., and Abo, M. (2013). Comparison of the effects of high- and low-frequency repetitive transcranial magnetic stimulation on upper limb hemiparesis in the early phase of stroke. *J. Stroke Cerebrovasc. Dis.* 22, 413–418. doi: 10.1016/j.jstrokecerebrovasdis.2011.10.004

Shah, S., Vanclay, F., and Cooper, B. (1989). Improving the sensitivity of the Barthel Index for stroke rehabilitation. *J. Clin. Epidemiol.* 42, 703–709. doi: 10.1016/0895-4356(89)90065-6

Stock, R., Thrane, G., Askim, T., Anke, A., and Mork, P. J. (2019). Development of grip strength during the first year after stroke. *J. Rehabil. Med.* 51, 248–256. doi: 10.2340/16501977-2530

Wolf, S. L., Winstein, C. J., Miller, J. P., Taub, E., Uswatte, G., Morris, D., et al. (2006). Effect of constraint-induced movement therapy on upper extremity function 3 to 9 months after strokethe EXCITE randomized clinical trial. *JAMA* 296, 2095–2104. doi: 10.1001/jama.296.17.2095

Zhang, Z. G., and Chopp, M. (2009). Neurorestorative therapies for stroke: underlying mechanisms and translation to the clinic. *Lancet Neurol.* 8, 491–500. doi: 10.1016/S1474-4422(09)70061-4

**Conflict of Interest:** The authors declare that the research was conducted in the absence of any commercial or financial relationships that could be construed as a potential conflict of interest.

frontiers in Aging Neuroscience

ORIGINAL RESEARCH
published: 26 May 2021
doi: 10.3389/fnagi.2021.632138

# Artificial Intelligence Can Effectively Predict Early Hematoma Expansion of Intracerebral Hemorrhage Analyzing Noncontrast Computed Tomography Image

*Linyang Teng[1†], Qianwei Ren[2†], Pingye Zhang[3], Zhenzhou Wu[3], Wei Guo[1] and Tianhua Ren[4*]*

[1]Department of Emergency, Beijing Tiantan Hospital, Capital Medical University, Beijing, China, [2]Department of Functional Neurosurgery, Beijing Tiantan Hospital, Capital Medical University, Beijing, China, [3]BioMind Technology, Beijing, China, [4]Department of International Medical, Beijing Tiantan Hospital, Capital Medical University, Beijing, China

This study aims to develop and validate an artificial intelligence model based on deep learning to predict early hematoma enlargement (HE) in patients with intracerebral hemorrhage. A total of 1,899 noncontrast computed tomography (NCCT) images of cerebral hemorrhage patients were retrospectively analyzed to establish a predicting model and 1,117 to validate the model. And a total of 118 patients with intracerebral hemorrhage were selected based on inclusion and exclusion criteria so as to validate the value of the model for clinical prediction. The baseline noncontrast computed tomography images within 6 h of intracerebral hemorrhage onset and the second noncontrast computed tomography performed at 24 ± 3 h from the onset were used to evaluate the prediction of intracerebral hemorrhage growth. In validation dataset 1, the AUC was 0.778 (95% CI, 0.768–0.786), the sensitivity was 0.818 (95% CI, 0.790–0.843), and the specificity was 0.601 (95% CI, 0.565–0.632). In validation dataset 2, the AUC was 0.780 (95% CI, 0.761–0.798), the sensitivity was 0.732 (95% CI, 0.682–0.788), and the specificity was 0.709 (95% CI, 0.658–0.759). The sensitivity of intracerebral hemorrhage hematoma expansion as predicted by an artificial intelligence imaging system was 89.3%, with a specificity of 77.8%, a positive predictive value of 55.6%, a negative predictive value of 95.9%, and a Yoden index of 0.671, which were much higher than those based on the manually labeled noncontrast computed tomography signs. Compared with the existing prediction methods through computed tomographic angiography (CTA) image features and noncontrast computed tomography image features analysis, the artificial intelligence model has higher specificity and sensitivity in the prediction of early hematoma enlargement in patients with intracerebral hemorrhage.

**Keywords: predict, hematoma expansion, convolutional neural network, artificial intelligence, intracerebral hematoma**

OPEN ACCESS

***Edited by:***
*Ramesh Kandimalla, Indian Institute of Chemical Technology (CSIR), India*

***Reviewed by:***
*Wanlin Yang, Southern Medical University, China*
*Marta Rubiera, Vall d'Hebron University Hospital, Spain*

***Correspondence:**
*Tianhua Ren*
*renth1970@163.com*

*†These authors have contributed equally to this work*

***Received:*** *22 November 2020*
***Accepted:*** *06 April 2021*
***Published:*** *26 May 2021*

***Citation:***
*Teng L, Ren Q, Zhang P, Wu Z, Guo W and Ren T (2021) Artificial Intelligence Can Effectively Predict Early Hematoma Expansion of Intracerebral Hemorrhage Analyzing Noncontrast Computed Tomography Image. Front. Aging Neurosci. 13:632138. doi: 10.3389/fnagi.2021.632138*

# INTRODUCTION

Intracerebral hemorrhage refers to hemorrhage caused by the rupture of the blood vessels in the brain parenchyma, with the mortality rate as high as 40% and 54% after 1 month and 1 year of the rupture, respectively (Zia et al., 2009; Hansen et al., 2013; Poon et al., 2014). More than 40% of the patients with acute intracerebral hemorrhage developed secondary hematoma enlargement (Van Asch et al., 2010). Past studies have shown that hematoma enlargement is an independent risk factor for the poor prognosis of intracerebral hemorrhage (Davis et al., 2006; Dowlatshahi et al., 2011; Delcourt et al., 2012). However, it has also been proved that the limited hematoma expansion therapy without selection shows no significant improvement on the prognosis (mortality and disability rate). In fact, it may even increase the incidence of the related adverse events (Anderson et al., 2013; Qureshi et al., 2016). Therefore, it is extremely important to identify the risk of hematoma enlargement in time for future clinical intervention.

Noncontrast computed tomography (NCCT) plays an extremely important role in the diagnosis and treatment of hematoma enlargement of the intracerebral hemorrhage. Past studies indicate that computed tomographic angiography (CTA) spot sign is an independent risk factor for hematoma enlargement (Goldstein et al., 2007; Wada et al., 2007; Demchuk et al., 2012; Brouwers et al., 2015; Caplan, 2016). However, due to the high requirements of emergency CTA for patients and the burden on hospitals, there are significant limitations in the application of CTA for early detection. NCCT is easy to operate and is widely applied. The recent years have witnessed a surge in research on the prediction of hematoma enlargement with NCCT imaging markers, with the concepts of black hole sign, blend sign, CT hypodensities, island sign, and hematoma enlargement border proposed and validated for their clinical value in the prediction of hematoma enlargement(Lu et al., 2007; Ji et al., 2009; Boulouis et al., 2016; Li et al., 2017; Sporns et al., 2017; Yu et al., 2017). However, these markers have to be interpreted by trained doctors only because it is easy to be influenced by the readers' experience and subjective judgment, and the related sensitivity is not high.

In recent years, segmentation methods based on deep learning have attracted increasing interest owing to their abilities of self-learning and generalization from large data volumes (Hosny et al., 2018; Wang et al., 2020). The application of artificial intelligence algorithm to further the intelligent analysis and mining of medical imaging information can better extract the image features in an image to obtain accurate internal correlation. In the entire analysis process, the interference of human subjective factors gets eliminated; as a result, the outcomes are more accurate and reproducible. In this study, we attempted to develop a prediction model of hematoma enlargement risk in patients with intracerebral hemorrhage based on the NCCT images so as to rapidly screen out the high-risk population of hematoma enlargement for preparing individualized clinical treatment and guidelines.

# MATERIALS AND METHODS

## Data Preparation

In this study, the NCCT images of patients with spontaneous intracerebral hemorrhage from 84 public hospitals were collected for retrospective analysis between November 2011 and May 2018. Meanwhile, a retrospective study cohort of eligible patients with spontaneous intracerebral hemorrhage admitted to 26 public hospitals between April and October 2018 was collected. All NCCT scans were taken as a part of the routine nursing care. The patient inclusion criteria were diagnosis with spontaneous ICH and admission to the emergency department within 6 h from the symptom onset, with the availability of the baseline values and follow-up NCCT data within 48 h of the symptom onset. The patient exclusion criteria included secondary ICH, patients undergoing acute treatment with the potential to limit the ICH volume, and NCCT images of insufficient quality.

In this study, we initially included 3,016 patients, of which only approximately 20% experienced hematoma enlargement (HE). Several proportional HE cases ($n$ = 1,183, 47.1%) were purposely accumulated in the retrospective dataset for use in the development of deep-learning systems. The retrospective dataset was randomly divided into the development set ($n$ = 1,899, 75.5%) and validation dataset 1 ($n$ = 615, 24.5%). Another retrospective dataset is validation dataset 2 ($n$ = 502).

For the clinical evaluation dataset, we retrospectively selected suitable patients from the Beijing Tiantan Hospital between June 2019 and April 2020 so as to assess the clinical behavior of the model. The inclusion criteria were patients diagnosed with spontaneous ICH and admitted to the Tiantan Hospital within 6 h from symptom onset, with the baseline images available, and who received a follow-up NCCT at 24 $\pm$ 3 h from the symptom onset. The exclusion criteria were secondary intracerebral hemorrhage that could not be recognized by the artificial intelligence model, patients treated with surgery within 24 h, and insufficient NCCT image quality. A total of 118 patients were finally involved in the dataset. Due to the sensitivity of the data used in the study, the data cannot be freely shared. We provided a flowchart of the process as **Figure 1**.

This study was conducted in accordance with the institutional review boards (IRBs) of Beijing Tiantan Hospital Affiliated to Capital Medical University, which also approved this study protocol. Patient information was anonymized and de-identified before the analysis.

## Image Processing

In order to reduce potential human errors, we employed a hierarchical marking method for all scans in the database. No conflict of interest was registered among the doctors who participated in the project. Eight master's degree candidates in neurology from the Beijing Tiantan Hospital received focused training for NCCT annotation and evaluation from a team of two experts (one neuroradiologist and one neurologist) with more than a decade of experience. The location and the presence of intracerebral hemorrhage were accordingly

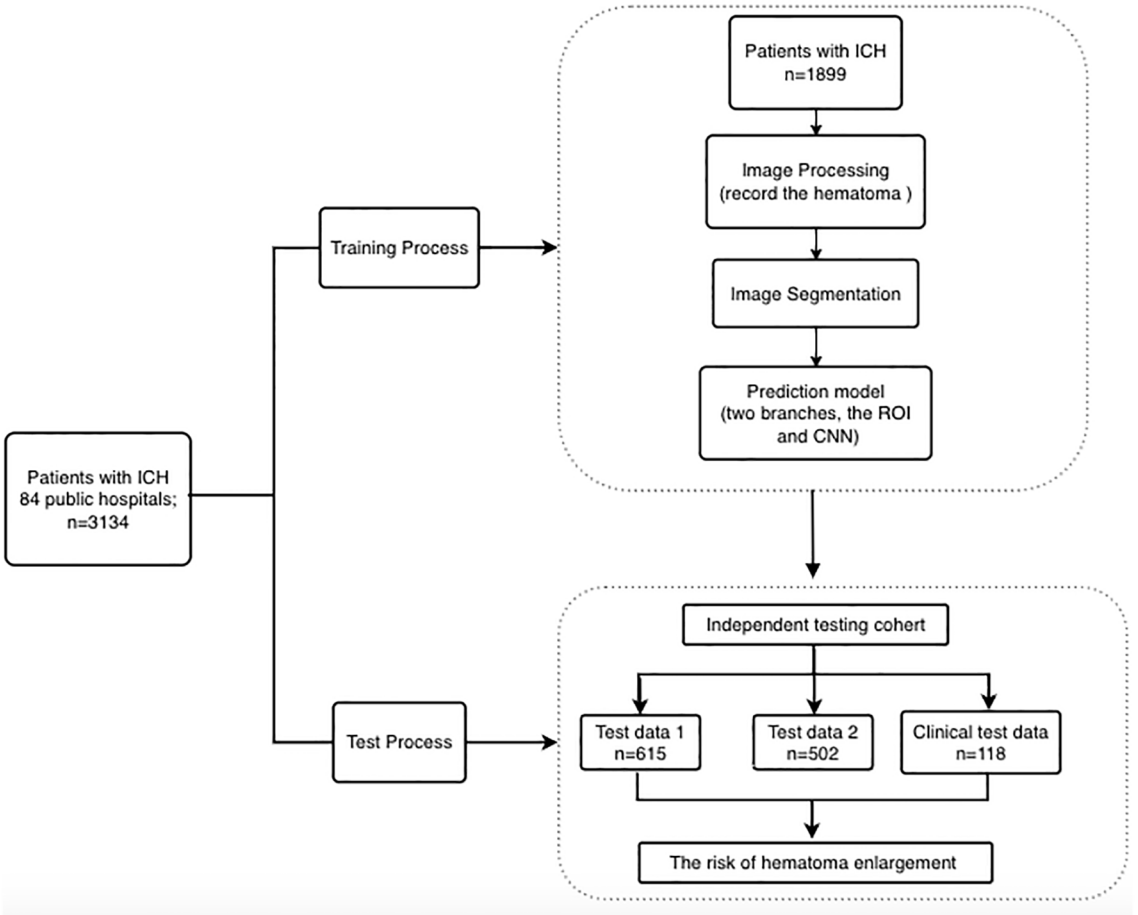


**FIGURE 1** | Flowchart of data preparation, image processing, system architecture, and evaluation.

recorded as shown in **Figure 2**. For hematoma segmentation training and ICH volume calculation, each slice of hematoma appearing on the NCCT images was first drawn manually using the 3D Slicer analysis software by a trained rater, followed by independent reviewing by a second rater. The ICH volumes of the baseline and follow-up NCCT were calculated using a planimetric method. During the manual drawing phase, both intraparenchymal and intraventricular hemorrhage accounted for the same percent of hematoma volume. HE was defined as an increase in the hematoma volume of >6 ml (Dowlatshahi et al., 2011).

## System Architecture

### Segmentation Model

The segmentation model is based on a convolutional neural network termed U-Net, albeit with some modifications. Before feeding into the network, each slice of the original NCCT image was fit to a 512 × 512 square by cropping and padding if necessary, followed by normalization by a Hounsfield unit (HU) value window 0–100. The U-Net architecture consisted of two stages, the downsampling stage and the upsampling stage. Each block of the downsampling stage was composed of two 3 × 3 convolution layers and a 2 × 2 max-pooling layer. At the upsampling stage, the feature map from the last downsampling block was upsampled by a 2 × 2 up-convolution layer, concatenated with a feature map of the corresponding downsampling block, and then through two 3 × 3 convolution layers. After the final upsampling block, a 1 × 1 convolution layer with sigmoid activation was employed to determine the class of each pixel. To better catch the feature of hematoma, we used dilated convolution on the second convolution layers of each downsampling block (**Figure 3**).

### Prediction Model

The inputs of the prediction model consisted of the original NCCT images of one patient and the segmentation results of the segmentation model that highlights the region of interest (ROI). The same inputs were propagated to the two branches of the prediction model.

The first branch generated radiomics features on the ROI. In this branch, image filters such as Laplacian of Gaussian and wavelet were applied on the images. Together with the original

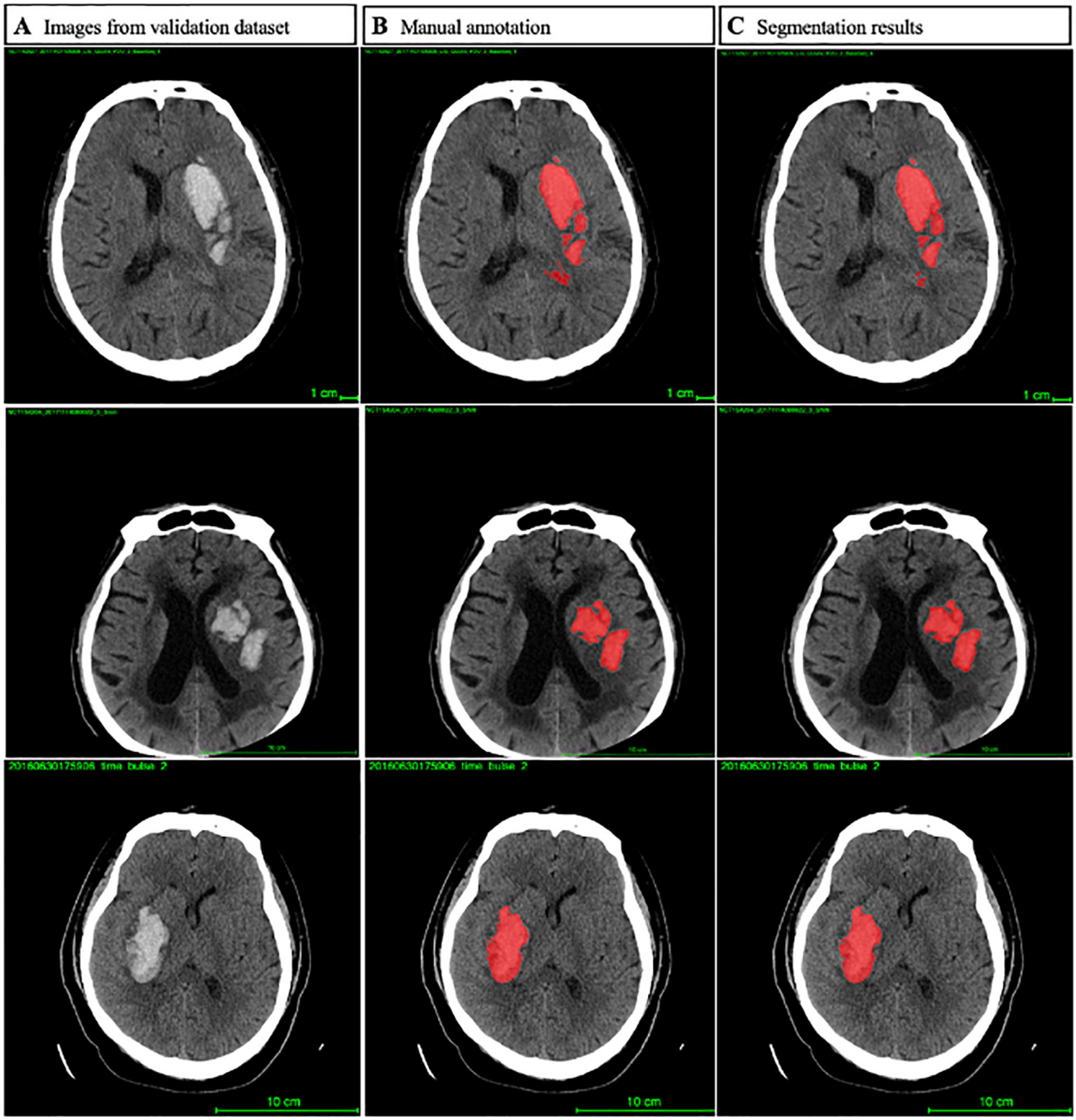


**FIGURE 2 |** Image processing of the predict model.

images, different classes of features including intensity, texture, and geometric were obtained on different image types. This process could yield 1379 quantitative features.

The other branch was a convolutional neural network (CNN) similar with the downsampling stage of U-Net, and a few repeated blocks consisted of convolution layers and a max pooling layer. The series of blocks terminates at a fully connected layer, and the final outputs were obtained from the last fully connected layer *via* softmax activation. Training was performed to optimize the prediction of the CNN, and the flattened output feature maps were extracted as the CNN features.

Finally, the radiomics features and the CNN features were concatenated and inputted to the gradient boosting

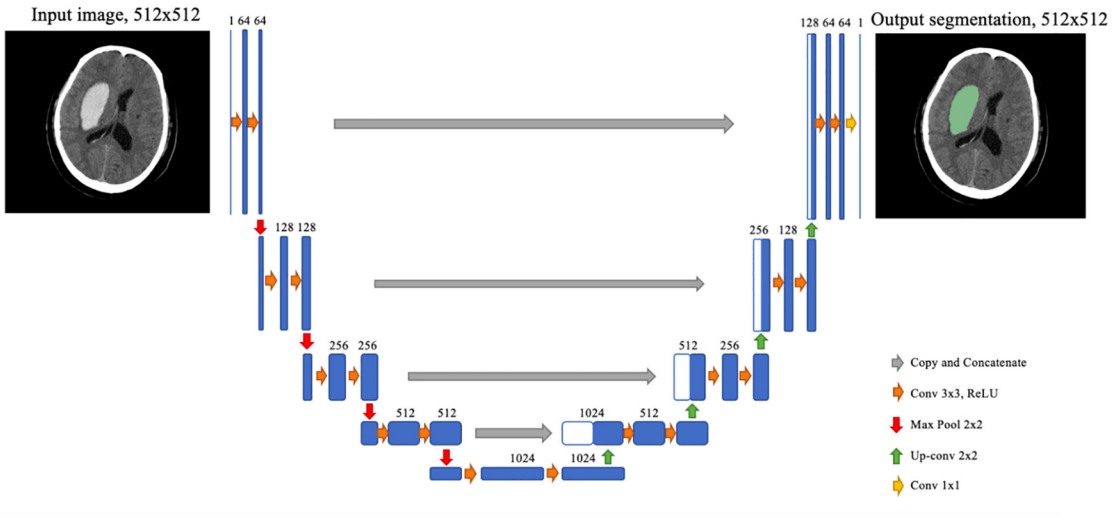


**FIGURE 3 |** The running process of convolutional neural network applied in this study.

classifier. Consequently, the outputs of the trained classifier were considered as the prediction results.

### Clinical Evaluation

The purpose of the prediction system for hematoma enlargement of intracerebral hemorrhage based on NCCT scan is to rapidly, conveniently, and without human interference predict whether secondary hematoma enlargement can occur in patients with spontaneous intracerebral hemorrhage. After the patients with suspected cerebral hemorrhage completed their head NCCT scan, the conventional process NCCT images were uploaded to the hospital imaging system PACS by imaging physicians, and the images were synchronized to the AI imaging system; the images were automatically identified, and the interpretation results were output. In order to facilitate the clinical decision-making, the risk of hematoma enlargement was set according to the AUC curve analysis. If the risk value was higher than the threshold value and the patient was considered to possess secondary hematoma enlargement, the hematoma was considered stable if it was lower than the critical value. The Tiantan Hospital evaluated the clinical application value of BioMind, mainly from the specificity, the sensitivity, the positive predictive value, the negative predictive value, and the Yoden index of hematoma enlargement prediction. This article analyzed the causes of the operation errors of the specific case model.

## Statistical Analysis

All analyses were performed using SPSS software version 26.0 (IBM, Armonk, NY, USA). The AUC curve was used to evaluate the prediction results of BioMind, and the sensitivity and specificity were calculated. The count data were expressed in percentage (%). Continuous data were expressed either as medians and interquartile ranges or as mean ± standard deviation (SD). The demographic and clinical characteristics were compared among the patients with hematoma growth and without it using Student's *t*-test or Mann–Whitney *U*-test, as appropriate. $P < 0.05$ was considered to be statistically significant.

# RESULTS

## Model Performance

The DLS model produces a segmentation mask indicating the location of hematoma and a confidence score representing the risk of HE. For hematoma segmentation, in validation dataset 1 ($n = 615$, 15,980 images), the slice-level pixel-wise IoU was 0.863 (95% CI, 0.848–0.877), and the patient-level IoU was 0.831 (95% CI, 0.811–0.856). The performance of the HE prediction was measured by the area under the receiver operating characteristic curve (AUC). **Figure 4** shows that in validation dataset 1, the AUC was 0.778 (95% CI, 0.768–0.786), the sensitivity was 0.818 (95% CI, 0.790–0.843), and the specificity was 0.601 (95% CI, 0.565–0.632). In validation dataset 2, the AUC was 0.780 (95% CI, 0.761–0.798), the sensitivity was 0.732 (95% CI, 0.682–0.788), and the specificity was 0.709 (95% CI, 0.658–0.759).

## Clinical Evaluation of BioMind

A total of 118 patients, including 84 (71.2%) male and 34 (28.8%) female, were enrolled in this study, with an average cohort age of 57.5 years. The basic characteristics of the patients included in the clinical validation datasets are summarized in **Table 1**. Among the 118 patients, 50 (42.4%) cases were with hematoma located in the basal ganglia, 26 (22.0%) cases in the thalamus, 30 (25.4%) cases in the lobe, and 12 (10.2%) in the cerebellum. Fifty-nine (50.0%) patients were found with an intraventricular hemorrhage on the baseline NCCT. Twenty-eight (23.7%) of the 118 patients suffered significant HE. We evaluated the ability of the model to predict hematoma enlargement in a clinical setting. In order to fit the clinical practice and facilitate the

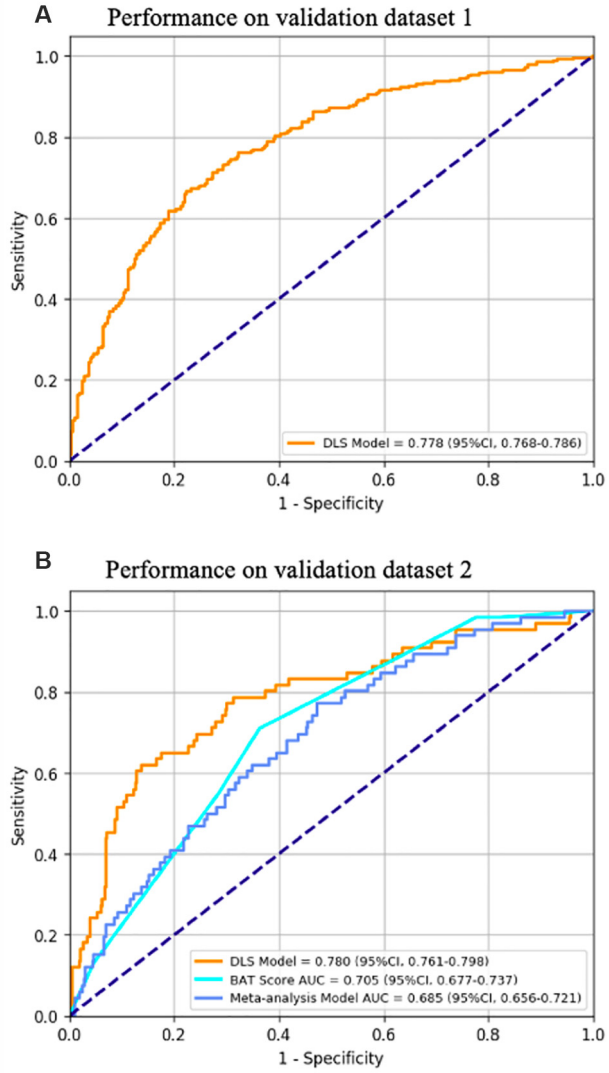


**FIGURE 4** | The performance of the HE prediction.

clinicians' decision-making, the risk of hematoma enlargement is considered to be a critical value through the statistical analysis of the prediction efficiency of the model. The following outputs are defined as stable hematoma, and the abovementioned output results are hematoma enlargement. Through the cross-table analysis (**Table 2**), the sensitivity of intracerebral hemorrhage hematoma expansion predicted by the artificial intelligence imaging system was found to be 89.3%, with a specificity of 77.8%, a positive predictive value of 55.6%, a negative predictive value of 95.9%, and a Yoden index of 0.671.

In addition, in the process of research, we found that the model cannot effectively operate in individual cases. The common feature of some cases is that the volume of hematoma is less than 3 ml, which leads to the result that the artificial intelligence model cannot judge the high-density shadow as the bleeding focus. Due to the small volume of the hematoma, the hematoma area on each slice is too small for the model to effectively distinguish the hematoma. The AI model also requires higher quality of images. Another part of patients may be anxious in the CT scanning process; in other words, they could not cooperate with the examination, resulting in lots of artifacts in the images. The strong interference made the model unable to identify and analyze effectively. These cases have been excluded in the data preparation.

## DISCUSSION

In this study, an innovative deep-learning algorithm based on NCCT was performed and validated for the prediction of hematoma enlargement in patients with intracerebral hemorrhage. Our results showed that the deep-learning algorithm could automatically complete the hematoma labeling and analysis to rapidly produce accurate prediction results. This type of artificial intelligence analysis based on NCCT scan offers several advantages, including universality, safety, time effectiveness, independence of the experience level of the reader, high sensitivity, and high specificity.

Previous studies have proposed several imaging predictors to identify hematoma expansion. CTA spot sign, leakage sign, and spot-and-tail sign are some of the proven independent predictors of hematoma enlargement (Goldstein et al., 2007; Wada et al., 2007; Sorimachi et al., 2013; Caplan, 2016; Orito et al., 2016). However, all of the above imaging markers have a common shortcoming of requiring initial CTA examination. Several patients are not eligible for CTA examination during the early stages of the disease; the examination cost is high, and the examination is not popular as the first diagnosis especially in the emergency department. Even many institutions do not have the capacity to conduct CTA. The application of CTA as a primary screening test presents with significant limitations. NCCT scan is simple and easy to operate. As a common and necessary examination step for patients with acute cerebral hemorrhage, the sign of hematoma enlargement has gained a hot spot in recent studies. Research about NCCT image features in the prediction of hematoma enlargement has already achieved positive results. The blend sign, CT hypodensities, and island sign in NCCT images have been reported in succession related with hematoma enlargement (Boulouis et al., 2016; Li et al., 2017; Sporns et al., 2017) However, the disadvantage of these imaging markers is that they are all highly subjective. On one hand, their interpretation needs to be conducted manually, which takes a relatively long time and the results cannot be obtained immediately. On the other hand, the results of their interpretation are influenced by the doctors who read the images, such that the results in clinical practice show a huge deviation and are not stable.

Moreover, there may be more imaging signs and more complex connections between them, which are difficult to identify and summarize by naked eyes alone. At present, the methods based on the analysis of NCCT image features to predict the hematoma enlargement of intracerebral hemorrhage need to pick out the variables before the prediction analysis, that is, researchers need to identify the image features that may be related to hematoma enlargement. This process is

**TABLE 1** | Comparison of the baseline demographic and clinical characteristics between patients with and without hematoma growth.

| Variables | Hematoma growth (*n* = 28) | Without hematoma growth (*n* = 90) | *P*-value |
|---|---|---|---|
| Demographic | | | |
| Age, year (IQR) | 48.5 (38.25–62.75) | 60 (53–65.25) | 0.012 |
| Sex, male, *n* (%) | 23 (82.1) | 61 (67.8) | 0.143 |
| Medical history | | | |
| Hypertension, *n* (%) | 18 (64.3) | 64 (71.1) | 0.493 |
| Diabetes mellitus, *n* (%) | 5 (17.9) | 18 (20.0) | 0.803 |
| Coronary heart disease, *n* (%) | 5 (17.9) | 12 (13.3) | 0.552 |
| Alcohol consumption, *n* (%) | 9 (32.1) | 25 (27.8) | 0.656 |
| Smoking, *n* (%) | 12 (42.9) | 25 (27.8) | 0.133 |
| Clinical features | | | |
| Admission SBP, mmHg (median) | 185.0 | 162.5 | 0.006 |
| Admission DBP, mmHg (SD) | 106.0 (21.2) | 93.8 (16.2) | 0.002 |
| Baseline GCS score, median (mean rank) | 8 (46.27) | 9 (63.62) | 0.018 |
| Admission heart rate, median | 96 (79.1) | 78 (53.4) | <0.001 |
| Location | | | 0.117 |
| Basal ganglia | 17 (60.7) | 33 (36.7) | |
| Thalamus | 3 (10.7) | 23 (25.6) | |
| Lobe | 5 (17.9) | 25 (27.8) | |
| Cerebellum | 3 (10.7) | 9 (10.0) | |
| Irregular hematoma | 28 (100) | 82 (91.1) | 0.195 |
| Intraventricular hemorrhage | 9 (32.1) | 50 (55.6) | 0.030 |
| Baseline ICH volume, ml (IQR) | 18.3 (14.8–20.3) | 13.9 (9.0–26.0) | 0.310 |

*IQR, interquartile range; SBP, systolic blood pressure; DBP, diastolic blood pressure; SD, standard deviation; GCS, Glasgow Coma Scale; ICH, intracerebral hemorrhage.*

**TABLE 2** | Cross-table analysis of diagnostic value of BioMind.

| | Actual Hematoma Growth *(n)* | Actual Hematoma Stable *(n)* | Total *(n)* |
|---|---|---|---|
| Predict Hematoma Growth *(n)* | 25 (a) | 17 (b) | 42 |
| Predict Hematoma Stable *(n)* | 3 (c) | 73 (d) | 76 |
| Total *(n)* | 28 | 90 | 118 |

*Sensitivity: $a/(a + c) \times 100\%$, Specificity: $d/(b + d) \times 100\%$, positive predictive value: $a/(a + b) \times 100\%$, negative predictive value: $d/(c + d) \times 100\%$, Yoden Index: sensitivity + specificity −1.*

likely to cause the loss of potential image features. But by the deep-learning model, we can directly import the processed images into the model without preset variables. The model can automatically learn and extract image features (Bengio et al., 2013; LeCun et al., 2015; Schmidhuber, 2015), greatly avoiding the loss of potential image feature information, so as to improve the specificity and sensitivity of prediction.

In addition, the deep-learning model and the convolutional neural network in image analysis have obvious strengths over other methods because of their own operational characteristics. Radiomics (Gillies et al., 2016; Lambin et al., 2017) is employed to extract a large number of high-dimensional quantitative imaging features from magnetic resonance imaging (MRI), positron emission tomography (PET), and NCCT images, which transform the conventional medical images into high-throughput imaging features that can be mined, quantitatively describe the spatial and temporal heterogeneity in the images, reveal the imaging features that cannot be recognized directly through the senses, effectively transform medical images into high-dimensional recognizable feature space, and analyze the generated spatial features with statistical analysis so as to establish models with predictive value that can provide worthy information for personalized diagnosis and treatment. The advantage of the deep convolution neural network is that it can automatically learn important low-level features (such as lines and edges) and can extract more complex and higher-level features (such as the shape) iteratively from low-level features (Fabijańska, 2018; Yasaka et al., 2018). Its end-to-end design provides more space for the model to automatically adjust according to the data and increase the overall fit of the model. Moreover, it retains the spatial relationship in filtering the input image, which can effectively extract the features of the images in the analysis of cerebral hemorrhage images. Moreover, the images are scaled and transformed in the training process, which greatly improves the stability of the output model.

Although our results are extremely promising, our study has some limitations. First, the learning process of the deep-learning model is known as a black box. Although we can develop and train the deep-learning model through data, we have no definite basis to explain the model. If the model predicts that a patient has a higher risk of early hematoma enlargement, we could not judge the imaging characteristics on which the prediction is based and could not explain the result. Second, only imaging data are included in the model at present, leaving the scope for including more statistically significant clinical features for comprehensive training through the analysis of clinical information of patients so as to further improve the clinical value of model prediction. Third, in this study, the predictive models did not automatically identify spontaneous intracerebral hemorrhage. There are some studies on the application of artificial intelligence to analyze the causes of cerebral hemorrhage with NCCT images with high accuracy. We believe that, if the two models can be combined, greater clinical benefits would be achieved. Fourth, this study was conducted with retrospective big data. As a result, we could not extract accurate past medical histories, such as the use of

anticoagulants and antiplatelet drugs, which may also affect the risk of hematoma enlargement. We will conduct a prospective study in the next step to validate the artificial intelligence model and explore the correlation between medical histories, drug use, and hematoma enlargement.

In conclusion, BioMind is a valuable hematoma expansion prediction system. As compared with existing hematoma prediction methods, it provides a time-saving, easy to implement, and subjective independent method to predict the risk of hematoma enlargement in patients with intracerebral hemorrhage. Presently, BioMind has realized the software transformation, and the artificial intelligence imaging analysis can be realized after installation to become a part of the diagnosis and treatment process of cerebral hemorrhage for more customized diagnosis and treatment of patients with cerebral hemorrhage.

## DATA AVAILABILITY STATEMENT

The raw data supporting the conclusions of this article will be made available by the authors, without undue reservation.

## ETHICS STATEMENT

The studies involving human participants were reviewed and approved by IRB of Beijing Tiantan Hospital Affiliated to Capital Medical University. The patients/participants provided their written informed consent to participate in this study.

## AUTHOR CONTRIBUTIONS

The studies were conceptualized, results analyzed, and manuscript drafted by LT and QR. PZ wrote the code, trained the models, and wrote the first draft of the manuscript, with guidance from TR. Also, PZ and ZW provided raw training data and overall study supervision. WG provided supervision of clinical data collection. All authors contributed to the article and approved the submitted version.

## FUNDING

This work has been supported by Beijing Tiantan Hospital, Capital Medical University "Emergency epidemiology study of Beijing Tiantan Hospital-952-01," Grant No. 2-952-01-DR.

## ACKNOWLEDGMENTS

Thanks for the support and convenience provided by the clinicians in the emergency department of Beijing Tiantan Hospital in data collection. Thanks for the contributions made by the people involved in this study.

## REFERENCES

Anderson, C. S., Heeley, E., Huang, Y., Wang, J., Stapf, C., Delcourt, C., et al. (2013). Rapid blood-pressure lowering in patients with acute intracerebral hemorrhage. *N. Engl. J. Med.* 368, 2355–2365. doi: 10.1056/NEJMoa1214609

Bengio, Y., Courville, A., and Vincent, P. (2013). Representation learning: a review and new perspectives. *IEEE Trans. Pattern Anal. Mach. Intell.* 35, 1798–1828. doi: 10.1109/TPAMI.2013.50

Boulouis, G., Morotti, A., Brouwers, H. B., Charidimou, A., Jessel, M. J., Auriel, E., et al. (2016). Association between hypodensities detected by computed tomography and hematoma expansion in patients with intracerebral hemorrhage. *JAMA Neurol.* 73, 961–968. doi: 10.1001/jamaneurol.2016.1218

Brouwers, H. B., Battey, T. W., Musial, H. H., Ciura, V. A., Falcone, G. J., Ayres, A. M., et al. (2015). Rate of contrast extravasation on computed tomographic angiography predicts hematoma expansion and mortality in primary intracerebral hemorrhage. *Stroke* 46, 2498–2503. doi: 10.1161/STROKEAHA.115.009659

Caplan, L. R. (2016). Recognizing and preventing intracerebral hematoma expansion. *JAMA Neurol.* 73, 914–915. doi: 10.1001/jamaneurol.2016.1899

Davis, S. M., Broderick, J., Hennerici, M., Brun, N. C., Diringer, M. N., Mayer, S. A., et al. (2006). Hematoma growth is a determinant of mortality and poor outcome after intracerebral hemorrhage. *Neurology* 66, 1175–1181. doi: 10.1212/01.wnl.0000208408.98482.99

Delcourt, C., Huang, Y., Arima, H., Chalmers, J., Davis, S. M., Heeley, E. L., et al. (2012). Hematoma growth and outcomes in intracerebral hemorrhage: the INTERACT1 study. *Neurology* 79, 314–319. doi: 10.1212/WNL.0b013e318260cbba

Demchuk, A. M., Dowlatshahi, D., Rodriguez-Luna, D., Molina, C. A., Blas, Y. S., Dzialowski, I., et al. (2012). Prediction of hematoma growth and outcome in patients with intracerebral hemorrhage using the CT-angiography spot sign (PREDICT): a prospective observational study. *Lancet Neurol.* 11, 307–314. doi: 10.1016/S1474-4422(12)70038-8

Dowlatshahi, D., Demchuk, A. M., Flaherty, M. L., Ali, M., Lyden, P. L., and Smith, E. E. (2011). Defining hematoma expansion in intracerebral hemorrhage: relationship with patient outcomes. *Neurology* 76, 1238–1244. doi: 10.1212/WNL.0b013e3182143317

Fabijańska, A. (2018). Segmentation of corneal endothelium images using a U-Net-based convolutional neural network. *Artif. Intell. Med.* 88, 1–13. doi: 10.1016/j.artmed.2018.04.004

Gillies, R. J., Kinahan, P. E., and Hricak, H. (2016). Radiomics: images are more than pictures, they are data. *Radiology* 278, 563–577. doi: 10.1148/radiol.2015151169

Goldstein, J. N., Fazen, L. E., Snider, R., Schwab, K., Greenberg, S. M., Smith, E. E., et al. (2007). Contrast extravasation on CT angiography predicts hematoma expansion in intracerebral hemorrhage. *Neurology* 68, 889–894. doi: 10.1212/01.wnl.0000257087.22852.21

Hansen, B. M., Nilsson, O. G., Anderson, H., Norrving, B., Säveland, H., and Lindgren, A. (2013). Long term (13 years) prognosis after primary intracerebral hemorrhage: a prospective population based study of long term mortality, prognostic factors and causes of death. *J. Neurol. Neurosurg. Psychiatry* 84, 1150–1155. doi: 10.1136/jnnp-2013-305200

Hosny, A., Parmar, C., Quackenbush, J., Schwartz, L. H., and Aerts, H. (2018). Artificial intelligence in radiology. *Nat. Rev. Cancer* 18, 500–510. doi: 10.1038/s41568-018-0016-5

Ji, N., Lu, J. J., Zhao, Y. L., Wang, S., and Zhao, J. Z. (2009). Imaging and clinical prognostic indicators for early hematoma enlargement after spontaneous intracerebral hemorrhage. *Neurol. Res.* 31, 362–366. doi: 10.1179/174313209X444035

Lambin, P., Leijenaar, R. T. H., Deist, T. M., Peerlings, J., De Jong, E. E. C., Van Timmeren, J., et al. (2017). Radiomics: the bridge between medical imaging and personalized medicine. *Nat. Rev. Clin. Oncol.* 14, 749–762. doi: 10.1038/nrclinonc.2017.141

LeCun, Y., Bengio, Y., and Hinton, G. (2015). Deep learning. *Nature* 521, 436–444. doi: 10.1038/nature14539

Li, Q., Liu, Q. J., Yang, W. S., Wang, X. C., Zhao, L. B., Xiong, X., et al. (2017). Island sign: an imaging predictor for early hematoma expansion and poor

outcome in patients with intracerebral hemorrhage. *Stroke* 48, 3019–3025. doi: 10.1161/STROKEAHA.117.017985

Lu, J. J., Ji, N., Zhao, Y. L., Wang, S., and Zhao, J. Z. (2007). Neuroimaging and clinical predictors of hematoma enlargement in spontaneous intracerebral hemorrhage. *Nat. Med. J. China* 87, 438–441.

Orito, K., Hirohata, M., Nakamura, Y., Takeshige, N., Aoki, T., Hattori, G., et al. (2016). Leakage sign for primary intracerebral hemorrhage: a novel predictor of hematoma growth. *Stroke* 47, 958–963. doi: 10.1161/STROKEAHA.115.011578

Poon, M. T., Fonville, A. F., and Al-Shahi Salman, R. (2014). Long-term prognosis after intracerebral hemorrhage systematic review and meta-analysis. *J. Neurol. Neurosurg. Psychiatry* 85, 660–667. doi: 10.1136/jnnp-2013-306476

Qureshi, A. I., Palesch, Y. Y., Barsan, W. G., Hanley, D. F., Hsu, C. Y., Martin, R. L., et al. (2016). Intensive blood-pressure lowering in patients with acute cerebral hemorrhage. *N. Engl. J. Med.* 375, 1033–1043. doi: 10.1056/NEJMoa1603460

Schmidhuber, J. (2015). Deep learning in neural networks: an overview. *Neural Netw.* 61, 85–117. doi: 10.1016/j.neunet.2014.09.003

Sorimachi, T., Osada, T., Baba, T., Inoue, G., Atsumi, H., Ishizaka, H., et al. (2013). The striate artery, hematoma and spot sign on coronal images of computed tomography angiography in putaminal intracerebral hemorrhage. *Stroke* 44, 1830–1832. doi: 10.1161/STROKEAHA.113.001498

Sporns, P. B., Schwake, M., Schmidt, R., Kemmling, A., Minnerup, J., Schwindt, W., et al. (2017). Computed tomographic blend sign is associated with computed tomographic angiography spot sign and predicts secondary neurological deterioration after intracerebral hemorrhage. *Stroke* 48, 131–135. doi: 10.1161/STROKEAHA.116.014068

Van Asch, C. J., Luitse, M. J., Rinkel, G. J., Van Der Tweel, I., Algra, A., and Klijn, C. J. (2010). Incidence, case fatality and functional outcome of intracerebral hemorrhage over time, according to age, sex and ethnic origin: a systematic review and meta-analysis. *Lancet Neurol.* 9, 167–176. doi: 10.1016/S1474-4422(09)70340-0

Wada, R., Aviv, R. I., Fox, A. J., Sahlas, D. J., Gladstone, D. J., Tomlinson, G., et al. (2007). CT angiography "spot sign" predicts hematoma expansion in acute intracerebral hemorrhage. *Stroke* 38, 1257–1262. doi: 10.1161/01.STR.0000259633.59404.f3

Wang, B., Jin, S., Yan, Q., Xu, H., Luo, C., Wei, L., et al. (2020). AI-assisted CT imaging analysis for COVID-19 screening: Building and deploying a medical AI system. *Appl. Soft Comput.* 98:106897. doi: 10.1016/j.asoc.2020.106897

Yasaka, K., Akai, H., Kunimatsu, A., Kiryu, S., and Abe, O. (2018). Deep learning with convolutional neural network in radiology. *Jpn. J. Radiol.* 36, 257–272. doi: 10.1007/s11604-018-0726-3

Yu, Z., Zheng, J., Ma, L., Guo, R., Li, M., Wang, X., et al. (2017). The predictive accuracy of the black hole sign and the spot sign for hematoma expansion in patients with spontaneous intracerebral hemorrhage. *Neurol. Sci.* 38, 1591–1597. doi: 10.1007/s10072-017-3006-6

Zia, E., Engström, G., Svensson, P. J., Norrving, B., and Pessah-Rasmussen, H. (2009). Three-year survival and stroke recurrence rates in patients with primary intracerebral hemorrhage. *Stroke* 40, 3567–3573. doi: 10.1161/STROKEAHA.109.556324

**Conflict of Interest**: Authors PZ and ZW were employed by company BioMind Technology.

The remaining authors declare that the research was conducted in the absence of any commercial or financial relationships that could be construed as a potential conflict of interest.

frontiers in Aging Neuroscience

ORIGINAL RESEARCH
published: 29 June 2021
doi: 10.3389/fnagi.2021.651614

# Time Course and Clinical Relevance of Neurological Deterioration After Endovascular Recanalization Therapy for Anterior Circulation Large Vessel Occlusion Stroke

*Zibao Li[1†], Hongchuan Zhang[2†], Jian Han[3†], Zhaohu Chu[1], Shoucai Zhao[1], Qian Yang[1], Xianjun Huang[1*] and Zhiming Zhou[1*]*

[1] Department of Neurology, Yijishan Hospital of Wannan Medical College, Wuhu, China, [2] Department of Radiology, Yijishan Hospital of Wannan Medical College, Wuhu, China, [3] Department of Neurology, Huangshan City People's Hospital, Huangshan, China

Neurological deterioration (ND) is a devastating complication for patients with ischemic stroke after endovascular recanalization therapy (EVT). We aimed to investigate the time course and clinical relevance of ND after EVT. Consecutive patients with acute ischemic stroke who underwent EVT for large arterial occlusions of the anterior cerebral circulation were enrolled. The National Institutes of Health Stroke Scale (NIHSS) scores were assessed before EVT, at the end of EVT, at 24 h (d1), on day 3 (d3), on day 15 (d15), at discharge and anytime when ND was indicated. ND was defined as an increase of $\geq$ 4 points in the NIHSS score and was divided into acute ND (AD, within 24 h), subacute ND (SD, d1–d3), and delayed ND (DD, d3–d15 or discharge). Using multivariable logistic regression analysis, we explored predictors and outcomes of ND at different time periods. As a result, of 343 patients, 129 (37.6%) experienced ND, including 90 (26.2%) with AD, 27 (7.9%) with SD and 12 (3.5%) with DD. Multivariable logistic regression analysis revealed that history of hypertension, cardioembolic stroke, lower Alberta Stroke Program Early Computed Tomography Score (ASPECTS), and poor collaterals were significantly associated with an increased risk of AD; history of hypertension, lower ASPECTS, poor collaterals, and unsuccessful recanalization, with SD; and high admission NIHSS score, with DD. In addition, patients who experienced AD (OR = 10.22, $P < 0.001$), SD (OR = 15.89, $P = 0.004$), or DD (OR = 8.31, $P = 0.015$) were more likely to have poor outcomes. ND was a strong predictor of poor stroke outcomes. Management of related risk factors at different ND time periods might improve the prognosis of EVT.

**Keywords: neurological deterioration, time course, stroke, recanalization, odds ratio**

OPEN ACCESS

***Edited by:***
*Yuanli Zhao,*
*Capital Medical University, China*

***Reviewed by:***
*Sheryl Martin-Schild,*
*Dr. Brain, Inc., United States*
*Yohei Tateishi,*
*Nagasaki University Hospital, Japan*

****Correspondence:***
*Xianjun Huang*
*doctorhuangxj@hotmail.com*
*Zhiming Zhou*
*neuro_depar@hotmail.com*

*† These authors have contributed equally to this work*

***Received:*** *10 January 2021*
***Accepted:*** *04 June 2021*
***Published:*** *29 June 2021*

***Citation:***
*Li Z, Zhang H, Han J, Chu Z, Zhao S, Yang Q, Huang X and Zhou Z (2021) Time Course and Clinical Relevance of Neurological Deterioration After Endovascular Recanalization Therapy for Anterior Circulation Large Vessel Occlusion Stroke. Front. Aging Neurosci. 13:651614. doi: 10.3389/fnagi.2021.651614*

## INTRODUCTION

With the aging of global population, stroke has become the second leading cause of disability-adjusted life-years (DALYs) for older adults underlying the need to deal with disabling outcome (GBD 2019 Diseases and Injuries Collaborators, 2020). Recently, several randomized controlled trials have confirmed the safety and efficacy of endovascular recanalization therapy (EVT) for

patients with large arterial occlusion strokes in anterior cerebral circulation (Berkhemer et al., 2015; Campbell et al., 2015; Goyal et al., 2015; Jovin et al., 2015; Saver et al., 2015). However, individual responses to EVT vary widely and clinical evolution is largely unpredictable. Less than half of patients achieve functional independence, while others become dependent or die at 90 days (Goyal et al., 2016). Previous studies had already suggested that early neurological deterioration (ND) predicted poor functional outcomes after EVT (Zhang et al., 2018; Kim et al., 2019a). The perioperative management of patients with EVT is a continuous and refined process during hospital. The incidence, predictors, and outcomes of ND in different time periods might be different. Thus, study of ND in different time periods after EVT contributed to a better individualized management.

Thus far, only few studies have reported the characteristics of ND after EVT. Regardless of the different definitions used, Kim et al. (2019a) showed that early ND occurs in 35.2% of patients and is significantly associated with large artery atherosclerosis (LAA) stroke, unsuccessful recanalization and a high National Institutes of Health Stroke Scale (NIHSS) score after EVT. Zhang et al. (2018) found that early ND occurred in 40.2% of patients, and high admission systolic blood pressure (SBP) and unsatisfactory recanalization of occluded arteries contributed to early ND. However, the clinical relevance for different ND time periods during hospitalization was not systematically investigated in either study. Therefore, we performed this prospective observational study to characterize the incidence, predictors, and outcomes of ND during different time periods to achieve refined management after EVT during hospitalization and to enrich enrollment in clinical trials of research interventions to decrease progression.

# MATERIALS AND METHODS

## Study Population

This study was a retrospective analysis of a prospectively collected stroke database. Consecutive patients with acute ischemic stroke undergoing EVT for large arterial occlusions of the anterior cerebral circulation on computed tomography angiography (CTA), magnetic resonance angiography (MRA), or digital-subtraction angiography (DSA) were enrolled from Yijishan Hospital of Wannan Medical College between May 2015 and September 2020. Patients with a modified Rankin Scale (mRS) score $>$ 2 before the index stroke were excluded from the study. This study was approved by the Ethical Review Board of Yijishan Hospital in Wuhu, China. Written informed consent was obtained from all enrolled patients or their surrogates.

## Endovascular Recanalization Therapy

The protocols of EVT and perioperative management strategies have been described previously (Hao et al., 2017; Huang et al., 2019; Li et al., 2019). Briefly, all patients received local anesthesia. Diazepam or dexmedetomidine was used in some patients who did not cooperate with the operation due to disturbance of consciousness. EVT was performed using a Solitaire stent retriever (Covidien, Irvine, CA, United States) or aspiration thrombectomy (Penumbra system, Alameda, CA, United States) as the first choice. If recanalization of targeting artery was not achieved, stent implantation, balloon dilation, or intra-arterial tirofiban administration were used as remedial measures.

## Clinical and Radiologic Assessment

Good collaterals were defined as $>$50% filling of the occluded area (Tan et al., 2007). Successful recanalization after EVT was defined as a modified Thrombolysis in Cerebral Infarction (mTICI) score of 2b or 3 (Zaidat et al., 2013). The NIHSS scores were recorded by certified neurologists before EVT, at the end of EVT, at 24 h (d1), on day 3 (d3), on day 15 (d15), at discharge and anytime when ND was indicated. For those patients receiving diazepam or dexmedetomidinem, the time of first postoperative evaluation was delayed to 24 h after EVT. ND was defined as an increase of four points or more in the NIHSS score compared to the best neurological status during hospitalization. We evaluated the time course of ND based on each time node of available clinical evaluations: acute ND (AD, within 24 h), subacute ND (SD, d1–d3), and delayed ND (DD, d3–d15 or discharge).

Non-contrast cranial CT scans were usually performed at 24 and 72 h after EVT or anytime ND was indicated by clinical manifestations. Symptomatic intracranial hemorrhage (sICH) was defined as parenchymal hemorrhage type 2 on non-contrast cranial CT with ND $\geq$ 4 NIHSS points from baseline (Kim et al., 2019b). A good functional outcome was defined as a mRS score $\leq$ 2 at 90-day follow-up. All clinical and imaging evaluations were performed in blind by two experienced neurologists. In cases of disagreement, a senior neuroscientist was consulted.

## Statistical Analysis

SPSS software (version 23.0; IBM, Armonk, NY, United States) was used for statistical analysis. Categorical variables are described by frequencies (percentages) and were compared using chi-square or Fisher exact tests. Continuous variables with normal distributions are presented as the mean (standard deviation, SD) and were compared using student t tests. Continuous variables without normal distributions are expressed as the median (interquartile range, IQR) and were compared using Mann-Whitney U tests. The association between potential predictive factors and outcome variables (ND and stroke outcome) was evaluated using logistic regression. Significant ($P < 0.1$) univariate predictive factors were candidates for inclusion in a multivariable logistic regression. A two-sided $P < 0.05$ was considered statistically significant.

# RESULTS

## Baseline Characteristics

We enrolled 343 patients with EVT in our study (**Table 1**). ND occurred in 129 (37.6%) patients, including 90 (26.2%) with AD, 27 (7.9%) with SD and 12 (3.5%) with DD, while 214 (62.4%) patients had no ND. Three patients without CT scan data in the ND group were discharged due to sudden neurological

**TABLE 1 |** Patient characteristics of the subgroups according to neurological deterioration status.

| Variables | Any Neurological Deterioration | | *P* | First Neurological Deterioration vs. No Deterioration by Category | | | | | |
|---|---|---|---|---|---|---|---|---|---|
| | Yes (*n* = 129) | No (*n* = 214) | | AD (*n* = 90) | *P* | SD (*n* = 27) | *P* | DD (*n* = 12) | *P* |
| **Demographic characteristics** | | | | | | | | | |
| Age, years, mean (SD) | 69.8 (11.5) | 67.7 (10.9) | 0.095 | 70.7 (10.7) | 0.031 | 67.0 (14.1) | 0.763 | 69.5 (10.6) | 0.585 |
| Female sex, *n* (%) | 60 (46.5) | 95 (44.4) | 0.702 | 45 (50.0) | 0.371 | 11 (40.7) | 0.719 | 4 (33.3) | 0.452 |
| **Past medical history, *n* (%)** | | | | | | | | | |
| Hypertension | 104 (80.6) | 139 (65.0) | 0.002 | 71 (78.9) | 0.016 | 24 (88.9) | 0.012 | 9 (75.0) | 0.551 |
| Diabetes mellitus | 27 (20.9) | 30 (14.0) | 0.096 | 16 (17.8) | 0.404 | 8 (29.6) | 0.048 | 3 (25.0) | 0.390 |
| Atrial fibrillation | 78 (60.5) | 94 (43.9) | 0.003 | 56 (62.2) | 0.004 | 15 (55.6) | 0.253 | 7 (58.3) | 0.329 |
| Antithrombotics | 43 (33.3) | 53 (24.8) | 0.087 | 31 (34.4) | 0.085 | 8 (29.6) | 0.584 | 4 (33.3) | 0.503 |
| **Clinical data** | | | | | | | | | |
| Admission SBP, mean (SD) | 151 (23) | 147 (23) | 0.069 | 151 (23) | 0.130 | 151 (24) | 0.322 | 153 (19) | 0.317 |
| Admission DBP, mean (SD) | 83 (14) | 81 (14) | 0.204 | 83 (15) | 0.362 | 85 (14) | 0.219 | 83 (8) | 0.776 |
| Admission NIHSS, median, (IQR) | 17 (14−20) | 14 (12−18) | <0.001 | 18 (14−20) | <0.001 | 17 (14−20) | 0.007 | 17 (14−21) | 0.034 |
| IV-rtPA, *n* (%) | 16 (12.4) | 24 (11.2) | 0.740 | 14 (15.6) | 0.296 | 1 (3.7) | 0.327 | 1 (8.3) | 1.000 |
| Occlusion site, *n* (%) | | | 0.021 | | 0.005 | | 0.827 | | 1.000 |
| ICA | 68 (52.7) | 80 (37.4) | | 52 (57.8) | | 12 (44.4) | | 4 (33.3) | |
| MCA-M1 | 52 (40.3) | 114 (53.3) | | 32 (35.6) | | 13 (48.1) | | 7 (58.3) | |
| MCA-M2, ACA | 9 (7.0) | 20 (9.3) | | 6 (6.7) | | 2 (7.4) | | 1 (8.3) | |
| TOAST type, *n* (%) | | | 0.003 | | 0.001 | | 0.435 | | 0.695 |
| CE | 89 (69.0) | 109 (50.9) | | 65 (72.2) | | 17 (63.0) | | 7 (58.3) | |
| LAA | 28 (21.7) | 81 (37.9) | | 14 (15.6) | | 9 (33.3) | | 5 (41.7) | |
| Others | 12 (9.3) | 24 (11.2) | | 11 (12.2) | | 1 (3.7) | | 0 (0.0) | |
| **Radiological findings and procedural aspects** | | | | | | | | | |
| ASPECTS, median (IQR) | 8 (7−9) | 9 (8−10) | <0.001 | 8 (7−9) | <0.001 | 7 (5−8) | <0.001 | 9 (8−10) | 0.689 |
| OTP, median (IQR) | 257(210−300) | 270 (222−330) | 0.282 | 245(210−300) | 0.114 | 296(220−360) | 0.420 | 253(200−293) | 0.568 |
| PT, median (IQR) | 74 (47−105) | 60 (44−90) | 0.010 | 79 (46−119) | 0.005 | 80 (54−100) | 0.118 | 51 (46−71) | 0.304 |
| Good collaterals, *n* (%) | 28 (21.7) | 112 (52.3) | <0.001 | 21 (23.3) | <0.001 | 3 (11.1) | <0.001 | 4 (33.3) | 0.200 |
| Procedural modes, *n* (%) | | | 0.120 | | 0.146 | | 0.106 | | 0.804 |
| Solitaire FR first | 94 (72.9) | 152 (71.0) | | 69 (76.7) | | 17 (63.0) | | 8 (66.7) | |
| Inspiration first | 28 (21.7) | 37 (17.3) | | 17 (18.9) | | 9 (33.3) | | 2 (16.7) | |
| Others, | 7 (5.4) | 25 (11.7) | | 4 (4.4) | | 1 (3.7) | | 2 (16.7) | |
| Remedial measures, *n* (%) | 18 (14.0) | 31 (14.5) | 0.891 | 14 (15.6) | 0.811 | 4 (14.8) | 0.999 | 0 (0.0) | 0.379 |
| mTICI (2b/3), *n* (%) | 80 (62.0) | 170 (79.4) | <0.001 | 55 (61.1) | 0.001 | 16 (59.3) | 0.027 | 9 (75.0) | 0.717 |

*SBP, systolic blood pressure; DBP, diastolic blood pressure; NIHSS, National Institutes of Health Stroke Scale; SD, standard deviation; IQR, Interquartile range; IV-rtPA, intravenous recombinant tissue plasminogen activator; ICA, internal carotid artery; MCA, middle cerebral artery; TOAST, Trial of Org 10172 in acute stroke treatment; CE, cardioembolic; LAA, large artery atherosclerosis; ASPECTS, the Alberta Stroke Program Early Computed Tomography Score; OTP, onset to puncture time; PT, procedural time; mTICI, modified Thrombolysis in Cerebral Infarction.*

deterioration. Compared to patients with no ND at any time point during hospitalization, patients with AD were more likely to have an older age (70.7 vs. 67.7 years, $P = 0.031$), higher rate of hypertension (78.9 vs. 65.0%, $P = 0.016$), higher rate of atrial fibrillation (62.2 vs. 43.9%, $P = 0.004$), higher NIHSS score on admission (18 vs. 14, $P < 0.001$), higher rate of an occlusion site in the internal carotid artery (ICA) (57.8 vs. 37.4%, $P = 0.005$), longer procedure time (PT) (79 vs. 60 min, $P = 0.005$), higher rate of cardioembolic stroke (CE) (72.2 vs. 50.9%, $P = 0.001$), lower Alberta Stroke Program Early Computed Tomography Score (ASPECTS) (8 vs. 9, $P < 0.001$), lower rate of good collaterals (23.3 vs. 52.3%, $P < 0.001$) and lower rate of successful reperfusion (61.1 vs. 79.4%, $P = 0.001$). Patients with SD were more likely to have a higher rate of hypertension (88.9 vs. 65.0%, $P = 0.012$), higher rate of diabetes mellitus (29.6 vs. 14.0%, $P = 0.048$), higher NIHSS score on admission (17 vs. 14, $P = 0.007$), lower ASPECTS (7 vs. 9, $P < 0.001$), lower rate of good collaterals (11.1 vs. 52.3%, $P < 0.001$) and lower rate of successful reperfusion (59.3 vs. 79.4%, $P = 0.027$). A higher NIHSS score on admission was significantly associated with DD (17 vs. 14, $P = 0.034$).

## Neurological Deterioration Free Survival Curves

A Kaplan-Meier curve was performed to test the effects of clinical variables on ND-free survival (**Figure 1**). ND was most likely to occur within the first 24 h (90/129, 69.8%, **Figure 1A**). The incidence of ND gradually decreased over time. Compared to patients with LAA stroke grouped by

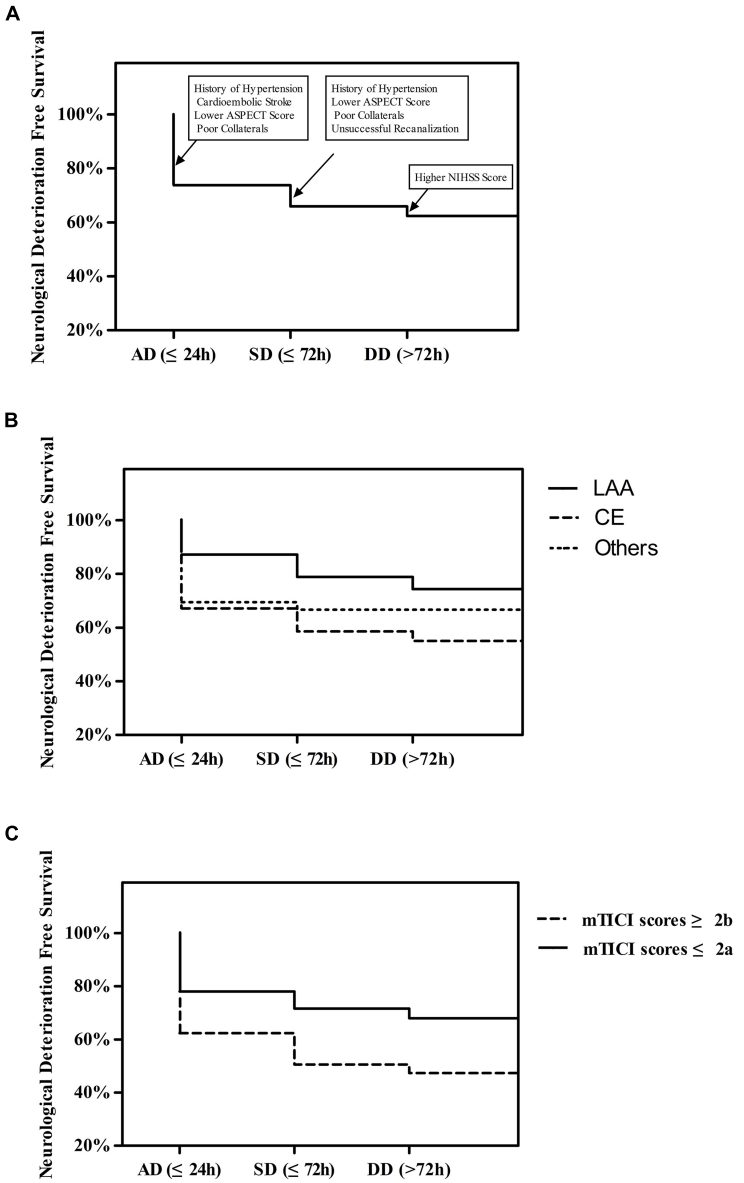


**FIGURE 1 | (A)** Time Course of First Neurological Deterioration. **(B)** The Course of First Neurological Deterioration grouped by TOAST type. **(C)** Time Course of First Neurological Deterioration grouped by mTICI scores.

Trial of Org 10172 in Acute Stroke Treatment (TOAST) type, patients with CE stroke and other stroke etiologies had a greater chance of ND (44.9 and 33.3%, respectively, vs. 25.7%, $P$ = 0.003, **Figure 1B**). We also observed that patients with successful recanalization after EVT had a decreased risk of ND (32.0 vs. 52.7%, OR = 0.423, $P < 0.001$, **Figure 1C**).

## Multivariable Model for Different ND Time Periods

The multivariable analysis of different ND time periods is shown in **Table 2** and **Figure 1A**. AD was significantly associated with history of hypertension (OR = 2.23, 95% CI = 1.09–4.55, $P$ = 0.028), TOAST type (LAA vs. CE, OR = 0.38, 95% CI = 0.15–0.97, $P$ = 0.043; others vs. CE, OR = 1.34, 95% CI = 0.45–4.02, $P$ = 0.602; total $P$ = 0.031), high ASPECTS (OR = 0.68, 95%CI = 0.54–0.86, $P$ = 0.001), and good collaterals (OR = 0.36, 95% CI = 0.19–0.68, $P$ = 0.002). SD was significantly associated with history of hypertension (OR = 6.25, 95% CI = 1.31–29.89, $P$ = 0.022), high ASPECTS (OR = 0.47, 95% CI = 0.34–0.66, $P < 0.001$), good collaterals (OR = 0.22, 95% CI = 0.06–0.83, $P$ = 0.026), and successful recanalization (OR = 0.26, 95% CI = 0.09–0.78, $P$ = 0.016). DD was significantly associated with a high admission NIHSS score (OR = 1.12, 95% CI = 1.00–1.26, $P$ = 0.048).

**TABLE 2 |** Factors associated with neurological deterioration according to time course.

| Variables | Odds ratio | Confidence interval | *P* value |
|---|---|---|---|
| **AD (≤24 h)** | | | |
| Age | 1.00 | 0.97–1.03 | 0.809 |
| Hypertension | 2.23 | 1.09–4.55 | 0.028 |
| Atrial fibrillation | 0.90 | 0.40–2.06 | 0.810 |
| Antithrombotics | 1.34 | 0.70–2.58 | 0.380 |
| Admission NIHSS | 1.02 | 0.95–1.09 | 0.633 |
| Occlusion site | | | 0.091 |
| MCA-M1 vs. ICA | 0.52 | 0.28–0.97 | 0.040 |
| MCA-M2 vs. ICA | 0.46 | 0.15–1.41 | 0.173 |
| TOAST | | | 0.031 |
| LAA vs. CE | 0.38 | 0.15–0.97 | 0.043 |
| Others vs. CE | 1.34 | 0.45–4.02 | 0.602 |
| ASPECTS | 0.68 | 0.54–0.86 | 0.001 |
| PT | 1.01 | 1.00–1.02 | 0.071 |
| Good collaterals | 0.36 | 0.19–0.68 | 0.002 |
| mTICI (2b/3) | 0.73 | 0.36–1.51 | 0.398 |
| **SD (1–3 days)** | | | |
| Hypertension | 6.25 | 1.31–29.89 | 0.022 |
| Diabetes mellitus | 2.70 | 0.86–8.41 | 0.088 |
| Admission NIHSS | 0.97 | 0.86–1.08 | 0.567 |
| ASPECTS | 0.47 | 0.34–0.66 | <0.001 |
| Good collaterals | 0.22 | 0.06–0.83 | 0.026 |
| mTICI (2b/3) | 0.26 | 0.09–0.78 | 0.016 |
| **DD (>3 days)** | | | |
| Admission NIHSS | 1.12 | 1.00–1.26 | 0.048 |

*AD, acute neurological deterioration; SD, subacute neurological deterioration; DD, delayed neurological deterioration; NIHSS, National Institutes of Health Stroke Scale; ICA, internal carotid artery; MCA, middle cerebral artery; PT, procedural time TOAST, Trial of Org 10172 in acute stroke treatment; CE, cardioembolic; LAA, large artery atherosclerosis; ASPECTS, the Alberta Stroke Program Early Computed Tomography Score; mTICI, modified thrombolysis in cerebral infarction.*

## Association Between the ND Time Course and Stroke Outcomes

Compared to patients with no ND, patients with ND were more likely to have poor outcomes (90.7 vs. 36.4%, $P < 0.001$). After adjustment for potential confounders (**Supplementary Table 1**), AD (OR = 10.22, 95% CI = 4.07–25.68, $P < 0.001$), SD (OR = 15.89, 95% CI = 2.47–102.14, $P = 0.004$) and DD (OR = 8.31, 95% CI = 1.51–45.90, $P = 0.015$) were significantly associated with poor outcomes (**Table 3** and **Figure 2**).

**TABLE 3 |** Association between time course of ND and poor outcome.

| Time course of ND | mRS > 2 | | |
|---|---|---|---|
| | Odds ratio | Confidence interval | *P* value |
| **ND vs. no ND** | | | |
| AD | 10.22 | 4.07–25.68 | <0.001 |
| SD | 15.89 | 2.47–102.14 | 0.004 |
| DD | 8.31 | 1.51–45.90 | 0.015 |

*ND, neurological deterioration; AD, acute neurological deterioration; SD, subacute neurological deterioration; DD, delayed neurological deterioration; mRS, modified Rankin Scale.*
*Adjusted for age, sex, diabetes mellitus, atrial fibrillation, antithrombotics, admission systolic blood pressure (SBP), National Institutes of Health Stroke Scale (NIHSS) score, occlusion site, Trial of Org 10172 in acute stroke treatment (TOAST), the Alberta Stroke Program Early Computed Tomography Score (ASPECTS), procedural time (PT), collateral score, procedural modes, modified Thrombolysis in Cerebral Infarction (mTICI).*

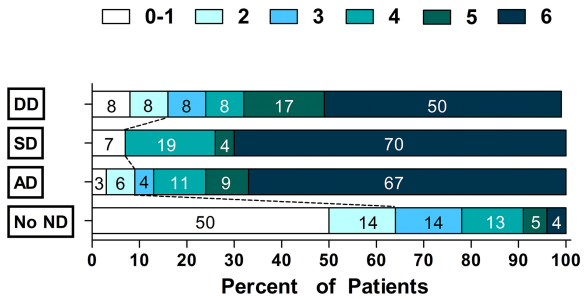


**FIGURE 2 |** Scores on the modified Rankin Scale grouped by Time Course of Neurological Deterioration status.

# DISCUSSION

Our study demonstrated that 37.6% of stroke patients experienced ND after EVT during hospitalization, especially in the first 24 h. We also revealed a striking association between ND at different time periods (AD, SD, and DD) and poor prognosis. Clinical strategies focused on prevention of different ND time courses are a logical step to improve outcomes after EVT.

Previous studies indicated that early ND occurs in 35.2–40.2% of patients, most of which occurs within 72 h. This was similar to the incidence in our study despite the different definitions (Zhang et al., 2018; Kim et al., 2019a). Kim et al. (2019a) found that more than half of patients with ICA occlusion experienced ND, which was attributed to the mechanisms of symptomatic hemorrhage, ischemia progression, and brain edema. The risk factors for ND were LAA stroke for ischemia progression, and successful recanalization and NIHSS score after thrombectomy for hemorrhage or brain edema. These findings are generally in line with our results. In this study, 52.7% of patients with ICA occlusion experienced ND, indicating that they were especially susceptible to secondary neuronal injury after EVT. Successful recanalization was also a protective factor for SD, which was consistent with the results from a clinical study in China (Zhang et al., 2018). We found that a high NIHSS score on admission was the only risk factor for DD, suggesting that the effects of baseline risk factors and procedure-related factors on ND elapse over time after EVT. However, compared to CE stroke, LAA stroke was a protective factor for AD, which was inconsistent with the results of Kim et al. (2019a). We speculated that this difference may be due to different ethnic groups, different definitions of ND, and different classification methods of ND. We found that CE stroke patients in our study had poor collaterals (CE vs. LAA, 69.9 vs. 30.1%, respectively, $P = 0.015$), while poor collaterals was a risk factor for both AD and SD. Previous studies indicated that poor collaterals was associated with a lower recanalization rate (Bang et al., 2011; Liebeskind et al., 2014a,b; Leng et al., 2016b), ischemia progression (Campbell et al., 2013; Chen et al., 2019),

a higher rate of sICH (Liebeskind et al., 2014a; Leng et al., 2016a; Hao et al., 2017) and malignant brain edema (Huang et al., 2019), which were common causes of ND after EVT. History of hypertension and lower ASPECTS were also observed to increase the risk of AD and SD. History of hypertension usually signifies a higher admission SBP (152 ± 22 vs. 139 ± 23 mmHg, $P < 0.001$ in our study) which only showed a moderate association with ND in this study ($P = 0.069$, **Table 1**). However, several studies have suggested that elevated admission SBP levels increase the risk of sICH (Mulder et al., 2017; Malhotra et al., 2020), ischemia progression (Goyal et al., 2017), early ischemic stroke recurrence (Leonardi-Bee et al., 2002) and cerebral edema (Leonardi-Bee et al., 2002), and consequently contribute to the occurrence of ND. A lower ASPECTS commonly indicates a higher NIHSS score with poor collaterals (Liebeskind et al., 2014a; Yoo et al., 2016), while both a higher NIHSS score and poor collaterals are considered major risk factors for ND.

There are limitations to this study. This was a retrospective single-center study with a limited sample size, especially for DD because of its low incidence. Further studies with a larger sample size in multiple centers are needed. Clinical confounding factors of ND are complicated, and not all of these factors were included. For example, post-stroke pneumonia, a common complication after stroke, was not included in this study because it is difficult to identify whether post-stroke pneumonia led to ND or ND resulted in post-stroke pneumonia in a logistic regression model. Finally, due to the unclear mechanism of ND and due to retrospective nature in this study, we failed to investigate the risk factors of ND according to its etiology, which needs to be explored in further studies.

Our study has clinical implications. ND at different time periods (AD, SD, and DD) predicted poor outcome, underlining the need to emphasize close neurological monitoring, especially within 24 h after EVT. The focus of monitoring should change as time progresses: history of hypertension, CE stroke, lower ASPECTS, and poor collaterals for AD (≤24 h); history of hypertension, ASPECTS, poor collaterals and unsuccessful recanalization for SD (24–72 h); and high NIHSS score for DD (>72 h). Recanalization rates should receive more attention during EVT. If recanalization is not achieved, prevention of hypovolemia (Arenillas et al., 2018), hypo- and hypertension (Biose et al., 2020; Raychev et al., 2020), hyperglycemia (Biose et al., 2020), and hyperuricemia (Menon et al., 2013) are primary targets for preserving collaterals. Other uncontrollable factors, including history of hypertension, CE stroke, lower ASPECTS and high NIHSS score, should also be considered in decision-making protocols before EVT. Families often expect patients to benefit more from EVT. We should prepare them with the fact that approximately 1/3 of patients experience ND, which implies a poor short-term prognosis.

Neurological deterioration by ≥4 NIHSS points occurring in one-third of patients with ischemic stroke undergoing EVT is a strong predictor for poor stroke outcomes. The risk factors for ND change as time progresses. Management of risk factors at different ND time periods might improve the prognosis of patients who undergo EVT in the future. Further large-scale studies are warranted to validate our findings and to delineate optimal criteria to prevent ND.

## DATA AVAILABILITY STATEMENT

The raw data supporting the conclusions of this article will be made available by the authors, without undue reservation.

## ETHICS STATEMENT

The studies involving human participants were reviewed and approved by the Ethical Review Board of Yijishan Hospital in Wuhu, China (2019-039). The patients/participants provided their written informed consent to participate in this study.

## AUTHOR CONTRIBUTIONS

ZL, HZ, and JH designed the study, analyzed all the data, and prepared the manuscript. ZZ and XH conceptualized the study, interpreted study data, and revised the manuscript. ZC and SZ performed the statistical analysis. QY collected clinical data and image data. All authors approved the final manuscript.

## FUNDING

ZL and XH were funded by the Natural Science Foundation of Wannan Medical College in China (WK2019F08 and WK2019F22, respectively). ZL was also received the Scientific Research Fund Project for Talent Introduction of Yijishan Hospital, Wannan Medical College in China (YR202111).

## ACKNOWLEDGMENTS

The authors thank Yang Xu for his statistical assistance.

## SUPPLEMENTARY MATERIAL

The Supplementary Material for this article can be found online at: https://www.frontiersin.org/articles/10.3389/fnagi.2021.651614/full#supplementary-material

## REFERENCES

Arenillas, J. F., Cortijo, E., Garcia-Bermejo, P., Levy, E. I., Jahan, R., Liebeskind, D., et al. (2018). Relative cerebral blood volume is associated with collateral status and infarct growth in stroke patients in SWIFT PRIME. *J. Cereb. Blood Flow Metab.* 38, 1839–1847. doi: 10.1177/0271678X17740293

Bang, O. Y., Saver, J. L., Kim, S. J., Kim, G.-M., Chung, C.-S., Ovbiagele, B., et al. (2011). Collateral flow predicts response to endovascular therapy for acute ischemic stroke. *Stroke* 42, 693–699. doi: 10.1161/strokeaha.110.595256

Berkhemer, O. A., Fransen, P. S., Beumer, D., Van Den Berg, L. A., Lingsma, H. F., Yoo, A. J., et al. (2015). A randomized trial of intraarterial treatment for acute ischemic stroke. *N. Engl. J. Med.* 372, 11–20. doi: 10.1056/NEJMoa1411587

Biose, I. J., Dewar, D., Macrae, I. M., and Mccabe, C. (2020). Impact of stroke co-morbidities on cortical collateral flow following ischaemic stroke. *J. Cereb. Blood Flow Metab.* 40, 978–990. doi: 10.1177/0271678X19858532

Campbell, B. C., Christensen, S., Tress, B. M., Churilov, L., Desmond, P. M., Parsons, M. W., et al. (2013). Failure of collateral blood flow is associated with infarct growth in ischemic stroke. *J. Cereb. Blood Flow Metab.* 33, 1168–1172. doi: 10.1038/jcbfm.2013.77

Campbell, B. C., Mitchell, P. J., Kleinig, T. J., Dewey, H. M., Churilov, L., Yassi, N., et al. (2015). Endovascular therapy for ischemic stroke with perfusion-imaging selection. *N. Engl. J. Med.* 372, 1009–1018. doi: 10.1056/NEJMoa1414792

Chen, C., Parsons, M. W., Levi, C. R., Spratt, N. J., Miteff, F., Lin, L., et al. (2019). Exploring the relationship between ischemic core volume and clinical outcomes after thrombectomy or thrombolysis. *Neurology* 93, e283–e292. doi: 10.1212/WNL.0000000000007768

GBD 2019 Diseases and Injuries Collaborators (2020). Global burden of 369 diseases and injuries in 204 countries and territories, 1990-2019: a systematic analysis for the global burden of disease study 2019. *Lancet* 396, 1204–1222. doi: 10.1016/s0140-6736(20)30925-9

Goyal, M., Demchuk, A. M., Menon, B. K., Eesa, M., Rempel, J. L., Thornton, J., et al. (2015). Randomized assessment of rapid endovascular treatment of ischemic stroke. *N. Engl. J. Med.* 372, 1019–1030. doi: 10.1056/NEJMoa1414905

Goyal, M., Menon, B. K., Van Zwam, W. H., Dippel, D. W. J., Mitchell, P. J., Demchuk, A. M., et al. (2016). Endovascular thrombectomy after large-vessel ischaemic stroke: a meta-analysis of individual patient data from five randomised trials. *Lancet* 387, 1723–1731. doi: 10.1016/s0140-6736(16)00163-x

Goyal, N., Tsivgoulis, G., Iftikhar, S., Khorchid, Y., Fawad Ishfaq, M., Doss, V. T., et al. (2017). Admission systolic blood pressure and outcomes in large vessel occlusion strokes treated with endovascular treatment. *J. Neurointerv. Surg.* 9, 451–454. doi: 10.1136/neurintsurg-2016-012386

Hao, Y., Yang, D., Wang, H., Zi, W., Zhang, M., Geng, Y., et al. (2017). Predictors for symptomatic intracranial hemorrhage after endovascular treatment of acute ischemic stroke. *Stroke* 48, 1203–1209. doi: 10.1161/strokeaha.116.016368

Huang, X., Yang, Q., Shi, X., Xu, X., Ge, L., Ding, X., et al. (2019). Predictors of malignant brain edema after mechanical thrombectomy for acute ischemic stroke. *J. Neurointerv. Surg.* 11, 994–998. doi: 10.1136/neurintsurg-2018-014650

Jovin, T. G., Chamorro, A., Cobo, E., De Miquel, M. A., Molina, C. A., Rovira, A., et al. (2015). Thrombectomy within 8 hours after symptom onset in ischemic stroke. *N. Engl. J. Med.* 372, 2296–2306. doi: 10.1056/NEJMoa1503780

Kim, J. M., Bae, J. H., Park, K. Y., Lee, W. J., Byun, J. S., Ahn, S. W., et al. (2019a). Incidence and mechanism of early neurological deterioration after endovascular thrombectomy. *J. Neurol.* 266, 609–615. doi: 10.1007/s00415-018-09173-0

Kim, T. J., Park, H. K., Kim, J. M., Lee, J. S., Park, S. H., Jeong, H. B., et al. (2019b). Blood pressure variability and hemorrhagic transformation in patients with successful recanalization after endovascular recanalization therapy: a retrospective observational study. *Ann. Neurol.* 85, 574–581. doi: 10.1002/ana.25434

Leng, X., Fang, H., Leung, T., Mao, C., Miao, Z., Liu, L., et al. (2016a). Impact of collaterals on the efficacy and safety of endovascular treatment in acute ischaemic stroke: a systematic review and meta-analysis. *J. Neurol. Neurosurg. Psychiatry* 87, 537–544. doi: 10.1136/jnnp-2015-310965

Leng, X., Fang, H., Leung, T. W., Mao, C., Xu, Y., Miao, Z., et al. (2016b). Impact of collateral status on successful revascularization in endovascular treatment: a systematic review and meta-analysis. *Cerebrovasc. Dis.* 41, 27–34. doi: 10.1159/000441803

Leonardi-Bee, J., Bath, P. M. W., Phillips, S. J., and Sandercock, P. A. G. (2002). Blood pressure and clinical outcomes in the international stroke trial. *Stroke* 33, 1315–1320. doi: 10.1161/01.str.0000014509.11540.66

Li, Z. B., Chu, Z. H., Zhao, S. C., Ma, L. S., Yang, Q., Huang, X. J., et al. (2019). Severe stroke patients with left-sided occlusion of the proximal anterior circulation benefit more from thrombectomy. *Front. Neurol.* 10:551. doi: 10.3389/fneur.2019.00551

Liebeskind, D. S., Jahan, R., Nogueira, R. G., Zaidat, O. O., and Saver, J. L. (2014a). Impact of collaterals on successful revascularization in Solitaire FR with the intention for thrombectomy. *Stroke* 45, 2036–2040. doi: 10.1161/strokeaha.114.004781

Liebeskind, D. S., Tomsick, T. A., Foster, L. D., Yeatts, S. D., Carrozzella, J., Demchuk, A. M., et al. (2014b). Collaterals at angiography and outcomes in the interventional management of stroke (IMS) III trial. *Stroke* 45, 759–764. doi: 10.1161/STROKEAHA.113.004072

Malhotra, K., Goyal, N., Katsanos, A. H., Filippatou, A., Mistry, E. A., Khatri, P., et al. (2020). Association of blood pressure with outcomes in acute stroke thrombectomy. *Hypertension* 75, 730–739. doi: 10.1161/hypertensionaha.119.14230

Menon, B. K., Smith, E. E., Coutts, S. B., Welsh, D. G., Faber, J. E., Goyal, M., et al. (2013). Leptomeningeal collaterals are associated with modifiable metabolic risk factors. *Ann. Neurol.* 74, 241–248. doi: 10.1002/ana.23906

Mulder, M., Ergezen, S., Lingsma, H. F., Berkhemer, O. A., Fransen, P. S. S., Beumer, D., et al. (2017). Baseline blood pressure effect on the benefit and safety of intra-arterial treatment in MR CLEAN (multicenter randomized clinical trial of endovascular treatment of acute ischemic stroke in the Netherlands). *Stroke* 48, 1869–1876. doi: 10.1161/STROKEAHA.116.016225

Raychev, R., Liebeskind, D. S., Yoo, A. J., Rasmussen, M., Arnaudov, D., Brown, S., et al. (2020). Physiologic predictors of collateral circulation and infarct growth during anesthesia – Detailed analyses of the GOLIATH trial. *J. Cereb. Blood Flow Metab.* 40, 1203–1212. doi: 10.1177/0271678X19865219

Saver, J. L., Goyal, M., Bonafe, A., Diener, H. C., Levy, E. I., Pereira, V. M., et al. (2015). Stent-retriever thrombectomy after intravenous t-PA vs. t-PA alone in stroke. *N. Engl. J. Med.* 372, 2285–2295. doi: 10.1056/NEJMoa1415061

Tan, J. C., Dillon, W. P., Liu, S., Adler, F., Smith, W. S., and Wintermark, M. (2007). Systematic comparison of perfusion-CT and CT-angiography in acute stroke patients. *Ann. Neurol.* 61, 533–543. doi: 10.1002/ana.21130

Yoo, A. J., Berkhemer, O. A., Fransen, P. S. S., Van Den Berg, L. A., Beumer, D., Lingsma, H. F., et al. (2016). Effect of baseline alberta stroke program early CT Score on safety and efficacy of intra-arterial treatment: a subgroup analysis of a randomised phase 3 trial (MR CLEAN). *Lancet Neurol.* 15, 685–694. doi: 10.1016/s1474-4422(16)00124-1

Zaidat, O. O., Yoo, A. J., Khatri, P., Tomsick, T. A., Von Kummer, R., Saver, J. L., et al. (2013). Recommendations on angiographic revascularization grading standards for acute ischemic stroke: a consensus statement. *Stroke* 44, 2650–2663. doi: 10.1161/strokeaha.113.001972

Zhang, Y. B., Su, Y. Y., He, Y. B., Liu, Y. F., Liu, G., and Fan, L. L. (2018). Early neurological deterioration after recanalization treatment in patients with acute ischemic stroke: a retrospective study. *Chin. Med. J. (Engl.).* 131, 137–143. doi: 10.4103/0366-6999.222343

**Conflict of Interest:** The authors declare that the research was conducted in the absence of any commercial or financial relationships that could be construed as a potential conflict of interest.

frontiers in Aging Neuroscience

ORIGINAL RESEARCH
published: 30 June 2021
doi: 10.3389/fnagi.2021.645649

# Transcriptome Analysis of Microglia Reveals That the TLR2/IRF7 Signaling Axis Mediates Neuroinflammation After Subarachnoid Hemorrhage

*Shenbin Xu[1†], Shuhao Mei[1†], Jianan Lu[1], Haijian Wu[1], Xiao Dong[1], Ligen Shi[1*], Jingyi Zhou[1*] and Jianmin Zhang[1,2,3*]*

[1] Department of Neurosurgery, Second Affiliated Hospital, School of Medicine, Zhejiang University, Hangzhou, China, [2] Brain Research Institute, Zhejiang University, Hangzhou, China, [3] Collaborative Innovation Center for Brain Science, Zhejiang University, Hangzhou, China

Microglia-mediated neuroinflammatory response in the early brain injury after subarachnoid hemorrhage (SAH) has been reported to have an impact on progress, and the mechanism is not completely understood. Here, we performed genome-wide transcriptome analysis of microglia purified from damaged hemisphere of adult mice at 3 days after SAH or sham operation. Robust transcriptional changes were observed between SAH-induced and healthy microglia, indicating rapid activation of microglia after suffering from SAH. We identified 1576 differentially expressed genes (DEGs; 928 upregulated and 648 downregulated) in SAH-induced microglia compared with sham microglia, representing a strong alteration of the genome (6.85% of total ∼23,000 genes). Functional enrichment of these DEGs indicated that cell division, inflammatory response, cytokine production, and leukocyte chemotaxis were strongly activated in SAH-induced microglia. Moreover, we identified and proved that the TLR2/IRF7 signaling axis was involved in the regulation of this microglia-mediated inflammation in SAH mice by performing flow cytometry and immunofluorescence. Together, these results provided a perspective of microglia-mediated neuroinflammatory response in the early stage of SAH and might give a new therapeutic target for SAH.

**Keywords: subarachnoid hemorrhage, microglia, flow cytometry, bulk RNA-seq, early brain injury**

OPEN ACCESS

***Edited by:***
*Shuo Wang,*
*Capital Medical University, China*

***Reviewed by:***
*Jianhua Peng,*
*The Affiliated Hospital of Southwest Medical University, China*
*Myoung-gwi Ryou,*
*Tarleton State University, United States*

***Correspondence:**
*Ligen Shi*
*slg0904@zju.edu.cn*
*Jingyi Zhou*
*2503027@zju.edu.cn*
*Jianmin Zhang*
*zjm135@zju.edu.cn*

*† These authors have contributed equally to this work*

***Received:*** *23 December 2020*
***Accepted:*** *19 April 2021*
***Published:*** *30 June 2021*

***Citation:***
*Xu S, Mei S, Lu J, Wu H, Dong X, Shi L, Zhou J and Zhang J (2021) Transcriptome Analysis of Microglia Reveals That the TLR2/IRF7 Signaling Axis Mediates Neuroinflammation After Subarachnoid Hemorrhage. Front. Aging Neurosci. 13:645649. doi: 10.3389/fnagi.2021.645649*

## INTRODUCTION

Subarachnoid hemorrhage (SAH), which is mainly caused by intracranial aneurysm rupture, is a severe subtype of stroke with high mortality, disability, and poor outcomes (Macdonald and Schweizer, 2017). It accounts for 5% of strokes and has an annual incidence of 6–10 cases per 100,000 persons (Amodio et al., 2020; Macdonald and Schweizer, 2017). Early brain injury (EBI), which occurs in the first 72 h after bleeding, has been considered as the most important pathophysiological mechanism contributing to delayed cerebral ischemia and poor prognosis (Rass and Helbok, 2019). EBI is associated with many pathological processes, such as neuroinflammation, brain edema, global ischemia, and excitotoxicity (Fujii et al., 2013). Among

them, neuroinflammation are considered to play a crucial role in EBI (Fujii et al., 2013). Microglia, the main resident immune cells in the central nervous system (CNS), is the most significant mediator in neuroinflammation. They constantly surveil the microenvironment and respond to damage and pathogens, acting as double-edged swords in different pathological states (Soulet and Rivest, 2008; Liu et al., 2019).

In the context of SAH, remarkable accumulation of microglia was observed within the first 3 days (Zheng et al., 2020) and lasted 28 days after bleeding (Schneider et al., 2015). In the acute phase, microglia are activated and secrete cytokines [e.g., interleukin-1β (IL-1β), IL-6, and tumor necrosis factor-α (TNF-α)], chemokines, and other potentially toxic chemicals, leading to inflammatory response and cell death (Schneider et al., 2015). However, microglia are also responsible for phagocytosis and clearance of blood and cell debris, indicating that microglia exhibit neuroprotective functions after bleeding (Schallner et al., 2015). Given the complex function of microglia, the specific role and underlying mechanisms of microglia in SAH remain largely obscure.

Toll-like receptors (TLRs), a class of pattern recognition receptors (PRRs) that are highly enriched in microglia, recognize the pathogen-associated molecular pattern (PAMP) ligands and the endogenous danger-associated molecular pattern (DAMP) ligands. Under pathological conditions, microglia initiate innate immune response *via* TLRs (Lalancette-Hebert et al., 2017). A previous study has shown that soluble TLR2 is elevated in cerebrospinal fluid (CSF) in patients with SAH (Sokol et al., 2016). 6-MP and glycyrrhizin treatment can attenuate TLR2 expression and SAH-induced brain injury (Chang et al., 2014, 2015). Additionally, TLR2 stimulation increases the leukocytosis in the CSF and blood flowing through choroid plexus (Rayasam et al., 2020). Interferon regulatory factor 7 (IRF7) is a multifunctional transcription factor that can be activated by PRRs (Ning et al., 2011). TLR2 can activate IRF7 in inflammatory monocytes and bone marrow-derived macrophages (Barbalat et al., 2009; Dietrich et al., 2010). Moreover, IRF7 participates in the M1-like microglial polarization switch (Tanaka et al., 2015). In conclusion, the TLR2/IRF7 signaling pathway may have influence on neuroinflammation. However, its exact function in mediating microglia, under SAH condition, is largely unknown.

To understand the microglial transcriptional changes after SAH and its potential role in SAH, we performed genome-wide transcriptome analysis of microglia isolated from damaged hemispheres of adult mice 3 days post-SAH and sham operation. We explored the functional implications of microglia in response to SAH and found that the microglia involved in neuroinflammation may be regulated by the TLR2/IRF7 signaling pathway.

# MATERIALS AND METHODS

## Animal

Eight- to 10-week-old male C57BL/6 mice (SLAC Laboratory Animal Co., Ltd., Shanghai, China) were housed in a temperature- and humidity-controlled room under a 12-h day/night cycle and had free access to food and water. All protocols were approved by the Institutional Ethics Committee of the Second Affiliated Hospital, Zhejiang University School of Medicine. The animal experiments were performed according to the National Institutes of Health's Guide for the Care and the Use of Laboratory Animals and the ARRIVE (Animal Research: Reporting *in vivo* Experiments) guidelines.

## Microglia Depletion

As previously described, PLX3397 (Selleckchem, Houston, TX, United States) was formulated in AIN-76 A standard chow at a concentration of 290 ppm. Mice were fed with PLX3397 chow for 21 consecutive days (Najafi et al., 2018) until the end of experiments.

## SAH Model

The endovascular perforation model was established as previously described (Muroi et al., 2015). Briefly, mice were anesthetized with pentobarbital sodium (40 mg/kg) *via* intraperitoneal injection. Left carotid artery and its bifurcation were exposed. Then, 5-0 sharpened nylon suture was inserted into the internal carotid artery (ICA) from the external carotid artery. Then, the suture was pushed until the tip reached the intracranial bifurcation of anterior cerebral artery and middle cerebral artery. The suture was pushed 1 mm further to perforate the vessel. The mice in the sham group underwent the same procedures except perforation. Since all procedures were performed on the left side, we collected the left hemisphere for all downstream experiments. Additionally, we assessed the degree of SAH *via* the grading system as previously described (Sugawara et al., 2008).

## Neurological Assessment

Modified Garcia test (range, 0–18) was used to assess the short-term neurological performance, by evaluating spontaneous activity, climbing, forelimb stretching, spontaneous movements of all limbs, body proprioception, and response to vibrissae touch (Shi et al., 2018).

## Adhesive Removal Test

To access the motor coordination and sensory neglect after SAH, adhesive test was performed following previous studies (Bouet et al., 2009). Small adhesive tape strips (2 mm × 3 mm) were applied to mice forepaws. Contact time and removal time were recorded with a maximum observation time of 120 s.

## Fluorescence-Activated Cell Sorting and Flow Cytometry

Mice were anesthetized with 40 mg/kg of pentobarbital sodium and transcardially perfused with ice-cold PBS. Brain tissues were obtained, and cerebrum was dissected and separated into ipsilateral and contralateral hemispheres. Ipsilateral hemispheres were mechanically dissociated using a razor blade and placed in a 15-ml conical tube with digestion solution [0.6 mg/ml of collagenase D (Sigma)]. Then, the mixture were incubated for 30 min at 37°C. After that, a 70-μm strainer was used to generate

a single-cell suspension (BD FALCON). Cells were isolated by centrifugation (30 min, 800 × *g* at 23°C) using 30–70% Percoll gradient solutions (GE Healthcare) (Agalave et al., 2020). Isolated cells were washed and resuspended in PBS with 0.01% bovine serum albumin (BSA) and then incubated with indicated anti-mouse antibodies for 30 min at 4°C [rat anti-mouse CD45 PerCP (BD Bioscience) and rat anti-mouse CD11b FITC (BD Bioscience)]. The population of microglia (CD45 positive and CD11b positive) was sorted.

In flow cytometry, rat anti-mouse Ly6G PE and rat anti-mouse Ly6C APC (BD Bioscience) antibodies were used and incubated with CD45 perCP and CD11b FITC.

## RNA Extraction and Sorted Microglia Sequencing

Total RNA from microglia sorted by FACS was isolated using TRIzol (Invitrogen, CA, United States) according to the manufacturer's protocol. The total RNA quantity and purity were checked by an Agilent 2100 bioanalyzer. High-quality samples (RIN number > 6.8) were used for downstream sequencing. Sequence libraries were constructed according to the standard SMART-seq protocol, and paired-end sequencing was performed with Illumina Novaseq 6000 (LC Bio) following the vendor's recommended protocol. Prior to assembly, low-quality reads that contain sequencing adaptors, sequencing primers, or low-quality nucleotides, were removed. The sequence quality was also checked with FastQC. HISAT was used to align and map reads to the UCSC[1] GRCm38 mouse reference genome. The mapped reads of each sample were assembled using StringTie. Then, all transcriptomes from the samples were merged to reconstruct a comprehensive transcriptome using perl scripts. After the final transcriptome was generated, StringTie and edgeR were used to estimate the expression levels of all transcripts. StringTie was used to perform expression level for mRNAs by calculating Fragment per Kilobase of transcript per Million mapped reads (FPKM). All raw sequence data have been uploaded to GSE167957.

## RNA-Seq Data Analysis

The expression matrixes were counter-checked to determine if there were any systematic errors or batch effects. The sva R package was used for identifying, estimating, and removing batch effects (Leek et al., 2012). The differentially expressed genes (DEGs) were selected with fold change > 2 or fold change < −2 and with statistical significance (Benjamini–Hochberg adjusted *p*-value < 0.01) by DESeq2 package (Love et al., 2014). FPKM were used for gene expression and were log2($x$ + 1) transformed. Principal components analysis (PCA) was performed on normalized counts. R package pheatmap was used to generate heatmap.

Functional enrichment analysis was conducted using *Metascape*[2] (Bhattacharya et al., 2018). All genes in mouse genome were used as background genes, and the default settings were used as enrichment criteria (minimum overlap = 3, *P*-value cutoff = 0.01, minimum enrichment score = 1.5). A gene ontology term was considered activated/increased with a *z*-score > 2 and a *p*-value < 0.01, and was predicted inhibited/decreased with a *z*-score < −2 and a *p*-value < 0.01.

Transcription factors (TFs) of selected DEGs were predicted using IRegulon plugin in Cytoscape (Janky et al., 2014). TFs were ranked by normalized enrichment score (NES), and NES > 3 was set as threshold.

The protein–protein interaction (PPI) network of selected DEGs was established using The Search Tool for the Retrieval of Interacting Genes (STRING[3]) (Szklarczyk et al., 2015) and then visualized in Cytoscape (Shannon et al., 2003). A combined score > 0.4 was set as a significant threshold. Furthermore, CytoHubba, a Cytoscape plugin, was used to explore hub genes in the constructed PPI network, and the top 10 genes were displayed based on degree method.

## Immunofluorescence Staining

Immunofluorescence staining was performed as described previously (Lu et al., 2019). In brief, mice were sacrificed and transcardially perfused with 0.9% NaCl, followed by 4% paraformaldehyde. Brain tissues were harvested and immersed in 4% paraformaldehyde for 24 h and then cryoprotected in 30% sucrose solution. Frozen serial coronal brain sections (9 μm) were prepared and fixed on slides. Slices were blocked with 5% donkey serum for 1 h and then incubated at 4°C overnight with primary antibodies, including goat anti-Iba1 antibody (1:500, Abcam, ab5076), rabbit anti-Tlr2 antibody (1:100, Abcam, ab209216), and mice anti-Irf7 antibody (1:200, Santa Cruz, sc-74471). After washing, the cryosections were incubated at 37°C for 1 h with the following secondary antibodies: donkey-anti-goat IgG(H + L) Alexa Fluor 594 (1:500, Thermo Fisher, A-11058), donkey-anti-rabbit IgG (H + L) Alexa Fluor 488 (1:500, Thermo Fisher, A-21206), and goat-anti-mouse IgG (H + L) Alexa Fluor 488 (1:500, Thermo Fisher, A-11001). Finally, the sections were observed and images were taken using an Olympus fluorescence microscope (Olympus Co., Japan).

## Statistical Analysis

RNA-seq data were analyzed as mentioned above. For other data, the statistical analyses were conducted using R software (version 3.6.3) and GraphPad Prism (version 8.0.2). Student's *t*-test and the Kruskal–Wallis test were employed in the two-group comparisons. A two-tailed *P*-value of <0.05 was considered statistically significant without specific annotation.

# RESULTS

## Microglia Lead to Poor Neurological Outcome in Acute Stage After SAH

At first, we induced SAH in adult C57BL/6 mice; the neurological scores and behavior tests were assessed in both SAH and sham group (**Figure 1A**). At 24 and 72 h after SAH, the average neurological scores were 11.714 ± 0.881

[1]http://genome.ucsc.edu/

[2]http://metascape.org/

[3]http://string-db.org/

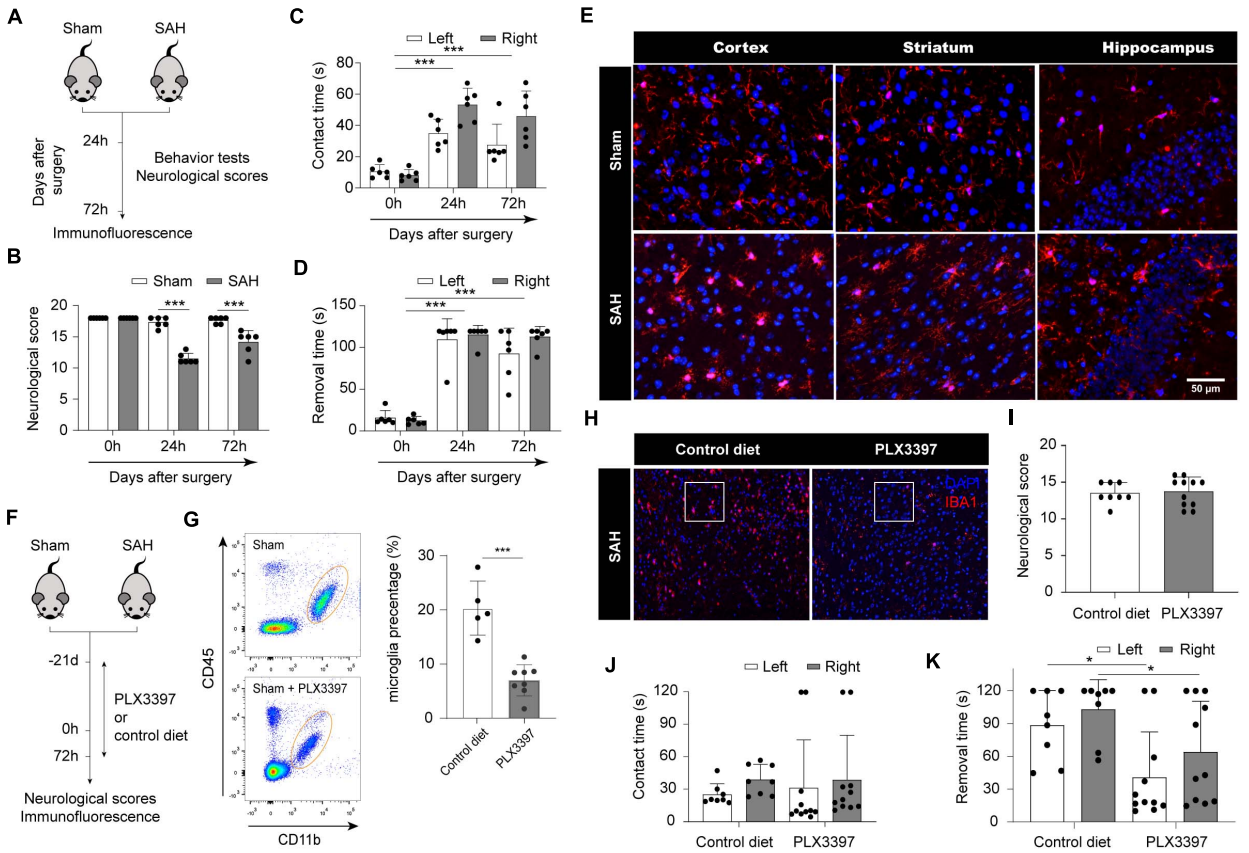


**FIGURE 1 |** Microglia lead to poor neurological outcome in acute stage after SAH. **(A)** Schematic diagram of experimental design. **(B)** Comparison of neurologic deficit scores among sham and SAH groups at 1 and 3 days after SAH. **(C,D)** Comparison of adhesive removal test results among sham and SAH groups at 1 and 3 days after SAH. **(E)** Immunofluorescence staining results of microglia in sham and SAH mice at 3 days after SAH, $n = 3$ per mice group. **(F)** Schematic diagram of microglia clearance. **(G)** Flow cytometry results proved that PLX3397 can clear microglia cells. **(H)** Immunofluorescence staining results of microglia in SAH mice fed with PLX3397 or control diet at 3 days after SAH. **(I)** Comparison of neurologic deficit scores among control diet and PLX3397 groups at 3 days after SAH. **(J,K)** Comparison of adhesive removal test results among control diet and PLX3397 groups at 3 days after SAH. SAH, subarachnoid hemorrhage; $^{*}P < 0.05$, $^{***}P < 0.001$.

and 14.167 ± 1.675, respectively. SAH mice showed worse neurological scores than the sham group ($p < 0.001$; **Figure 1B**). At 24 h after SAH, compared with the sham group, SAH mice showed significantly increased contact times and removal times, respectively ($p < 0.001$; **Figures 1C,D**). Similarly, at 72 h, increased contact times and removal times were observed in SAH mice compared to sham mice ($p < 0.001$; **Figures 1C,D**). Representative images of Iba1 staining in cortex, striatum, and hippocampus are shown in **Figure 1E**. Significant morphological changes, like larger bodies, thicker pseudopodia, and ameboid morphology, were displayed in SAH mice, indicating microglia activation at 72 h after SAH.

To examine whether microglia play a detrimental role in SAH, we administrated the CSF1R inhibitor PLX3397 or control diet in chow to deplete microglia (**Figure 1F**). The number of microglia ($CD45^{low}/CD11b^{+}$) was assessed through flow cytometry. Administration of PLX3397 to sham mice resulted in an 65% reduction in microglia compared to control mice ($p < 0.0001$; **Figure 1G**). Next, we induced SAH in mice pretreated with PLX3397 or control diet, and maintained their chow until sacrifice (**Figure 1F**). Immunofluorescence showed that the number of microglia in the PLX3397-fed group was significantly lower than the control diet group at 72 h after SAH (**Figure 1H**). PLX3397 treatment had no apparent effect on the neurological scores at 72 h after SAH (**Figure 1I**). In the adhesive removal test, there was no difference in average contact times between the PLX3397-fed group and the control diet group (**Figure 1J**). However, PLX3397-fed mice spent less time removing the tape at 72 h after SAH compared with the control diet group ($p < 0.05$; **Figure 1K**). Taken together, these data suggested that microglia were activated after SAH, and they may positively correlate with neurological dysfunction.

## SAH Induces Strong Transcriptomic Alterations in Microglia

To elucidate the functional roles of microglia after SAH, we used FACS to purify the microglia population ($CD45^{+}/CD11b^{+}$) from the brains of mice 72 h after SAH or sham operation. Sorted microglia cells were subjected to bulk RNA-seq (**Figure 2A**).

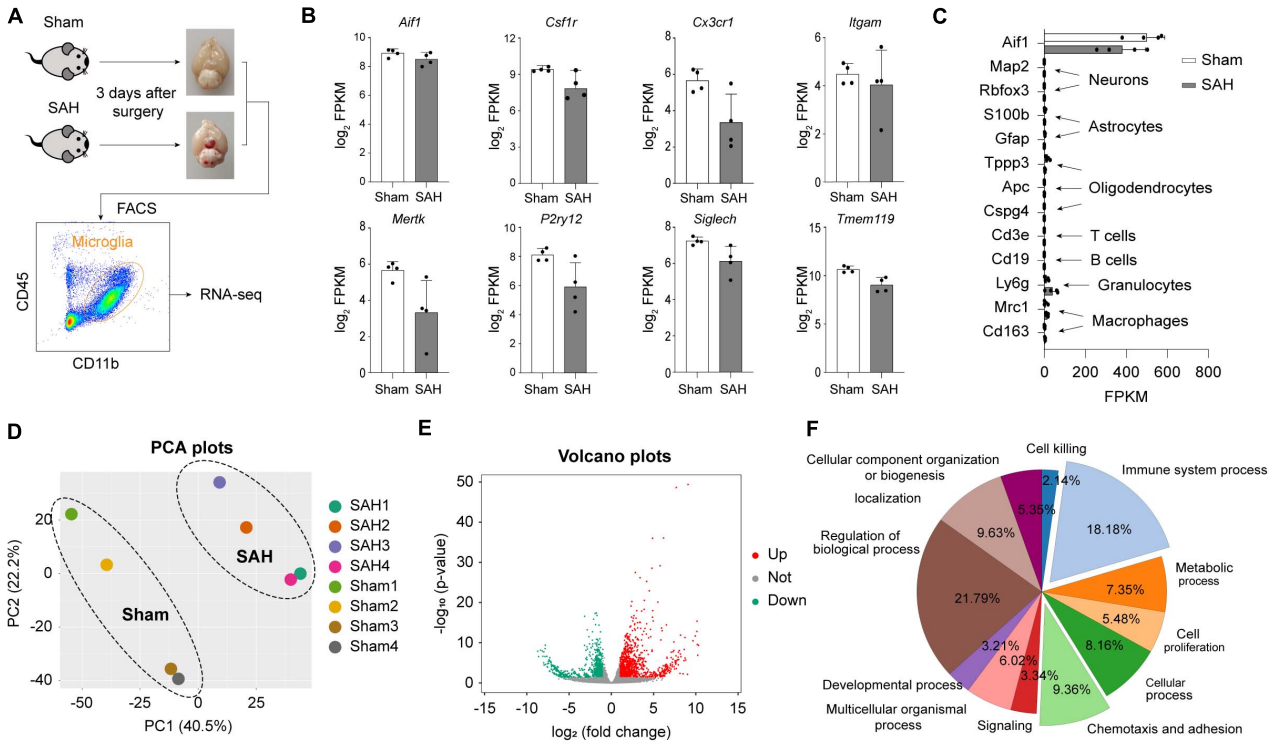


**FIGURE 2 |** Subarachnoid hemorrhage induces strong transcriptomic alterations in microglia. **(A)** Microglia cell sorting strategy. **(B)** mRNA expression levels of microglia marker genes. **(C)** mRNA expression levels of microglia (*Aif1*), neuron (*Map2, Rabfox3*), astrocyte (*S100b*, *Gfap*), ependymal cell (*Tppp3*), oligodendrocyte progenitor cells (*Apc*, *Cspg4*), T cell (*Cd3e*), B cell (*Cd19*), neutrophil (*Ly6g*), macrophage (*Mrc1*, *Cd163*), and marker genes. **(D)** PCA plots of microglia transcriptome sequencing results. **(E)** Volcano plots show the DEGs (fold change > 2 or <−2, adj_pval < 0.01) in microglia from SAH brain versus sham brain. **(F)** Shown are the percentages of significantly overrepresented GO terms. Twelve major clusters of functions were identified.

We confirmed the high expression level of microglial marker in FACS-sorted cells, such as *Itgam* (encoding CD11b), *Cx3cr1*, *Aif1* (encoding Iba1), *Csf1r*, *Mertk*, *Tmem119*, *Siglech*, and *P2ry12* (**Figure 2B**). The established markers of neurons (*Map2* and *Rbfox3*), astrocytes (*S100b* and *Gfap*), oligodendrocytes (*Tppp3, Apc*, and *Cspg4*), and other immune cells (*Cd3e, Cd19, Ly6g, Mrc1*, and *Cd163*) were all expressed at low level (**Figure 2C**). The result of PCA performed on RNA-seq data showed that samples in the same group clustered together, and samples in different groups separated clearly (**Figure 2D**), indicating robust transcriptomic differences between the SAH and Sham group.

Next, to determine the transcriptomic changes of microglia induced by SAH, differential expression analysis was performed. A total of 1576 genes were identified as DEGs (fold change > 2 or <−2, Benjamini–Hochberg adjusted *p*-value < 0.01), which contained 928 upregulated genes and 648 downregulated genes in post-SAH microglia compared with sham hemispheres (**Figure 2E** and **Supplementary Table 1**), indicating strong alterations of the genome (6.85% of total ∼23,000 genes). To elucidate the functional alterations in post-SAH microglia, pathway enrichment analysis was performed on the DEGs by an online tool *Metascape*. Regulation of biological process (21.79%), immune system process (18.18%), and chemotaxis and adhesion (9.36%) accounted for a major proportion of GO terms obtained from *Metascape* (**Figure 2F**). The top 20 clustered GO terms and specific GO terms obtained by *Metascape* are shown in **Supplementary Tables 2, 3**, respectively.

## Immune Response and Chemotaxis Were Activated in Post-SAH Microglia

We analyzed the biological processes related to *immune inflammatory responses* in microglia after SAH, and the Top 20 GO terms predicted to be activated (*z*-score > 2) are shown in **Figure 3A**. The inflammatory response, defense response, innate immune response, adaptive immune response, and neuroinflammatory response were all involved.

As chemotaxis was a large cluster that participates in immune inflammatory response, we further compared the pathways that related to cytokines and chemokines. 17 GO terms were exhibited in **Figure 3B**, all of them were predicted to be activated (*z*-score > 2). We also screened the expression level of a panel of cytokine and chemokine genes (Bhattacharya et al., 2018), and there were 17 significantly upregulated genes. The upregulated genes involved seven chemokine-encoding genes (*Cxcl1*, *Cxcl2*, *Cxcl3*, *Cxcl10*, *Cxcl11*, *Cxcl14*, and *Cxcl16*), and 10 cytokine-encoding genes, such as *Ccl6*, *Ccl9*, *Il1b*, *Il23a*, *Ifng*, *Il33*, and *Mif* (**Figure 3C**). These data indicated that a variety of pro-inflammatory cytokines and chemokines were released from post-SAH microglia, to recruit peripheral immune cells into

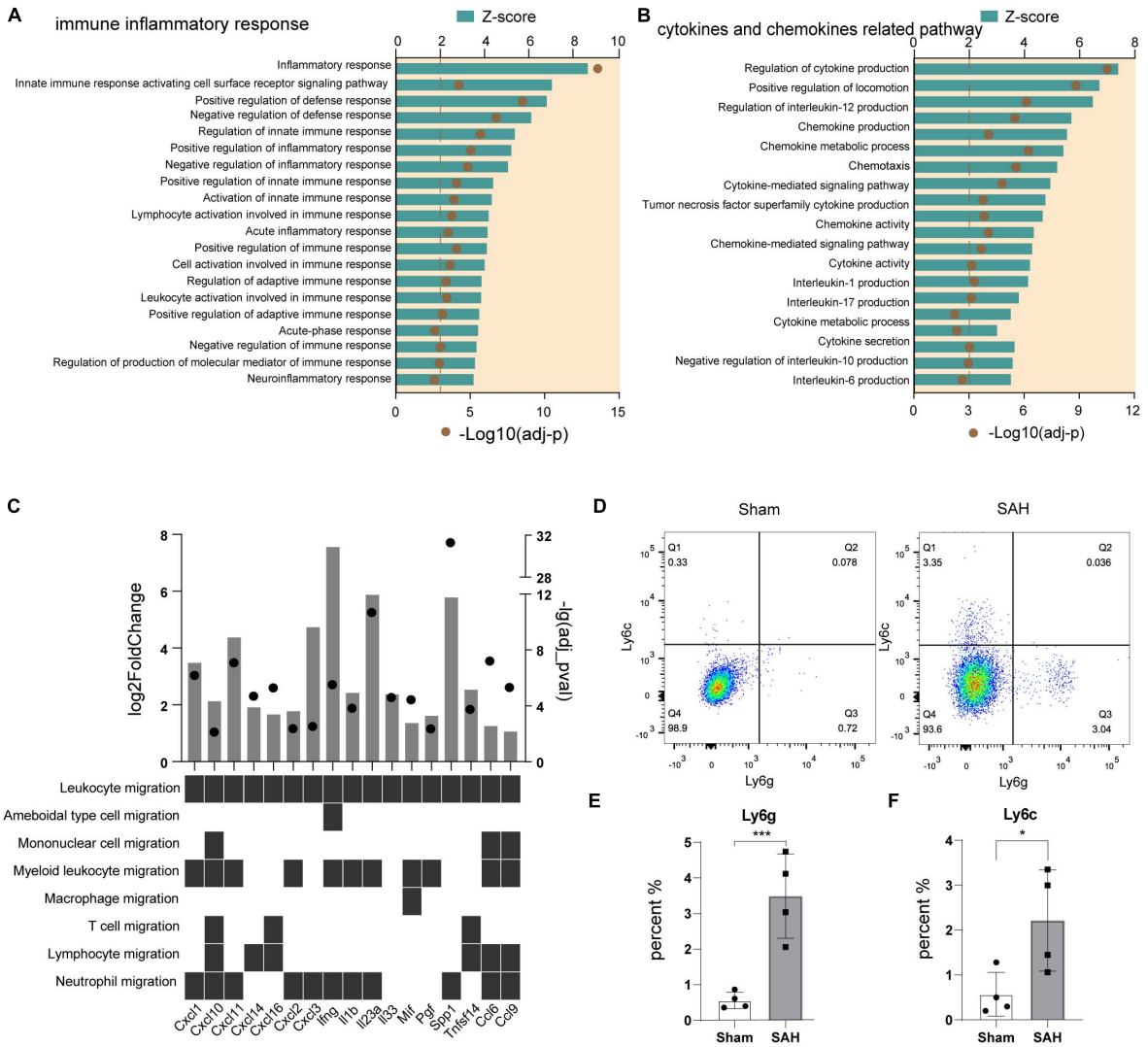


**FIGURE 3 |** Immune response and chemotaxis term were activated in post-SAH microglia. **(A)** GO enrichment analysis was performed by Metascape on all DEGs in sham and SAH microglia. Shown are the *z*-scores of biological functions on inflammatory and immune response-related pathways. **(B)** Shown are the *z*-scores of biological functions on cytokine and chemokine-related pathways. **(C)** Expression profiles of DEGs (fold change > 2, adj_pval < 0.01) in SAH microglia related to leukocyte recruitment pathways. **(D–F)** Flow cytometric analysis showed that the number of Ly6c+ and Ly6g+ cells increased after SAH, $n = 4$ per mice group. DEG, differentially expressed gene. $^{*}P < 0.05$, $^{***}P < 0.001$.

brain parenchyma, and it also suggested that myeloid cells were the main target of upregulated cytokines and chemokines (**Figure 3C**). Then, we detected the different populations of myeloid cells in ipsilateral hemispheres of SAH and sham mice by flow cytometry. Compared to sham mice, there were significant increases in the amount of infiltrating immune cells in post-SAH hemispheres, such as $CD45^{+}Ly6C^{+}Ly6G^{-}$ monocytes ($p < 0.01$) and $CD45^{+}Ly6C^{-}Ly6G^{+}$ neutrophils ($p < 0.05$) (**Figures 3D–F**).

## Irf7 Is a Master Regulator Involved in the Post-SAH Microglia

Next, we investigated the DEGs involved in cytokine- and chemokine-related pathways. These upregulated products could also be defined as receptors (e.g., TLR2), cytokines (e.g., IFNG and IL1B), and chemokines (e.g., CXCL1 and CXCL10). The top 15 genes, including *Ifng*, *Cxcl1*, *Cxcl10*, *Tlr2*, and *Il1b*, were associated with at least three functional subcategories of cytokine- and chemokine-related pathways (**Figure 4A**). In addition, we also screened out the genes that contribute multiple steps in immune inflammatory response, including inflammatory response, regulation of innate immune response, neuroinflammatory response, and so on (**Figure 4B**). The products of these genes predicted to be active included TFs (e.g., NR1H3 and IRF7), receptors on the membrane (e.g., CD40 and TLR2), nuclear receptor (e.g., PLSCR1), enzyme (e.g., DNASE1L3), and inflammatory-related proteins (e.g., ADAM8, RSAD2, and ZBP1).

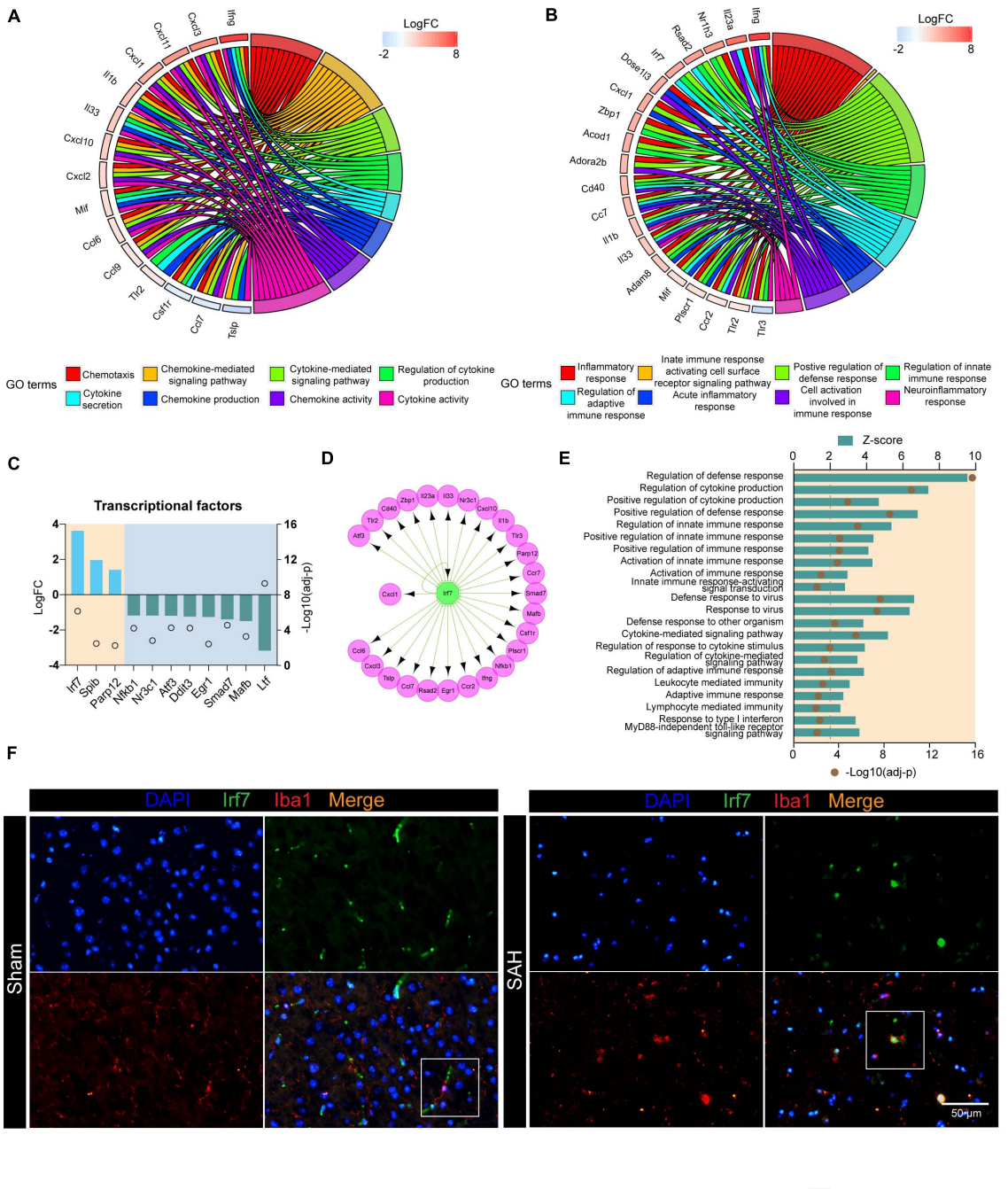


**FIGURE 4 |** Irf7 is a transcription factor involved in the post-SAH microglia. **(A)** Circular plot showed the DEGs involved in cytokine- and chemokine-related pathways. **(B)** Circular plot showed the DEGs involved in inflammatory and immune response-related pathways. **(C)** Expression profiles of differentially expressed transcriptional factors (fold change > 2, adj_pval < 0.01) in SAH microglia. **(D)** Regulatory network of *Irf7*. **(E)** Shown are the *z*-scores of biological functions that are correlated with *Irf7*. **(F)** Immunofluorescence staining results of Irf7 and Iba1 in sham and ICH mice, $n = 3$ per mice group. DEG, differentially expressed gene.

In order to investigate the upstream regulators of these biological processes, the interactions between all DEGs, which consisted of 985 nodes and 11,456 edges, were constructed based on STRING database (**Supplementary Table 5**). Then, the nodes related to high-frequency DEGs in **Figures 4A,B** were retrieved, out of which 11 unigenes were TFs (**Figure 4C**). In our dataset, the expression of *Irf7*, *Spib*, and *Parp12* were significantly upregulated, whereas *Nfkb1* was downregulated in post-SAH microglia. The upstream regulator analysis was performed by IRegulon, a plugin in Cytoscape. The top 10 potential TFs that target the selected DEGs are shown in **Table 1**. According to the transcriptional level and the

results from IRegulon, IRF7 was predicted to be a potent master regulator of the transcriptional processes related to *immune inflammatory response* and *chemotaxis*. In the TF target gene network, IRF7 was predicted to target 19 genes in the selected high-frequency DEGs (e.g., *Cd40*, *Il1b*, *Cxcl10*, and *Il23a*) (**Figure 4D**). Moreover, **Figure 4E** demonstrated that IRF7 involved a GO term that was predicted to be activated. Using dual immunofluorescence staining of Iba1 and IRF7, we confirmed that IRF7 expression was induced in microglia at 72 h after SAH (**Figure 4F**). IRF7 immunosignal was detected in the cortex from sham mice, while the IRF7 was hardly colocalized with Iba1.

## The TLR2/IRF7 Signaling Axis Potentially Mediates Neuroinflammation After SAH

Following SAH, microglia were activated to cope with the disruption of brain homeostasis. We examined the GO terms related to "cellular response" and found that response to stimulus (e.g., response to virus and response to external stimulus) and response to cytokines (e.g., response to interferon and response to macrophage colony-stimulating factor) were enriched in post-SAH microglia (**Figure 5A**). We also examined SAH-induced gene expression changes of receptor on the membrane in microglia (**Figure 5B**), most of which were upregulated (e.g., *Bst1*, *Gpnmb*, *Fgr*, and *Tlr2*). **Figure 5B** also showed that several receptors participated in microglia "cellular response," including response to external stimulus and response to interferon. Additionally, hub genes of the selected high-frequency genes were identified by CytoHubba, and the top 10 genes were calculated based on Degree algorithm (**Figure 5C** and **Supplementary Table 4**). All of the hub genes were upregulated except *Tlr3*, and *Irf7* was the only one identified as TF. In addition, *Tlr2* was also regarded as a hub gene, and the interaction between TLR2 and IRF7 indicates that the TLR2/IRF7 signaling axis may mediate the immune inflammatory response and chemotaxis in post-SAH microglia. Furthermore, immunostaining confirmed that the expression of TLR2 was elevated and colocalized with Iba1 in post-SAH brain (**Figure 5D**).

**TABLE 1 |** Top 10 transcription factors obtained by IRegulon.

| Transcription factor | NES | Target genes |
|---|---|---|
| *Irf8* | 8.7502 | *Parp12, Zbp1, Tlr3, Atf3, Cxcl10, Cd40, Ccr7, Irf7, Ccl6, Ccr2, Tlr2, Mafb, Egr1, Nr3c1, Il33, Tslp, Rsad2* |
| *Nfkb2* | 8.20316 | *Cxcl10, Egr1, Nfkb1, Cd40, Cxcl1, Il1b, Cxcl3, Tslp, Ccr7, Atf3, Cxcl2, Spib, Smad7, Plscr1, Il23a, Tlr2, Csf1r, Mafb, Il33* |
| *Irf7* | 6, 986 | *Atf3, Tlr2, Cd40, Zbp1, Il23a, Irf7, Il33, Nr3c1, Cxcl10, Il1b, Tlr3, Parp12, Ccr7, Smad7, Mafb, Csf1r, Plscr1, Nfkb1, Ifng, Ccr2, Egr1, Rsad2, Ccl6, Ccl7, Tslp, Cxcl3, Cxcl1* |
| *Homez* | 4.708 | *Nr3c1, Egr1, Smad7, Mafb, Atf3, Csf1r, Ccr7, Nfkb1* |
| *Cebpb* | 4.674 | *Atf3, Smad7, Il23a, Ltf, Ddit3, Spib, Il1b, Ccr7, Cxcl1, Cxcl3, Tslp, Nfkb1, Egr1, Zbp1, Nr3c1, Il33* |
| *Pbx1* | 4.529 | *Smad7, Egr1, Ccr7, Atf3, Nr3c1, Mafb, Cxcl1, Nfkb1, Il33, Ccr2, Ltf, Ifng, Irg1, Tslp, Parp12, Tlr2, Zbp1, Tlr3, Cxcl3* |
| *Yy1* | 4.118 | *Egr1, Nr3c1, Tlr2, Mafb, Smad7, Ccr2, Il23a, Atf3, Zbp1* |
| *Cebpa* | 4.080 | *Il23a, Ddit3, Atf3, Ccr2, Il1b* |
| *Tbx5* | 4.042 | *Cxcr3, Ddit3, Nfkb1, Irf7, Ccr7, Nr3c1, Smad7, Plscr1, Atf3* |
| *Scrt2* | 3.999 | *Nfkb1, Ccr7, Nr3c1, Irf7* |

## DISCUSSION

In this work, we presented, for the first time, genome-wide transcriptional analyses of microglia isolated from the brain at 72 h after SAH, compared with sham mice. The results demonstrated that (i) post-SAH microglia have robust transcriptomic changes that drive them into an activated state; (ii) transcriptional alteration contributes to SAH-induced neuroinflammation, especially the functional terms related to immune inflammatory response and chemotaxis; and (iii) the TLR2/IRF7 signaling axis may mediate the microglial activation.

Previous studies have reported that microglia contribute to both neuroinflammation and brain recovery, during the acute stage and recovery phase after stroke, respectively (Jiang et al., 2020; Xu et al., 2020). Elmore et al. (2014) found that microglia depletion by PLX3397 for either 21 days or 2 months does not affect learning, memory, motor function, or behavior in adult mice. Furthermore, the blood–brain barrier (BBB) remains intact in microglia-depleted mice (Elmore et al., 2014). However, other researchers claimed that microglia depletion could have unexpected effects, including increased pro- and anti-inflammatory cytokines, circadian system disruption, and increased BBB leakage under hypoxia condition (Miron and Priller, 2020; Sominsky et al., 2021; Yegla et al., 2021). In our study, pharmacological depletion of microglia using PLX3397 ameliorates short-term neurological deficits in post-SAH mice, and long-term neurological functions still need to be tested.

Since microglia are heterogeneous cells, many specific markers are pathologically decreased. However, the expression level of CD45 is increased in injury conditions (Plemel et al., 2020). Therefore, we choose $CD45^{+}CD11b^{+}$ to sort out microglia in this study.

We discovered dramatic transcriptomic changes between microglia in the post-SAH and sham mice. A total of 1576 DEGs were identified (6.85% of total ∼23,000 genes), including 928 upregulated DEGs and 648 downregulated DEGs. The functional enrichment analysis showed that biological processes related to inflammatory response were significantly enriched, including inflammatory response, regulation of defense response, chemotaxis, leukocyte migration, cytokine production, and chemokine production. Flow cytometry data examined the infiltration of neutrophils and monocytes into the cortex at 72 h after SAH. These results suggested that microglia switched to pro-inflammatory state at 72 h after SAH compared to sham mice. As expected, this finding is consistent with previous studies that showed increased pro-inflammatory cytokines after SAH

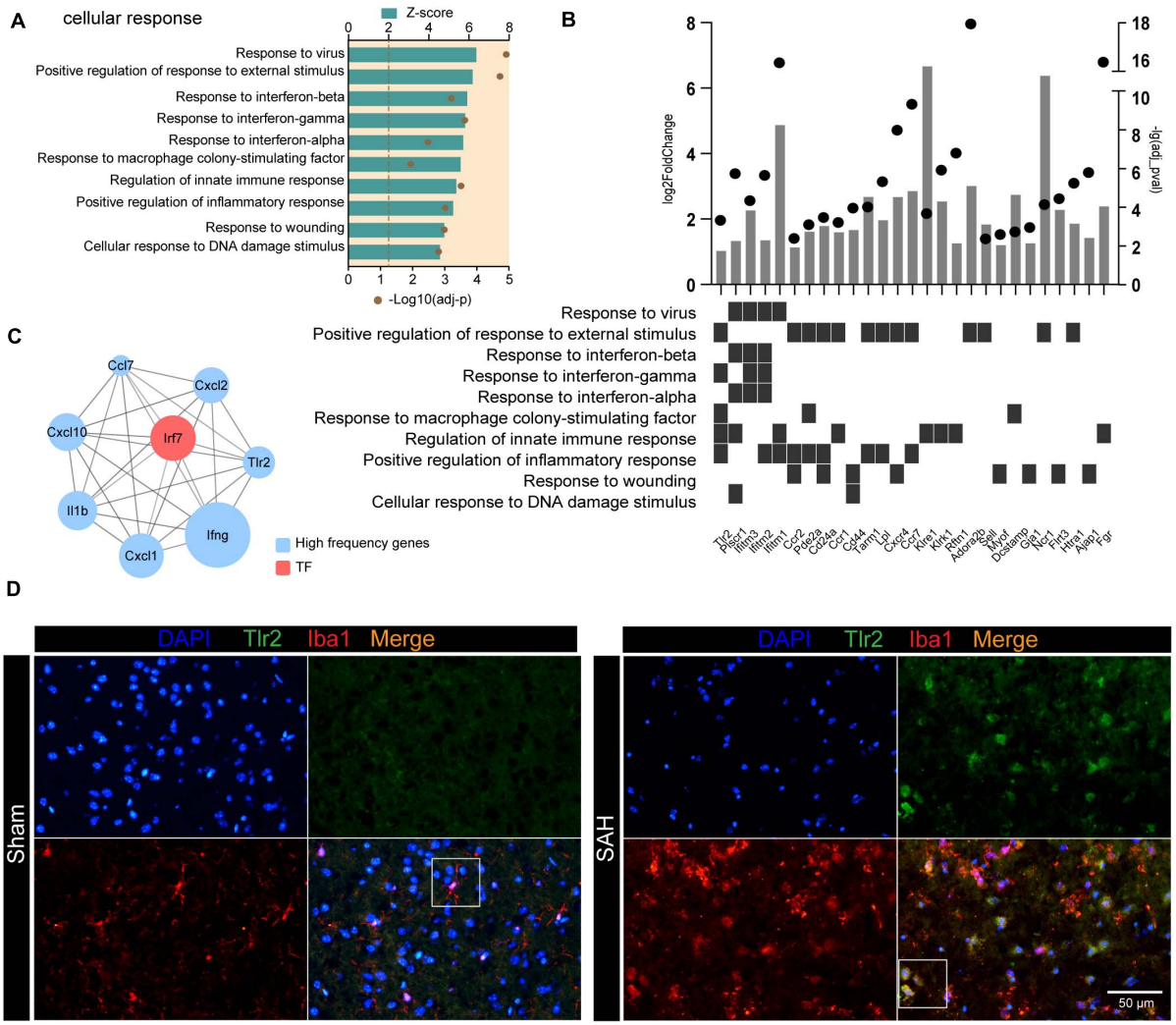


**FIGURE 5 |** TLR2/IRF7 signaling axis potentially mediates neuroinflammation after SAH. **(A)** GO enrichment analysis was performed by Metascape on all DEGs in sham and SAH microglia. Shown are the *z*-scores of biological functions on cell response-related pathways. **(B)** Expression profiles of DEGs (fold change > 2, adj_pval < 0.01) in SAH microglia related to cell response-related pathways. **(C)** Top 10 hub genes identified by CytoHubba. **(D)** Immunofluorescence staining results of Tlr2 and Iba1 in sham and SAH mice, $n = 3$ per mice group. DEG, differentially expressed gene.

(Zheng et al., 2020). However, the underlying mechanisms of these processes remain elusive.

IRF7, as a TF, mainly plays a role in interferon production pathway. IRF7 is also involved in apoptosis and TLR4 pathway. According to the analysis conducted by IRegulon, IRF7 was predicted to be a master regulator whose targets are involved in immune response and cytokine production (e.g., *Cd40*, *Il1b*, *Cxcl10*, *Ifng*, *Ccl6*, *Il33*, and *Tlr2*). Besides, *Irf7* was also predicted to be a hub gene mediating inflammatory response and chemokines. We examined the protein expression level of IRF7 in post-SAH microglia. Some of these effects have been previously reported. Sin et al. (2020) reported that IRF7 promotes IL-1β production. CXCL10 production is IRF7-dependent in macrophages (Tsiantoulas et al., 2018). IRF7 also participates in monocyte differentiation and other inflammatory cytokine production (e.g., TNF-α, IL6, CCL2, and IL33) (Ning et al., 2011; Sun et al., 2014; Simons et al., 2019). Tanaka et al. (2015) demonstrated that the expression level of IRF7 increased during the M2 to M1-like switch in microglia. However, another study found that Irf7 expression induced by spinal cord injury reduced microglial pro-inflammatory activity (Cohen et al., 2014).

Toll-like receptor 2 (TLR2), a member of the TLR family, recognizes PAMPs and DAMPs, leading to upregulation of signaling pathways to modulate inflammatory response (Lalancette-Hebert et al., 2017). We observed an increasing expression level of *Tlr2* in microglia at 72 h after SAH, and it participated in biological processes, such as the cellular response to interferon, response to external stimulus, defense response, inflammatory response, cytokine production, and chemotaxis. According to the results from CytoHubba, *Tlr2* was confirmed as a hub gene in activating immune inflammatory response and pathways related to cytokines and chemokines. Consistent

with the results of the present study, Jiang et al. (2020) have reported an elevated expression level of *Tlr2* in microglia purified from post-ischemic stroke mice. Mottahedin et al. (2019) and Deng et al. (2020) have demonstrated that TLR2 participates in microglia activation and peripheral immune cell infiltration in ischemic stroke. Administration of the inhibitor targeting TLR2 decreased the release of pro-inflammatory cytokines (Wang et al., 2020).

According to the results from the PPI network and CytoHubba calculation, we identified the TLR2/IRF7 signaling axis that potentially mediates an inflammatory response in microglia after SAH. As previous studies reported, TLR2 activation induces IFN *via* IRF7, leading to CXCL10 production (Dietrich et al., 2010).

Several limitations of our study should be noted. Firstly, bulk RNA-seq was performed on the sorted cells, which measured the average expression level in a sample, thus limiting us to distinguish the subpopulations of cells within each sample. Combining bulk RNA-seq with single-cell RNA-seq technology may help to improve this problem. Secondly, because microglia are heterogeneous, it is hard to distinguish them from infiltration macrophages and perivascular macrophages, and more specific markers should be considered to refine our FACS strategy. Thirdly, we obtained the data from a single time point (3 days) after SAH, because the number of microglia reached the maximum at 72 h (Xu et al., 2019). However, 24 h after SAH is a critical time point to investigate microglial activation, and further studies should expand the time window to confirm the protein expression levels and investigate microglia transcriptional profiles at different time points. Fourthly, the verification of the TLR2/IRF7 signaling axis is limited; *in vivo* and *in vitro* functional/mechanical experiments should be conducted in further studies.

In summary, we report that microglia at 72 h after SAH harbor robust transcriptional changes compared to sham mice. The alteration in post-SAH microglia genes may contribute to immune inflammatory response, cytokine and chemokine production, and chemotaxis, which then lead to a poor outcome. The TLR2/IRF7 signaling axis is considered to be capable of regulating neuroinflammatory processes after SAH. Based on these findings, further investigation targeting the TLR2/IRF7 axis may help to improve the outcome of SAH patients.

## DATA AVAILABILITY STATEMENT

The datasets generated for this study can be found in online repositories. The names of the repository/repositories and accession number(s) can be found below: https://www.ncbi.nlm.nih.gov/geo/query/acc.cgi?acc=GSE167957.

## ETHICS STATEMENT

The animal study was reviewed and approved by Institutional Ethics Committee of the Second Affiliated Hospital, Zhejiang University School of Medicine.

## AUTHOR CONTRIBUTIONS

SX, SM, and JL drafted the manuscript. HW and XD reviewed and modified the manuscript. LS, JYZ, and JMZ revised the manuscript. All authors agreed on the final version.

## FUNDING

This work was supported by grants from the Key Program of Science and Technology Development of Zhejiang Province (2017C03021), the Zhejiang Provincial Natural Science Foundation of China (LQ17H090003), and the National Natural Science Foundation of China (81870916 and 82071287).

## SUPPLEMENTARY MATERIAL

The Supplementary Material for this article can be found online at: https://www.frontiersin.org/articles/10.3389/fnagi.2021.645649/full#supplementary-material

## REFERENCES

Agalave, N. M., Lane, B. T., Mody, P. H., Szabo-Pardi, T. A., and Burton, M. D. (2020). Isolation, culture, and downstream characterization of primary microglia and astrocytes from adult rodent brain and spinal cord. *J. Neurosci. Methods* 340:108742. doi: 10.1016/j.jneumeth.2020.108742

Amodio, S., Bouzat, P., Robba, C., and Taccone, F. S. (2020). Rethinking brain injury after subarachnoid hemorrhage. *Crit. Care* 24:612.

Barbalat, R., Lau, L., Locksley, R. M., and Barton, G. M. (2009). Toll-like receptor 2 on inflammatory monocytes induces type I interferon in response to viral but not bacterial ligands. *Nat. Immunol.* 10, 1200–1207. doi: 10.1038/ni.1792

Bhattacharya, S., Dunn, P., Thomas, C. G., Smith, B., Schaefer, H., Chen, J., et al. (2018). ImmPort, toward repurposing of open access immunological assay data for translational and clinical research. *Sci. Data* 5:180015.

Bouet, V., Boulouard, M., Toutain, J., Divoux, D., Bernaudin, M., Schumann-Bard, P., et al. (2009). The adhesive removal test: a sensitive method to assess sensorimotor deficits in mice. *Nat. Protoc.* 4, 1560–1564. doi: 10.1038/nprot.2009.125

Chang, C. Z., Wu, S. C., and Kwan, A. L. (2014). Glycyrrhizin attenuates toll like receptor-2, -4 and experimental vasospasm in a rat model. *J. Immunol. Res.* 2014:740549.

Chang, C. Z., Wu, S. C., and Kwan, A. L. (2015). A purine antimetabolite attenuates toll-like receptor-2, -4, and subarachnoid hemorrhage-induced brain apoptosis. *J. Surg. Res.* 199, 676–687. doi: 10.1016/j.jss.2015.06.011

Cohen, M., Matcovitch, O., David, E., Barnett-Itzhaki, Z., Keren-Shaul, H., Blecher-Gonen, R., et al. (2014). Chronic exposure to TGFbeta1 regulates myeloid cell inflammatory response in an IRF7-dependent manner. *EMBO J.* 33, 2906–2921. doi: 10.15252/embj.201489293

Deng, W., Mandeville, E., Terasaki, Y., Li, W., Holder, J., Chuang, A. T., et al. (2020). Transcriptomic characterization of microglia activation in a rat model of ischemic stroke. *J. Cereb. Blood Flow Metab.* 40, S34–S48.

Dietrich, N., Lienenklaus, S., Weiss, S., and Gekara, N. O. (2010). Murine toll-like receptor 2 activation induces type I interferon responses from endolysosomal compartments. *PLoS One* 5:e10250. doi: 10.1371/journal.pone.0010250

Elmore, M. R., Najafi, A. R., Koike, M. A., Dagher, N. N., Spangenberg, E. E., Rice, R. A., et al. (2014). Colony-stimulating factor 1 receptor signaling is necessary

for microglia viability, unmasking a microglia progenitor cell in the adult brain. *Neuron* 82, 380–397. doi: 10.1016/j.neuron.2014.02.040

Fujii, M., Yan, J., Rolland, W. B., Soejima, Y., Caner, B., and Zhang, J. H. (2013). Early brain injury, an evolving frontier in subarachnoid hemorrhage research. *Transl. Stroke Res.* 4, 432–446. doi: 10.1007/s12975-013-0257-2

Janky, R., Verfaillie, A., Imrichova, H., Van de Sande, B., Standaert, L., Christiaens, V., et al. (2014). iRegulon: from a gene list to a gene regulatory network using large motif and track collections. *PLoS Comput. Biol.* 10:e1003731. doi: 10.1371/journal.pcbi.1003731

Jiang, L., Mu, H., Xu, F., Xie, D., Su, W., Xu, J., et al. (2020). Transcriptomic and functional studies reveal undermined chemotactic and angiostimulatory properties of aged microglia during stroke recovery. *J. Cereb. Blood Flow Metab.* 40, S81–S97.

Lalancette-Hebert, M., Faustino, J., Thammisetty, S. S., Chip, S., Vexler, Z. S., and Kriz, J. (2017). Live imaging of the innate immune response in neonates reveals differential TLR2 dependent activation patterns in sterile inflammation and infection. *Brain Behav. Immun.* 65, 312–327. doi: 10.1016/j.bbi.2017.05.020

Leek, J. T., Johnson, W. E., Parker, H. S., Jaffe, A. E., and Storey, J. D. (2012). The sva package for removing batch effects and other unwanted variation in high-throughput experiments. *Bioinformatics* 28, 882–883. doi: 10.1093/bioinformatics/bts034

Liu, W., Li, R., Yin, J., Guo, S., Chen, Y., Fan, H., et al. (2019). Mesenchymal stem cells alleviate the early brain injury of subarachnoid hemorrhage partly by suppression of Notch1-dependent neuroinflammation: involvement of Botch. *J. Neuroinflamm.* 16:8.

Love, M. I., Huber, W., and Anders, S. (2014). Moderated estimation of fold change and dispersion for RNA-seq data with DESeq2. *Genome Biol.* 15:550.

Lu, J., Sun, Z., Fang, Y., Zheng, J., Xu, S., Xu, W., et al. (2019). Melatonin suppresses microglial necroptosis by regulating deubiquitinating enzyme A20 after intracerebral hemorrhage. *Front. Immunol.* 10:1360. doi: 10.3389/fimmu.2019.01360

Macdonald, R. L., and Schweizer, T. A. (2017). Spontaneous subarachnoid haemorrhage. *Lancet* 389, 655–666.

Miron, V. E., and Priller, J. (2020). Investigating microglia in health and disease: challenges and opportunities. *Trends Immunol.* 41, 785–793. doi: 10.1016/j.it.2020.07.002

Mottahedin, A., Joakim, E. K. C., Truve, K., Hagberg, H., and Mallard, C. (2019). Choroid plexus transcriptome and ultrastructure analysis reveals a TLR2-specific chemotaxis signature and cytoskeleton remodeling in leukocyte trafficking. *Brain Behav. Immun.* 79, 216–227. doi: 10.1016/j.bbi.2019.02.004

Muroi, C., Fujioka, M., Marbacher, S., Fandino, J., Keller, E., Iwasaki, K., et al. (2015). Mouse model of subarachnoid hemorrhage: technical note on the filament perforation model. *Acta Neurochir. Suppl.* 120, 315–320. doi: 10.1007/978-3-319-04981-6_54

Najafi, A. R., Crapser, J., Jiang, S., Ng, W., Mortazavi, A., West, B. L., et al. (2018). A limited capacity for microglial repopulation in the adult brain. *Glia* 66, 2385–2396. doi: 10.1002/glia.23477

Ning, S., Pagano, J. S., and Barber, G. N. (2011). IRF7: activation, regulation, modification and function. *Genes Immun.* 12, 399–414. doi: 10.1038/gene.2011.21

Plemel, J. R., Stratton, J. A., Michaels, N. J., Rawji, K. S., Zhang, E., Sinha, S., et al. (2020). Microglia response following acute demyelination is heterogeneous and limits infiltrating macrophage dispersion. *Sci. Adv.* 6:eaay6324. doi: 10.1126/sciadv.aay6324

Rass, V., and Helbok, R. (2019). Early brain injury after poor-grade subarachnoid hemorrhage. *Curr. Neurol. Neurosci. Rep.* 19:78.

Rayasam, A., Faustino, J., Lecuyer, M., and Vexler, Z. S. (2020). Neonatal stroke and TLR1/2 ligand recruit myeloid cells through the choroid plexus in a CX3CR1-CCR2- and context-specific manner. *J. Neurosci.* 40, 3849–3861. doi: 10.1523/jneurosci.2149-19.2020

Schallner, N., Pandit, R., LeBlanc, R. III, Thomas, A. J., Ogilvy, C. S., Zuckerbraun, B. S., et al. (2015). Microglia regulate blood clearance in subarachnoid hemorrhage by heme oxygenase-1. *J. Clin. Invest.* 125, 2609–2625. doi: 10.1172/jci78443

Schneider, U. C., Davids, A. M., Brandenburg, S., Muller, A., Elke, A., Magrini, S., et al. (2015). Microglia inflict delayed brain injury after subarachnoid hemorrhage. *Acta Neuropathol.* 130, 215–231. doi: 10.1007/s00401-015-1440-1

Shannon, P., Markiel, A., Ozier, O., Baliga, N. S., Wang, J. T., Ramage, D., et al. (2003). Cytoscape: a software environment for integrated models of biomolecular interaction networks. *Genome Res.* 13, 2498–2504. doi: 10.1101/gr.1239303

Shi, L., Liang, F., Zheng, J., Zhou, K., Chen, S., Yu, J., et al. (2018). Melatonin regulates apoptosis and autophagy via ROS-MST1 pathway in subarachnoid hemorrhage. *Front. Mol. Neurosci.* 11:93. doi: 10.3389/fnmol.2018.00093

Simons, K. H., de Vries, M. R., de Jong, R. C. M., Peters, H. A. B., Jukema, J. W., and Quax, P. H. A. (2019). IRF3 and IRF7 mediate neovascularization via inflammatory cytokines. *J. Cell Mol. Med.* 23, 3888–3896. doi: 10.1111/jcmm.14247

Sin, W. X., Yeong, J. P., Lim, T. J. F., Su, I. H., Connolly, J. E., and Chin, K. C. (2020). IRF-7 mediates Type I IFN responses in Endotoxin-challenged mice. *Front. Immunol.* 11:640. doi: 10.3389/fimmu.2020.00640

Sokol, B., Wasik, N., Jankowski, R., Holysz, M., Wieckowska, B., and Jagodzinski, P. (2016). Soluble Toll-Like receptors 2 and 4 in cerebrospinal fluid of patients with acute hydrocephalus following aneurysmal subarachnoid haemorrhage. *PLoS One* 11:e0156171. doi: 10.1371/journal.pone.0156171

Sominsky, L., Dangel, T., Malik, S., De Luca, S. N., Singewald, N., and Spencer, S. J. (2021). Microglial ablation in rats disrupts the circadian system. *FASEB J.* 35:e21195.

Soulet, D., and Rivest, S. (2008). Microglia. *Curr. Biol.* 18, R506–R508.

Sugawara, T., Ayer, R., Jadhav, V., and Zhang, J. H. (2008). A new grading system evaluating bleeding scale in filament perforation subarachnoid hemorrhage rat model. *J. Neurosci. Methods* 167, 327–334. doi: 10.1016/j.jneumeth.2007.08.004

Sun, L., Zhu, Z., Cheng, N., Yan, Q., and Ye, R. D. (2014). Serum amyloid A induces interleukin-33 expression through an IRF7-dependent pathway. *Eur. J. Immunol.* 44, 2153–2164. doi: 10.1002/eji.201344310

Szklarczyk, D., Franceschini, A., Wyder, S., Forslund, K., Heller, D., Huerta-Cepas, J., et al. (2015). STRING v10: protein-protein interaction networks, integrated over the tree of life. *Nucleic Acids Res.* 43, D447–D452.

Tanaka, T., Murakami, K., Bando, Y., and Yoshida, S. (2015). Interferon regulatory factor 7 participates in the M1-like microglial polarization switch. *Glia* 63, 595–610. doi: 10.1002/glia.22770

Tsiantoulas, D., Sage, A. P., Goderle, L., Ozsvar-Kozma, M., Murphy, D., Porsch, F., et al. (2018). B Cell-activating factor neutralization aggravates atherosclerosis. *Circulation* 138, 2263–2273. doi: 10.1161/circulationaha.117.032790

Wang, X., Tian, S., Wang, H., Liu, P., Zheng, H., Wu, L., et al. (2020). Botulinum toxin type A alleviates neuropathic pain and suppresses inflammatory cytokines release from microglia by targeting TLR2/MyD88 and SNAP23. *Cell Biosci.* 10:141.

Xu, W., Mo, J., Ocak, U., Travis, Z. D., Enkhjargal, B., Zhang, T., et al. (2020). Activation of Melanocortin 1 receptor attenuates early brain injury in a rat model of subarachnoid hemorrhage viathe suppression of neuroinflammation through AMPK/TBK1/NF-kappaB pathway in rats. *Neurotherapeutics* 17, 294–308. doi: 10.1007/s13311-019-00772-x

Xu, Z., Shi, W. H., Xu, L. B., Shao, M. F., Chen, Z. P., Zhu, G. C., et al. (2019). Resident Microglia activate before peripheral Monocyte infiltration and p75NTR blockade reduces microglial activation and early brain injury after subarachnoid hemorrhage. *ACS Chem. Neurosci.* 10, 412–423. doi: 10.1021/acschemneuro.8b00298

Yegla, B., Boles, J., Kumar, A., and Foster, T. C. (2021). Partial microglial depletion is associated with impaired hippocampal synaptic and cognitive function in young and aged rats. *Glia* 69, 1494–1514. doi: 10.1002/glia.23975

Zheng, Z. V., Lyu, H., Lam, S. Y. E., Lam, P. K., Poon, W. S., and Wong, G. K. C. (2020). The dynamics of Microglial polarization reveal the resident neuroinflammatory responses after subarachnoid hemorrhage. *Transl. Stroke Res.* 11, 433–449. doi: 10.1007/s12975-019-00728-5

**Conflict of Interest:** The authors declare that the research was conducted in the absence of any commercial or financial relationships that could be construed as a potential conflict of interest.

frontiers in Aging Neuroscience

ORIGINAL RESEARCH
published: 02 July 2021
doi: 10.3389/fnagi.2021.681998

# The Effect of Preoperative Antiplatelet Therapy on Early Postoperative Rehemorrhage and Outcomes in Patients With Spontaneous Intracranial Hematoma

*Junhua Yang[1,2,3,4], Qingyuan Liu[1,2,3,4], Shaohua Mo[1,2,3,4], Kaiwen Wang[1,2,3,4], Maogui Li[1,2,3,4], Jun Wu[1,2,3,4], Pengjun Jiang[1,2,3,4], Shuzhe Yang[1,2,3,4], Rui Guo[1,2,3,4], Yi Yang[1,2,3,4], Jiaming Zhang[1,2,3,4], Yang Liu[1,2,3,4], Yong Cao[1,2,3,4] and Shuo Wang[1,2,3,4]**

[1] Department of Neurosurgery, Beijing Tiantan Hospital, Capital Medical University, Beijing, China, [2] China National Clinical Research Center for Neurological Diseases, Beijing, China, [3] Center of Stroke, Beijing Institute for Brain Disorders, Beijing, China, [4] Beijing Key Laboratory of Translational Medicine for Cerebrovascular Disease, Beijing, China

OPEN ACCESS

**Edited by:**
Aurel Popa-Wagner,
University of Medicine and Pharmacy of Craiova, Romania

**Reviewed by:**
Archana Hinduja,
The Ohio State University, United States
Zhouping Tang,
Huazhong University of Science and Technology, China
Mehmet Akif Topçuoğlu,
Hacettepe University, Turkey

***Correspondence:**
Shuo Wang
captain9858@126.com

**Received:** 17 March 2021
**Accepted:** 31 May 2021
**Published:** 02 July 2021

**Citation:**
Yang J, Liu Q, Mo S, Wang K, Li M, Wu J, Jiang P, Yang S, Guo R, Yang Y, Zhang J, Liu Y, Cao Y and Wang S (2021) The Effect of Preoperative Antiplatelet Therapy on Early Postoperative Rehemorrhage and Outcomes in Patients With Spontaneous Intracranial Hematoma. Front. Aging Neurosci. 13:681998. doi: 10.3389/fnagi.2021.681998

**Background and Purpose:** The effect of antiplatelet therapy (APT) on early postoperative rehemorrhage and outcomes of patients with spontaneous intracerebral hemorrhage (ICH) is still unclear. This study is to evaluate the effect of preoperative APT on early postoperative rehemorrhage and outcomes in ICH patients.

**Methods:** This was a multicenter cohort study. ICH patients undergoing surgery were divided into APT group and no antiplatelet therapy (nAPT) group according to whether patients received APT or not. Chi-square test, *t*-test, and Mann–Whitney *U* test were used to compare the differences in variables, postoperative rehematoma, and outcomes between groups. Multivariate logistics regression analysis was used to correct for confounding variables, which were different in group comparison.

**Results:** One hundred fifty ICH patients undergoing surgical treatment were consecutively included in this study. Thirty five (23.33%) people were included in the APT group, while 115 (76.67%) people were included in the nAPT group. The incidence of early postoperative rehemorrhage in the APT group was significantly higher than that in the nAPT group (25.7% VS 10.4%, $p = 0.047 < 0.05$). After adjustment for age, ischemic stroke history, and ventricular hematoma, preoperative APT had no significant effect on early postoperative rehemorrhage ($p = 0.067$). There was no statistical difference between the two groups in early poorer outcomes ($p = 0.222$) at 14 days after surgery. After adjustment for age, ischemic stroke history, and ventricular hematoma, preoperative APT also had no significant effect on early poorer modified Rankin Scale (mRS) ($p = 0.072$).

**Conclusion:** In conclusion, preoperative APT appears to be safe and have no significant effect on early postoperative rehematoma and outcomes in ICH patients.

**Keywords: spontaneous intracranial hematoma, stroke, surgery, antiplatelet, complications**

## INTRODUCTION

The incidence of spontaneous intracranial hemorrhage (ICH) increases with age (An et al., 2017). According to reports (Cordonnier et al., 2018; Luzzi et al., 2019), the mortality rate of ICH can be as high as 50%. Although there is no specific treatment for ICH patients, emergency surgery may reduce the mortality rate of ICH patients (Wu et al., 2020). Surgical methods mainly include craniectomy with hematoma evacuation, endoscopic surgery, minimally invasive puncture, and thrombolysis (Luzzi et al., 2019). These procedures can effectively reduce the intracranial pressure and hematoma volume of ICH patients (Luzzi et al., 2019; Wu et al., 2020). However, surviving ICH patients may be at risk of postoperative complications, especially postoperative rehemorrhage, which may seriously affect the prognosis of patients (Yu et al., 2016).

According to report, antiplatelet therapy (APT) is widely used in neurosurgery patients at the time of consultation (Fiaschi et al., 2020). Although the impact of APT on tumor patients can be reduced by delaying surgery (Rahman et al., 2015), patients with ICH usually do not have enough time to completely eliminate the impact of APT before surgery. Previous studies mainly focused on the effect of APT on hematoma volume or hematoma expansion in ICH patients (Sansing et al., 2009; Khan et al., 2017). The evidence for the effect of preoperative APT on early postoperative rehemorrhage and prognosis of ICH patients is still insufficient.

Thus, to evaluate the impact of APT on early postoperative rehemorrhage and outcomes in ICH patients, we designed this cohort study.

## MATERIALS AND METHODS

This was a multicenter cohort study that has been registered on the website of the Chinese Clinical Trial Registry (trial registration number: ChiCTR1900024406)[1] and has received the support of the Institutional Review Board of Beijing Tiantan Hospital, Capital Medical University (reference number: KY2019-096-02).

### Study Population

The population of the current study was consecutively enrolled from a retrospective and a prospective ICH cohort according the inclusion and exclusion criteria. Patients in the retrospective cohort were those who received surgical treatment in Beijing Tiantan Hospital, Capital Medical University between January 1, 2015 and July 31,2019, while patients in prospective cohort were those who received surgical treatment in Beijing Tiantan Hospital, Beijing Chaoyang Hospital, Beijing Friendship Hospital, Beijing Anzhen Hospital, Beijing Shunyi District Hospital, Beijing Pinggu District Hospital, or Guangzhou Red Cross Hospital between August 1, 2019 and December 31, 2019. All patients' informed consent forms were signed by themselves or their family members.

[1]http://www.chictr.org.cn/

### Inclusion and Exclusion Criteria

Inclusion criteria were as follows: (1) patients older than 18 years old, (2) patients diagnosed as ICH, and (3) patients received surgery treatment within 7 days after the onset of symptoms.

Exclusion criteria were as follows: (1) ICH caused by secondary causes such as trauma, tumor, moyamoya disease, aneurysm, venous thrombosis, cerebral ischemic infarction, etc.; (2) patients accompanied by primary and secondary coagulopathy; (3) patients accompanied by malignant tumor or liver or renal dysfunction; (4) patients receiving any form of anticoagulation therapy within 7 days before surgery; (5) patients with incomplete clinical data; and (6) patients without informed consent.

### Surgery

All ICH patients in this study received standard care in accordance with guidelines (Hemphill et al., 2015) and received craniotomy, endoscopic, or minimally invasive surgery to remove hematoma within 7 days after the onset of symptoms. Two or three experienced neurosurgeons jointly decided on the surgical plan and performed the operation. The selection of surgical methods has been described in our previous reports (Wu et al., 2020), and the surgical indications included supratentorial hematoma greater than 30 ml, subtentorial hematoma greater than 10 ml, midline displacement larger than 1 cm, and brain herniation. In addition, APT before the onset of ICH was not considered an absolute contraindication to surgery. However, the patients with insufficient platelet count or decreased platelet activity may be treated with platelet transfusion. After operation, the first follow-up computerized tomography (CT) scan was routinely performed in 24 h. Then, follow-up CTs were performed every 2–3 days or when patients had new neurological symptoms.

### Data Collection

The collected characteristics of ICH patients included (1) demographic characteristics, such as patients' age and gender; (2) vascular risk factors, such as patients' history of smoking and alcohol; (3) medical history, such as patients' history of hypertension, diabetes, coronary heart disease, ischemic stroke, cerebral hemorrhage, and antiplatelet agent types (including aspirin, clopidogrel, or aspirin plus clopidogrel); (4) radiography characteristics analyzed by three neurosurgeons who were blinded to the information of enrolled patients, such as hematoma side, localization (the basal ganglia, thalamus, internal capsule, brain stem, and cerebellum were defined as deep; the frontal, temporal, parietal, and occipital were defined as lobar), hematoma volume calculated by $A \times B \times C/2$ method (Kothari et al., 1996), hemorrhage expansion, ventricular hematoma, and subarachnoid hemorrhage; (5) surgery information, such as time from symptom onset to surgery, surgical approach, intraoperative blood loss, and hematoma evacuation rate; (6) laboratory characteristics, such as platelets (PLT) count, international normalized ratio (INR), activated partial thromboplastin time (APTT), and platelet transfusion; and (7) functional status, such as modified Rankin Scale (mRS) and mortality.

**TABLE 1 |** Patient's baseline characteristics according to preoperative APT.

| Variables | nAPT (*N* = 115, 76.67%) | APT (*N* = 35, 23.33%) | *P*-value |
|---|---|---|---|
| **Demographic characteristics** | | | |
| Gender | | | 0.175 |
| Male | 97 (84.35%) | 26 (74.29%) | |
| Female | 18 (15.65%) | 9 (25.71%) | |
| Age (years) | 48.39 ± 12.713 | 57.29 ± 13.024 | 0.001 |
| **Vascular risk factors** | | | |
| Smoking | 59 (51.30%) | 12 (34.29%) | 0.077 |
| Alcohol | 73 (63.48%) | 16 (45.71%) | 0.061 |
| **Medical history** | | | |
| Hypertension | 107 (93.04%) | 32 (91.43%) | 0.719 |
| Diabetes | 11 (9.57%) | 6 (17.14%) | 0.230 |
| Coronary heart disease | 6 (5.22%) | 5 (14.29%) | 0.129 |
| Ischemic stroke history | 5 (4.35%) | 14 (40.00%) | 0.000 |
| Cerebral hemorrhage history | 4 (3.49%) | 3 (8.57%) | 0.355 |
| **Imaging** | | | |
| Side | | | 0.709 |
| Left | 60 (52.17%) | 17 (48.57%) | |
| Right | 55 (47.83%) | 18 (51.43%) | |
| Localization | | | 0.096 |
| Lobar | 21 (18.26%) | 11 (31.43%) | |
| Deep | 94 (81.74%) | 24 (68.57%) | |
| Hematoma volume (ml) | 46.37 (31.36, 58.58) | 54.11 (33.36, 76.90) | 0.077 |
| Hemorrhage expansion | 43 (37.39%) | 10 (28.57%) | 0.629 |
| Ventricular hematoma | 52 (45.22%) | 29 (82.86%) | 0.000 |
| Subarachnoid hemorrhage | 25 (21.74%) | 7 (20.00%) | 0.826 |
| **Surgery** | | | |
| Time from symptom onset to surgery (h) | 45 (22, 93) | 32 (15, 60) | 0.149 |
| Surgery | | | 0.368 |
| Craniotomy | 50 (43.48%) | 19 (54.29%) | |
| Endoscopic surgery | 10 (8.70%) | 4 (11.43%) | |
| Minimally invasive surgery | 55 (47.83%) | 12 (34.29%) | |
| Intraoperative blood loss (ml) | 200 (100, 400) | 300 (200, 500) | 0.053 |
| Rate of hematoma evacuation (%) | 92.30 (75.90, 96.77) | 89.00 (70.42, 93.40) | 0.226 |
| Postoperative residual hematoma volume (ml) | 2.63 (1.03, 12.79) | 4.33 (1.12, 21.14) | 0.645 |
| **Laboratory test** | | | |
| PLT 10'9/l | | | 0.102 |
| <125 | 2 (1.74%) | 3 (8.57%) | |
| 125–350 | 107 (93.04%) | 29 (82.8%) | |
| >350 | 6 (5.22%) | 3 (8.57%) | |
| INR | 0.96 (0.89, 1.02) | 0.99 (0.94, 1.04) | 0.087 |
| APTT (s) | 26.00 (23.50, 28.48) | 26.80 (24.20, 30.40) | 0.109 |
| Platelet transfusion | 7 (6.09%) | 5 (14.29%) | 0.152 |
| Neurological condition at admission | | | 1.000 |
| mRS (0–3) | 12 (10.43%) | 4 (11.43%) | |
| mRS (4–5) | 103 (89.57%) | 31 (88.57%) | |

*APT, antiplatelet therapy; nAPT, no antiplatelet therapy; N, number; PLT, platelets; INR, international normalized ratio; mRS, postoperative modified Rankin Scale; APTT, activated partial thromboplastin time.*

## Outcomes and Definition

Taking into account the effective time of antiplatelet drugs (Cahill et al., 2005; Hornor et al., 2018), outcomes were determined according to the mRS and all-cause mortality at 14 days after surgery.

The definition of postoperative hemorrhage is as follows: compared with the previous postoperative CT scan, the volume of the hematoma increased by >33% (the ICH volume decreased significantly after minimally invasive surgery), or the CT scan at the follow-up after the operation found that the volume of hematoma was completely high-density shadows that appeared again in the excised primary site (Wu et al., 2017; Shen et al., 2018).

Preoperative APT is defined as the continuous administration of aspirin (100 mg), clopidogrel (75 mg), or aspirin plus clopidogrel for more than 7 days due to coronary heart disease, cerebral infarction, or other ischemic lesions before the operation, and the interruption time is less than 7 days (Ford, 2015; Hornor et al., 2018).

## Statistical Analysis

Platelets count and mRS values were transformed into categorical variables. Categorical variables were described by percentage, and continuous variables were described by means (standard deviations) or medians (quartiles) when appropriate. Categorical variables were analyzed by chi-square test. According to whether continuous variables conformed to normal distribution, the *t* or Mann–Whitney *U* test were used for analysis. Multivariate logistics regression analysis was used to correct confounding factors whose *p*-value was less than 0.05 in the comparison between groups. All statistical tests were performed by SPSS statistical software (IBM, version 26). A *p*-value of <0.05 on both sides was considered statistically significant.

# RESULTS

## Study Population

From January 1, 2015 to July 31, 2019, 1,548 patients were diagnosed with ICH in Beijing Tiantan Hospital, Capital

**TABLE 2 |** The association between preoperative APT and postoperative rehemorrhage or outcomes.

| | nAPT (*N* = 115, 76.67%) | APT (*N* = 35, 23.33%) | *P*-value |
|---|---|---|---|
| Postoperative rehemorrhage | 12 (10.43%) | 9 (25.71%) | 0.047 |
| Postoperative hematoma expansion volume (ml) | 15.76 (3.26, 24.48) | 8.50 (3.80, 13.99) | 0.286 |
| Outcomes | | | 0.222 |
| mRS (0–3) | 19 (16.52%) | 9 (25.71%) | |
| mRS (4–5) | 94 (81.74%) | 23 (65.72%) | |
| Mortality | 2 (1.74%) | 3 (8.57%) | |

*APT, antiplatelet therapy; nAPT, no antiplatelet therapy; N, number; mRS, postoperative modified Rankin Scale.*

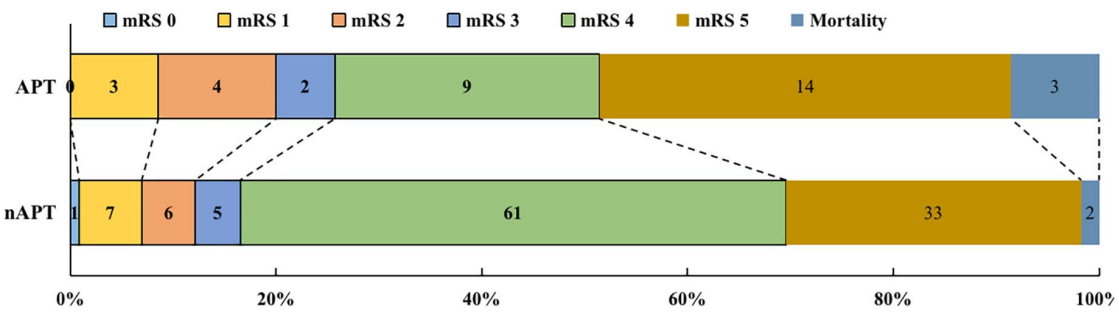


**FIGURE 1 |** The outcomes of patients with ICH after surgery. APT, antiplatelet therapy; nAPT, no antiplatelet therapy; mRS, modified Rankin Scale.

Medical University. Among them, 176 adult patients received surgery treatment; 38 patients were excluded because they were diagnosed with aneurysm, arteriovenous malformation, moyamoya disease, etc.; eight patients were excluded due to receiving anticoagulation therapy within 7 days before surgery; and eight patients were excluded due to incomplete data. In the end, 122 patients in the retrospective cohort were included in this study. And according to the inclusion and exclusion criteria, from January 2019 to December 2019, a total of 28 patients in the prospective cohort were consecutively enrolled into current study. Totally, 150 ICH patients were involved in this study.

## Baseline Characteristics

The enrolled population was divided into APT group and no antiplatelet therapy (nAPT) group according to whether they accept APT or not. Thirty five (23.33%) people were included in the APT group, while 115 (76.67%) people were included in the nAPT group. The baseline characteristics of the two groups are shown in **Table 1**. As shown, the age of patients in the APT group was older than that in the nAPT group ($p = 0.001$); patients in the APT group were more likely to have a history of ischemic stroke than patients in the nAPT group ($p = 0.000$); patients in the APT group were also more prone to ventricular hemorrhage when ICH occurred than patients in the APT group ($p = 0.000$) (**Table 1**). In addition, there was no statistical difference between the two groups in variables of hematoma volume, hemorrhage expansion, surgical methods, intraoperative blood loss, hematoma evacuation rate, postoperative residual hematoma volume, APTT, and other factors (**Table 1**).

## Differences in Postoperative Rehemorrhage and Outcomes Between Groups

Nine (25.7%) patients in the APT group developed early postoperative rehematoma, and 12 (10.4%) patients in the nAPT group developed early postoperative rehematoma (**Table 2**). As **Table 2** shows, the incidence of early postoperative rehemorrhage in the APT group was significantly higher than that in the nAPT group ($p = 0.047 < 0.05$). However, there was no significant difference (0.286) in postoperative hematoma expansion volume between the two groups.

In the APT group, 9 (25.7%) patients had a good early prognosis, while 26 (74.3%) patients had a poor early prognosis, of which 3 (8.6%) patients died early after surgery (**Figure 1**). In the nAPT group, 19 patients (16.5%) had a better early prognosis, while 96 patients (83.5%) had a poor early prognosis and two patients (1.7%) died earlier after surgery (**Figure 1**). As **Table 2** shows, there was no statistical difference between the two groups in early poorer outcomes ($p = 0.222$) at 14 days after surgery.

## Effect of APT on Postoperative Rehemorrhage and Outcomes

After adjusting for age, history of ischemic stroke, and ventricular hematoma variables, preoperative APT had no significant effect on early postoperative rehemorrhage [$p = 0.067$; 95% confidence interval (CI), 3.046 (0.926, 10.031)], as shown in **Table 3**.

As shown in **Table 4**, preoperative APT also had no significant effect on early poorer outcomes [$p = 0.072$; 95% CI, 0.324 (0.095, 1.105)] after adjusting for age, history of ischemic stroke, and ventricular hematoma.

**TABLE 3 |** The effects of preoperative APT on postoperative rehemorrhage after adjustment.

| Variables | Odds ratio (95% CI) | *P*-value |
|---|---|---|
| APT | 3.046 (0.926, 10.031) | 0.067 |
| Age (years) | 0.998 (0.962, 1.036) | 0.920 |
| Ischemic stroke history | 0.941 (0.237, 3.735) | 0.931 |
| Ventricular hematoma | 1.034 (0.368, 2.906) | 0.949 |

*APT, antiplatelet therapy; CI, confidence interval.*

**TABLE 4 |** The effects of APT on outcomes after adjustment.

| Variables | Odds ratio (95% CI) | *P*-value |
|---|---|---|
| APT | 0.324 (0.095, 1.105) | 0.072 |
| Age (years) | 0.991 (0.958, 1.026) | 0.620 |
| Ischemic stroke history | 1.160 (0.279, 4.813) | 0.838 |
| Ventricular hematoma | 3.792 (1.408, 10.213) | 0.008 |

*APT, antiplatelet therapy; CI, confidence interval.*

## DISCUSSION

Postoperative rehemorrhage seriously affects the prognosis of ICH patients. Previous research reported that postoperative rehemorrhage is an independent risk factor of poor outcome (Ren et al., 2018). However, there is still a lack of evidence in neurosurgery to support the hypothesis that preoperative APT may increase the risk of early postoperative rehemorrhage and affect early prognosis. So based on the hypothesis, we designed this study.

The results of the current study found that although the proportion of early postoperative rehemorrhage in ICH patients receiving APT is higher than that of patients not receiving APT, after adjusting for age, history of ischemic stroke, and ventricular hematoma, preoperative APT did not significantly increase the probability of early postoperative rehemorrhage in ICH patients. Similarly, preoperative APT did not significantly affect early poorer prognosis (mRS and mortality) of ICH patients undergoing surgery.

The results of current study were consistent with previous studies on the effects of APT on neurosurgery. Hanalioglu et al. (2020) studied 1,346 cases of intracranial tumor surgery and reported that discontinued APT before surgery and continued APT during perioperative period all did not significantly increase the probability of postoperative rehematoma. The same conclusion was also obtained in patients with traumatic brain injury undergoing craniotomy or craniectomy (Greuter et al., 2019). Although there were reports that preoperative APT was an independent risk factor for postoperative rehematoma in patients with ICH, the population of this study excluded deep ICH, which was the majority part of ICH (Biffi et al., 2010). This may cause bias in the results of their study. Besides, in another observational study on lobar and deep ICH, APT did not affect the recurrence of ICH after ICH (Weimar et al., 2011). Although its population included ICH patients who have not undergone surgery, it showed that APT had no significant effect on rehematoma, which indirectly proved the conclusion of the current study.

However, some studies in the field of non-neurosurgery have reached the opposite conclusion. In 2016, a retrospective research analyzed more than 4,500 patients undergoing thyroid surgery and found that patients who received preoperative APT had a significantly higher risk of postoperative hematoma than patients who did not undergo preoperative APT ($p < 0.01$) (Oltmann et al., 2016). Noteworthy, the population in this study took aspirin at a dose of 325 mg, which is higher than the low dose (100 mg) for cerebrovascular disease. Therefore, the conclusion of this study may not be applicable to patients with cerebrovascular disease. Subsequently, Luni et al. (2017) reported in a meta-analysis of cardiac surgery patients that patients who did not discontinue aspirin in time (>5 days) suffered a higher risk of postoperative rehemorrhage ($p = 0.04$). It seems that preoperative aspirin abuse increases the risk of postoperative rehemorrhage. However, its $p$-value was at a critical point, and the studies included in this meta-analysis have a moderate degree of heterogeneity (Luni et al., 2017), which may lead to controversial results.

Although previous studies have shown that preoperative APT does not significantly affect the occurrence of postoperative rehemorrhage, platelet transfusion is still used before surgery in ICH patients to prevent hemorrhage and postoperative rehemorrhage by improving platelet function. However, majority of evidences (Naidech et al., 2012; Suzuki et al., 2014; Baschin et al., 2017) supporting the efficacy of platelet transfusion on ICH come from observational studies, and such studies (Naidech et al., 2012; Suzuki et al., 2014; Baschin et al., 2017) are susceptible to various confounding factors and cannot accurately reflect the impact of platelet transfusion on ICH. In 2016, a randomized controlled trial conducted by PATCH showed that platelet transfusion after ICH in people receiving APT increased the patient's chance of death (Baharoglu et al., 2016). Subsequently, the research of Al-Shahi Salman et al. (2018) also reached the same conclusion, and some researchers (Magid-Bernstein et al., 2021) proposed that the poor efficacy after platelet transfusion may be related to the mismatch of ABO blood type. In the current study, only a small percentage of ICH patients received platelet transfusion before surgery and no significant difference was observed between the two groups. Therefore, this study cannot clarify the effect of platelet transfusion on postoperative rehemorrhage in ICH patients. More researches need to be implemented to clarify the effect of platelet transfusion in ICH patients.

On the other hand, some previous observational studies have shown that preoperative APT was a risk factor for poorer prognosis and mortality (Roquer et al., 2005; Yang et al., 2014; Won et al., 2017; Maas et al., 2018; Würtz et al., 2018), but this result was not observed in our study. The group comparison and correction analysis in our study showed preoperative APT did not affect the early outcome of ICH patients. This may be related to different study populations and observation periods from previous studies. Unlike previous studies (Roquer et al., 2005; Yang et al., 2014; Won et al., 2017; Maas et al., 2018; Würtz et al., 2018), our study only included ICH patients undergoing surgical treatment and the observation period was shorter. Recently, two studies (Khan et al., 2017; Franco et al., 2020) have challenged previous conclusions that preoperative APT is a risk factor for poor prognosis and death in ICH patients. Khan et al. (2017) analyzed the data of 82,576 ICH patients and found that single APT did not significantly increase the risk of in-hospital mortality. Franco et al. (2020) found a similar conclusion that previous APT was not an independent predictor of in-hospital mortality, which was exactly the conclusion of our research.

This study explored the effect of preoperative APT on early postoperative rehemorrhage and prognosis in ICH patients undergoing surgery and may provide some evidence for the clinical application of APT in ICH patients. In addition, this is a multi-center cohort study, which could avoid certain case limitations and bias. The research still has certain shortcomings. The current study is only based on the effective time of antiplatelet drugs to determine the study observation time, but did not detect the patient's platelet function during this period, which may have a certain impact on the accuracy of the results. Besides, this study was non-random and the included population was small, which inevitably had a certain impact on the accuracy

of the results. Therefore, large randomized controlled trials are needed to verify the accuracy of this conclusion.

## CONCLUSION

Preoperative APT appears to be safe and has no significant effect on early postoperative rehematoma and outcomes in ICH patients.

## DATA AVAILABILITY STATEMENT

The original contributions presented in the study are included in the article/supplementary material, further inquiries can be directed to the corresponding author/s.

## ETHICS STATEMENT

The studies involving human participants were reviewed and approved by the Institutional Review Board of Beijing Tiantan Hospital, Capital Medical University. The patients/participants provided their written informed consent to participate in this study.

## AUTHOR CONTRIBUTIONS

SW made significant contributions in the conceptualization of the study. JY, QL, SM, and ML made significant contributions in the methodology of the study. JY, SM, KW, and SY made significant contributions in the formal analysis and investigation. JY made significant contributions in the original draft preparation. JW, RG, YY, JZ, and YL made significant contributions in reviewing and editing of the manuscript. PJ, YC, and SW made significant contributions in the supervision of the study. All authors contributed to the article and approved the submitted version.

## FUNDING

This work was supported by the National Natural Science Foundation of China (Grant Nos. 81471210 and 81671129) and major special projects in the 13th Five-Year Plan (Grant No. 2016YFC1301800).

## ACKNOWLEDGMENTS

We gratefully thank all authors in this research and the projects for providing funding.

## REFERENCES

Al-Shahi Salman, R., Law, Z. K., Bath, P. M., Steiner, T., and Sprigg, N. (2018). Haemostatic therapies for acute spontaneous intracerebral haemorrhage. *Cochrane Database Syst. Rev.* 4:CD005951.

An, S. J., Kim, T. J., and Yoon, B.-W. (2017). Epidemiology, risk factors, and clinical features of intracerebral hemorrhage: an update. *J. Stroke* 19, 3–10. doi: 10.5853/jos.2016.00864

Baharoglu, M. I., Cordonnier, C., Al-Shahi Salman, R., de Gans, K., Koopman, M. M., Brand, A., et al. (2016). Platelet transfusion versus standard care after acute stroke due to spontaneous cerebral Haemorrhage associated with antiplatelet therapy (PATCH): a randomised, open-label, phase 3 trial. *Lancet* 387, 2605–2613. doi: 10.1016/s0140-6736(16)30392-0

Baschin, M., Selleng, S., Zeden, J.-P., Westphal, A., Kohlmann, T., Schroeder, H. W., et al. (2017). Platelet transfusion to reverse antiplatelet therapy before decompressive surgery in patients with intracranial haemorrhage. *Vox Sang.* 112, 535–541. doi: 10.1111/vox.12542

Biffi, A., Halpin, A., Towfighi, A., Gilson, A., Busl, K., Rost, N., et al. (2010). Aspirin and recurrent intracerebral hemorrhage in cerebral amyloid angiopathy. *Neurology* 75, 693–698.

Cahill, R. A., McGreal, G. T., Crowe, B. H., Ryan, D. A., Manning, B. J., Cahill, M. R., et al. (2005). Duration of increased bleeding tendency after cessation of aspirin therapy. *Clin. Trial.* 200, 564–573. doi: 10.1016/j.jamcollsurg.2004.11.002

Cordonnier, C., Demchuk, A., Ziai, W., and Anderson, C. S. (2018). Intracerebral haemorrhage: current approaches to acute management. *Lancet* 392, 1257–1268. doi: 10.1016/S0140-6736(18)31878-6

Fiaschi, P., Iaccarino, C., Stefini, R., Prior, E., Prior, A., and Zona, G. (2020). Clinical practice for antiplatelet and anticoagulant therapy in neurosurgery: data from an Italian survey and summary of current recommendations - part I, antiplatelet therapy. *Neurosurg. Rev.* 44, 485–493. doi: 10.1007/s10143-019-01229-7

Ford, I. (2015). Coming safely to a stop: a review of platelet activity after cessation of antiplatelet drugs. *Therap. Adv. Drug Saf.* 6, 141–150. doi: 10.1177/2042098615588085

Franco, L., Paciaroni, M., Enrico, M. L., Scoditti, U., Guideri, F., Chiti, A., et al. (2020). Mortality in patients with intracerebral hemorrhage associated with antiplatelet agents, oral anticoagulants or no antithrombotic therapy. *Eur. J. Intern. Med.* 75, 35–43. doi: 10.1016/j.ejim.2019.12.016

Greuter, L., Ullmann, M., Mariani, L., Guzman, R., and Soleman, J. (2019). Effect of preoperative antiplatelet or anticoagulation therapy on hemorrhagic complications in patients with traumatic brain injury undergoing craniotomy or craniectomy. *Neurosurg. Focus* 47:E3. doi: 10.3171/2019.8.FOCUS19546

Hanalioglu, S., Sahin, B., Sahin, O. S., Kozan, A., Ucer, M., Cikla, U., et al. (2020). Effect of perioperative aspirin use on hemorrhagic complications in elective craniotomy for brain tumors: results of a single-center, retrospective cohort study. *J. Neurosurg.* 132, 1529–1538. doi: 10.3171/2018.12.jns182483

Hemphill, J. C. rd, Greenberg, S. M., Anderson, C. S., Becker, K., Bendok, B. R., Cushman, M., et al. (2015). Guidelines for the management of spontaneous intracerebral hemorrhage: A guideline for healthcare professionals from the American Heart Association/American Stroke Association. *Stroke.* 46, 2032–2060. doi: 10.1161/STR.0000000000000069

Hornor, M. A., Duane, T. M., Ehlers, A. P., Jensen, E. H., Brown, P. S. J., Pohl, D., et al. (2018). American College of Surgeons' guidelines for the perioperative management of antithrombotic medication. *J. Am. Coll. Surg.* 227, 521–536.e1. doi: 10.1016/j.jamcollsurg.2018.08.183

Khan, N. I., Siddiqui, F. M., Goldstein, J. N., Cox, M., Xian, Y., Matsouaka, R. A., et al. (2017). Association between previous use of antiplatelet therapy and intracerebral hemorrhage outcomes. *Stroke* 48, 1810–1817. doi: 10.1161/strokeaha.117.016290

Kothari, R. U., Brott, T., Broderick, J. P., Barsan, W. G., Sauerbeck, L. R., Zuccarello, M., et al. (1996). The ABCs of measuring intracerebral hemorrhage volumes. *Stroke* 27, 1304–1305. doi: 10.1161/01.str.27.8.1304

Luni, F. K., Riaz, H., Khan, A. R., Riaz, T., Husnain, M., Riaz, I. B., et al. (2017). Clinical outcomes associated with per-operative discontinuation of aspirin in patients with coronary artery disease: a systematic review and meta-analysis. *Catheter Cardiovasc. Interv.* 89, 1168–1175. doi: 10.1002/ccd.26807

Luzzi, S., Elia, A., Del Maestro, M., Morotti, A., Elbabaa, S. K., Cavallini, A., et al. (2019). Indication, timing, and surgical treatment of spontaneous intracerebral hemorrhage: systematic review and proposal of a management algorithm. *World Neurosurg.* 124:e00769-78.

Maas, M. B., Naidech, A. M., Kim, M., Batra, A., Manno, E. M., Sorond, F. A., et al. (2018). Medication history versus point-of-care platelet activity testing in

patients with intracerebral hemorrhage. *J. Stroke Cerebrovasc. Dis.* 27, 1167–1173. doi: 10.1016/j.jstrokecerebrovasdis.2017.11.033

Magid-Bernstein, J., Beaman, C. B., Carvalho Poyraz, F., Boehme, A., Hod, E., Francis, R. O., et al. (2021). Impacts of ABO incompatible platelet transfusions on platelet recovery and outcomes after intracerebral hemorrhage. *Blood* 137, 2699–2703. doi: 10.1182/blood.2020008381

Naidech, A. M., Liebling, S. M., Rosenberg, N. F., Lindholm, P. F., Bernstein, R. A., Batjer, H. H., et al. (2012). Early platelet transfusion improves platelet activity and may improve outcomes after intracerebral hemorrhage. *Neurocrit. Care* 16, 82–87. doi: 10.1007/s12028-011-9619-3

Oltmann, S. C., Alhefdhi, A. Y., Rajaei, M. H., Schneider, D. F., Sippel, R. S., and Chen, H. (2016). Antiplatelet and anticoagulant medications significantly increase the risk of postoperative hematoma: review of over 4500 Thyroid and Parathyroid procedures. *Ann. Surg. Oncol.* 23, 2874–2882. doi: 10.1245/s10434-016-5241-0

Rahman, M., Donnangelo, L. L., Neal, D., Mogali, K., Decker, M., and Ahmed, M. M. (2015). Effects of perioperative acetyl salicylic acid on clinical outcomes in patients undergoing craniotomy for brain tumor. *World Neurosurg.* 84, 41–47. doi: 10/f7fptw

Ren, Y., Zheng, J., Liu, X., Li, H., and You, C. (2018). Risk factors of Rehemorrhage in postoperative patients with spontaneous intracerebral hemorrhage?: a case-control study. *J. Korean Neurosurg. Soc.* 61, 35–41. doi: 10.3340/jkns.2017.0199

Roquer, J., Rodríguez Campello, A., Gomis, M., Ois, A., Puente, V., and Munteis, E. (2005). Previous antiplatelet therapy is an independent predictor of 30-day mortality after spontaneous supratentorial intracerebral hemorrhage. *J. Neurol.* 252, 412–416. doi: 10.1007/s00415-005-0659-5

Sansing, L. H., Messe, S. R., Cucchiara, B. L., Cohen, S. N., Lyden, P. D., Kasner, S. E., et al. (2009). Prior antiplatelet use does not affect hemorrhage growth or outcome after ICH. *Neurology* 72, 1397–1402. doi: 10.1212/01.wnl.0000342709.31341.88

Shen, Z., Wang, L., Wu, G., Li, Q., Ren, S., and Mao, Y. (2018). Computed tomographic black hole sign predicts postoperative Rehemorrhage in patients with spontaneous intracranial hemorrhage following Stereotactic minimally invasive surgery. *World Neurosurg.* 120:e00153-60. doi: 10.1016/j.wneu.2018.07.256

Suzuki, Y., Kitahara, T., Soma, K., Konno, S., Sato, K., Suzuki, S., et al. (2014). Impact of platelet transfusion on survival of patients with intracerebral hemorrhage after administration of anti-platelet agents at a tertiary emergency center. *PLoS One* 9:e97328. doi: 10.1371/journal.pone.0097328

Weimar, C., Benemann, J., Terborg, C., Walter, U., Weber, R., Diener, H.-C., et al. (2011). Recurrent stroke after lobar and deep intracerebral hemorrhage: a hospital-based cohort study. *Cerebrovasc. Dis.* 32, 283–288. doi: 10.1159/000330643

Won, S.-Y., Dubinski, D., Bruder, M., Cattani, A., Seifert, V., and Konczalla, J. (2017). Acute subdural hematoma in patients on oral anticoagulant therapy: management and outcome. *Neurosurg. Focus* 43:E12.

Wu, G., Shen, Z., Wang, L., Sun, S., Luo, J., and Mao, Y. (2017). Post-operative re-bleeding in patients with hypertensive ICH is closely associated with the CT blend sign. *BMC Neurol.* 17:131. doi: 10.1186/s12883-017-0910-6

Wu, J., Liu, Q., Wang, K., Yang, J., Jiang, P., Li, M., et al. (2020). Emergency surgery is an effective way to improve the outcome of severe spontaneous intracerebral hemorrhage patients on long-term oral antiplatelet therapy. *Neurosurg. Rev.* 44, 1205–1216. doi: 10.1007/s10143-020-01319-x

Würtz, M., Schmidt, M., Grove, E. L., Horváth-Puhó, E., Henderson, V. W., Christiansen, C. F., et al. (2018). Pre-admission use of platelet inhibitors and short-term stroke mortality: a population-based cohort study. *Eur. Heart J. Cardiovasc. Pharmacother.* 4, 158–165. doi: 10.1093/ehjcvp/pvy010

Yang, N. R., Kim, S. J., and Seo, E. K. (2014). Spontaneous intracerebral hemorrhage with antiplatelets/anticoagulants/none: a comparison analysis. *Acta Neurochir.* 156, 1319–1325. doi: 10.1007/s00701-014-2080-2

Yu, S.-X., Zhang, Q.-S., Yin, Y., Liu, Z., Wu, J.-M., and Yang, M.-X. (2016). Continuous monitoring of intracranial pressure for prediction of postoperative complications of hypertensive intracerebral hemorrhage. *Eur. Rev. Med. Pharmacol. Sci.* 20, 4750–4755.

**Conflict of Interest:** The authors declare that the research was conducted in the absence of any commercial or financial relationships that could be construed as a potential conflict of interest.

frontiers in Aging Neuroscience

ORIGINAL RESEARCH
published: 05 July 2021
doi: 10.3389/fnagi.2021.620763

# Measurement of Cortical Atrophy and Its Correlation to Memory Impairment in Patients With Asymptomatic Carotid Artery Stenosis Based on VBM-DARTEL

*Peijiong Wang[1,2,3,4], Husule Cai[1,2,3,4], Rutao Luo[5], Zihao Zhang[6], Dong Zhang[1,2,3,4] and Yan Zhang[1,2,3,4]**

[1] Department of Neurosurgery, Beijing Tiantan Hospital, Capital Medical University, Beijing, China, [2] China National Clinical Research Center for Neurological Diseases (NCRC-ND), Beijing, China, [3] Center of Stroke, Beijing Institute for Brain Disorders, Beijing, China, [4] Beijing Key Laboratory of Translational Medicine for Cerebrovascular Disease, Beijing, China, [5] Department of Neurosurgery, Beijing Children's Hospital, Capital Medical University, National Center for Children's Health, Beijing, China, [6] State Key Laboratory of Brain and Cognitive Science, Beijing MRI Center for Brain Research, Institute of Biophysics, Chinese Academy of Sciences, Beijing, China

**Objective:** Severe carotid artery stenosis (CAS) can lead to atrophy of gray matter (GM) and memory impairment; however, the underlying mechanism is unknown. Thus, we aimed to identify memory impairment and GM atrophy and explore the possible correlation between them in patients with asymptomatic severe CAS.

**Methods:** Twenty-four patients with asymptomatic severe CAS and 10 healthy controls completed the mini-mental state examination (MMSE) and clinical memory scale (CMS) and underwent 7T magnetic resonance imaging (MRI) scan. Field intensity inhomogeneities were corrected. Images were processed using VBM8, and GM images were flipped. First, 11 flipped and 10 non-flipped images of patients with unilateral CAS and 5 flipped and 5 non-flipped images of controls were pre-processed using DARTEL algorithm and analyzed using an analysis of variance (ANOVA). Second, flipped and non-flipped images of unilateral patients were similarly pre-processed and analyzed using the paired *t*-test. Third, pre-processed non-flipped GM images and CMS scores of 24 patients were analyzed by multiple regression analysis. Nuisance variables were corrected accordingly.

**Results:** Basic information was well matched between patients and controls. MMSE scores of patients were in the normal range; however, memory function was significantly reduced (all $P < 0.05$). GM volumes of patients were significantly reduced in the anterior circulation regions. The stenosis-side hemispheres showed greater atrophy. GM volumes of the left pars opercularis, pars triangularis, and middle frontal gyrus were strongly positively correlated with the total scores of CMS (all $r > 0.7$, $P = 0.001$). Additionally, the left middle frontal gyrus was strongly positively correlated with

OPEN ACCESS

**Edited by:**
Shaohua Yang,
University of North Texas Health Science Center, United States

**Reviewed by:**
Zaizhu Han,
Beijing Normal University, China
Xin Lou,
Chinese PLA General Hospital, China

***Correspondence:**
Yan Zhang
yanzhang135@163.com

**Received:** 28 January 2021
**Accepted:** 14 May 2021
**Published:** 05 July 2021

**Citation:**
Wang P, Cai H, Luo R, Zhang Z, Zhang D and Zhang Y (2021) Measurement of Cortical Atrophy and Its Correlation to Memory Impairment in Patients With Asymptomatic Carotid Artery Stenosis Based on VBM-DARTEL. Front. Aging Neurosci. 13:620763. doi: 10.3389/fnagi.2021.620763

associative memory ($r$ = 0.853, $P$ = 0.001). The left pars opercularis was moderately positively correlated with semantic memory ($r$ = 0.695, $P$ = 0.001).

**Conclusion:** Patients with asymptomatic CAS suffer from memory impairment. Bilateral anterior circulation regions showed extensive atrophy. The hemisphere with stenosis showed severer atrophy. Memory impairment in patients may be related to atrophy of the left frontal gyrus and atrophy of different regions may result in different memory impairments.

**Keywords: asymptomatic carotid stenosis, memory deficiency, VBM analysis, cerebral gray matter atrophy, 7T-MRI**

## INTRODUCTION

Carotid artery stenosis (CAS), a type of vascular degenerative disease, can cause cerebral ischemic events, such as amaurosis, transient ischemic attack (TIA), and stroke, which threaten life and health. Several large-sample studies, such as the Cardiovascular Health Study and the Framingham Study, have revealed that CAS can lead to cortical atrophy (Newman et al., 2005; Romero et al., 2009) and the MART-MR study confirmed progressive loss of gray matter (GM) in patients with severe CAS during long-term follow-up (Muller et al., 2011). However, these studies focused primarily on whole brain GM volumes and left specific areas of atrophy unexplored. Despite some recent researches reporting that cortical atrophy mainly occurs in cerebral areas supplied by the anterior circulation (Asllani et al., 2016; Avelar et al., 2016; Marshall et al., 2017), few studies have investigated the location and characteristics of atrophy, especially difference in cerebral atrophy between the hemisphere affected by severe stenosis and the contralateral hemisphere.

Moreover, cognitive impairment was detected in around 50% of patients with severe CAS (Pettigrew et al., 2000; Smith, 2017), and memory decline, one of the most common complaints, was reported in 25.5% patients approximately (Luo et al., 2018). Furthermore, thinning of the cortex is considered a potential biomarker, which has shown to be associated with cognitive impairment in aging, neurodegenerative disease, and small vascular disease (Seo et al., 2010; Kim et al., 2014; Pettigrew et al., 2016; Weston et al., 2016). All these studies raise the possibility that cortical thinning in CAS patients may contribute to memory decline; however, this has not been clarified. Furthermore, locating the specific correlating cortex may allow a better understanding of the mechanism of memory impairment in CAS patients.

Thus, we acquired 7T-MRI T1 images and cognitive scores from patients with severe asymmetric CAS and healthy controls. This study aimed to show the changes in memory function and gray matter volumes of patients to delineate whether cerebral atrophy in patients was asymmetric between the stenosis-side hemisphere and the contralateral hemisphere and to better understand the correlation between memory impairment and GM atrophy.

**Abbreviations:** ANOVA, analysis of variance; CAS, carotid artery stenosis; CBF, cerebral blood flow; CMS, clinical memory scale; CSF, cerebrospinal fluid; CTA, computed tomography angiography; DLPFC, dorsolateral prefrontal cortex; DSA, digital subtraction angiography; FDR, false discovery rate; GE, gradient echo; GM, gray matter; MMSE, mini-mental state examination; MQ, memory quotient; MRI, magnetic resonance imaging; PFC, prefrontal cortex; ROI, region of interest; TIA, transient ischemic attack; TIV, total intracranial volume; TPM, tissue probability map; VBM, voxel-based morphometry; VLPFC, ventrolateral prefrontal cortex; WM, white matter.

## MATERIALS AND METHODS

This study was approved by the ethics committee of Beijing Tiantan Hospital, Capital Medical University. All patients and healthy volunteers were voluntarily involved in this study and provided consent. The inclusion criteria of CAS patients were as follows: (1) severe CAS (grade of stenosis ≥70%), based on either or both computed tomography angiography (CTA) and digital subtraction angiography (DSA), following the guidelines for CAS (criteria of the North American Symptomatic Carotid Endarterectomy Trial) (Barnett et al., 1998); and (2) asymptomatic CAS, where no cerebral ischemic events (amaurosis, TIA, and stroke) had occurred during the last 6 months. The exclusion criteria of CAS patients were as follows: (1) contraindications to magnetic resonance imaging (MRI), such as claustrophobia or metal implants in the body; (2) history of any other cognitive impairment disease, such as Alzheimer's disease; and (3) history of surgery of the carotid artery. The inclusion criteria of healthy volunteers were as follows: (1) no carotid stenosis; (2) no history of cerebral disease; and (3) no history of cognitive impairment. To match healthy volunteers with patients, volunteers were recruited online using random stratified sampling according to age, sex, and educational background.

A total of 24 patients with severe asymptomatic CAS and 10 healthy volunteers were recruited from April 2016 to August 2018. All patients and healthy volunteers completed cognitive scales and underwent 7T-MRI scan. Baseline information obtained for the study included age, sex, and educational background.

### Cognitive Examination

The cognitive function of patients and volunteers were assessed using the mini-mental state examination (MMSE) and clinical memory scale (CMS), which was completed several days before the MRI scan. All tests and reports were conducted by doctors.

The MMSE was used to estimate general cognitive function and detect moderate and severe cognitive impairment. MMSE

consists of 30 items, which include evaluation of temporal and spatial orientation, verbal memory, attention and calculation, short-term memory, object naming, retelling, reading comprehension, language comprehension, speech articulation, and graphic drawing, among others. Reference scores for cognitive impairment are defined as ≤18 for illiteracy, ≤21 for primary school education, and ≤25 for middle school education and above.

Clinical memory scale was employed to assess memory function. CMS was adapted by the Institute of Psychology of Chinese Academy of Sciences and is composed of five tests, which include directed memory, associative memory, meaningless graphic recognition, free image recall, and portrait characteristic recall. After the test, original scale scores were converted into scores according to age and educational background, according to user guide. Then, the five scores were summed up to obtain the total scale score. The total scale score was transformed into a memory quotient (MQ) according to the user guide. The grades of memory function were defined as follows: MQ ≥ 130 as super-excellence, 120–129 as excellence, 110–119 as upper level, 90–109 as moderate level, 80–89 as lower level, 70–79 as poor, and MQ < 70 as very poor. Directed memory test and associative learning tests were used to assess the semantic memory function, and these two scores were summed up to obtain a semantic memory score.

## 7T-MRI Acquisition

MRI data were acquired at the Beijing Brain MRI Center using the 7T-MRI investigational system (Magnetom 7T, Siemens Healthineers, Erlangen, Germany), which was equipped with a Nova 32 channel phased-array head coil. We chose T1-MPRAGE as researching MRI sequence with the following parameters: TR 2200 ms, TE 3.01 ms, flip angle 7°, FOV 224 × 224 $mm^2$, matrix 320 × 320, slice thickness 0.70 mm, and voxel size 0.7 × 0.7 × 0.7 $mm^3$.

## Processing and Analysis of MRI Images

Because 7T T1-MPRAGE images are not acquired with additional gradient echo (GE) images to correct intensity inhomogeneities of the bias field, we followed a two-step pre-processing pipeline. First, the non-parametric non-uniform intensity normalization (N3) algorithm was used before VBM processing. This step was implemented in the FreeSurfer software and followed the optimal parameters (proto-iters = 1000, distance = 15, $n$ = 1), proposed by Lüsebrink et al. (2013) Second, two parameters were adapted for VBM processing to correct any remaining intensity inhomogeneities using the following parameters: bias regularization changed from the default of "very light" to "extremely light, bias FWHM cutoff changed from the default of 60 to 30 mm (Lüsebrink et al., 2013).

After processing using the N3 algorithm, three-dimensional (3D) T1 images were processed automatically using voxel-based morphometry (VBM) analysis in VBM8 software running in SPM8 under MATLAB 2012a. During this procedure, two parameters were adapted as above, and a symmetric tissue probability map (TPM) provided by Kurth et al. (2015) was used instead of the default unsymmetrical TPM. The T1 images were spatially normalized and then segmented into gray matter (GM), white matter (WM) and cerebrospinal fluid (CSF). Meanwhile, the absolute volumes (ml) of GM, WM, and CSF were calculated. Total intracranial volume (TIV) was calculated as the sum of the absolute volumes of GM, WM, and CSF. GM images of all subjects were then flipped in the right–left orientation to obtain corresponding mirror GM images in SPM8 using image calculation.

### Patients vs. Controls

We defined the left cerebral hemisphere as the stenosis-side hemisphere and the right hemisphere as the contralateral hemisphere. Thus, flipped GM images of patients with right CAS should be involved, and an equal proportion of flipped images of controls should be involved for comparison. The flipped images of controls were selected at random. In total, there were 11 flipped GM images of patients with right CAS, 10 non-flipped GM images of patients with left CAS, and 5 flipped and 5 non-flipped GM images of healthy volunteers. All these images were processed using the DARTEL algorithm, modulated by flow field files and smoothed at an 8-mm full width at half maximum. The GM template was used to make a mask to limit analysis to the cortex. The grayscale threshold was a minimum of 0.3. Finally, the smoothed GM images were analyzed using an analysis of variance (ANOVA) of all factors (a 2 × 2 ANOVA) in SPM8 software to verify the impact of CAS on cerebral atrophy and eliminate the effect of sides. The nuisance variables TIV, sex, age, and educational background were used for correction. Statistical significance was defined as $P < 0.05$ using false discovery rate (FDR) correction and a minimum of 200 contiguous voxels. After comparison, atrophic cerebral areas on the left hemisphere demonstrated the effect of CAS on the stenosis-side hemisphere, and areas on the right hemisphere demonstrated the effect of CAS on the contralateral hemisphere. This enabled us to determine whether atrophy caused by unilateral CAS was unilateral or bilateral and where it was located, while eliminating the impact of laterality.

### Stenosis-Side Hemisphere vs. Contralateral Hemisphere

We defined the left cerebral hemisphere as the region of interest (ROI). The non-flipped and flipped GM images of 21 patients were processed using the DARTEL algorithm, and then images were modulated by flow field files and smoothed at an 8-mm full width at half maximum. The left-hemisphere mask was made using the GM template with grayscale threshold >0.3, which limited the analysis to the left hemisphere. Finally, smoothed non-flipped and flipped GM images were analyzed using the paired $t$-test to compare the contralateral hemisphere with the stenosis-side hemisphere on the left side defined by the left-hemisphere mask. The statistical significance was defined as $P_{FDR} < 0.05$ and a minimum of 100 contiguous voxels. The diagram is shown in **Figure 1**.

### Memory-Related Cortex

The non-flipped GM images of 24 patients were processed using the DARTEL algorithm to create templates and then these images

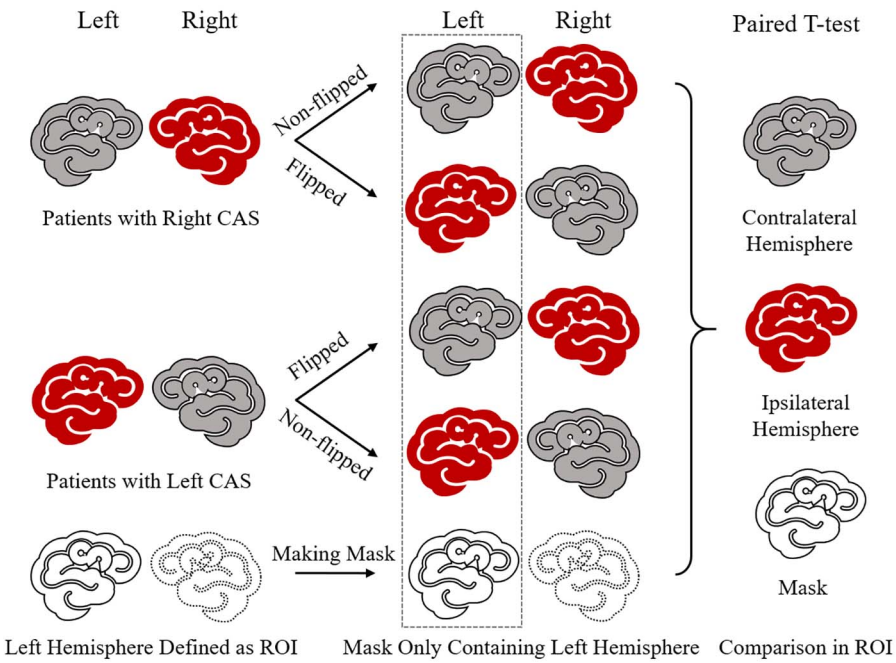


**FIGURE 1 |** Diagram of stenosis-side hemisphere vs. contralateral hemisphere. First, in each unilateral CAS patient, ipsilateral hemisphere and contralateral hemisphere cannot be paired and compared directly. So, the GM image of each patient needs to be flipped in the right–left orientation and then each patient had one non-flipped image and one paired flipped image. In this way, each patient had a stenosis hemisphere and a contralateral image on the left side when his/her non-flipped image and flipped image were paired together. Thus, patients' non-flipped images and flipped GM images were analyzed by paired *t*-test following mode of contralateral hemisphere vs. stenosis-side hemisphere on the left side defined by left-hemisphere mask.

were modulated and smoothed at an 8-mm full width at half maximum. The mask was made using the GM template with a grayscale threshold of 0.3. The smoothed GM images and CMS scores, including the total scores, the five subtest scores, and semantic memory scores, were analyzed successively using multiple regression analysis in SPM8 software. The nuisance variables TIV, sex, and degrees of carotid stenosis on each side were used for correction. Age and educational background were not used for correction because they had already been adjusted for during scoring. Statistical significance was defined as $P_{FDR} < 0.05$ and a minimum of 100 contiguous voxels.

If correlated regions were detected, these were each defined as an ROI and a corresponding mask was created. A customized script referring to Kurth's "extract" script was used to extract the volume ($mm^3$) from each GM image in MATLAB R2012a, and each volume was divided by corresponding TIV to obtain the relative volume (Kurth et al., 2015). Relative volumes and CMS scores were analyzed by Pearson correlation analysis in SPSS (Windows version 23.0, IBM).

## Statistical Analysis

Statistical analyses were conducted in SPSS (Windows version 23.0, IBM). Continuous variables are shown as means ± standard deviations, and categorical values are described as percentages (numbers). Absolute volumes of GM, WM, CSF, and TIV were used as references to correct results during analysis but were not used as explicit values for data comparison. We focused mainly on the relative volumes, which were obtained by dividing the absolute volumes by the corresponding TIV. A chi-square test was used to compare categorical data. Student's *t*-test and rank sum test were used to compare continuous data. Pearson correlation analysis was used to correlate relative volumes of correlated cerebral areas with CMS scores, and the Pearson correlation coefficient ($r$) indicated the strength of correlation. Correlation was considered strong when $1 > r \geq 0.7$, moderate when $0.7 > r \geq 0.4$, and weak when $0.4 > r > 0$ (Dancey and Reidy, 2007). Statistical significance was defined as $P < 0.05$. VBM results were shown as 3D reconstructed images and slice views using xjView software.

# RESULTS

Baseline information, including age, gender, details of stenosis, and education background, is listed in **Table 1**, and there were no statistical differences between patients with asymptomatic severe CAS and healthy controls. For cognitive function, MMSE scores of patients with CAS were in normal range and were similar to those of healthy controls (all $P \geq 0.05$). For CMS, the total scores, MQ, and memory function grade of the patient group were much lower than those of the control group (all $P < 0.05$). Moreover, the scores of the four subtests (i.e., directed

**TABLE 1 |** Basic information of CAS patients and healthy controls.

| | CAS patients (*n* = 24) | Healthy controls (*n* = 10) | *P*-value |
|---|---|---|---|
| Age (years) | 63.8 ± 5.6 | 65.0 ± 5.1 | 0.585 |
| Gender (male) | 15 (62.5%) | 6 (60.0%) | 1.000 |
| **Carotid stenosis** | | | |
| Bilateral | 3 (12.5%) | – | – |
| Unilateral | 21 (0.875) | – | – |
| Left | 10 (47.6%) | – | – |
| Right | 11 (52.4%) | – | – |
| **Contralateral** | | | |
| Moderate | 5 (23.8%) | – | – |
| Mild | 5 (23.8%) | – | – |
| None | 11 (52.3%) | – | – |
| **Education** | | | 0.493 |
| None | 2 (8.3%) | 0 (0.0%) | |
| Primary school | 5 (20.8%) | 1 (10.0%) | |
| High school | 14 (58.4%) | 7 (70.0%) | |
| University/above | 3 (12.5%) | 2 (20.0%) | |

memory, associative learning, free image recall, and portrait characteristic recall) were lower in patients with CAS than in healthy controls (all $P < 0.05$). Meaningless graphic recognition test scores were lower in patients than in healthy controls; however, this did not reach statistical significance ($P = 0.080$; **Table 2**). Compared with healthy controls, the relative GM volumes of patients were significantly lower ($P = 0.027$), and the relative CSF volumes were significantly higher ($P = 0.001$), whereas relative WM volumes were similar between the two groups ($P = 0.082$). The reduction in relative GM volume was approximately 3.1% (**Table 3**).

**TABLE 2 |** Cognitive function assessment of CAS patients and healthy controls.

| | CAS patients (*n* = 24) | Healthy controls (*n* = 10) | *P*-value |
|---|---|---|---|
| **MMSE** | | | |
| Scores | 26.2 ± 2.1 | 27.3 ± 0.9 | 0.050 |
| Grade of MMSE | | | 1.000 |
| Normal | 24 (100%) | 10 (100%) | |
| Impairment | 0 (0%) | 0 (0%) | |
| **CMS** | | | |
| Directed memory | 10.6 ± 5.8 | 19.6 ± 2.0 | 0.001 |
| Associative memory | 11.1 ± 4.5 | 22.1 ± 3.0 | 0.001 |
| Meaningless graphic recognition | 11.6 ± 5.1 | 21.0 ± 2.7 | 0.001 |
| Free image recall | 15.4 ± 8.1 | 18.8 ± 1.9 | 0.080 |
| Portrait characteristic recall | 15.0 ± 5.5 | 19.2 ± 3.1 | 0.037 |
| Semantic memory | 41.7 ± 4.7 | 22.1 ± 9.3 | 0.001 |
| Total scores | 64.3 ± 19.5 | 99.4 ± 11.2 | 0.001 |
| MQ | 80.4 ± 14.9 | 108.4 ± 9.3 | 0.001 |
| **Grade of memory** | | | 0.001 |
| Super-excellence (≥130) | 0 (0%) | 0 (0%) | |
| Excellence (120–129) | 0 (0%) | 1 (10%) | |
| Upper level (110–119) | 1 (4.8%) | 3 (30%) | |
| Moderate level (90–109) | 6 (28.6%) | 5 (50%) | |
| Lower level (80–89) | 2 (9.5%) | 1 (10%) | |
| Poor (70–79) | 6 (28.6%) | 0 (0%) | |
| Very poor (≤69) | 6 (28.6%) | 0 (0%) | |

As shown in **Figure 2** and **Table 4**, loss of GM volume in patients was not only limited to the stenosis-side hemisphere, but also observed in the contralateral hemisphere. Atrophy was widely distributed in the frontal, temporal, and parietal lobes as well as in smaller regions of the occipital lobes on both the ipsilateral and contralateral hemispheres. Meanwhile, large parts of the occipital lobes and cerebellar lobes were unaffected bilaterally. Furthermore, the stenosis-side hemisphere showed more severe atrophy of the inferior parietal lobule and cingulate gyrus compared with the contralateral hemisphere (**Figure 3** and **Table 5**).

**Figure 4** and **Table 5** illustrate the positive correlation of GM volumes of the left middle frontal gyrus, left frontal pars triangularis, and left frontal pars opercularis with the total scores of CMS and their Pearson correlations being strong (left middle frontal gyrus: $r = 0.841$, $P = 0.001$; left frontal pars triangularis: $r = 0.724$, $P = 0.001$; left frontal pars opercularis: $r = 0.798$, $P = 0.001$).

Moreover, GM volumes of the left medial frontal gyrus were strongly positively correlated with the associative memory scores ($r = 0.853$, $P = 0.001$; **Figure 5** and **Table 5**). GM volumes of the left posterior inferior frontal gyrus were moderately positively correlated with the semantic memory scores ($r = 0.695$, $P = 0.001$; **Figure 6** and **Table 5**).

# DISCUSSION

## Cortical Atrophy

This study confirmed cortical atrophy and increased CSF volumes in patients with CAS by analyzing relative GM and CSF volumes and VBM, which were consistent with several previous studies (Newman et al., 2005; Romero et al., 2009; Muller et al., 2011). Large-sample cross-sectional studies, such as the Cardiovascular Health Study and the Framingham Study, reported that moderate and severe CAS leads to brain atrophy, which mainly manifest as enlarged ventricles and sulci and reduced GM volumes (Newman et al., 2005; Romero et al., 2009). Furthermore, a SMART-MR study demonstrated that during a long-term follow-up of 3–9 years, unilateral severe CAS and bilateral CAS caused severe progressive atrophy of the cortex (Muller et al., 2011).

We found that the average reduction in cerebral GM in patients with asymptomatic severe CAS was 3.1%, which is close to 3.7% published by Iris et al. previously (Asllani et al., 2016). Although 3.1% may not seem substantial, the proportion is clinically significant when compared with those of other cognitive diseases. As reported in previous studies, cortical atrophy due to aging is roughly 0.2% every year in middle-aged healthy people (Shaw et al., 2016). The hippocampal cortices has been reported to be 1.2–1.5% thinner in patients with mild cognitive

**TABLE 3 |** Brain volumes of different parts in CAS patients and healthy controls.

| | Healthy controls ($n$ = 10) | Total CAS patients ($n$ = 24) | | Unilateral CAS patients ($n$ = 21) | | Bilateral CAS patients ($n$ = 3) | |
|---|---|---|---|---|---|---|---|
| | | Data | $P$ | Data | $P$ | Data | $P$ |
| **Absolute volume** | | | | | | | |
| GM volume/ml | 596.0 ± 50.2 | 527.7 ± 50.14 | 0.001 | 534.00 ± 50.06 | 0.003 | 483.87 ± 23.68 | 0.004 |
| WM volume/ml | 539.5 ± 71.2 | 475.77 ± 51.29 | 0.006 | 484.60 ± 47.97 | 0.017 | 413.99 ± 26.46 | 0.014 |
| CSF volume/ml | 231.1 ± 26.4 | 244.2 ± 37.9 | 0.327 | 245.90 ± 37.07 | 0.267 | 232.35 ± 50.44 | 0.953 |
| TIV volume/ml | 1366.1 ± 139.4 | 1247.7 ± 113.5 | 0.014 | 1264.50 ± 110.87 | 0.014 | 1130.22 ± 40.98 | 0.017 |
| **Relative volume** | | | | | | | |
| GM volume/% | 43.69 ± 1.24 | 42.34 ± 2.17 | 0.029 | 42.26 ± 2.16 | 0.027 | 42.85 ± 2.63 | 0.640 |
| WM volume/% | 39.39 ± 1.59 | 38.11 ± 1.80 | 0.058 | 38.31 ± 1.56 | 0.082 | 36.68 ± 3.06 | 0.057 |
| CSF volume/% | 17.03 ± 0.90 | 19.28 ± 2.43 | 0.001 | 19.28 ± 2.43 | 0.001 | 20.47 ± 3.65 | 0.012 |
| Reduced GM volume/% | – | 3.1 | – | 3.3 | – | 1.9 | – |

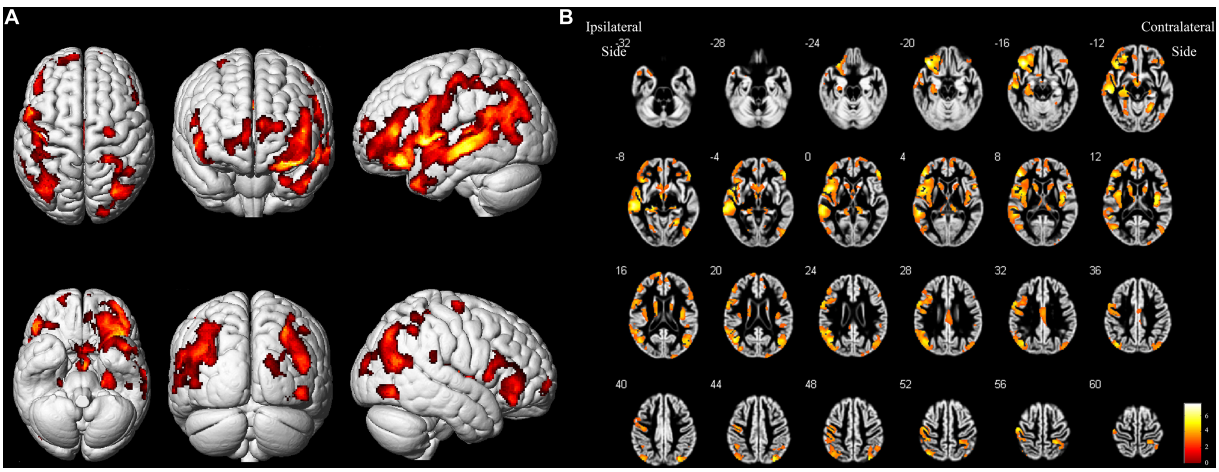


**FIGURE 2 |** Asymptomatic CAS patients vs. healthy controls. **(A)** Three-dimensional image. **(B)** Slice view. Cortical atrophy was observed in bilateral frontal, temporal, and parietal lobes, but occipital lobe and cerebellum were barely affected. L: left, R: right.

impairment (Das et al., 2012) and 4.7% thinner in patients with Alzheimer's disease who carry the APOEε4 allele (Harrison et al., 2016). Thus, cortical atrophy in patients with asymptomatic severe CAS deserve clinical attention.

Our VBM analysis revealed that cortical atrophy was widely distributed bilaterally in the frontal, temporal, and parietal lobes; however, the occipital lobes and cerebellum were largely unaffected, which is consistent with the areas of the anterior circulation. This finding is in line with those of several previous studies (Asllani et al., 2016; Avelar et al., 2016; Marshall et al., 2017). This phenomenon may be caused by hypoperfusion, a patent circle of Willis, and susceptibility to hypoperfusion. First, in regard to hypoperfusion, Gabriella et al. (2018) confirmed that carotid artery occlusion can lead to cortical atrophy in a mouse model and found a correlation between cortical atrophy and cerebral hypoperfusion. Marshall et al. (2017) further reported in a human MRI study that anterior circulation hypoperfusion caused by CAS leads to atrophy of the primary motor cortex, and these were positively correlated. Second, a patent circle of Willis may compensate for hypoperfusion by directing blood from the contralateral to the stenosis-side hemisphere, which may result in general hypoperfusion across the whole brain. Previous studies have found that the opening rate of the anterior communicating artery in patients with CAS was significantly higher than that of healthy controls (Lee et al., 2004). Marshall et al. (2017) showed that cerebral blood flow (CBF) of both the anterior and posterior circulation regions of both hemispheres in patients with CAS was lower than that of healthy controls. Third, the same study found that the posterior circulation regions also showed hypoperfusion, whereas the occipital and cerebellar cortices were barely affected, which led them to speculate that the anterior circulation region, but not the but posterior circulation, is susceptible to hypoperfusion (Marshall et al., 2017).

We also found that atrophy of the stenosis-side hemisphere was more severe than that of the contralateral hemisphere. Previous study findings on asymmetrical atrophy are inconsistent. Nickel et al. (2019) did not find significant reductions in cortical thickness in brain regions ipsilateral to the stenosis. Asllani et al. (2016) reported significant reductions in cortical thickness on the stenosis-side hemisphere, but

**TABLE 4 |** Details of gray matter regions reaching statistical significance in comparison between CAS patients and healthy controls.

| Anatomical structure | Brodmann area | MNI coordinates | | | Voxel size | $P_{FDR}$ | *t* | *z* |
|---|---|---|---|---|---|---|---|---|
| | | *x* | *y* | *z* | | | | |
| ***On Stenosis Side*** | | | | | | | | |
| Frontal and temporal lobe | 21, 22, 13, 40, 11 | -42 | 34.5 | 6 | 25300 | 0.001 | 7.47 | 5.27 |
| Limbic lobe | 36, 25 | −22.5 | −24 | −7.5 | 4029 | 0.001 | 6.03 | 4.62 |
| Basal ganglia | | −24 | −43.5 | −10.5 | 378 | 0.013 | 3.72 | 3.26 |
| Superior frontal gyrus | 10, 32 | −12 | 66 | 15 | 1262 | 0.006 | 4.39 | 3.70 |
| Cingulate gyrus | 23, 24 | 0 | −12 | 31.5 | 787 | 0.010 | 3.94 | 3.41 |
| ***On contralateral side*** | | | | | | | | |
| Inferior frontal gyrus | 47, 44, 45 | 51 | 36 | −3 | 1766 | 0.002 | 5.48 | 4.34 |
| Limbic lobe | 19, 36 | 22.5 | −55.5 | −7.5 | 531 | 0.002 | 5.63 | 4.42 |
| Middle occipital gyrus | 19, 37 | 45 | −73.5 | −7.5 | 593 | 0.004 | 4.70 | 3.90 |
| Parahippocampal gyrus | 27, 28 | 22.5 | −24 | −9 | 569 | 0.003 | 5.10 | 4.13 |
| Medial frontal gyrus | 10, 32 | 7.5 | 52.5 | 13.5 | 1017 | 0.005 | 4.43 | 3.73 |
| Insular lobe | 13 | 39 | −9 | 10.5 | 1259 | 0.001 | 6.29 | 4.75 |
| Occipital cuneus | 18, 19 | 18 | −94.5 | 18 | 369 | 0.012 | 3.79 | 3.30 |
| Superior parietal lobule | 39, 40 | 30 | −73.5 | 45 | 3406 | 0.001 | 5.84 | 4.53 |
| Superior temporal gyrus | 13, 40 | 45 | −37.5 | 16.5 | 219 | 0.004 | 4.70 | 3.90 |
| Superior frontal gyrus | 6 | 25.5 | −12 | 67.5 | 279 | 0.007 | 4.22 | 3.59 |

*MNI, Montreal Neurological Institute.*

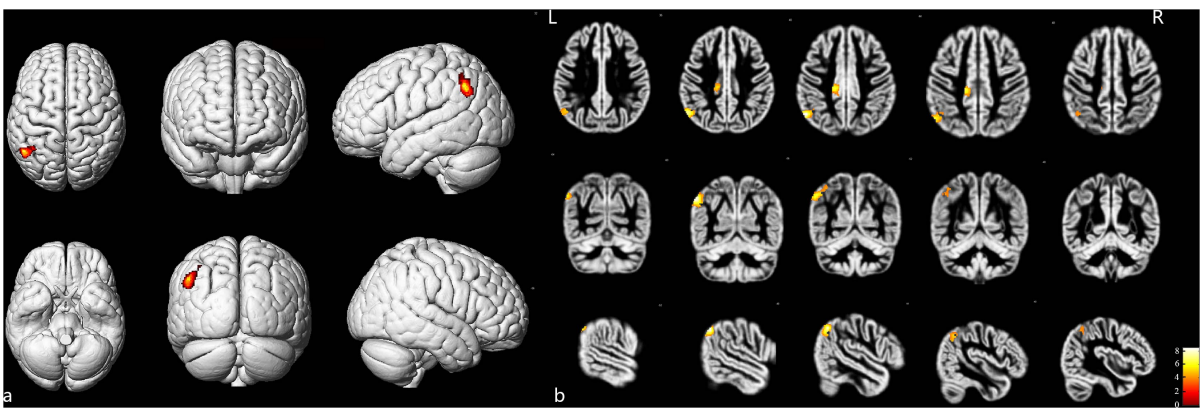


**FIGURE 3 |** Stenosis-side hemisphere vs. contralateral hemisphere. **(a)** Three-dimensional image. **(b)** Slice view. The stenosis-side hemisphere suffered more severe atrophy on inferior parietal lobule and cingulate gyrus, compared with contralateral hemisphere. L: left, R: right.

no difference was observed in cortical volumes between the stenosis and the contralateral hemispheres. Marshall and Avelar drew similar conclusions by confirming a greater reduction of cortical volumes of the stenosis-side hemisphere (Avelar et al., 2016; Marshall et al., 2017). Differences in the inclusion and exclusion criteria and algorithms may contribute to the inconsistent findings.

Comparisons between the two hemispheres carry the issue of structural asymmetries of the brain, and detection of brain asymmetries requires methods that can establish accurate spatial correspondence not only across subjects, but also across an individual's hemispheres. VBM was proven to be capable of capturing gray matter asymmetries with an extremely high voxel-based regional accuracy. Thus, we followed the VBM guideline published by Kurth et al. to analyze the structural asymmetries in cortical atrophy in CAS patients. According to this guideline, regional specificity and accurate spatial correspondence is ensured by the spatial normalization of images into the symmetrical TPM, using the DARTEL algorithm (Kurth et al., 2015). Moreover, we used an explicit brain mask to avoid the blurring of information across hemispheres and to control the possible impact of noise in the data. These modifications were included in our study to maximize the accuracy of our study.

## Cognitive Impairment

In this study, we found that patients with asymptomatic unilateral severe CAS performed poorly in the CMS examination, which indicated memory impairment in patients with CAS. Numerous studies have reported similar levels of memory decline in patients with CAS (Hayashi et al., 2004; Lee et al.,

**TABLE 5 |** Details of gray matter regions reaching statistical significance in the ipsilateral and the contralateral comparison and memory function-related cortex.

| Anatomical structure | Brodmann area | MNI coordinates | | | Voxel size | $P_{FDR}$ | *t* | *z* | *r** | *P** |
|---|---|---|---|---|---|---|---|---|---|---|
| | | *x* | *y* | *z* | | | | | | |
| Ipsilateral vs. Contralateral ‡ | | | | | | | | | | |
| Left inferior parietal lobule | 40 | −51 | −58.5 | 39 | 236 | 0.001 | 8.50 | 5.47 | – | – |
| Left cingulate gyrus | 31 | −15 | −27 | 42 | 124 | 0.004 | 6.64 | 4.77 | – | – |
| Memory function related cortex§ | | | | | | | | | | |
| General memory | | | | | | | | | | |
| Left middle frontal gyrus | 10 | −22.5 | 46.5 | 22.5 | 312 | 0.022 | 5.82 | 4.31 | 0.841 | 0.001 |
| Left frontal pars triangularis | 46 | −42 | 27 | 19.5 | 252 | 0.022 | 5.78 | 4.29 | 0.724 | 0.001 |
| Left frontal pars opercularis | 44 | −60 | 6 | 12 | 473 | 0.022 | 6.16 | 4.46 | 0.798 | 0.001 |
| Associative memory | | | | | | | | | | |
| Left middle frontal gyrus | 10 | −30.5 | 51 | 13.5 | 137 | 0.048 | 6.86 | 4.75 | 0.853 | 0.001 |
| Semantic memory | | | | | | | | | | |
| Left frontal pars opercularis | 44 | −58.5 | 3 | 15 | 157 | 0.015 | 6.47 | 4.59 | 0.695 | 0.001 |

‡*Paired t-test.* §*Multiple regression analysis.* **Pearson correlation analysis.*
*MNI, Montreal Neurological Institute.*

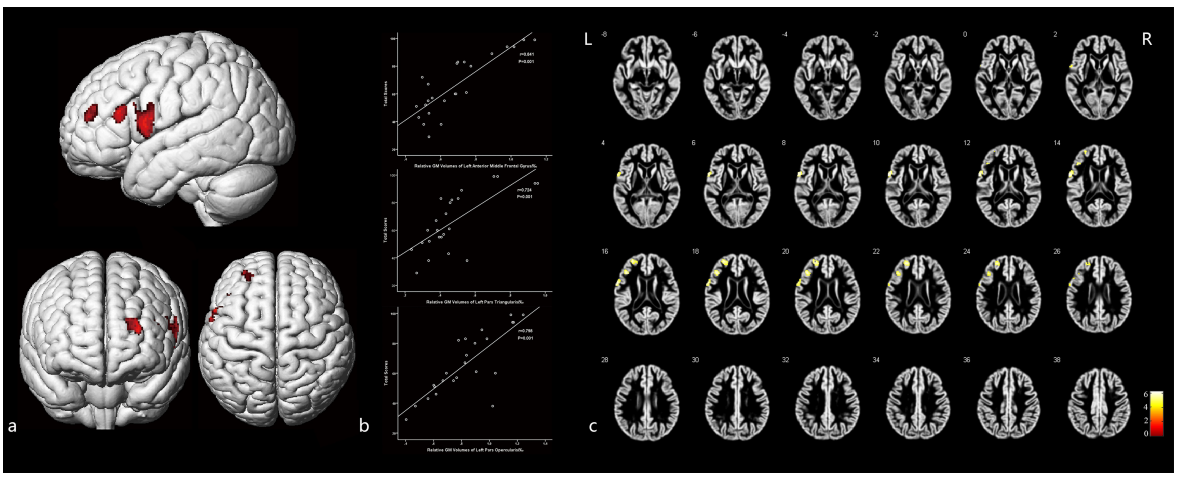


**FIGURE 4 |** The cortex related with general memory function and their Pearson correlation coefficients. **(a)** Three-dimensional image. **(b)** Correlation between the total scores of CMS and regional relative GM volumes. **(c)** Slice view. GM volumes of the left pars opercularis gyri frontalis inferioris, left pars triangularis gyri frontalis inferioris, and the frontal part of left middle frontal gyrus were positively related with the total clinical memory scores closely. L: left, R: right.

2004; Laura et al., 2012). Scores of directed memory, associative learning, free image recall, and portrait characteristic recall were significantly lower in patients than in healthy controls, which indicated that the corresponding memory functions were impaired. Furthermore, lower scores in the direct memory and associative learning test indicated impaired semantic memory function. Lower scores in the free image recall and portrait characteristic recall test proved that non-verbal memory was also impaired in patients with CAS. Previous studies have also reported similar results (Newman et al., 2005; Laura et al., 2012). However, scores in the meaningless graphic recognition test were lower than those of healthy controls, but not significantly so. Our relatively small sample size may account for this result. Furthermore, this may also indicate that non-verbal memory decline may not have been as prominent as semantic memory impairment.

Mini-mental state examination was used in our research to detect moderate and severe cognitive impairment (Folstein et al., 1978). The MMSE scores of patients with CAS were slightly lower than those of healthy controls; however, the scores were defined as normal, which is consistent with previous studies (Martinić-Popović et al., 2009; Luo et al., 2018). This indicated that cognitive impairment in asymptomatic patients is relatively mild.

## The Relationship Between Memory Impairment and Regional GM Volumes

### General Memory Function

We found that the GM volumes of the left frontal pars triangularis, left frontal pars opercularis, and the frontal part of the left middle frontal gyrus were strongly positively correlated with the total score of CMS. This indicated that GM atrophy

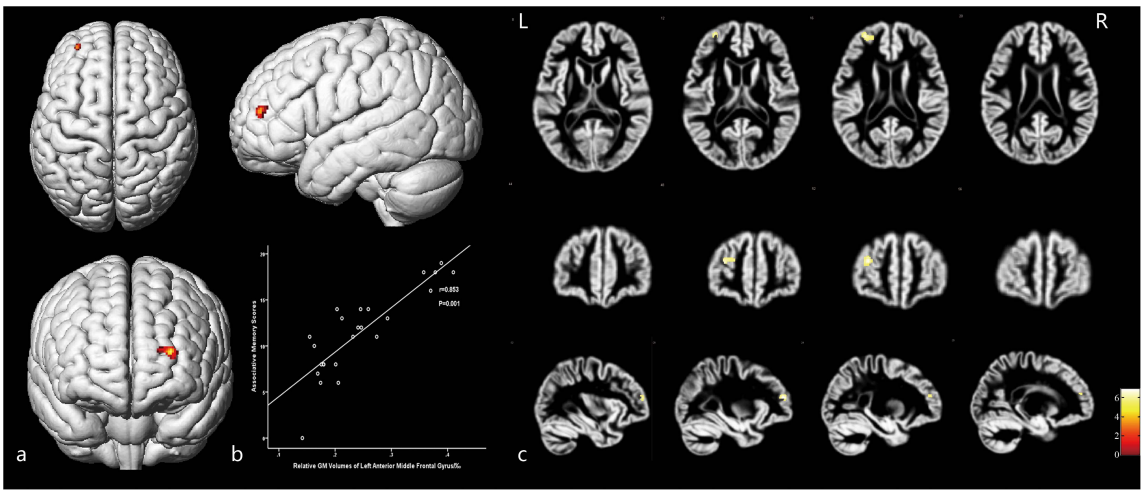


**FIGURE 5 |** The cortex related to associative memory and their Pearson correlation coefficients. **(a)** Three-dimensional image. **(b)** Correlation between associative scores and regional relative GM volumes. **(c)** Slice view. GM volumes of the anterior medial frontal gyrus cortex were positively related with the associative memory scores. L: left, R: right.

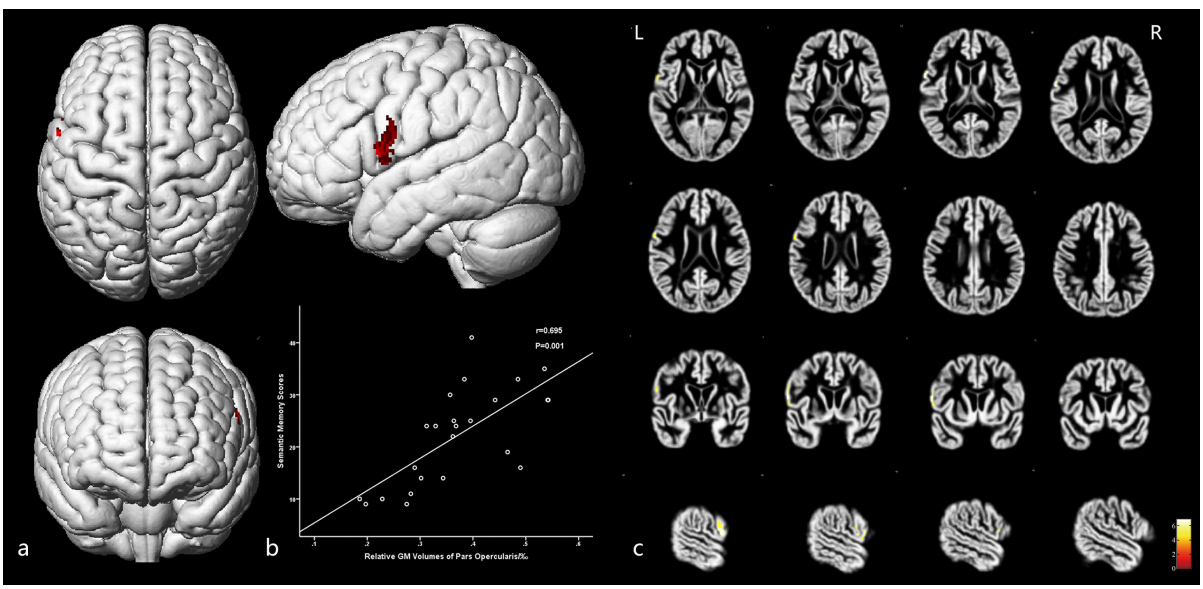


**FIGURE 6 |** The cortex related to semantic memory and their Pearson correlation coefficients. **(a)** Three-dimensional image. **(b)** Correlation between semantic memory scores and regional relative GM volumes. **(c)** Slice view. GM volumes of the posterior inferior frontal gyrus were positively related with the semantic memory scores. L: left, R: right.

in these areas caused by CAS may be an important factor underlying the memory impairment in patients. Several studies have also found that cerebral atrophy may account for the decline in memory, execution, attention, and other functions, although focus was primarily on whole brain volume rather than specific regional GM volume (Hayashi et al., 2004; Newman et al., 2005; Romero et al., 2009). In this study, we not only identified the specific correlated cortical areas form extensive atrophied areas but also demonstrated how they correlated with memory function. These findings may provide theoretical support and inspiration for clinical practice and further studies.

In cognitive neuroscience, the prefrontal cortex (PFC) has been shown to play an important role in memory functions. D'Esposito and Postle (1999) reported that damage to the PFC may not affect short-term memory but may impair the maintenance and processing of memory. Fuster et al. (1985) demonstrated that a hypothermic PFC reduced performance of delayed memory, which supports our results. Furthermore, the PFC can be divided into the dorsolateral prefrontal cortex

(DLPFC), at or near Brodmann's areas (BA) 9/10 and 46, and the ventrolateral prefrontal cortex (VLPFC), at or near BA 6/8, 44, 45, and 47, according to their cognitive functions and anatomical structure (Ranganath, 2006). In our study, the pars opercularis and pars triangularis of the inferior frontal gyrus were a part of the VPFC and the frontal part of left middle frontal gyrus belonged to the DLPFC. The VLPFC is activated in tasks that require transient encoding (Paller and Wagner, 2002), organizing, reordering (Blumenfeld, 2006), and maintaining relevant items (Ranganath et al., 2004) and inhibiting distractions (Konishi et al., 1999). More specifically, the area near BA 6 and 8 is involved in encoding spatial items (Courtney et al., 1998), the area near left BA 45 and 47 is activated during classification and comparison of semantic items (Wagner et al., 2001b), the area near BA 44 and 47 is engaged during non-verbal memory (Braver et al., 2001), and that near BA 44 and 45 is involved in resisting distractions (Thompson-Schill and D'Esposito, 1997). Moreover, the DLPFC is activated in memory tasks that require reasoning and relating (Kroger et al., 2002; Blumenfeld, 2006; Murray and Ranganath, 2007), especially in tasks involving reasoning abstract relation (Kroger et al., 2002; Badre and Wagner, 2004), encoding relationships between items (Davachi and Goldman-Rakic, 2001), and reordering relevant items (Blumenfeld, 2006). Taken together, these findings explain why extensive atrophy of both the VLPFC and DLPFC due to CAS can lead to a decline in general memory functions. These findings also offer theoretical support for our findings.

### Associative Memory

We found that GM volumes of the frontal part of the left middle frontal gyrus were positively correlated with associative memory scores, which indicated that atrophy of this region leads to associative memory decline. In previous studies, the DLPFC has been shown to be involved in memory tasks that require relating and reasoning (Kroger et al., 2002; Blumenfeld, 2006). Blumenfeld (2006) reported that the DLPFC was activated in tasks requiring reordering items, and Wagner et al. (2001a) found that the DLPFC was involved in encoding relationships among relevant items. These findings explained why atrophy of the left middle frontal gyrus results in associative memory impairment. Although some studies have found that the middle temporal gyrus and hippocampus are also involved in associative memory (Diana et al., 2007; Mayes et al., 2007), Becker et al. (2015) found that atrophy of these regions due to aging was not severe and Brehmer et al. (2020) demonstrated that atrophy of the frontal lobe can predict memory function more precisely in older adults. Similarly, atrophy of the middle temporal gyrus and hippocampus may not have been severe enough, or alternatively, they may not be closely correlated with associative memory in CAS patients.

### Semantic Memory

The GM volumes of the left pars opercularis were positively correlated with semantic memory scores, which suggested that GM atrophy may lead to semantic memory decline. The left pars opercularis is located in the posterior VLPFC, which has been shown to be involved in semantic memory processes (Wagner et al., 2001b; Murray and Ranganath, 2007). Poldrack et al. (1999) reported that the VLPFC is specifically activated in memory tasks requiring semantic processing, and the posterior/dorsal region is active in both semantic and phonological processing. In a review of previous studies, they found that the posterior/dorsal VLPFC is also involved in semantic generation, semantic decision, lexical tasks, and viewing the world (Poldrack et al., 1999). Additionally, Stebbins et al. (2002) reported that semantic memory decline caused by aging was related to the reduced function of the DLPFC. These studies support our findings and suggest that atrophy of the VLPFC may be a leading risk factor of semantic memory impairment in patients with CAS.

## 7T-MRI

Benefiting from ultra-high resolution, 7T-MRI has become more widely used in clinical work and scientific research. Wei et al. (2018) demonstrated that 7T-MRI could visualize the superficial temporal artery as well as DSA. Furthermore, Matsushige et al. (2016a) succeeded in visualizing the triple-layered microstructure of the giant aneurysm wall using 7T-MRI. They also applied 7T TOF-MRI to detect submillimeter-range microaneurysms that are invisible under DSA and 3T-MRI (Matsushige et al., 2016b). Furthermore, Lüsebrink et al. (2013) further found that 7T-MRI T1 images are more precise than 3T-MRI for segmentation for structural analyses. However, there is still some debate regarding structural analyses of 7T-MRI images (Seiger et al., 2015; Chen et al., 2017) and further studies are needed.

## Limitation

We analyzed the 7T-MRI data of 24 patients with asymptomatic severe CAS and 10 healthy controls. Although our sample size is the largest among previous reports, the absolute number of patients is still small, which may result in false positives or negatives. In addition, we only analyzed memory functions and did not investigate other cognitive functions. Finally, structural analysis of 7T-MRI images remains controversial at this stage. Despite using the best available correction and processing procedures, insufficiencies are still likely and further studies are required.

# CONCLUSION

Patients with asymptomatic severe CAS show greater memory impairment compared with healthy controls. Patients with asymptomatic severe unilateral CAS showed extensive GM atrophy in the frontal, temporal, and parietal lobes and in small parts of the occipital lobe in both the stenosis-side and the contralateral hemispheres. The areas were consistent with the anterior circulation region. GM atrophy of the stenosis hemisphere was more severe than that of contralateral hemisphere. Memory impairment in patients with asymptomatic severe CAS may be related to GM atrophy of the left inferior frontal and middle frontal gyri. Moreover, the atrophy of the anterior medial frontal gyrus may be responsible for the decline

of associative memory, whereas atrophy of the posterior inferior frontal gyrus may contribute to the decline of semantic memory.

## DATA AVAILABILITY STATEMENT

The datasets presented in this article are not readily available in order to protect the subjects' privacy. Requests to access the datasets should be directed to YZ, yanzhang135@163.com.

## ETHICS STATEMENT

The studies involving human participants were reviewed and approved by the Ethics Committee of Beijing Tiantan Hospital, Capital Medical University. The patients/participants provided their written informed consent to participate in this study.

## AUTHOR CONTRIBUTIONS

PW, RL, and YZ: conception and design. PW and RL: acquisition of data. PW: analysis and interpretation of data and drafting the article. HC, RL, ZZ, DZ, and YZ: technical, administrative, and material support. YZ: approving the final version of the manuscript on behalf of all authors. YZ: study supervision. All authors critically revised the article and reviewed the submitted version of the manuscript.

## FUNDING

This work was supported by the Program of the National Natural Science Foundation of China (81870833) and the Capital Health Research and Development of Special Project (2016-2-2043).

## REFERENCES

Asllani, I., Slatterya, P., Fafarda, A., Pavol, M., Lazar, R. M., and Marshall, R. S. (2016). Measurement of cortical thickness asymmetry in carotid occlusive disease. *NeuroImage Clin.* 12, 640–644. doi: 10.1016/j.nicl.2016.09.013

Avelar, W. M., D'Abreu, A., Coan, A. C., Lima, F. O., Guimarães, R., Yassuda, C. L., et al. (2016). Asymptomatic carotid stenosis is associated with gray and white matter damage. *Int. J. Stroke* 10, 1197–1203. doi: 10.1111/ijs.12574

Badre, D., and Wagner, A. D. (2004). Selection, integration, and conflict monitoring; assessing the nature and generality of prefrontal cognitive control mechanisms. *Neuron* 41, 473–487. doi: 10.1016/s0896-6273(03)00851-1

Barnett, H. J., Taylor, D. W., Eliasziw, M., Fox, A. J., Ferguson, G. G., Haynes, R. B., et al. (1998). Benefit of Carotid Endarterectomy in Patients with Symptomatic Moderate or Severe Stenosis. *N. Engl. J. Med.* 339, 1415–1425. doi: 10.1056/NEJM199811123392002

Becker, N., Laukka, E. J., Kalpouzos, G., Naveh-Benjamin, M., Bäckman, L., and Brehmer, Y. (2015). Structural brain correlates of associative memory in older adults. *NeuroImage* 118, 146–153. doi: 10.1016/j.neuroimage.2015.06.002

Blumenfeld, R. S. (2006). Dorsolateral prefrontal cortex promotes long-term memory formation through its role in working memory organization. *J. Neurosci.* 26, 916–925. doi: 10.1523/JNEUROSCI.2353-05.2006

Braver, T. S., Barch, D. M., Kelley, W. M., Buckner, R. L., Cohen, N. J., Miezin, F. M., et al. (2001). Direct Comparison of Prefrontal Cortex Regions Engaged by Working and Long-Term Memory Tasks. *NeuroImage* 14, 48–59. doi: 10.1006/nimg.2001.0791

Brehmer, Y., Nilsson, J., Berggren, R., Schmiedek, F., and Lövdén, M. (2020). The importance of the ventromedial prefrontal cortex for associative memory in older adults: A latent structural equation analysis. *NeuroImage* 209:116475. doi: 10.1016/j.neuroimage.2019.116475

Chen, Z., Liu, M. Q., and Ma, L. (2017). Surface-Based Morphometry of Human Brain: Intra-Individual Comparison Between 3T and 7T High Resolution Structural MR Imaging. *Chin. Med. Sci. J.* 32, 226–231. doi: 10.24920/J1001-9294.2017.031

Courtney, S. M., Petit, L., Maisog, J. M., Ungerleider, L. G., and Haxby, J. V. (1998). An area specialized for spatial working memory in human frontal cortex. *Science* 279, 1347–1351. doi: 10.1126/science.279.5355.1347

D'Esposito, M., and Postle, B. R. (1999). The dependence of span and delayed-response performance on prefrontal cortex. *Neuropsychologia* 37, 1303–1315. doi: 10.1016/s0028-3932(99)00021-4

Dancey, C. P., and Reidy, J. (2007). *Statistics without Maths for Psychology*. Hoboken, NJ: Prentice-Hall, Inc.

Das, S. R., Avants, B. B., Pluta, J., Wang, H., Suh, J. W., Weiner, M. W., et al. (2012). Measuring longitudinal change in the hippocampal formation from in vivo high-resolution T2-weighted MRI. *NeuroImage* 60, 1266–1279. doi: 10.1016/j.neuroimage.2012.01.098

Davachi, L., and Goldman-Rakic, P. S. (2001). Primate rhinal cortex participates in both visual recognition and working memory tasks: functional mapping with 2-DG.[J]. *J. Neurophysiol.* 85, 2590–2601. doi: 10.1152/jn.2001.85.6.2590

Diana, R. A., Yonelinas, A. P., and Ranganath, C. (2007). Imaging recollection and familiarity in the medial temporal lobe: A three-component model. *Trends Cogn. Sci.* 11, 379–386. doi: 10.1016/j.tics.2007.08.001

Folstein, M. F., Folstein, S. E., and Mchugh, P. R. (1978). "Mini-mental state". A practical method for grading the cognitive state of patients for the clinician. *J. Psychiatr. Res.* 12, 189–198. doi: 10.1016/0022-3956(75)90026-6

Fuster, J. M., Bauer, R. H., and Jervey, J. P. (1985). Functional interactions between inferotemporal and prefrontal cortex in a cognitive task. *Brain Res.* 330, 299–307. doi: 10.1016/0006-8993(85)90689-4

Gabriella, N., Tamás, S., Zsófia, S., Dávid, G., Pálma, D., Zsigmond, K. T., et al. (2018). Stepwise occlusion of the carotid arteries of the rat: MRI assessment of the effect of donepezil and hypoperfusion-induced brain atrophy and white matter microstructural changes. *PLoS One* 13:e0198265. doi: 10.1371/journal.pone.0198265

Harrison, T. M., Mahmood, Z., Lau, E. P., Karacozoff, A. M., Burggren, A. C., Small, G. W., et al. (2016). An Alzheimer's Disease Genetic Risk Score Predicts Longitudinal Thinning of Hippocampal Complex Subregions in Healthy Older Adults. *eNeuro* 3, e98–e16. doi: 10.1523/ENEURO.0098-16.2016

Hayashi, A., Kosaka, M., Kimura, A., Wako, Y., Kawasako, K., and Hamada, S. (2004). Reduced neuropsychological test performance in asymptomatic carotid stenosis: The Troms Study. *Neurology* 62, 695–701. doi: 10.1016/j.jvs.2004.08.008

Kim, H. J., Ye, B. S., Yoon, C. W., Noh, Y., and Sang, W. S. (2014). Cortical thickness and hippocampal shape in pure vascular mild cognitive impairmentand dementia. *Eur. J. Neurol.* 21, 744–751. doi: 10.1111/ene.12376

Konishi, S., Nakajima, K., Uchida, I., Kikyo, H., Kameyama, M., and Miyashita, Y. (1999). Common Inhibitory Mechanism in Human Inferior Prefrontal Cortex Revealed by Event-Related Functional MRI. *Brain* 122, 981–991. doi: 10.1093/brain/122.5.981

Kroger, J. K., Sabb, F. W., Fales, C. L., Bookheimer, S. Y., Cohen, M. S., and Holyoak, K. J. (2002). Recruitment of anterior dorsolateral prefrontal cortex in human reasoning: a parametric study of relational complexity. *Cereb. Cortex* 5, 477–485. doi: 10.1093/cercor/12.5.477

Kurth, F., Gaser, C., and Luders, E. (2015). A 12-step user guide for analyzing voxel-wise gray matter asymmetries in statistical parametric mapping (SPM). *Nat. Protoc.* 10, 293–304. doi: 10.1038/nprot.2015.014

Laura, C. H., Maite, G., Dolors, B. G., Carlos, C. B. J., Josep, R., and Miquel, A. (2012). The effect of carotid occlusion in cognition before endarterectomy. *Arch. Clin. Neuropsychol.* 27, 879–890. doi: 10.1093/arclin/acs075

Lee, J. H., Choi, C. G., Kim, D. K., Kim, G. E., Lee, H. K., and Suh, D. C. (2004). Relationship between circle of Willis morphology on 3D time-of-flight MR angiograms and transient ischemia during vascular clamping of the internal

carotid artery during carotid endarterectomy. *AJNR Am. J. Neuroradiol.* 25, 558–564. doi: 10.1080/02841850410004418

Luo, R. T., Wang, P. J., Deng, X. F., Zhou, S. J., Zhao, M., Qian, J., et al. (2018). An Integrated Analysis of Risk Factors of Cognitive Impairment in Patients with Severe Carotid Artery Stenosis. *Biomed Environ. Sci.* 31, 797–804. doi: 10.3967/bes2018.107

Lüsebrink, F., Wollrab, A., and Speck, O. (2013). Cortical thickness determination of the human brain using high resolution 3T and 7T MRI data. *NeuroImage* 70, 122–131. doi: 10.1016/j.neuroimage.2012.12.016

Marshall, R. S., Asllani, I., Pavol, M. A., Cheung, Y., and Lazar, R. M. (2017). Altered cerebral hemodyamics and cortical thinning in asymptomatic carotid artery stenosis. *PLoS One* 12:e0189727. doi: 10.1371/journal.pone.0189727

Martinić-Popović, I., Lovrenciæ-Huzjan, A., and Demarin, V. (2009). Assessment of subtle cognitive impairment in stroke-free patients with carotid disease. *Acta Clin. Croat.* 48, 231–240.

Matsushige, T., Chen, B., Ringelstein, A., Umutlu, L., Forsting, M., Quick, H. H., et al. (2016a). Giant Intracranial Aneurysms at 7T MRI. *AJNR Am. J. Neuroradiol.* 37, 636–641. doi: 10.3174/ajnr.A4569

Matsushige, T., Kraemer, M., Schlamann, M., Berlit, P., Forsting, M., Ladd, M. E., et al. (2016b). Ventricular Microaneurysms in Moyamoya Angiopathy Visualized with 7T MR Angiography. *AJNR Am. J. Neuroradiol.* 37, 1669–1672. doi: 10.3174/ajnr.A4786

Mayes, A., Montaldi, D., and Migo, E. (2007). Associative memory and the medial temporal lobes. *Trends Cogn. Sci.* 11, 126–135. doi: 10.1016/j.tics.2006.12.003

Muller, M., van der Graaf, Y., Algra, A., Hendrikse, J., Mali, W. P., and Geerlings, M. I. (2011). Carotid atherosclerosis and progression of brain atrophy: the SMART-MR study. *Ann. Neurol.* 70, 237–244. doi: 10.1016/j.jalz.2011.05.860

Murray, L. J., and Ranganath, C. (2007). The Dorsolateral Prefrontal Cortex Contributes to Successful Relational Memory Encoding. *J. Neurosci.* 27, 5515–5522. doi: 10.1523/JNEUROSCI.0406-07.2007

Newman, A. B., Fitzpatrick, A. L., Lopez, O., Jackson, S., and Kuller, L. H. (2005). Dementia and Alzheimer's disease incidence in relationship to cardiovascular disease in the Cardiovascular Health Study cohort. *J. Am. Geriatr. Soc.* 53, 1101–1107. doi: 10.1111/j.1532-5415.2005.53360.x

Nickel, A., Kessner, S., Niebuhr, A., Schrder, J., and Thomalla, G. (2019). Cortical thickness and cognitive performance in asymptomatic unilateral carotid artery stenosis. *BMC Cardiovasc. Disord.* 19:154. doi: 10.1186/s12872-019-1127-y

Paller, K. A., and Wagner, A. D. (2002). Observing the transformation of experience into memory. *Trends Cogn. Sci.* 6, 93–102. doi: 10.1016/s1364-6613(00)01845-3

Pettigrew, C., Soldan, A., Zhu, Y., Wang, M. C., Moghekar, A., Brown, T., et al. (2016). Cortical thickness in relation to clinical symptom onset in preclinical AD. *Neuroimage Clin.* 12, 116–122. doi: 10.1016/j.nicl.2016.06.010

Pettigrew, L. C., Thomas, N., Howard, V. J., Veltkamp, R., and Toole, J. F. (2000). Low mini-mental status predicts mortality in asymptomatic carotid arterial stenosis. *Asymptomat. Carotid Atheroscler. Study investigat. Neurol.* 55, 30–34. doi: 10.1212/WNL.55.1.30

Poldrack, R. A., Wagner, A. D., Prull, M. W., Desmond, J. E., Glover, G. H., and Gabrieli, J. D. (1999). Functional specialization for semantic and phonological processing in the left inferior prefrontal cortex. *NeuroImage* 10, 15–35. doi: 10.1006/nimg.1999.0441

Ranganath, C. (2006). Working memory for visual objects: Complementary roles of inferior temporal, medial temporal, and prefrontal cortex. *Neuroscience* 139, 277–289. doi: 10.1016/j.neuroscience.2005.06.092

Ranganath, C., Cohen, M. X., Dam, C., and D'Esposito, M. (2004). Inferior Temporal, Prefrontal, and Hippocampal Contributions to Visual Working Memory Maintenance and Associative Memory Retrieval. *J. Neurosci.* 26, 916–925. doi: 10.1523/JNEUROSCI.5053-03.2004

Romero, J. R., Beiser, A., Seshadri, S., Benjamin, E. J., and Wolf, P. A. (2009). Carotid Artery Atherosclerosis, MRI Indices of Brain Ischemia, Aging, and Cognitive Impairment The Framingham Study. *Stroke* 40, 1590–1596. doi: 10.2352/J.ImagingSci.Technol.200751:2(127)

Seiger, R., Hahn, A., Hummer, A., Kranz, G. S., Ganger, S., Küblböck, M., et al. (2015). Voxel-based morphometry at ultra-high fields. A comparison of 7T and 3T MRI data. *NeuroImage* 113, 207–216. doi: 10.1016/j.neuroimage.2015.03.019

Seo, S. W., Ahn, J., Yoon, U., Im, K., Lee, J. M., and Tae Kim, S. (2010). Cortical thinning in vascular mild cognitive impairment and vascular dementia of subcortical type. *J. Neuroimaging* 20, 37–45. doi: 10.1111/j.1552-6569.2008.00293.x

Shaw, M. E., Abhayaratna, W. P., Sachdev, P. S., Anstey, K. J., and Cherbuin, N. (2016). Cortical Thinning at Midlife: The PATH Through Life Study. *Brain Topogr.* 29, 1–10. doi: 10.1007/s10548-016-0509-z

Smith, E. E. (2017). Clinical presentations and epidemiology of vascular dementia. *Clin. Sci.* 131, 1059–1068. doi: 10.1042/CS20160607

Stebbins, G. T., Carrillo, M. C., Dorfman, J., Dirksen, C., Desmond, J. E., Turner, D. A., et al. (2002). Aging effects on memory encoding in the frontal lobes. *Psychol. Aging* 17, 44–55. doi: 10.1037//0882-7974.17.1.44

Thompson-Schill, S. L., and D'Esposito, M. (1997). Aguirre1 GK, Farah MJ. Role of left inferior prefrontal cortex in retrieval of semantic knowledge: A reevaluation. *Proc. Natl. Acad. Sci. U S A.* 94, 14792–14797. doi: 10.1073/pnas.94.26.14792

Wagner, A. D., Maril, A., Bjork, R. A., and Schacter, D. L. (2001a). Prefrontal Contributions to Executive Control: fMRI Evidence for Functional Distinctions within Lateral Prefrontal Cortex. *NeuroImage* 14, 1337–1347. doi: 10.1006/nimg.2001.0936

Wagner, A. D., Pare-Blagoev, E. J., Clark, J., and Poldrack, R. A. (2001b). Recovering meaning: left prefrontal cortex guides controlled semantic retrieval. *Neuron* 31, 329–338. doi: 10.1016/s0896-6273(01)00359-2

Wei, N., Zhang, Z., An, J., Weng, D., and Zhuo, Y. (2018). Improved visualization of superficial temporal artery using segmented time-of-flight MR angiography with venous suppression at 7T. *Neuroradiology* 60, 1243–1246. doi: 10.1007/s00234-018-2099-9

Weston, P. S., Nicholas, J. M., Lehmann, M., Ryan, N. S., Liang, Y., Macpherson, K., et al. (2016). Presymptomatic cortical thinning in familial Alzheimer disease: A longitudinal MRI study. *Neurology* 87, 2050–2057. doi: 10.1212/WNL.0000000000003322

**Conflict of Interest:** The authors declare that the research was conducted in the absence of any commercial or financial relationships that could be construed as a potential conflict of interest.

frontiers in Aging Neuroscience

ORIGINAL RESEARCH
published: 08 July 2021
doi: 10.3389/fnagi.2021.630437

# Development and Validation of a LASSO Prediction Model for Better Identification of Ischemic Stroke: A Case-Control Study in China

*Zirui Meng[1†], Minjin Wang[1†], Shuo Guo[1], Yanbing Zhou[1], Mingxue Zheng[1], Miaonan Liu[1], Yongyu Chen[1], Zhumiao Yang[1], Bi Zhao[2*] and Binwu Ying[1*]*

[1] Department of Laboratory Medicine, West China Hospital, Sichuan University, Chengdu, China, [2] Department of Neurology, West China Hospital, Sichuan University, Chengdu, China

OPEN ACCESS

**Edited by:**
Denis Gris,
Université de Sherbrooke, Canada

**Reviewed by:**
Jia-Da Li,
Central South University, China
Rüdiger Christoph Pryss,
Julius Maximilian University of Würzburg, Germany

***Correspondence:**
Binwu Ying
binwuying@126.com
Bi Zhao
bueaty84@126.com

[†] These authors have contributed equally to this work

**Received:** 17 November 2020
**Accepted:** 07 June 2021
**Published:** 08 July 2021

**Citation:**
Meng Z, Wang M, Guo S, Zhou Y, Zheng M, Liu M, Chen Y, Yang Z, Zhao B and Ying B (2021) Development and Validation of a LASSO Prediction Model for Better Identification of Ischemic Stroke: A Case-Control Study in China. Front. Aging Neurosci. 13:630437. doi: 10.3389/fnagi.2021.630437

**Background:** Timely diagnosis of ischemic stroke (IS) in the acute phase is extremely vital to achieve proper treatment and good prognosis. In this study, we developed a novel prediction model based on the easily obtained information at initial inspection to assist in the early identification of IS.

**Methods:** A total of 627 patients with IS and other intracranial hemorrhagic diseases from March 2017 to June 2018 were retrospectively enrolled in the derivation cohort. Based on their demographic information and initial laboratory examination results, the prediction model was constructed. The least absolute shrinkage and selection operator algorithm was used to select the important variables to form a laboratory panel. Combined with the demographic variables, multivariate logistic regression was performed for modeling, and the model was encapsulated within a visual and operable smartphone application. The performance of the model was evaluated on an independent validation cohort, formed by 304 prospectively enrolled patients from June 2018 to May 2019, by means of the area under the curve (AUC) and calibration.

**Results:** The prediction model showed good discrimination (AUC = 0.916, cut-off = 0.577), calibration, and clinical availability. The performance was reconfirmed in the more complex emergency department. It was encapsulated as the Stroke Diagnosis Aid app for smartphones. The user can obtain the identification result by entering the values of the variables in the graphical user interface of the application.

**Conclusion:** The prediction model based on laboratory and demographic variables could serve as a favorable supplementary tool to facilitate complex, time-critical acute stroke identification.

**Keywords: ischemic stroke, prediction model, laboratory variables, demographic variables, least absolute shrinkage and selection operator, smartphone app**

## INTRODUCTION

Stroke is currently the second cause of death worldwide and the leading cause of death in China. Approximately 70% of all strokes are ischemic and this will significantly increase the health burden due to the aging population (Zhou et al., 2016; GBD 2016 Causes of Death Collaborators, 2017; Wang et al., 2017). When it comes to treatment, intravenous tPA (tissue-type plasminogen activator) has been used to treat most acute ischemic strokes (AISs). However, it is highly risky and can be lethal in the case of intracerebral hemorrhage (ICH) (Zerna et al., 2018). Therefore, determining the stroke subtype in an early, timely, and accurate manner is essential to achieve proper treatment and good prognosis (Hankey, 2017; Deboevere et al., 2019). Furthermore, stroke mimics, which present with an acute neurological deficit simulating AIS and represent a significant percentage of all acute stroke hospital admissions, pose a diagnostic challenge to emergency physicians (Vilela, 2017; Liberman et al., 2019). A recent meta-analysis was performed on 23 studies, including a total of 15,721 patients and reported that the initial diagnosis was misdiagnosed in 26–40% of the cases. Besides, 2–26% of ischemic stroke (IS) patients were misdiagnosed (Tarnutzer et al., 2017). This might be due to the absence of acute ischemic signs or the presence of non-specific stroke symptoms on initial computed tomography (CT) imaging, as well as the interference of stroke mimics (Walsh, 2019). In such cases, the diagnosis may not be confirmed until additional imaging tests are performed several hours or even a day later, which results in missing the optimal intervention time (Martins et al., 2020). In addition, neuroimaging examination needs to be performed in a qualified medical institution with specialized equipment and under the guidance of professional physicians; these conditions seem overly ideal and unreliable for community hospitals and hospitals in most underdeveloped regions in Asia and Africa (Clarke et al., 2017). In China, only 10–20% of stroke patients can reach the medical institution qualified to complete neuroimaging examination within 3 h (Jin et al., 2012; Jiang et al., 2016). In addition, these neurological examination equipments are usually expensive, bulky, difficult to popularize, and in need for highly educated, trained, and skilled operators. Obviously, this is not conductive to the early clinical diagnosis and treatment in the case of inadequate medical conditions, such as community hospitals, primary hospitals, and clinics in regions where patients often do not have rapid access to imaging examinations (Chen et al., 2018; Mathur et al., 2019). Therefore, clinicians need a useful supplementary tool to promote early diagnosis and provide possible directions for the triage process and referral management at the initial visit, which is not to replace CT/magnetic resonance imaging but to complement its work and provide a necessary supplement.

The comprehensive diagnostic efficacy of blood biomarkers has been seriously underestimated or even ignored in stroke. However, with the recent research development, their application value has been revisited (El-Serag et al., 2014; Valappil et al., 2017; Lee et al., 2018; Dagonnier et al., 2021). Unlike univariate analysis in neuroimaging, some preliminary studies related to stroke classification have focused on models that combine blood biomarkers, showing great potential (Misra et al., 2017; Makris et al., 2018). As a result, more attention has been paid to blood biomarkers that can be objectively measured in the laboratory at hyperacute phase, hoping to assist in the accurate identification of ISs. The application of fast, reliable, and inexpensive blood biomarkers as an auxiliary tool, along with CT characteristics, would provide more diagnostic information that may improve stroke identification and management, especially in atypical or hyperacute IS (Wu et al., 2019; Fan et al., 2020; Baez et al., 2021).

In this study, we propose a stroke prediction model that combines demographic and laboratory variables to provide an early and accurate stroke prediction. Then, we validate the model in a more complex emergency department. This model can serve as a supplemental tool to help clinicians get more information to improve the identification of IS in the acute phase and provide the patients with an accurate treatment, which could significantly promote the prognosis.

## MATERIALS AND METHODS

### Study Subjects

The derivation cohort consisted of 322 patients with IS and 305 patients with other intracranial hemorrhagic diseases, including hemorrhagic stroke, subarachnoid hemorrhage, subdural hematoma, and brain tumor–associated ICH, who were admitted to West China Hospital of Sichuan University from March 2017 to June 2018. These patients were retrospectively enrolled to construct the prediction model. The exclusion criteria included patients younger

**Abbreviations:** IS, ischemic stroke; HP, hypertension; DM, diabetes mellitus; HLP, hyperlipidemia; RBC, red blood cell; Hb, hemoglobin; Hct, hematocrit; RDW, red cell distribution width; CV, coefficient of variation; SD, standard deviation; PLT, platelets; WBC, white blood cell; PT, prothrombin time; APTT, activated partial thromboplastin time; TT, thromboplastin time; FIB, fibrinogen; AT-III, antithrombin III; TBIL, total bilirubin; DBIL, direct bilirubin; ALT, alanine aminotransferase; IBIL, indirect bilirubin; TP, total protein; Alb, albumin; CREA, serum creatinine; URIC, uric acid; GLU, glucose; AST, glutamic oxaloacetic transaminase; ALP, alkaline phosphatase; CK, creatine kinase; GGT, γ-glutamyl transpeptidase; LDH, lactate dehydrogenase; HBDH, hydroxybutyrate dehydrogenase; TG, triglyceride; CHOL, cholesterol; HDLC, high-density lipoprotein cholesterol; LDLC, low-density lipoprotein cholesterol; TBA, total bile acid; DCA, decision curve analysis; AUC, area under the curve.

than 18 years or those treated with anticoagulation therapy before hospitalization. All the patients underwent a preliminary clinical evaluation, including the demographic characteristics, physical examination, electrocardiogram, laboratory examinations, and neuroimaging. The laboratory examinations were completed within 45 min after admission. The final diagnosis of all the patients was reconfirmed by a team of experienced vascular neurologists (three independent neurologists) based on the World Health Organization definitions, clinical symptoms, and neuroimaging findings.

The validation cohort consisted of 304 patients from the emergency department with suspected stroke symptoms (headache, dizziness, nausea, walking instability, partial sensory disturbance, language dysfunction, coma, etc.) on admission from June 2018 to May 2019. These patients were prospectively and consecutively included for the model validation. The same preliminary clinical evaluation was performed on all the patients, and their final definite diagnosis was obtained (IS, subarachnoid hemorrhage, hemorrhagic stroke, or stroke mimics) by a team of neurologists. The research process is shown in **Figure 1**.

Informed consents were obtained from all the participants. This study was approved by the Clinical Trials and Biomedical Ethics Committee of West China (no. 812) and was performed in accordance with the ethical standards as laid down in the 1964 Declaration of Helsinki and its later amendments or comparable ethical standards.

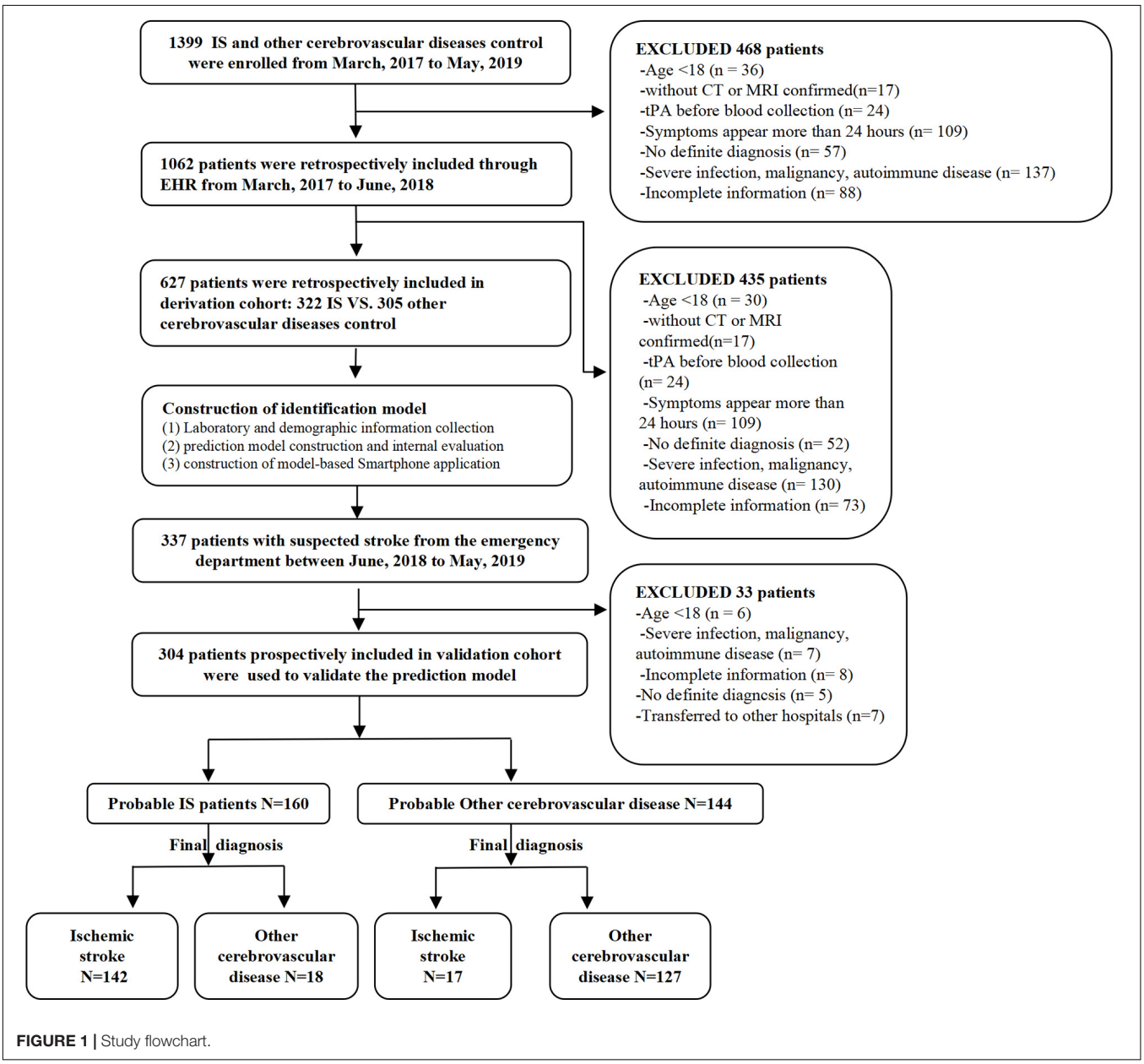


**FIGURE 1 |** Study flowchart.

## Variable Collection

The demographic characteristics (**Table 1**), including the age, smoking habits, drinking, hypertension, hyperlipidemia, and diabetes, were collected according to the uniform format by the resident physicians on admission. If the patients were dysphasic, aphasic, or unconscious, the information was then provided orally by their close relatives or legal representatives and documented in the patient's medical history.

The laboratory findings before therapy were collected through the laboratory management system of West China Hospital, including 35 indicators (**Table 1**) of complete blood count (SYSMEXXN-10, Sysmex, Japan), coagulation tests (SYSMEXCS-5100, Sysmex, Japan), and biochemical examination (Cobas c702, Roche, Germany). All tests were conducted according to the standard operating procedure (**Supplementary 1**).

## Variable Selection and Laboratory Panel Construction

In the derivation cohort, in order to select the IS predicting factors and obtain the corresponding coefficients, we first performed a statistical consolidation of all the laboratory variables using the least absolute shrinkage and selection operator (LASSO). First proposed by Robert Tibshirani in 1996, LASSO is a method of shrinkage estimate based on model reduction. The main idea of LASSO is to construct a first-order penalty function to shrink the regression coefficient of each variable to a certain range, independent of variable selection based on statistical significance. The variables with a coefficient of 0 are eliminated, and a panel of optimal and representative variables is finally obtained. Thus, the coefficients are optimized, and relatively unimportant variables are excluded. This can effectively avoid the influence of factors such as the number of variables, different orders of magnitude, various units, and possible colinearity between the indicators on the classical analysis methods. In this regard, the LASSO program can choose the truly valuable variables to constitute the model and has been well applied in multiple types of studies on different subjects (radiomics, genomics, and histology). In this work, the resulting predictors were combined to form a scoring formula called the "laboratory panel." As a result, a large number of laboratory variables were integrated into a single variable associated with IS.

## Construction of the Prediction Model and Smartphone Application

The prediction model was constructed based on the demographic variables together with the laboratory panel using univariate and multivariate logistic regression. Through 10-fold cross-validation, the model with the highest accuracy was selected and encapsulated as a visual Java-based smartphone application (app) (Wojciechowski et al., 2015). The app can be easily used by both patients and clinicians, who can input the required predictors into the graphical user interface to obtain the probability of IS.

## Evaluation of the Prediction Model

The model was evaluated by comparing the predicted results with the confirmed diagnoses in the validation cohort to calculate the metrics of sensitivity, specificity, positive predictive value (PPV), and negative predictive value (NPV). The area under the curve (AUC) and calibration curve were used to comprehensively evaluate the model's discrimination and consistency (Muntner et al., 2014).

## Statistical Analysis

Continuous variables are represented by the median (upper and lower quartiles). Categorical variables are expressed in terms of frequency. Comparisons of the categorical variables and continuous variables were performed using the $\chi^2$ test and Mann–Whitney *U* test. The LASSO algorithm was used to select laboratory variables and construct the "laboratory panel." Univariate logistic regression was used to select predictors of IS, and the model was constructed using multivariate logistic regression. All statistical analyses were completed using the R software version 3.5.0. The LASSO algorithm was performed by the "glmmet" R package, and the logistic regression model was constructed by the "glm" R package. The app was developed in Java.

# RESULTS

## Patient and Clinical Characteristics

A total of 931 patients were included in this study, among which 627 patients (322 IS vs. 305 controls) were enrolled in the derivation cohort, and 304 patients (159 IS vs. 145 controls) were enrolled in the validation cohort. There was no statistically significant difference in the frequency of IS between the derivation cohort (51.35%) and validation cohort (52.30%). The comparison of both control groups (derivation vs. validation) and IS groups (derivation vs. validation) is listed in **Supplementary 2**.

## Development of the Laboratory Panel and Prediction Model

Fourteen representative variables were screened by the LASSO method and integrated into a laboratory panel (**Table 2** and **Figures 2A,B**), which could obtain a C-index of 82%. The formula is as follows:

Laboratory score = $-2.4449367225 + 0.0324156962 \times$ age $+ 0.3467528672 \times$ hematocrit (Hct) $- 0.0328739639 \times$ red cell distribution width standard deviation (RDWSD) $+ 0.0023251346 \times$ platelets (PLT) $- 0.1514963590 \times$ white blood cell (WBC) $+ 0.0880501180 \times$ thromboplastin time (TT) $+ 0.2269026873 \times$ fibrinogen (FIB) $+ 0.0037785538 \times$ antithrombin III (AT-III) $+ 0.0023879174 \times$ alanine aminotransferase (ALT) $+ 0.0075773496 \times$ indirect bilirubin (IBIL) $- 0.0010988689 \times$ serum creatinine (CREA) $- 0.0493824972 \times$ glucose (GLU) $- 0.0002345279 \times$ creatine kinase (CK) $+ 0.0558149527 \times$ urea.

**TABLE 1 |** Baseline patient characteristics.

| Group | Derivation cohort (627) | | Validation cohort (304) | |
|---|---|---|---|---|
| | **Study group (322)** | **Control group (305)** | **Study group (159)** | **Control group (145)** |
| Subtype | IS (322) | HS (176) | IS (159) | HS (60) |
| | | SAH (45) | | SAH (21) |
| | | SDH (62) | | SDH (14) |
| | | Brain tumor–associated ICH (22) | | Brain tumor–associated ICH (11) |
| | | – | | SM (39) |
| Age, y | 63 (52.25–73.75) | 53 (43–64) | 65 (54–75) | 54 (45–65) |
| Sex (female) | 114 (35.40%) | 99 (32.46%) | 55 (34.59%) | 50 (34.48%) |
| Drinking | 136 (42.24%) | 103 (33.77%) | 63 (39.62%) | 48 (33.10%) |
| Smoking | 148 (45.96%) | 100 (32.79%) | 78 (49.06%) | 48 (33.10%) |
| Height | 163 (157–170) | 165 (159–170) | 165 (158–170) | 165 (158–170) |
| Weight | 65 (55.62–70) | 65 (55–72) | 65 (59.50–72.50) | 65 (61–75) |
| HP | 223 (69.25%) | 201 (65.90%) | 113 (71.07%) | 102 (70.34%) |
| DM | 114 (35.40%) | 25 (8.20%) | 42 (26.42%) | 13 (8.97%) |
| HLP | 51 (15.84%) | 4 (1.31%) | 18 (11.32%) | 1 (0.69%) |
| RBC | 4.63 (4.21–4.96) | 4.58 (4.17–5.00) | 4.59 (4.28–4.93) | 4.46 (4.02–4.92) |
| Hct | 0.41 (0.38–0.44) | 0.41 (0.38–0.45) | 0.41 (0.38–0.44) | 0.41 (0.37–0.44) |
| Hb | 139 (127–150) | 139 (125–152) | 137 (124–149.50) | 137 (123–149) |
| RDW-CV | 13.50 (12.90–14.30) | 13.60 (13.00–14.50) | 13.60 (13.00–14.60) | 13.70 (13.00–14.40) |
| RDW-SD | 43.70 (41.02–46.68) | 43.90 (41.40–46.50) | 44.20 (41.70–47.65) | 44.10 (40.90–47.30) |
| WBC | 7.63 (6.20–9.39) | 10.80 (7.95–14.37) | 7.63 (6.56–9.32) | 10.92 (7.41–13.29) |
| PLT | 181 (134.25–219.75) | 172 (130–213) | 177 (137.50–230) | 165 (124–222) |
| PT | 11.50 (10.90–12.30) | 11.30 (10.70–11.90) | 11.00 (10.50–11.80) | 11.20 (10.60–12.00) |
| APTT | 27.50 (25.22–29.70) | 26.00 (23.80–28.20) | 26.50 (24.95–28.30) | 25.20 (23.40–27.60) |
| TT | 18.20 (17.50–18.90) | 18.00 (17.30–18.90) | 17.90 (17.30–18.60) | 18.00 (17.30–18.60) |
| FIB | 2.85 (2.40–3.58) | 2.58 (2.07–3.23) | 2.83 (2.41–3.42) | 2.60 (2.14–3.35) |
| AT-III | 90.50 (82.43–99.60) | 90.10 (81.70–98.90) | 87.90 (80.65–95.20) | 89.60 (78.40–98.10) |
| D-dimer | 0.44 (0.23–1.03) | 0.73 (0.31–1.68) | 0.63 (0.27–1.64) | 0.64 (0.27–1.38) |
| TBIL | 12.65 (8.83–18.98) | 13.00 (9.50–18.00) | 12.00 (9.50–17.00) | 11.00 (8.60–15.90) |
| DBIL | 4.65 (3.30–6.88) | 4.90 (3.30–6.50) | 3.90 (2.80–5.75) | 3.90 (3.00–5.70) |
| IBIL | 7.95 (5.50–11.78) | 8.10 (5.80–11.20) | 8.20 (6.15–11.20) | 6.90 (5.10–10.30) |
| TP | 71.70 (68.32–75.60) | 72.00 (68.40–77.00) | 72.50 (68.60–75.90) | 72.50 (68.40–76.40) |
| Alb | 42.65 (39.80–45.00) | 43.00 (40.50–46.00) | 42.70 (39.35–45.00) | 43.40 (40.10–45.60) |
| Globin | 29.05 (26.40–32.30) | 29.10 (26.00–32.10) | 29.60 (26.95–32.40) | 29.80 (25.80–32.80) |
| CREA | 74 (61–91) | 72 (60–86) | 72 (63–86) | 67 (55–82) |
| URIC | 338 (273.25–403) | 318 (248–409) | 329 (263.50–407.50) | 315 (243–382) |
| GLU | 6.75 (5.88–8.36) | 7.46 (6.13–9.72) | 6.74 (5.93–8.61) | 7.76 (6.37–9.75) |
| ALT | 19 (13–27.75) | 19 (14–30) | 19 (13.50–31) | 20 (15–28) |
| AST | 20.50 (17–27) | 23 (18–31) | 20 (16–27) | 22 (17–28) |
| ALP | 81 (67–96) | 80 (66–97) | 83 (68–97.50) | 77 (67–103) |
| CK | 86 (56–131.75) | 110 (72–176) | 86 (56.50–128) | 95 (64–125) |
| GGT | 29 (18–46.75) | 25 (15–50) | 28 (19–51.50) | 31 (16–53) |
| LDH | 185 (155–220) | 205 (176–252) | 185 (159–215) | 202 (177–240) |
| HBDH | 148 (125–179.75) | 167 (142–203) | 151 (132.50–180) | 165 (144–198) |
| TG | 1.39 (0.96–2.01) | 1.16 (0.75–1.82) | 1.27 (0.95–1.92) | 1.08 (0.73–1.49) |
| CHOL | 4.29 (3.54–5.09) | 4.30 (3.71–4.93) | 4.22 (3.37–5.08) | 4.25 (3.69–4.96) |
| HDL-C | 1.17 (0.93–1.42) | 1.27 (0.98–1.55) | 1.12 (0.92–1.38) | 1.32 (1.08–1.62) |
| LDL-C | 2.48 (1.93–3.14) | 2.56 (2.04–3.09) | 2.64 (1.90–3.30) | 2.58 (2.07–3.14) |
| TBA | 3.50 (1.70–6.18) | 2.30 (1.10–4.50) | 3.20 (1.70–5.50) | 2.20 (1.20–4.80) |
| Urea | 5.60 (4.50–7.09) | 5.00 (3.90–6.30) | 5.10 (4.20–6.67) | 4.90 (3.90–6.26) |

*Data are presented as n (%) for categorical variables and as median (upper and lower quartiles) for continuous variables. *$p < 0.05$.*

**TABLE 2 |** Indicators in the Stroke Diagnosis Aid app.

| | Derivation cohort (627) | | | Validation cohort (304) | | |
|---|---|---|---|---|---|---|
| | *p*-Value | OR | 95% CI | *p*-Value | OR | 95% CI |
| Age | <0.001 | 0.945 | 0.928, 0.963 | <0.001 | 0.917 | 0.890, 0.945 |
| Smoking | <0.001 | 2.342 | 1.473, 3.723 | 0.005 | 2.289 | 1.206, 4.346 |
| HP | 0.370 | 0.539 | 0.335, 0.867 | 0.890 | 0.447 | 0.210, 0.954 |
| DM | <0.001 | 6.790 | 3.294, 13.997 | <0.001 | 8.157 | 2.576, 25.827 |
| HLP | <0.001 | 8.634 | 2.632, 28.324 | <0.001 | 35.415 | 3.735, 335.760 |
| Hct | 0.869 | 0.173 | 0.002, 13.43 | 0.370 | 0.004 | 0.000, 2.198 |
| RDWSD | 0.630 | 1.087 | 1.030, 1.147 | 0.792 | 1.046 | 0.970, 1.127 |
| PLT | 0.143 | 0.996 | 0.992, 0.999 | 0.249 | 0.992 | 0.987, 0.997 |
| WBC | <0.001 | 1.250 | 1.172, 1.334 | <0.001 | 1.228 | 1.115, 1.352 |
| TT | 0.186 | 0.739 | 0.619, 0.882 | 0.783 | 1.033 | 0.847, 1.262 |
| FIB | <0.001 | 0.631 | 0.480, 0.828 | 0.020 | 0.762 | 0.558, 1.042 |
| ATIII | 0.753 | 0.979 | 0.961, 0.997 | 0.501 | 0.969 | 0.942, 0.996 |
| ALT | 0.194 | 0.989 | 0.981, 0.997 | 0.916 | 0.985 | 0.970, 1.000 |
| IBIL | 0.939 | 0.965 | 0.930, 1.001 | 0.028 | 0.936 | 0.874, 1.003 |
| CREA | 0.124 | 1.006 | 1.001, 1.011 | 0.013 | 1.004 | 0.998, 1.010 |
| GLU | 0.009 | 1.134 | 1.048, 1.228 | 0.004 | 1.281 | 1.120, 1.465 |
| UREA | <0.001 | 0.793 | 0.700, 0.897 | 0.171 | 0.823 | 0.715, 0.949 |
| CK | <0.001 | 1.001 | 1.000, 1.002 | 0.179 | 1.000 | 0.999, 1.001 |

*Data are presented as n (%) for categorical variables and as median (upper and lower quartiles) for continuous variables. *p < 0.05.*

Next, we combined the demographic variables and laboratory panel and constructed a model through univariate and multivariate logistic regression. The formula is as follows:

Risk = 1/{1 + EXP [−(1.624515 × laboratory score + 0.2387812 + 0.8346704 × smoke − 0.5875043 × hypertension (HP) + 2.2938255 × hyperlipidemia (HLP) + 1.7165673 × diabetes mellitus (DM))]}, AUC = 0.916, cut-off = 0.577.

This prediction model was further encapsulated as the Stroke Diagnosis Aid app. It is freely available, and Android users can download it through the link[1] or QR code (**Supplementary 3**). In addition, we also provide an operational and free Web app for the Stroke Diagnosis Aid app at[2] to reduce usage restrictions (**Supplementary 4**).

## Independent Validation

The performance of the proposed model was evaluated using the data of 304 patients with suspected stroke from the emergency department, among which 159 patients had confirmed IS, and 145 had confirmed hemorrhagic stroke, subarachnoid hemorrhage, or stroke mimics, including subdural hematoma, intracranial tumor, hypoglycemic encephalopathy, epileptic seizures, hepatic encephalopathy, hysteria, intracranial infections, or moyamoya disease. The results showed that the sensitivity, specificity, PPV, and NPV values were 89.31% [95% confidence interval (CI), 83.18–93.46%], 87.59% (95% CI, 80.83–92.28%), 88.75% (95% CI, 82.56–93.01%), and 88.19% (95% CI, 81.51–92.77%), respectively. The AUC was 0.896 (**Figure 3C**). The calibration curve showed good performance (**Figures 3A,B**) in both the derivation and validation cohorts. The *p*-value of the Hosmer–Lemeshow test was much greater than 0.05.

[1]http://t.cn/A6AKOPTJ

[2]https://zirui.shinyapps.io/shiny/

# DISCUSSION

Our research showed an excellent performance of the laboratory and demographic variables in assisting the identification of AIS. On the one hand, the predictors in our model are objective, biologically plausible, and initially available. All the laboratory variables are common and have a short turnaround time, which is convenient for primary health care and community hospitals. Besides, they can provide possible management directions for the patients with no immediate access to CT scans. On the other hand, the computational predictions can be less influenced by subjective judgments, especially that they do not rely on the experience of the clinicians. For patients with atypical symptoms, the predicted results can be used to strengthen the awareness and reduce the chance of misdiagnosing stroke. It can be a good complementary tool for stroke management, especially for atypical or hyperacute IS, although it cannot be used as an independent diagnostic method. To the best of our knowledge, our study presents the most comprehensive, timely, and practical laboratory method to assist in the early identification of stroke.

Notably, many previous studies used variables with statistically significant differences in disease diagnosis (Kadayifci et al., 2017; Zhang et al., 2018; Han et al., 2019; Sui et al., 2019). However, it has been indicated that too much reliance on the statistically significant threshold could result in wasted

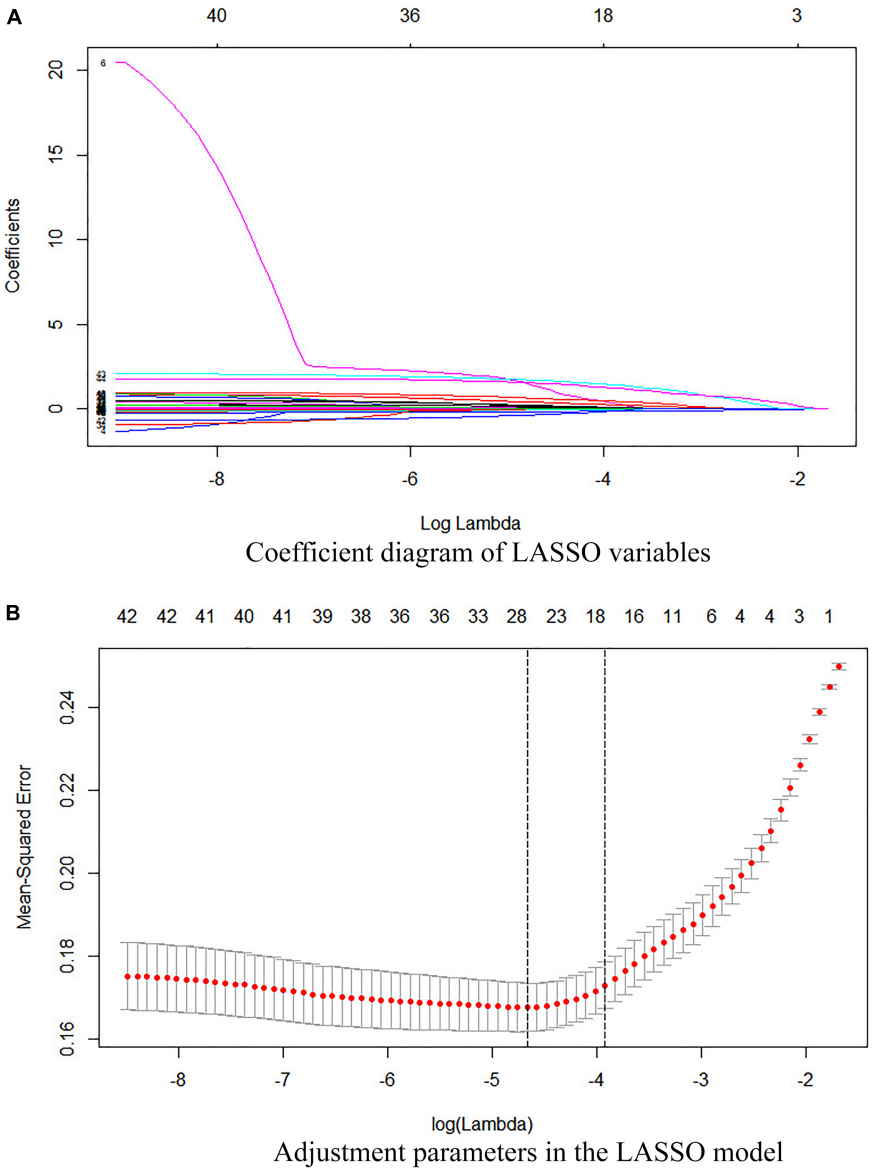


**FIGURE 2 | (A)** Coefficient diagram of the LASSO variables. Each curve in the figure represents the trajectory of the coefficient of an independent variable. The ordinate is the value of the coefficient. The lower abscissa, λ, is the parameter that controls the severity of the penalty. The upper abscissa is the number of non-zero coefficients in the model under the penalty parameter. **(B)** Adjustment parameters in the LASSO model. The λ is screened by 10-fold cross-validation. A dashed vertical line is drawn at 1 standard error (1-SE standard) of the minimum and maximum standards. λ.1se corresponds to a model that has a good performance with the fewest number of arguments.

resources and even misleading decisions (Amrhein et al., 2019). To this end, we adopted the LASSO algorithm, which does not depend on statistical significance for regularization but shrinks the coefficients of complex laboratory variables and excludes relatively unimportant ones. Finally, a set of valid and concise variables was selected and synthesized into a laboratory panel. This normalization can also avoid the difference of the same index caused by different laboratory methods to a certain extent.

Although the selected predictors are not specific to IS or the brain, and one single index does not play a decisive role in identifying IS, they may reflect the changes in different pathways (coagulation function, inflammatory response, and oxidative stress damage) in the body during the occurrence and development of IS. Besides, the joint assessment of these predictors with a suitable weighting model can help us to achieve a more comprehensive IS identification.

Another inspiring finding in this work might be that the model also showed a relatively precise identification in the validation cohort, which contains more various cerebrovascular diseases (IS, hemorrhagic stroke, subarachnoid hemorrhage, or stroke mimics). This indicates that the model has a stable performance even under real and complex clinical conditions.

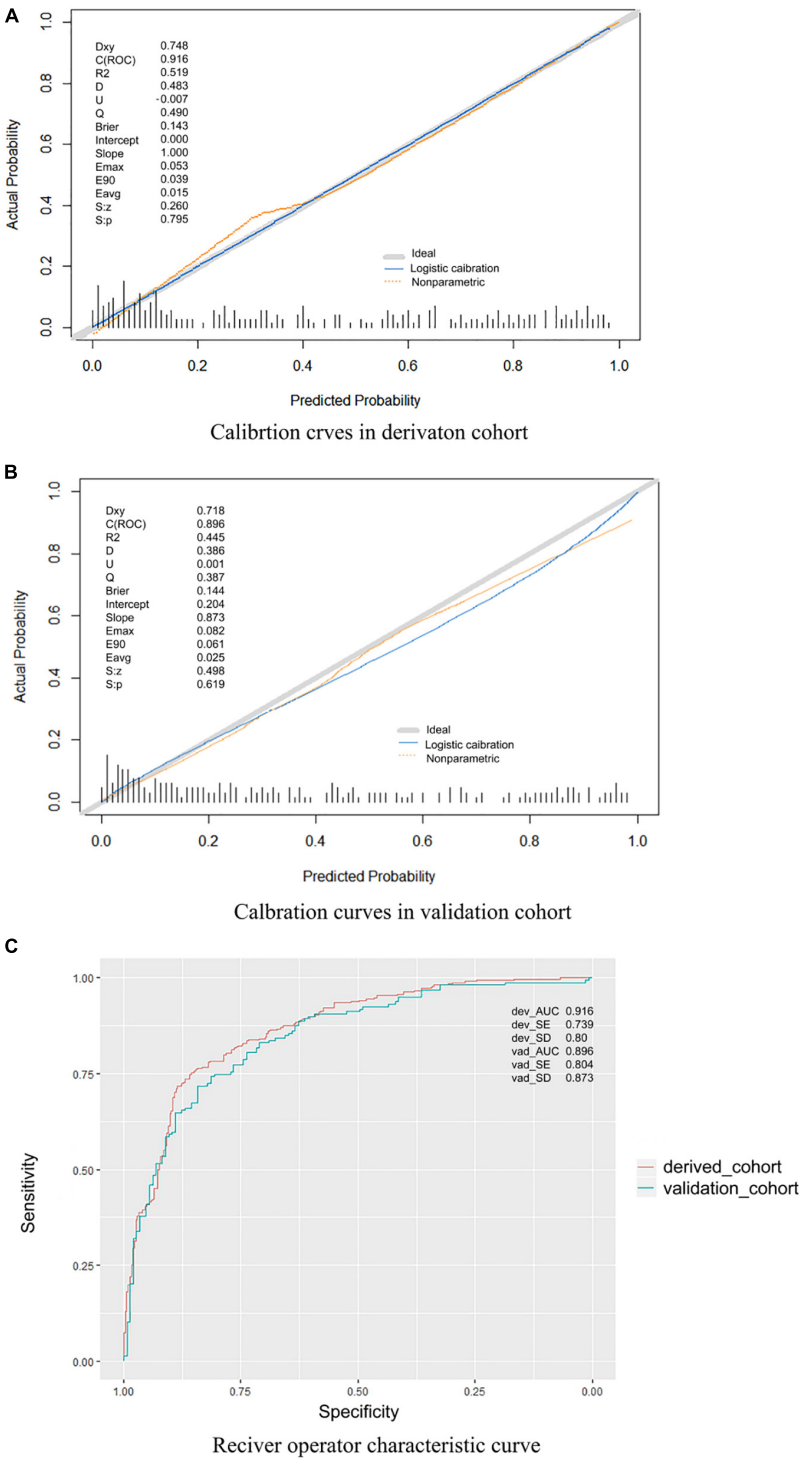


**FIGURE 3 | (A)** Calibration curves in the derivation cohort. **(B)** Calibration curves in the validation cohort. The calibration curve was drawn based on the consistency between the prediction and the label. The *y*-axis represents the actual results, and the *x*-axis represents the predicted results. Diagonal lines represent perfect predictions of the ideal models. Solid lines represent the performance of the model, and a closer fit to the dotted diagonal line indicates better prediction. The ideal model is a perfectly fitting curve, where the predicted probability is equal to the actual probability. The non-parametric part is the calibration result obtained by fitting the sample data through non-parametric regression, which is a built-in fitting method of the R software. The logistic calibration is the calibration result obtained by the fitting method used to construct our model. Dxy, Somer *D* rank correlation; $R^2$, Nagelkerke–Cox–Snell–Maddala–Magee $R^2$ index; *D*, discrimination index; U, unreliability index; Q, quality index; Emax, maximum absolute difference in predicted and calibrated probabilities; S: *z*, Spiegelhalter *Z* test; S: *p*, two-tailed *p*-value of the Spiegelhalter *Z* test. **(C)** Receiver operating characteristic curve. This model had an area under the receiver operating characteristic curve of 0.916 in the derivation cohort and 0.896 in the validation cohort.

The results showed high specificity and PPV, which means that the rate of misdiagnosis is low, and our model can help to avoid the risk of misusing tPA. Meanwhile, the model showed high sensitivity and NPV, which indicates that it can well recognize the presence of IS, providing additional incremental evidence for the clinicians to identify AIS. The results also showed a satisfactory discrimination ability (AUC = 0.896) and a prediction curve that is close to the actual curve, which indicates that the model can correctly identify IS and provide prediction results that are highly consistent with the actual ones. Therefore, it may be more applicable to Asian populations and certain conditions than some of the currently recommended screening scales and biomarkers (with a specificity of 37–75%) (Demir et al., 2015; Wendt et al., 2015).

Although some of the previously proposed diagnostic models based on programming have the feature of visualization, they require specific programming experience, which greatly limits their convenient app and promotion. In this study, we developed a more user-friendly design of the app, called the Stroke Diagnosis Aid app. Our app is qualified with visualization and also has a strong operability (Lynch, 2015). Both clinicians and patients can use this app on their own smartphones. By entering the value of the required indicators, dragging the slider, or selecting individual items to enter the corresponding parameters on the app client or web app, the user can intuitively obtain the probability of having an IS.

Our model can be applied to the following conditions to improve the diagnosis of IS. First, it can help the patients to receive reference information in the case of inadequate medical conditions, such as in community hospitals, primary hospitals, and clinics in the remote areas of low- to middle-income countries. In these conditions, patients often do not have rapid access to imaging examinations; thus, our model can provide possible directions for the early triage and referral management at the initial visit. Second, it can act as a decision-support system for clinicians when the patients have atypical clinical characteristics and imaging manifestations. In fact, 70% of IS patients have atypical CT features in the hyperacute phase (<24 h of onset) (Lin and Liebeskind, 2016). This tool can assist in identifying and assessing the patient's condition from different perspectives. In addition, our app is an open-source, web-based online prediction model, which can be installed on the personal mobile of the clinical staff in all kinds of medical and health institutions at all levels to build a communication network between medical institutions. Furthermore, we can safely implant this software into the laboratory reporting system once the agency's permission is granted. The probability of IS can be directly calculated as the laboratory test is completed to save more time.

In this work, we do not deny the important role of imaging technology in the stroke diagnosis or intend to replace it. The purpose is to present our app as a necessary and important supplement. We hope that our research can help the physicians to obtain reference information concerning stroke evaluation when the medical conditions can benefit from support, such as community hospitals, primary hospitals, and clinics in regions with relatively scarce medical resources. The patients in these areas are often limited by insufficient CT inspection equipment or high costs and are unable to quickly obtain the imaging results. Under these circumstances, our model can provide valuable preinspection auxiliary information. While the contribution of our model might be less significant in developed countries or capitals, the vast majority of the world's population lives in areas lacking basic medical resources, where our model can be of great benefit. It is worth mentioning that expensive imaging techniques are far more difficult to promote than experimental diagnostic techniques. In fact, training qualified medical imaging physicians also requires a huge investment in the medical resources. Still, there is a clinical need for early and rapid diagnosis of stroke, and with the popularization of digital medical and mobile terminals, we believe that our research can provide better diagnostic services in this regard.

Our study has some limitations. First, because of the urgency of emergency stroke, we did not repeatedly measure the laboratory indicators, and dynamic testing results may correlate with the disease progression and prognosis, which is of great importance. Second, this model can be used only as a supplementary tool in the earlier period of stroke identification to provide predictive insights rather than an independent diagnosis app. Finally, as this work is a hospital-based, case–control study, inherent selection bias cannot be completely excluded. Our study was designed as a nested case–control study that involved a prospective collection of the validation cohort to avoid extreme selection bias that can affect inference and conclusions (Sallam, 2015; Simmons et al., 2019). In the future, we plan to enhance the model with some specific markers and clinical symptoms to improve its diagnostic efficiency. In addition, we intend to dynamically detect the laboratory indicators to explore their value in the prognosis of stroke. We will also validate this model in various mimicking diseases and across many centers to ensure its generalization capabilities. The smooth development of these tasks may greatly enhance the early identification and treatment of IS.

## CONCLUSION

In conclusion, our study confirmed the important value of the laboratory variables and demographic variables in the identification of stroke and used these variables to construct a new, universal, and applicable supplementary tool to provide more reference information to increase awareness. The proposed model can help to improve the identification of AIS, even in the absence of specific manifestations or adequate medical resources.

## DATA AVAILABILITY STATEMENT

The original contributions presented in the study are included in the article/**Supplementary Material**, further inquiries can be directed to the corresponding author/s.

## ETHICS STATEMENT

The studies involving human participants were reviewed and approved by the Clinical Trials and Biomedical Ethics Committee of West China Hospital, Sichuan University (no. 812). Written informed consent for participation was not required for this study in accordance with the national legislation and the institutional requirements.

## AUTHOR CONTRIBUTIONS

BY, BZ, ZM, and MW: contributed to study conception and design of the work. ZM, MW, ML, YC, and ZY: acquisition, analysis, or interpretation of the data. ZM and MW: drafting of the manuscript. BY and BZ: critical revision of the manuscript for important intellectual content. ZM, SG, and YZ: statistical analysis. BY: administrative, technical, or material support. BY and BZ: supervision. All authors contributed to the article and approved the submitted version.

## FUNDING

This research was supported by the National Science & Technology Pillar Program during the 13th Five-year Plan Period (Grant No. 2018ZX10715003).

## ACKNOWLEDGMENTS

The authors would like to express their gratitude to EditSprings (https://www.editsprings.com/) for the expert linguistic services provided.

## SUPPLEMENTARY MATERIAL

The Supplementary Material for this article can be found online at: https://www.frontiersin.org/articles/10.3389/fnagi.2021.630437/full#supplementary-material

## REFERENCES

Amrhein, V., Greenland, S., and McShane, B. (2019). Scientists rise up against statistical significance. *Nature* 567, 305–307.

Baez, S. C., García del Barco, D., Hardy-Sosa, A., Guillen Nieto, G., Bringas-Vega, M. L., Llibre-Guerra, J. J., et al. (2021). Scalable bio marker combinations for early stroke diagnosis: a systematic review. *Front. Neurol.* 12:638693. doi: 10.3389/fneur.2021.638693

Chen, Z. C., Zhang, R. T., Xu, F. Z., Gong, X. X., Shi, F. N., Zhang, M. X., et al. (2018). Novel prehospital prediction model of large vessel occlusion using artificial neural network. *Front. Aging Neurosci.* 10:181. doi: 10.3389/fnagi.2018.00181

Clarke, R., Du, H., Kurmi, O., Parish, S., Yang, M., Arnold, M., et al. (2017). Burden of carotid artery atherosclerosis in Chinese adults: implications for future risk of cardiovascular diseases. *Eur. J. Prev. Cardiol.* 24, 647–656. doi: 10.1177/2047487317689973

Dagonnier, M., Donnan, G. A., Davis, S. M., Dewey, H. M., and Howells, D. W. (2021). Acute stroke biomarkers: are we there yet? *Front. Neurol.* 12:619721. doi: 10.3389/fneur.2021.619721

Deboevere, N., Marjanovic, N., Sierecki, M., Marchetti, M., Dubocage, M., Magimel, E., et al. (2019). Value of copeptin and the S-100b protein assay in ruling out the diagnosis of stroke-induced dizziness pattern in emergency departments. *Scand. J. Trauma Resusc. Emerg. Med.* 27:72.

Demir, R., Saritemur, M., Atis, O., Ozel, L., Kocaturk, I., Emet, M., et al. (2015). Can we distinguish stroke and stroke mimics via red cell distribution width in young patients? *Arch. Med. Sci.* 11, 958–963.

El-Serag, H. B., Kanwal, F., Davila, J. A., Kramer, J., and Richardson, P. (2014). A new laboratory-based algorithm to predict development of hepatocellular carcinoma in patients witsh hepatitis C and cirrhosis. *Gastroenterology* 146, 1249–55.e1.

Fan, J. F., Saft, M., Sadanandan, N., Gonzales-Portillo, B., Park, Y. J., Sanberg, P. R., et al. (2020). LncRNAs stand as potent biomarkers and therapeutic targets for stroke. *Front. Aging Neurosci.* 12:594571. doi: 10.3389/fnagi.2020.594571I

GBD 2016 Causes of Death Collaborators (2017). Global, regional, and national age-sex specific mortality for 264 causes of death, 1980-2016: a systematic analysis for the Global Burden of Disease Study 2016. *Lancet* 390, 1151–1210.

Han, R. L., Wang, J., Zhang, F. J., Zhao, N., and Gao, B. L. (2019). Ultrasound risk assessment combined with molecular markers of galectin-3, c-MET, HBME-1 and CK19 for diagnosis of malignant and benign thyroid nodules. *Pathol. Oncol. Res.* 25, 1075–1081. doi: 10.1007/s12253-018-0485-6

Hankey, G. J. (2017). Stroke. *Lancet* 389, 641–654.

Jiang, B., Ru, X., Sun, H., Liu, H., Sun, D., Liu, Y., et al. (2016). Pre-hospital delay and its associated factors in first-ever stroke registered in communities from three cities in China. *Sci. Rep.* 6:29795.

Jin, H., Zhu, S., Wei, J. W., Wang, J., Liu, M., Wu, Y., et al. (2012). Factors associated with prehospital delays in the presentation of acute stroke in urban China. *Stroke* 43, 362–370. doi: 10.1161/strokeaha.111.623512

Kadayifci, A., Atar, M., Wang, J. L., Forcione, D. G., Casey, B. W., Pitman, M. B., et al. (2017). Value of adding GNAS testing to pancreatic cyst fluid KRAS and carcinoembryonic antigen analysis for the diagnosis of intraductal papillary mucinous neoplasms. *Dig. Endosc.* 29, 111–117. doi: 10.1111/den.12710

Lee, S., Kim, S., Chang, H., Jung, H., Kim, Y., Hwang, S., et al. (2018). A new scoring system for the differential diagnosis between tuberculous meningitis and viral meningitis. *J. Korean Med. Sci.* 33:e201.

Liberman, A. L., Choi, H. J., French, D. D., and Prabhakaran, S. (2019). Is the cost-effectiveness of stroke thrombolysis affected by proportion of stroke mimics? *Stroke* 50, 463–468. doi: 10.1161/strokeaha.118.022857

Lin, M. P., and Liebeskind, D. S. (2016). Imaging of ischemic stroke. *Continuum (Minneap Minn.)* 22, 1399–1423.

Lynch, A. (2015). Crambled: a Shiny application to enable intuitive resolution of conflicting cellularity estimates. *F1000Res.* 4:1407. doi: 10.12688/f1000research.7453.1

Makris, K., Haliassos, A., Chondrogianni, M., and Tsivgoulis, G. (2018). Blood biomarkers in ischemic stroke: potential role and challenges in clinical practice and research. *Crit. Rev. Clin. Lab. Sci.* 55, 294–328. doi: 10.1080/10408363.2018.1461190

Martins, S. C. O., Weiss, G., Almeida, A. G., Brondani, R., Carbonera, L. A., de Souza, A. C., et al. (2020). Validation of a smartphone application in the evaluation and treatment of acute stroke in a comprehensive stroke center. *Stroke* 51, 240–246. doi: 10.1161/strokeaha.119.026727

Mathur, S., Walter, S., Grunwald, I. Q., Helwig, S. A., Lesmeister, M., and Fassbender, K. (2019). Improving prehospital stroke services in rural and underserved settings with mobile stroke units. *Front. Neurol.* 10:159. doi: 10.3389/fneur.2019.00159

Misra, S., Kumar, A., Kumar, P., Yadav, A. K., Mohania, D., Pandit, A. K., et al. (2017). Blood-based protein biomarkers for stroke differentiation: a systematic review. *Proteom. Clin. Appl.* 11:1700007. doi: 10.1002/prca.201700007

Muntner, P., Colantonio, L. D., Cushman, M., Goff, D. C. Jr., Howard, G., Howard, V. J., et al. (2014). Validation of the atherosclerotic cardiovascular disease Pooled Cohort risk equations. *JAMA* 311, 1406–1415. doi: 10.1001/jama.2014.2630

Sallam, R. M. (2015). Proteomics in cancer biomarkers discovery: challenges and applications. *Dis. Markers* 2015:321370.

Simmons, A. R., Fourkala, E. O., Gentry-Maharaj, A., Ryan, A., Sutton, M. N., Baggerly, K., et al. (2019). Complementary longitudinal serum biomarkers to CA125 for early detection of ovarian cancer. *Cancer Prev. Res.* 12, 391–399. doi: 10.1158/1940-6207.capr-18-0377

Sui, Y. B., Zou, Z. X., Li, F. F., and Hao, C. J. (2019). Application value of MRI diffuse weighted imaging combined with PET/CT in the diagnosis of stomach cancer at different stages. *Oncol. Lett.* 18, 43–48.

Tarnutzer, A. A., Lee, S. H., Robinson, K. A., Wang, Z., Edlow, J. A., and Newman-Toker, D. E. (2017). misdiagnosis of cerebrovascular events in the era of modern neuroimaging: a meta-analysis. *Neurology* 88, 1468–1477. doi: 10.1212/wnl.0000000000003814

Valappil, A. V., Thiruvoth, S., Peedikayil, J. M., Raghunath, P., and Thekkedath, M. (2017). Differential diagnosis of scrub typhus meningitis from tuberculous meningitis using clinical and laboratory features. *Clin. Neurol. Neurosurg.* 163, 76–80. doi: 10.1016/j.clineuro.2017.10.022

Vilela, P. (2017). Acute stroke differential diagnosis: stroke mimics. *Eur. J. Radiol.* 96, 133–144. doi: 10.1016/j.ejrad.2017.05.008

Walsh, K. B. (2019). Non-invasive sensor technology for prehospital stroke diagnosis: current status and future directions. *Int. J. Stroke* 14, 592–602. doi: 10.1177/1747493019866621

Wang, W., Jiang, B., Sun, H., Ru, X., Sun, D., Wang, L., et al. (2017). Prevalence, Incidence, and Mortality of Stroke in China: results from a Nationwide Population-Based Survey of 480 687 Adults. *Circulation* 135, 759–771. doi: 10.1161/circulationaha.116.025250

Wendt, M., Ebinger, M., Kunz, A., Rozanski, M., Waldschmidt, C., Weber, J. E., et al. (2015). Copeptin Levels in patients with acute ischemic stroke and stroke mimics. *Stroke* 46, 2426–2431. doi: 10.1161/strokeaha.115.009877

Wojciechowski, J., Hopkins, A. M., and Upton, R. N. (2015). Interactive pharmacometric applications using r and the shiny package. *CPT Pharmacomet. Syst. Pharmacol.* 4, 146–159. doi: 10.1002/psp4.21

Wu, S., Wu, B., Liu, M., Chen, Z., Wang, W., Anderson, C. S., et al. (2019). Stroke in China: advances and challenges in epidemiology, prevention, and management. *Lancet Neurol.* 18, 394–405.

Zerna, C., Thomalla, G., Campbell, B. C. V., Rha, J. H., and Hill, M. D. (2018). Current practice and future directions in the diagnosis and acute treatment of ischaemic stroke. *Lancet* 392, 1247–1256. doi: 10.1016/s0140-6736(18)31874-9

Zhang, X., Yu, H., Zhang, Y., Liu, X. N., Yu, X., and Chen, X. J. (2018). The application of RNFL thickness detection in early differential diagnosis among various types of idiopathic optic neuritis. *J. Clin. Neurosci.* 55, 82–85. doi: 10.1016/j.jocn.2018.06.052

Zhou, M., Wang, H., Zhu, J., Chen, W., Wang, L., Liu, S., et al. (2016). Cause-specific mortality for 240 causes in China during 1990-2013: a systematic subnational analysis for the Global Burden of Disease Study 2013. *Lancet* 387, 251–272.

**Conflict of Interest:** The authors declare that the research was conducted in the absence of any commercial or financial relationships that could be construed as a potential conflict of interest.

frontiers in Aging Neuroscience

ORIGINAL RESEARCH
published: 09 July 2021
doi: 10.3389/fnagi.2021.691518

# Hemispheric Difference of Regional Brain Function Exists in Patients With Acute Stroke in Different Cerebral Hemispheres: A Resting-State fMRI Study

*Jingchun Gao[1,2], Canhong Yang[3], Qixiong Li[1], Lanpin Chen[4], Yijing Jiang[5], Songyan Liu[6], Jing Zhang[6], Gang Liu[7]* and Junqi Chen[1]**

[1] Department of Rehabilitation Medicine, Third Affiliated Hospital of Southern Medical University, Guangzhou, China, [2] Department of Rehabilitation Medicine, Foshan Hospital of Traditional Chinese Medicine, Foshan, China, [3] Department of Neurology, Third Affiliated Hospital of Southern Medical University, Guangzhou, China, [4] School of Traditional Chinese Medicine, Southern Medical University, Guangzhou, China, [5] Department of Rehabilitation Medicine, Rehabilitation Hospital, Fujian University of Traditional Chinese Medicine, Fuzhou, China, [6] Department of Neurology, China-Japan Union Hospital of Jilin University, Changchun, China, [7] Department of Rehabilitation Medicine, Nanfang Hospital, Southern Medical University, Guangzhou, China

OPEN ACCESS

**Edited by:**
Shuo Wang,
Capital Medical University, China

**Reviewed by:**
Ángel Céspedes Rubio,
Universidad del Tolima, Colombia
Deepali Mathur,
University of Valencia, Spain

***Correspondence:**
Gang Liu
lg2781@smu.edu.cn
orcid.org/0000-0002-6426-3155
Junqi Chen
meixibao@126.com
orcid.org/0000-0001-6847-0891

**Received:** 06 April 2021
**Accepted:** 14 June 2021
**Published:** 09 July 2021

**Citation:**
Gao JC, Yang CH, Li QX, Chen LP, Jiang YJ, Liu SY, Zhang J, Liu G and Chen JQ (2021) Hemispheric Difference of Regional Brain Function Exists in Patients With Acute Stroke in Different Cerebral Hemispheres: A Resting-State fMRI Study. Front. Aging Neurosci. 13:691518. doi: 10.3389/fnagi.2021.691518

**Objective:** To explore the different compensatory mechanisms of brain function between the patients with brain dysfunction after acute ischemic stroke (AIS) in the dominant hemisphere and the non-dominant hemisphere based on Resting-state Functional Magnetic Resonance Imaging (Rs-fMRI).

**Methods:** In this trial, 15 healthy subjects (HS) were used as blank controls. In total, 30 hemiplegic patients with middle cerebral artery acute infarction of different dominant hemispheres were divided into the dominant hemisphere group (DH) and the non-dominant hemisphere group (NDH), scanned by a 3.0 T MRI scanner, to obtain the amplitude of low-frequency fluctuations (ALFF) and regional homogeneity (ReHo) and compare the differences.

**Results:** Compared with the HS, increased ALFF values in the brain areas, such as the bilateral midbrain, were observed in DH. Meanwhile decreased ReHo values in the brain areas, such as the right postcentral gyrus (BA3), were also observed. Enhanced ALFF values in the brain areas, such as the left BA6, and enhanced ReHo values in the brain areas, such as the left precuneus, were observed in the NDH. The ALFF and ReHo values of the right BA9 and precentral gyrus were both increased. Compared with DH, the NDH group showed lower ALFF values in the left supplementary motor area and lower ReHo values in the right BA10.

**Conclusion:** After acute infarction in the middle cerebral artery of the dominant hemisphere, a compensation mechanism is triggered in brain areas of the ipsilateral cortex regulating motor-related pathways, while some brain areas related to cognition, sensation, and motor in the contralateral cortex are suppressed, and the connection

with the peripheral brain regions is weakened. After acute infarction in the middle cerebral artery of the non-dominant hemisphere, compensatory activation appears in motor control-related brain areas of the dominant hemisphere. After acute middle cerebral artery infarction in the dominant hemisphere, compared with the non-dominant hemisphere, functional specificity in the bilateral supplementary motor area weakens. After acute middle cerebral artery infarction in different hemispheres, there are hemispheric differences in the compensatory mechanism of brain function.

**Keywords: resting-state functional magnetic resonance imaging, AIS, amplitude of low frequency fluctuations, regional homogeneity, dominant hemisphere, non-dominant hemisphere**

## INTRODUCTION

The brain is the most complex organ in humans, and research on it is the most advanced and popular field in life science. With the implementation of the "Brain Plan," more researchers nowadays are exploring cerebral functional changes with an aim to study various cerebral diseases.

As one of the cerebral diseases in the "brain program," stroke is listed as the primary cause of disability and death (Wang et al., 2013, 2017) due to its characteristics of high incidence, high disability rate, and high mortality rate. The existing basic researches mainly concentrate on proteomics, genomics, and metabolomics (Nguyen et al., 2016; Hasin et al., 2017; Wang et al., 2020). Neuroimaging technology is a research focus in the field of *in vivo* research on post-stroke injury. With the continuous development of neuroimaging technology, neuroimaging diagnosis is no longer limited to observing the changes in brain histomorphology but has entered the stage of comprehensive diagnosis by combining brain morphology with function (Hojjati et al., 2019). In particular, understanding of cerebral reorganization after the injury in the central nervous system has been increased significantly through the non-invasive examination of functional MRI.

Functional magnetic resonance imaging (fMRI) is one of the representative neuroimaging techniques and can be divided into task-state fMRI technology and resting-state fMRI technology (resting-state fMRI, rs-fMRI). Under the rest state, Rs-fMRI (Li et al., 2016; Wang et al., 2016) receives feedback on neuronal activity by detecting the change of the hemodynamics in the local brain area after the spontaneous cerebral function activity and measuring the change of deoxyhemoglobin content. It can also reflect the pathophysiological changes of cerebral functions in the resting state and directly display the location, range, and size of the activated area of cerebral functions with accurate positioning. This is beneficial to compare the rs-fMRI results of acute ischemic stroke in different lesions and is more meaningful for stroke patients with dysfunction in clinical diagnosis and treatment evaluation (Golestani et al., 2013).

**Abbreviations:** ALFF, amplitude of low-frequency fluctuations; ReHo, regional homogeneity; AIS, acute ischemic stroke; MRI, Magnetic Resonance Imaging; Rs-fMRI, Resting-state Functional Magnetic Resonance Imaging; BA, Brodmann area; fALFF, fractional amplitude of low frequency fluctuations; FC, Functional Connectivity; HS, healthy subjects; DH, the dominant hemisphere group; NDH, the non-dominant hemisphere group; NHISS, National Institute of Health stroke scale; tDCS, transcranial direct current stimulation.

At present, clinical researchers have utilized different analytical methods of rs-fMRI to study a variety of brain diseases. However, most studies only use a single parameter (ALFF/fALFF/ReHo/FC) of rs-fMRI to observe local or overall functional changes in the brain after stroke (Yin et al., 2013; van Hees et al., 2014). Moreover, functional disorders in patients with acute stroke in the dominant hemisphere (left hemisphere) differ significantly from those in the non-dominant hemisphere (right hemisphere) clinically. Physiologically, there are hemispheric differences between the dominant hemisphere and non-dominant hemisphere in neuroanatomy, physiology, neurotransmitters, and the control of sympathetic nerves (Yoon et al., 1997).

However, specific effects of dominant hemispheric and non-dominant hemispheric infarctions on brain function reorganization have not been reported in human trials, and there is a lack of rs-MRI studies on hemispheric differences in brain function after acute stroke.

Therefore, this study aims to explore the difference of brain function between dominant hemisphere and non-dominant hemisphere after acute middle cerebral artery infarction using two parameters of rs-fMRI: amplitude of low-frequency fluctuation (ALFF) and regional homogeneity (ReHo).

## MATERIALS AND METHODS

### Study Design

This study was conducted as an exploratory case-control study.

### Participants

Ethical approval was obtained from the Ethics Committee of China-Japan Union Hospital of Jilin University on July 18, 2016 (No: 2016ks043). Participants aged 40–70 years old were recruited from January to December 2017 in this hospital, and written informed consent was obtained from each participant.

#### Healthy Subjects

In total, 15 healthy subjects were recruited into the normal group (HS). The inclusion criteria included the following: (1) moderate figure, regardless of gender; (2) regular diet and normal sleep, no addiction to smoking or alcohol, no tea or coffee for 24 h; (3) no head acupuncture and physiotherapy performed in the last month; (4) right handed. All of the

above conditions were met. The exclusion criteria included the following: (1) having a history of stroke; (2) sensory aphasia/mixed aphasia/claustrophobia/dementia or other factors affecting communication and operation during the experiment; (3) pregnant and lactating women; (4) having metallic substances in the body (e.g., heart stents); (5) cerebral vascular pathological variation; (6) cardiovascular, renal, and liver diseases, tumors, or other diseases affecting the test results; (7) having underlying hypertension or diabetes or thyroid disease, and the recent disease control is not stable. Any of the above conditions were excluded.

### Patients

A total of 1983 stroke patients with acute stroke were consecutively selected from the Department of Neurology. Based on the complexity and particularity of fMRI image acquisition and data statistics of stroke patients, this article estimates the sample size of the fMRI study. Referring to the systematic review (Guo et al., 2014) and statistical analyses (Desmond and Glover, 2002) on estimating sample size in functional MRI, and considering the 20% shedding rate, 15 patients were included in the dominant hemisphere group (DH) and the non-dominant hemisphere group (NDH), respectively. The inclusion criteria included the following: (1) meet the diagnostic criteria of Chinese Guidelines for Diagnosis and Treatment of Acute Ischemic Stroke, 2014 by the Neurology Branch of Chinese Medical Association and the Cerebrovascular Disease Group of the Neurology Branch of Chinese Medical Association; (2) first-ever ischemic stroke within 72 h after symptoms appear; (3) limb motor and sensory deficits; (4) stroke lesions located within the right or left middle cerebral artery (MCA) territory, as verified by magnetic resonance imaging (MRI) or computed tomography (CT); (5) in stable condition; (6) normal diet and sleep and no addiction to smoking, alcohol, tea, or coffee; (7) right handed. All of the above conditions were met. The exclusion criteria included: (1) hemorrhagic stroke, as verified by CT; (2) sensory aphasia/mixed aphasia/claustrophobia/dementia or other factors affecting communication and operation during the experiment; (3) pregnant and lactating women; (4) having metallic substances in the body (e.g., heart stents); (5) cerebral vascular pathological variation; (6) cardiovascular, renal and liver diseases, tumors, or other diseases affecting the test results; (7) having underlying hypertension or diabetes or thyroid disease, and the recent disease control is not stable. Any of the above conditions were excluded.

## MRI Data Acquisition

The MRI system (Siemens 3.0T, Siemens Healthineers, Germany) and the standard head coil were used to obtain data of T1MPRAGE and rs-fMRI (EPI sequence). The technician asked the participants to lie on the MRI scanning bed and fixed their heads in the coil with foam pads to keep their heads still. Participants were required to remain awake, maintain calm breathing, cover their eyes with a black eye mask, plug their ears with sponge earplugs, and try not to engage in specific thinking activities during the scanning.

T1MPRAGE scanning parameters were as follows: three D TFE sequence cross-section scans, and a high-resolution anatomical image T1WI of the whole brain is obtained. Scanning parameters were repetition, time/echo time ratio = 2300 ms/2.45 ms, flip angle = 8°, field of view (FOV) = 250 mm × 250 mm, slice thickness = 1 mm, Voxel = 1.0 mm × 1.0 mm, Matrix = 256 × 256, number of slices = 192.

Functional magnetic resonance imaging-BOLD scanning parameters were as follows: the single excitation echo plane imaging (EPI) technique was used for horizontal axis scanning, and Pulse time (TR) = 2000 ms, echo time (TE) = 30 ms, flip Angle = 90°, slice thickness = 3.5 mm, slice spacing = 0.7 mm, voxel = 3.5 mm × 3.5 mm × 3.5 mm, field of view (FOV) = 224 cm × 224 mm, phases per location = 240, matrix = 64 × 64, and number of slices = 37, covering a total of 8 min.

## Data Processing

Amplitude of low-frequency fluctuations and ReHo values of the three groups were calculated, respectively, based on the Matlab 2012a platform and by using the DPABI toolkit to launch statistical parameter maps (SPM 12) after removing time point, time correction, head movement correction, registration, de-linear drift, covariate removal, and image filtering, etc. Then, based on the two independent samples *t* test in the rest 1.8 software package, the three sets of data were compared and analyzed to get statistical parameters maps. We identified and corrected (AlphaSim correction, Cluster Size 27, rmm = 4, $P < 0.005$) the statistical parameter maps to achieve the anatomical location and activation intensity of brain regions with significant changes in ALFF and ReHo. The maps were finally calibrated by an experienced neurologist with anatomical knowledge and clinical experience. When DH or NDH was compared with HS, sex, age, and head movements were used as covariates; when DH and the NDH were compared, sex, age, course of disease, systolic blood pressure, diastolic blood pressure, and NHISS score were used as covariates.

In addition, data such as gender were measured by $\chi 2$ test and other data like age were checked by *t*-test. Statistical analysis was completed with statistical software SPSS20.0.

# RESULTS

## General Information

According to the diagnostic inclusion and exclusion criteria, 30 patients were selected into patient groups from 1983 patients suspected of acute ischemic stroke. A total of five cases in DH and three in NDH failed to complete fMRI-BOLD data collection as participants were unable to withstand long magnetic resonance scans. The EPI scanning parameters of two cases in NDH were different from the experimental design and the data were thus stripped out. Participants in one case of the normal group fell asleep during the test, and two cases had different T1 MPRAGE scanning parameters from the experimental design, and the

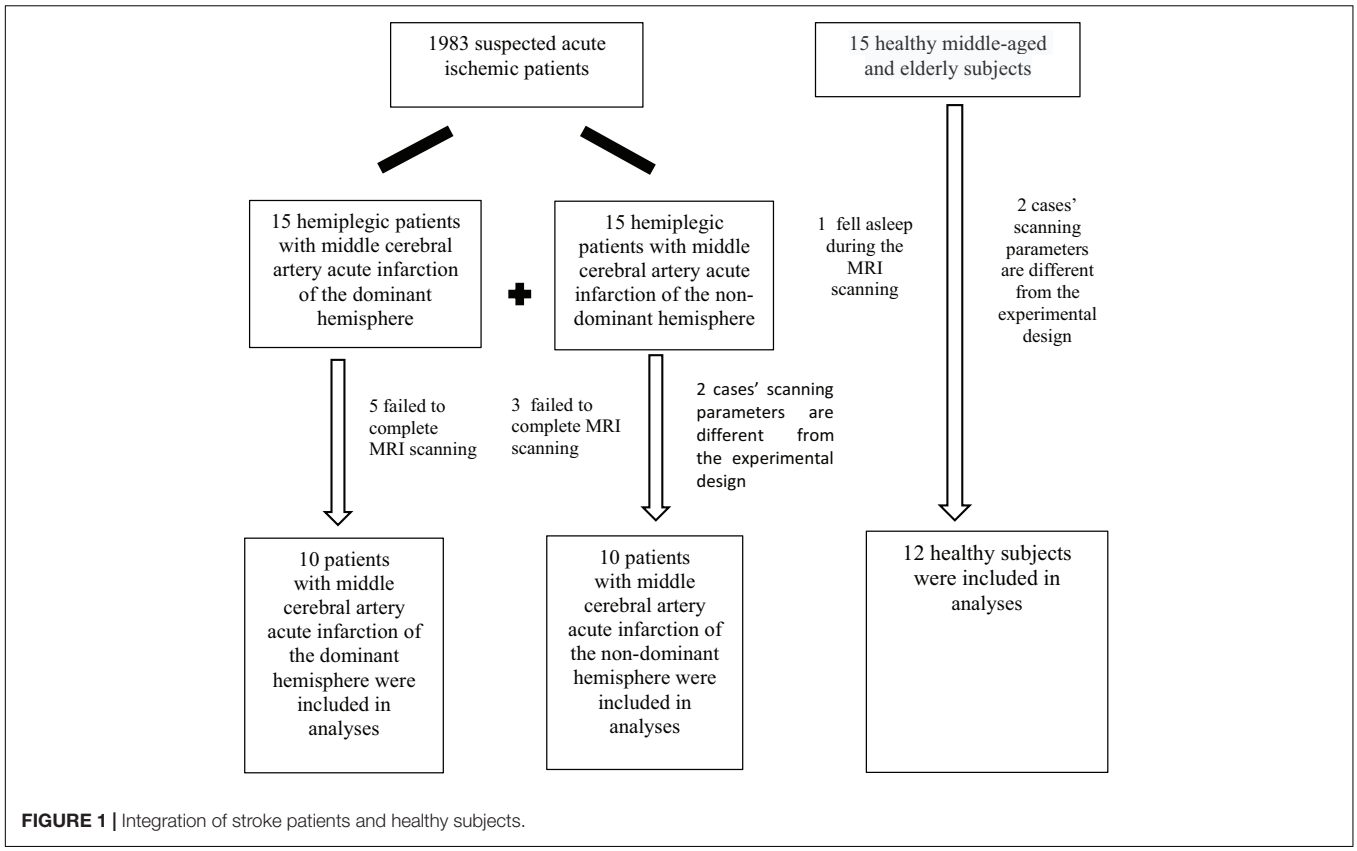


**FIGURE 1 |** Integration of stroke patients and healthy subjects.

**TABLE 1 |** Demographic and clinical characteristics of all patients in three groups.

| Group | Case (n) | Gender (case) | | Age (year) | Course of disease | Systolic pressure (mmHg) | Diastolic pressure (mmHg) | NHISS |
|---|---|---|---|---|---|---|---|---|
| | | Male | Female | | | | | |
| HS | 12 | 4 | 8 | 56.17 ± 3.83 | \ | \ | \ | \ |
| DH | 10 | 7 | 3 | 63.70 ± 6.00 | 2.15 ± 0.94 | 147.80 ± 13.14 | 84.90 ± 10.07 | 5.30 ± 4.99 |
| NDH | 10 | 8 | 2 | 59.40 ± 7.65 | 2.10 ± 0.88 | 152.90 ± 12.34 | 90.40 ± 10.74 | 3.80 ± 1.03 |
| Statistics | | $\chi^2 = 5.728$ | | $F = 4.437$ | $t = 0.123$ | $t = -0.895$ | $t = -1.181$ | $t = 0.931$ |
| *P* Value | | 0.057 | | 0.021 | 0.904 | 0.383 | 0.253 | 0.374 |

*Values presented are mean ± SD (range) or median [IQR]. NIHSS, National Institutes of Health Stroke Scale.*

data were all removed. A flowchart of participants is shown in **Figure 1**.

There were no significant differences among the three groups in their gender, course of disease, systolic and diastolic blood pressure, and NHISS scores ($P > 0.05$) (**Table 1**). However, the age difference of the included subjects in the three groups was statistically significant ($P < 0.05$) (**Table 1**).

## fMRI Results

### Normal Group vs. Dominant Hemisphere Group

Compared with HS, DH showed significantly increased ALFF values in the right midbrain and lobus anterior cerebelli, extending to the vermis (including cerebellar lingual), and in the left midbrain and mammillary body.

Increased ReHo values appeared mainly in the left caudate tai, extending to the pulvinar in DH. On the contrary, the ReHo values decreased mainly in right inferior orbital gyrus (including BA47), triangular inferior frontal gyrus (BA45), and the supra marginal and postcentral gyrus (mostly in BA3), extending to the precentral gyrus (BA4) (**Table 2** and **Figures 2**, **3**).

### Normal Group vs. Non-dominant Hemisphere Group

Compared with HS, ALFF values of NDH increased significantly mainly in the left inferior orbital gyrus (including BA47), extending to left BA25, mainly in the left cerebellum anterior lobe (including cerebellar lingual) and Vermis, in left lentiform nuclei and globus pallidus, in the medial dorsal nucleus, extending to left midbrain, in the right caudate head, and in left BA6 and the paracentral lobule. On the contrary, the ALFF values decreased in the right BA9 and precentral gyrus.

**TABLE 2 |** Regions of DH showing significant changes in ALFF and ReHo values compared with HS.

| Parameter | Effect | Brain region | MNI coordinate | | | Intensity (*T*-value) |
|---|---|---|---|---|---|---|
| | | | *X* | *Y* | *Z* | |
| ALFF | Enhanced | Right midbrain, lobus anterior cerebelli and Vermis | 9 | −33 | −18 | 5.6226 |
| | Enhanced | Left Midbrain and Mammillary Body | −3 | −12 | −12 | 5.0006 |
| ReHo | Enhanced | Left Caudate Tai and Pulvinar | −21 | −36 | 15 | 5.3222 |
| | Reduced | Right inferior orbital gyrus (including BA47) | 27 | 33 | −9 | −5.1493 |
| | Reduced | Right triangular inferior frontal gyrus (BA45) | 48 | 30 | 24 | −7.3696 |
| | Reduced | Right supramarginal gyrus | 66 | −42 | 30 | −4.876 |
| | Reduced | Right postcentral gyrus (mostly in BA3) and precentral gyrus (BA4) | 60 | −15 | 30 | −6.2719 |

*X, Y, Z represent the brain space position axis, respectively, in the MiNi standardized spatial coordinate system in the left and right, front and back, and up and down position of the coordinate position.*

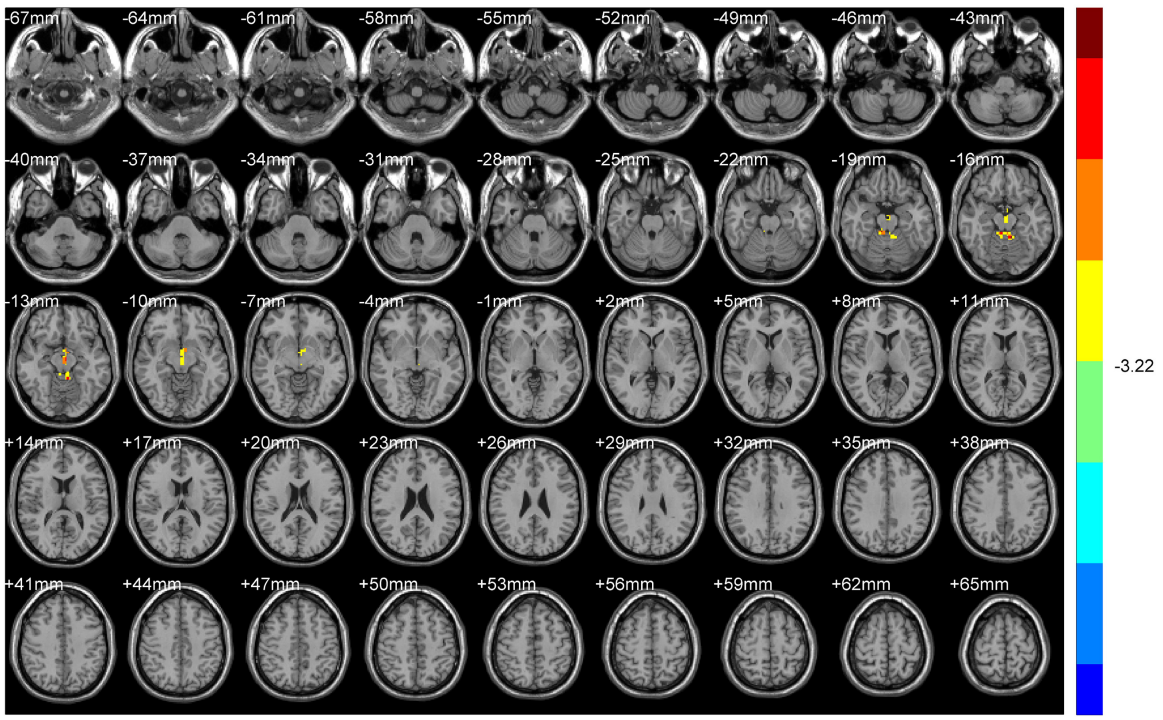


**FIGURE 2 |** ALFF (Dominant hemisphere vs. Normal).

ReHo values were increased mainly in the left Precuneus (BA7) and rectal gyrus, extending to the orbital gyrus (including BA11), mainly in the left parahippocampal gyrus, extending to BA47.

In contrast, the ReHo values decreased mainly in the left cerebellum posterior lobe, tubera valvulae, right BA9, and precentral gyrus (**Table 3** and **Figures 4**, **5**).

### Non-dominant Hemisphere Group vs. Dominant Hemisphere Group

Compared with NDH, DH indicated significantly decreased ALFF values mainly in the left supplementary motor area (including BA6). While decreased ReHo values appeared mainly in the right BA10 (**Table 4** and **Figures 6**, **7**).

## DISCUSSION

In this study, changes in brain function in patients after acute stroke were observed, and differences between the dominant hemisphere and the non-dominant hemisphere were explored through ReHo and ALFF. For now, this is the first rs-fMRI study to compare the hemispheric differences of brain functions after stroke, especially in the acute period. Analyses of these differences are demonstrated as follows.

### Normal Group (HS) vs. Dominant Hemisphere Group (DH)

Compared with HS, the ALFF values of changed brain regions in DH were mainly activated, which means the focal neuronal activities of these regions were enhanced.

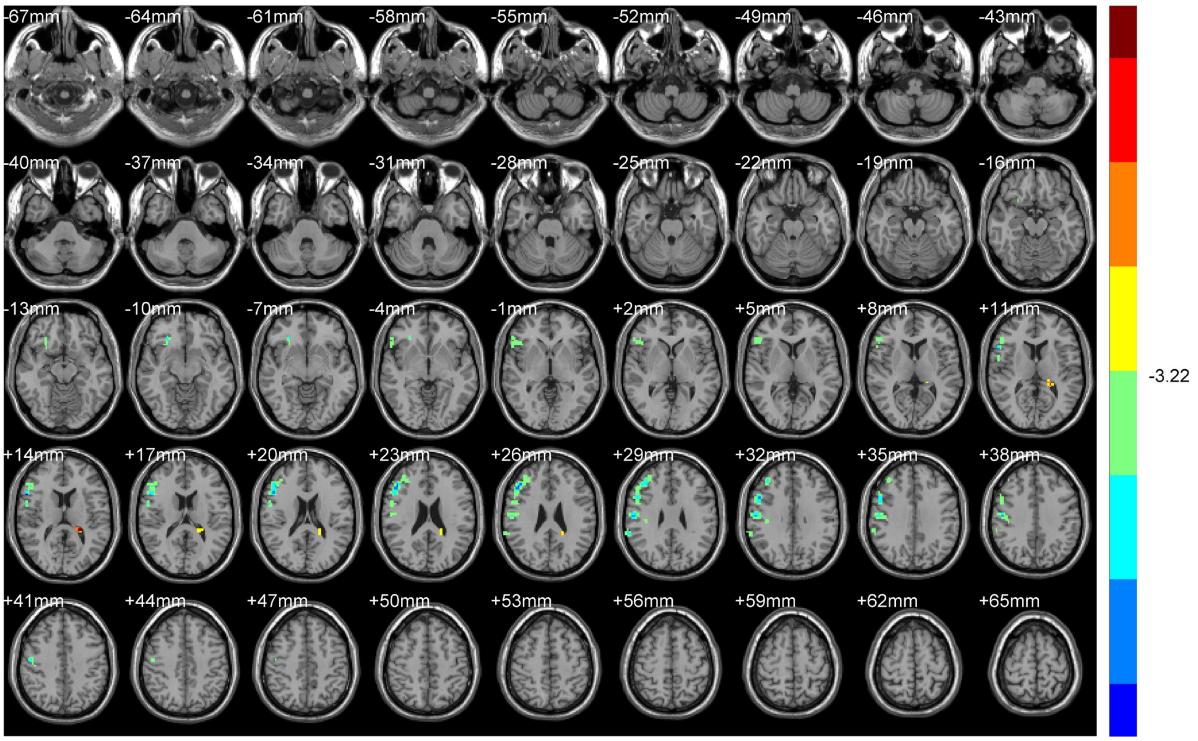


**FIGURE 3 |** ReHo (Dominant hemisphere vs. Normal).

**TABLE 3 |** Regions of NDH showing significant changes in ALFF and ReHo values compared with HS.

| Parameter | Effect | Brain region | MNI coordinate | | | Intensity (*T*-value) |
|---|---|---|---|---|---|---|
| | | | *X* | *Y* | *Z* | |
| ALFF | Enhanced | Left inferior orbital gyrus (including BA47), BA25 | −15 | 12 | −24 | 6.8358 |
| | Enhanced | Left cerebellum anterior lobe (including cerebellar lingual) and Vermis | 0 | −39 | −28 | 4.633 |
| | Enhanced | Left lentiform nuclei and globus pallidus | −9 | 3 | 3 | 7.4651 |
| | Enhanced | Left medial dorsal nucleus and midbrain | −3 | −12 | 3 | 5.3041 |
| | Enhanced | Right caudate head | 9 | 6 | 0 | 6.6047 |
| | Enhanced | Left BA6 and paracentral lobule | −3 | −15 | 66 | 5.0251 |
| | Reduced | Right BA9 and precentral gyrus | 57 | 9 | 36 | −4.9502 |
| ReHo | Enhanced | Left precuneus (BA7) | −9 | −54 | 45 | 5.1723 |
| | Enhanced | Left rectal gyrus and orbital gyrus (including BA11) | −6 | 33 | −27 | 4.5542 |
| | Enhanced | Left parahippocampal gyrus and BA47 | −15 | 6 | −24 | 4.386 |
| | Reduced | Left cerebellum posterior lobe and tubera valvulae | −30 | −75 | −36 | −5.4037 |
| | Reduced | Right BA9 and precentral gyrus | 54 | 12 | 36 | −5.0544 |

*X, Y, Z represent the brain space position axis, respectively, in the MiNi standardized spatial coordinate system in the left and right, front and back, and up and down position of the coordinate position.*

The midbrain, as the reflex center of vision and hearing, participates in the information feedback link of the closed-loop control system and can modify an executing movement in time. This is part of the typical theory of motion control (Faul et al., 2020). The cerebellar vermis (including cerebellar lingual) belongs to the anterior cerebellum and plays an important role in the transmission and feedback of the brain-cerebellar sensorimotor network (Cano-de-la-Cuerda et al., 2015; Zuk and Bertrand, 2019). The mammillary body related to the operation of emotions is a part of the limbic system of the brain. According to some literature (Habas et al., 2009), fierce emotions can affect the control of movement and produce significant behavioral responses to posture patterns or motor strategies.

Both the ALFF and ReHo values were enhanced in the left caudate tai and pulvinar. The pulvinar receives fibers from the inner and outer geniculate body and participates in the visual and auditory pathways (Tamietto et al., 2009, 2012; Pessoa and Adolphs, 2010; Faivre et al., 2012; Gainotti, 2012). The caudate

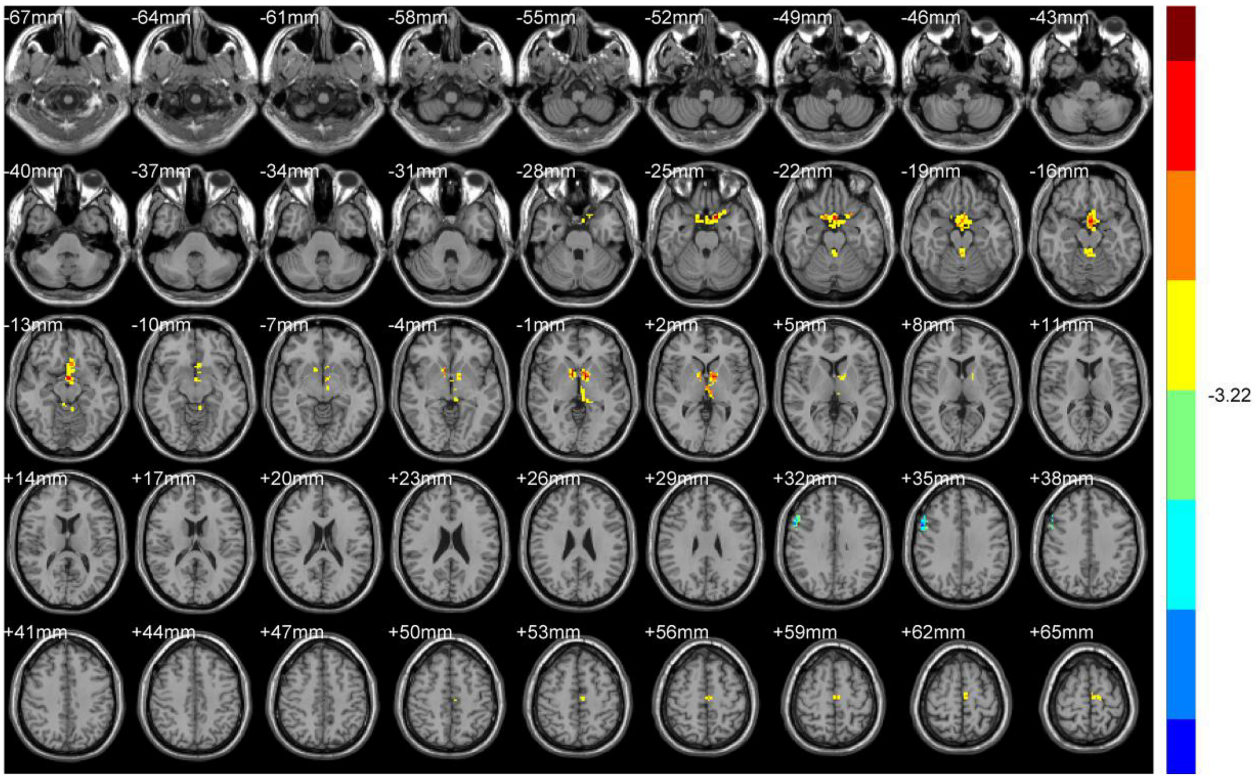


**FIGURE 4 |** ALFF (Non-dominant hemisphere vs. Normal).

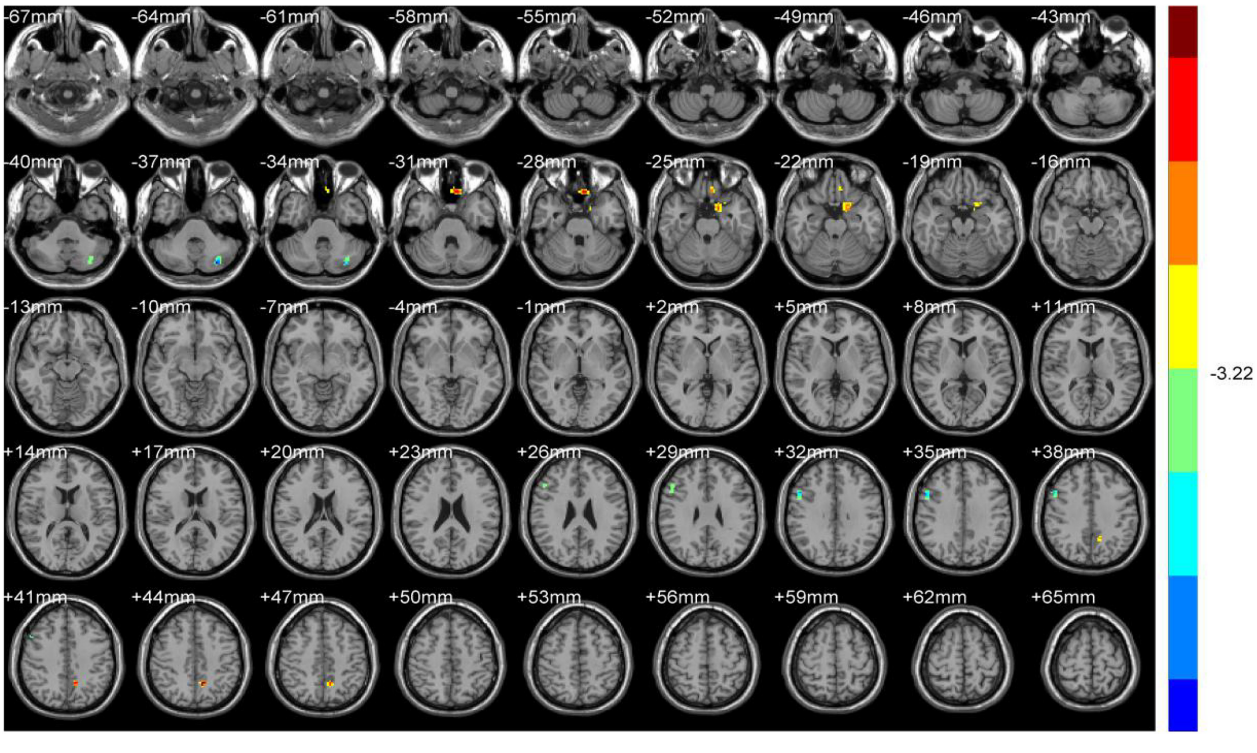


**FIGURE 5 |** ReHo (Non-dominant hemisphere vs. Normal).

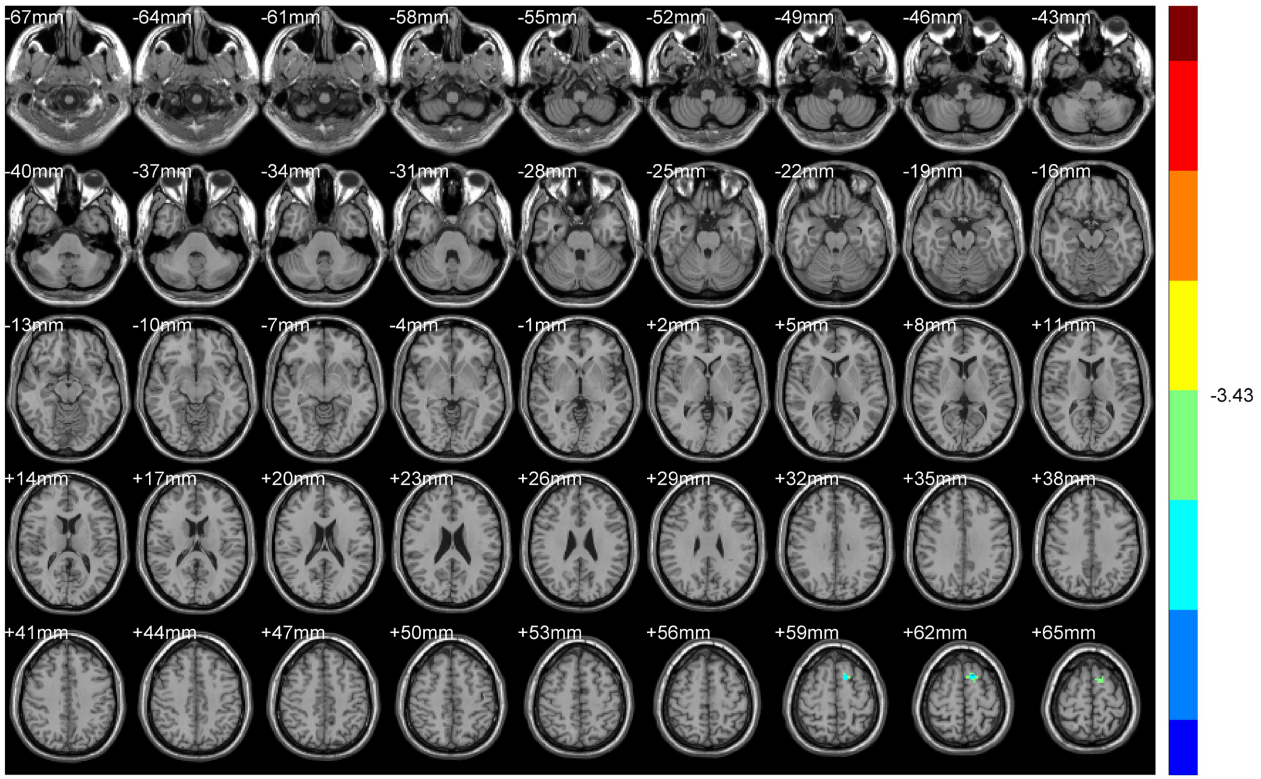


**FIGURE 6 |** ALFF (Dominant hemisphere vs. Non-dominant hemisphere).

**TABLE 4 |** Regions of DH showing significant changes in ALFF and ReHo values compared with NDH.

| Parameter | Effect | Brain region | MNI coordinate | | | Intensity (*T*-value) |
|---|---|---|---|---|---|---|
| | | | *X* | *Y* | *Z* | |
| ALFF | Reduced | Left supplementary motor area (including BA6) | −12 | 15 | 63 | −4.9172 |
| ReHo | Reduced | Right BA10 | 30 | 69 | 9 | −5.6143 |

*X, Y, Z represent the brain space position axis, respectively, in the MiNi standardized spatial coordinate system in the left and right, front and back, and up and down position of the coordinate position.*

tail is one of the important components of the extravertebral motor pathway, which engages in the generation and regulation of motor planning.

As is well known, when the brain receives a specific action command, a signal sent by the cerebral cortex will pass through the outgoing fiber to the skeletal muscle motor endplate and finally complete the action. Motor planning generation, coordinated control of the action, and the feedback for correction are assisted by the cortex, basal ganglia, cerebellum, and midbrain. Therefore, it is speculated that due to the infarction of the middle cerebral artery in the dominant hemisphere, it is difficult for the motor cortex to send out accurate action task signals in contrast to healthy subjects. The signal and function of the brain areas involved in the regulation of movement are strengthened as compensation to ensure the integrity and accuracy of movement.

In addition, ReHo values of the right inferior orbital gyrus (including BA47), triangular inferior frontal gyrus (including BA45), postcentral gyrus (mostly BA3), central anterior gyrus (BA4), and supramarginal gyrus decreased. These brain areas are distributed in the blood supply area of the middle cerebral artery. Vincent has shown that there is a high correlation between bilateral hemispheric ipsilateral brain interval neural activity (Vincent et al., 2007). Therefore, after an acute stroke in the dominant hemisphere, the connection between the homologous brain regions of the non-dominant hemisphere and the peripheral brain regions weakens. Among these brain regions, BA45 is responsible for performing semantic tasks and text production (Jacot-Descombes et al., 2012), BA47 is related to grammar processing of language (Levitin and Menon, 2003), the precentral gyrus (BA4) can control behavior and movement (Levitin and Menon, 2003; Jacot-Descombes et al., 2012; Itabashi et al., 2016) the postcentral gyrus (BA3) manages somatosensory, and the upper marginal gyrus (BA40) is relevant with fine movement (Hämäläinen et al., 2002). ALFF and ReHo values of some brain areas were not reduced in the dominant hemisphere, which may be related to the ischemic stroke classification (TOAST) and the compensation mechanism of cerebral collateral circulation (Liebeskind, 2003).

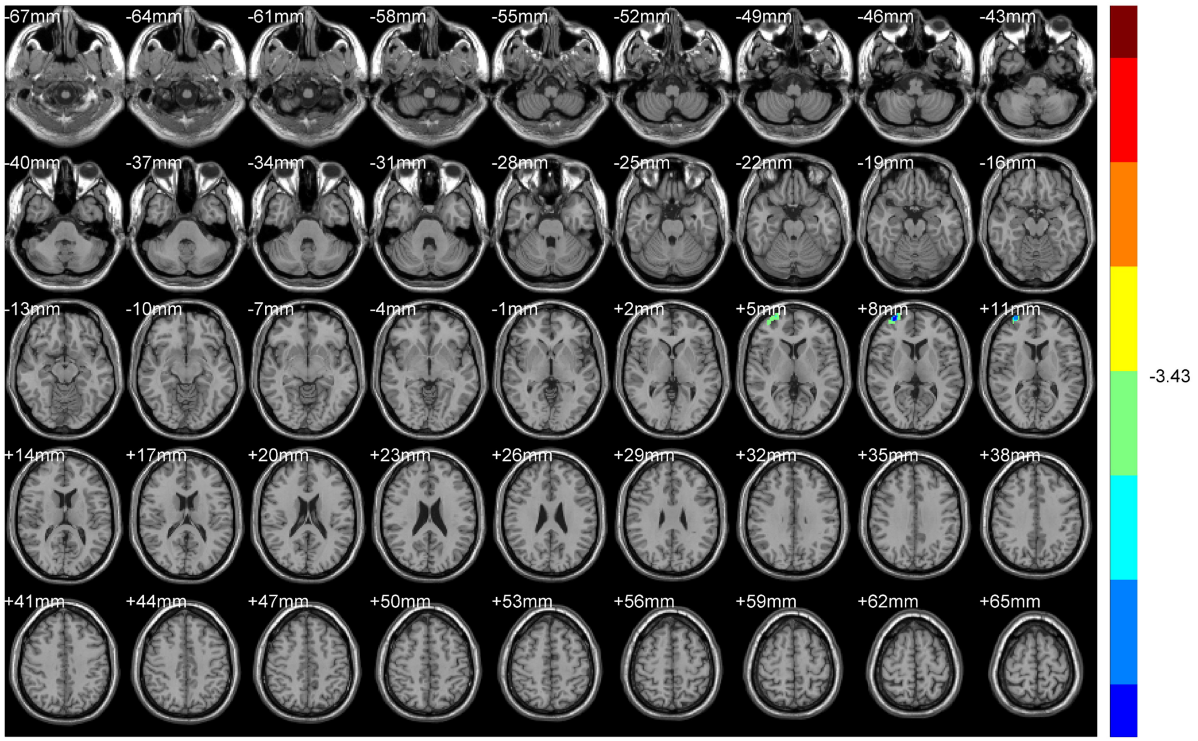


**FIGURE 7 |** ReHo (Dominant hemisphere vs. Non-dominant hemisphere).

## Normal Group vs. Non-dominant Hemisphere Group

Compared with HS, neuronal activities of the injured side and precentral gyrus in the non-dominant hemisphere weakened in the NDH. The connection with peripheral brain regions was also reduced, which is consistent with the physiological changes caused by the responsible lesions. The precentral gyrus is the advanced motor control center, and BA9, BA6, and BA8 constitute the supplementary motor area. They serve as the main brain regions for motor sequence management and participate in the learning, planning, preparation, starting, and production of movement (Kwan et al., 1978; Meier et al., 2008). Negative activation of these two brain regions matches the hemiplegic symptoms of patients.

Interestingly, brain regions with activated ALFF and ReHo values were mainly located in the dominant hemisphere. We believe this is due to the compensation of the uninjured hemisphere (Zaaimi et al., 2012). The paracentral lobule and the precentral gyrus constitute the primary motor cortex and participate in the stage of motor execution. BA6 belongs to part of the premotor cortex and mainly engages in the initial stage of motor preparation and planning (Kwan et al., 1978; Meier et al., 2008). The supramarginal gyrus is related to the fine motor (Hämäläinen et al., 2002). Thalamus and lentiform nuclei are basal ganglia nuclei and play an important role in regulating complex and voluntary movement (Groenewegen, 2003). The lentiform nucleus, dorsomedial nucleus of the left thalamus, and the midbrain can control and purposefully perform active movement through two pathways: cortex-striatum (globus pallidus)-dorsal thalamus cortex and striatum midbrain (substantia nigra)-striatum. The precuneus are brain regions related to the cerebrum's cognitive function (Cavanna and Trimble, 2006), which can analyze external stimuli and adjust the movement. As part of the cerebellum, the anterior lobe and superior vermis (including lingula of the cerebellum) can coordinate the motor through the feedback path of cerebellum-thalamus-(pre) motor cortex. On the other hand, the parahippocampal gyrus and cingulate cortex in BA25 are components of the limbic system and can make the cerebral cortex form higher cognitive connection and program movement to achieve an ideal motor control effect (Geyer et al., 1996). According to the theory of motor control, sensation, cognition, and activity act together in the process of motor control. Based on the theory of neuroplasticity, activation of the upper brain areas indicates a new motor control network has established in the uninjured hemisphere soon after a stroke, which can strengthen body movement coordination in many aspects and ensure active movement to the greatest extent.

In addition, the orbital gyrus (including BA47), the orbital part of the left inferior frontal gyrus, and the rectal gyrus (including BA11) were activated (Berlin et al., 2004; Camille et al., 2004; Kringelbach and Rolls, 2004; Rolls, 2004). Related to the emotion control of humans, these are components of the orbitofrontal cortex and regulate motor together with brain regions of the motor network mentioned above.

### Dominant Hemisphere Group vs. Non-dominant Hemisphere Group

Compared with the NDH, focal neuronal activities in BA6, the area responsible for motor guidance and sequence control, were lessened in the left supplementary motor area in DH. BA10 is the brain area related to emotion control movement. After Stroke, the connection between BA10 and its peripheral brain areas also reduced at the uninjured-side hemisphere. This may be related to the specific influence on the functional impairment of the brain regions responsible for the sequential control of motor guidance in the motor brain network after the injury of the dominant hemisphere (Russo et al., 2020).

### Hemispheric Differences in Stroke Can Conduct the Clinical Application of Transcranial Direct Current Stimulation

Early studies have found that when the cathode of tDCS (transcranial direct current stimulation) is close to the cell body or dendrite of nerve cells, the resting potential threshold increases and the discharge of neurons decreases, while the anode reduces the threshold of resting potential and increases the discharge of neurons (Yavari et al., 2018). Therefore, tDCS can regulate cortical excitability and has the function of nerve regulation. We believe that exploring the changes in brain function after acute stroke in different hemispheres is of great clinical significance for conducting the application of tDCS in the early phase. The cathode can be placed in the abnormal activation enhanced brain area to inhibit the local neuronal activity, while for the brain area with reduced function, the anode should be placed in the corresponding position to enhance the excitability of the neurons.

### Limitations of the Study

This study also has some limitations. First of all, due to the high requirement of resting-state functional magnetic resonance imaging on patients, although the sample size of this study was estimated according to the literature, there was still a large drop-off rate (33.3%), resulting in the study's sample size of only 10–12 cases. But the volunteers of this study were patients with acute stroke in the middle cerebral artery, which made the recruitment difficult. Additionally, the sample size of the same type of fMRI study in stroke patients was around 10–15 cases (Guo et al., 2014). Therefore, it can be considered that the sample size of this study is sufficient to illustrate the conclusion. Secondly, this study only used ALFF and ReHo, the focal indicators of the rs-fMRI, to observe the changes in brain function of patients after acute stroke. And the results were not further discussed by the association between cerebral hemispheres after acute stroke, which needs to be verified in animal experiments.

## CONCLUSION

The findings of this study are as follows. Firstly, after acute infarction in the middle cerebral artery of the dominant hemisphere, a compensation mechanism is triggered in brain areas of the ipsilateral cortex regulating motor-related pathways, while some brain areas related to cognition, sensation, and motor in the contralateral cortex are suppressed, and the connection with the peripheral brain regions is weakened. Secondly, after acute infarction in the middle cerebral artery of the non-dominant hemisphere, compensatory activation appears in motor control-related brain areas of the dominant hemisphere. Thirdly, after acute middle cerebral artery infarction in the dominant hemisphere, compared with the non-dominant hemisphere, functional specificity in the bilateral supplementary motor area weakens. After acute middle cerebral artery infarction in different hemispheres, there are hemispheric differences in the compensatory mechanism of brain function.

## DATA AVAILABILITY STATEMENT

The original contributions presented in the study are included in the article/supplementary material, further inquiries can be directed to the corresponding authors.

## ETHICS STATEMENT

The studies involving human participants were reviewed and approved by the Ethics Committee of the China-Japan Union Hospital at Jilin University approval. The patients/participants provided their written informed consent to participate in this study. Written informed consent was obtained from the individual(s) for the publication of any potentially identifiable images or data included in this article.

## AUTHOR CONTRIBUTIONS

JQC was the project holder. JQC and GL contributed to conception and study design. JCG, CHY, and QXL were responsible for study follow-up and contributed to this article are tied for first place. YJJ were responsible for fcMRI acquisition. LPC and YJJ analyzed the data. SYL and JZ were responsible for patients' recruitment, diagnosis, and treatment. JCG wrote the manuscript. CHY and QXL revised the manuscript. All authors approved the final version of the manuscript.

## FUNDING

This study was supported by the National Natural Science Foundation of China (Grant No: 81403455) and the Program for College Students' innovation and entrepreneurship training of Southern Medical University in 2019 (Grant No: S201912121172).

## ACKNOWLEDGMENTS

The authors thank for the technical support from all colleagues in the imaging department and Neurology Department of China-Japan Union Hospital, Jilin University.

## REFERENCES


Berlin, H. A., Rolls, E. T., and Kischka, U. (2004). Impulsivity, time perception, emotion and reinforcement sensitivity in patients with orbitofrontal cortex lesions. *Brain* 127(Pt 5), 1108–1126. doi: 10.1093/brain/awh135

Camille, N., Coricelli, G., Sallet, J., Pradat-Diehl, P., Duhamel, J. R., and Sirigu, A. (2004). The involvement of the orbitofrontal cortex in the experience of regret. *Science* 304, 1167–1170. doi: 10.1126/science.1094550

Cano-de-la-Cuerda, R., Molero-Sánchez, A., Carratalá-Tejada, M., Alguacil-Diego, I. M., Molina-Rueda, F., Miangolarra-Page, J. C., et al. (2015). Theories and control models and motor learning: clinical applications in neuro-rehabilitation. *Neurologia* 30, 32–41.

Cavanna, A. E., and Trimble, M. R. (2006). The precuneus: a review of its functional anatomy and behavioural correlates. *Brain* 129(Pt 3), 564–583. doi: 10.1093/brain/awl004

Desmond, J. E., and Glover, G. H. (2002). Estimating sample size in functional MRI (fMRI) neuroimaging studies: statistical power analyses. *J. Neurosci. Methods* 118, 115–128. doi: 10.1016/s0165-0270(02)00121-8

Faivre, N., Charron, S., Roux, P., Lehéricy, S., and Kouider, S. (2012). Nonconscious emotional processing involves distinct neural pathways for pictures and videos. *Neuropsychologia* 50, 3736–3744. doi: 10.1016/j.neuropsychologia.2012.10.025

Faul, L., Knight, L. K., Espay, A. J., Depue, B. E., and LaFaver, K. (2020). Neural activity in functional movement disorders after inpatient rehabilitation. *Psychiatry Res. Neuroimaging* 303:111125. doi: 10.1016/j.pscychresns.2020.111125

Gainotti, G. (2012). Unconscious processing of emotions and the right hemisphere. *Neuropsychologia* 50, 205–218. doi: 10.1016/j.neuropsychologia.2011.12.005

Geyer, S., Ledberg, A., Schleicher, A., Kinomura, S., Schormann, T., Bürgel, U., et al. (1996). Two different areas within the primary motor cortex of man. *Nature* 382, 805–807. doi: 10.1038/382805a0

Golestani, A. M., Tymchuk, S., Demchuk, A., Goodyear, B. G., and Vision-2 Study Group. (2013). Longitudinal evaluation of resting-state FMRI after acute stroke with hemiparesis. *Neurorehabil. Neural Repair* 27, 153–163. doi: 10.1177/1545968312457827

Groenewegen, H. J. (2003). The basal ganglia and motor control. *Neural Plast.* 10:108384.

Guo, Q., Thabane, L., Hall, G., McKinnon, M., Goeree, R., and Pullenayegum, E. (2014). A systematic review of the reporting of sample size calculations and corresponding data components in observational functional magnetic resonance imaging studies. *Neuroimage* 86, 172–181. doi: 10.1016/j.neuroimage.2013.08.012

Habas, C., Kamdar, N., Nguyen, D., Prater, K., Beckmann, C. F., Menon, V., et al. (2009). Distinct cerebellar contributions to intrinsic connectivity networks. *J. Neurosci.* 29:8586. doi: 10.1523/jneurosci.1868-09.2009

Hämäläinen, H., Hiltunen, J., and Titievskaja, I. (2002). Activation of somatosensory cortical areas varies with attentional state: an fMRI study. *Behav. Brain Res.* 135, 159–165. doi: 10.1016/s0166-4328(02)00145-6

Hasin, Y., Seldin, M., and Lusis, A. (2017). Multi-omics approaches to disease. *Genome Biol.* 18:83.

Hojjati, S. H., Ebrahimzadeh, A., and Babajani-Feremi, A. (2019). Identification of the early stage of alzheimer's disease using structural mri and resting-state fMRI. *Front. Neurol.* 10:904. doi: 10.3389/fneur.2019.00904

Itabashi, R., Nishio, Y., Kataoka, Y., Yazawa, Y., Furui, E., Matsuda, M., et al. (2016). Damage to the left precentral gyrus is associated with apraxia of speech in acute stroke. *Stroke* 47, 31–36. doi: 10.1161/strokeaha.115.010402

Jacot-Descombes, S., Uppal, N., Wicinski, B., Santos, M., Schmeidler, J., Giannakopoulos, P., et al. (2012). Decreased pyramidal neuron size in Brodmann areas 44 and 45 in patients with autism. *Acta Neuropathol.* 124, 67–79. doi: 10.1007/s00401-012-0976-6

Kringelbach, M. L., and Rolls, E. T. (2004). The functional neuroanatomy of the human orbitofrontal cortex: evidence from neuroimaging and neuropsychology. *Prog. Neurobiol.* 72, 341–372. doi: 10.1016/j.pneurobio.2004.03.006

Kwan, H. C., MacKay, W. A., Murphy, J. T., and Wong, Y. C. (1978). Spatial organization of precentral cortex in awake primates. II. motor outputs. *J. Neurophysiol.* 41, 1120–1131. doi: 10.1152/jn.1978.41.5.1120

Levitin, D. J., and Menon, V. (2003). Musical structure is processed in "language" areas of the brain: a possible role for Brodmann area 47 in temporal coherence. *Neuroimage* 20, 2142–2152. doi: 10.1016/j.neuroimage.2003.08.016

Li, J., Zhang, X. W., Zuo, Z. T., Lu, J., Meng, C. L., Fang, H. Y., et al. (2016). Cerebral functional reorganization in ischemic stroke after repetitive transcranial magnetic stimulation: an fmri study. *CNS Neurosci. Ther.* 22, 952–960. doi: 10.1111/cns.12593

Liebeskind, D. S. (2003). Collateral circulation. *Stroke* 34, 2279–2284.

Meier, J. D., Aflalo, T. N., Kastner, S., and Graziano, M. S. (2008). Complex organization of human primary motor cortex: a high-resolution fMRI study. *J. Neurophysiol.* 100, 1800–1812. doi: 10.1152/jn.90531.2008

Nguyen, V. A., Carey, L. M., Giummarra, L., Faou, P., Cooke, I., Howells, D. W., et al. (2016). A pathway proteomic profile of ischemic stroke survivors reveals innate immune dysfunction in association with mild symptoms of depression - a pilot study. *Front. Neurol.* 7:85. doi: 10.3389/fneur.2016.00085

Pessoa, L., and Adolphs, R. (2010). Emotion processing and the amygdala: from a 'low road' to 'many roads' of evaluating biological significance. *Nat. Rev. Neurosci.* 11, 773–783. doi: 10.1038/nrn2920

Rolls, E. T. (2004). The functions of the orbitofrontal cortex. *Brain Cogn.* 55, 11–29. doi: 10.1016/S0278-2626(03)00277-X

Russo, A. A., Khajeh, R., Bittner, S. R., Perkins, S. M., Cunningham Laurence, J. P., Abbott, F., et al. (2020). Neural trajectories in the supplementary motor area and motor cortex exhibit distinct geometries, compatible with different classes of computation. *Neuron* 107, 745–758. doi: 10.1016/j.neuron.2020.05.020

Tamietto, M., Castelli, L., Vighetti, S., Perozzo, P., Geminiani, G., Weiskrantz, L., et al. (2009). Unseen facial and bodily expressions trigger fast emotional reactions. *Proc. Natl. Acad. Sci. U.S.A.* 106, 17661–17666. doi: 10.1073/pnas.0908994106

Tamietto, M., Pullens, P., de Gelder, B., Weiskrantz, L., and Goebel, R. (2012). Subcortical connections to human amygdala and changes following destruction of the visual cortex. *Curr. Biol.* 22, 1449–1455. doi: 10.1016/j.cub.2012.06.006

van Hees, S., McMahon, K., Angwin, A., de Zubicaray, G., Read, S., and Copland, D. A. (2014). A functional MRI study of the relationship between naming treatment outcomes and resting state functional connectivity in post−stroke aphasia. *Hum. Brain Mapp.* 35, 3919–3931. doi: 10.1002/hbm.22448

Vincent, J. L., Patel, G. H., Fox, M. D., Snyder, A. Z., Baker, J. T., Van Essen, D. C., et al. (2007). Intrinsic functional architecture in the anaesthetized monkey brain. *Nature* 447, 83–86. doi: 10.1038/nature05758

Wang, D., Liu, J., Liu, M., Lu, C., Brainin, M., and Zhang, J. (2017). Patterns of stroke between university hospitals and nonuniversity hospitals in mainland china: prospective multicenter hospital-based registry study. *World Neurosurg.* 98, 258–265. doi: 10.1016/j.wneu.2016.11.006

Wang, M., Gui, X., Wu, L., Tian, S., Wang, H., Xie, L., et al. (2020). Amino acid metabolism, lipid metabolism, and oxidative stress are associated with post-stroke depression: a metabonomics study. *BMC Neurol.* 20:250. doi: 10.1186/s12883-020-01780-7

Wang, Y., Zheng, Y., Qu, S., Zhang, J., Zhong, Z., Zhang, J., et al. (2016). Cerebral targeting of acupuncture at combined acupoints in treating essential hypertension: an Rs-fMRI study and curative effect evidence. *Evid. Based Complement. Alternat. Med.* 2016:5392954.

Wang, Z., Li, J., Wang, C., Yao, X., Zhao, X., Wang, Y., et al. (2013). Gender differences in 1-year clinical characteristics and outcomes after stroke: results from the China National Stroke Registry. *PLoS One* 8:e56459. doi: 10.1371/journal.pone.0056459

Yavari, F., Jamil, A., Mosayebi, S. M., Vidor, L. P., and Nitsche, M. A. (2018). Basic and functional effects of transcranial Electrical Stimulation (tES)-An introduction. *Neurosci. Biobehav. Rev.* 85, 81–92. doi: 10.1016/j.neubiorev.2017.06.015

Yin, D., Luo, Y., Song, F., Xu, D., Peterson, B. S., Sun, L., et al. (2013). Functional reorganization associated with outcome in hand function after stroke revealed by regional homogeneity. *Neuroradiology* 55, 761–770. doi: 10.1007/s00234-013-1146-9

Yoon, B. W., Morillo, C. A., Cechetto, D. F., and Hachinski, V. (1997). Cerebral hemispheric lateralization in cardiac autonomic control. *Arch. Neurol.* 54, 741–744. doi: 10.1001/archneur.1997.00550180055012

Zaaimi, B., Edgley, S. A., Soteropoulos, D. S., and Baker, S. N. (2012). Changes in descending motor pathway connectivity after corticospinal tract lesion in macaque monkey. *Brain* 135, 2277–2289. doi: 10.1093/brain/aws115

Zuk, N. J., and Bertrand, D. (2019). Neural coding and perception of auditory motion direction based on interaural time differences. *J. Neurophysiol.* 122, 1821–1842. doi: 10.1152/jn.00081.2019

**Conflict of Interest:** The authors declare that the research was conducted in the absence of any commercial or financial relationships that could be construed as a potential conflict of interest.

frontiers in Aging Neuroscience

ORIGINAL RESEARCH
published: 28 July 2021
doi: 10.3389/fnagi.2021.706544

# Intracranial Atherosclerotic Plaque Characteristics and Burden Associated With Recurrent Acute Stroke: A 3D Quantitative Vessel Wall MRI Study

*Beibei Sun[1†], Lingling Wang[1†], Xiao Li[1], Jin Zhang[1], Jianjian Zhang[1], Xiaosheng Liu[1,2], Hengqu Wu[3], Mahmud Mossa-Basha[4], Jianrong Xu[1], Bing Zhao[5], Huilin Zhao[1*], Yan Zhou[1*] and Chengcheng Zhu[4*]*

[1] Department of Radiology, Renji Hospital, School of Medicine, Shanghai Jiaotong University, Shanghai, China, [2] Department of Nuclear Medicine, Fudan University Shanghai Cancer Center, Shanghai, China, [3] Department of Neurology, Renji Hospital, School of Medicine, Shanghai Jiaotong University, Shanghai, China, [4] Department of Radiology, University of Washington, Seattle, WA, United States, [5] Department of Neurosurgery, Renji Hospital, School of Medicine, Shanghai Jiaotong University, Shanghai, China

OPEN ACCESS

**Edited by:**
Shuo Wang,
Capital Medical University, China

**Reviewed by:**
Yisen Zhang,
Capital Medical University, China
Xiaolin Chen,
Capital Medical University, China

***Correspondence:**
Huilin Zhao
huilinzhao2013@163.com
Yan Zhou
yaner1475@163.com
Chengcheng Zhu
zhucheng@uw.edu

[†]These authors have contributed equally to this work and share first authorship

**Received:** 07 May 2021
**Accepted:** 21 June 2021
**Published:** 28 July 2021

**Citation:**
Sun B, Wang L, Li X, Zhang J, Zhang J, Liu X, Wu H, Mossa-Basha M, Xu J, Zhao B, Zhao H, Zhou Y and Zhu C (2021) Intracranial Atherosclerotic Plaque Characteristics and Burden Associated With Recurrent Acute Stroke: A 3D Quantitative Vessel Wall MRI Study. Front. Aging Neurosci. 13:706544. doi: 10.3389/fnagi.2021.706544

**Background:** Intracranial atherosclerotic disease (ICAD) tends to affect multiple arterial segments, and previous studies rarely performed a comprehensive plaque analysis of the entire circle of Willis for the evaluation of recurrent stroke risk. We aimed to investigate the features of circle of Willis ICAD on 3D magnetic resonance vessel wall imaging (MR-VWI) and their relationships with recurrent acute stroke.

**Methods:** Patients with either acute ischemic stroke (within 4 weeks after stroke) or chronic ischemic stroke (after 3 months of stroke) due to intracranial atherosclerotic plaque underwent 3D contrast-enhanced MR-VWI covering major cerebral arteries. Participants were divided into three groups: first-time acute stroke, recurrent acute stroke, and chronic stroke. Culprit plaque (defined as the only lesion or the most stenotic lesion when multiple plaques were present within the same vascular territory of the stroke) and non-culprit plaque characteristics, including total plaque number, plaque thickness, plaque area, plaque burden (calculated as plaque area divided by outer wall area), enhancement ratio (ER), eccentricity, and stenosis, were measured and compared across the three groups. Associations between plaque characteristics and recurrent acute stroke were investigated by multivariate analysis.

**Results:** A total of 176 participants (aged 61 ± 10 years, 109 men) with 702 intracranial plaques were included in this study. There were 80 patients with first-time acute stroke, 42 patients with recurrent acute stroke, and 54 patients with chronic stroke. More intracranial plaques were found per patient in the recurrent acute stroke group than in the first-time acute stroke or chronic stroke group (5.19 ± 1.90 vs. 3.71 ± 1.96 and 3.46 ± 1.33, $p < 0.001$). Patients in the recurrent acute stroke group had greater culprit plaque burden ($p < 0.001$) and higher culprit ER ($p < 0.001$) than the other two groups. After adjustment of clinical demographic factors, in multivariate analysis, coronary artery disease (CAD)

(odds ratio, $OR = 4.61$; $p = 0.035$), total plaque number ($OR = 1.54$; $p = 0.003$), culprit plaque ER ($OR = 2.50$; $p = 0.036$), and culprit plaque burden ($OR$ per 10% increment = 2.44; $p = 0.010$) were all independently associated with recurrent acute stroke compared to the first-time acute stroke.

**Conclusion:** Increased intracranial atherosclerotic plaque number, higher culprit plaque ER, greater culprit plaque burden, and CAD are independently associated with recurrent acute stroke.

**Keywords: intracranial artery, atherosclerosis, recurrent acute stroke, culprit plaque, 3D high-resolution vessel wall MR imaging**

## BACKGROUND

Intracranial atherosclerotic disease (ICAD) is a common cause of ischemic stroke in Asians (Holmstedt et al., 2013; Wang et al., 2014) and is associated with a high risk of stroke recurrence (as high as 10–24% annually) (Mazighi et al., 2006). Determination of the factors associated with stroke recurrence is critical for the secondary prevention of stroke. Previous studies suggest that several vascular risk factors such as high blood pressure, diabetes, the circle of Willis variations, and previous coronary artery disease (CAD) are well-known risk factors for recurrent stroke (Holmstedt et al., 2013; Wang et al., 2014; Kang et al., 2016). Patients with severe symptomatic intracranial stenosis (70–99% of the diameter of a major intracranial artery) are at particularly high risk for recurrent stroke in the territory of the stenotic artery (5–23% at 1 year) despite under standard medication (Kasner et al., 2006; Zaidat et al., 2008; Chimowitz et al., 2011; Wang et al., 2014). Besides, ICAD is a systemic disease and can affect multiple arterial segments and vascular beds (Hoshino et al., 2018). Many large prospective studies have documented that the presence of multiple intracranial atherosclerotic stenoses (ICAS) or concurrent extracranial atherosclerosis, on computed tomography angiography (CTA) (Lau et al., 2013), magnetic resonance angiography (MRA) (Man et al., 2009; Wang et al., 2014; Sun et al., 2018), or digital subtraction angiography (DSA) (Zhao et al., 2018), was an independent predictor of stroke recurrence. Coexisting cerebrovascular atherosclerosis involving both intracranial and extracranial arterial beds is an independent predictor for subsequent vascular events (including ischemic stroke) (Li et al., 2020).

During the past decades, the development of vessel wall MRI has enabled the evaluation of intracranial plaque features *in vivo*, and recently, three-dimensional (3D) MR vessel wall imaging (MR-VWI) allows for the evaluation of plaque in the entire Circle of Willis with high isotropic resolution (Qiao et al., 2011; Xie et al., 2016). The intracranial plaque enhancement detected by gadolinium-contrasted MRI is associated with vasa vasorum, which is possibly a surrogate marker of vessel wall inflammation (Portanova et al., 2013), and it was associated with stroke risk (Rudd and Fayad, 2008; Qiao et al., 2014). There were a few studies that investigated the association between plaque features using MR-VWI and recurrent stroke risk and found that contrast enhancement and plaque burden were the potential factors associated with recurrent stroke (Kim et al., 2016; Ran et al., 2020; Shi et al., 2021). However, these studies were limited in the use of two-dimensional (2D) imaging, only one single segment [middle cerebral artery (MCA) stenosis], and only in patients with anterior circulation stroke.

We hypothesize that the number of intracranial plaques and vulnerable plaque features revealed on 3D contrast-enhanced MR-VWI are associated with stroke recurrence. This study sought to investigate whether these features are associated with patients with recurrent acute stroke in both the anterior and posterior circulation.

## METHODS

### Study Population

This was a prospective, cross-sectional study, and the study protocol was approved by the institutional review board, and informed written consent was obtained from all patients. Patients with ischemic stroke symptoms prospectively and consecutively underwent 3D contrast-enhanced MR-VWI covering major cerebral arteries from October 2017 to December 2020, and we reviewed these images in 1 week after scans (from October 2017 to January 2021). Inclusion criteria for this study were as follows: (1) patients with intracranial arterial stenosis detected on MRA or CTA (including bilateral C6-7 segment of internal carotid artery, A1-2 segment of anterior cerebral artery, M1-2 segment of MCA, V4 segment of vertebral artery, P1-2 segment of posterior cerebral artery and basilar artery); (2) ischemic infarct confirmed by diffusion-weighted imaging (DWI) for the acute group, and chronic infarct was identified from T2-fluid attenuated inversion recovery imaging (FLAIR) and DWI; and (3) stroke etiology determined to be ICAS by the identification of intracranial artery plaque on 3D MR-VWI. Exclusion criteria were as follows: (1) intracranial artery occlusion; (2) coexistence of >50% stenosis or unstable plaques (presence of at least three

**Abbreviations:** ACA, anterior cerebral artery; BMI, body mass index; BA, basilar artery; CVD, cerebro-cardiovascular disease; CAD, coronary artery disease; DBP, diastolic blood pressure; DM, diabetes mellitus; DWI, diffusion-weighted imaging; ER, enhancement ratio; FLAIR, fluid-attenuated inversion recovery imaging; HDL, high-density lipoprotein; Hs-CRP, high-sensitivity C-reactive protein; ICAD, intracranial atherosclerosis disease; ICA, internal carotid artery; LDL, low-density lipoprotein; MCA, middle cerebral artery; MR-VWI, MR vessel wall imaging; NIHSS, NIH Stroke Score; PCA, posterior cerebral artery; SBP, systolic blood pressure; TG, triglyceride; TC, total cholesterol; T1-VISTA, T1WI volume isotropic turbo spin-echo acquisition; VA, vertebral artery.

of the following features: calcification, hemorrhage, superficial irregularity, and being lipid-rich) of the ipsilateral extracranial carotid artery detected by imaging (ultrasound, MRA, CTA, or DSA); (3) evidence of cardioembolic source ischemic stroke (recent myocardial infarction within 3 weeks, atrial fibrillation or flutter, evidence of cardiac or valvular thrombus on echocardiography, or other imaging; (4) clinical evidence of the presence of vasculopathy other than atherosclerosis (e.g., vasculitis, reversible cerebral vasoconstriction syndrome or other vasospastic processes, Moyamoya disease, or dissection); (5) degraded image quality of 3D MR-VWI that limited accurate delineation of the artery boundaries for quantitative analysis; and (6) patients with subacute stroke (time from onset:1–3 months). Recurrent acute stroke events were defined as new neurological deficits that fit the definition of acute ischemic stroke occurring 24 h after the incident strokes in the same vascular territory and were not attributable to cerebral edema, mass effect, or hemorrhagic transformation (Coull and Rothwell, 2004). Participants were divided into three groups: first-time acute stroke, recurrent acute stroke, and chronic stroke.

Clinical information including age, gender, body mass index (BMI), vascular risk factors (hypertension, hyperlipidemia, diabetes mellitus, smoking status, CAD), and relevant medications (statins and antiplatelet agents) was recorded for each patient. Hypertension was defined as a systolic blood pressure ≥140 mmHg, a diastolic blood pressure ≥90 mmHg, or current treatment with antihypertensive agents. Dyslipidemia was defined as TC/HDL-C ratio ≥5, measured LDL-C ≥ 3.5 mmol/l, or taking lipid-modifying medications. Smoking status was assessed at the time of the ischemic event, and the patients were dichotomized into two groups: current smoker (defined as a patient who had smoked continuously for 6 months with ≥1 cigarette per day) (Wang et al., 2014) or not a current smoker. Clinical history of previous strokes was recorded for patients in the recurrent acute stroke group.

## 3D MR-VWI Protocol

All the subjects underwent brain MRI on a 3.0T whole-body scanner (Philips Ingenia, Philips Healthcare, Best, The Netherlands). The MR protocol included three-dimensional time-of-flight (3D-TOF) MRA and 3D MR-VWI. The imaging parameters of these sequences were as follows: (1) 3D-TOF MRA: TR/TE: 23/3.5 ms, flip angle 18°, field of view 199 mm × 199 mm; slice thickness 1.2 mm, and acquisition matrix 500 × 332; (2) T1WI volume isotropic turbo spin-echo acquisition (T1-VISTA): coronal imaging orientation, TR/TE 500/25 ms, TSE factor 45, with variable flip angle, number of slices 120, FOV 230 m × 250 mm × 50 mm, voxel size 0.6 × 0.6 × 0.6 mm, scan time 7 min 10 s; (3) Simultaneous Non-contrast Angiography and intraPlaque hemorrhage (SNAP): FFE, TR/TE 9.9/4.8 ms, flip angle 11/5°. Post-contrast T1-VISTA images were acquired 5 min after intravenous gadolinium contrast agent (Bayer Schering Pharma AG, Germany) injection (with a dose of 0.1 mmol/kg, at a rate of 1.5 ml/s) with similar imaging parameters as pre-contrast. DWI and T2-FLAIR were used for infarct identification.

## Image Analysis

Evaluation of MR-VWI was conducted by two experienced radiologists (XL and LW, each with 5 years of experience in intracranial artery imaging) who were blinded to patient clinical information and performed a quantitative evaluation of plaque characteristics. A subgroup of 30 cases was randomly selected from the studied population (10 cases in the first-time acute stroke group, 10 cases in the recurrent acute stroke group, and 10 cases in the chronic stroke group) for a reproducibility study. Two readers (XL and LW) independently performed all measurements on the 30 cases for the evaluation of inter- and intra-reader agreement. One reviewer (XL) re-evaluated the same 30 cases independently after 2 months. Image quality rating was assigned using a four-point scale (1, poor; 2, marginal; 3, good; and 4, excellent) depending on the overall signal-to-noise ratio and the clarity of the vessel wall boundaries (Zhao et al., 2013), and the MR images with image quality ≥3 were qualified for analysis. All atherosclerotic plaques on pre-contrast MR-VWI were then identified using a previously reported definition, that is, the presence of focal wall thickening (Qiao et al., 2014). Lumen and outer wall boundaries were manually segmented on both pre-contrast and post-contrast T1-VISTA, using medical imaging viewer software (Vue PACS Livewire, Carestream, Rochester, NY, United States). The contouring of the plaques in each patient took 10–20 min depending on the number of plaques per patient.

Plaque quantitative parameters assessed included plaque thickness, plaque length, plaque area, plaque burden, plaque enhancement ratio (ER) and enhancement score, and luminal stenotic rate. Qualitative parameters included eccentricity, enhancement grade, and intraplaque hemorrhage (IPH). Luminal stenotic rate, plaque length, plaque burden, and ER were measured on the reconstructed pre-contrast and post-contrast images at the site of the most stenotic lesion or the most apparent wall thickening for each participant. The degree of stenosis was measured on black blood T1-VISTA images using WASID criteria:

$Degree\ of\ stenosis = \left(1 - \frac{D_{stenosis}}{D_{normal}}\right) \times 100\%$ (Samuels et al., 2000), where $D_{stenosis}$ denotes the diameter of the artery at the site of the most severe stenosis and $D_{normal}$ denotes the diameter of the proximal normal artery. The use of 3D MR-VWI for intracranial stenosis measurements has been validated against luminal imaging techniques with the excellent agreement (Tian et al., 2021). The plaque burden was calculated as:

$$Plaque\ burden = \frac{total\ wall\ area - lumen\ area}{total\ wall\ area} \times 100\%$$

(Qiao et al., 2016).

Diagram for the measurements of plaque morphology is shown in **Supplementary Figure 1**.

The ER was measured at the slice of greatest enhancement, using adjacent gray matter (in a region of ∼15 $mm^2$) to normalize the signal intensity (SI). The ER was calculated as $Enhancement\ ratio = \frac{\frac{SI\_Plaque_{postcontrast}}{\overline{SI\_gray\ matter}_{postcontrast}} - \frac{SI\_Plaque_{precontrast}}{\overline{SI\_gray\ matter}_{precontrast}}}{\frac{SI\_Plaque_{precontrast}}{\overline{SI\_gray\ matter}_{precontrast}}}$ (Shi et al., 2018) (SI short for signal intensity). Plaque enhancement

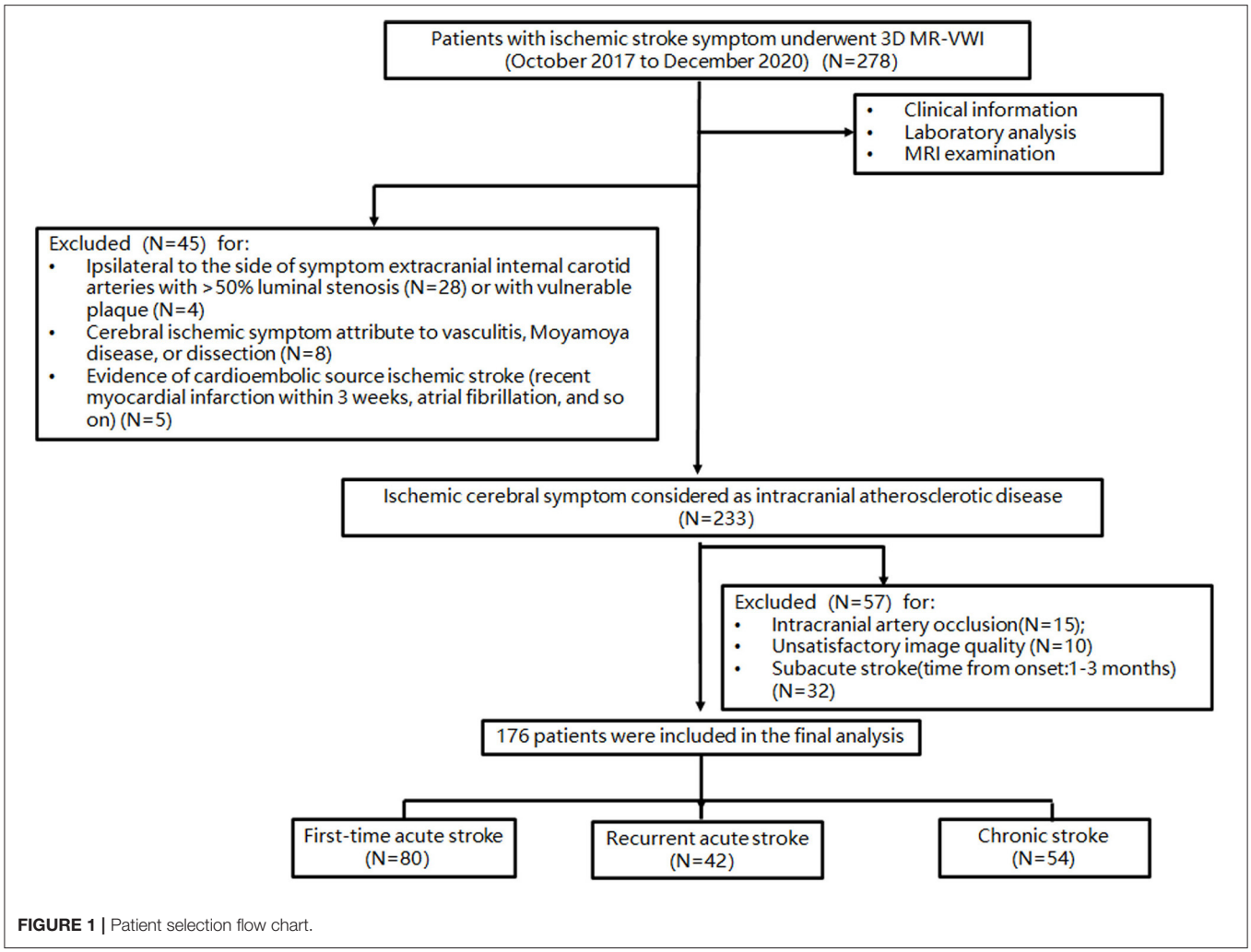


**FIGURE 1 |** Patient selection flow chart.

grade was classified into three grades on post-contrast T1-VISTA images by using published criteria (Qiao et al., 2014; Hartman et al., 2019): grade 0, no enhancement, defined as the SI of plaque was similar to that of adjacent normal vessel wall; grade 1, mild to moderate enhancement, defined as the SI of plaque was lower than that of the pituitary infundibulum but higher than that of adjacent normal vessel wall; and grade 2, significant enhancement, defined as the SI of plaque was similar to or greater than that of the pituitary infundibulum. The plaque enhancement score of each patient was calculated by summing all enhancement grades of all plaques in intracranial arteries (Cui et al., 2020).

Eccentricity was defined as a localized plaque surrounding <75% of the vessel wall (Chung et al., 2012). The presence of IPH was defined as >150% signal relative to muscles within the covered anatomy on pre-contrast T1-weighted images (Zhu C. et al., 2018).

The culprit plaque was defined as (a) the only lesion within the vascular territory of the stroke or (b) the most stenotic lesion when multiple plaques were present within the same vascular territory of the stroke (Qiao et al., 2014). The other plaques that were not culprit plaque were defined as non-culprit.

## Statistical Analysis

Quantitative and categorical data are presented as mean ± SD or median (range) and counts or percentages, respectively. Comparisons between groups were made using chi-square/Fisher's test for categorical data and the Mann–Whitney *U*-test or Student's *t*-test for continuous data. The inter- and intra-observer agreement was calculated through the Cohen κ value for categorical data, and by intraclass correlation coefficient (ICC) and Bland–Altman analysis for continuous data. A value of κ and ICC > 0.80 was used to indicate an excellent agreement. Parameters with a $p < 0.1$ from univariate analysis were included in the following multivariate logistic regression analysis, which was used to determine the independent factors associated with recurrent stroke. Multicollinearity testing was performed using variance inflation factor (VIF) as an evaluation standard. A VIF that equals 1 indicates no multicollinearity among factors; a VIF

**TABLE 1 |** Demographic information of the study population.

| | Group 1, patients with first-time acute stroke (*N* = 80) | Group 2, patients with recurrent acute stroke (*N* = 42) | Group 3, patients with chronic stroke (*N* = 54) | $p^a$-value | Between-group $p^b$ values: group 1 vs. 2; group 2 vs. 3, group 1 vs. 3 |
|---|---|---|---|---|---|
| Male, *n* (%) | 53 (66.3%) | 24 (57.1%) | 32 (59.3%) | 0.547 | 0.322, 0.835, 0.410 |
| Age, year | 59.45 ± 9.85 | 60.64 ± 9.40 | 63.32 ± 9.37 | 0.075 | 0.515, 0.178, 0.025 |
| BMI, kg/m$^2$ | 24.60 ± 2.89 | 24.58 ± 2.34 | 24.68 ± 2.21 | 0.978 | 0.957, 0.845, 0.866 |
| Interval between symptom and MRI scan[#] | 20d (2d−30d) | 15d (2d−30d) | 6M (3M−48M) | NA | 0.158[†] |
| Baseline NIHSS[#] | 2 (0–8) | 2.5 (0–6) | 2 (0–8) | 0.107 | 0.587, 0.051, 0.090 |
| **Risk factors** | | | | | |
| Current smoking, *n* (%) | 15 (18.8%) | 10 (23.8%) | 7 (13.0%) | 0.387 | 0.511, 0.188, 0.375 |
| Alcohol, *n* (%) | 7 (8.8%) | 7(16.7%) | 3(5.6%) | 0.175 | 0.235, 0.098, 0.739 |
| Family history of CVD, *n* (%) | 18 (22.5%) | 10 (23.8%) | 16 (29.6%) | 0.633 | 0.870, 0.949, 0.352 |
| DM, *n* (%) | 36 (45.0%) | 17 (40.5%) | 16 (29.6%) | 0.199 | 0.632, 0.524, 0.073 |
| CAD, *n* (%) | 4 (5.0%) | 8 (19.0%) | 7 (13.0%) | 0.042 | 0.022, 0.415, 0.118 |
| Hypertension, *n* (%) | 56 (70.0%) | 34 (81.0%) | 42 (77.8%) | 0.353 | 0.191, 0.704, 0.319 |
| SBP, mmHg | 145.05 ± 21.59 | 144.02 ± 23.02 | 143.33 ± 19.23 | 0.897 | 0.800, 0.875, 0.647 |
| DBP, mmHg | 84.00 ± 12.39 | 83.64 ± 13.79 | 83.65 ± 11.18 | 0.982 | 0.880, 0.998, 0.872 |
| Dyslipidemia, *n* (%) | 26 (33.3%) | 9 (21.4%) | 16 (31.4%) | 0.381 | 0.171, 0.282, 0.816 |
| **Laboratory findings** | | | | | |
| Blood glucose, mmol/L | 6.33 ± 2.15 | 5.81 ± 1.40 | 5.96 ± 1.54 | 0.269 | 0.137, 0.691, 0.250 |
| HDL cholesterol, mmol/L | 1.00 ± 0.31 | 1.05 ± 0.31 | 1.02 ± 0.36 | 0.751 | 0.452, 0.687, 0.731 |
| LDL cholesterol, mmol/L | 2.06 ± 0.83 | 2.03 ± 0.76 | 2.20 ± 0.88 | 0.555 | 0.874, 0.339, 0.349 |
| TG, mmol/L | 2.16 ± 1.33 | 1.76 ± 1.31 | 2.21 ± 1.30 | 0.199 | 0.112, 0.104, 0.847 |
| TC, mmol/L | 2.98 ± 1.38 | 3.18 ± 1.12 | 3.12 ± 1.59 | 0.720 | 0.451, 0.824, 0.578 |
| Hs-CRP, mg/L[#] | 2.15 (0.19–25.4) | 3.48 (0.33–38.34) | 1.25 (0.18–18.56) | 0.167 | 0.397, 0.060, 0.197 |
| **Medication** | | | | | |
| Pre-admission statin use (%) (>3months) | 9 (11.3%) | 22 (52.4%) | 8 (14.8%) | <0.001 | <0.001, <0.001, 0.543 |
| Pre-admission aspirin use (%) (>3months) | 3 (3.8%) | 14 (33.3%) | 6 (11.1%) | <0.001 | <0.001, 0.008, 0.157 |
| Pre-admission dual antiplatelet therapy use (%) (>3months) | 5 (6.3%) | 7 (16.7%) | 1 (1.9%) | 0.024 | 0.106, 0.020, 0.401 |

*[†] Comparison confined to between group 1 and group 2 for comparability.*

*[#] Medium (range); d, day; m, month.*

*BMI, body mass index; CVD, cerebro-cardiovascular disease; CAD, coronary artery disease; DM, diabetes mellitus; SBP, systolic blood pressure; DBP, diastolic blood pressure; HDL, high-density lipoprotein; LDL, low-density lipoprotein; TG, triglyceride; TC, total cholesterol; Hs-CRP, high-sensitivity C-reactive protein. NIHSS, NIH Stroke Score.*

*$p^a$ values are calculated by ANOVA or chi-square test among three groups, as appropriate; $p^b$ values are calculated by independent-samples t-test or Mann–Whitney U-test or chi-square test between group 1 and 2, group 2 and 3, or group 1 and 3, as appropriate.*

between 1 and 5 indicates moderate collinearity; a VIF between 5 and 10 indicates a high correlation that may be problematic; a VIF > 10 indicates a significant correlation leading to unreliability of the regression analysis (Kim, 2019). All tests were two-tailed, and $p < 0.05$ were considered significant. The receiver-operating characteristic (ROC) curves were plotted for parameters with independent significance, and area under curves (AUC) were calculated. SPSS (Statistics version 22) was used for data analysis. MedCalc version 19.1 was used for drawing ROC curves.

# RESULTS

## Characteristics of Patients

The patient selection flowchart is shown in **Figure 1**. From October 2017 to December 2020, 278 patients met the inclusion criteria. After the exclusion of 102 patients, 176 patients [aged 61 ± 10 years; 109 (61.9%) men] were included in the final analysis. The demographic information of patients is listed in **Table 1**. Of these patients, 132 (75%) had hypertension, 69 (39.2%) had diabetes, 51 (28.9%) had dyslipidemia, 44 (25%) had family

**TABLE 2 |** Comparisons of plaque features among the three group patients.

| | Group 1, patients with first-time acute stroke ($N = 80$) | Group 2, patients with recurrent acute stroke ($N = 42$) | Group 3, patients with chronic stroke ($N = 54$) | $p^a$-value | Between-group $p^b$-values: group 1 vs. 2; group 2 vs. 3, group 1 vs. 3 |
|---|---|---|---|---|---|
| **PLAQUE CHARACTERISTICS** | | | | | |
| Multiple plaque, *n* (%) | 69 (86.2%) | 39 (92.9%) | 50 (92.6%) | 0.371 | 0.376, 0.999, 0.253 |
| Average plaque number, *n* | 3.71 ± 1.96 | 5.19 ± 1.90 | 3.46 ± 1.33 | <0.001 | <0.001, <0.001, 0.417 |
| Total plaque enhancement score | 3.24 ± 2.12 | 4.29 ± 2.24 | 2.65 ± 1.80 | 0.001 | 0.008, <0.001, 0.106 |
| **CULPRIT PLAQUE LOCATION** | | | | | |
| **Anterior circulation** | | | | | |
| ICA (C6-C7), *n* (%) | 2 (2.5%) | 3 (7.1%) | 1 (1.9%) | 0.956 | 0.388, 0.316, 0.999 |
| ACA (A1-A2), *n* (%) | 0 | 0 | 0 | NA | |
| MCA (M1-M2), *n* (%) | 55 (68.8%) | 32 (76.2%) | 35 (64.8%) | 0.482 | 0.388, 0.229, 0.634 |
| **Posterior circulation** | | | | | |
| VA (V4), *n* (%) | 14 (17.5%) | 2 (4.8%) | 8 (14.8%) | 0.143 | 0.048, 0.178, 0.681 |
| BA, *n* (%) | 9 (11.3%) | 5 (11.9%) | 10 (18.5%) | 0.452 | 0.999, 0.376, 0.237 |
| PCA (P1-P2), *n* (%) | 0 | 0 | 0 | NA | |
| **CULPRIT PLAQUE FEATURES** | | | | | |
| Eccentricity, *n* (%) | 28 (35.0%) | 18 (42.9%) | 19 (35.2%) | 0.660 | 0.395, 0.444, 0.982 |
| Stenosis>50%, *n* (%) | 71 (88.8%) | 38 (90.5%) | 46 (85.2%) | 0.707 | 0.769, 0.437, 0.543 |
| Stenosis, % | 75.31 ± 18.04 | 80.00 ± 19.36 | 71.85 ± 16.09 | 0.087 | 0.169, 0.027, 0.271 |
| Plaque length, mm | 8.30 ± 4.14 | 8.71 ± 5.93 | 6.92 ± 3.73 | 0.112 | 0.632, 0.056, 0.086 |
| Plaque thickness, mm | 1.70 ± 0.74 | 1.70 ± 0.71 | 1.63 ± 0.78 | 0.845 | 0.996, 0.647, 0.590 |
| Plaque area, $mm^2$ | 10.68 ± 8.36 | 9.02 ± 7.24 | 9.33 ± 7.87 | 0.463 | 0.276, 0.850, 0.339 |
| Plaque burden, % | 79.10 ± 9.28 | 83.42 ± 6.42 | 74.48 ± 13.64 | <0.001 | 0.029, <0.001, 0.012 |
| Plaque hemorrhage, *n* (%) | 8 (10.0%) | 4 (9.5%) | 7 (13.0%) | 0.829 | 0.933, 0.600, 0.594 |
| **PLAQUE ENHANCEMENT** | | | | | |
| Grade 0, *n* (%) | 11(13.8%) | 5 (11.9%) | 15(27.8%) | 0.060 | 0.774, 0.057, 0.044 |
| Grade 1, *n* (%) | 35(43.8%) | 10 (23.8%) | 22 (40.7%) | 0.087 | 0.030, 0.081, 0.730 |
| Grade 2, *n* (%) | 34(42.5%) | 27 (64.3%) | 17 (31.5%) | 0.005 | 0.022, 0.001, 0.198 |
| Plaque ER | 1.77 ± 0.63 | 2.06 ± 0.39 | 1.53 ± 0.37 | <0.001 | 0.003, <0.001, 0.009 |
| **NON-CULPRIT PLAQUE FEATURES** | | | | | |
| Stenosis, % | 31.48 ± 19.55 | 34.64 ± 16.46 | 39.82 ± 19.74 | 0.046 | 0.382, 0.185, 0.013 |
| Max plaque thickness, mm | 1.22 ± 0.73 | 1.44 ± 0.62 | 1.27 ± 0.58 | 0.219 | 0.083, 0.238, 0.616 |
| Enhanced plaque number, *n* (%) | 118 (49.4%) | 89 (50.6%) | 65 (45.5%) | 0.273 | 0.303, 0.110, 0.458 |
| Grade 2 enhanced plaque number, *n* (%) | 33 (13.8%) | 18 (10.2%) | 16 (11.2%) | 0.636 | 0.414, 0.968, 0.459 |

*ICA, internal carotid artery; ACA, anterior cerebral artery; MCA, middle cerebral artery; VA, vertebral artery; BA, basilar artery; PCA, posterior cerebral artery, ER, enhancement ratio. $p^a$ values are calculated by ANOVA or chi-square test among three groups, as appropriate; $p^b$ values are calculated by independent-samples t-test or Mann–Whitney U-test or chi-square test between group 1 and 2, group 2 and 3, or group 1 and 3, as appropriate.*

history of cerebro-cardiovascular disease, 19 (10.8%) had CAD, and 32 (18.2%) were current smokers at the time of imaging. There were 80 first-time acute stroke patients, 42 recurrent acute stroke patients, and 54 chronic stroke patients. Recurrent acute stroke occurred with a mean of 12.6 ± 23.9 months (median 3.5 months, interquartile range 1–10.5 months) after the previous events. The age of chronic stroke patients was older than that of the first-time acute stroke patients ($p = 0.025$). The prevalence of CAD of recurrent acute stroke patients was higher than that of the first-time acute stroke patients ($p = 0.022$). Pre-admission statin and aspirin use was more common in the recurrent acute stroke group than in the other two groups, while dual antiplatelet

use was more common in the recurrent acute stroke group compared with the chronic stroke group, but no different from the first-time acute stroke patients. No significant difference was observed in other clinical characteristics among the three groups.

## Comparison of Intracranial Plaque Features Among the Three Groups

The comparison of intracranial plaque features among the three groups is shown in **Table 2**. Seven hundred and two intracranial plaques were identified in all participants (297 in the first-time acute stroke group; 218 in the recurrent acute stroke group, and 187 in the chronic stroke group). A mean of 4.0 ± 1.9 (median 4, range 1–9) plaques were identified per patient, with a mean of 3.7 ± 1.9 (median 3, range 1–9) plaques in anterior circulation stroke patients and 4.7 ± 1.8 (median 5, range 1–9) plaques in posterior circulation stroke patients. Recurrent acute stroke patients had more plaques than the other two groups ($p < 0.001$).

As for culprit plaque, there was the following arterial segment involvement: 6 (3.4%) intracranial internal carotid artery, 122 (69.3%) M1-2 segment of the MCA, 24 (13.6%) V4 segment of vertebral artery, and 24 (13.6%) were found in basilar artery. Patients with acute stroke (first-time and recurrent) had significantly larger culprit plaque burden and higher plaque ER than patients with chronic stroke ($p < 0.001$, $p < 0.001$, respectively). Patients in the recurrent acute stroke group had larger culprit plaque burden ($p < 0.001$) and higher plaque ER ($p < 0.001$) than the other two groups. The degree of stenosis of culprit plaques was not significantly different among the three groups ($p = 0.087$) but was significantly different between the recurrent acute stroke group and the chronic stroke group ($p = 0.027$). Culprit plaque length ($p = 0.112$), culprit plaque thickness ($p = 0.845$), culprit plaque area ($p = 0.463$), and culprit plaque eccentricity ($p = 0.660$) were not significantly different among the three groups. The prevalence of culprit IPH was generally low in all three groups. Box plots are shown in **Figure 2**, and the representative cases are shown in **Figures 3**, **4**.

No significant difference was detected in the investigated plaque features of non-culprit plaques among the three groups.

## Association Between Intracranial Plaque Characteristics and Recurrent Acute Stroke

**Table 3** shows univariate and multivariate analysis results for the parameters associated with recurrent acute stroke compared with the first-time acute stroke. The VIF values between intracranial plaque enhancement score and culprit plaque ER, culprit plaque enhancement grade, total plaque number are 1.279, 1.313, and 1.258, respectively, indicating a moderate collinearity, which is unlikely to substantially affect the following multivariate analysis significantly, whereas culprit plaque ER had no collinearity with culprit plaque enhancement grade ($VIF = 1.0$) (**Supplementary Table 1**). After the adjustment of clinical demographic factors, CAD [odds ratio, 4.61 (95% CI, 1.11–19.18); $p = 0.035$), total plaque number [odds ratio, 1.54, (95% CI, 1.16–2.03); $p = 0.003$], culprit plaque ER [odds ratio, 2.50, (95% CI, 1.06–5.89); $p = 0.036$], and culprit plaque burden [odds ratio, 2.44, per 10% increase (95% CI, 1.24–4.79); $p = 0.010$] were all independently associated with recurrent acute stroke.

The ROC curves of differentiating patients with the first-time and recurrent acute strokes are shown in **Figure 5**. The areas under the curve for CAD, culprit plaque burden, culprit plaque ER, and total plaque number were 0.570, 0.636, 0.704, and 0.716, respectively. The AUCs for CAD, culprit plaque burden, culprit plaque ER, and total plaque number were 0.570, 0.636, 0.704, and 0.716, respectively. The cutoff values of culprit plaque burden, culprit plaque ER, and total plaque number were 81.60% (sensitivity = 69.05%, specificity = 55.0%), 1.91 (sensitivity = 78.57%, specificity = 66.25%), and 4 (sensitivity = 76.19%, specificity = 66.25%), respectively. The AUC was 0.804 for the total plaque number combined with culprit plaque burden, culprit plaque ER, and CAD (sensitivity = 78.57%; specificity = 73.75%), and the corresponding cutoff values of culprit plaque burden, culprit ER, and total plaque number were 88.88%, 1.13, and 5, respectively.

The logistic regression analysis and ROC curves for differentiating between chronic and recurrent acute stroke groups were also performed in **Supplementary Table 2** and **Supplementary Figure 2**. We found that culprit plaque ER and total plaque numbers were independently associated with recurrent acute stroke compared with chronic stroke patients ($OR = 51.01$ and $OR = 2.30$, respectively). The AUCs of culprit ER and total plaque number were 0.836 and 0.783, and a combination of the two factors achieved an excellent AUC of 0.916.

## Reliability Assessment

There were excellent intra- and inter-reader agreements for the identification of intracranial plaque, plaque enhancement grade, IPH, measurement of stenosis, plaque length, plaque thickness, plaque burden, ER, enhancement score, and total plaque number. The *kappa* values or ICC values were all higher than 0.8 (**Table 4**). Bland–Altman analysis results are shown in **Supplementary Figure 3**. Good agreement was shown on the Bland–Altman plots without significant bias. The above quantitative results of the plaque analysis were based on one reviewer (LW) because of the excellent intra- and inter-reader agreements.

# DISCUSSION

In this study, a group of plaque features of intracranial atherosclerotic lesions in patients with ischemic stroke was evaluated with 3D contrast-enhanced MR-VWI. We found that plaque number, culprit plaque ER, plaque burden, and CAD were independently associated with acute stroke recurrence. Our study highlights the importance of performing whole-brain vessel wall imaging and evaluating not only the culprit artery but also the entire cerebral artery tree, considering the significant associations between the total plaque number and the recurrence of acute stroke events. Different from the previous vessel wall MRI studies of recurrent ICAD stroke, the novelty of our study is that we evaluated all the arterial plaques in the Circle of

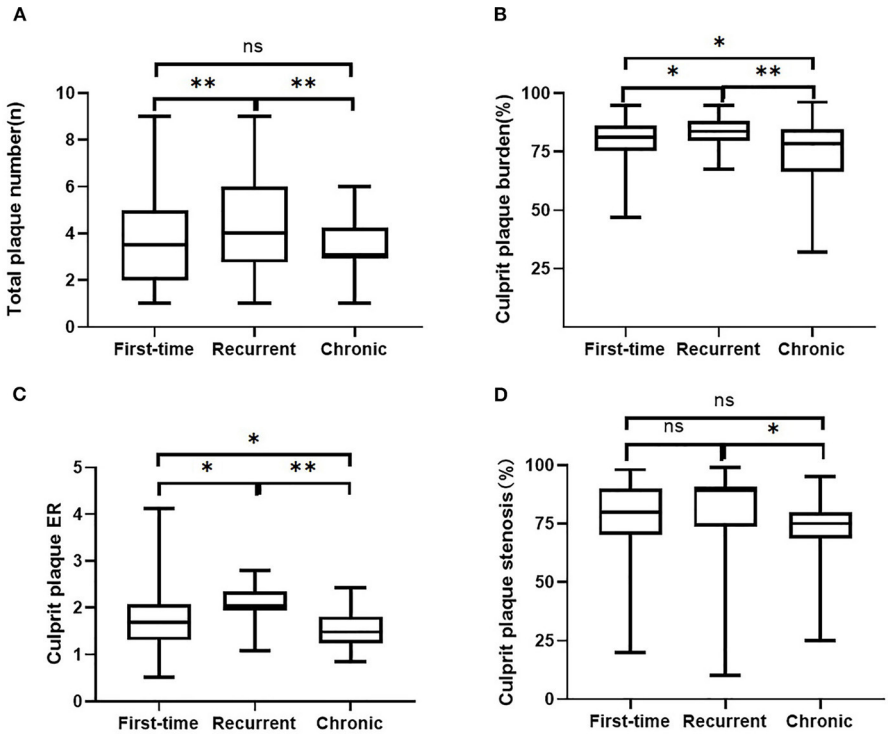


**FIGURE 2 |** Comparisons of intracranial plaque features among the three groups. Intracranial plaque numbers **(A)** and culprit plaque features (**B**, plaque burden, **C**, enhancement ratio, **D**, degree of stenosis) on 3D MR-VWI in patient groups with the first-time acute stroke, recurrent acute stroke, and in patients with chronic stroke. ER, enhancement ratio. $^{**}p < 0.001$, $^{*}p < 0.05$, ns, no significant.

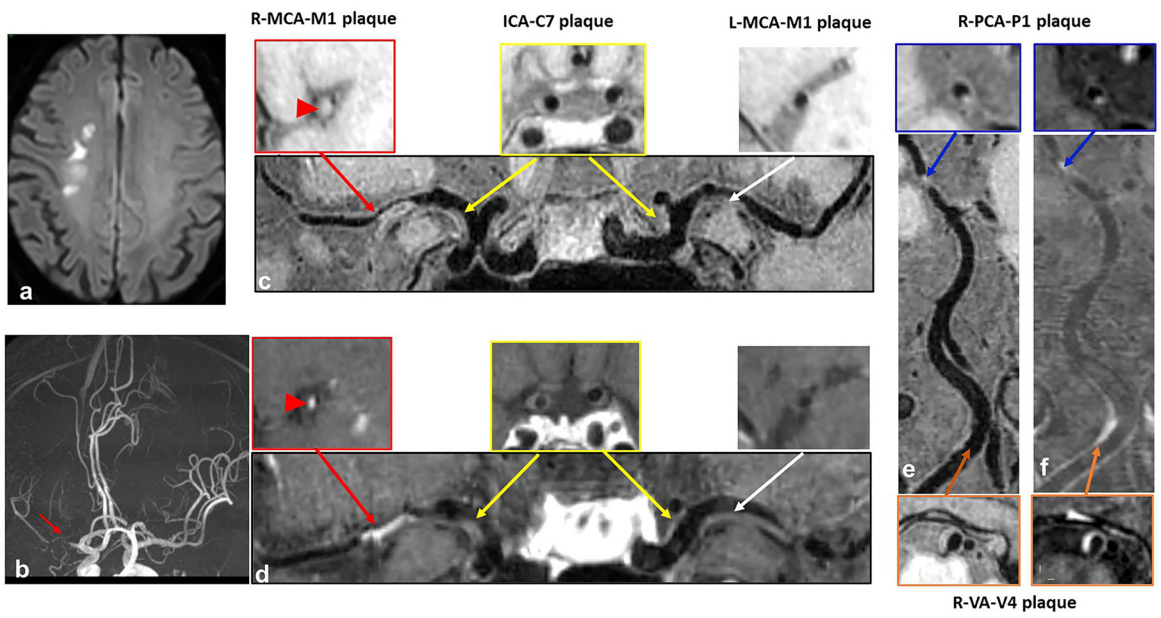


**FIGURE 3 |** A case with recurrent acute stroke. A 62-year-old male patient presented with recurrent acute stroke. **(a)** Axial diffusion-weighted imaging detects high-signal-intensity lesions in the right corona radiata. **(b)** Time-of-flight magnetic resonance angiography image shows severe stenosis on the M1 segment of right middle cerebral artery (MCA) (red arrow) and no obvious stenosis on the left MCA, basilar artery (BA) or posterior cerebral artery (PCA). **(c–f)** curved planar reconstruction images from pre-contrast and post-contrast whole-brain vessel wall imaging show multiple plaques in the right MCA (red arrow) and left MCA (white arrow), bilateral C7 segment of internal carotid artery (ICA) (yellow arrow), P1 segment of right PCA (blue arrow), and V4 segment of vertebral artery (VA) (orange arrow). Grade 2 enhancement pattern and obvious contrast enhancement are detected in the culprit plaque of the M1 segment of right MCA (red arrowhead).

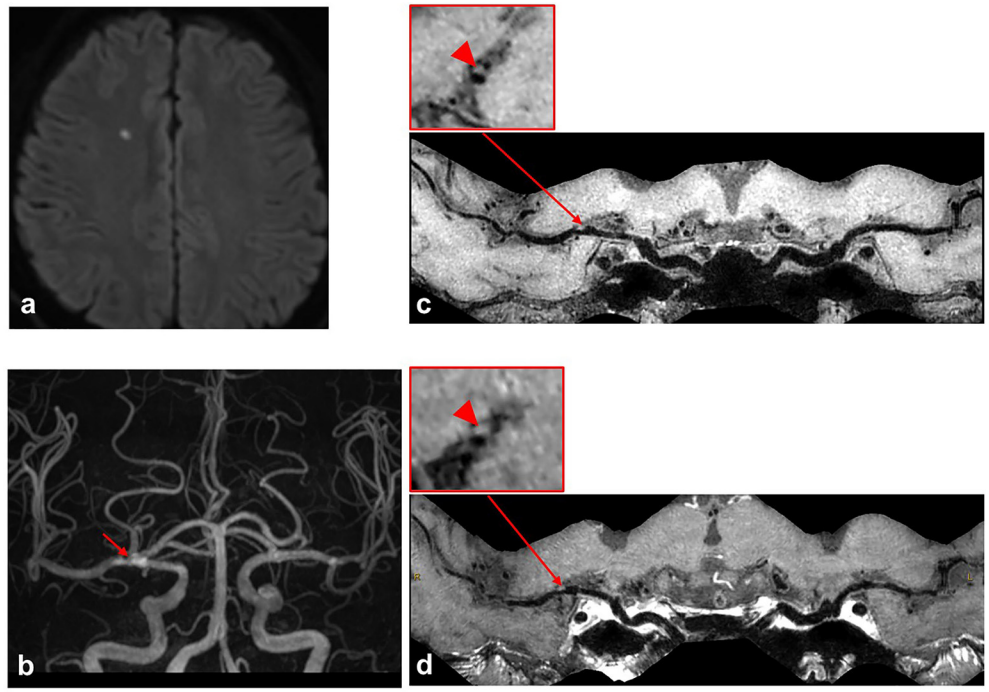


**FIGURE 4 |** A case with first-time acute stroke. A 68-year-old male patient with the first-time acute stroke. **(a)** Axial diffusion-weighted imaging detects high-signal-intensity lesion in the right corona radiata. **(b)** Time-of-flight magnetic resonance angiography image shows moderate stenosis on the M1 segment of right middle cerebral artery (MCA) (red arrow) and no stenosis on the left MCA. **(c,d)** Curved planar reconstruction images from pre-contrast and post-contrast whole-brain vessel wall imaging show a focal plaque in the right M1 segment of MCA. No obvious contrast enhancement is identified in the culprit plaque of the right MCA M1 segment (red arrowhead).

**TABLE 3 |** Univariate and multivariate analyses for factors associated with recurrent stroke in comparison with the first-time stroke.

| Parameters | Univariate analysis | | Multivariate analysis | |
|---|---|---|---|---|
| | OR (95% CI) | *p*-value | OR (95% CI) | *p*-value |
| Male | 0.68 (0.32–1.46) | 0.323 | | |
| Age, year | 1.01 (0.97–1.05) | 0.517 | | |
| BMI, kg/m$^2$ | 0.10(0.87–1.15) | 0.958 | | |
| Hypertension | 1.82 (0.74–4.51) | 0.195 | | |
| Dyslipidemia | 0.55 (0.23–1.31) | 0.174 | | |
| Current smoking | 1.35 (0.55–3.35) | 0.512 | | |
| Alcohol use | 2.09 (0.68–6.41) | 0.199 | | |
| DM | 1.13 (0.53–2.34) | 0.761 | | |
| CAD | 4.47 (1.26–15.86) | 0.020 | 4.61 (1.11–19.18) | 0.035 |
| Hs–CRP, mg/L | 1.01 (0.96–1.11) | 0.429 | | |
| Culprit plaque stenosis, % [a] | 1.25 (0.96–1.53) | 0.101 | | |
| Culprit plaque thickness, mm | 1.00 (0.60–1.67) | 0.996 | | |
| Culprit plaque length, mm | 1.02 (0.94–1.10) | 0.652 | | |
| Culprit plaque area, mm$^2$ | 0.97 (0.92–1.02) | 0.280 | | |
| Culprit plaque burden, % [a] | 2.03 (1.18–3.50) | 0.011 | 2.44 (1.24–4.79) | 0.010 |
| Culprit plaque ER | 2.51 (1.23–5.12) | 0.011 | 2.50 (1.06–5.89) | 0.036 |
| Total plaque enhancement score | 1.24 (1.04–1.48) | 0.015 | 0.93 (0.72–1.19) | 0.544 |
| Total plaque number | 1.47 (1.19–1.82) | <0.001 | 1.54 (1.16–2.03) | 0.003 |

[a] *OR based on every 10% increase.*

*BMI, body mass index; CAD, coronary artery disease; DM, diabetes mellitus; Hs-CRP, high-sensitivity C-reactive protein; ER, enhancement ratio.*

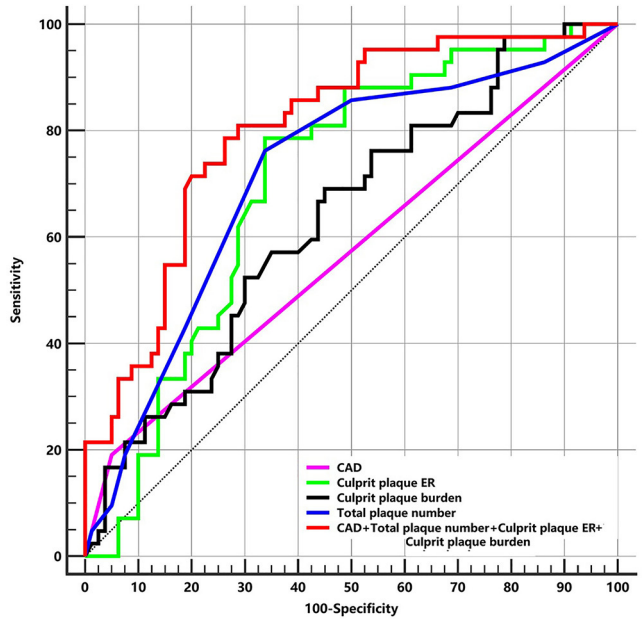


**FIGURE 5 |** The ROC of plaque features for differentiating patients with the first-time and recurrent acute stroke. ER, enhancement ratio; CAD, coronary artery disease; ROC, receiver-operating characteristic curves; AUC, area under curve. CAD: AUC = 0.570. Culprit plaque ER: AUC = 0.704 (cutoff = 1.91, sensitivity = 78.57% specificity = 66.25%). Culprit plaque burden: AUC = 0.636 (cutoff = 81.60%, sensitivity = 69.05%, specificity = 55.0%). Total plaque number: AUC = 0.716 (cutoff = 4, sensitivity = 76.19%, specificity = 66.25%). CAD + Total plaque number + Culprit plaque ER + Culprit plaque burden: AUC = 0.804 (sensitivity = 78.57%, specificity = 73.75%).

Willis instead of only evaluated the features of a single culprit plaque (mostly MCA plaque or basilar artery plaque) (Kim et al., 2016; Ran et al., 2020; Shi et al., 2021). Some other studies were assessing multiple plaques in ICAD, but they didn't evaluate recurrent stroke patients (Qiao et al., 2014; Zwartbol et al., 2020). Another strength of this study is the relatively large sample size (176 patients with 702 plaques), and our results demonstrate the added value of performing 3D contrast-enhanced VWI and multiplaque analysis.

Compared with traditional 2D high-resolution contrast-enhanced MRI that was commonly used to assess intracranial plaque, 3D quantitative MRI has several major advantages. First, it covers the multiple plaques in the entire circle of Willis in a single scan, while 2D scans need multiple scans for each plaque and the slice position has inter-operator variations. Second, it provides high isotropic resolution (voxel size 0.6mm$^3$ in our study); thus, the vessels can be reconstructed in any plane, while 2D imaging has larger slice thickness (2 mm mostly), which is challenging to evaluate the tortuous segments. The partial volume effect of the thick slice also reduces the accuracy when quantifying the plaque thickness, area, and plaque burden. Our study found that intracranial plaque number was independently associated with recurrent acute stroke. As a systemic disease, atherosclerosis tends to affect multiple arterial segments. Several studies have documented that multiple intracranial stenoses were associated with recurrent stroke. The Chinese Intracranial Atherosclerosis Study (CICAS) (Wang et al., 2014; Sun et al., 2018) and Clopidogrel in High-Risk Patients With Acute Nondisabling Cerebrovascular Events trial (CHANCE) (Zhu B. et al., 2018) were two multicenter, prospective MRA trials, which found that multiple ICAS was significantly associated with recurrent stroke in patients with previous stroke or transient ischemic attack. A retrospective DSA study with 576 non-disabling ischemic stroke patients established that asymptomatic ICAS was an independent risk factor for 30-days recurrent stroke (odds ratio = 2.37, 95% CI, 1.14–5.63) in patients undergoing symptomatic ICAS stenting (Zhao et al., 2018). In a prospective, long-term transcranial Doppler (TCD) follow-up study, Arenillas et al. reported that the number of coexisting asymptomatic ICAS showed a trend toward a higher recurrence rate (Arenillas et al., 2001). This supports the importance of evaluating the entire cerebral artery tree. Also, the use of 3D black blood MRI can potentially detect more plaques without stenosis than DSA (up to 27% more by a recent study) (Tian et al., 2021). Recent 3D MR-VWI studies showed that the total plaque number involving both the symptomatic intracranial and extracranial arteries had a strong predictive value for recurrent stroke (Xu et al., 2016; Li et al., 2020). Compared to previous studies, our study with 3D MR-VWI evaluated the entire cerebral vasculature out to the second-order branches, rather than only the symptomatic arterial territory; our approach enriched the existing evidence that multiple intracranial plaques are related to stroke recurrence. One potential mechanism for this finding could be that the higher atherosclerosis burden is the result of poor control of vascular risk factors that may contribute to stroke recurrence. Genetic contributors could also be a consideration, but further investigation is needed for a better understanding of the mechanisms. Besides, longitudinal studies are needed to confirm these relationships.

Previous studies showed that several intracranial plaque features were associated with recurrent stroke (Kim et al., 2016; Ran et al., 2020). Kim et al. (2016) reported that the presence of plaque enhancement predicted future stroke recurrence among stroke patients with intracranial atherosclerosis. Ran et al. (2020) found that plaque burden was associated with recurrent stroke in patients with MCA stenosis in a cross-sectional analysis comparing the first-time stroke and recurrent stroke patients. Our study showed that quantitative culprit plaque ER and plaque burden both as independent factors were associated with recurrent acute stroke, which was different from the previous studies. Disparities between our study and Kim's as compared to the study by Ran et al. could have arisen from the fact that we included both anterior and posterior circulation ICAD, while Ran et al. only analyzed symptomatic atherosclerotic MCA. Another difference between the studies was the degree of stenosis of culprit arteries. Our study included mostly patients with severe stenosis (median 80%), and the previous studies included mild–moderate stenosis patients (23.3–51.8% stenosis in Ran's study). Kim's study was longitudinal and qualitative, Ran's study was a cross-sectional and quantitative using 2D MRI, and our study was a cross-sectional and quantitative using 3D MR-VWI. The different results of these studies indicate that future

**TABLE 4 |** Inter-observer and intra-observer reproducibility ($N = 30$).

| Parameters | Inter-observer agreement | | | Intra-observer agreement | | |
|---|---|---|---|---|---|---|
| | Bias (LOA) | *p*-value | ICC/κ (95%CI) | Bias (LOA) | *p*-value | ICC/κ (95%CI) |
| Identification of intracranial plaque | – | – | 0.870 (0.620–1.000) | – | – | 0.870 (0.620–1.000) |
| Plaque enhancement grade | – | – | 0.904 (0.775–1.000) | – | – | 0.842 (0.674–1.000) |
| Intraplaque hemorrhage | – | – | 1.000 | – | – | 1.000 |
| Culprit plaque ER | −0.09 (−0.92–0.74) | 0.456 | 0.839 (0.689–0.920) | 0.12 (−0.66–0.90) | 0.271 | 0.819 (0.658–0.909) |
| Culprit plaque enhancement score | −0.07 (−1.77–1.64) | 0.893 | 0.897 (0.796–0.950) | 0.13 (−1.77–2.04) | 0.776 | 0.858 (0.724–0.929) |
| Culprit plaque length, mm | −0.18 (−2.81–2.45) | 0.777 | 0.932 (0.863–0.967) | −0.78 (−2.88–1.33) | 0.344 | 0.937 (0.875–0.969) |
| Culprit plaque stenosis, % | 1.07 (−8.64–10.78) | 0.453 | 0.977 (0.953–0.989) | 3.30 (−6.19–12.79) | 0.102 | 0.969 (0.937–0.985) |
| Culprit plaque burden, % | 0.97 (−10.41–12.35) | 0.502 | 0.879 (0.762–0.941) | 1.62 (−10.03–13.28) | 0.356 | 0.863 (0.735–0.932) |
| Culprit plaque thickness, mm | −0.04 (−0.60–0.53) | 0.771 | 0.891 (0.784–0.947) | −0.20 (−0.83–0.43) | 0.189 | 0.823 (0.675–0.915) |
| Total plaque number | 0.20 (−1.88–2.28) | 0.746 | 0.863 (0.733–0.933) | 0.30 (−1.89–2.49) | 0.545 | 0.826 (0.668–0.913) |

*ICC, intraclass correlation coefficient; LoA, limitation of agreement.*

larger-scale longitudinal studies with standardization of plaque measurements are needed to further establish vulnerable plaque features predicting stroke recurrence. IPH in the intracranial plaque is another culprit plaque feature that is associated with acute stroke (Xu et al., 2012; Zhu C. et al., 2018), but it hasn't been found to be associated with recurrent stroke. In our study, the prevalence of IPH was low (10.8%), which agreed with previous studies (MCA, 10.1%, BA, 17.5%) (Xu et al., 2012; Zhu C. et al., 2018). The low prevalence of IPH may be the reason why it was not significant in our study, and future larger-scale study may help better indent the role of IPH with recurrent stroke.

Previous large prospective studies showed that patients with severe symptomatic ICAS (70 to 99%) are at particularly high risk for recurrent stroke in the stenotic artery territory (5–23% at 1 year) despite standard medical therapy and control of vascular risk factors (Kasner et al., 2006; Zaidat et al., 2008; Chimowitz et al., 2011; Wang et al., 2014; Sun et al., 2018). We, however, did not find stenosis as an independent factor for recurrent stroke, possibly because our study was single-center study and all our patients had advanced atherosclerosis with acute ischemic stroke, so the stenosis range was narrow (median 80% and interquartile range, 70–90%).

Coexisting CAD is common in patients with stroke (Bae et al., 2006; Liu et al., 2020). An observational multicenter survey reported that 15.8% of patients with recent atherothrombotic cerebral infarction had a history of CAD (Leys et al., 2006). Cheng et al. found that CAD carried a 1.5-fold risk in 1-year recurrent ischemic stroke in men (Cheng et al., 2020). Man et al. (2010) reported that ischemic stroke patients with concurrent stenoses and CAD had a high risk of poor outcomes and recurrent vascular events. Our findings agree with these previous studies that CAD is associated with recurrent ischemic stroke.

Our study and most previous vessel wall MRI studies of intracranial plaque rely on manual contouring of the plaque boundaries, which is limited by the experience of readers and is time-consuming. Automatic segmentation of the intracranial vessel wall boundaries will improve the reproducibility of plaque measurements and save time. However, the segmentation of the intracranial vessel wall is a challenging task mostly due to the small size of intracranial plaque (around 2 mm thick or less), the tortuous course of intracranial arteries, and the lack of contrast between the vessel wall and surrounding tissues (Mandell et al., 2017). Therefore, the investigation of the automatic segmentation of the intracranial vessel wall is still rare. Shi et al. developed a U-net-like fully convolutional network (FCN) method to automate vessel wall segmentation in a cohort of 56 patients with intracranial plaque and achieve a Dice coefficient of 0.77 for vessel wall segmentation (Shi et al., 2019). With the strong efforts of the research community on developing methods in intracranial vessel wall segmentation, and the continuous improvement in imaging techniques with novel sequences and ultra-high-field strength (Zhu et al., 2016), more robust and automatic techniques will be available for clinical applications soon.

This study has several limitations. First, this is a cross-sectional study, and all MRIs were performed after the ischemic stroke event. The plaque morphology may change after stroke. Therefore, our results could only demonstrate the possible association between plaque features and recurrent acute stroke, but not the causality. Our results should be interpreted with caution, and our findings require a validation with future larger-scale longitudinal studies. Second, we did not evaluate collateral circulation and concurrent extracranial stenosis, both of which might play an important role in the assessment of cerebral hemodynamics and stroke risk. Future development of a risk stratification model incorporating ICAD burden, concurrent extracranial stenosis, and collateral status could provide a valuable tool for assessing the risk of recurrent ischemic events. Third, although we excluded patients with strong flow artifacts that affect the evaluation of the plaque features, there were still some moderate flow artifacts that existed. Additional blood suppression techniques, including MSDE (Zhu et al., 2014) and DANTE (Zhu et al., 2019), should be used in future studies to reduce the flow artifacts and improve the image quality. Fourth, the exact mechanism accounting for intracranial plaque enhancement remains unknown due to the

lack of histology validation, and its relationship with intracranial plaque inflammation is not well-understood. Future studies using contrast agents directly targeting inflammation [like ultra-small superparamagnetic iron oxides (USPIOs)] (Hope et al., 2015) will allow the evaluation of vessel wall inflammation directly. And quantitative 3D analysis methods, including radiomics (Shi et al., 2018), will improve the evaluation of contrast enhancement.

## CONCLUSION

Increased intracranial atherosclerotic plaque number, higher culprit plaque ER, greater culprit plaque burden, and CAD are independently associated with recurrent acute stroke.

## DATA AVAILABILITY STATEMENT

The raw data supporting the conclusions of this article will be made available by the authors, without undue reservation.

## ETHICS STATEMENT

The studies involving human participants were reviewed and approved by Research Ethics Committee of Renji Hospital, School of Medicine, Shanghai Jiaotong University. The patients/participants provided their written informed consent to participate in this study.

## AUTHOR CONTRIBUTIONS

LW, XLi, and JinZ performed the MR examination. BS, LW, and JiaZ performed the image analysis. BS and LW performed the statistical analysis. CZ and HZ participated in the study design. YZ, XLiu, and JX reviewed the manuscript. BS was a major contributor in writing the manuscript. All authors read and approved the final manuscript, contributed to the discussion, read, and approved the final manuscript.

## FUNDING

This study was supported by the National Natural Science Foundation of China (Grants 81801650 and 81571630), Shanghai Municipal Population and Family Planning Commission (201940060 and 20204Y0089), and Renji Hospital School of Medicine Shanghai Jiaotong University (RJZZ18-002 and 2019NYBSZX01). CZ is supported by the US National Institutes of Health (NIH) grant R00HL 136883.

## SUPPLEMENTARY MATERIAL

The Supplementary Material for this article can be found online at: https://www.frontiersin.org/articles/10.3389/fnagi.2021.706544/full#supplementary-material

## REFERENCES

Arenillas, J. F., Molina, C. A., Montaner, J., Abilleira, S., Gonzalez-Sanchez, M. A., and Alvarez-Sabin, J. (2001). Progression and clinical recurrence of symptomatic middle cerebral artery stenosis: a long-term follow-up transcranial Doppler ultrasound study. *Stroke* 32, 2898–2904. doi: 10.1161/hs1201.099652

Bae, H. J., Yoon, B. W., Kang, D. W., Koo, J. S., Lee, S. H., Kim, K. B., et al. (2006). Correlation of coronary and cerebral atherosclerosis: difference between extracranial and intracranial arteries. *Cerebrovasc. Dis.* 21, 112–119. doi: 10.1159/000090209

Cheng, C. G., Chu, H., Lee, J. T., Chien, W. C., and Cheng, C. A. (2020). Increased one-year recurrent ischemic stroke after first-ever ischemic stroke in males with benign prostatic hyperplasia. *Int. J. Environ. Res. Public Health* 17:5360. doi: 10.3390/ijerph17155360

Chimowitz, M. I., Lynn, M. J., Derdeyn, C. P., Turan, T. N., Fiorella, D., Lane, B. F., et al. (2011). Stenting versus aggressive medical therapy for intracranial arterial stenosis. *N. Engl. J. Med.* 365, 993–1003. doi: 10.1056/NEJMoa1105335

Chung, G. H., Kwak, H. S., Hwang, S. B., and Jin, G. Y. (2012). High resolution MR imaging in patients with symptomatic middle cerebral artery stenosis. *Eur. J. Radiol.* 81, 4069–4074. doi: 10.1016/j.ejrad.2012.07.001

Coull, A. J., and Rothwell, P. M. (2004). Underestimation of the early risk of recurrent stroke: evidence of the need for a standard definition. *Stroke* 35, 1925–1929. doi: 10.1161/01.STR.0000133129.58126.67

Cui, B., Yang, D., Zheng, W., Wu, Y., Yang, Q., Wang, Z., et al. (2020). Plaque enhancement in multi-cerebrovascular beds associates with acute cerebral infarction. *Acta Radiol.* 2020:284185120915604. doi: 10.1177/0284185120915604

Hartman, J. B., Watase, H., Sun, J., Hippe, D. S., Kim, L., Levitt, M., et al. (2019). Intracranial aneurysms at higher clinical risk for rupture demonstrate increased wall enhancement and thinning on multicontrast 3D vessel wall MRI. *Br. J. Radiol.* 92:20180950. doi: 10.1259/bjr.20180950

Holmstedt, C. A., Turan, T. N., and Chimowitz, M. I. (2013). Atherosclerotic intracranial arterial stenosis: risk factors, diagnosis, and treatment. *Lancet Neurol.* 12, 1106–1114. doi: 10.1016/S1474-4422(13)70195-9

Hope, M. D., Hope, T. A., Zhu, C., Faraji, F., Haraldsson, H., Ordovas, K. G., et al. (2015). Vascular imaging with ferumoxytol as a contrast agent. *AJR Am. J. Roentgenol.* 205, W366–W373. doi: 10.2214/AJR.15.14534

Hoshino, T., Sissani, L., Labreuche, J., Ducrocq, G., Lavallee, P. C., Meseguer, E., et al. (2018). Prevalence of systemic atherosclerosis burdens and overlapping stroke etiologies and their associations with long-term vascular prognosis in stroke with intracranial atherosclerotic disease. *JAMA Neurol.* 75, 203–211. doi: 10.1001/jamaneurol.2017.3960

Kang, K., Park, T. H., Kim, N., Jang, M. U., Park, S. S., Park, J. M., et al. (2016). Recurrent stroke, myocardial infarction, and major vascular events during the first year after acute ischemic stroke: the multicenter prospective observational study about recurrence and its determinants after acute ischemic stroke I. *J. Stroke Cerebrovasc. Dis.* 25, 656–664. doi: 10.1016/j.jstrokecerebrovasdis.2015.11.036

Kasner, S. E., Chimowitz, M. I., Lynn, M. J., Howlett-Smith, H., Stern, B. J., Hertzberg, V. S., et al. (2006). Predictors of ischemic stroke in the territory of a symptomatic intracranial arterial stenosis. *Circulation* 113, 555–563. doi: 10.1161/CIRCULATIONAHA.105.578229

Kim, J. H. (2019). Multicollinearity and misleading statistical results. *Korean J. Anesthesiol.* 72, 558–569. doi: 10.4097/kja.19087

Kim, J. M., Jung, K. H., Sohn, C. H., Moon, J., Shin, J. H., Park, J., et al. (2016). Intracranial plaque enhancement from high resolution vessel wall magnetic resonance imaging predicts stroke recurrence. *Int. J. Stroke* 11, 171–179. doi: 10.1177/1747493015609775

Lau, A. Y., Wong, K. S., Lev, M., Furie, K., Smith, W., and Kim, A. S. (2013). Burden of intracranial steno-occlusive lesions on initial computed tomography angiography predicts poor outcome in patients with acute stroke. *Stroke* 44, 1310–1316. doi: 10.1161/STROKEAHA.111.672741

Leys, D., Woimant, F., Ferrieres, J., Bauters, C., Touboul, P. J., Guerillot, M., et al. (2006). Detection and management of associated atherothrombotic locations in

patients with a recent atherothrombotic ischemic stroke: results of the DETECT survey. *Cerebrovasc. Dis*. 21, 60–66. doi: 10.1159/000090004

Li, J., Li, D., Yang, D., Huo, R., Chen, X., Xu, Y., et al. (2020). Co-existing cerebrovascular atherosclerosis predicts subsequent vascular event: a multi-contrast cardiovascular magnetic resonance imaging study. *J. Cardiovasc. Magn. Reson*. 22:4. doi: 10.1186/s12968-019-0596-6

Liu, B., Zhou, F., Hua, Y., Liu, Y., and Ji, X. (2020). Evaluation of intracranial and extracranial atherosclerotic lesions in patients with symptomatic coronary artery disease. *Neurol. Res*. 42, 547–553. doi: 10.1080/01616412.2020.1754653

Man, B. L., Fu, Y. P., Chan, Y. Y., Lam, W., Hui, C. F., Leung, W. H., et al. (2009). Use of magnetic resonance angiography to predict long-term outcomes of ischemic stroke patients with concurrent stenoses in Hong Kong. *Cerebrovasc. Dis*. 28, 112–118. doi: 10.1159/000223435

Man, B. L., Fu, Y. P., Chan, Y. Y., Lam, W., Hui, C. F., Leung, W. H., et al. (2010). Long-term outcomes of ischemic stroke patients with concurrent intracranial and extracranial stenoses and ischemic heart disease. *Cerebrovasc. Dis*. 29, 236–241. doi: 10.1159/000267847

Mandell, D. M., Mossa-Basha, M., Qiao, Y., Hess, C. P., Hui, F., Matouk, C., et al. (2017). Intracranial vessel wall MRI: principles and expert consensus recommendations of the american society of neuroradiology. *AJNR Am. J. Neuroradiol*. 38, 218–229. doi: 10.3174/ajnr.A4893

Mazighi, M., Tanasescu, R., Ducrocq, X., Vicaut, E., Bracard, S., Houdart, E., et al. (2006). Prospective study of symptomatic atherothrombotic intracranial stenoses: the GESICA study. *Neurology* 66, 1187–1191. doi: 10.1212/01.wnl.0000208404.94585.b2

Portanova, A., Hakakian, N., Mikulis, D. J., Virmani, R., Abdalla, W. M., and Wasserman, B. A. (2013). Intracranial vasa vasorum: insights and implications for imaging. *Radiology* 267, 667–679. doi: 10.1148/radiol.13112310

Qiao, Y., Anwar, Z., Intrapiromkul, J., Liu, L., Zeiler, S. R., Leigh, R., et al. (2016). Patterns and implications of intracranial arterial remodeling in stroke patients. *Stroke* 47, 434–440. doi: 10.1161/STROKEAHA.115.009955

Qiao, Y., Steinman, D. A., Qin, Q., Etesami, M., Schar, M., Astor, B. C., et al. (2011). Intracranial arterial wall imaging using three-dimensional high isotropic resolution black blood MRI at 3.0 Tesla. *J. Magn. Reson. Imaging* 34, 22–30. doi: 10.1002/jmri.22592

Qiao, Y., Zeiler, S. R., Mirbagheri, S., Leigh, R., Urrutia, V., Wityk, R., et al. (2014). Intracranial plaque enhancement in patients with cerebrovascular events on high-spatial-resolution MR images. *Radiology* 271, 534–542. doi: 10.1148/radiol.13122812

Ran, Y., Wang, Y., Zhu, M., Wu, X., Malhotra, A., Lei, X., et al. (2020). Higher plaque burden of middle cerebral artery is associated with recurrent ischemic stroke: a quantitative magnetic resonance imaging study. *Stroke* 51, 659–662. doi: 10.1161/STROKEAHA.119.028405

Rudd, J. H., and Fayad, Z. A. (2008). Imaging atherosclerotic plaque inflammation. *Nat. Clin. Pract. Cardiovasc. Med*. 5 (Suppl. 2), S11–S17. doi: 10.1038/ncpcardio1160

Samuels, O. B., Joseph, G. J., Lynn, M. J., Smith, H. A., and Chimowitz, M. I. (2000). A standardized method for measuring intracranial arterial stenosis. *AJNR Am. J. Neuroradiol*. 21, 643–646.

Shi, F., Yang, Q., Guo, X., Qureshi, T. A., Tian, Z., Miao, H., et al. (2019). Intracranial vessel wall segmentation using convolutional neural networks. *IEEE Trans. Biomed. Eng*. 66, 2840–2847. doi: 10.1109/TBME.2019.2896972

Shi, Z., Li, J., Zhao, M., Zhang, X., Degnan, A. J., Mossa-Basha, M., et al. (2021). Progression of plaque burden of intracranial atherosclerotic plaque predicts recurrent stroke/transient ischemic attack: a pilot follow-up study using higher-resolution MRI. *J. Magn. Reson. Imaging*. doi: 10.1002/jmri.27561. [Epub ahead of print].

Shi, Z., Zhu, C., Degnan, A. J., Tian, X., Li, J., Chen, L., et al. (2018). Identification of high-risk plaque features in intracranial atherosclerosis: initial experience using a radiomic approach. *Eur. Radiol*. 28, 3912–3921. doi: 10.1007/s00330-018-5395-1

Sun, P., Liu, L., Pan, Y., Wang, X., Mi, D., Pu, Y., et al. (2018). Intracranial atherosclerosis burden and stroke recurrence for symptomatic intracranial artery stenosis (sICAS). *Aging Dis*. 9, 1096–1102. doi: 10.14336/AD.2018.0301

Tian, X., Tian, B., Shi, Z., Wu, X., Peng, W., Zhang, X., et al. (2021). Assessment of intracranial atherosclerotic plaques using 3D black-blood MRI: comparison with 3D time-of-flight MRA and DSA. *J. Magn. Reson. Imaging* 53, 469–478. doi: 10.1002/jmri.27341

Wang, Y., Zhao, X., Liu, L., Soo, Y. O., Pu, Y., Pan, Y., et al. (2014). Prevalence and outcomes of symptomatic intracranial large artery stenoses and occlusions in China: the Chinese Intracranial Atherosclerosis (CICAS) Study. *Stroke* 45, 663–669. doi: 10.1161/STROKEAHA.113.003508

Xie, Y., Yang, Q., Xie, G., Pang, J., Fan, Z., and Li, D. (2016). Improved black-blood imaging using DANTE-SPACE for simultaneous carotid and intracranial vessel wall evaluation. *Magn. Reson. Med*. 75, 2286–2294. doi: 10.1002/mrm.25785

Xu, W. H., Li, M. L., Gao, S., Ni, J., Yao, M., Zhou, L. X., et al. (2012). Middle cerebral artery intraplaque hemorrhage: prevalence and clinical relevance. *Ann Neurol*. 71, 195–198. doi: 10.1002/ana.22626

Xu, Y., Yuan, C., Zhou, Z., He, L., Mi, D., Li, R., et al. (2016). Co-existing intracranial and extracranial carotid artery atherosclerotic plaques and recurrent stroke risk: a three-dimensional multicontrast cardiovascular magnetic resonance study. *J. Cardiovasc. Magn. Reson*. 18:90. doi: 10.1186/s12968-016-0309-3

Zaidat, O. O., Klucznik, R., Alexander, M. J., Chaloupka, J., Lutsep, H., Barnwell, S., et al. (2008). The NIH registry on use of the Wingspan stent for symptomatic 70-99% intracranial arterial stenosis. *Neurology* 70, 1518–1524. doi: 10.1212/01.wnl.0000306308.08229.a3

Zhao, H., Zhao, X., Liu, X., Cao, Y., Hippe, D. S., Sun, J., et al. (2013). Association of carotid atherosclerotic plaque features with acute ischemic stroke: a magnetic resonance imaging study. *Eur. J. Radiol*. 82:e465–e470. doi: 10.1016/j.ejrad.2013.04.014

Zhao, J., Li, X., Chi, L. X., Ma, B. W., Du, Y. H., Chen, G. S., et al. (2018). Concomitant asymptomatic intracranial atherosclerotic stenosis increase the 30-day risk of stroke in patients undergoing symptomatic intracranial atherosclerotic stenosis stenting. *J. Stroke Cerebrovasc. Dis*. 27, 479–485. doi: 10.1016/j.jstrokecerebrovasdis.2017.09.032

Zhu, B., Liu, H., Pan, Y., Jing, J., Li, H., Zhao, X., et al. (2018). Elevated neutrophil and presence of intracranial artery stenosis increase the risk of recurrent stroke. *Stroke* 49, 2294–2300. doi: 10.1161/STROKEAHA.118.022126

Zhu, C., Cao, L., Wen, Z., Ahn, S., Raithel, E., Forman, C., et al. (2019). Surveillance of abdominal aortic aneurysm using accelerated 3D non-contrast black-blood cardiovascular magnetic resonance with compressed sensing (CS-DANTE-SPACE). *J. Cardiovasc. Magn. Reson*. 21:66. doi: 10.1186/s12968-019-0571-2

Zhu, C., Graves, M. J., Yuan, J., Sadat, U., Gillard, J. H., and Patterson, A. J. (2014). Optimization of improved motion-sensitized driven-equilibrium (iMSDE) blood suppression for carotid artery wall imaging. *J Cardiovasc. Magn. Reson*. 16:61. doi: 10.1186/s12968-014-0061-5

Zhu, C., Haraldsson, H., Tian, B., Meisel, K., Ko, N., Lawton, M., et al. (2016). High resolution imaging of the intracranial vessel wall at 3 and 7 T using 3D fast spin echo MRI. *MAGMA* 29, 559–570. doi: 10.1007/s10334-016-0531-x

Zhu, C., Tian, X., Degnan, A. J., Shi, Z., Zhang, X., Chen, L., et al. (2018). Clinical significance of intraplaque hemorrhage in low- and high-grade basilar artery stenosis on high-resolution MRI. *AJNR Am. J. Neuroradiol*. 39, 1286–1292. doi: 10.3174/ajnr.A5676

Zwartbol, M. H. T., van der Kolk, A. G., Ghaznawi, R., van der Graaf, Y., Hendrikse, J., Geerlings, M. I., et al. (2020). Intracranial atherosclerosis on 7T MRI and cognitive functioning: The SMART-MR study. *Neurology* 95, e1351–e61. doi: 10.1212/WNL.0000000000010199

**Conflict of Interest:** The authors declare that the research was conducted in the absence of any commercial or financial relationships that could be construed as a potential conflict of interest.

**Publisher's Note:** All claims expressed in this article are solely those of the authors and do not necessarily represent those of their affiliated organizations, or those of the publisher, the editors and the reviewers. Any product that may be evaluated in this article, or claim that may be made by its manufacturer, is not guaranteed or endorsed by the publisher.

frontiers in Aging Neuroscience

ORIGINAL RESEARCH
published: 30 July 2021
doi: 10.3389/fnagi.2021.675158

# Gut-Derived Metabolite Phenylacetylglutamine and White Matter Hyperintensities in Patients With Acute Ischemic Stroke

*Fang Yu*[1†], *Xianjing Feng*[1†], *Xi Li*[1], *Yunfang Luo*[1], *Minping Wei*[1], *Tingting Zhao*[1] *and Jian Xia*[1,2,3*]

[1] *Department of Neurology, Xiangya Hospital, Central South University, Changsha, China,* [2] *Clinical Research Center for Cerebrovascular Disease of Hunan Province, Central South University, Changsha, China,* [3] *National Clinical Research Center for Geriatric Disorders, Xiangya Hospital, Central South University, Changsha, China*

**Background:** White matter hyperintensity (WMH) burden is associated with a higher risk of ischemic stroke. Phenylacetylglutamine (PAGln) is a gut microbiota-derived metabolite that may induce cardiovascular events by activating platelets and increasing the risk of thrombosis. The relationship between plasma PAGln and WMH burden in patients with ischemic stroke is unknown. This study was designed to investigate the association between plasma PAGln and WMH burden in patients with acute ischemic stroke.

**Methods:** A total of 595 patients with acute ischemic stroke were enrolled in this study within 14 days of symptom onset. The burden of WMH was evaluated using the Fazekas scale based on the fluid-attenuated inversion recovery sequence. The severity of overall WMH was defined as none–mild WMH (total Fazekas score 0–2) or moderate–severe WMH (total Fazekas score 3–6). Based on the severity of periventricular WMH (P-WMH) and deep WMH (D-WMH), patients were categorized into either a none–mild (Fazekas score 0–1) group or a moderate–severe (Fazekas score 2–3) group. Plasma PAGln levels were quantified using liquid chromatography–mass spectrometry.

**Results:** We found that patients with moderate–severe overall WMH showed higher plasma PAGln levels than patients with none–mild overall WMH, and similar results were found in the analyses according to P-WMH and D-WMH. The logistic regression analysis showed that the fourth PAGln quartile was independently associated with moderate–severe overall WMH (adjusted 95% CI 1.134–4.018) and P-WMH (adjusted 95% CI 1.174–4.226).

**Conclusion:** These findings suggest that higher plasma PAGln levels are associated with moderate–severe overall WMH and P-WMH in patients with acute ischemic stroke.

**Keywords: metabolomics, phenylacetylglutamine, white matter hyperintensities, ischemic stroke, biomarkers**

OPEN ACCESS

***Edited by:***
*Shuo Wang,*
*Capital Medical University, China*

***Reviewed by:***
*Ewa Maria,*
*Polish Academy of Sciences, Poland*
*Christoph Reinhardt,*
*Johannes Gutenberg University Mainz, Germany*

***Correspondence:**
*Jian Xia*
*xjian1216@csu.edu.cn*

*[†]These authors have contributed equally to this work and share first authorship*

***Received:*** *02 March 2021*
***Accepted:*** *25 June 2021*
***Published:*** *30 July 2021*

***Citation:***
*Yu F, Feng X, Li X, Luo Y, Wei M, Zhao T and Xia J (2021) Gut-Derived Metabolite Phenylacetylglutamine and White Matter Hyperintensities in Patients With Acute Ischemic Stroke. Front. Aging Neurosci. 13:675158. doi: 10.3389/fnagi.2021.675158*

## INTRODUCTION

Stroke is a major cause of disability and death in China (Wu et al., 2019). White matter hyperintensity (WMH) is the most common radiological marker of small vessel disease (SVD) (Joutel and Chabriat, 2017), and mounting evidence has shown that WMH burden is related to the risk of first stroke, recurrent stroke, and poorer outcomes after stroke (Arsava et al., 2009; Park et al., 2019). Age and hypertension are widely considered to be the main risk factors for WMH (Rist et al., 2019), but they do not account for all the pathophysiological mechanisms of WMH. Therefore, identifying novel risk factors is crucial to improve our understanding of the etiology and consequences of WMH in patients with ischemic stroke.

Recently, altered circulating metabolites have been identified as contributing factors in stroke and cerebral small vessel disease (CSVD) (Nie et al., 2018; Janes et al., 2019). For instance, asymmetric dimethylarginine (ADMA) levels were found to be positively correlated with WMH burden in young asymptomatic patients (Janes et al., 2019). Phenylacetylglutamine (PAGln), a gut microbiota-derived metabolite, has been associated with adverse cardiovascular events, such as coronary artery disease and stroke (Nemet et al., 2020). PAGln is formed by the conjugation of glutamine and phenylacetate, which is derived from bacterial phenylalanine metabolism (Moldave and Meister, 1957). Higher plasma PAGln levels increase the risk of cardiovascular events which may be due to enhanced platelet activation and thrombosis potential (Nemet et al., 2020).

However, the relationship between circulating PAGln and WMH burden in ischemic stroke patients is unknown. Therefore, to enhance our knowledge of the predictive role of PAGln in WMH impairment, we prospectively investigated the relationship between circulating PAGln and WMH impairment in patients with ischemic stroke. This study represents the first cross-sectional study examining whether plasma PAGln levels are associated with WMH burden in ischemic stroke patients.

## MATERIALS AND METHODS

### Study Participants

This study included consecutive patients with ischemic stroke confirmed between August 2017 and October 2020. We recruited 595 patients with ischemic stroke confirmed by diffusion-weighted imaging of the brain within 14 days of symptom onset. The other inclusion criterion was age $\geq$18 years. We excluded patients with disabilities (Modified Rankin Scale score $\geq$2) before stroke onset and those without fluid-attenuated inversion recovery sequence (FLAIR). This study was approved by the Ethics Committee of Xiangya Hospital. All participants provided written informed consent.

### Clinical Assessments

We assessed demographic characteristics and medical history, including age, sex, vascular risk factors [i.e., hypertension, diabetes mellitus, dyslipidemia, coronary heart disease (CAD), smoking, and drinking], based on the definitions previously described in detail (Feng et al., 2021). Complete blood count, liver and kidney function, blood glucose, homocysteine, and serum lipids were determined from overnight fasting venous blood samples from each participant on the second day of admission.

### Fluid-Attenuated Inversion Recovery Sequence Magnetic Resonance Imaging Assessment of WMH

Periventricular WMH (P-WMH) and deep WMH (D-WMH) were assessed on FLAIR images using the Fazekas scale, which ranges from 0 to 3. We categorized the severity of P-WMH and D-WMH as none–mild (Fazekas score 0–1) or moderate–severe (Fazekas score 2–3) (Yu et al., 2018). The total Fazekas score was classified based on the sum of P-WMH and D-WMH (range 0–6). The severity of overall WMH was identified as follows: none–mild WMH (Fazekas score 0–2) or moderate–severe WMH (Fazekas score 3–6) (Zhu et al., 2020).

### Quantification of PAGln

Overnight fasting venous blood samples were collected as soon as possible on the second day of admission. The whole blood sample was centrifuged into plasma and stored at −80°C until analysis. Plasma PAGln was quantified on an AB SCIEX TripleTOF 6500 system (AB SCIEX, Foster City, CA, USA) using liquid chromatography-mass spectrometry with $D_5$-PAGln (CDN Isotopes, Cat # D-6900) as an internal standard. First, plasma was diluted 10-fold with $ddH_2O$, then 2 μl of 1 ppm D5-PAGln was added to 48 μl of diluted plasma, and the mixture was diluted 4-fold with ice-cold methanol and vortexed for 1 min. The supernatant was then centrifuged at 21,000×*g* at 4°C for 15 min and transferred to a clean vial for testing. Finally, 1 μl of the supernatant was injected into an Acquity UPLC BEH C18 column (Waters, Herts, UK) for analysis (50 × 2.1 mm, 1.7 μm). The column temperature was 40°C, and the flow rate was 0.3 ml/min, with the mobile phase A containing 0.1% acetic acid in water and mobile phase B containing 0.1% acetic acid in water. We used known PAGln concentrations to establish a standard curve for the determination of PAGln concentrations. The PAGln concentration of the standard was 10 ng/ml. The intra-day coefficients of variation were 0.80–1.39%, and the inter-day coefficients of variation were 4.80–6.00%.

### Statistical Analysis

We used SPSS 22.0 (IBM Corp., Armonk, NY, USA) and GraphPad Prism 8 (GraphPad Software, San Diego, CA, USA) for the statistical analysis. The participants were dichotomized according to WMH burden into none–mild and moderate–severe groups using the Fazekas scores. In addition, participants were divided into four groups according to the quartiles of plasma PAGln concentrations. Categorical variables were described as proportions, and continuous variables were described as mean ± SD or medians [interquartile range (IQR)]. Continuous variables were compared using an ANOVA, Kruskal–Wallis test, or Mann–Whitney *U* test, as appropriate. Categorical variables were analyzed using the Pearson's $\chi^2$ test. We conducted a logistic regression analysis using the following three models: an unadjusted model, a model adjusted for age and sex, and a model adjusted for age, sex, and the variables showing

**TABLE 1 |** Baseline characteristics of patients with ischemic stroke according to PAGln quartiles.

| Variables | First quartile $n = 149$ | Second quartile $n = 149$ | Third quartile $n = 149$ | Fourth quartile $n = 148$ | *P* value |
|---|---|---|---|---|---|
| Fazekas score | 2.0 (1.5–4.0) | 3.0 (2.0–4.0) | 2.0 (2.0–4.0) | 4.0 (2.0–5.0) | <0.001 |
| Age (years) | 54 (48–62) | 60 (51–66) | 63 (54–70) | 67 (60–72) | <0.001 |
| Sex (male, *N*, %) | 95 (63.8%) | 106 (71.1%) | 103 (69.1%) | 99 (66.9%) | 0.562 |
| HBP (*N*, %) | 93 (62.4%) | 113 (75.8%) | 99 (66.4%) | 119 (80.4%) | 0.002 |
| DM (*N*, %) | 26 (17.4%) | 47 (31.5%) | 45 (30.2%) | 54 (36.5%) | 0.003 |
| Hyperlipidemia (*N*, %) | 46 (30.9%) | 42 (28.2%) | 40 (26.8%) | 45 (30.4%) | 0.855 |
| CAD (*N*, %) | 19 (12.8%) | 15 (10.1%) | 29 (19.5%) | 39 (26.4%) | <0.001 |
| Smoking (*N*, %) | 68 (45.6%) | 81 (54.4%) | 71 (47.7%) | 64 (43.2%) | 0.253 |
| Drinking (*N*, %) | 48 (32.2%) | 58 (38.9%) | 59 (39.6%) | 48 (32.4%) | 0.372 |
| SBP (mmHg) | 140.0 (125.0–154.0) | 144.0 (129.0–157.0) | 143.0 (130.0–156.0) | 142.5 (134.8–158.5) | 0.135 |
| DBP (mmHg) | 84.0 (74.0–93.0) | 82.0 (74.0–92.0) | 82.0 (74.0–90.0) | 81.0 (72.0–91.2) | 0.632 |
| BMI | 23.5 (22.0–25.1) | 23.6 (21.9–25.9) | 22.9 (21.5–25.7) | 23.0 (21.0–25.7) | 0.678 |
| White blood cell count ($\times 10^9$/L) | 6.2 (5.2–7.9) | 6.7 (5.7–8.2) | 6.5 (5.5–8.1) | 7.0 (5.8–8.1) | 0.064 |
| Platelet ($\times 10^9$/L) | 208.0 (164.0–251.0) | 209.0 (167.0–240.0) | 196.0 (162.0–246.0) | 203.5 (167.8–235.0) | 0.615 |
| BUN (mmol/L) | 4.6 (3.9–5.6) | 4.9 (4.1–6.0) | 5.2 (4.1–6.2) | 5.6 (4.6–7.2) | <0.001 |
| eGFR (ml/min/1.73 $m^2$) | 89.4 (76.7–102.6) | 86.6 (74.6–96.3) | 81.5 (69.7–92.5) | 72.7 (57.8–89.1) | <0.001 |
| Uric acid (μmol/L) | 335.9 (96.4) | 341.1 (270.6–385.4) | 307.3 (245.0–381.8) | 332.3 (273.2–387.4) | 0.175 |
| TC (mmol/L) | 3.9 (3.3–5.0) | 4.4 (3.6–5.2) | 4.2 (3.5–5.0) | 4.3 (3.5–5.2) | 0.110 |
| TG (mmol/L) | 1.5 (1.0–2.2) | 1.6 (1.1–2.3) | 1.5 (1.1–2.0) | 1.5 (1.2–2.3) | 0.525 |
| HDL (mmol/L) | 1.0 (0.8–1.2) | 1.0 (0.8–1.2) | 1.0 (0.9–1.2) | 1.0 (0.9–1.1) | 0.757 |
| LDL (mmol/L) | 2.4 (1.9–3.1) | 2.6 (2.1–3.2) | 2.6 (2.1–3.3) | 2.7 (2.2–3.3) | 0.078 |
| Fasting blood-glucose (mmol/L) | 5.4 (4.8–6.3) | 5.8 (5.0–7.4) | 5.9 (5.1–7.7) | 5.7 (5.1–8.1) | 0.065 |
| HbA1c (%) | 5.7(5.4–6.3) | 5.9 (5.5–6.9) | 5.9 (5.5–7.4) | 6.0 (5.5–7.3) | 0.017 |
| Homocysteine (μmol/L) | 12.3 (10.6–14.6) | 13.4 (11.5–16.7) | 13.2 (11.3–15.6) | 14.7 (11.9–19.3) | <0.001 |

*PAGln, phenylacetylglutamine; HBP, hypertension; DM, diabetes mellitus; CAD, coronary artery disease; SBP, systolic blood pressure, DBP, diastolic blood pressure; BMI, body mass index; BUN, blood urea nitrogen; eGFR, estimated glomerular filtration rate; TC, total cholesterol; TG, triglycerides; HDL, high-density lipoprotein; LDL, low-density lipoprotein; HbA1c, glycosylated hemoglobin A1c.*

$P < 0.05$ in the univariate analyses. We used the median to classify these confounding continuous variables in the regression analysis. Odds ratio (OR) and the 95% CI were obtained. A Spearman rank correlation was used to identify the association between plasma PAGln levels and Fazekas scores. The value of PAGln for the prediction of WMH severity was evaluated using a receiver operating characteristics (ROC) curve, and the area under the ROC curve (AUC) was calculated. All tests were two-sided. Statistical significance was set at $P < 0.05$.

# RESULTS

## Clinical Characteristics of Patients With Ischemic Stroke

A total of 595 patients (67.7% male; median age, 61 years) with ischemic stroke were enrolled in our study. The median plasma PAGln level at admission was 2.06 μmol/L. Quartiles of PAGln levels were as follows: first quartile, <1.21 μmol/L; second quartile, 1.21–2.06 μmol/L; third quartile, >2.06–3.34 μmol/L; fourth quartile, >3.34 μmol/L. Higher PAGln quartiles were associated with high Fazekas scores, old age, high frequency of hypertension, diabetes mellitus, CAD, high levels of blood urea nitrogen and homocysteine, and low levels of estimated glomerular filtration rate (eGFR) (**Table 1**).

## The Association Between Plasma PAGln and the Severity of Overall WMH According to Total Fazekas Scores

There were 283 patients with none–mild overall WMH (total Fazekas score 0–2) and 312 patients with moderate–severe overall WMH (total Fazekas score 3–6). When compared with patients with none–mild WMH, patients with moderate–severe WMH were older and had a higher frequency of hypertension, diabetes mellitus, CAD, and higher levels of blood urea nitrogen and homocysteine. Lower levels of platelet count, eGFR, and total cholesterol were observed in moderate–severe WMH subjects (**Table 2**). We found higher plasma PAGln levels in patients with moderate–severe WMH than in patients with none–mild WMH [median 2.3 (IQR 1.5–3.8) vs. median 1.8 (IQR 1.0–2.8) μmol/L, $P < 0.001$] (**Figure 1A**). Moreover, PAGln levels showed a limited correlation with the Fazekas score ($r = 0.221$, $P < 0.001$) (**Figure 2**).

The results of the logistic regression analyses are shown in **Table 3**. In the unadjusted model, when using the first quartile as a reference, the second and fourth quartiles of PAGln levels

**TABLE 2 |** Baseline characteristics of all patients according to the degree of overall WMH.

| Variables | None-mild WMH *n* = 283 | Moderate-severe WMH *n* = 312 | *P* value |
|---|---|---|---|
| Age (years) | 55 (49–63) | 66 (59–72) | <0.001 |
| Sex (male, *N*, %) | 200 (70.7%) | 203 (65.1%) | 0.144 |
| HBP (*N*, %) | 176 (62.2%) | 248 (79.5%) | <0.001 |
| DM (*N*, %) | 70 (24.7%) | 102 (32.7%) | 0.032 |
| Hyperlipidemia (*N*, %) | 83 (29.3%) | 90 (28.8%) | 0.897 |
| CAD (*N*, %) | 33 (11.7%) | 69 (22.1%) | <0.001 |
| Smoking (*N*, %) | 143 (50.5%) | 141 (45.2%) | 0.193 |
| Drinking (*N*, %) | 101 (35.7%) | 112 (35.9%) | 0.958 |
| SBP (mmHg) | 142.0 (127.5–154.0) | 143.0 (130.0–159.2) | 0.086 |
| DBP (mmHg) | 83.0 (74.0–93.0) | 82.0 (73.0–91.0) | 0.391 |
| BMI | 23.4 (22.0–25.2) | 23.3 (20.9–25.8) | 0.652 |
| PAGln (μmol/L) | 1.8 (1.0–2.8) | 2.3 (1.5–3.8) | <0.001 |
| White blood cell count ($\times 10^9$/L) | 6.7 (5.4–8.2) | 6.6 (5.6–8.0) | 0.946 |
| Platelet ($\times 10^9$/L) | 208.0 (171.0–250.5) | 199.0 (162.8–236.2) | 0.043 |
| BUN (mmol/L) | 4.9 (3.9–6.0) | 5.2 (4.2–6.3) | 0.043 |
| eGFR (ml/min/1.73 $m^2$) | 88.5 (74.5–98.6) | 78.6 (64.5–90.2) | <0.001 |
| Uric acid (μmol/L) | 315.8 (272.9–380.1) | 331.4 (268.3–391.9) | 0.598 |
| TC (mmol/L) | 4.2 (3.4–5.2) | 4.2 (3.5–4.9) | 0.234 |
| TG (mmol/L) | 1.6 (1.2–2.2) | 1.5 (1.0–2.2) | 0.035 |
| HDL (mmol/L) | 1.0 (0.8–1.2) | 1.0 (0.9–1.2) | 0.318 |
| LDL (mmol/L) | 2.6 (2.1–3.4) | 2.6 (2.0–3.1) | 0.231 |
| Fasting blood–glucose (mmol/L) | 5.6 (5.0–7.1) | 5.6 (5.0–7.7) | 0.702 |
| HbA1c (%) | 5.8 (5.4–6.7) | 5.9 (5.5–7.0) | 0.100 |
| Homocysteine (μmol/L) | 12.7 (10.8–15.2) | 13.8 (11.4–17.7) | 0.002 |

*WMH, white matter hyperintensity; HBP, hypertension; DM, diabetes mellitus; CAD, coronary artery disease; SBP, systolic blood pressure, DBP, diastolic blood pressure; BMI, body mass index; PAGln, phenylacetylglutamine; BUN, blood urea nitrogen; eGFR, estimated glomerular filtration rate; TC, total cholesterol; TG, triglycerides; HDL, high-density lipoprotein; LDL, low-density lipoprotein; HbA1c, glycosylated hemoglobin A1c.*

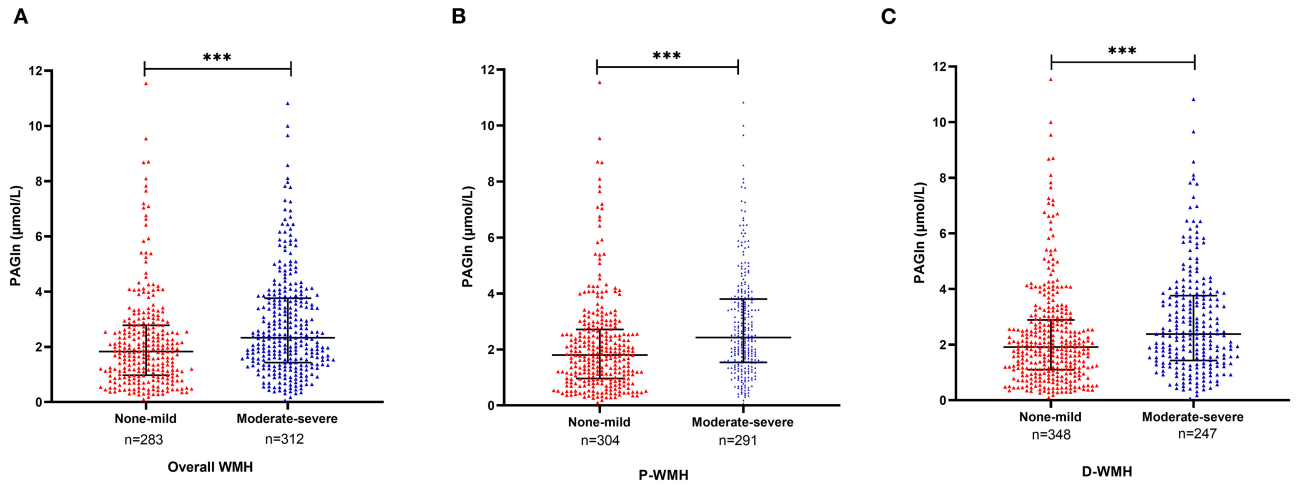


**FIGURE 1 |** Plasma PAGln levels in different groups according to the severity of WMH. **(A)** Patients with moderate–severe overall WMH had higher plasma PAGln levels than patients with none–mild overall WMH [median 2.3 (IQR 1.5–3.8) vs. median 1.8 (IQR 1.0–2.8) μmol/L, $P < 0.001$]. **(B)** Patients with moderate–severe P-WMH had higher plasma PAGln levels than none–mild P-WMH group [median 2.4 (IQR 1.5–3.8) vs. median 1.8 (IQR 1.0–2.7) μmol/L, $P < 0.001$]. **(C)** Patients with moderate–severe D-WMH had higher PAGln levels than none–mild D-WMH group [median 2.4 (IQR 1.5–3.8) vs. median 1.9 (IQR 1.1–2.9) μmol/L, $P < 0.001$]. Horizontal lines represent median and interquartile ranges. WMH, white matter hyperintensity; PAGln, phenylacetylglutamine; P-WMH, periventricular white matter hyperintensity; D-WMH, deep white matter hyperintensity. Mann–Whitney *U* test, $^{***}P < 0.001$.

were independently associated with moderate–severe WMH (OR 2.212 and 95% CI 1.390–3.522 for the second quartile and OR 4.296 and 95% CI 2.639–6.994 for the fourth quartile). These results remained significant when adjusted for age and sex. When the multivariable model was further adjusted for age, sex, hypertension, diabetes mellitus, CAD, platelet counts, eGFR, triglycerides, and homocysteine levels, only the fourth quartile of PAGln level was independently associated with moderate–severe WMH (OR 2.134 and 95% CI 1.134–4.018).

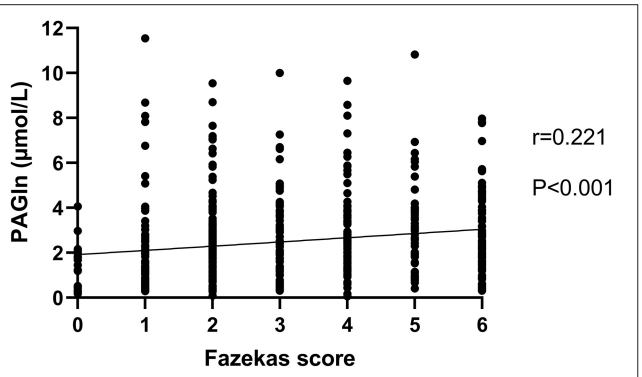


**FIGURE 2 |** Correlation between PAGln levels and Fazekas score. PAGln levels showed a significant, although limited, relationship with the total Fazekas score ($r = 0.221$, $P < 0.001$, and Spearman rank correlation analysis). PAGln, phenylacetylglutamine.

## The Association Between Plasma PAGln and the Severity of WMH According to the Location of WMH

To further explore the relationship between plasma PAGln and different areas of WMH burden, we divided all patients into a P-WMH group and a D-WMH group. We categorized the severity of P-WMH and D-WMH as none–mild (Fazekas score 0–1) and moderate–severe (Fazekas score 2–3), respectively. There were 304 patients with none–mild P-WMH and 291 patients with moderate–severe P-WMH. Compared with patients with none-mild P-WMH, patients with moderate–severe P-WMH were older and had a higher frequency of hypertension, diabetes mellitus, and CAD, higher levels of blood urea nitrogen and homocysteine, and lower levels of eGFR and triglycerides.

**TABLE 3 |** Logistic regression analyses of the association between PAGln levels and overall WMH.

| | *P* value | OR | 95% CI for OR | |
|---|---|---|---|---|
| | | | Lower | Upper |
| **Unadjusted model** | | | | |
| PAGln levels | | | | |
| First quartile | Reference | | | |
| Second quartile | 0.001 | 2.212 | 1.390 | 3.522 |
| Third quartile | 0.061 | 1.559 | 0.980 | 2.479 |
| Fourth quartile | <0.001 | 4.296 | 2.639 | 6.994 |
| **Adjusted model[a]** | | | | |
| PAGln levels | | | | |
| First quartile | Reference | | | |
| Second quartile | 0.020 | 1.818 | 1.098 | 3.010 |
| Third quartile | 0.755 | 0.921 | 0.549 | 1.544 |
| Fourth quartile | 0.009 | 2.053 | 1.195 | 3.528 |
| Age (years) | <0.001 | 1.080 | 1.059 | 1.100 |
| Sex (male) | 0.781 | 0.946 | 0.642 | 1.396 |
| **Adjusted model[b]** | | | | |
| PAGln levels | | | | |
| First quartile | Reference | | | |
| Second quartile | 0.085 | 1.670 | 0.932 | 2.994 |
| Third quartile | 0.963 | 0.986 | 0.547 | 1.778 |
| Fourth quartile | 0.019 | 2.134 | 1.134 | 4.018 |
| Age (years) | <0.001 | 1.065 | 1.041 | 1.089 |
| Sex (male vs. female) | 0.324 | 0.776 | 0.469 | 1.285 |
| HBP | 0.399 | 1.235 | 0.757 | 2.015 |
| DM | 0.804 | 1.060 | 0.668 | 1.685 |
| CAD | 0.799 | 1.077 | 0.610 | 1.900 |
| Platelet $>204\times10^9$ /L | 0.195 | 0.755 | 0.494 | 1.155 |
| eGFR $\leq$ 83.85 mL/min/1.73 $m^2$ | 0.125 | 1.421 | 0.908 | 2.224 |
| TG >1.52 mmol/L | 0.262 | 0.785 | 0.514 | 1.198 |
| Homocysteine >13.28 μmol/L | 0.181 | 1.359 | 0.867 | 2.129 |

*Adjusted model[a]: adjusted for age and sex.*

*Adjusted model[b]: adjusted for age, sex, HBP, DM, CAD, platelet counts, eGFR, TG, and homocysteine levels.*

*WMH, white matter hyperintensity; OR, odds ratio; CI, confidence interval; PAGln, phenylacetylglutamine; HBP, hypertension; DM, diabetes mellitus; CAD, coronary artery disease; eGFR, estimated glomerular filtration rate; TG, triglycerides.*

When classified by D-WMH, 348 and 247 patients were in the none–mild and moderate–severe D-WMH groups, respectively. Patients with moderate–severe D-WMH were more likely to have hypertension and CAD, higher systolic blood pressure, higher levels of blood urea nitrogen, high-density lipoprotein, and homocysteine, and lower levels of eGFR (**Table 4**).

Levels of PAGln in the P-WMH and D-WMH groups are shown in **Figures 1B,C**. PAGln levels were elevated in patients with moderate–severe WMH. Binary logistic regression analyses demonstrated that the fourth PAGln quartile was independently associated with severe P-WMH (OR 2.227 and 95% CI 1.174–4.226) (using the first quartile as the reference) when adjusted for age, sex, hypertension, diabetes mellitus, CAD, blood urea nitrogen, eGFR, triglycerides, and homocysteine levels. However, the significant association between the second and fourth quartiles of PAGln levels with severe D-WMH disappeared when adjustments were made for age, sex, vascular risk factors, and laboratory biomarkers (**Table 5**).

## Receiver Operating Characteristic Analyses of PAGln Levels According to the Severity of WMH

The diagnostic value of PAGln in distinguishing ischemic stroke patients according to WMH burden was evaluated using the ROC analysis. The AUCs for overall WMH, P-WMH, and D-WMH were 0.616, 0.635, and 0.579 (**Figure 3**), respectively. The optimal PAGln cut-off values were 3.348, 3.075, and 3.341 μmol/L for overall WMH, P-WMH, and D-WMH, respectively.

# DISCUSSION

In this study, we conducted a targeted metabolomic analysis to explore the association between PAGln levels and WMH in patients with ischemic stroke. Our results demonstrated that plasma PAGln levels at admission were associated with the severity of WMH in patients with ischemic stroke. After adjusting for age, sex, and confounding factors, higher PAGln levels were independently associated with moderate–severe overall WMH. These associations were also found with P-WMH but not with D-WMH.

The pathophysiology of WMH remains unclear. Traditional vascular risk factors such as age, hypertension, diabetes mellitus, and smoking may play crucial roles in the pathological process of WMH and SVD (Rost et al., 2010; Giese et al., 2020). Previous studies have uncovered biomarkers of endothelial dysfunction, inflammation, and impaired fibrinolysis for WMH in stroke patients and the general population (Poggesi et al., 2016). Metabolomic biomarkers such as uric acid, homocysteine,

**TABLE 4 |** Characteristics of patients according to the scales of P-WMH and D-WMH.

| Variables | P-WMH | | | D-WMH | | |
|---|---|---|---|---|---|---|
| | None–mild $n = 304$ | Moderate–severe $n = 291$ | *P* value | None–mild $n = 348$ | Moderate–severe $n = 247$ | *P* value |
| Age (years) | 55.0 (49.0–63.0) | 67.0 (60.0–72.0) | <0.001 | 57.0 (50.0–64.0) | 67.0 (59.0–72.0) | <0.001 |
| Sex (male, *N*, %) | 87 (28.6%) | 105 (36.1%) | 0.052 | 244 (70.1%) | 159 (64.4%) | 0.140 |
| HBP (*N*, %) | 191 (62.8%) | 233 (80.1%) | <0.001 | 223 (64.1%) | 201 (81.4%) | <0.001 |
| DM (*N*, %) | 73 (24.0%) | 99 (34.0%) | 0.007 | 98 (28.2%) | 74 (30.0%) | 0.633 |
| Hyperlipidemia (*N*, %) | 88 (28.9%) | 85 (29.2%) | 0.944 | 95 (27.3%) | 78 (31.6%) | 0.257 |
| CAD (*N*, %) | 37 (12.2%) | 65 (22.3%) | 0.001 | 44 (12.6%) | 58 (23.5%) | <0.001 |
| Smoking (*N*, %) | 153 (50.3%) | 131 (45.0%) | 0.195 | 169 (48.6%) | 115 (46.6%) | 0.630 |
| Drinking (*N*, %) | 108 (35.5%) | 105 (36.1%) | 0.888 | 124 (35.6%) | 89 (36.0%) | 0.920 |
| SBP (mmHg) | 142.0 (127.0–155.0) | 143.0 (130.0–158.5) | 0.096 | 141.0 (129.0–154.0) | 145.0 (130.0–161.0) | 0.017 |
| DBP (mmHg) | 83.0 (74.0–94.0) | 82.0 (73.0–90.0) | 0.190 | 83.0 (74.0–92.0) | 82.0 (73.0–91.5) | 0.613 |
| BMI | 23.6 (22.0–25.2) | 23.0 (20.8–25.8) | 0.279 | 23.3 (21.9–25.6) | 23.4 (20.9–25.7) | 0.720 |
| PAGln (μmmol/L) | 1.8 (1.0–2.7) | 2.4 (1.5–3.8) | <0.001 | 1.9 (1.1–2.9) | 2.4 (1.5–3.8) | <0.001 |
| White blood cell count ($\times 10^9$ /L) | 6.7 (5.4–8.2) | 6.7 (5.6–8.0) | 0.884 | 6.7 (5.5–8.1) | 6.7 (5.5–8.0) | 0.904 |
| Platelet ($\times 10^9$/L) | 207.0 (167.8–249.0) | 199.0 (163.0–239.5) | 0.113 | 207.0 (167.8–249.0) | 199.0 (163.0–239.5) | 0.113 |
| BUN (mmol/L) | 4.9 (3.9–5.9) | 5.2 (4.2–6.4) | 0.009 | 5.0 (3.9–6.0) | 5.1 (4.2–6.3) | 0.033 |
| eGFR (ml/min/1.73 $m^2$) | 88.5 (74.0–98.7) | 77.7 (64.2–89.1) | <0.001 | 88.4 (74.6–98.2) | 76.7 (62.2–88.2) | <0.001 |
| Uric acid (μmol/L) | 318.6 (273.1–385.7) | 328.1 (267.1–385.8) | 0.799 | 315.0 (272.3–379.1) | 339.8 (271.2–393.2) | 0.204 |
| TC (mmol/L) | 4.2 (3.4–5.2) | 4.2 (3.4–4.9) | 0.143 | 4.2 (3.4–5.2) | 4.3 (3.5–5.0) | 0.415 |
| TG (mmol/L) | 1.6 (1.2–2.2) | 1.5 (1.0–2.2) | 0.045 | 1.6 (1.1–2.2) | 1.5 (1.0–2.3) | 0.154 |
| HDL (mmol/L) | 1.0 (0.8–1.2) | 1.0 (0.9–1.2) | 0.669 | 1.0 (0.8–1.1) | 1.0 (0.9–1.2) | 0.004 |
| LDL (mmol/L) | 2.6 (2.1–3.4) | 2.6 (2.0–3.1) | 0.123 | 2.6 (2.0–3.3) | 2.6 (2.1–3.2) | 0.565 |
| Fasting blood–glucose (mmol/L) | 5.6 (4.9–6.9) | 5.7 (5.0–7.7) | 0.213 | 5.6 (5.0–7.4) | 5.7 (5.0–7.3) | 0.882 |
| HbA1c (%) | 5.8 (5.4–6.5) | 6.0 (5.5–7.1) | 0.314 | 5.8 (5.4–7.2) | 5.9 (5.6–6.8) | 0.647 |
| Homocysteine (μmol/L) | 12.7 (10.8–15.1) | 14.0 (11.4–17.8) | <0.001 | 12.8 (10.8–15.5) | 14.0 (11.6–18.3) | 0.001 |

*P-WMH, periventricular white matter hyperintensity; D-WMH, deep white matter hyperintensity; HBP, hypertension; DM, diabetes mellitus; CAD, coronary artery disease; SBP, systolic blood pressure; DBP, diastolic blood pressure; BMI, body mass index; PAGln, phenylacetylglutamine; BUN, blood urea nitrogen; eGFR, estimated glomerular filtration rate; TC, total cholesterol; TG, triglycerides; HDL, high-density lipoprotein; LDL, low-density lipoprotein; HbA1c, glycosylated hemoglobin A1c.*

**TABLE 5 |** Logistic regression analyses of the association between PAGln levels and P-WMH and D-WMH.

| | P-WMH | | | | | D-WMH | | | |
|---|---|---|---|---|---|---|---|---|---|
| | ***P* value** | **OR** | **95% CI for OR** | | | ***P* value** | **OR** | **95% CI for OR** | |
| | | | **Lower** | **Upper** | | | | **Lower** | **Upper** |
| **Unadjusted model** | | | | | **Unadjusted model** | | | | |
| PAGln levels | | | | | PAGln levels | | | | |
| First quartile | Reference | | | | First quartile | Reference | | | |
| Second quartile | 0.003 | 2.021 | 1.263 | 3.235 | Second quartile | 0.022 | 1.748 | 1.083 | 2.823 |
| Third quartile | 0.024 | 1.719 | 1.073 | 2.755 | Third quartile | 0.177 | 1.396 | 0.860 | 2.266 |
| Fourth quartile | <0.001 | 4.816 | 2.9491 | 7.867 | Fourth quartile | <0.001 | 3.220 | 1.993 | 5.201 |
| **Adjusted model[a]** | | | | | **Adjusted model[a]** | | | | |
| PAGln levels | | | | | PAGln levels | | | | |
| First quartile | Reference | | | | First quartile | Reference | | | |
| Second quartile | 0.062 | 1.637 | 0.976 | 2.747 | Second quartile | 0.171 | 1.428 | 0.858 | 2.379 |
| Third quartile | 0.983 | 0.994 | 0.585 | 1.689 | Third quartile | 0.629 | 0.878 | 0.518 | 1.488 |
| Fourth quartile | 0.004 | 2.247 | 1.297 | 3.890 | Fourth quartile | 0.065 | 1.648 | 0.970 | 2.799 |
| Age (years) | <0.001 | 1.088 | 1.067 | 1.110 | Age (years) | <0.001 | 1.068 | 1.049 | 1.088 |
| Sex (male) | 0.494 | 0.872 | 0.588 | 1.291 | Sex (male) | 0.684 | 0.924 | 0.633 | 1.349 |
| **Adjusted model[b]** | | | | | **Adjusted model[b]** | | | | |
| PAGln levels | | | | | PAGln levels | | | | |
| First quartile | Reference | | | | First quartile | Reference | | | |
| Second quartile | 0.286 | 1.383 | 0.762 | 2.511 | Second quartile | 0.475 | 1.243 | 0.685 | 2.255 |
| Third quartile | 0.859 | 1.056 | 0.577 | 1.933 | Third quartile | 0.730 | 0.899 | 0.489 | 1.651 |
| Fourth quartile | 0.014 | 2.227 | 1.174 | 4.226 | Fourth quartile | 0.057 | 1.819 | 0.981 | 3.372 |
| Age (years) | <0.001 | 1.077 | 1.051 | 1.103 | Age (years) | <0.001 | 1.054 | 1.031 | 1.078 |
| Sex (male vs. female) | 0.377 | 0.796 | 0.480 | 1.321 | Sex (male vs. female) | 0.750 | 1.082 | 0.665 | 1.761 |
| HBP | 0.377 | 1.255 | 0.759 | 2.075 | HBP | 0.076 | 1.609 | 0.951 | 2.723 |
| DM | 0.414 | 1.215 | 0.761 | 1.939 | CAD | 0.724 | 1.103 | 0.640 | 1.901 |
| CAD | 0.974 | 0.990 | 0.561 | 1.749 | SBP >142 mmHg | 0.692 | 1.092 | 0.708 | 1.684 |
| BUN >5.01 mmol/L | 0.899 | 0.972 | 0.623 | 1.515 | BUN >5.01 mmol/L | 0.307 | 0.795 | 0.512 | 1.235 |
| eGFR ≤ 83.85mL/min/1.73 $m^2$ | 0.305 | 1.277 | 0.800 | 2.038 | eGFR ≤ 83.85mL/min/1.73 $m^2$ | 0.051 | 1.584 | 0.998 | 2.513 |
| TG >1.52 mmol/L | 0.154 | 0.733 | 0.479 | 1.123 | HDL >1.00 mmol/L | 0.006 | 1.847 | 1.196 | 2.853 |
| Homocysteine >13.28 μmol/L | 0.119 | 1.437 | 0.910 | 2.268 | Homocysteine >13.28 μmol/L | 0.260 | 1.303 | 0.822 | 2.067 |

*Adjusted model[a]: adjusted for age and sex.*

*P-WMH adjusted model[b]: adjusted for age, sex, HBP, DM, CAD, BUN, eGFR, TG, and homocysteine levels.*

*D-WMH adjusted model[b]: adjusted for age, sex, HBP, CAD, SBP, BUN, eGFR, HDL, and homocysteine levels.*

*WMH, white matter hyperintensity; P-WMH, periventricular white matter hyperintensity; D-WMH, deep white matter hyperintensity; OR, odds ratio; CI, confidence interval; PAGln, phenylacetylglutamine; HBP, hypertension; DM, diabetes mellitus; CAD, coronary artery disease; BUN, blood urea nitrogen; eGFR, estimated glomerular filtration rate; TG, triglycerides; HDL, high-density lipoprotein; SBP, systolic blood pressure.*

AMDA, and ceramides have been reported to be related to WMH (Han et al., 2016). Of note, these altered metabolites might be involved in the pathological process of WMH through their common role in endothelial dysfunction. Many studies have investigated the role of microbiota in neurological disorders, but studies on WMH and SVD are relatively rare. Recently, Cai et al. reported on the role of the gut-immune-brain axis in arteriosclerotic SVD pathophysiology (Cai et al., 2021). Another cross-sectional study indicated that some microbiota may increase the risk of WMH and SVD (Saji et al., 2021).

Gut microbiota can produce metabolites or toxins that influence the health of the host. Gut microbiota-derived metabolites, such as trimethylamine-*N*-oxide (TMAO), tryptophan, and indole derivatives, may play critical roles in the pathogenesis of cardiovascular and cerebrovascular diseases (Ascher and Reinhardt, 2018; Wang and Zhao, 2018). TMAO has been the most studied gut microbiota-derived metabolite in recent years. Accumulating evidence has proven the causal links among TMAO, CAD, and stroke (Witkowski et al., 2020). Elevated TMAO and choline levels have recently been found to be associated with severe WMHs, especially P-WMH (Chen et al., 2021).

Phenylacetylglutamine, another gut microbial metabolite, has been reported to correlate with chronic kidney disease, diabetes mellitus, cardiovascular disease, and Parkinson's disease (Poesen et al., 2016; Urpi-Sarda et al., 2019; Shao et al., 2021). In 2020, Hazen et al. identified a causal contribution of PAGln to incident

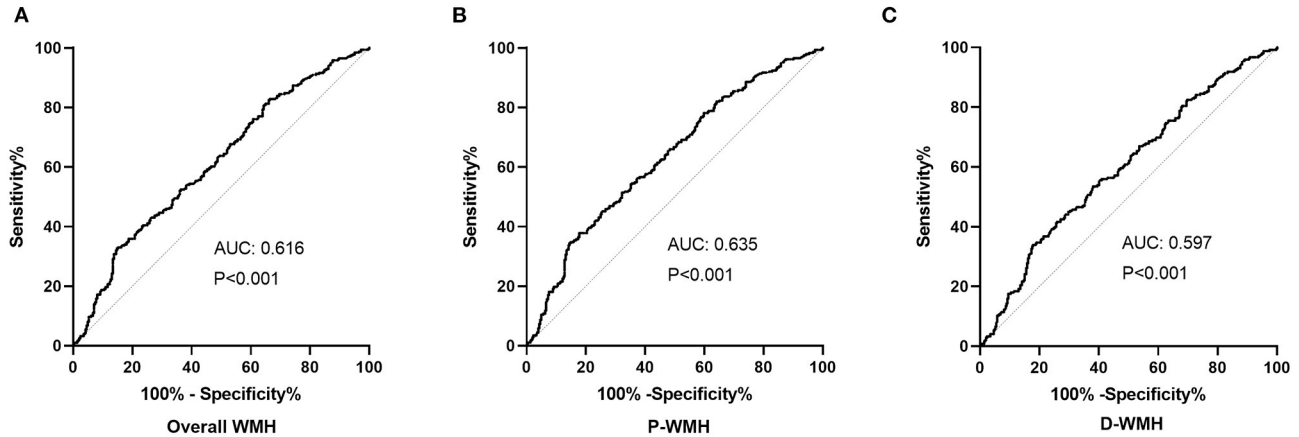


**FIGURE 3 |** Receiver operating characteristic analysis of PAGln according to the severity of WMH. **(A)** The AUC was 0.616, and the optimal PAGln level cut-off value was 3.348 μmol/L for overall WMH. **(B)** The AUC was 0.635, and the optimal PAGln level cut-off value was 3.075μmol/L for P-WMH. **(C)** The AUC was 0.597, and the optimal PAGln level cut-off value was 3.341 μmol/L for D-WMH. ROC, receiver operating characteristic curve; PAGln, phenylacetylglutamine; WMH, white matter hyperintensity; P-WMH, periventricular white matter hyperintensity; D-WMH, deep white matter hyperintensity; AUC, area under the curve.

cardiovascular disease risks in a large sample clinical study (Nemet et al., 2020). This study suggested a clinical association between elevated PAGln levels and the overall burden of WMH and P-WMH. The possible mechanisms are as follows: first, studies have shown that PAGln levels are positively associated with age (Swann et al., 2013; Poesen et al., 2016), and our data also showed an increase in PAGln levels with increasing age, which is a known factor contributing to the pathology of WMH (Urpi-Sarda et al., 2019). Second, traditional vascular risk factors, such as hypertension and diabetes mellitus, are involved in the process of WMH (Tamura and Araki, 2015). As shown in **Table 1**, the group of patients with higher PAGln levels had higher rates of hypertension and diabetes, and studies have also suggested higher PAGln levels in patients with diabetes (Nemet et al., 2020), and therefore the relationship between PAGln and WMH might be due to the underlying mechanism of small vessel abnormalities of hypertension and diabetes (Tamura and Araki, 2015). Our data showed a decrease in eGFR with increasing PAGln levels, and previous observations also showed that kidney impairment measured by eGFR was strongly associated with high serum PAGln levels (Wang and Zhao, 2018). Furthermore, we found that decreased eGFR was associated with moderate–severe WMH, consistent with the previous results (Steinicke et al., 2012; Zong et al., 2016).

In this study, WMH was divided into P-WMH and D-WMH. A limited number of studies have investigated the differences between P-WMH and D-WMH; however, the underlying mechanism has not yet been fully elucidated. Our results suggest the involvement of PAGln in the development of P-WMH, but not D-WMH, and the detailed mechanisms require further investigation. Previous pathology studies have shown that P-WMH is more likely to be associated with inflammation and chronic hypoperfusion, whereas D-WMH is related to ischemic damage (Fazekas et al., 1993). These differences may provide possible explanations for the relationship between PAGln and P-WMH. Previous studies have found a relationship between PAGln levels and human immunodeficiency virus-associated dementia and impaired cognitive function in patients receiving hemodialysis (Cassol et al., 2014; Kurella Tamura et al., 2016). As a uremic metabolite, PAGln can lead to blood–brain barrier disruption and impair P-WMH. In addition, there are some controversies regarding the relationship between diabetes and P-WMH and D-WMH. In our data, we found a higher rate of diabetes in patients with moderate–severe P-WMH; however, no difference was found in patients with D-WMH. Limited studies (Urpi-Sarda et al., 2019; Nemet et al., 2020) have revealed the associations between diabetes and PAGln levels. The closer relationship between diabetes and P-WMH might be the reason why PAGln is associated more with P-WMH than D-WMH.

There were some limitations to this study. First, this was a cross-sectional study, so we could not establish a causal relationship between PAGln and WMH. Second, participants in our study were recruited from a single center, and this could have led to patient selection bias. Third, PAGln levels were only analyzed at a single time point, and information on dynamic changes in PAGln was missing. Fourth, investigations of the gut microbiota were lacking in this study. Finally, we used a less precise visual rating scale to assess the degree of WMH. Quantification of WMH is needed to further investigate the relationship between PAGln and WMH volume.

## CONCLUSION

In conclusion, higher plasma PAGln levels might be a biomarker of moderate–severe WMH, especially moderate–severe P-WMH. Further studies concerning the cause–effect relationship between PAGln and WMH are needed.

## DATA AVAILABILITY STATEMENT

The datasets generated for this study are available on request to the corresponding author.

## ETHICS STATEMENT

The studies involving human participants were reviewed and approved by Xiangya Hospital Ethics Committee. The patients/participants provided their written informed consent to participate in this study.

## AUTHOR CONTRIBUTIONS

FY and XF: methodology and writing—original draft preparation. XL, YL, MW, and TZ: investigation and data curation. JX: conceptualization and writing—reviewing and editing. All authors contributed to the article and approved the submitted version.

## FUNDING

This study was supported by the Project Program of National Clinical Research Center for Geriatric Disorders (Xiangya Hospital, Grant No. 2020LNJJ16), the National Natural Science Foundation of China (Grant No. 81671166), the Fundamental Research Funds for the Central Universities of Central South University (Grant No. 2019zzts902), and the Provincial Key Plan for Research and Development of Hunan (Grant No. 2020SK2067).

## ACKNOWLEDGMENTS

We thank Zhimin Long, Haihong Zha, and Mengqin Xiao from SCIEX, Analytical Instrument Trading Co., Ltd, Shanghai, China for their help in sample testing and analysis of metabolomics data. We also thank Editage (www.editage.cn) for their linguistic assistance during the revision of this manuscript.

## REFERENCES

Arsava, E. M., Rahman, R., Rosand, J., Lu, J., Smith, E. E., Rost, N. S., et al. (2009). Severity of leukoaraiosis correlates with clinical outcome after ischemic stroke. *Neurology* 72, 1403–1410. doi: 10.1212/WNL.0b013e3181a18823

Ascher, S., and Reinhardt, C. (2018). The gut microbiota: an emerging risk factor for cardiovascular and cerebrovascular disease. *Eur. J. Immunol.* 48, 564–575. doi: 10.1002/eji.201646879

Cai, W., Chen, X., Men, X., Ruan, H., Hu, M., Liu, S., et al. (2021). Gut microbiota from patients with arteriosclerotic CSVD induces higher IL-17A production in neutrophils via activating RORγt. *Sci. Adv.* 7: eabe4827. doi: 10.1126/sciadv.abe4827

Cassol, E., Misra, V., Dutta, A., Morgello, S., and Gabuzda, D. (2014). Cerebrospinal fluid metabolomics reveals altered waste clearance and accelerated aging in HIV patients with neurocognitive impairment. *AIDS* 28, 1579–1591. doi: 10.1097/QAD.0000000000000303

Chen, Y., Xu, J., Pan, Y., Yan, H., Jing, J., Yang, Y., et al. (2021). Association of trimethylamine N-oxide and its precursor with cerebral small vessel imaging markers. *Front. Neurol.* 12:648702. doi: 10.3389/fneur.2021.648702

Fazekas, F., Kleinert, R., Offenbacher, H., Schmidt, R., Kleinert, G., Payer, F., et al. (1993). Pathologic correlates of incidental MRI white matter signal hyperintensities. *Neurology* 43, 1683–1689. doi: 10.1212/WNL.43.9.1683

Feng, X., Yu, F., Zhou, X., Liu, Z., Liao, D., Huang, Q., et al. (2021). MMP9 rs17576 Is simultaneously correlated with symptomatic intracranial atherosclerotic stenosis and white matter hyperintensities in Chinese population. *Cerebrovasc. Dis.* 50, 4–11. doi: 10.1159/000511582

Giese, A. K., Schirmer, M. D., Dalca, A. V., Sridharan, R., Donahue, K. L., Nardin, M., et al. (2020). White matter hyperintensity burden in acute stroke patients differs by ischemic stroke subtype. *Neurology* 95, e79–e88. doi: 10.1212/WNL.0000000000009728

Han, S. W., Song, T. J., Bushnell, C. D., Lee, S. S., Kim, S. H., Lee, J. H., et al. (2016). Serum uric acid is associated with cerebral white matter hyperintensities in patients with acute lacunar infarction. *J. Neuroimaging* 26, 351–354. doi: 10.1111/jon.12308

Janes, F., Cif,ù, A., Pessa, M. E., Domenis, R., Gigli, G. L., Sanvilli, N., et al. (2019). ADMA as a possible marker of endothelial damage. A study in young asymptomatic patients with cerebral small vessel disease. *Sci. Rep.* 9:14207. doi: 10.1038/s41598-019-50778-w

Joutel, A., and Chabriat, H. (2017). Pathogenesis of white matter changes in cerebral small vessel diseases: beyond vessel-intrinsic mechanisms. *Clin. Sci.* 131, 635–651. doi: 10.1042/CS20160380

Kurella Tamura, M., Chertow, G. M., Depner, T. A., Nissenson, A. R., Schiller, B., Mehta, R. L., et al. (2016). Metabolic profiling of impaired cognitive function in patients receiving dialysis. *J. Am. Soc. Nephrol.* 27, 3780–3787. doi: 10.1681/ASN.2016010039

Moldave, K., and Meister, A. (1957). Synthesis of phenylacetylglutamine by human tissue. *J. Biol. Chem.* 229, 463–476. doi: 10.1016/S0021-9258(18)70632-7

Nemet, I., Saha, P. P., Gupta, N., Zhu, W., Romano, K. A., Skye, S. M., et al. (2020). A cardiovascular disease-linked gut microbial metabolite acts via adrenergic receptors. *Cell* 180, 862–877.e822. doi: 10.1016/j.cell.2020.02.016

Nie, J., Xie, L., Zhao, B. X., Li, Y., Qiu, B., Zhu, F., et al. (2018). Serum trimethylamine N-oxide concentration is positively associated with first stroke in hypertensive patients. *Stroke* 49, 2021–2028. doi: 10.1161/STROKEAHA.118.021997

Park, J. H., Heo, S. H., Lee, M. H., Kwon, H. S., Kwon, S. U., and Lee, J. S. (2019). White matter hyperintensities and recurrent stroke risk in patients with stroke with small-vessel disease. *Eur. J. Neurol.* 26, 911–918. doi: 10.1111/ene.13908

Poesen, R., Claes, K., Evenepoel, P., de Loor, H., Augustijns, P., Kuypers, D., et al. (2016). Microbiota-derived phenylacetylglutamine associates with overall mortality and cardiovascular disease in patients with CKD. *J. Am. Soc. Nephrol.* 27, 3479–3487. doi: 10.1681/ASN.2015121302

Poggesi, A., Pasi, M., Pescini, F., Pantoni, L., and Inzitari, D. (2016). Circulating biologic markers of endothelial dysfunction in cerebral small vessel disease: a review. *J. Cereb. Blood Flow Metab.* 36, 72–94. doi: 10.1038/jcbfm.2015.116

Rist, P. M., Buring, J. E., Rexrode, K. M., Cook, N. R., and Rost, N. S. (2019). Prospectively collected lifestyle and health information as risk factors for white matter hyperintensity volume in stroke patients. *Eur. J. Epidemiol.* 34, 957–965. doi: 10.1007/s10654-019-00546-x

Rost, N. S., Rahman, R., Sonni, S., Kanakis, A., Butler, C., Massasa, E., et al. (2010). Determinants of white matter hyperintensity volume in patients with acute ischemic stroke. *J. Stroke Cerebrovasc. Dis.* 19, 230–235. doi: 10.1016/j.jstrokecerebrovasdis.2009.05.007

Saji, N., Murotani, K., Hisada, T., Tsuduki, T., Sugimoto, T., Kimura, A., et al. (2021). The association between cerebral small vessel disease and the gut microbiome: a cross-sectional analysis. *J. Stroke Cerebrovasc. Dis.* 30, 105568. doi: 10.1016/j.jstrokecerebrovasdis.2020.105568

Shao, Y., Li, T., Liu, Z., Wang, X., Xu, X., Li, S., et al. (2021). Comprehensive metabolic profiling of Parkinson's disease by liquid chromatography-mass spectrometry. *Mol. Neurodegener.* 16:4. doi: 10.1186/s13024-021-00425-8

Steinicke, R., Gaertner, B., Grittner, U., Schmidt, W., Dichgans, M., Heuschmann, P. U., et al. (2012). Kidney function and white matter disease in young stroke patients: analysis of the stroke in young fabry patients study population. *Stroke* 43, 2382–2388. doi: 10.1161/STROKEAHA.111.645713

Swann, J. R., Spagou, K., Lewis, M., Nicholson, J. K., Glei, D. A., Seeman, T. E., et al. (2013). Microbial-mammalian cometabolites dominate the age-associated urinary metabolic phenotype in Taiwanese and American populations. *J. Proteome Res.* 12, 3166–3180. doi: 10.1021/pr4000152

Tamura, Y., and Araki, A. (2015). Diabetes mellitus and white matter hyperintensity. *Geriatr. Gerontol. Int.* 15 (Suppl 1), 34–42. doi: 10.1111/ggi.12666

Urpi-Sarda, M., Almanza-Aguilera, E., Llorach, R., Vázquez-Fresno, R., Estruch, R., Corella, D., et al. (2019). Non-targeted metabolomic biomarkers and metabotypes of type 2 diabetes: a cross-sectional study of PREDIMED trial participants. *Diabetes Metab.* 45, 167–174. doi: 10.1016/j.diabet.2018.02.006

Wang, Z., and Zhao, Y. (2018). Gut microbiota derived metabolites in cardiovascular health and disease. *Protein Cell* 9, 416–431. doi: 10.1007/s13238-018-0549-0

Witkowski, M., Weeks, T. L., and Hazen, S. L. (2020). Gut microbiota and cardiovascular disease. *Circ. Res.* 127, 553–570. doi: 10.1161/CIRCRESAHA.120.316242

Wu, S., Wu, B., Liu, M., Chen, Z., Wang, W., Anderson, C. S., et al. (2019). Stroke in China: advances and challenges in epidemiology, prevention, and management. *Lancet Neurol.* 18, 394–405. doi: 10.1016/S1474-4422(18)30500-3

Yu, L., Yang, L., Zhang, X., Yuan, J., Li, Y., Yang, S., et al. (2018). Age and recurrent stroke are related to the severity of white matter hyperintensities in lacunar infarction patients with diabetes. *Clin. Interv. Aging* 13, 2487–2494. doi: 10.2147/CIA.S184463

Zhu, S., Qian, S., Xu, T., Peng, H., Dong, R., Wang, D., et al. (2020). White matter hyperintensity, immediate antihypertensive treatment, and functional outcome after acute ischemic stroke. *Stroke* 51, 1608–1612. doi: 10.1161/STROKEAHA.119.028841

Zong, L., Yao, M., Ni, J., Zhou, L., Yuan, J., Peng, B., et al. (2016). Kidney function is associated with severity of white matter hyperintensity in patients with acute ischemic stroke/TIA. *BMC Neurol.* 16, 193. doi: 10.1186/s12883-016-0714-0

**Conflict of Interest:** The authors declare that the research was conducted in the absence of any commercial or financial relationships that could be construed as a potential conflict of interest.

**Publisher's Note:** All claims expressed in this article are solely those of the authors and do not necessarily represent those of their affiliated organizations, or those of the publisher, the editors and the reviewers. Any product that may be evaluated in this article, or claim that may be made by its manufacturer, is not guaranteed or endorsed by the publisher.

frontiers in Aging Neuroscience

ORIGINAL RESEARCH
published: 16 August 2021
doi: 10.3389/fnagi.2021.716068

# Association Between Body Mass Index and Intracranial Aneurysm Rupture: A Multicenter Retrospective Study

*Sifang Chen[1], Jianyao Mao[1], Xi Chen[1], Zhangyu Li[1], Zhi Zhu[2], Yukui Li[1], Zhengye Jiang[1], Wenpeng Zhao[1], Zhanxiang Wang[3,4], Ping Zhong[5]* and Qinghai Huang[6]**

[1] Department of Neurosurgery, The First Affiliated Hospital of Xiamen University, Xiamen, China, [2] Department of Neurosurgery, Heze Municipal Hospital, Heze, China, [3] Department of Neurosurgery, Xiamen Key Laboratory of Brain Center, The First Affiliated Hospital of Xiamen University, Xiamen, China, [4] Department of Neuroscience, School of Medicine, Institute of Neurosurgery, Xiamen University, Xiamen, China, [5] BE and Phase I Clinical Trial Center, The First Affiliated Hospital of Xiamen University, Xiamen, China, [6] Department of Neurosurgery, Changhai Hospital, Second Military Medical University, Shanghai, China

**Background and Aims:** It has recently emerged the concept of "obesity paradox," a term used to describe an inverse association between obesity and clinical outcomes in cardiovascular diseases and stroke. The purpose of this study was to investigate the association between body mass index (BMI) and the risk of intracranial aneurysm rupture.

**Methods:** In this study, we conducted a retrospective analysis of a prospectively maintained database of patients with intracranial aneurysms from 21 medical centers in China. A total of 3,965 patients with 4,632 saccular intracranial aneurysms were enrolled. Patients were separated into unruptured ($n$ = 1,977) and ruptured groups ($n$ = 1,988). Univariable and multivariable logistic regression analyses were performed to determine the association between BMI and intracranial aneurysm rupture.

**Results:** Compared to the patients with normal BMI (18.5 to < 24.0 kg/m$^2$), the odds of intracranial aneurysm rupture were significantly lower in patients with BMI 24.0 to < 28.0 kg/m$^2$ (OR = 0.745, 95% CI = 0.638–0.868, $P$ = 0.000) and patients with BMI ≥ 28.0 kg/m$^2$ (OR = 0.628, 95% CI = 0.443–0.890, $P$ = 0.009). Low BMI (<18.0 kg/m$^2$) was not associated with intracranial aneurysm rupture (OR = 0.894, 95% CI = 0.483–1.657, $P$ = 0.505). For males, both the BMI 24.0 to < 28.0 kg/m$^2$ (OR = 0.606, 95% CI = 0.469–0.784, $P$ = 0.000) and the BMI ≥ 28.0 kg/m$^2$ (OR = 0.384, 95% CI = 0.224–0.658, $P$ = 0.001) were associated with a lower rupture risk, whereas the inverse association was not observed in females. Both the BMI 24.0 to < 28.0 kg/m$^2$ (OR = 0.722 for aged 50–60y, 95% CI = 0.554–0.938, $P$ = 0.015; OR = 0.737 for aged >60y, 95% CI = 0.586–0.928, $P$ = 0.009) and the BMI ≥ 28.0 kg/m$^2$ (OR = 0.517 for aged 50–60y, 95% CI = 0.281–0.950, $P$ = 0.0034; OR = 0.535 for aged >60y, 95% CI = 0.318–0.899, $P$ = 0.0018) was associated with a lower rupture risk in patients aged ≥50 years, whereas the association was not significant in patients aged <50 years.

**Conclusions:** Increased BMI is significantly and inversely associated with saccular intracranial aneurysm rupture in males and patients aged ≥50 years.

**Keywords: body mass index, intracranial aneurysms, stroke, cerebrovascular disease, subarachnoid hemorrhage**

OPEN ACCESS

***Edited by:***
*Yuanli Zhao,*
*Capital Medical University, China*

***Reviewed by:***
*Chengcheng Zhu,*
*University of Washington, United States*
*Talitha Best,*
*Central Queensland University, Australia*

****Correspondence:***
*Ping Zhong*
*jgszp2004@163.com*
*orcid.org/0000-0002-4415-2992*
*Qinghai Huang*
*ocinhqh@163.com*

***Received:*** *28 May 2021*
***Accepted:*** *20 July 2021*
***Published:*** *16 August 2021*

***Citation:***
*Chen S, Mao J, Chen X, Li Z, Zhu Z, Li Y, Jiang Z, Zhao W, Wang Z, Zhong P and Huang Q (2021) Association Between Body Mass Index and Intracranial Aneurysm Rupture: A Multicenter Retrospective Study. Front. Aging Neurosci. 13:716068. doi: 10.3389/fnagi.2021.716068*

## INTRODUCTION

Subarachnoid hemorrhage (SAH) is a life-threatening subtype of stroke, leading to loss of many years of productive life owing to the high morbidity and mortality (Macdonald and Schweizer, 2017; Maher et al., 2020). The overall incidence of SAH is ∼9 per 100,000 person-years, ranging from 4.2 per 100,000 person-years to 22.7 per 100,000 person-years worldwide (de Rooij et al., 2007). The incidence of SAH is age-related and peaks in the 60s, and elderly patients commonly experience poor outcomes following SAH compared with the young population. Particularly, there is an increase in mean age over time with a remarkable rise in the proportion of octogenarian patients and a reduction in patients younger than 50 years in recent years (Feghali et al., 2021). In general, the rupture of an intracranial aneurysm is the underlining cause of SAH, accounting for about 85% of cases (Macdonald and Schweizer, 2017). Currently, there is high agreement among neurosurgeons that older age, female sex, smoking, hypertension, multiple aneurysms, size, and location are among pivotal risk factors for rupture of an intracranial aneurysm (Wermer et al., 2007; Greving et al., 2014; Wang Y. et al., 2021). However, these well-established risk factors only explain a small proportion of the risk of intracranial aneurysm rupture (Andreasen et al., 2013; Kleinloog et al., 2018). Thus, the prediction of the risk of intracranial aneurysm rupture for individual patients is still poorly explored, and therefore the search for new risk factors is urgently needed to continue, especially for aging patients.

Traditionally, obesity has been regarded as a well-established risk factor for cardiovascular diseases and stroke. Nevertheless, a growing body of evidence has suggested that an "obesity paradox"-namely that there is an inverse association between obesity and clinical outcomes-exists for patients with hypertension (Kleinloog et al., 2018) coronary artery diseases (Uretsky et al., 2007; Wang et al., 2015), atrial fibrillation (Sandhu et al., 2016), intracerebral hemorrhage (Persaud et al., 2019), and ischemic stroke (Rodríguez-Castro et al., 2019; Liu et al., 2021). Likewise, this paradoxical phenomenon was also observed in patients with SAH (Rinaldo et al., 2019; Rautalin et al., 2020), suggesting a potential protective effect of increased BMI on the risk of adverse events after presenting intracranial aneurysms. Moreover, several metabolic abnormalities similar to obesity, including hypercholesterolemia and diabetes mellitus, seem to could reduce the risk of intracranial aneurysm rupture (Lindgren et al., 2013; Vlak et al., 2013). Furthermore, recent population-based cohort studies have demonstrated that overweight or obesity was associated with a reduced risk of SAH in the general population (Sandvei et al., 2012; Kroll et al., 2016). In addition, the "obesity paradox" phenomenon seems to be pronounced in the elderly population (Wang and Ren, 2018). Accordingly, overweight and obesity might be associated with a decreased risk of intracranial aneurysm rupture.

However, previous results of the effect of BMI on the incidence of SAH are inconsistent (Feigin et al., 2005; Sandvei et al., 2012; Kroll et al., 2016; Kawate et al., 2017), especially in the Asian population (Feigin et al., 2005; Kawate et al., 2017). Particularly, the control groups of the previous population-based cohort studies were general populations rather than patients with unruptured intracranial aneurysms, and therefore whether higher BMI is associated with a decreased risk of intracranial aneurysm rupture remains largely unknown. To date, data examining the association between BMI and the risk of intracranial aneurysm rupture are sparse. Considering that over one-third of the world's population is now classified as BMI-defined overweight and obesity and the population is aging worldwide (Chooi et al., 2019), there is an urgent need to understand the effect of BMI on the intracranial aneurysm rupture. We hypothesized that increased BMI is inversely associated with intracranial aneurysm rupture. Therefore, the purpose of this study was to explore the association between BMI and the risk of intracranial aneurysm rupture based on a prospectively maintained database.

## METHODS

### Study Population

The study population was from the National Research and Development Project of Intracranial Aneurysms, which was led by Naval Medical University Changhai Hospital and performed at 21 tertiary academic medical centers in China. Patients with saccular intracranial aneurysms registered in this project between 2017 and 2020 were included. The diagnosis of intracranial aneurysms was based on the results of CT angiography (CTA), 3-dimensional time-of-flight magnetic resonance angiography (3D-TOF-MRA), or digital subtraction angiography (DSA). Both ruptured and unruptured intracranial aneurysms were included. Exclusion criteria included non-definitive aneurysms on angiography imaging, feeding artery aneurysms to arteriovenous malformations (AVM), traumatic aneurysms, fusiform aneurysms, and patients whose aneurysms were treated before a presentation. The patients with unruptured intracranial aneurysms were diagnosed incidentally in cerebrovascular angiography during evaluations for headache, dizziness, neurologic symptoms, or screening for other diseases. The diagnosis of aneurysmal subarachnoid hemorrhage (aSAH) was made if CT scans and/or lumbar punctures revealed blood in the subarachnoid space. Patients who presented with aSAH were categorized as harboring a ruptured status. According to the ruptured status, the patients were separated into ruptured and unruptured groups. This study was approved by the local institutional review board and considered minimal risk. Patient informed consent was, therefore, waived by the institutional review board (IRB). All methods were carried out following the Declaration of Helsinki.

### Exposure Assessment

We conducted a retrospective analysis of a prospectively maintained database of patients with intracranial aneurysms from 21 medical centers. Initially, an electronic data capture (EDC) system had been designed using the Delphi method before the study. Based on the EDC system, information on patient demographic and clinical characteristics was collected. The demographic characteristics included age, sex, height,

**TABLE 1 |** Baseline demographic and clinical characteristics between the two groups.

| Characteristics | Unruptured ($n_1$ = 1,977, $n_2$ = 2,270) | Ruptured ($n_1$ = 1,988, $n_2$ = 2,362) | *P* |
|---|---|---|---|
| Age (years) | 59.05 ± 11.14 | 59.47 ± 10.47 | 0.225 |
| <50 [*n* (%)] | 384 (19.42) | 308 (15.49) | 0.002 |
| 50–60 [*n* (%)] | 683 (34.55) | 684 (34.41) | |
| >60 [*n* (%)] | 910 (46.03) | 996 (50.10) | |
| Sex [*n* (%)] | | | |
| Male | 775 (39.20) | 671 (33.75) | 0.000 |
| Female | 1,202 (60.80) | 1,317 (66.25) | |
| Ethnic [*n* (%)] | | | |
| Han | 1,944 (98.33) | 1,939 (97.54) | 0.078 |
| Others | 33 (1.67) | 49 (2.46) | |
| BMI (kg/m$^2$) | 24.19 ± 2.60 | 23.65 ± 2.74 | 0.000 |
| 18.5–23.9 [*n* (%)] | 918 (46.43) | 1,111 (55.88) | 0.000 |
| <18.5 [*n* (%)] | 24 (1.21) | 29 (1.46) | |
| 24.0–27.9 [*n* (%)] | 908 (45.94) | 771 (38.78) | |
| ≥28.0 [*n* (%)] | 127 (6.42) | 77 (3.88) | |
| Smoking [*n* (%)] | 243 (12.29) | 320 (16.10) | 0.001 |
| Former | 32 (1.62) | 32 (1.61) | 0.001 |
| Current | 211 (10.67) | 288 (14.49) | |
| Drinking [*n* (%)] | 157 (7.94) | 195 (9.81) | 0.039 |
| Hypertension [*n* (%)] | 883 (44.66) | 970 (48.79) | 0.009 |
| Diabetes [*n* (%)] | 193 (9.76) | 90 (4.53) | 0.000 |
| Polycystic kidney diseases [*n* (%)] | 3 (0.15) | 4 (0.20) | 1.000 |
| Atrial fibrillation [*n* (%)] | 3 (0.15) | 2 (0.10) | 0.686 |
| Acute coronary syndrome [*n* (%)] | 20 (1.01) | 28 (1.41) | 0.253 |
| Heart failure [*n* (%)] | 37 (1.87) | 11 (0.55) | 0.000 |
| Hyperlipidemia [*n* (%)] | 96 (4.86) | 14 (0.70) | 0.000 |
| Ischemic stroke [*n* (%)] | 233 (11.63) | 77 (3.87) | 0.000 |
| Genetic diseases [*n* (%)] | 9 (0.46) | 5 (0.25) | 0.280 |
| Peripheral vascular diseases [*n* (%)] | 12 (0.61) | 5 (0.25) | 0.087 |
| No. of aneurysms per patient [mean (SD)] | 1.15 (0.45) | 1.19 (0.52) | 0.000 |
| Location of aneurysms [*n* (%)] | | | |
| Anterior circulation artery | 2,104 (88.72) | 1,819 (77.01) | 0.000 |
| Posterior circulation artery | 256 (11.28) | 543 (22.99) | |
| Size of aneurysm (mm) | 4.00 [3.00–5.80] | 4.60 [3.40–6.00] | 0.000 |
| <5 mm [*n* (%)] | 1,477 (65.07) | 1,271 (53.81) | 0.000 |
| ≥5 mm [*n* (%)] | 793 (34.93) | 1,091 (46.19) | |
| Multiple aneurysms [*n* (%)] | 239 (12.09) | 289 (14.53) | 0.008 |
| Irregular shape [*n* (%)] | 57 (2.51) | 414 (17.53) | 0.000 |

*$n_1$ represents the number of patients, $n_2$ represents the number of aneurysms; BMI, body mass index.*

weight, and ethnicity. The clinical characteristics included pre-existing comorbidities (e.g., hypertension, diabetes, polycystic kidney diseases, atrial fibrillation, acute coronary syndrome, heart failure, hyperlipidemia, history of ischemic stroke, genetic diseases, and peripheral vascular diseases), information on smoking, and alcohol use, and aneurysmal parameters. Aneurysmal parameters included the number, maximum size, shape irregularity, and location of intracranial aneurysms. The height and weight had been measured using a validated measuring instrument in each center. BMI was calculated as measured weight in kilograms divided by the standing height in meters squared. We divided BMI into four groups according to the guideline for prevention and control of overweight and obesity in Chinese adults: <18.5 kg/m$^2$ (BMI-defined underweight), 18.5 to <24.0 kg/m$^2$ (BMI-defined normal weight), 24.0 to <28.0 kg/m$^2$ (BMI-defined overweight), ≥28.0 kg/m$^2$ (BMI-defined obesity) (Chen and Lu, 2004). For MRA or CTA, three-dimensional models of aneurysms and their surrounding vasculature had been generated using corresponding software in the offline workstation in each medical center. Measurements of maximal neck-width, neck to dome length (length from the neck center to the dome of the aneurysm), and aneurysm width (measured perpendicular to the neck to dome length) had been performed using the standard projection of 2-dimensional conventional angiograms in DSA and 3-dimensional reconstructions in MRA or CTA. The maximum measurement of aneurysm width or aneurysm neck-to-dome length was defined as the maximum aneurysm size. The locations of intracranial aneurysms were categorized as anterior circulation artery and posterior circulation artery. The irregular shape was defined as that the aneurysm fundus was bi- or multi-lobular or small bleb(s) or secondary aneurysm(s) were protruding from the aneurysm fundus (Lindgren et al., 2016; Wang Y. et al., 2021). Based on this definition, the shape irregularity was independently assessed by two attending neurointerventional surgeons (both with over 15 years of experience in neurointerventional surgery) who were blinded to this study, and the inter-reader agreement was good due to their extensive experience in this field. Finally, the shape irregularity of intracranial aneurysms was categorized as regular and irregular shape.

## Statistical Analysis

The sample size was roughly estimated using the method of event per variable (EPV), which recommends that the sample size with logistical regression should be at least ten times the number of predictors. Since there were over 4,000 cases in the EDC system, the sample size was sufficient to achieve the statistical power. The Shapiro-Wilk test, stem-leaf plot, and normal P-P plot were used for the test of data distribution of continuous variables. Continuous variables were expressed as the median [interquartile range (IQR)] or mean [standard deviation (S.D.)], as appropriate. The Student's *t*-test was used for variables with parametric distribution and the Mann-Whitney test for variables with the non-parametric distribution. Categorical variables were expressed as numbers (frequencies), and the differences between the two groups were analyzed using $\chi^2$-test or Fisher's exact test.

To determine the association between BMI and intracranial aneurysm rupture in the study population, univariable and multivariable logistic regression models were performed. Candidate variables with a $P \leq 0.10$ in univariable analysis were included in the multivariable model. Given the fact that multiple aneurysms are common in patients with intracranial

aneurysms, there is probably some kind of random effect of aneurysmal parameters on the result. Hence, a mixed effect logistic regression model was performed in the multivariable analysis. In this model, three aneurysmal parameters including size, location, and shape of intracranial aneurysms were included in the random effect model and other variables were included in the fixed-effect model. Furthermore, to explore age and sex differences in the association of BMI and intracranial aneurysm rupture, subgroup analyses were performed according to age and sex stratifications. All data were handled and analyzed using SPSS statistic 25.0 (SPSS Inc., Chicago, USA) and R programming environment (R Foundation for Statistical Computing, Vienna, Austria). All statistical significance was defined as $P < 0.05$.

# RESULTS

## Comparisons of Demographic and Clinical Characteristics Between Ruptured and Unruptured Groups

We enrolled 3,965 patients with 4,632 intracranial aneurysms who met our inclusion criteria, of whom 1,977 patients (49.86%) were unruptured and 1,988 patients (50.14%) were ruptured. There were 1,446 males (36.46%) and 2,519 females (63.54%). The average age was (59.26 ± 10.81) years in the study population, the majority of which (82.55%) was aged ≥50 years. Comparisons of demographic and clinical characteristics between ruptured and unruptured groups before matching are presented in **Table 1**. There were significant differences in age, sex, BMI, drinking, smoking, hypertension, heart failure, hyperlipidemia, history of ischemic stroke, multiple aneurysms, size, shape irregularity, and location between the two groups (all $P < 0.05$).

## Univariable and Multivariable Analyses for the Risk Factors of Intracranial Aneurysm Rupture

The results of the univariable and multivariable analyses for the risk factors of intracranial aneurysm rupture are shown in **Table 2**. A total of 16 variables (3 variables in the random effect model and 13 variables in the fixed-effect model) were included in the mixed-effect logistic regression model. In the multivariable analysis, older age (OR = 1.448 for >60 years 95% CI = 1.174–1.784), female sex (OR = 1.381, 95% CI = 1.163–1.639), smoking (OR = 1.542, 95% CI = 1.177–2.202), hypertension (OR = 1.392, 95% CI = 1.195–1.623), aneurysm located in posterior circulation artery (OR = 2.293, 95% CI = 1.883–2.793), irregular shape (OR = 7.956, 95% CI = 5.778–10.913, $P = 0.000$), and aneurysm size with ≥5.0 mm (OR = 1.249, 95% CI = 1.077–1.449) were significantly associated with a higher risk of intracranial aneurysm rupture. In contrast, pre-existing diabetes (OR = 0.501, 95% CI = 0.369–0.679), heart failure (OR = 0.404, 95% CI = 0.181–0.899), hyperlipidemia (OR = 0.146, 95% CI = 0.076–0.281), and ischemic stroke (OR = 0.258, 95% CI = 0.188- 0.354) were significantly associated with a lower risk of intracranial aneurysm rupture.

## Evaluation of the Association Between BMI and Intracranial Aneurysm Rupture

Evaluation of the association between BMI and intracranial aneurysm rupture is shown in **Table 2** and **Figure 1**. Compared with the patients with normal BMI (18.5 to < 24.0 kg/m$^2$), patients with BMI 24.0 to < 28.0 kg/m$^2$ (OR = 0.745, 95% CI = 0.638–0.868) and patients with BMI ≥ 28.0 kg/m$^2$ (OR = 0.628, 95% CI = 0.443–0.890) had significantly lower odds of intracranial aneurysm rupture. Low BMI (<18.0 kg/m$^2$) was not associated with intracranial aneurysm rupture (OR = 0.894, 95% CI = 0.483–1.657, $P = 0.505$). Taking the patients with BMI < 24 kg/m$^2$ as a reference, the patients with BMI ≥ 24.0 kg/m$^2$ had a lower odds of intracranial aneurysm rupture as well (OR = 0.733, 95% CI = 0.632–0.850, $P = 0.000$).

## Associations Between BMI and Intracranial Aneurysm Rupture Stratified by Sex and Age

Subgroup analyses of associations between BMI and intracranial aneurysm rupture stratified by sex and age are shown in **Figures 2**, **3**. For males, both the BMI 24.0 to < 28.0 kg/m$^2$ (OR = 0.606, 95% CI = 0.469–0.784, $P = 0.000$) and the BMI ≥ 28.0 kg/m$^2$ (OR = 0.384, 95% CI = 0.224–0.658, $P = 0.000$) were associated with a lower risk of intracranial aneurysm rupture. However, no association was found between BMI and intracranial aneurysm rupture in females. Both the BMI 24.0 to < 28.0 kg/m$^2$ (OR = 0.722 for aged 50–60y, 95% CI = 0.554–0.938, $P = 0.015$; OR = 0.737 for aged >60y, 95% CI = 0.586–0.928, $P = 0.009$) and the BMI ≥ 28.0 kg/m$^2$ (OR = 0.517 for aged 50–60y, 95% CI = 0.281–0.950, $P = 0.0034$; OR = 0.535 for aged >60y, 95% CI = 0.318–0.899, $P = 0.0018$) was associated with a lower rupture risk in patients aged ≥50 years, whereas no significant association between BMI and intracranial aneurysm rupture was found in patients aged <50 years.

# DISCUSSION

In the present study, our results demonstrated that increased BMI was significantly and inversely associated with saccular intracranial aneurysm rupture. Patients with BMI 24.0 to < 28.0 kg/m$^2$ and those with BMI ≥ 28.0 kg/m$^2$ had significantly lower odds of intracranial aneurysm rupture compared with patients with normal BMI (18.5 to < 24.0 kg/m$^2$). In particular, this inverse association was significant in males and patients aged ≥50 years, whereas the association was not significant in females and patients aged <50 years. To the best of our knowledge, this is the largest multicenter study to date to investigate the association between BMI and intracranial aneurysm rupture.

In line with existing literature (Wermer et al., 2007; Greving et al., 2014; Lindgren et al., 2016; Wang Y. et al., 2021), our study demonstrated that older age, female sex, smoking, hypertension, large size, shape irregularity, and aneurysms in the posterior circulation artery were significantly associated with a higher risk of intracranial aneurysm rupture. Moreover, since risk factors for rupture of an unruptured aneurysm are theoretically similar to those for aneurysm formation and SAH (Macdonald and

**TABLE 2 |** Univariable and multivariable analyses for the risk factors of intracranial aneurysm rupture.

| Variables | Univariable analysis | | Multivariable analysis | |
|---|---|---|---|---|
| | OR [95% CI] | *P* | OR [95% CI] | *P* |
| Age (years) | | | | |
| <50 | Reference | | Reference | |
| 50–60 | 1.249 [1.039–1.500] | 0.018 | 1.212 [0.977–1.504] | 0.080 |
| >60 | 1.365 [1.146–1.625] | 0.000 | 1.448 [1.174–1.784] | 0.001 |
| Sex | | | | |
| Male | Reference | | Reference | |
| Female | 1.265 [1.112–1.441] | 0.000 | 1.381 [1.163–1.639] | 0.000 |
| Ethnic | | | | |
| Han | Reference | | | |
| Others | 1.489 [0.953–2.325] | 0.080 | 1.290 [0.780–2.190] | 0.153 |
| BMI (kg/m$^2$) | | | | |
| 18.5–23.9 | Reference | | Reference | |
| <18.5 | 0.998 [0.577–1.727] | 0.996 | 0.894 [0.483–1.657] | 0.505 |
| 24.0–27.9 | 0.702 [0.616–0.799] | 0.000 | 0.745 [0.638–0.868] | 0.000 |
| ≥28.0 | 0.501 [0.373–0.674] | 0.000 | 0.628 [0.443–0.890] | 0.009 |
| Smoking | 1.369 [1.144–1.639] | 0.001 | 1.542 [1.177–2.020] | 0.002 |
| Drinking | 1.261 [1.012–1.571] | 0.039 | 1.361 [0.978–1.893] | 0.068 |
| Hypertension | 1.181 [1.042–1.338] | 0.009 | 1.392 [1.195–1.623] | 0.000 |
| Diabetes | 0.438 [0.339–0.568] | 0.000 | 0.501 [0.369–0.679] | 0.000 |
| Heart failure | 0.292 [0.148–0.574] | 0.000 | 0.404 [0.181–0.899] | 0.026 |
| Hyperlipidemia | 0.139 [0.079–0.244] | 0.000 | 0.146 [0.076–0.281] | 0.000 |
| Ischemic stroke | 0.302 [0.231–0.393] | 0.000 | 0.258 [0.188–0.354] | 0.000 |
| Peripheral vascular diseases | 0.413 [0.145–1.174] | 0.097 | 0.838 [0.229–3.062] | 0.789 |
| Location of aneurysms | | | | |
| Anterior circulation artery | Reference | | Reference | |
| Posterior circulation artery | 2.605 [2.191–3.099] | 0.000 | 2.293 [1.883–2.793] | 0.000 |
| Size of aneurysm (mm) | | | | |
| <5 | Reference | | Reference | |
| ≥5 | 1.767 [1.557–2.006] | 0.000 | 1.249 [1.077–1.449] | 0.003 |
| Multiple aneurysms | 1.282 [1.068–1.540] | 0.008 | 1.359 [1.135–1.629] | 0.001 |
| Irregular shape | 9.576 [6.992–13.116] | 0.000 | 7.956 [5.778–10.913] | 0.000 |

Schweizer, 2017), our study importantly extends previous studies of the association between BMI and the incidence of SAH. Consistent with previous studies (Sandvei et al., 2012; Kroll et al., 2016), our result showed that the higher BMI was negatively associated with intracranial aneurysm rupture. In Sandvei et al.'s (2012) study, there was no association between obesity and the risk of aSAH. However, patients with BMI-defined obesity (≥28.0 kg/m$^2$) had lower odds of intracranial aneurysm rupture in this study. Particularly, the higher BMI showed a lower OR for the rupture risk, suggesting that this association tends to be linear. In accordance with the present results, Kroll et al. (2016) demonstrated that higher BMI was linearly associated with a decreased risk of SAH. Similarly, one standard deviation higher BMI was reported to be associated with a risk ratio (RR) of 0.94 (95% CI = 0.91–0.99) for the incidence of SAH in a Sweden cohort of 950,000 adults (Sundström et al., 2019).

It is difficult to explain this inverse association. However, there are several possible explanations for this result. First, since BMI does not accurately account for the regional fat distribution, high BMI is not necessarily about being true overweight or obese. Besides, about 12% of obese individuals belong to the metabolically healthy obese individuals (obese but fit individuals) (van Vliet-Ostaptchouk et al., 2014), which have lower cardiovascular diseases risk compared to normal weight but unfit individuals (*the "fat but fit" hypothesis*) (Ortega et al., 2016; Antonopoulos and Tousoulis, 2017). This is the reason that we interpret the inverse association restricting in higher BMI instead of overweight and obesity. Second, the vascular wall mechanical properties, such as wall stress on the lumen, are currently considered to play a key role in the initiation, growth, and rupture of intracranial aneurysms (Turjman et al., 2014). High wall shear stress could promote the migration of smooth muscle cells (SMCs) and phenotypic changes, resulting in smooth muscle cells' secretion of inflammatory mediators and factors involved in the degradation of the vessel wall of the intracranial aneurysm (Staarmann et al., 2019). This process was suggested

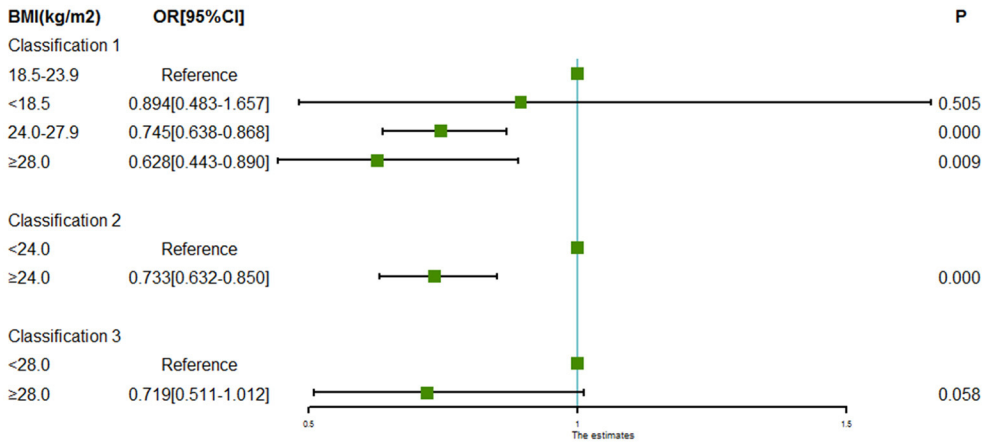


**FIGURE 1 |** Forest plot of ORs for the association between BMI and intracranial aneurysm rupture. Compared to the patients with normal BMI (18.5 to < 24.0 kg/m$^2$), odds of intracranial aneurysm rupture were significantly lower in the patients with BMI 24.0 to < 28.0 kg/m$^2$ and patients with BMI ≥ 28.0 kg/m$^2$. Low BMI (<18.0 kg/m$^2$) was not associated with intracranial aneurysm rupture. Taking the patients with BMI < 24 kg/m$^2$ as a reference, the patients with BMI ≥ 24.0 kg/m$^2$ had a lower odds of intracranial aneurysm rupture as well.

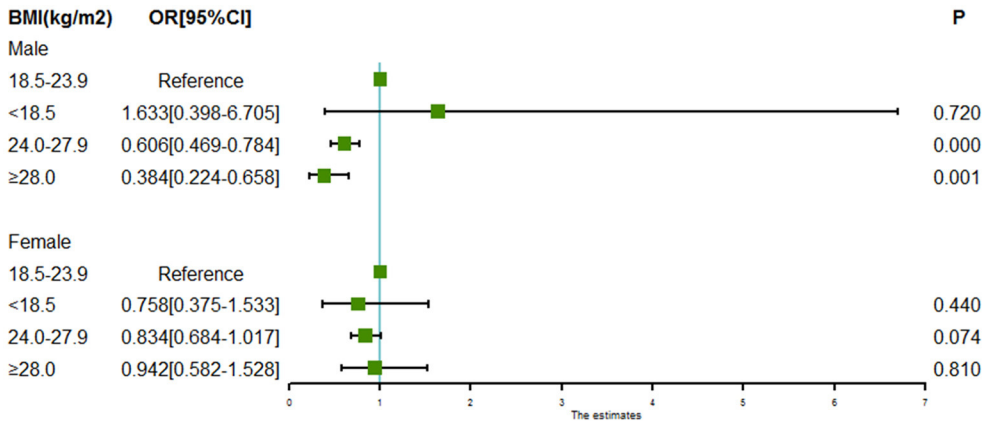


**FIGURE 2 |** Forest plot of ORs for the association between BMI and intracranial aneurysm rupture stratified by sex. Both the BMI 24.0 to < 28.0 kg/m$^2$ and the BMI ≥ 28.0 kg/m$^2$ were associated with a lower risk of intracranial aneurysm rupture in males. However, no association was found between BMI and intracranial aneurysm rupture in females.

to be associated with the growth and rupture of the small or secondary bleb aneurysm phenotype of intracranial aneurysms (Meng et al., 2014). Coincidentally, low BMI was reported to be inversely associated with the peak wall stress in patients with abdominal aortic aneurysm (AAA), leading to an increased rupture risk of abdominal aortic aneurysm (Sweeting et al., 2012; Lindquist Liljeqvist et al., 2017). Given this result and the fact that the majority of the study population presented a small aneurysm (size < 10 mm), patients with a relatively lower level of BMI might have higher wall shear stress and then increase the rupture risk of small intracranial aneurysms. Third, patients with higher BMI are more likely to take statins for secondary prevention to reduce the risk of cardiovascular diseases and ischemic stroke in clinical practice. The experimental animal models, as well as clinical studies, suggest that statins have various pleiotropic effects including anti-inflammatory and anti-thrombotic that could reduce the risk of intracranial aneurysm rupture (Sweeting et al., 2009; Can et al., 2018). However, the pathophysiological basis accounting for the inverse association remains unclear, and therefore further research is recommended to be undertaken to draw these inferences.

In the subgroup analysis, we found that there was a significant sex difference in the inverse association between BMI and intracranial aneurysm rupture. Our sex-strata result is similar to several previous cardiovascular and cerebrovascular studies where they also observed that the inverse association between BMI and adverse events is more prominent in males than in females (Hong et al., 2018; Liu et al., 2021). This result may be partly explained by the fact that there is a sex difference in the prevalence of obesity. A recent study, based on the

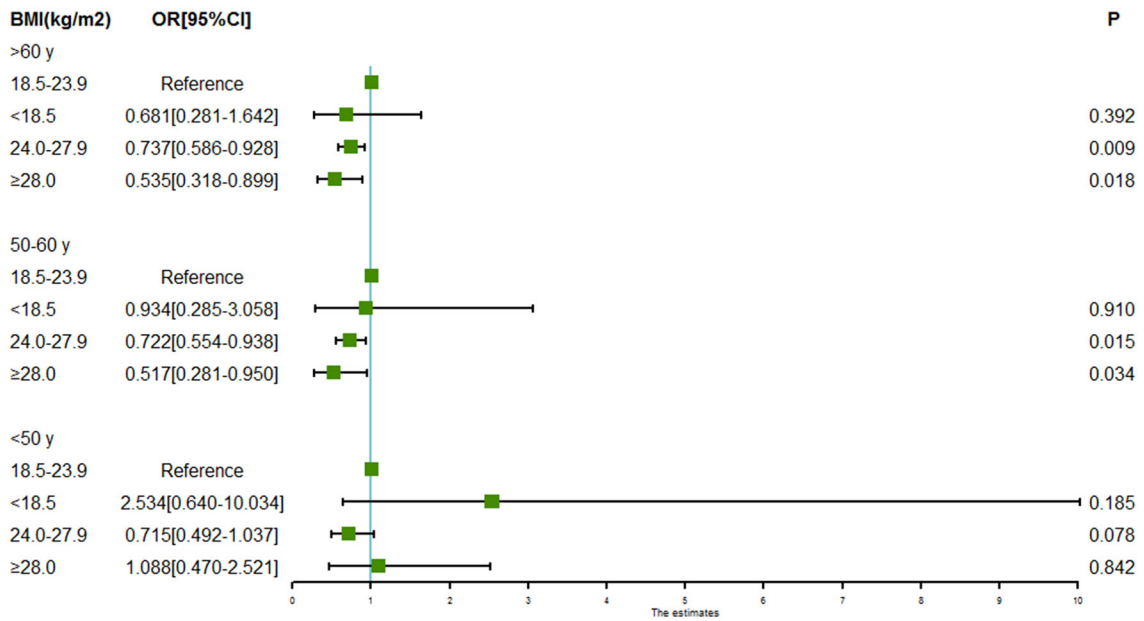


**FIGURE 3 |** Forest plot of ORs for the association between BMI and intracranial aneurysm rupture stratified by age. Both the BMI 24.0 to < 28.0 kg/m$^2$ and the BMI ≥ 28.0 kg/m$^2$ were associated with a lower risk of intracranial aneurysm rupture in patients aged 50–60 years and patients aged >60 years. However, no association was found between BMI and intracranial aneurysm rupture in patients aged <50 years.

China Chronic Disease and Risk Factors Surveillance program, demonstrated that males have significantly higher proportions of overweight and obesity than females in China, especially in recent years (Wang L. et al., 2021). Similarly, male patients had higher proportions of BMI-defined overweight and obesity in the present study (data not showed). Looking back, it makes sense that overweight and obesity were not or even positively associated with the incidence of SAH in a Japanese cohort study due to its disproportionally high percentage of females (Kawate et al., 2017). Besides, it is easy to understand the phenomenon that male sex is related to a lower risk of intracranial aneurysm rupture from the perspective of sex difference in this inverse association. At the same time, our results contrast with the Sweden cohort study where the inverse association of BMI with risk of SAH was found in females (Sundström et al., 2019). In addition to the difference in controls, this inconsistency might be attributed to the regional difference in the epidemiology of obesity as well as the racial difference in the fat distribution between the Asian and Caucasian populations (Deurenberg et al., 2002; Lim et al., 2011). For instance, visceral adiposity, a fat that is thought to be more dangerous than subcutaneous adiposity, was reported to be more prominent in Asian females than Caucasian females with similar BMI (Lim et al., 2011).

Consistent with the literature, the majority of patients with intracranial aneurysms were aged ≥50 years and about half of them were elderly. Interestingly, our results demonstrated that BMI was negatively associated with intracranial aneurysm rupture both in patients aged 50–60 years and those aged >60 years, whereas the inverse association was not found in younger patients. This study supports evidence from previous observations that older individuals have a more significant inverse association between BMI and the incidence of SAH (Sundström et al., 2019). Besides, this result further confirms the phenomenon that the "obesity paradox" seems to be profound in aging patients (Wang and Ren, 2018). Since there is a complex relationship between aging, metabolism, and relevant disease, it is difficult to explain this result. However, one possible explanation for this might be the loss of skeletal mass due to the aging process in older individuals. On the one hand, weight loss, especially for the loss of skeletal mass, is common in the elderly population, and advanced age (>65 years) is particularly vulnerable to loss of skeletal mass (Bischof and Park, 2015), which in turn has been shown to be highly related to the growth of intracranial aneurysms (aneurysmal growth easily leads to a rupture) (Giordan et al., 2018). On the other hand, loss of skeletal mass is thought to be negatively associated with BMI (Iannuzzi-Sucich et al., 2002). In this perspective, elderly patients with relatively high BMI would have less likelihood of loss of skeletal mass, resulting in a lower risk of intracranial aneurysm rupture. Similarly, Kuo et al. (2006) suggested that elderly individuals with elevated BMI present better cognitive performance in terms of reasoning and visuospatial speed of processing than those with normal BMI, in which a high level of skeletal mass was inferred to be an important contributor. Consequently, if loss of skeletal mass is the accountable factor, more efforts to reduce the risk of intracranial aneurysm rupture as well as improve the structure and function of the aging brain, including adequate protein intake and moderate physical exercise, are warranted in aging patients with intracranial aneurysms. However, the impact of a loss of skeletal mass on the intracranial aneurysm rupture is

still needed to be validated, and further prospective studies are therefore suggested to be undertaken in the future.

Strengths of our study include the comprehensive collection of directly measured data from prospective hospital-based samples, the large sample size, the many harmonized exposure variables, and a multicenter design, which could largely reduce the likelihood of random error, selection bias, and measurement bias. With an increasing number of BMI-defined overweight and obesity and increasing mean age in patients with intracranial aneurysms in recent years, this study addresses a clinically relevant question for the clinicians. Our findings could help clinicians to fully understand the effect of BMI on the natural history of unruptured intracranial aneurysms, providing important implications in deciding on the optimal management of unruptured intracranial aneurysms in patients with higher BMI, especially for aging patients.

Despite the intriguing findings of the present study, several important limitations should be taken into account. First, our study design is retrospective, which has less power to estimate the cause-effect. Besides, as patients with ruptured intracranial aneurysms might have weight loss owing to the negative nitrogen balance at presentation, the sudden weight loss might have an impact on the results. Despite that, the majority of the study population was admitted to the hospitals within 1 day, and thereby the impact of weight loss on the results could be thought to be minor. In any case, a large prospective cohort study is needed to confirm our results in the future. Second, since nearly one-fourth of patients with SAH would die before admission to a hospital, the cases in the present study may not be fully representative of all cases of ruptured intracranial aneurysms. There is some kind of prevalence-incidence bias (Neyman bias) in the present study. Third, although we adjusted a set of crucial covariates in multivariable models, there are still potential confounders that could influence our results. Particularly, previous SAH is independently associated with intracranial aneurysm rupture. Since the relevant information was not available in the database, this important covariate was not included in the multivariable model. The absence of the important factor in the multivariable model might have an impact on the results. Further studies, which take these variables into account, will need to be undertaken. Fourth, although the loss of skeletal mass was inferred to contribute to the significant inverse association between BMI and intracranial aneurysm rupture in aging patients, no direct evidence could be presented. Thus, to draw this inference, further prospective studies on the exact benefit of life and behavioral change are therefore suggested to be undertaken in the future. Last but not least, the results of the present study were based on the Chinese population. As there are regional and racial differences in the epidemiology of obesity across countries, replication of the results in other populations is suggested. This is an important issue for future research.

## CONCLUSIONS

In summary, the findings of our study demonstrated that increased BMI was significantly and inversely associated with saccular intracranial aneurysm rupture in males and patients aged $\geq$50 years. With an increasing number of BMI-defined overweight and obesity and increasing mean age in patients with intracranial aneurysms in recent years, our findings could provide important implications in deciding on the optimal management of unruptured intracranial aneurysms in patients with higher BMI, especially for aging patients. However, a large prospective cohort study is needed to confirm our results in the future.

## DATA AVAILABILITY STATEMENT

The raw data supporting the conclusions of this article will be made available by the authors, without undue reservation.

## ETHICS STATEMENT

The studies involving human participants were reviewed and approved by the Institutional Review Board of the First Affiliated Hospital of Xiamen University. Written informed consent for participation was not required for this study in accordance with the national legislation and the institutional requirements.

## AUTHOR CONTRIBUTIONS

SC, XC, ZL, JM, YL, ZZ, ZJ, and WZ collected the data and performed the research. SC and PZ analyzed the data and drafted the manuscript. PZ and QH conceived and designed the research. ZW and QH initiated and organized this study. All authors reviewed and edited the manuscript and approved the final version of the manuscript.

## FUNDING

This study was funded by the National Research and Development Project of Key Chronic Diseases (Grant No. 2016YFC1300703).

## ACKNOWLEDGMENTS

We are grateful to the investigators from the 21 tertiary academic medical centers who participated in the National Research and Development Project of Intracranial Aneurysms for their prospectively comprehensive collection of patients' data. Meanwhile, we are also grateful to Dr. Zaixing Shi, the assistant professor of statistics from the Public Health School of Xiamen University, for his professional suggestions regarding the mixed effect model.

## REFERENCES


Andreasen, T. H., Bartek, J. Jr., Andresen, M., Springborg, J. B., and Romner, B. (2013). Modifiable risk factors for aneurysmal subarachnoid hemorrhage. *Stroke* 44, 3607–3612. doi: 10.1161/STROKEAHA.113.001575

Antonopoulos, A. S., and Tousoulis, D. (2017). The molecular mechanisms of obesity paradox. *Cardiovasc. Res.* 113, 1074–1086. doi: 10.1093/cvr/cvx106

Bischof, G. N., and Park, D. C. (2015). Obesity and aging: consequences for cognition, brain structure, and brain function. *Psychosom. Med.* 77, 697–709. doi: 10.1097/PSY.0000000000000212

Can, A., Castro, V. M., Dligach, D., Finan, S., Yu, S., Gainer, V., et al. (2018). Lipid-lowering agents and high HDL (high-density lipoprotein) are inversely associated with intracranial aneurysm rupture. *Stroke* 49, 1148–1154. doi: 10.1161/STROKEAHA.117.019972

Chen, C., and Lu, F. C. (2004). The guidelines for prevention and control of overweight and obesity in Chinese adults. *Biomed. Environ. Sci.* 17, 1–36.

Chooi, Y. C., Ding, C., and Magkos, F. (2019). The epidemiology of obesity. *Metab. Clin. Exp.* 92, 6–10. doi: 10.1016/j.metabol.2018.09.005

de Rooij, N. K., Linn, F. H., van der Plas, J. A., Algra, A., and Rinkel, G. J. (2007). Incidence of subarachnoid haemorrhage: a systematic review with emphasis on region, age, gender and time trends. *J. Neurol. Neurosurg. Psychiatry* 78, 1365–1372. doi: 10.1136/jnnp.2007.117655

Deurenberg, P., Deurenberg-Yap, M., and Guricci, S. (2002). Asians are different from Caucasians and from each other in their body mass index/body fat per cent relationship. *Obes. Rev.* 3, 141–146. doi: 10.1046/j.1467-789X.2002.00065.x

Feghali, J., Gami, A., Rapaport, S., Bender, M. T., Jackson, C. M., Caplan, J. M., et al. (2021). Aging patient population with ruptured aneurysms: trend over 28 years. *Neurosurgery* 88, 658–665. doi: 10.1093/neuros/nyaa494

Feigin, V., Parag, V., Lawes, C. M., Rodgers, A., Suh, I., Woodward, M., et al. (2005). Smoking and elevated blood pressure are the most important risk factors for subarachnoid hemorrhage in the Asia-Pacific region: an overview of 26 cohorts involving 306,620 participants. *Stroke* 36, 1360–1365. doi: 10.1161/01.STR.0000170710.95689.41

Giordan, E., Sorenson, T. J., Brinjikji, W., Vine, R., and Lanzino, G. (2018). Risk factors for growth of conservatively managed unruptured intracranial aneurysms. *Acta Neurochir.* 160, 2419–2423. doi: 10.1007/s00701-018-3729-z

Greving, J. P., Wermer, M. J., Brown, R. D. Jr., Morita, A., Juvela, S., Yonekura, M., et al. (2014). Development of the PHASES score for prediction of risk of rupture of intracranial aneurysm: a pooled analysis of six prospective cohort studies. *Lancet Neurol.* 13, 59–66. doi: 10.1016/S1474-4422(13)70263-1

Hong, S., Lee, J. H., Kim, K. M., Lee, J. W., Youn, Y. J., Ahn, M. S., et al. (2018). Is there a sex-related difference in the obesity paradox in systolic heart failure? Sex-related difference in the obesity paradox. *Yonsei Med. J.* 59, 57–62. doi: 10.3349/ymj.2018.59.1.57

Iannuzzi-Sucich, M., Prestwood, K. M., and Kenny, A. M. (2002). Prevalence of sarcopenia and predictors of skeletal muscle mass in healthy, older men and women. *J. Gerontol. A Biol. Sci. Med. Sci.* 57, M772–M777. doi: 10.1093/gerona/57.12.M772

Kawate, N., Kayaba, K., Hara, M., Hamaguchi, T., Kotani, K., and Ishikawa, S. (2017). Body mass index and incidence of subarachnoid hemorrhage in japanese community residents: the Jichi Medical School Cohort study. *J. Stroke Cerebrovasc. Dis.* 26, 1683–1688. doi: 10.1016/j.jstrokecerebrovasdis.2017.03.029

Kleinloog, R., de Mul, N., Verweij, B. H., Post, J. A., Rinkel, G. J. E., and Ruigrok, Y. M. (2018). Risk factors for intracranial aneurysm rupture: a systematic review. *Neurosurgery* 82, 431–440. doi: 10.1093/neuros/nyx238

Kroll, M. E., Green, J., Beral, V., Sudlow, C. L., Brown, A., Kirichek, O., et al. (2016). Adiposity and ischemic and hemorrhagic stroke: prospective study in women and meta-analysis. *Neurology* 87, 1473–1481. doi: 10.1212/WNL.0000000000003171

Kuo, H. K., Jones, R. N., Milberg, W. P., Tennstedt, S., Talbot, L., Morris, J. N., et al. (2006). Cognitive function in normal-weight, overweight, and obese older adults: an analysis of the advanced cognitive training for independent and vital elderly cohort. *J. Am. Geriatr. Soc.* 54, 97–103. doi: 10.1111/j.1532-5415.2005.00522.x

Lim, U., Ernst, T., Buchthal, S. D., Latch, M., Albright, C. L., Wilkens, L. R., et al. (2011). Asian women have greater abdominal and visceral adiposity than Caucasian women with similar body mass index. *Nutr. Diabetes* 1:e6. doi: 10.1038/nutd.2011.2

Lindgren, A. E., Koivisto, T., Björkman, J., von Und Zu Fraunberg, M., Helin, K., Jääskeläinen, J. E., et al. (2016). Irregular shape of intracranial aneurysm indicates rupture risk irrespective of size in a population-based cohort. *Stroke* 47, 1219–1226. doi: 10.1161/STROKEAHA.115.012404

Lindgren, A. E., Kurki, M. I., Riihinen, A., Koivisto, T., Ronkainen, A., Rinne, J., et al. (2013). Type 2 diabetes and risk of rupture of saccular intracranial aneurysm in eastern Finland. *Diabetes Care* 36, 2020–2026. doi: 10.2337/dc12-1048

Lindquist Liljeqvist, M., Hultgren, R., Siika, A., Gasser, T. C., and Roy, J. (2017). Gender, smoking, body size, and aneurysm geometry influence the biomechanical rupture risk of abdominal aortic aneurysms as estimated by finite element analysis. *J. Vasc. Surg.* 65, 1014–1021.e4. doi: 10.1016/j.jvs.2016.10.074

Liu, Z., Sanossian, N., Starkman, S., Avila-Rinek, G., Eckstein, M., Sharma, L. K., et al. (2021). Adiposity and outcome after ischemic stroke: obesity paradox for mortality and obesity parabola for favorable functional outcomes. *Stroke* 52, 144–151. doi: 10.1161/STROKEAHA.119.027900

Macdonald, R. L., and Schweizer, T. A. (2017). Spontaneous subarachnoid haemorrhage. *Lancet* 389, 655–666. doi: 10.1016/S0140-6736(16)30668-7

Maher, M., Schweizer, T. A., and Macdonald, R. L. (2020). Treatment of spontaneous subarachnoid hemorrhage: guidelines and gaps. *Stroke* 51, 1326–1332. doi: 10.1161/STROKEAHA.119.025997

Meng, H., Tutino, V. M., Xiang, J., and Siddiqui, A. (2014). High WSS or low WSS? Complex interactions of hemodynamics with intracranial aneurysm initiation, growth, and rupture: toward a unifying hypothesis. *AJNR Am. J. Neuroradiol.* 35, 1254–1262. doi: 10.3174/ajnr.A3558

Ortega, F. B., Lavie, C. J., and Blair, S. N. (2016). Obesity and cardiovascular disease. *Circ. Res.* 118, 1752–1770. doi: 10.1161/CIRCRESAHA.115.306883

Persaud, S. R., Lieber, A. C., Donath, E., Stingone, J. A., Dangayach, N. S., Zhang, X., et al. (2019). Obesity paradox in intracerebral hemorrhage. *Stroke* 50, 999–1002. doi: 10.1161/STROKEAHA.119.024638

Rautalin, I., Kaprio, J., and Korja, M. (2020). Obesity paradox in subarachnoid hemorrhage: a systematic review. *Neurosurg. Rev.* 43, 1555–1563. doi: 10.1007/s10143-019-01182-5

Rinaldo, L., Rabinstein, A. A., and Lanzino, G. (2019). Increased body mass index associated with reduced risk of delayed cerebral ischemia and subsequent infarction after aneurysmal subarachnoid hemorrhage. *Neurosurgery* 84, 1035–1042. doi: 10.1093/neuros/nyy104

Rodríguez-Castro, E., Rodríguez-Yáñez, M., Arias-Rivas, S., Santamaría-Cadavid, M., López-Dequidt, I., Hervella, P., et al. (2019). Obesity paradox in ischemic stroke: clinical and molecular insights. *Transl. Stroke Res.* 10, 639–649. doi: 10.1007/s12975-019-00695-x

Sandhu, R. K., Ezekowitz, J., Andersson, U., Alexander, J. H., Granger, C. B., Halvorsen, S., et al. (2016). The 'obesity paradox' in atrial fibrillation: observations from the ARISTOTLE (Apixaban for Reduction in Stroke and Other Thromboembolic Events in Atrial Fibrillation) trial. *Eur. Heart J.* 37, 2869–2878. doi: 10.1093/eurheartj/ehw124

Sandvei, M. S., Lindekleiv, H., Romundstad, P. R., Müller, T. B., Vatten, L. J., Ingebrigtsen, T., et al. (2012). Risk factors for aneurysmal subarachnoid hemorrhage - BMI and serum lipids: 11-year follow-up of the HUNT and the Tromsø Study in Norway. *Acta Neurol. Scand.* 125, 382–388. doi: 10.1111/j.1600-0404.2011.01578.x

Staarmann, B., Smith, M., and Prestigiacomo, C. J. (2019). Shear stress and aneurysms: a review. *Neurosurg. Focus* 47:E2. doi: 10.3171/2019.4.FOCUS19225

Sundström, J., Söderholm, M., Söderberg, S., Alfredsson, L., Andersson, M., Bellocco, R., et al. (2019). Risk factors for subarachnoid haemorrhage: a nationwide cohort of 950 000 adults. *Int. J. Epidemiol.* 48, 2018–2025. doi: 10.1093/ije/dyz163

Sweeting, M. J., Thompson, S. G., Brown, L. C., and Powell, J. T. (2012). Meta-analysis of individual patient data to examine factors affecting growth and rupture of small abdominal aortic aneurysms. *Br. J. Surg.* 99, 655–665. doi: 10.1002/bjs.8707

Sweeting, M. J., Thompson, S. G., Brown, L. C., Powell, J. T., and RESCAN Collaborators (2009). Pitavastatin suppresses formation and progression of cerebral aneurysms through inhibition of the nuclear

factor kappaB pathway. *Neurosurgery* 64, 357–365; discussion: 365–6. doi: 10.1227/01.NEU.0000336764.92606.1D

Turjman, A. S., Turjman, F., and Edelman, E. R. (2014). Role of fluid dynamics and inflammation in intracranial aneurysm formation. *Circulation* 129, 373–382. doi: 10.1161/CIRCULATIONAHA.113.001444

Uretsky, S., Messerli, F. H., Bangalore, S., Champion, A., Cooper-Dehoff, R. M., Zhou, Q., et al. (2007). Obesity paradox in patients with hypertension and coronary artery disease. *Am. J. Med.* 120, 863–870. doi: 10.1016/j.amjmed.2007.05.011

van Vliet-Ostaptchouk, J. V., Nuotio, M. L., Slagter, S. N., Doiron, D., Fischer, K., Foco, L., et al. (2014). The prevalence of metabolic syndrome and metabolically healthy obesity in Europe: a collaborative analysis of ten large cohort studies. *BMC Endocr. Disord.* 14:9. doi: 10.1186/1472-6823-14-9

Vlak, M. H., Rinkel, G. J., Greebe, P., and Algra, A. (2013). Risk of rupture of an intracranial aneurysm based on patient characteristics: a case-control study. *Stroke* 44, 1256–1259. doi: 10.1161/STROKEAHA.111.000679

Wang, L., Zhou, B., Zhao, Z., Yang, L., Zhang, M., Jiang, Y., et al. (2021). Body-mass index and obesity in urban and rural China: findings from consecutive nationally representative surveys during 2004-18. *Lancet* 398, 53–63. doi: 10.1016/S0140-6736(21)00798-4

Wang, S., and Ren, J. (2018). Obesity paradox in aging: from prevalence to pathophysiology. *Prog. Cardiovasc. Dis.* 61, 182–189. doi: 10.1016/j.pcad.2018.07.011

Wang, Z. J., Zhou, Y. J., Galper, B. Z., Gao, F., Yeh, R. W., and Mauri, L. (2015). Association of body mass index with mortality and cardiovascular events for patients with coronary artery disease: a systematic review and meta-analysis. *Heart* 101, 1631–1638. doi: 10.1136/heartjnl-2014-307119

Wang, Y., Cheng, M., Liu, S., Xie, G., Liu, L., Wu, X., et al. (2021). Shape related features of intracranial aneurysm are associated with rupture status in a large Chinese cohort. *J Neurointerv Surg.* doi: 10.1136/neurintsurg-2021-017452. [Epub ahead of print].

Wermer, M. J., van der Schaaf, I. C., Algra, A., and Rinkel, G. J. (2007). Risk of rupture of unruptured intracranial aneurysm in relation to patient and aneurysm characteristics: an updated meta-analysis. *Stroke* 38, 1404–1410. doi: 10.1161/01.STR.0000260955.51401.cd

**Conflict of Interest:** The authors declare that the research was conducted in the absence of any commercial or financial relationships that could be construed as a potential conflict of interest.

**Publisher's Note:** All claims expressed in this article are solely those of the authors and do not necessarily represent those of their affiliated organizations, or those of the publisher, the editors and the reviewers. Any product that may be evaluated in this article, or claim that may be made by its manufacturer, is not guaranteed or endorsed by the publisher.

frontiers in Aging Neuroscience

ORIGINAL RESEARCH
published: 17 August 2021
doi: 10.3389/fnagi.2021.720061

# Severe Brain Atrophy Predicts Poor Clinical Outcome After Endovascular Treatment of Acute Basilar Artery Occlusion: An Automated Volumetric Analysis of a Nationwide Registry

*Chang Liu[1], Hansheng Liu[1], Deping Wu[1], Zhiming Zhou[2], WenGuo Huang[3], Zhilin Wu[4], Wenjie Zi[1]* and Qingwu Yang[1]**

[1] Department of Neurology, Xinqiao Hospital and The Second Affiliated Hospital, Army Medical University (Third Military Medical University), Chongqing, China, [2] Department of Neurology, Yijishan Hospital of Wannan Medical College, Wuhu, China, [3] Department of Neurology, Chinese Medical Hospital of Maoming, Maoming, China, [4] Department of Neurology, Yunfu People's Hospital, Yunfu, China

**Background:** Brain atrophy globally reflects the effects of preexisting risk factors and biological aging on brain structures and normally predicts poor outcomes in anterior circulation stroke. However, comparing with these patients, acute basilar artery occlusion (ABAO) impairs infratentorial regions frequently and might benefit from brain atrophy due to the resulting residual space to reduce tissue compression and thus improve prognosis, which raises doubts that current understandings for prognostic roles of brain atrophy are also applicable for ABAO. Therefore, this study aims to evaluate brain atrophy automatically from CT images and investigates its impact on outcomes of ABAO following endovascular treatment (EVT).

**Methods:** A total of 231 ABAO who underwent EVT from the BASILAR registry were enrolled. Brain atrophy was quantified as the ratio of brain parenchymal volume to cerebrospinal fluid volume on baseline CT. The primary outcome was the modified Rankin Scale (mRS) score at 3 months.

**Results:** The frequency of favorable outcomes (90-day mRS $\leq 3$) was significantly lower in the severe atrophy group ($P = 0.014$). Adjusted logistic models revealed that severe brain atrophy was significantly negatively associated with favorable outcome incidence ($P = 0.006$), with no relationship with either in-hospital or 90-day overall mortality (all $P > 0.05$). Adding a severe atrophy index into the baseline model obviously enhanced its discriminatory ability in predicting the outcome by obviously increasing areas under the receiver operating characteristic curve, net reclassification improvement algorithm, and integrated discrimination improvement algorithm values (all $P < 0.05$).

**Conclusion:** Severe brain atrophy did not improve in-hospital or overall mortality but impaired the long-term recovery after EVT. This objective and automated marker has the potential to be incorporated into decision-support methods for treating ABAO.

**Keywords: brain atrophy, acute basilar artery occlusion, computed tomography, endovascular treatment, automatical analysis**

OPEN ACCESS

***Edited by:***
*Yuanli Zhao,*
*Capital Medical University, China*

***Reviewed by:***
*Qinghai Huang,*
*Changhai Hospital, China*
*Liqun Jiao,*
*Capital Medical University, China*

***Correspondence:**
*Wenjie Zi*
*ziwenjie@126.com*
*Qingwu Yang*
*yangqwmlys@163.com*

***Received:*** *03 June 2021*
***Accepted:*** *20 July 2021*
***Published:*** *17 August 2021*

***Citation:***
*Liu C, Liu H, Wu D, Zhou Z, Huang W, Wu Z, Zi W and Yang Q (2021) Severe Brain Atrophy Predicts Poor Clinical Outcome After Endovascular Treatment of Acute Basilar Artery Occlusion: An Automated Volumetric Analysis of a Nationwide Registry. Front. Aging Neurosci. 13:720061. doi: 10.3389/fnagi.2021.720061*

# INTRODUCTION

Acute basilar artery occlusion (ABAO) accounts for nearly 1% of all forms of ischemic stroke (Mattle et al., 2011). It is a devastating neurological disorder with high mortality that leaves a substantial part of survivors severely disabled (Mattle et al., 2011). Although endovascular treatment (EVT) has been increasingly applied as a common strategy in daily clinical practice for patients with ABAO, the latest BASICS randomized controlled trial focusing on the management of ABAO failed to demonstrate statistically the benefit of this intervention over medical management therapy under current EVT indications (Langezaal et al., 2021). To further ameliorate the outcomes of patients with ABAO treated with EVT, novel key prognostic markers are urgently needed to improve clinical decision-making systems and to identify patients suitable for EVT.

Brain atrophy, indicating the loss of brain cells or their connections, has recently been presented as a new, reliable imaging marker for predicting poor functional outcomes in patients with anterior circulation stroke treated with intravenous thrombolysis or EVT (Lauksio et al., 2020; Pedraza et al., 2020). However, compared with anterior circulation stroke, which damages cerebral hemispheres, in patients with ABAO, the subtentorial structures are frequently impaired; such patients might benefit from brain atrophy, which provides compensation space and increases tolerance of space-occupying conditions, thereby decreasing the probability of brain herniation, decreasing mortality, and promoting recovery (Mattle et al., 2011; Delcourt et al., 2020). The markedly different infarction locations between ABAO and anterior circulation stroke have raised doubts that the current understanding of the prognostic roles of brain atrophy is applicable to ABAO. However, due to the relatively low incidence of ABAO, the association between brain atrophy and outcomes of these patients with ABAO after EVT has not been explored to the best of our knowledge.

Previous methods of evaluating brain atrophy have mainly relied on the subjective visual experience of the neurologists performing the evaluation, which might limit the use of brain atrophy for outcome evaluation in clinical practice (Appleton et al., 2020). Nevertheless, a recently developed automated volumetric algorithm named CTseg has enabled the rapid and objective estimation of the degree of global brain atrophy after mapping to the standard brain map and quantifying brain parenchymal volume (BPV) and cerebrospinal fluid volume (CFV) by CT, which is the most frequent type of brain image used to diagnose ischemic stroke (Adduru et al., 2020; Brudfors et al., 2020). Therefore, based on our previous multicenter BASILAR registry and the CTseg automatic algorithm, this study aims to explore the role of brain atrophy in determining clinical outcomes among patients with ABAO treated with EVT.

# MATERIALS AND METHODS

## Study Design and Participants

The BASILAR study was a nationwide, prospective registry of EVT plus medical management vs. medical management alone for patients who were confirmed with an acute symptomatic and radiological ABAO from 47 comprehensive stroke centers in China between January 2014 and May 2019. The details of the study protocol have been previously published (Writing Group for the BASILAR Group et al., 2020).

In the present analysis, we evaluated the degree of atrophy automatically from CT slices to further explore the impact of brain atrophy on clinical outcomes among patients with ABAO after EVT (Adduru et al., 2020; Brudfors et al., 2020). We included consecutive patients in the BASILAR registry who met the following criteria: (1) treated with EVT, (2) accepted non-contrast-enhanced CT (NECT) scanning before the endovascular intervention, and (3) NECT slice thickness $\leq 5$ mm (to guarantee the accuracy of the analysis). From 829 patients in the BASILAR registry, a total of 231 patients treated with EVT were enrolled in this study. In addition, another 66 patients with ABAO who had been treated with medical management alone (NECT thickness also $\leq$5 mm) were further enrolled to verify whether brain atrophy data can improve clinical decision-making.

## Standard Protocol Approvals, Registrations, and Patient Consents

The BASILAR was registered on the Chinese Clinical Trial Registry (ChiCTR1800014759). This study was approved by the research board at each participating center, and informed consent was obtained from all patients or their authorized representatives.

## Procedures and Data Collection

In addition to CT images acquired at admission, we retrospectively collected data on baseline characteristics, including age, sex, vascular risk factors (i.e., diabetes mellitus, hypertension, atrial fibrillation, and hyperlipidemia), National Institute of Health Stroke Scale (NIHSS) at admission, and posterior circulation-Alberta Stroke Program Early scores (PC-ASPECTS). Collateral circulation status was assessed by the posterior circulation collateral score (PC-CS) based on the presence of potential collateral pathways on CT angiography (van der Hoeven et al., 2016). Successful reperfusion was defined as a modified thrombolysis-in-cerebral-infarction (mTICI) score higher than 2a at the end of the intervention. An independent core imaging laboratory, blinded to clinical outcomes, assessed all digital subtraction angiographies and imaging data.

Primary functional outcomes at follow-up were assessed using the 90-day modified Rankin Scale (mRS). A score on the 90-day mRS of 4–6 was defined as a poor outcome. sICH was defined as a newly observed intracranial hemorrhage leading to an increase of four points on the NIHSS before worsening or an increase of two points in one category (Liu et al., 2020; Writing Group for the BASILAR Group et al., 2020). Early neurological improvement (ENI) was defined as a reduction of the NIHSS score from the baseline score of $>$8, or a return to 0, 24 h after EVT (Guenego et al., 2021).

## Brain Atrophy Degree Evaluation

We estimated brain atrophy automatically based on the CTseg algorithm (https://github.com/WCHN/CTseg), developed by the Ashburner group at the Wellcome Trust Centre for Neuroimaging (Brudfors et al., 2020). This routine spatially

**TABLE 1 |** Baseline characteristics of the study population.

| | All patients (*N* = 231) | mRS ≤ 3 (*N* = 79) | mRS > 3 (*N* = 152) | *P* |
|---|---|---|---|---|
| Age, years, mean ± SD | 62.74 ± 12.18 | 61.23 ± 13.35 | 63.52 ± 11.49 | 0.175 |
| Men, (*n*%) | 172 (74.46) | 56 (70.89) | 116 (76.32) | 0.460 |
| Baseline NIHSS, median (IQR) | 26.0 (17.0–32.0) | 23.0 (11.0–30.0) | 29.0 (20.0–34.0) | <0.001 |
| Initial PC-ASPECTS, median (IQR) | 8 (7–9) | 9 (8–10) | 7 (6–8) | <0.001 |
| Admission SBP, mmHg, mean ± SD | 144.94 ± 23.42 | 146.52 ± 23.72 | 144.12 ± 23.30 | 0.461 |
| Admission DBP, mmHg, mean ± SD | 83.86 ± 15.17 | 83.38 ± 16.09 | 84.11 ± 14.71 | 0.729 |
| 24 h NIHSS after EVT, median (IQR) | 27.0 (12.0–34.0) | 9.0 (3.0–17.5) | 32.0 (23.0–35.0) | <0.001 |
| 7 d NIHSS after EVT, median(IQR) | 19.0 (6.5–35.0) | 3.0 (1.0–8.0) | 31.5 (18.0–36.0) | <0.001 |
| Pre-onset mRS | | | | |
| 0 | 206 (89.18) | 71 (89.87) | 135 (88.82) | 0.794 |
| 1 | 20 (8.66) | 7 (8.86) | 13 (8.55) | |
| 2 | 5 (2.16) | 1 (1.27) | 4 (2.63) | |
| BPV/CFV | 3.20 (0.45) | 3.30 (0.41) | 3.16 (0.47) | 0.022 |
| **History of risk factors, *n* (%)** | | | | |
| Hypertension | 152 (65.80) | 56 (70.89) | 96 (63.16) | 0.304 |
| Diabetes mellitus | 53 (22.94) | 16 (20.25) | 37 (24.34) | 0.592 |
| Dyslipidemia | 73 (31.60) | 30 (37.97) | 43 (28.29) | 0.176 |
| Atrial fibrillation | 45 (19.48) | 19 (24.05) | 26 (17.11) | 0.276 |
| Smoking | 85 (36.80) | 32 (40.51) | 53 (34.87) | 0.484 |
| TIA | 5 (2.16) | 1 (1.27) | 4 (2.63) | 0.841 |
| **TOAST classification, *n* (%)** | | | | 0.262 |
| LAA | 151 (65.37) | 45 (56.96) | 106 (69.74) | |
| CE | 58 (25.11) | 25 (31.65) | 33 (21.71) | |
| SOE | 6 (2.60) | 2 (2.53) | 4 (2.63) | |
| SUE | 16 (6.93) | 7 (8.86) | 9 (5.92) | |
| **Imaging parameters** | | | | |
| Occlusion site, *n* (%) | | | | 0.044 |
| BA distal | 76 (32.90) | 34 (43.04) | 42 (27.63) | |
| BA middle | 70 (30.30) | 16 (20.25) | 54 (35.53) | |
| BA proximal | 42 (18.18) | 13 (16.46) | 29 (19.08) | |
| V4 | 43 (18.61) | 16 (20.25) | 27 (17.76) | |
| PC-CS score, median (IQR) | 4 (3–6) | 5 (4–6) | 4 (3–6) | <0.001 |
| **Treatment procedure, *n* (%)** | | | | |
| Intravenous thrombolysis | 49 (21.21) | 15 (18.99) | 34 (22.37) | 0.330 |
| Anesthesia | | | | 0.450 |
| General | 83 (35.93) | 31 (39.24) | 52 (34.21) | |
| Local | 148 (64.07) | 48 (60.76) | 100 (65.79) | |
| **Reperfusion status, *n* (%)** | | | | |
| mTICI | | | | |
| 0–2a | 42 (18.18) | 5 (6.33) | 37 (24.34) | 0.009 |
| 2b−3[a] | 189 (81.18) | 74 (93.67) | 115 (75.66) | |
| **Treatment delay, median (IQR), min** | | | | |
| Onset to puncture | 324.5 (230.5, 494.2) | 266.0 (172.0, 384.0) | 354.0 (250.0, 506.0) | 0.005 |
| Puncture to recanalization | 103.0 (69.5, 144.5) | 86.0 (60.0, 120.0) | 113.0 (79.0, 167.0) | <0.001 |
| Onset to recanalization | 449.0 (326.0, 627.7) | 365.0 (279.0, 499.0) | 485.0 (365.0, 649.0) | <0.001 |

[a]*mTICI score of 2b or 3 indicates satisfied recanalization.*

*BA, basilar artery; mTICI, modified thrombolysis in cerebral infarction; PCA, posterior cerebral artery; V4, V4 segment of vertebral artery; CE, cardioembolism; NIHSS, National Institutes of Health Stroke Scale; PC-ASPECTS, posterior circulation Alberta Stroke Program Early CT Score; SBP, systolic blood pressure; DBP, diastolic blood pressure; SOE, stroke of other determined cause; SUE, stroke of undetermined cause; TIA, transient ischemic attack; TOAST, Trial of ORG 10172 in Acute Stroke Treatment; BPV, brain parenchymal volume; CFV, cerebrospinal fluid volume.*

normalized brain CT images in the standard brain space at the Montreal Neurological Institute by flexible Bayesian modeling and further segmented the total BPV and CFV after skull stripping. Compared with previous methods, CTseg leads to a more robust segmentation that can better handle images with considerable noise and/or large morphological variability (Brudfors et al., 2020). Brain atrophy was then categorized by tertiles in the ratio of BPV–CFV as follows: first tertile (>3.349), mild atrophy; second tertile (3.018–3.349), intermediate atrophy; and third tertile (<3.018), severe atrophy.

## Statistical Analysis

Depending on the normality of the distribution as assessed by the Kolmogorov–Smirnov test, continuous variables were compared using Student's *t*-test for independent samples, or the Mann–Whitney *U*-test or Kruskal–Wallis test for non-normal data. Proportion tests for categorical variables were performed using the chi-square test or Fisher's exact test. The data were presented as mean ± SD, median [interquartile range (IQR)], or as number (percentage), where appropriate. To determine the independent prognostic factors for favorable outcomes, the binary and multivariable logistic regression analyses were performed, and the results were summarized as odds ratios (ORs) with 95% CIs. The restricted cubic spline analyses were employed to characterize the dose–response association and to explore the potential linear or nonlinear relationship between atrophy status and clinical outcome. We used three predefined "knots" (inter-spline dividing values of the independent variable) for transforming the BPV/CFV values for restricted cubic spline analysis (10, 33, and 90th percentiles). The tests for nonlinearity were performed first. If this test was not statistically significant, the test result for overall association and linearity was checked, with a significant result indicating a linear association. We also analyzed the heterogeneity of the effect of brain atrophy status within subgroups based on sex, age (≤65 or >65 years), mTICI (0–2a or 2b−3), NIHSS score (<25 or ≥25), and ASITN/SIR (<2 or ≥2). The areas under the receiver operating characteristic curves (AUCs) were calculated and compared using the DeLong's test. The incremental effects of the severe level of the brain atrophy index for outcome prediction were examined using the net reclassification improvement algorithm (NRI) and the integrated discrimination improvement algorithm (IDI), with the baseline model as a reference. The threshold for statistical significance was set at $P < 0.05$. All statistical analyses were performed using the R software version 3.6.1 (https://www.r-project.org).

# RESULTS

## Baseline Characteristics of the Study Population

The clinical manifestations of the study population at admission are shown in **Table 1**. The average age was 62.74 years and 74.46% of them were men. A total of 152 patients (65.80%) had a history of hypertension and 53 (22.94%) patients had a history of diabetes mellitus. A total of 79 (34.20%) patients achieved favorable outcomes. The PC-ASPECTS score, the PC-CS, and the proportion of mTICI ≥ 2b were significantly higher in patients with favorable outcomes than in those with poor outcomes (90-day mRS ≤3 vs. >3; all $P < 0.01$). In addition, the baseline NIHSS score, the onset-to-puncture time, the puncture-to-recanalization time, and the onset-to-recanalization were significantly elevated in patients with poor outcomes (all $P < 0.05$).

Patients were stratified into three groups according to their brain atrophy levels (**Table 2**). The average age in the highest tertile group was obviously elevated compared with the others [lowest tertile ($N = 77$): 58.19 ± 11.15; intermediate tertile ($N = 77$): 60.26 ± 10.45; highest tertile ($N = 77$): 69.75 ± 11.75, $P < 0.001$]. We also detected significant differences in the proportions of men, atrial fibrillation, and dyslipidemia among these three groups (all $P < 0.05$). None of the other risk factors, including systolic blood pressure, diastolic blood pressure, initial PC-ASPECTS score, and baseline NIHSS, were remarkably affected by the degree of atrophy (all $P > 0.05$).

## The Impact of Brain Atrophy on Clinical Outcome

As shown in **Table 3**, favorable outcomes were least likely among patients with severe atrophy, with lower percentages than in the other atrophy subgroups (mild atrophy vs. intermediate vs. severe: mRS ≤ 3, 41.56 vs. 37.66 vs. 23.38%, $P = 0.044$; mRS ≤ 2, 40.25 vs. 28.57 vs. 22.08%, $P = 0.045$). In the adjusted analysis, intermediate brain atrophy had the same prognostic values as mild brain atrophy (all $P > 0.05$). However, compared with mild brain atrophy, favorable outcomes were less likely to occur in the severe atrophy group [adjusted OR with 95% CI: mRS ≤ 3, 0.21 (0.07–0.62), $P = 0.006$; mRS ≤ 2, 0.18 (0.05–0.58), $P = 0.006$; mRS ≤ 1, 0.22 (0.06, 0.69), $P = 0.014$; **Table 3**).

Previous studies have demonstrated that brain atrophy can promote the survival of patients with anterior circulation stroke (Lee et al., 2010). However, we found no significant correlations between brain atrophy degree and NIHSS score alterations at 24 h, NIHSS score alterations at 5–7 days, or the proportion of ENI (all $P > 0.05$). Both the unadjusted model and the multivariate analysis with adjustment for confounders indicated that brain atrophy level could not improve in-hospital or 90-day mortality (all $P > 0.05$).

## Association of Severe Brain Atrophy With Traditional Risk Factors in Predicting Outcomes of ABAO Treated With EVT

Our restricted cubic spline analysis detected a significant nonlinear association of brain atrophy levels, with favorable clinical outcomes at 3 months ($P$ for non-linear = 0.034, **Figure 1A**) among patients treated with EVT. With all OR and CI values falling below 1, the unique OR and CI distribution patterns of severe atrophy supported the previous results provided in **Table 3** and indicated obviously differential

**TABLE 2 |** Baseline clinical characteristics according to brain atrophy levels.

| | Mild atrophy ($N = 77$)[a] | Intermediate atrophy ($N = 77$)[a] | Severe atrophy ($N = 77$)[a] | *P* |
|---|---|---|---|---|
| Age, years, mean ± SD | 58.19 ± 11.15 | 60.26 ± 10.45 | 69.75 ± 11.75 | <0.001 |
| Male, (*n* %) | 53 (68.83) | 70 (90.91) | 49 (63.64) | <0.001 |
| Baseline NIHSS, median (IQR) | 26.0 (18.0–32.0) | 26.0 (18.0–34.0) | 27.0 (16.0–32.0) | 0.914 |
| PC-ASPECTS, median (IQR) | 8.0 (7.0–9.0) | 8.0 (7.0–9.0) | 8.0 (6.0–9.0) | 0.608 |
| Admission SBP, mmHg, mean ± SD | 142.49 ± 26.00 | 143.90 ± 21.21 | 148.43 ± 21.98 | 0.260 |
| Admission DBP, mmHg, mean ± SD | 84.00 ± 17.30 | 83.86 ± 12.57 | 83.73 ± 15.44 | 0.994 |
| NIHSS at 24 h after EVT, median (IQR) | 23.0 (9.0–35.0) | 27.0 (15.0–34.0) | 30.0 (13.0–35.0) | 0.780 |
| NIHSS at 7 days after EVT, median (IQR) | 15.0 (5.0–35.0) | 18.0 (9.0–35.0) | 23.0 (8.0–35.0) | 0.443 |
| Pre-onset mRS (%) | | | | 0.267 |
| 0 | 72 (93.51) | 64 (83.12) | 70 (90.91) | |
| 1 | 4 (5.19) | 11 (14.29) | 5 (6.49) | |
| 2 | 1 (1.30) | 2 (2.60) | 2 (2.60) | |
| **History of risk factors, *n* (%)** | | | | |
| Hypertension | 48 (62.34) | 52 (67.53) | 52 (67.53) | 0.735 |
| Diabetes mellitus | 24 (31.17) | 17 (22.08) | 12 (15.58) | 0.069 |
| Dyslipidemia | 26 (33.77) | 36 (46.75) | 11 (14.29) | <0.001 |
| Atrial fibrillation | 13 (16.88) | 9 (11.69) | 23 (29.87) | 0.013 |
| TIA | 2 (2.60) | 2 (2.60) | 1 (1.30) | 0.815 |
| **TOAST classification, *n* (%)** | | | | 0.139 |
| LAA | 51 (66.23) | 58 (75.32) | 42 (54.55) | |
| CE | 17 (22.08) | 13 (16.88) | 28 (36.36) | |
| SOE | 2 (2.60) | 2 (2.60) | 2 (2.60) | |
| SUE | 7 (9.09) | 4 (5.19) | 5 (6.49) | |
| **Imaging parameters** | | | | |
| Occlusion site, *n* (%) | | | | 0.326 |
| BA distal | 25 (32.47) | 19 (24.68) | 32 (41.56) | |
| BA middle | 22 (28.57) | 25 (32.47) | 23 (29.87) | |
| BA proximal | 13 (16.88) | 16 (20.78) | 13 (16.88) | |
| V4 | 17 (22.08) | 17 (22.08) | 9 (11.69) | |
| PC-CS score, median (IQR) | 5 (4–6) | 4 (2–5) | 5 (3.5–6) | 0.026 |
| **Treatment procedure, *n* (%)** | | | | |
| Intravenous thrombolysis | 18 (23.38) | 16 (20.78) | 15 (19.48) | 0.834 |
| Anesthesia | | | | 0.073 |
| General | 30 (38.96) | 33 (42.86) | 20 (25.97) | |
| Local | 47 (61.04) | 44 (57.14) | 57 (74.03) | |
| **Reperfusion status, *n* (%)** | | | | |
| mTICI | | | | 0.542 |
| 0–2a | 11 (14.29) | 15 (19.48) | 16 (20.78) | |
| 2b−3[b] | 66 (85.71) | 62 (80.52) | 61 (79.22) | |
| **Treatment delay, median (IQR), min** | | | | |
| Onset to puncture | 315.0 (240.7, 475.7) | 330.0 (191.0, 589.5) | 324.0 (250.1, 440.5) | 0.977 |
| Puncture to recanalization | 102.0 (69.8, 148.0) | 107.0 (79.5, 144.8) | 99.50 (58.0, 136.5) | 0.508 |
| Onset to recanalization | 430.0 (345.8, 617.0) | 454.0 (315.0, 710.0) | 449.5 (331.3, 569.8) | 0.836 |

[a] *Brain atrophy was categorized by tertile based on the ratio of brain parenchymal volume–cerebrospinal fluid volume (BPV–CFV); mild atrophy (first tertile): BPV–CFV >3.349; intermediate atrophy (second tertile): BPV–CFV 3.018–3.349; severe atrophy (third tertile): BPV–CFV < 3.018.*

[b] *mTICI score of 2b or 3 indicates complete recanalization.*

*PC-CS, posterior circulation collateral system score; BA, basilar artery; mTICI, modified thrombolysis in cerebral infarction; PCA, posterior cerebral artery; V4, V4 segment of vertebral artery; CE, cardioembolism; NIHSS, National Institutes of Health Stroke Scale; PC-ASPECTS, posterior circulation Alberta Stroke Program Early CT Score; SBP, systolic blood pressure; DBP, diastolic blood pressure; SOE, stroke of other determined cause; SUE, stroke of undetermined cause; TIA, transient ischemic attack; TOAST, Trial of ORG 10172 in Acute Stroke Treatment.*

**TABLE 3 |** The impact of brain atrophy on clinical outcome.

| Characteristics | Atrophy levels | No./No. (%) | *P*-value | OR (95%CI) | *P* | Adjusted OR (95%CI) | *P* |
|---|---|---|---|---|---|---|---|
| **EFFICACY OUTCOME** | | | | | | | |
| **90-day outcome** | | | | | | | |
| mRS, median (IQR) | Mild | 5 (1–6) | 0.137[a] | Reference | Reference | Reference | Reference |
| | Intermediate | 5 (2–6) | | 1.23 (0.68, 2.34)[c] | 0.493 | 0.69 (0.34, 1.41)[d] | 0.311 |
| | Severe | 5 (3–6) | | 1.96 (1.06, 3.65)[c] | 0.033 | 2.43 (1.17, 5.12)[d] | 0.018 |
| mRS 0-3 | Mild | 32 (41.56) | 0.044[b] | Reference | Reference | Reference | Reference |
| Intermediate | 29 (37.66) | | 0.85 (0.44, 1.62) | 0.621 | 2.11 (0.82, 5.74) | 0.131 | |
| | Severe | 18 (23.38) | | 0.43 (0.21, 0.85) | 0.017 | 0.21 (0.07, 0.62) | 0.006 |
| mRS 0-2 | Mild | 31 (40.25) | 0.045[b] | Reference | Reference | Reference | Reference |
| | Intermediate | 22 (28.57) | | 0.59 (0.30, 1.16) | 0.128 | 1.13 (0.42, 3.08) | 0.814 |
| | Severe | 17 (22.08) | | 0.42 (0.20, 0.84) | 0.016 | 0.18 (0.05, 0.58) | 0.006 |
| mRS 0-1 | Mild | 26 (33.77) | 0.066[b] | Reference | Reference | Reference | Reference |
| | Intermediate | 17 (22.08) | | 0.56 (0.27, 1.13) | 0.108 | 0.93 (0.32, 2.70) | 0.890 |
| | Severe | 14 (18.18) | | 0.44 (0.20, 0.91) | 0.029 | 0.22 (0.06, 0.69) | 0.014 |
| **NIHSS SCORE** | | | | | | | |
| Change from baseline at | Mild | 0.00 (−4.00–2.00) | 0.455[a] | Reference | Reference | Reference | Reference |
| 24 h, median (IQR) | Intermediate | 0.00 (−4.00, 2.00) | | 1.78 (−1.44 to 5.00)[e] | 0.278 | 0.39 (−2.71 to 3.49)[e] | 0.805 |
| | Severe | 0.00 (2.00, 2.00) | | 2.48 (−0.74 to 5.70)[e] | 0.131 | 1.54 (−1.68 to 4.77)[f] | 0.346 |
| Change from baseline at | Mild | −4.0 (−14.00, 2.00) | 0.285[a] | Reference | Reference | Reference | Reference |
| 5–7 d, median (IQR) | Intermediate | −2.00 (−15.00, 2.00) | | 1.69 (−2.44 to 5.81)[f] | 0.421 | −0.87 (−4.56 to 2.82)[f] | 0.642 |
| | Severe | 0.00 (−9.00, 4.00) | | 3.78 (−0.35 to 7.90)[f] | 0.072 | 2.02 (−1.82 to 5.86)[f] | 0.300 |
| ENI[g] | Mild | 14 (18.18) | 0.916[b] | Reference | Reference | Reference | Reference |
| | Intermediate | 13 (16.88) | | 0.91 (0.39, 2.11) | 0.832 | 2.50 (0.77, 8.94) | 0.139 |
| | Severe | 15 (19.48) | | 1.09 (0.48, 2.46) | 0.837 | 1.99 (0.65, 6.51) | 0.227 |
| **SAFETY OUTCOMES** | | | | | | | |
| Mortality in hospital | Mild | 15 (19.48) | 0.770[b] | Reference | Reference | Reference | Reference |
| | Intermediate | 15 (19.48) | | 1.00 (0.45, 2.23) | 1.000 | 0.90 (0.35, 2.34) | 0.832 |
| | Severe | 12 (15.58) | | 0.76 (0.33,1.76) | 0.526 | 0.69 (0.22, 2.07) | 0.511 |
| Mortality at 90 d | Mild | 29 (37.66) | 0.502[b] | Reference | Reference | Reference | Reference |
| | Intermediate | 34 (44.16) | | 1.18 (0.62, 2.25) | 0.621 | 0.59 (0.22, 1.52) | 0.285 |
| | Severe | 36 (46.75) | | 1.45 (0.77, 2.78) | 0.254 | 1.26 (0.47, 3.36) | 0.636 |
| SICH | Mild | 4 (5.19) | 0.768[b] | Reference | Reference | Reference | Reference |
| | Intermediate | 3 (3.90) | | 0.74 (0.14, 3.47) | 0.700 | 0.86 (0.13, 5.57) | 0.870 |
| | Severe | 5 (6.49) | | 1.27 (0.32, 5.30) | 0.732 | 0.47 (0.08, 2.83) | 0.404 |

[a] *Wilcoxon test.*
[b] *Chi-square test.*
[c] *Common odds ratio.*
[d] *Adjusted common odds ratio; adjusted estimates of outcome were calculated using multiple regression, taking the following variables into account: age, sex, dyslipidemia, atrial fibrillation, baseline NIHSS score, baseline PC-ASPECTS, mTICI, PC-CS, and onset to recanalization time.*
[e] *β-values were estimated from a univariate linear regression model.*
[f] *β-values were estimated from a multivariable linear regression model; adjusted estimates of outcome were calculated using multiple regression, taking the following variables into account: age, sex, dyslipidemia, atrial fibrillation, baseline NIHSS score, baseline PC-ASPECTS, mTICI, PC-CS, and onset to recanalization time.*
[g] *ENI: early neurological improvement was estimated by a reduction of > 8 or return to 0 on NIHSS compared with baseline score at 24 h after EVT.*
*EVT, endovascular treatment; NIHSS, National Institutes of Health Stroke Scale; mRS, modified Rankin Scale score at 90 days.*

prognostic roles of severe brain atrophy from mild and intermediate atrophy.

The frequency of favorable outcomes (mRS $\leq$ 3) in patients with severe brain atrophy was significantly lower than that of the other groups (severe vs. non-severe: 23.38 vs. 39.61%, $P = 0.014$; **Figure 1B**). In the multivariate analysis with adjustment for confounders, the severe brain atrophy level was found to be significantly negatively correlated with the incidence of mRS $\leq$3 [adjusted OR with 95% CI 0.22 (0.08–0.53), $P = 0.001$, **Figure 1C**].

The univariate and multivariate analyses were used to explore the association of severe brain atrophy with traditional risk factors in predicting the outcomes for patients with ABAO after EVT (**Table 4**). Univariate logistic regression showed that severe brain atrophy, NIHSS score at baseline, PC-ASPECTS, and PC-CS were related to the outcomes in patients with ABAO

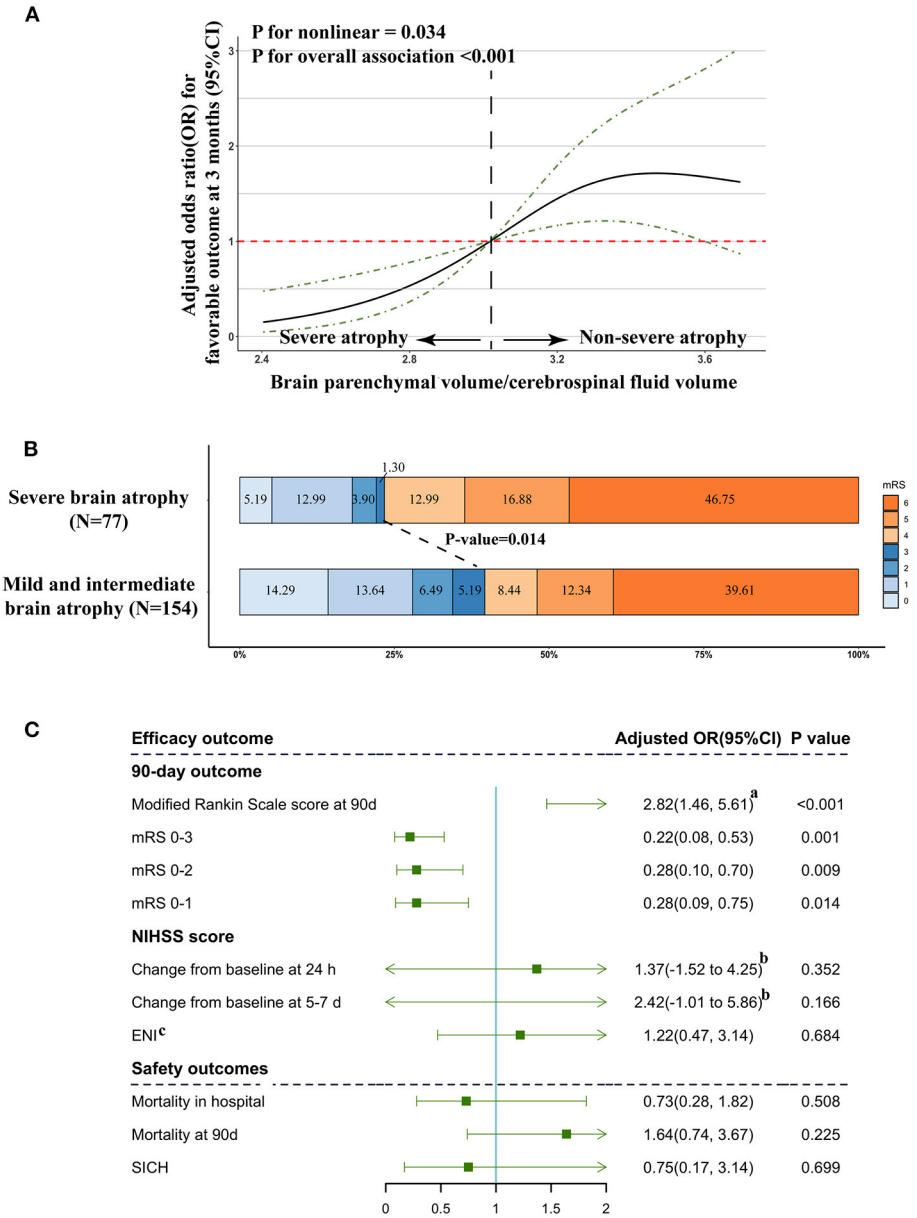


**FIGURE 1 |** Association of severe brain atrophy with clinical outcome. **(A)** Association of brain atrophy with favorable outcome (mRS ≤ 3) in a restricted cubic spline model. Brain atrophy was estimated by quantifying BPV/CFV. ORs, solid line; 95% CI, dashed lines. **(B)** Primary outcomes according to brain atrophy status. Distribution of modified Rankin Scale (mRS) scores at 3 months in patients treated with endovascular treatment. **(C)** Multivariable logistic regression analysis revealed the relationship between brain atrophy and efficacy outcome and safety outcome. Adjusted estimates of outcome were calculated using multiple regression, taking the following variables into account: age, sex, dyslipidemia, atrial fibrillation, baseline NIHSS score, baseline PC-ASPECTS, mTICI, PC-CS, and onset to recanalization time. (a) Common odds ratio; (b) $\beta$ and 95% CI values were estimated from a multivariable linear regression model, which was adjusted by multiple regression, taking the following variables into account: age, sex, dyslipidemia, atrial fibrillation, baseline NIHSS score, baseline PC-ASPECTS, mTICI, PC-CS score, and onset to recanalization time. (c) ENI: early neurological improvement was estimated by a reduction of > 8 or return to 0 on NIHSS compared with baseline score at 24 h after EVT.

after EVT (all $P < 0.05$). Multivariable logistic regression that included predictors identified by using the univariate analysis (at $P < 0.05$) further identified the following independent predictors of favorable outcomes (mRS ≤ 3) after EVT: severe brain atrophy [adjusted OR with 95% CI, 0.33 (0.15, 0.70), $P = 0.005$], NIHSS score at baseline [adjusted OR with 95% CI, 0.97 (0.93–1.00), $P = 0.072$], PC-ASPECTS [adjusted OR with 95% CI, 1.82 (1.44, 2.36), $P < 0.001$], mTICI [adjusted OR with 95% CI,

**TABLE 4 |** The association of severe brain atrophy and traditional risk factors in predicting outcome.

| | Univariate analysis | | Multivariate analysis | |
|---|---|---|---|---|
| | **OR (95% CI)** | ***p*-value** | **Adjusted OR (95% CI)** | ***p*-value** |
| Severe atrophy | 0.47 (0.25, 0.85) | 0.015 | 0.33 (0.15, 0.70) | 0.005 |
| Age | 0.98 (0.96, 1.01) | 0.176 | | |
| Sex | 0.76 (0.41, 1.41) | 0.370 | | |
| Dyslipidemia | 1.55 (0.87, 2.76) | 0.134 | | |
| Diabetes mellitus | 0.79 (0.4, 1.51) | 0.484 | | |
| Hypertension | 1.42 (0.8, 2.58) | 0.241 | | |
| Atrial fibrillation | 1.53 (0.78, 2.98) | 0.208 | | |
| SBP | 1.00 (0.99, 1.02) | 0.460 | | |
| DBP | 1.00 (0.98, 1.01) | 0.727 | | |
| TIA | 0.47 (0.02, 3.27) | 0.508 | | |
| TOAST | 1.11 (0.78, 1.56) | 0.555 | | |
| Occlusion Sites | 0.90 (0.70, 1.15) | 0.392 | | |
| Thrombolysis treatment | 0.81 (0.40, 1.58) | 0.551 | | |
| Preonset mRS | 0.85 (0.39, 1.69) | 0.659 | | |
| Anesthesia | 1.13 (0.81, 1.57) | 0.463 | | |
| Onset to recanalization time | 0.99 (0.99, 1.00) | 0.591 | | |
| NIHSS baseline | 0.94 (0.91, 0.97) | <0.001 | 0.97 (0.93, 1.00) | 0.072 |
| PC-ASPECTS | 1.98 (1.59, 2.51) | <0.001 | 1.82 (1.44, 2.36) | <0.001 |
| mTICI | 1.68 (1.33, 2.19) | <0.001 | 1.80 (1.35, 2.50) | <0.001 |
| PC-CS score | 1.89 (1.43, 2.54) | <0.001 | 1.31 (1.09, 1.60) | 0.005 |

*SBP, systolic blood pressure; DBP, diastolic blood pressure; TIA, transient ischemic attack; TOAST, Trial of ORG 10172 in Acute Stroke Treatment; PC-CS score, posterior circulation collateral system score; mTICI, modified thrombolysis in cerebral infarction; PC-ASPECTS, posterior circulation Alberta Stroke Program Early CT Score.*

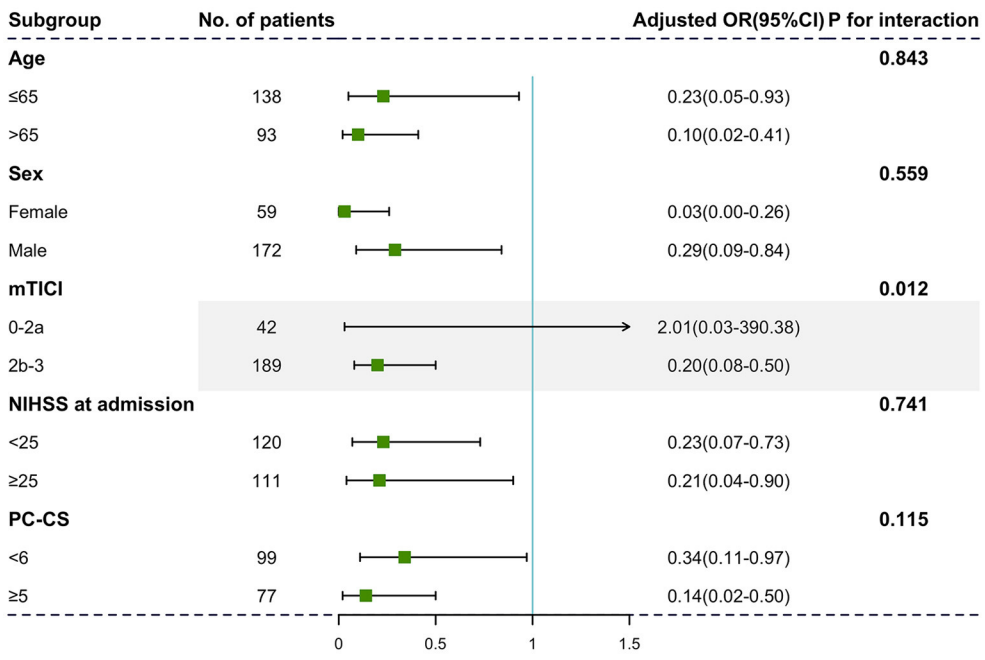


**FIGURE 2 |** Subgroup analyses of primary outcomes. The forest plot showed the differences in odds ratios for favorable outcomes (defined as the modified Rankin Scale score of 0–3) at 3 months in the prespecified subgroups. Adjusted variables are as follows: age, sex, dyslipidemia, atrial fibrillation, baseline NIHSS score, baseline PC-ASPECTS, mTICI, PC-CS, and onset to recanalization time.

1.80 (1.35, 2.50), $P < 0.001$], and PC-CS score [adjusted OR with 95% CI, 1.31 (1.09, 1.60), $P = 0.005$].

## Subgroup Analysis

Identical negative effects of severe brain atrophy on 90-day outcome were found in patients in different age strata [**Figure 2**, age ≤65: adjusted OR with 95% CI, 0.23 (0.05–0.93); age >65: adjusted OR with 95% CI, 0.10 (0.02–0.41)]. Although we did not identify significant interactions between sex and initial NIHSS score, the relationship between severe brain atrophy and unfavorable outcome was more obvious in those with satisfied reperfusion levels (mTICI ≥ 2b, $P$ for interaction = 0.012).

## Incremental Effect of the Severe Brain Atrophy Index on the Predictive Value of the Baseline Model

The addition of the severe brain atrophy index significantly increased the ability of the baseline model to predict the outcomes in individuals with satisfactory reperfusion levels (mTICI ≥ 2b) and yielded a statistically elevated AUC value [baseline model vs. baseline model + severe atrophy: 0.809 (95% CI: 0.75–0.87) vs. 0.851 (95% CI: 0.80–0.91), $P = 0.022$ by using the DeLong's test; **Figure 3**]. Significant improvements in risk reclassification and discrimination were also detected after adding the severe brain atrophy index into the baseline model, with an NRI of 0.40 (95% CI: 0.12–0.69, $P = 0.006$) and an IDI of 0.04 (95% CI: 0.01–0.07, $P = 0.005$).

The roles of brain atrophy can play in assisting clinical decision-making, namely, receiving medicine or EVT has also been explored. The clinical manifestations of patients receiving medical treatment only are given in **Supplementary Table 1**, and the outcomes obtained by comparing patients treated with EVT with those treated with medical management only are given in **Supplementary Table 2**. No differences were observed in favorable outcomes or mortality between patients with ABAO with severe brain atrophy who received different treatment methods (all $P > 0.05$). However, in patients without severe brain atrophy, the EVT cohort presented a remarkably higher rate of favorable functional outcome (39.61 vs. 6.82%; $P < 0.001$) than the medical management only group. As given in **Supplementary Table 3**, the multivariate analysis confirmed that the following measures were associated with favorable outcome in patients with ABAO without severe brain atrophy: initial NIHSS score [adjusted OR with 95% CI: 0.96 (0.92–0.99), $P = 0.030$], PC-ASPECTS [adjusted OR with 95% CI: 1.78 (1.38–2.36), $P < 0.001$], and intervention treatment [adjusted OR with 95% CI: 11.76 (3.53–55.76), $P < 0.001$]. However, intervention treatment was not significantly related to favorable outcomes in patients with ABAO with severe brain atrophy ($P > 0.05$).

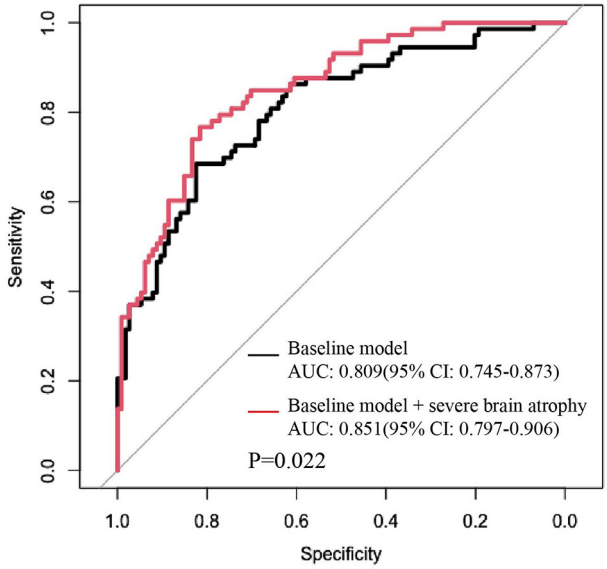


**FIGURE 3 |** Adding severe brain atrophy index into the baseline model obviously increased its discrimination ability in predicting favorable outcomes among patients with a satisfied reperfusion level (mTICI ≥ 2b). Baseline model: multivariable logistic model constructed by age, sex, dyslipidemia, atrial fibrillation, baseline NIHSS score, baseline PC-ASPECTS, mTICI, PC-CS, and onset to recanalization time.

# DISCUSSION

Based on a multi-centered cohort derived from the BASILAR research, this is, to our knowledge, the first study to explore the association between brain atrophy and clinical outcomes for patients with ABAO treated with EVT. Our findings revealed that (1) severe brain atrophy implied poor long-term recovery status, (2) severe brain atrophy could not promote either overall 90-day mortality or in-hospital mortality in patients with ABAO treated with EVT, and (3) adding a severe brain atrophy index to the baseline model yielded a statistically significant improvement in predictions of poor outcomes. The automatic quantitative analysis of brain atrophy applied in this study ensured the reliability of the present analysis and remarkably extended the applicability of our findings.

In the acute stage following EVT, no significant association between brain atrophy and in-hospital mortality was detected in patients with ABAO, a remarkably different result from that of patients with anterior circulation stroke. Candica et al. detected an inverse association between severe atrophy and 7-day death in patients with anterior circulation stroke (Delcourt et al., 2020). Lee et al. demonstrated that brain atrophy might be protective in anterior circulation stroke due to the presence of greater residual intracerebral space available for absorbing the disruption of space-occupying lesions, thus preventing herniation and death (Lee et al., 2010). Two factors might contribute to these discrepancies. First, due to the limited subtentorial space at baseline, severe global brain atrophy might not provide enough room to compensate for the increased regional volume caused by the edema of infratentorial infarctions (Neugebauer et al., 2013). Second, multiple key brain areas such as the midbrain and pons, which regulate a variety of crucial physiological functions, are frequently impaired in patients with ABAO, which

might directly result in poor outcomes in the acute phase after EVT, and this dysfunction will not be relieved by the increased residual space available from brain atrophy (Meinel et al., 2019). Overall, the evidence shows that the failure of brain atrophy to improve patient survival guarantees the safety of using severe brain atrophy as a novel prognostic indicator for EVT for ABAO.

As for the long-term prognosis after EVT, this study demonstrated severe cerebral atrophy to be strongly associated with unfavorable 90-day clinical outcomes, which is in line with previous studies on anterior circulation stroke (Pedraza et al., 2020). The decreased ischemic tolerance ability and impaired capacity to adapt and reorganize after stroke might be the dominant mechanisms underlying the prognostic roles of severe brain atrophy in ABAO after EVT (Adduru et al., 2020). Interestingly, we did not detect significant alterations in NIHSS or PC-ASPECTS at admission among different brain atrophy levels. This result agreed with previous findings from the Lauksio, Lee, and Pranita groups focusing on the roles of brain atrophy in outcome evaluation for patients with anterior circulation stroke (Lee et al., 2010; Lauksio et al., 2020; Kaginele et al., 2021). The effect of brain atrophy on prognosis might reflect a reduced ability of recovery after stroke rather than a blunting of the initial stroke severity or PC-ASPECTS (Lee et al., 2010; Schaapsmeerders et al., 2015). In addition, PC-ASPECTS and NIHSS scores were significantly related to onset to treatment time, occlusion sites, and collateral circulation, which might not be affected by brain atrophy status and were also identical among different atrophy groups in this study (Yoshimura et al., 2018; Aoki et al., 2019; Guillaume et al., 2019; Sang et al., 2021). Taken together, the significant relationships that we observed between brain atrophy and favorable outcomes demonstrate the effectiveness of incorporating brain atrophy into the prognosis assessment system for patients with ABAO treated with EVT.

Aging is considered an important contributor to brain atrophy (Moroni et al., 2020). However, the role of aging in determining outcomes in ABAO remains controversial. Kang et al. showed that younger age was significantly associated with a favorable shift in the overall distribution of 90-day mRS (Kang et al., 2018). In contrast, Bouslama et al. found that age was not associated with good outcomes (Bouslama et al., 2017). Our results show that age does not result in significantly greater odds of a poorer clinical outcome after EVT in patients with ABAO, while brain atrophy was a more reliable outcome predictor than age in both univariate and multivariate analyses. Compared with biological aging alone, brain atrophy is the end-organ effect of cumulative risk factors on brain structures that include aging, disease history, education, and vascular risk factors, which might be more directly related to the health status of brain tissues than aging and lead to its outperformance when predicting outcomes (Cole et al., 2015; Pini et al., 2016). These findings proved the necessity of incorporating brain atrophy besides age into the inclusion criteria of future clinical trials on ABAO.

This study had several limitations. First, compared with the CT used in this study, MRI detects cerebral atrophy with better accuracy and provides a more comprehensive imaging assessment of brain region volume. However, CT is the most frequent type of brain image used to diagnose ischemic stroke and has few contraindications. Our approach reflects the clinical practice and generalizes the clinical application of this index. Second, besides atrophy, old infarcts and white matter hyperintensity are also biomarkers for brain frailty (Delcourt et al., 2020). The interaction of old infarcts, white matter hyperintensity, brain atrophy, and clinical outcomes requires further exploration. Third, although we estimated the degree of global brain atrophy automatically and objectively, the atrophy level of specific brain regions such as subtentorial tissues might provide additional prognostic information, and we are carrying out research to further identify imaging markers from specific brain regions.

## CONCLUSION

Severe brain atrophy might be an independent risk factor for unfavorable clinical outcomes among ABAO subjects after EVT and add prognostic information to the conventional model. Brain atrophy could serve as a novel imaging biomarker to be integrated into the clinical decision-making system to better identify suitable patients for EVT.

## DATA AVAILABILITY STATEMENT

The raw data supporting the conclusions of this article will be made available by the authors, without undue reservation.

## CODE AVAILABILITY STATEMENT

The analyzing codes of this study are available from the corresponding author upon reasonable request.

## ETHICS STATEMENT

The studies involving human participants were reviewed and approved by the *post-hoc* analysis of BASILAR registry, which was registered on the Chinese Clinical Trial Registry (ChiCTR1800014759). The study was approved by the research board at each participating center and informed consents were obtained from all patients or their authorized representatives. The patients/participants provided their written informed consent to participate in this study.

## AUTHOR CONTRIBUTIONS

CL performed most of the experiments, interpreted data, and wrote the first draft of the paper. HL and DW performed a part of experiments and analyzed the data. ZZ, WH, and ZW took part to conceive the study and a part of sample collection. WZ and QY critically edited the manuscript and supervised the study. QY mainly provided funding and designed

the study. All authors contributed to the article and approved the submitted version.

## FUNDING

This work was supported by the National Natural Science Foundation of China (Nos. 81901236, 82071323, and 82001264), the Chongqing Natural Science Foundation (No. cstc2020jcyj-msxmX0926), and the Clinical Medical Research Talent Training Program of Army Medical University (Nos. 2019XLC2008 and 2019XLC3016).

## ACKNOWLEDGMENTS

The authors thank the Ashburner group in Wellcome Trust Centre for Neuroimaging for providing the CT-based automated analysis.

## SUPPLEMENTARY MATERIAL

The Supplementary Material for this article can be found online at: https://www.frontiersin.org/articles/10.3389/fnagi.2021.720061/full#supplementary-material

## REFERENCES

Adduru, V., Baum, S. A., Zhang, C., Helguera, M., Zand, R., Lichtenstein, M., et al. (2020). A method to estimate brain volume from head CT images and application to detect brain atrophy in Alzheimer disease. *Am. J. Neuroradiol.* 41, 224–230. doi: 10.3174/ajnr.A6402

Aoki, J., Suzuki, K., Kanamaru, T., Kutsuna, A., Katano, T., Takayama, Y., et al. (2019). Association between initial NIHSS score and recanalization rate after endovascular thrombectomy. *J. Neurol. Sci.* 403, 127–132. doi: 10.1016/j.jns.2019.06.033

Appleton, J. P., Woodhouse, L. J., Adami, A., Becker, J. L., Berge, E., Cala, L. A., et al. (2020). Imaging markers of small vessel disease and brain frailty, and outcomes in acute stroke. *Neurology* 94, e439–e452. doi: 10.1212/WNL.0000000000008881

Bouslama, M., Haussen, D. C., Aghaebrahim, A., Grossberg, J. A., Walker, G., Rangaraju, S., et al. (2017). Predictors of good outcome after endovascular therapy for vertebrobasilar occlusion stroke. *Stroke* 48, 3252–3257. doi: 10.1161/STROKEAHA.117.018270

Brudfors, M., Balbastre, Y., Flandin, G., Nachev, P., and Ashburner, J. (2020). "Flexible bayesian modelling for nonlinear image registration," in *Medical Image Computing and Computer Assisted Intervention - MICCAI 2020. MICCAI 2020. Lecture Notes in Computer Science*, Vol. 12263, eds A. L. Martel et al. (Cham: Springer). doi: 10.1007/978-3-030-59716-0_25

Cole, J. H., Leech, R., and Sharp, D. J. (2015). Alzheimer's disease neuroimaging I prediction of brain age suggests accelerated atrophy after traumatic brain injury. *Ann. Neurol.* 77, 571–581. doi: 10.1002/ana.24367

Delcourt, C., Wang, X., Zhou, Z., Wardlaw, J. M., Mair, G., Robinson, T. G., et al. (2020). Brain imaging abnormalities and outcome after acute ischaemic stroke: the ENCHANTED trial. *J. Neurol. Neurosurg. Psychiatr.* 91, 1290–1296. doi: 10.1136/jnnp-2020-323015

Guenego, A., Bourcier, R., Guillen, M., Weisenburger-Lile, D., Lapergue, B., Gory, B., et al. (2021). Neurological improvement predicts clinical outcome after acute basilar artery stroke thrombectomy. *Eur. J. Neurol.* 28, 117–123. doi: 10.1111/ene.14487

Guillaume, M., Lapergue, B., Gory, B., Labreuche, J., Consoli, A., Mione, G., et al. (2019). Rapid successful reperfusion of basilar artery occlusion strokes with pretreatment diffusion-weighted imaging posterior-circulation ASPECTS <8 is associated with good outcome. *J. Am. Heart Assoc.* 8:e010962. doi: 10.1161/JAHA.118.010962

Kaginele, P., Beer-Furlan, A., Joshi, K. C., Kadam, G., Achanaril, A., Levy, E., et al. (2021). Brain atrophy and leukoaraiosis correlate with futile stroke thrombectomy. *J. Stroke Cerebrovasc. Dis.* 30:105871. doi: 10.1016/j.jstrokecerebrovasdis.2021.105871

Kang, D. H., Jung, C., Yoon, W., Kim, S. K., Baek, B. H., Kim, J. T., et al. (2018). Endovascular thrombectomy for acute basilar artery occlusion: a multicenter retrospective observational study. *J. Am. Heart Assoc.* 7:9419. doi: 10.1161/JAHA.118.009419

Langezaal, L. C. M., van der Hoeven, E., Mont'Alverne, F. J. A., de Carvalho, J. J. F., Lima, F. O., Dippel, D. W. J., et al. (2021). Endovascular therapy for stroke due to basilar-artery occlusion. *N. Engl. J. Med.* 384, 1910–1920. doi: 10.1056/NEJMoa2030297

Lauksio, I., Lindstrom, I., Khan, N., Sillanpaa, N., Hernesniemi, J., Oksala, N., et al. (2020). Brain atrophy predicts mortality after mechanical thrombectomy of proximal anterior circulation occlusion. *J. Neurointerv. Surg.* 2020:16168. doi: 10.1136/neurintsurg-2020-016168

Lee, S. H., Oh, C. W., Han, J. H., Kim, C. Y., Kwon, O. K., Son, Y. J., et al. (2010). The effect of brain atrophy on outcome after a large cerebral infarction. *J. Neurol.* Neurosurg. Psychiatr. 81, 1316–1321. doi: 10.1136/jnnp.2009.197335

Liu, X., Dai, Q., Ye, R., Zi, W., Liu, Y., Wang, H., et al. (2020). Endovascular treatment versus standard medical treatment for vertebrobasilar artery occlusion (BEST): an open-label, randomised controlled trial. *Lancet Neurol.* 19, 115–122. doi: 10.1016/S1474-4422(19)30395-3

Mattle, H. P., Arnold, M., Lindsberg, P. J., Schonewille, W. J., and Schroth, G. (2011). Basilar artery occlusion. *Lancet Neurol.* 10, 1002–1014. doi: 10.1016/S1474-4422(11)70229-0

Meinel, T. R., Kaesmacher, J., Chaloulos-Iakovidis, P., Panos, L., Mordasini, P., Mosimann, P. J., et al. (2019). Mechanical thrombectomy for basilar artery occlusion: efficacy, outcomes, and futile recanalization in comparison with the anterior circulation. *J. Neurointerv. Surg.* 11, 1174–1180. doi: 10.1136/neurintsurg-2018-014516

Moroni, F., Ammirati, E., Hainsworth, A. H., and Camici, P. G. (2020). Association of white matter hyperintensities and cardiovascular disease: the importance of microcirculatory disease. *Circ. Cardiovasc. Imag.* 13:e010460. doi: 10.1161/CIRCIMAGING.120.010460

Neugebauer, H., Witsch, J., Zweckberger, K., and Juttler, E. (2013). Space-occupying cerebellar infarction: complications, treatment, and outcome. *Neurosurg. Focus* 34:E8. doi: 10.3171/2013.2.FOCUS12363

Pedraza, M. I., de Lera, M., Bos, D., Calleja, A. I., Cortijo, E., Gomez-Vicente, B., et al. (2020). Brain atrophy and the risk of futile endovascular reperfusion in acute ischemic stroke. *Stroke* 51, 1514–1521. doi: 10.1161/STROKEAHA.119.028511

Pini, L., Pievani, M., Bocchetta, M., Altomare, D., Bosco, P., Cavedo, E., et al. (2016). Brain atrophy in Alzheimer's disease and aging. *Ageing Res. Rev.* 30, 25–48. doi: 10.1016/j.arr.2016.01.002

Sang, H., Li, F., Yuan, J., Liu, S., Luo, W., Wen, C., et al. (2021). Values of baseline posterior circulation acute stroke prognosis early computed tomography score for treatment decision of acute basilar artery occlusion. *Stroke* 52, 811–820. doi: 10.1161/STROKEAHA.120.031371

Schaapsmeerders, P., van Uden, I. W., Tuladhar, A. M., Maaijwee, N. A., van Dijk, E. J., Rutten-Jacobs, L. C., et al. (2015). Ipsilateral hippocampal atrophy is associated with long-term memory dysfunction after ischemic stroke in young adults. *Hum. Brain Mapp.* 36, 2432–2442. doi: 10.1002/hbm.22782

van der Hoeven, E. J., McVerry, F., Vos, J. A., Algra, A., Puetz, V., Kappelle, L. J., et al. (2016). Collateral flow predicts outcome after basilar artery occlusion: the posterior circulation collateral score. *Int. J. Stroke* 11, 768–775. doi: 10.1177/1747493016641951

Writing Group for the BASILAR Group, Zi, W., Qiu, Z., Wu, D., Li, F., Liu, H., et al. (2020). Assessment of endovascular treatment for acute basilar artery occlusion *via* a nationwide prospective registry. *J. Am. Med. Assoc. Neurol.* 77, 561–573. doi: 10.1001/jamaneurol.2020.0156

Yoshimura, S., Lindley, R. I., Carcel, C., Sato, S., Delcourt, C., Wang, X., et al. (2018). NIHSS cut point for predicting outcome in supra- vs. infratentorial acute ischemic stroke. *Neurology* 91, e1695–e1701. doi: 10.1212/WNL.0000000000006437

**Conflict of Interest:** The authors declare that the research was conducted in the absence of any commercial or financial relationships that could be construed as a potential conflict of interest.

**Publisher's Note:** All claims expressed in this article are solely those of the authors and do not necessarily represent those of their affiliated organizations, or those of the publisher, the editors and the reviewers. Any product that may be evaluated in this article, or claim that may be made by its manufacturer, is not guaranteed or endorsed by the publisher.

frontiers in Aging Neuroscience

ORIGINAL RESEARCH
published: 01 September 2021
doi: 10.3389/fnagi.2021.692615

# Rebleeding of Ruptured Intracranial Aneurysm After Admission: A Multidimensional Nomogram Model to Risk Assessment

*Qingyuan Liu[1], Yi Yang[1], Junhua Yang[1], Maogui Li[1], Shuzhe Yang[1], Nuochuan Wang[2], Jun Wu[1], Pengjun Jiang[1]* and Shuo Wang[1,3]**

[1] Department of Neurosurgery, Beijing Tiantan Hospital, Capital Medical University, Beijing, China, [2] Department of Blood Transfusion, Beijing Tiantan Hospital, Capital Medical University, Beijing, China, [3] China National Clinical Research Center for Neurological Diseases, Beijing, China*

**Objective:** Rebleeding is recognized as the main cause of mortality after intracranial aneurysm rupture. Though timely intervention can prevent poor prognosis, there is no agreement on the surgical priority and choosing medical treatment for a short period after rupture. The aim of this study was to investigate the risk factors related to the rebleeding after admission and establish predicting models for better clinical decision-making.

**Methods:** The patients with ruptured intracranial aneurysms (RIAs) between January 2018 and September 2020 were reviewed. All patients fell to the primary and the validation cohort by January 2020. The hemodynamic parameters were determined through the computational fluid dynamics simulation. Cox regression analysis was conducted to identify the risk factors of rebleeding. Based on the independent risk factors, nomogram models were built, and their predicting accuracy was assessed by using the area under the curves (AUCs).

**Result:** A total of 577 patients with RIAs were enrolled in this present study, 86 patients of them were identified as undergoing rebleeding after admission. Thirteen parameters were identified as significantly different between stable and rebleeding aneurysms in the primary cohort. Cox regression analysis demonstrated that six parameters, including hypertension [hazard ratio (HR), 2.54; $P = 0.044$], bifurcation site (HR, 1.95; $P = 0.013$), irregular shape (HR, 4.22; $P = 0.002$), aspect ratio (HR, 12.91; $P < 0.001$), normalized wall shear stress average (HR, 0.16; $P = 0.002$), and oscillatory stress index (HR, 1.14; $P < 0.001$) were independent risk factors related to the rebleeding after admission. Two nomograms were established, the nomogram including clinical, morphological, and hemodynamic features (CMH nomogram) had the highest predicting accuracy (AUC, 0.92), followed by the nomogram including clinical and morphological features (CM nomogram; AUC, 0.83), ELAPSS score (AUC, 0.61), and PHASES score (AUC, 0.54). The calibration curve for the probability of rebleeding showed good agreement between prediction by nomograms and actual observation. In the validation cohort, the

OPEN ACCESS

**Edited by:**
*Kewei Chen,*
*Banner Alzheimer's Institute,*
*United States*

**Reviewed by:**
*Philipp Berg,*
*Otto von Guericke University Magdeburg, Germany*
*Shengzhang Wang,*
*Fudan University, China*
*Xinjian Yang,*
*Capital Medical University, China*

***Correspondence:**
*Shuo Wang*
*captain9858@126.com*
*Pengjun Jiang*
*yizhefly@126.com*

**Received:** *08 April 2021*
**Accepted:** *28 June 2021*
**Published:** *01 September 2021*

**Citation:**
*Liu Q, Yang Y, Yang J, Li M, Yang S, Wang N, Wu J, Jiang P and Wang S (2021) Rebleeding of Ruptured Intracranial Aneurysm After Admission: A Multidimensional Nomogram Model to Risk Assessment. Front. Aging Neurosci. 13:692615. doi: 10.3389/fnagi.2021.692615*

discrimination of the CMH nomogram was superior to the other models (AUC, 0.93 vs. 0.86, 0.71 and 0.48).

**Conclusion:** We presented two nomogram models, named CMH nomogram and CM nomogram, which could assist in identifying the RIAs with high risk of rebleeding.

**Keywords: ruptured intracranial aneurysms, rebleeding, morphology, hemodynamics, multidimensional predicting model**

## INTRODUCTION

Intracranial aneurysms (IAs), a common cerebrovascular disease in the aging population, refer to the main cause of subarachnoid hemorrhage. Rebleeding is recognized as a catastrophic event with high mortality after aneurysmal subarachnoid hemorrhage (aSAH) (Rosenørn et al., 1987; Jaechan et al., 2015; Kienzler et al., 2016). Though timely surgical intervention can effectively protect aSAH patients from poor outcome (Ko et al., 2011; Cordonnier et al., 2018; Darkwah Oppong et al., 2018), for several reasons, a notable number of patients cannot receive treatment as soon as they are sent to a hospital. For the reason that the most rebleeding occurs within 6 h after the initial hemorrhage (Rosenørn et al., 1987; Hijdra et al., 1988; Jaechan et al., 2015), patients to be prioritized should be determined.

The key to making medical decisions for this condition is to identify the rebleeding risk of ruptured intracranial aneurysms (RIAs). However, a predicting model has not been built, or reliable factors have not been set to discriminate the RIAs at high risk of rebleeding. There are several aspects involved in the mechanism of IAs rupture, which primarily include the structure damage of the aneurysm wall (Frösen et al., 2012) and the hemodynamic condition of IAs (Meng et al., 2012, 2014; Dolan et al., 2013). Though some comorbidities could elevate the risk of rebleeding (e.g., hypertension), rebleeding still occurred in approximately 22% of patients after they had received the effective management (Boogaarts et al., 2015). It is noteworthy that some existing studies reported that morphological characteristics could predict the risk of rebleeding after aSAH (Starke et al., 2011; Boogaarts et al., 2015). However, a meta-analysis revealed the low quality of current evidence and low predicting accuracy of reported parameters (Boogaarts et al., 2015), which may be insufficient in clinical risk assessment. As indicated from our preliminary study, the hemodynamic characteristics could help discriminate the RIAs at high risk of rebleeding (Liu et al., 2019). Based on the mentioned facts, this study assumed that building a multidimensional predicting model can effectively discriminate the RIAs at high risk of rebleeding.

**Abbreviations:** IA, intracranial aneurysm; RIA, ruptured intracranial aneurysm; aSAH, aneurysmal subarachnoid hemorrhage; CT, computational tomography; mFS, modified Fisher scale; AR, aspect ratio; SR, size ratio; NSI, non-sphericity index; UI, undulation index; WSS, wall shear stress; WSSA, wall shear stress average; WSSM, wall shear stress maximum; PA, pressure average; WSSG, wall shear stress gradient; NWSSA, normalized wall shear stress average; NWSSM, normalized wall shear stress maximum; NPA, normalized pressure average; LSAR, low shear area rate; RRT, relative resident time; OSI, oscillatory shear index; VA, vessel angle; AA, aneurysm angle.

The present study aimed to build a risk assessment model by exploiting multidimensional characteristics of RIAs. The clinical, morphological, and hemodynamic characteristics of a group of RIAs in a neurosurgical center were retrospectively reviewed. This study considered that this current can present more insights into the factors of rebleeding and contribute to better medical decisions.

## MATERIALS AND METHODS

### Patient Selected and Study Design

The patients with RIAs from January 2018 to September 2020 were retrospectively reviewed. Patients were enrolled by complying with the following standards: (1) an angiogram (CT angiogram, CTA) was performed after IA rupture; (3) the patients were sent to our institution within 12 h as soon as aSAH was identified (by symptoms, e.g., acute headache and sudden coma); and (4) clinical records were complete, or clinical history can be traced.

This study excluded the patients (1) having other intracranial tumors, angiostenosis and angio-malformation (e.g., arteriovenous malformation and cavernous malformation); (2) having a family history of IAs or connective tissue disease; (3) having multiple IAs, causing the source of the bleeding or rebleeding difficult to identify; (4) with dissecting or thrombus IAs; and (5) receiving special treatment for RIAs in other medical institutions before admission.

Rebleeding was the primary endpoint in this study and was diagnosed based on radiological findings: the magnitude of subarachnoid, intracerebral, or intraventricular blood significantly increased on CT after the admission, and the magnitude of bleeding did not increase and remained stable at/before admission.

The IAs which underwent rebleeding after the admission were identified as the rebleeding aneurysms, whereas the IAs without rebleeding before surgical intervention were found as the stable aneurysms. Rebleeding events were identified by two experienced neurosurgeons (PJ and JW, who were blind to clinical information and had worked as cerebral vascular neurosurgeons for more than 5 years) in accordance with the bleeding presentation on medical record and CT after the admission. Furthermore, the discrepancies were solved by consulting a senior neurosurgeon (SW, who had worked as a cerebral vascular neurosurgeon for more than 15 years).

Patients enrolled from August 2018 to December 2019 formed the primary cohort (411 patients with 411 IAs), which was

adopted to develop the predictive model; while patients enrolled from January 2020 to September 2020 were classified as the validation cohort (127 patients with 127 IAs). The ratio of numbers of unruptured IAs in the primary cohort and the validation cohort reached approximately 3:1.

## Perioperative Management

After admission, acute lowering of systolic pressure to 120–140 mmHg was the target (Connolly et al., 2012; American Society of Anesthesiologists Task Force on Perioperative Blood Management., 2015); all patients with Hunt-Hess I-II received surgical intervention within 72 h. However, once neurological condition progressively deteriorated, an emergency intervention would be performed.

Specific to patients with Hunt-Hess grade III-V at the admission, immediate surgical intervention was not recommended (Connolly et al., 2012). The patients who had not received immediate intervention would receive standard care following the guidelines (Connolly et al., 2012). After the admission, a CT would be performed per day, or when the patient had a sudden disorder of consciousness, or gradually worsening neurological states or convulsion after the admission. Surgical intervention was only considered when the patient's neurological status progressively deteriorated, or a rebleeding or a cerebral hernia was found in the radiological examination.

## Clinical Information and Morphology Assessment

Clinical information was collected from electronical medical records about age, gender, comorbidities (e.g., hypertension, dyslipidemia, diabetes mellitus, coronary heart disease, and ischemic stroke), Hunt-Hess grade at the admission, time from the admission to the rebleeding (the time from admission to neurological symptoms) or intervention, blood pressure at the admission, and blood pressure before rebleeding/intervention. Moreover, the time interval from admission to rebleeding or intervention was recorded. Furthermore, Modified Fisher scale (mFS) and IA site were collected from the radiological data.

The morphology assessment was performed according to our previous studies (Liu et al., 2019; Chen S. et al., 2021; Yang et al., 2021). The reconstruction of vascular model and measurement of morphological parameters were conducted by two neurosurgeons (QL and YY, who were blind to clinical information and had worked as cerebral vascular neurosurgeons for more than 3 years). The Digital Imaging and Communications in Medicine data were introduced into Mimics 17.0 (Mimics Research 17.0, Materialize, Belgium) and then reconstructed for subsequent studies. The pathological protruding region was recognized as the IA sac and was separated from the parent artery for further analysis. Two neurosurgeons separated the IA sacs independently, the discrepancy was solved by consulting a senior

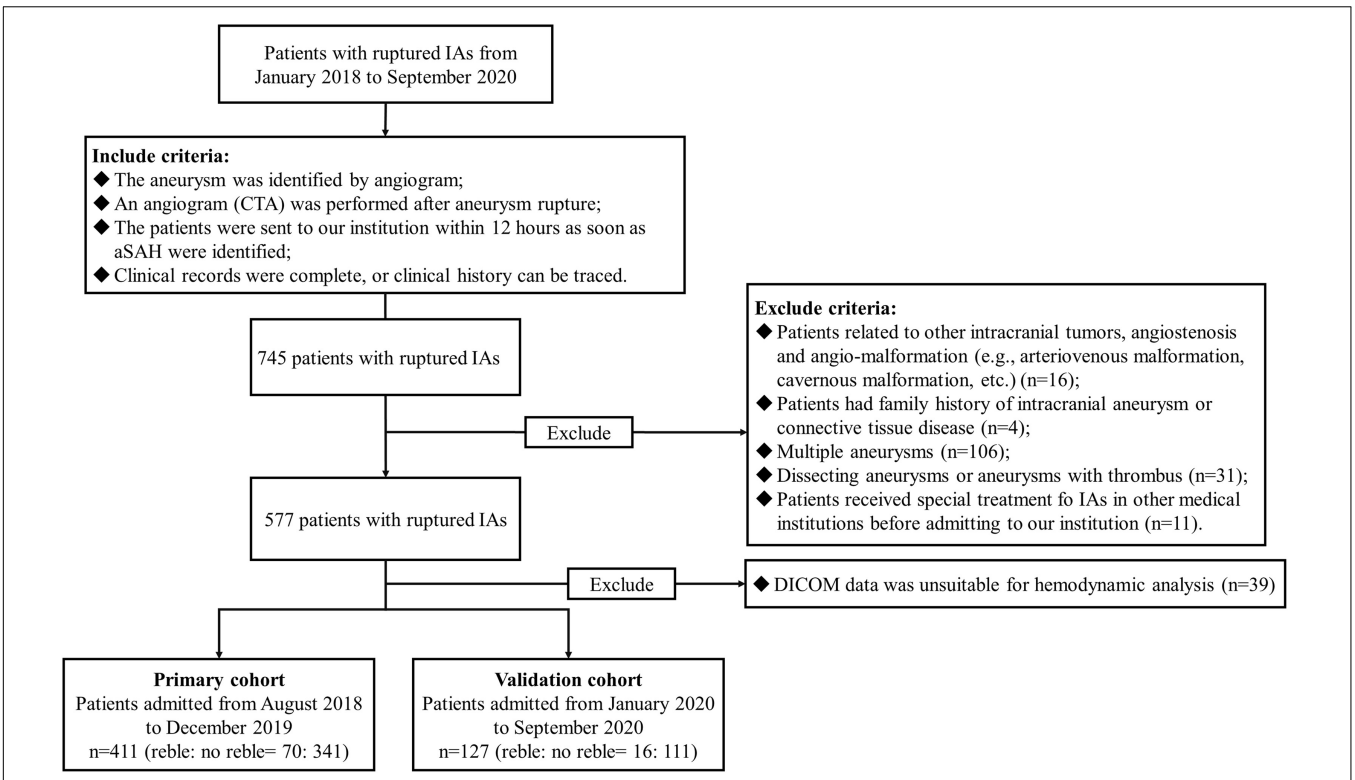


**FIGURE 1 |** The study flow chart. In this study, 411 appropriate patients with ruptured IAs were reviewed. A total of 70 patients were identified as rebleeding after the admission. Patients enrolled from August 2018 to December 2019 formed the primary cohort (411 patients with 411 IAs), which was adopted to develop the predictive model; while patients enrolled from January 2020 to September 2020 were classified as the validation cohort (127 patients with 127 IAs). IAs, intracranial aneurysms; DICOM, Digital Imaging and Communications in Medicine data.

neurosurgeon (HWH, who had worked in neurointervention for more than 15 years).

This study measured aneurysm size (S), diameter of dome (D), perpendicular height (H), diameter of parent artery, vessel angle (VA), aneurysm inclination angle (AA), volume, and surface area according to our previous study (Jiang et al., 2018a). The same neurosurgeons measured these morphological parameters independently, the discrepancy was solved by consulting a senior neurosurgeon (SW). The averages of measurements from each neurosurgeon were taken to be analyzed in depth. The morphological parameters involved here are also listed in **Supplementary Table 1**. Aspect ratio (AR), size ratio (SR), undulation index (UI), and non-sphericity index (NSI) were calculated according to previous study (Dhar et al., 2008). An irregular shape was defined as small bleb(s) or secondary aneurysm(s) protruding from the IA fundus or bi-/multi-lobular IA fundus.

## Computational Fluid Dynamics Simulating and Hemodynamic Assessment

The hemodynamic analysis protocol was referred to our previously conducted studies (Liu et al., 2019; Chen S. et al., 2021; Yang et al., 2021). For no saccular IAs sited in A3–A5 (anterior cerebral artery), M3–M5 (middle cerebral artery), P3–P4 (posterior cerebral artery), and vertebral artery in this study, we kept the vascular from internal carotid artery to M2 and A2 for IAs sited in anterior circulation and the vascular from basilar artery to P2 for IAs sited in posterior circulation. Meshing was performed using STAR-CCM (STAR-CCM + 12, Siemens, German), which automatically created 4 to 5 million unites of finite tetrahedral, prism elements and optimal boundary layers. The simulations were performed using STAR-CCM fluid workstation (STAR-CCM + 12, Siemens, Germany). The Navier-Stokers equation was employed as the solver in pulsatile blood. To conduct in-depth analyses, the pulsatile waveform of the internal carotid artery (waveform at cervical segmentation, for IAs sited in anterior circulation) and basilar artery (for IAs sited in posterior circulation) from a representative patient (**Supplementary Figure 1**) were adopted. The pulsatile waveform was obtained using Origin 2018b (OriginLab Corporation, Massachusetts, United States) and was exported to a comma-separated value file for further analysis. Blood was assumed as the incompressible Newtonian fluid. We set the blood as density $\rho = 1056\ kg/m^3$ and viscosity $\mu = 0.0035$ Poise. Pulsatile curve was set as the velocity inlet boundary condition, and velocity boundary condition (the mass flow rate was obtained from a population-based study (Tegeler et al., 2013)) was set at the outlet. Under the residuals $< 10^{-5}$, the results would be considered converged (Tian et al., 2016). A time step of 0.0001s was used. A cardiac cycle was divided into 800 steps (total 0.8 s per cycle). Four pulsatile cycles were simulated. The last cycle was yielded for subsequent studies.

Based on separated IA sacs, we extracted the time-averaged WSS and pressure over a cycle. The oscillatory shear index (OSI) and relative resident time (RRT) were calculated. In addition, the spatially average WSS, pressure, RRT and OSI over the aneurysm surface were obtained. Moreover, the hemodynamic parameters involved here are also listed in **Supplementary Table 1**. Specific to each model, WSS maximum (WSSM), WSS average (WSSA), WSS gradient (WSSG), and pressure average (PA), were obtained from the IA region, and parent pressure average, parent WSS average were determined according to the parent artery region. Low shear area was defined as the area with WSS < 10% of WSS of parent artery according to previous study (Xiang et al., 2011), and the percentage of low WSS area in IA dome (i.e., low shear area ratio, LSAR) was determined. The normalization of pressure and WSS was performed based on the hemodynamic status of parent artery. Furthermore, the normalized WSS average (NWSSA), normalized pressure average (NPA), and normalized WSS maximum (NWSSM) were calculated, respectively.

## Statistical Analysis

Measurement variables were compared using chi-square test or Fisher's exact test. Continuous variables were compared using the

**TABLE 1 |** The demographic and baseline information of patients in the primary cohort.

| Characteristics | With stable IAs $n = 341$ | With rebleeding IAs $n = 70$ | *P* value |
|---|---|---|---|
| Male, n (%) | 129 (37.8%) | 32 (45.7%) | 0.219 |
| Age, years, M ± SD | 54.8 ± 10.4 | 54.0 ± 8.9 | 0.467 |
| **Comorbidities, n (%)** | | | |
| Hypertension | 111 (32.6%) | 39 (11.4%) | <0.001+ |
| Dyslipidemia | 28 (8.2%) | 10 (14.3%) | 0.110 |
| Diabetes mellitus | 11 (3.2%) | 3 (4.3%) | 0.656 |
| Coronary heart disease | 8 (2.3%) | 3 (4.3%) | 0.360 |
| Ischemic stroke | 10 (2.9%) | 3 (4.3%) | 0.556 |
| **Modified Fisher scale at admission, n (%)** | | | 0.517 |
| I–II | 121 (35.5%) | 22 (31.4%) | |
| III–IV | 220 (64.5%) | 48 (68.6%) | |
| **Hunt-Hess grade at admission, n (%)** | | | 0.829 |
| I–II | 219 (64.2%) | 44 (62.9%) | |
| III–V | 122 (35.8%) | 26 (37.1%) | |
| **Blood pressure** | | | |
| At admission, n (%) | | | 0.578 |
| <160/90 mmHg | 114 (33.4%) | 21 (30.0%) | |
| >160/90 mmHg | 227 (66.6%) | 49 (70.0%) | |
| Before rebleeding/surgery, n (%) | | | 0.951 |
| <140/80 mmHg | 311 (91.2%) | 64 (91.4%) | |
| >140/80 mmHg | 30 (8.8%) | 6 (8.6%) | |
| **Treatment, n (%)** | | | |
| Dead before surgical intervention | 7 (2.1%) | 14 (20.0%) | |
| Endovascular intervention | 189 (55.4%) | 36 (51.4%) | |
| Microsurgical clipping | 145 (42.5%) | 20 (28.6%) | |
| PHASES, m (IQR) | 2 (0–4) | 2 (1–5) | 0.265 |
| ELAPSS, m (IQR) | 9 (5–14) | 12.5 (7–15) | 0.004+ |

+*The parameter was significant.*
*IAs, intracranial aneurysms.*

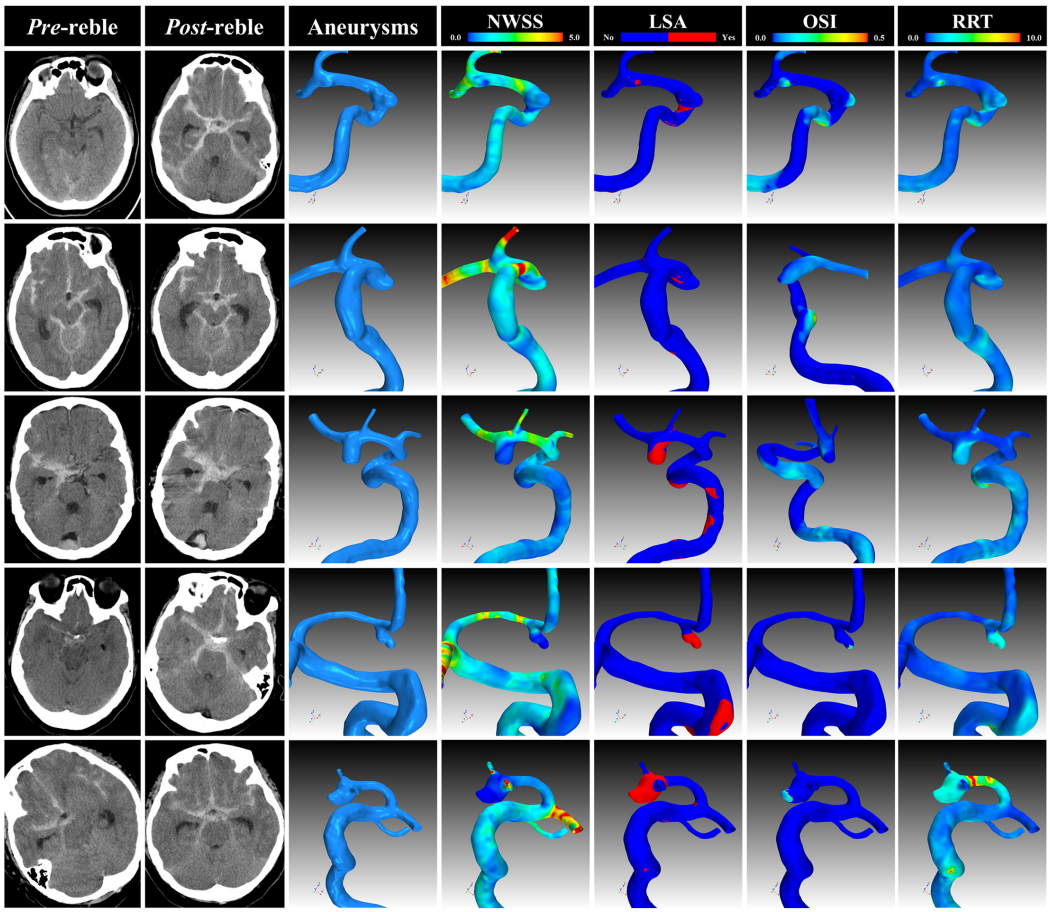


**FIGURE 2 |** Representative cases. The CT, angiogram and hemodynamic analysis of several representative cases. CT, computational tomography; NWSS, normalized wall shear stress; LSA, low shear area; OSI, oscillatory shear index; RRT, relative resident time.

independent samples' t-test. PHASES score and ELAPSS score were calculated by complying with previous protocols (Greving et al., 2014; Backes et al., 2017). The parameters with significance in univariable analysis were inputted into Cox regression model to identify the independent risk factors. The result was expressed as hazard ratio (HR) and 95% confidence interval (CI). The performance of the nomograms to predict the rebleeding was measured with AUCs in receiver operating characteristic curve (ROC) analyses. An AUC > 0.7 was considered a clinical utility. The cutoff value was calculated using the Youden index. To further assess the predictive accuracy of nomograms, the risk, assessed by using nomogram models, was adopted to categorize patients as the high-risk group and the low-risk group at the risk as 50% (with the highest Youden index). The survival analysis was conducted by using Kaplan-Meier model. The statistical analyses were conducted by employing SPSS 24.0 (SPSS, Chicago, IL, United States), with two-sided $P < 0.05$ showing statistical significance.

Subsequently, nomograms to predict the rebleeding were formulated. All parameters of interest as described above fell to three categories, i.e., clinical, morphological and hemodynamic features (**Supplementary Table 2**). Based on results of the multivariate Cox regression analyses, this study developed two nomogram models incorporating factors independently associated with the primary endpoint, i.e., the clinical + morphological model (CM model) and clinical + morphological + hemodynamic model (CMH model). In addition, the calibration curves were plotted to assess the calibration of the nomograms. The nomograms were subjected to bootstrapping validation (1000 bootstrap resamples). Furthermore, the nomograms were developed with the package of "rms" in R version 3.6.2.

# RESULTS

## Demographic, Clinical, Radiological, and Hemodynamic Difference in the Primary Cohort

On the whole, 411 appropriate patients with ruptured IAs were reviewed (**Figure 1**). 70 patients were identified as rebleeding after the admission ranged in age from 49 to 68 years (mean: 58.4 ± 6.0 years). The rebleeding rate was 17.0%. The

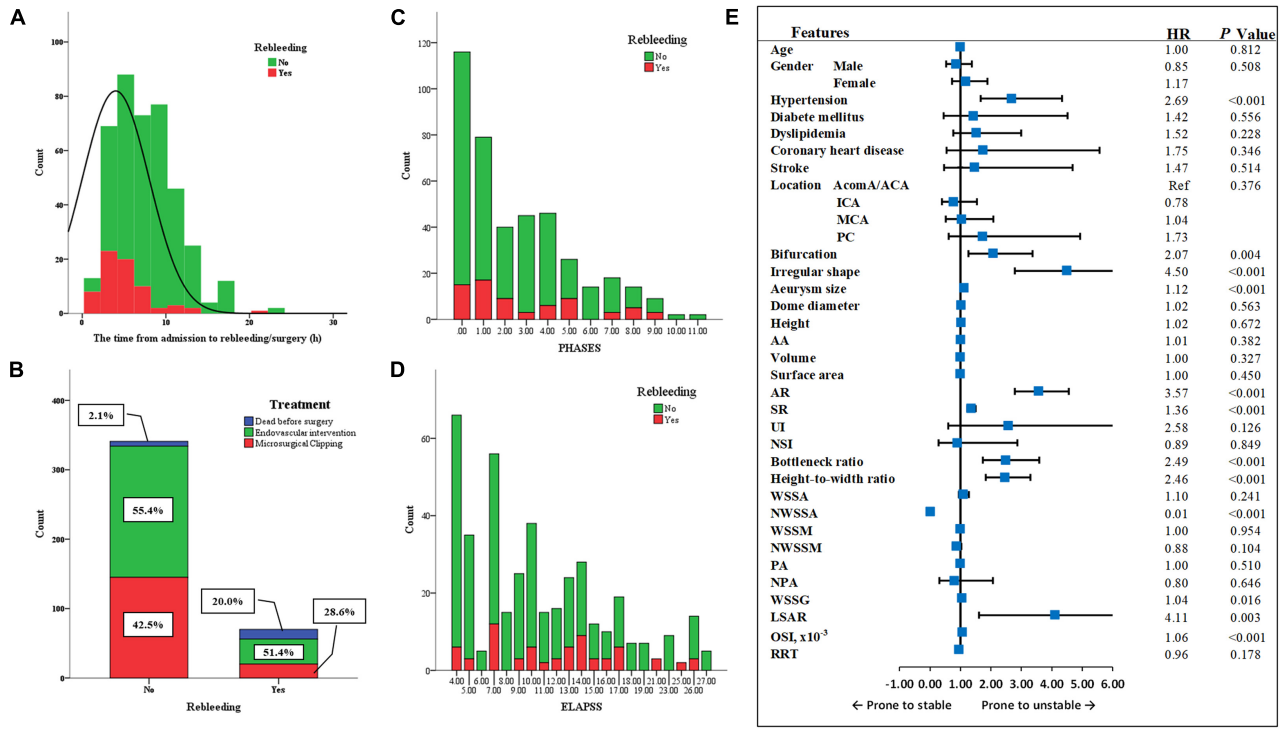


**FIGURE 3 |** The factors related to the rebleeding after admission. **(A)** The average time from admission to the rebleeding was 4.4 ± 4.7 h. **(B)** 54.7% patients received endovascular intervention, and 40.2% patients received microsurgical clipping, whereas 5.1% died before the surgery, of which 66.7% patients underwent rebleeding after the admission. **(C,D)** The PHASES score and ELAPSS score were presented here. **(E)** The forest plot summarized the result of univariate Cox regression analysis. MCA, middle cerebral artery; ICA, internal carotid artery; AcomA, anterior communicating artery; ACA, anterior cerebral artery; PC, posterior circulation; AA, aneurysm inclination angle; AR, aspect ratio; SR, size ratio; UI, undulation index; NSI, non-sphericity index; WSSA, wall shear stress average; NWSSA, normalized wall shear stress average; WSSM, wall shear stress maximum; NWSSM, normalized wall shear stress maximum; PA, pressure average; NPA, normalized pressure average; WSSG, wall shear stress gradient; LSAR, low shear area ratio; OSI, oscillatory shear index; RRT, relative resident time; Ref, reference; HR, hazard ratio.

demographic and clinical information was given in **Table 1**. Of all patients in the primary cohort, the percentage of male patients was 39.2% (161/411). 34.1% (150/411) patients had hypertension. Several representative cases were presented in **Figure 2**.

After standardly caring, the blood pressure of 91.2% (375/411) of patients was controlled in a reasonable range before rebleeding/intervention. The average time from admission to the rebleeding was 4.4 ± 4.7 h (**Figure 3A**). 54.7% (225/411) of patients received endovascular intervention, whereas 5.1% (21/411) died before the intervention, of which 66.7% (14/21) of patients underwent rebleeding after the admission (**Figure 3B**).

**Table 2** lists the morphological and hemodynamic characteristics. Several characteristics, including the history of hypertension ($P < 0.001$), bifurcation ($P = 0.005$), irregular shape ($P < 0.001$), size ($P < 0.001$), AR ($P < 0.001$), SR ($P < 0.001$), bottleneck factor ($P < 0.001$), height-to-width ratio ($P < 0.001$), NWSSA ($P < 0.001$), WSSG ($P = 0.008$), LSAR ($P = 0.010$), OSI ($P < 0.001$), and RRT ($P < 0.001$), were significantly different between stable and rebleeding IAs.

The ELAPSS score was significantly higher in rebleeding IAs compared with stable IAs [12.5 (7–15) vs. 9 (5–14), $P = 0.004$]; however, the PHASES score was not significant between rebleeding and stable IAs ($P = 0.265$). **Figures 3C,D** present the distributions of rebleeding cases in PHASES score and ELAPSS score.

## Risk Factors of Rebleeding After the Admission

The significant parameters in univariate analysis were inputted into univariate Cox regression model. The results are summarized as a forest plot (**Figure 3E**). Hypertension ($P < 0.001$), bifurcation ($P = 0.004$), irregular shape ($P < 0.001$), size ($P < 0.001$), AR ($P < 0.001$), SR ($P < 0.001$), bottleneck ratio ($P < 0.001$), height-to-width ratio ($P < 0.001$), NWSSA ($P < 0.001$), WSSG ($P = 0.016$), LSAR ($P = 0.003$), and OSI ($P < 0.001$) were identified as the risk factors of rebleeding after the admission.

These parameters were then inputted into a multivariate Cox regression model. The result was summarized in **Table 3**. The parameters were demonstrated as independent risk factors for the rebleeding after the admission, including hypertension (HR = 2.54; 95% CI, 1.02–6.31, $P = 0.044$), bifurcation (HR = 1.95; 95% CI, 1.12–3.07, $P = 0.013$), irregular shape (HR = 4.22; 95% CI, 1.68–10.62, $P = 0.002$), AR (HR = 12.91; 95% CI, 4.74–35.13, $P < 0.001$), and NWSSA

**TABLE 2 |** The morphological and hemodynamic features of IAs in the primary cohort.

| | Stable IAs $n = 341$ | Rebleeding IAs $n = 70$ | *P* value |
|---|---|---|---|
| Location, n (%) | | | 0.470 |
| AcomA/ACA | 52 (15.2%) | 12 (17.1%) | |
| ICA | 159 (46.6%) | 27 (38.6%) | |
| MCA | 117 (34.3%) | 26 (37.1%) | |
| PC | 13 (3.8%) | 5 (7.1%) | |
| Bifurcation, n (%) | 142 (41.6%) | 42 (60.0%) | 0.005+ |
| Irregular shape, n (%) | 58 (17.0%) | 38 (54.3%) | <0.001+ |
| IAsize, mm, M ± SD | 5.6 ± 2.9 | 7.0 ± 2.7 | <0.001+ |
| Dome diameter, mm, M ± SD | 4.9 ± 3.5 | 5.0 ± 3.1 | 0.248 |
| Height, mm, M ± SD | 4.5 ± 2.4 | 4.7 ± 1.9 | 0.057 |
| AA,°, M ± SD | 88.8 ± 19.0 | 91.3 ± 23.2 | 0.859 |
| Volume, $mm^3$, m (IQR) | 38.4 (19.7–69.4) | 40.1 (22.3–90.5) | 0.958 |
| Surface area, $mm^2$, m (IQR) | 54.8 (33.2–132.1) | 50.2 (33.4–180.9) | 0.949 |
| AR, M ± SD | 1.2 ± 0.4 | 2.1 ± 0.8 | <0.001+ |
| SR, M ± SD | 2.1 ± 1.4 | 3.1 ± 2.2 | <0.001+ |
| UI, M ± SD | 0.3 ± 0.2 | 0.4 ± 0.3 | 0.541 |
| NSI, M ± SD | 0.3 ± 0.2 | 0.3 ± 0.2 | 0.732 |
| Bottleneck factor, M ± SD | 1.2 ± 0.4 | 1.5 ± 0.5 | <0.001+ |
| Height-to-width ratio, M ± SD | 1.5 ± 0.5 | 2.0 ± 0.9 | <0.001+ |
| WSSA, Pa, m (IQR) | 2.2 (1.2–3.7) | 2.7 (1.3–4.1) | 0.093 |
| NWSSA, m (IQR) | 0.42 (0.26–0.63) | 0.22 (0.18–0.28) | <0.001+ |
| WSSM, Pa, m (IQR) | 6.4 (4.0–9.9) | 6.7 (3.3–9.8) | 0.580 |
| NWSSM, m (IQR) | 1.4 (0.68–2.8) | 1.0 (0.57–2.6) | 0.227 |
| PA, kPa, m (IQR) | 2.3 (1.6–2.8) | 2.1 (1.3–2.5) | 0.173 |
| NPA, m (IQR) | 0.62 (0.44–0.80) | 0.57 (0.44–0.77) | 0.184 |
| WSSG, m (IQR) | 23.0 (16.5–29.1) | 16.5 (14.2–25.8) | 0.008+ |
| LSAR, m (IQR) | 0.28 (0.15–0.45) | 0.38 (0.23–0.54) | 0.010+ |
| OSI, $x10^{-2}$, m (IQR) | 0.58 (0.20–0.97) | 0.70 (0.43–1.73) | <0.001+ |
| RRT, m (IQR) | 5.79 (3.74–8.22) | 4.57 (3.02–7.80) | 0.059 |

+*The parameter with significant.*
*IAs, intracranial aneurysms; MCA, middle cerebral artery; ICA, internal carotid artery; AcomA, anterior communicating artery; ACA, anterior cerebral artery; PC, posterior circulation; AA, aneurysm inclination angle; AR, aspect ratio; SR, size ratio; UI, undulation index; NSI, non-sphericity index; WSSA, wall shear stress average; NWSSA, normalized wall shear stress average; WSSM, wall shear stress maximum; NWSSM, normalized wall shear stress maximum; PA, pressure average; NPA, normalized pressure average; WSSG, wall shear stress gradient; LSAR, low shear area ratio; OSI, oscillatory shear index; RRT, relative resident time.*

(HR = 0.16; 95% CI, 0.01–0.28, $P = 0.002$), as well as OSI (HR = 1.14; 95% CI, 1.06–1.23, $P < 0.001$).

## Nomogram Models to Predict the Rebleeding After the Admission

Based on the result of multivariate Cox regression analysis and parameter category, two nomograms, i.e., clinical + morphological model (CM model, **Figure 4A**) and clinical + morphological + hemodynamic model (CMH model, **Figure 4B**) were built. With the risk as 50%, all patients were categorized as the high-risk group and the low-risk group.

**TABLE 3 |** Multivariate Cox analysis for rebleeding before surgery in the primary cohort.

| Characteristics | HR | 95% CI | *P* value |
|---|---|---|---|
| Hypertension (Yes vs. No) | 2.54 | (1.02–6.31) | 0.044+ |
| Bifurcation (Yes vs. No) | 1.95 | (1.12–3.07) | 0.013+ |
| Irregular shape (Yes vs. No) | 4.22 | (1.68–10.62) | 0.002+ |
| Aneurysm size | 1.07 | (0.90–1.28) | 0.450 |
| AR | 12.91 | (4.74–35.13) | <0.001+ |
| SR | 0.93 | (0.65–1.34) | 0.659 |
| Bottleneck ratio | 0.93 | (0.35–2.42) | 0.704 |
| Height-to-width ratio | 3.52 | (0.73–16.97) | 0.496 |
| NWSSA | 0.16 | (0.01–0.28) | 0.002+ |
| WSSG | 1.09 | (0.93–1.26) | 0.153 |
| LSAR | 0.15 | (0.01–2.87) | 0.226 |
| OSI | 1.14 | (1.06–1.23) | <0.001+ |

+*The independent risk factor associated with rebleeding.*
*AR, aspect ratio; SR, size ratio; NWSSA, normalized wall shear stress average; WSSG, wall shear stress gradient; LSAR, low shear area ratio; OSI, oscillatory shear index.*

The survival curves are presented as **Figures 4C,D**. Here, the patients in the high-risk group, recognized by the CM model and CMH model respectively, had higher risk of rebleeding after the admission (both $P < 0.001$). The calibration plots display a substantial agreement between the prediction by each nomogram and the actual observation, in the risk of rebleeding before the intervention (**Figures 5A,B**). The ROC analyses based on the primary cohort showed a good predicting accuracy of two nomogram models (AUC = 0.83 and 0.92, respectively), whereas a poor predicting accuracy of PHASES and ELAPSS score was found (AUC = 0.54 and 0.61, respectively). The CMH model had a higher predicting accuracy compared with the CM model ($P < 0.05$). The results of ROC analyses are summarized as **Figures 5C,C'** and given in **Table 4**.

## Validation of Predicting Accuracy of Nomogram Models to the Rebleeding After the Admission

The information of the validation cohort was given in **Table 5**. No significant difference was identified between the primary cohort and the validation cohort (**Supplementary Table 3**). As indicated from the ROC analyses (**Figures 5D,D'**), the CMH model exhibited the highest predicting accuracy (AUC = 0.93), followed by CM model (AUC = 0.86); however, the PHASES and ELAPSS score performed poorly (AUC = 0.53 and 0.51, respectively) in predicting the rebleeding after the admission. The result of ROC analyses based on the validation cohort is also listed in **Table 4**.

# DISCUSSION

Rebleeding refers to a main cause of morbidity for aSAH patients. Existing study reported that the morphology and hemodynamics of IAs would change after aSAH, which makes IAs prone to be stable (Skodvin et al., 2017). However, some RIAs may not reach

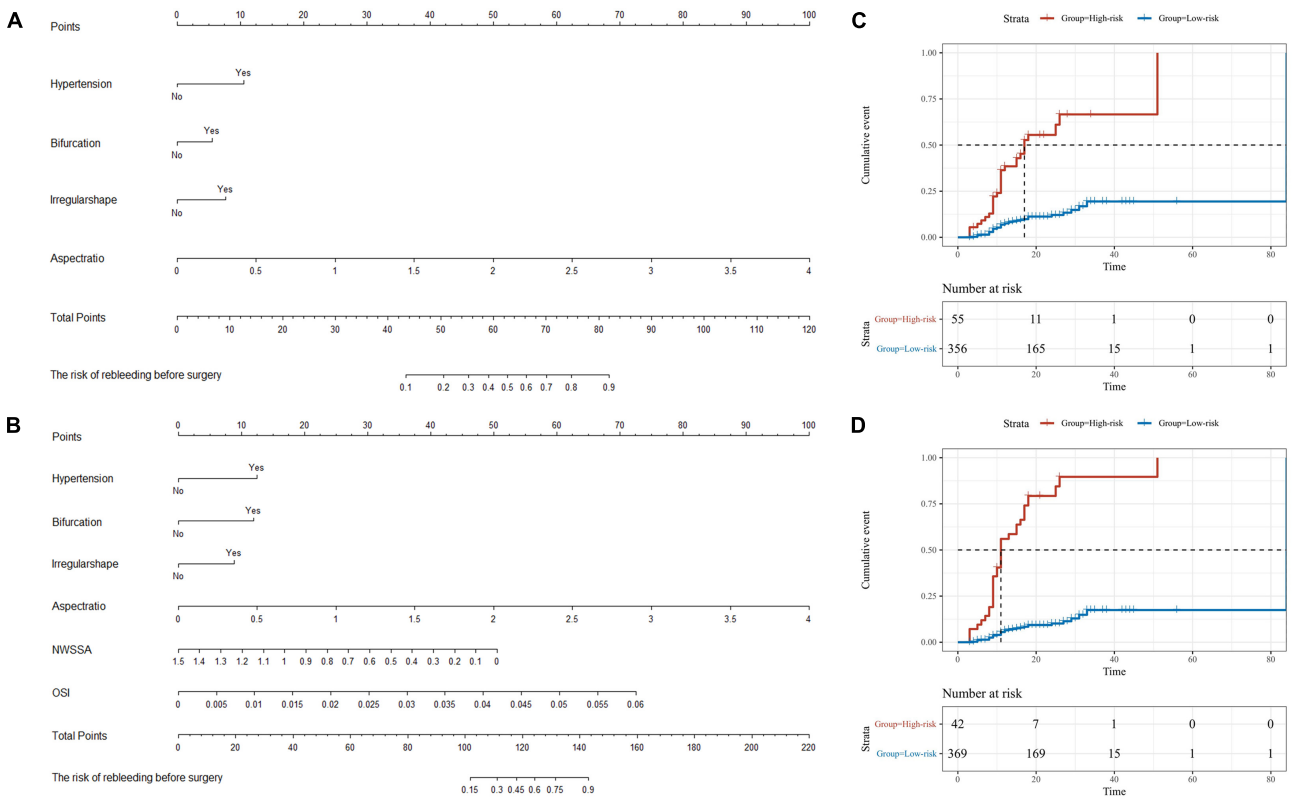


**FIGURE 4 |** The nomograms for the risk of rebleeding after admission. **(A,B)** Two nomograms, i.e., clinical + morphological model (CM model) and clinical + morphological + hemodynamic model (CMH model), were presented here. **(C,D)** With the risk at 50%, all patients were categorized as the high-risk group and the low-risk group. The survival curves showed that the RIAs in the high-risk group might rebleed in a short period after admission. NWSSA, normalized wall shear stress average; OSI, oscillatory shear index.

a stable condition and had a high risk of rebleeding. In this study, we confirmed the predictive value of hemodynamic parameters for rebleeding after the admission and build a predicting model to discriminate the RIAs at high risk of rebleeding.

This study demonstrated the relationship between the history of hypertension and rebleeding after the admission. Systematic artery hypertension was recognized as the major cause of cardiovascular disease. Previous cohort and animal studies confirmed that hypertension could increase the risk of IA natural rupture (Lindgren et al., 2014; Tada et al., 2014); thus, the hypertension was considered in subsequent predicting models (Greving et al., 2014; Backes et al., 2017). Here, the hypertension was also found as the independent risk factor for the rebleeding after the admission, demonstrating that the risk of rebleeding of RIA patients with hypertension was approximately 2.7 times that of patients without hypertension. Though the blood pressure was well under control after the admission, the systematic artery hypertension had caused damage to vessels throughout the body before the IAs rupture. Accordingly, this study considered that the risk of rebleeding was higher in patients with hypertension as compared to patients without hypertension.

In this study, the RIAs sited in bifurcation, with irregular shape, and larger AR were found with a high risk of rebleeding after the admission. The IAs sited in bifurcation were more possible to suffer from the impact of blood flow; the dynamic change from direct impact area to surrounding area could cause physical injury to the endothelia of vessels, and thus to the aneurysm wall (Metaxa et al., 2010). In addition to the bifurcation site, irregular shape is also a sign of high risk of rupture. Irregular shape generally suggested a more significantly fragile area in IAs, which could present as bled or second aneurysm protruding from the primary IAs, as compared with the surrounding area in the aneurysm dome. As revealed from existing studies, the bled or second aneurysm in an irregular aneurysm was generally thin and blood-blister like, and the rupture areas were commonly associated with these bled or second aneurysms (Kawaguchi et al., 2012; Jiang et al., 2020). Notably, the hemodynamic condition of the bled aneurysm is generally low WSS and high OSI (Kawaguchi et al., 2012). Thus, it is easy to understand that the RIAs sited in bifurcation with an irregular shape has a higher risk of rebleeding after the admission. The IAs with large AR generally have large size and relatively narrow neck, often with unstable hemodynamic condition and severe damage in the aneurysm wall (Qiu et al., 2017); therefore, this parameter was confirmed as a predictor for IA natural rupture (Backes et al., 2017). Our preliminary study also reported that the AR was a predictor for rebleeding of RIAs. This study demonstrated that the risk of rebleeding increased by 12.9 per 1 of AR, suggesting that AR is

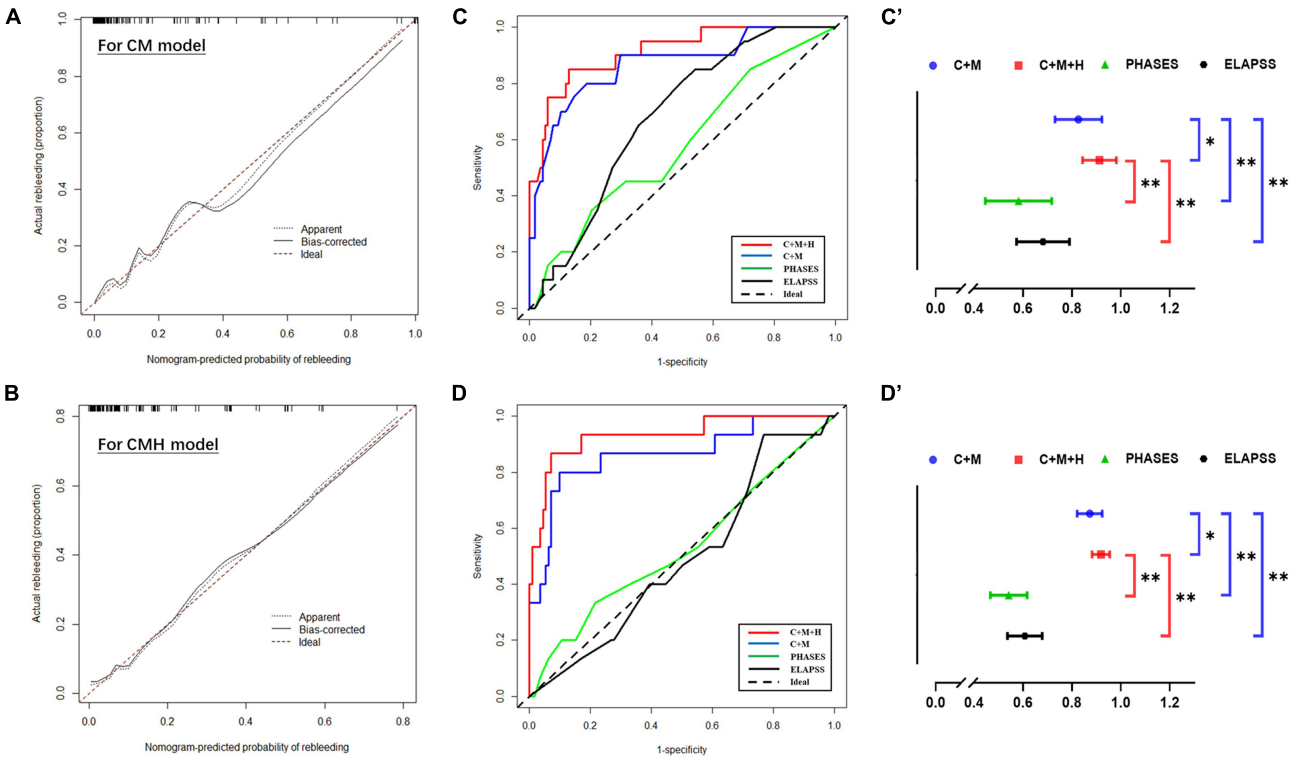


**FIGURE 5 |** The predictive accuracy of models for rebleeding. **(A,B)** The calibration plots display a substantial agreement between the prediction by each nomogram and the actual observation, in the risk of rebleeding before the surgery. **(C,C',D,D')** The ROC analyses based on the primary cohort and validation cohort showed a good predicting accuracy of two nomogram models, whereas a poor predicting accuracy of PHASES and ELAPSS score was found. *$P < 0.05$; **$P < 0.01$.

a vital parameter to identify the RIAs at high risk of rebleeding after the admission.

This study also confirmed the role of hemodynamic parameters, mainly the WSSA and OSI, in predicting the risk of rebleeding after the admission. The hemodynamic condition could induce inflammation filtration and vessel remodeling in the vascular wall (Albarran-Juarez et al., 2018; Lu et al., 2019; Zhang et al., 2020), which would cause atherosclerosis, IA growth/rupture, etc. Recent studies reported that oscillator flow could induce the inflammation in the vascular wall and inhibit the expression of vascular protective factors (Albarran-Juarez et al., 2018) (e.g., endothelial nitric oxide synthase). Moreover, the low WSS could activate the inflammatory pathway (Chen J. et al., 2021) (e.g., ROS pathway, pyroptosis pathway and nuclear factor kappa B pathway) to induce inflammation, which could promote the damage of vessels. This study demonstrated that the RIAs with low WSSA and high OSI had a high risk of rebleeding after the admission. Notably, as suggested by existing pathological research, the inflammation in the aneurysm wall is the main cause of IA rupture and growth (Frösen et al., 2004, 2012; Jiang et al., 2018b; Tulamo et al., 2018). According to Frosen et al., the pathological characteristics of the aneurysm wall fell to four levels by largely complying with the inflammation; the severer the level, the higher the risk of aneurysm rupture will be (Frösen et al., 2004). Since WSS and OSI could induce the inflammation in the vascular wall, the low WSS and the high OSI in RIAs suggested that the damage for the aneurysm wall was continuous after initial hemorrhage; besides, for rebleeding aneurysms, the bleeding stopped before IA reaching a stable status. The mentioned result also demonstrated the clinical utility of computational fluid dynamics.

Based on the independent risk factors, two nomogram models were set to identify the RIAs at high risk of rebleeding. The CM model included the clinical and morphological characteristics (e.g., hypertension, bifurcation site, irregular shape, and AR). The hemodynamic characteristics were further integrated with the

**TABLE 4 |** The predicting value of each model.

| | Primary cohort | | | Validation cohort | | |
|---|---|---|---|---|---|---|
| | **AUC** | **95%CI** | ***P* value** | **AUC** | **95%CI** | ***P* value** |
| **Nomogram models** | | | | | | |
| CM model[a] | 0.83 | (0.78–0.90) | <0.001 | 0.86 | (0.75–0.98) | <0.001 |
| CMH model[b] | 0.92 | (0.88–0.95) | <0.001 | 0.93 | (0.86–1.00) | <0.001 |
| **Clinical scores** | | | | | | |
| PHASES | 0.54 | (0.47–0.62) | 0.273 | 0.53 | (0.36–0.70) | 0.712 |
| ELAPSS | 0.61 | (0.54–0.68) | 0.004 | 0.51 | (0.36–0.65) | 0.917 |

[a]*CM model, clinical and morphological model.*
[b]*CMH model, clinical, morphological and hemodynamic model.*
*AUC, area under the curve; CI, confidence interval.*

**TABLE 5 |** The information of patients and IAs in the validation cohort.

| Characteristics | Stable IAs $n = 111$ | Rebleeding IAs $n = 16$ | *P* value |
|---|---|---|---|
| Age, years, M ± SD | 54.6 ± 10.5 | 53.4 ± 5.8 | 0.588 |
| Male, n (%) | 43 (38.7%) | 8 (50.0%) | 0.392 |
| **Comorbidities, n (%)** | | | |
| Hypertension | 40 (36.0%) | 10 (62.5%) | 0.044+ |
| Dyslipidemia | 9 (8.1%) | 3 (18.8%) | 0.175 |
| Diabetes mellitus | 5 (4.5%) | 1 (6.3%) | 0.759 |
| Coronary heart disease | 2 (1.8%) | 0 (0.0%) | 0.590 |
| Ischemic stroke | 3 (2.7%) | 1 (6.3%) | 0.449 |
| History of aSAH | 16 (14.4%) | 2 (12.5%) | 0.837 |
| Modified Fisher scale at admission, n (%) | | | 0.742 |
| I–II | 37 (33.3%) | 6 (37.5%) | |
| III–IV | 74 (66.7%) | 10 (62.5%) | |
| Hunt-Hess grade at admission, n (%) | | | 0.106 |
| I–II | 67 (60.4%) | 13 (81.2%) | |
| III–V | 44 (39.6%) | 3 (18.8%) | |
| **Blood pressure** | | | |
| At admission, n (%) | | | 0.117 |
| <160/90 mmHg | 35 (31.5%) | 2 (12.5%) | |
| >160/90 mmHg | 76 (68.5%) | 14 (87.5%) | |
| Before rebleeding/surgery, n (%) | | | 0.574 |
| <140/80 mmHg | 99 (89.2%) | 15 (93.8%) | |
| >140/80 mmHg | 12 (9.8%) | 1 (6.2%) | |
| Location, n (%) | | | 0.244 |
| AcomA/ACA | 16 (14.4%) | 5 (31.3%) | |
| ICA | 53 (47.7%) | 6 (37.5%) | |
| MCA | 40 (36.1%) | 5 (31.3%) | |
| PC | 2 (1.8%) | 0 (0.0%) | |
| Bifurcation, n (%) | 42 (37.8%) | 13 (81.3%) | 0.001+ |
| Irregular shape, n (%) | 17 (15.3%) | 9 (56.3%) | <0.001+ |
| IAsize, mm, M ± SD | 4.7 (3.8–7.1) | 6.4 (4.5–7.5) | 0.130 |
| Dome diameter, mm, M ± SD | 3.9 (2.9–5.6) | 4.3 (3.2–6.0) | 0.472 |
| Height, mm, M ± SD | 3.8 (3.0–5.7) | 3.9 (3.5–5.4) | 0.520 |
| AA,°, M ± SD | 86.8 (79.9–98.3) | 85.6 (81.3–103.3) | 0.757 |
| Volume, $mm^3$, m (IQR) | 41.6 (19.7–121.9) | 40.3 (29.3–75.5) | 0.870 |
| Surface area, $mm^2$, m (IQR) | 60.7 (34.6–144.84) | 52.2 (46.6–161.0) | 0.951 |
| AR, m (IQR) | 1.2 (0.9–1.5) | 1.9 (1.3–2.3) | <0.001+ |
| SR, m (IQR) | 1.6 (1.2–2.6) | 2.3 (1.3–5.0) | 1.116 |
| UI, m (IQR) | 0.26 (0.15–0.42) | 0.19 (0.12–0.49) | 0.525 |
| NSI, m (IQR) | 0.29 (0.06–0.44) | 0.21 (0.07–0.43) | 0.525 |
| Bottleneck factor, m (IQR) | 1.1 (1.0–1.3) | 1.3 (1.1–1.7) | 0.064 |
| HWR, m (IQR) | 1.4 (1.2–1.7) | 1.9 (1.4–2.5) | 0.024+ |
| WSSA, Pa, m (IQR) | 2.3 (1.4–4.0) | 2.2 (1.0–3.8) | 0.773 |
| NWSSA, m (IQR) | 0.42 (0.26–0.61) | 0.22 (0.18–0.27) | 0.001+ |
| WSSM, Pa, m (IQR) | 6.7 (3.9–11.3) | 6.0 (2.9–10.0) | 0.606 |
| NWSSM, m (IQR) | 1.31 (0.68–2.38) | 1.25 (0.65–2.45) | 0.922 |
| PA, Pa, m (IQR) | 2319.3 (1737.6–2910.7) | 1912.9 (1270.8–2217.9) | 0.008+ |
| NPA, m (IQR) | 0.60 (0.42–0.76) | 0.64 (0.44–0.77) | 0.719 |
| WSSG, m (IQR) | 6.9 (5.4–10.7) | 7.9 (6.3–13.0) | 0.1123 |
| LSAR, m (IQR) | 0.27 (0.16–0.44) | 0.41 (0.26–0.55) | 0.072 |
| OSI, $x10^{-2}$, m (IQR) | 0.60 (0.17–0.91) | 0.84 (0.51–1.64) | 0.009+ |
| RRT, m (IQR) | 5.3 (3.6–7.2) | 4.5 (3.0–5.9) | 0.286 |

+*The parameter was significant.*

*IAs, intracranial aneurysms; MCA, middle cerebral artery; ICA, internal carotid artery; AcomA, anterior communicating artery; ACA, anterior cerebral artery; PC, posterior circulation; AA, aneurysm inclination angle; AR, aspect ratio; SR, size ratio; UI, undulation index; NSI, non-sphericity index; WSSA, wall shear stress average; NWSSA, normalized wall shear stress average; WSSM, wall shear stress maximum; NWSSM, normalized wall shear stress maximum; PA, pressure average; NPA, normalized pressure average; WSSG, wall shear stress gradient; LSAR, low shear area ratio; OSI, oscillatory shear index; RRT, relative resident time.*

other characteristics to build the CMH model. The predicting value of the CM model and CMH model was confirmed as good for clinical utility. Using the risk as 50% assessed by each nomogram model, we confirmed that the rupture risk was higher and interval from initial hemorrhage to rebleeding was shorter in the high-risk group as compared with the low-risk group. As indicated from the further comparison, these two nomogram models exhibited higher predicting accuracy as compared with PHASES and ELAPSS models. Interestingly, the CMH model had higher predicting accuracy as compared with the CM model. For this phenomenon, this study considered that the stability of IAs mainly involved two aspects, i.e., internal hemodynamic condition and pathological characteristics of the aneurysm wall. Taking multidimensional risk factors into consideration could help to comprehensively understand the stability of RIAs, demonstrating that the CMH model would have a higher predicting accuracy as compared with the CM model. However, the CM model could be more easily handled in clinical work as compared with the CMH model, especially in emergency conditions. Though the hemodynamic analysis is limited in clinical work for its technical barrier and time-consumption now, the tool, i.e., aView, has been reported in previous study (Xiang et al., 2017); therefore, the clinical practical hemodynamic analysis tool would arise to assist in quickly identifying the hemodynamic characteristics of RIAs in the future.

In the developing nations, because of large populations but limited medical resources (Bian et al., 2012), the sequence of treatment is essential to make a treatment strategy for IAs. This fact reveals that a patient has to wait a long time for appropriate treatment immediately to get medical intervention after IA rupture. Though the bleeding stopped in some RIAs, RIAs may not reach a real stable condition. This study built two models with good accuracy to identify the high-risk RIAs. To avoid rebleeding, an immediate surgical intervention was recommended for the RIAs at high risk of rebleeding, and a priority should be given to IAs with higher scores.

There are several limitations here. First, the inlet boundary condition was from a representative patient, which can affect the result of computational fluid dynamics since this method is sensitive to velocity and waveform (Xiang et al., 2014). However,

this study used normalized parameters that can reduce the effects exerted by this problem. Second, the morphology can significantly impact the hemodynamics. Due to the change of morphology and hemodynamics after indiscoverable IA rupture (Skodvin et al., 2017) and the effect of hemorrhage on the quality of radiological images, our conclusion may be limited. Third, this study was a single center and retrospective study, which may limit our conclusion. Fourth, this study only considered the utility of PHASES and ELAPSS score in predicting the risk of rebleeding. There were several other models which could help in discriminating the high-risk IAs, e.g., Detmer's model (Detmer et al., 2018). However, the PHASES and ELAPSS score were representative models to discriminate the high-risk IAs; thus, we compared the predictive accuracy between our nomograms and these models. Indications remain the focus in IA treatment, and our models have their clinical utility to help clinical work identify the optimal sequence of treatment, though some limitations remain.

## CONCLUSION

Hemodynamic parameters could serve as the predictors for rebleeding after admission. Two nomogram models were presented, i.e., CMH nomogram and CM nomogram, helping to identify the RIAs at high risk of rebleeding. For RIAs at high risk of rebleeding, intervention should be prioritized, and medical treatment is not recommended after rupture.

## DATA AVAILABILITY STATEMENT

The original contributions presented in the study are included in the article/**Supplementary Material**, further inquiries can be directed to the corresponding authors.

## ETHICS STATEMENT

This study was approved by the Institutional Review Board of Beijing Tiantan Hospital. Written informed consents were obtained and the privacy of patients was effectively protected.

## AUTHOR CONTRIBUTIONS

QL and PJ: conception and design. QL, YY, JY, PJ, ML, SY, and NW: acquisition of data. QL and YY: analysis and interpretation of data. QL: drafting the article. PJ and SW: critically revising the article. SW: approving the final version of the manuscript on behalf of other authors and study supervision. All authors: reviewing the submitted version of manuscript.

## FUNDING

This study was supported by the "National Natural Science Foundation of China" (Grant Nos. 82071296, 81671129, and 81471210) and "Major special projects in the 13th 5-year plan" (Grant No. 2016YFC1301800).

## ACKNOWLEDGMENTS

The authors thank Hongwei He for helping in separation of IAs.

## SUPPLEMENTARY MATERIAL

The Supplementary Material for this article can be found online at: https://www.frontiersin.org/articles/10.3389/fnagi.2021.692615/full#supplementary-material

## REFERENCES

Albarran-Juarez, J., Iring, A., Wang, S., Joseph, S., Grimm, M., Strilic, B., et al. (2018). Piezo1 and Gq/G11 promote endothelial inflammation depending on flow pattern and integrin activation. *J. Exp. Med.* 215, 2655–2672. doi: 10.1084/jem.20180483

American Society of Anesthesiologists Task Force on Perioperative Blood Management. (2015). Practice guidelines for perioperative blood management: an updated report by the American Society of Anesthesiologists Task Force on Perioperative Blood Management*. *Anesthesiology* 122, 241–275. doi: 10.1097/aln.0000000000000463

Backes, D., Rinkel, G. J. E., Greving, J. P., Velthuis, B. K., Murayama, Y., Takao, H., et al. (2017). ELAPSS score for prediction of risk of growth of unruptured intracranial aneurysms. *Neurology* 88, 1600–1606.

Bian, L. H., Liu, Y. F., Nichols, L. T., Wang, C. X., Wang, Y. L., Liu, G. F., et al. (2012). Epidemiology of subarachnoid hemorrhage, patterns of management, and outcomes in China: a hospital-based multicenter prospective study. *CNS Neurosci. Ther.* 18, 895–902. doi: 10.1111/cns.12001

Boogaarts, H. D., van Lieshout, J. H., van Amerongen, M. J., de Vries, J., Verbeek, A. L., Grotenhuis, J. A., et al. (2015). Aneurysm diameter as a risk factor for pretreatment rebleeding: a meta-analysis. *J. Neurosurg.* 122, 921–928. doi: 10.3171/2014.12.jns14931

Chen, J., Zhang, J., Wu, J., Zhang, S., Liang, Y., Zhou, B., et al. (2021). Low shear stress induced vascular endothelial cell pyroptosis by TET2/SDHB/ROS pathway. *Free Radic. Biol. Med.* 162, 582–591. doi: 10.1016/j.freeradbiomed.2020.11.017

Chen, S., Liu, Q., Ren, B., Li, M., Jiang, P., Yang, Y., et al. (2021). A scoring system to discriminate blood blister-like aneurysms: a multidimensional study using patient-specific model. *Neurosurg. Rev.* [Preprint].

Connolly, E. S. Jr., Rabinstein, A. A., Carhuapoma, J. R., Derdeyn, C. P., Dion, J., Higashida, R. T., et al. (2012). Guidelines for the management of aneurysmal subarachnoid hemorrhage: a guideline for healthcare professionals from the American Heart Association/american Stroke Association. *Stroke* 43, 1711–1737. doi: 10.1161/str.0b013e3182587839

Cordonnier, C., Demchuk, A., Ziai, W., and Anderson, C. S. (2018). Intracerebral haemorrhage: current approaches to acute management. *Lancet* 392, 1257–1268. doi: 10.1016/s0140-6736(18)31878-6

Darkwah Oppong, M., Skowronek, V., Pierscianek, D., Gembruch, O., Herten, A., Saban, D. V., et al. (2018). Aneurysmal intracerebral hematoma: Risk factors and surgical treatment decisions. *Clin. Neurol. Neurosurg.* 173, 1–7. doi: 10.1016/j.clineuro.2018.07.014

Detmer, F. J., Chung, B. J., Mut, F., Slawski, M., Hamzei-Sichani, F., Putman, C., et al. (2018). Development and internal validation of an aneurysm rupture probability model based on patient characteristics and aneurysm location, morphology, and hemodynamics. *Int. J. Comput. Assist Radiol. Surg.* 13, 1767–1779. doi: 10.1007/s11548-018-1837-0

Dhar, S., Tremmel, M., Mocco, J., Kim, M., Yamamoto, J., Siddiqui, A. H., et al. (2008). Morphology Parameters for Intracranial Aneurysm Rupture

Risk Assessment. *Neurosurgery* 63:185. doi: 10.1227/01.neu.0000316847.64140.81

Dolan, J. M., Kolega, J., and Meng, H. (2013). High wall shear stress and spatial gradients in vascular pathology: a review. *Ann. Biomed. Eng.* 41, 1411–1427. doi: 10.1007/s10439-012-0695-0

Frösen, J., Piippo, A., Paetau, A., Kangasniemi, M., Niemelä, M., Hernesniemi, J., et al. (2004). Remodeling of saccular cerebral artery aneurysm wall is associated with rupture: histological analysis of 24 unruptured and 42 ruptured cases. *Stroke* 35, 2287–2293. doi: 10.1161/01.str.0000140636.30204.da

Frösen, J., Tulamo, R., Paetau, A., Laaksamo, E., Korja, M., Laakso, A., et al. (2012). Saccular intracranial aneurysm: pathology and mechanisms. *Acta Neuropathol.* 123, 773–786. doi: 10.1007/s00401-011-0939-3

Greving, J. P., Wermer, M. J., Brown, R. D. Jr., Morita, A., Juvela, S., Yonekura, M., et al. (2014). Development of the PHASES score for prediction of risk of rupture of intracranial aneurysms: a pooled analysis of six prospective cohort studies. *Lancet Neurol.* 13, 59–66. doi: 10.1016/s1474-4422(13)70263-1

Hijdra, A., van Gijn, J., Nagelkerke, N. J., Vermeulen, M., and van Crevel, H. (1988). Prediction of delayed cerebral ischemia, rebleeding, and outcome after aneurysmal subarachnoid hemorrhage. *Stroke* 19, 1250–1256. doi: 10.1161/01.str.19.10.1250

Jaechan, P., Hyunjin, W., Dong-Hun, K., Yong-Sun, K., Young, K. M., Im Hee, S., et al. (2015). Formal protocol for emergency treatment of ruptured intracranial aneurysms to reduce in-hospital rebleeding and improve clinical outcomes. *J. Neurosurg.* 122:383. doi: 10.3171/2014.9.jns131784

Jiang, P., Liu, Q., Wu, J., Chen, X., Li, M., Li, Z., et al. (2018a). A Novel Scoring System for Rupture Risk Stratification of Intracranial Aneurysms: A Hemodynamic and Morphological Study. *Front. Neurosci.* 12, doi: 10.3389/fnins.2018.00596

Jiang, P., Liu, Q., Wu, J., Chen, X., Li, M., Yang, F., et al. (2020). Hemodynamic findings associated with intraoperative appearances of intracranial aneurysms. *Neurosurg. Rev.* 43, 203–209. doi: 10.1007/s10143-018-1027-0

Jiang, P., Wu, J., Chen, X., Ning, B., Liu, Q., Li, Z., et al. (2018b). Quantitative proteomics analysis of differentially expressed proteins in ruptured and unruptured cerebral aneurysms by iTRAQ. *J. Proteom.* 182, 45–52. doi: 10.1016/j.jprot.2018.05.001

Kawaguchi, T., Nishimura, S., Kanamori, M., Takazawa, H., Omodaka, S., Sato, K., et al. (2012). Distinctive flow pattern of wall shear stress and oscillatory shear index: similarity and dissimilarity in ruptured and unruptured cerebral aneurysm blebs. *J. Neurosurg.* 117, 774–780. doi: 10.3171/2012.7.jns111991

Kienzler, J., Marbacher, S., Remonda, L., Soleman, J., Ai Schlaeppi, J., Leupold, U., et al. (2016). Outcome after In-Hospital Rebleeding of Rupture of Intracranial Aneurysms. *J. Neurol. Surg. A Cent. Eur. Neurosurg.* 77, 207–221. doi: 10.1055/s-0035-1570007

Ko, S. B., Choi, H. A., Carpenter, A. M., Helbok, R., Schmidt, J. M., Badjatia, N., et al. (2011). Quantitative analysis of hemorrhage volume for predicting delayed cerebral ischemia after subarachnoid hemorrhage. *Stroke* 42, 669–674. doi: 10.1161/strokeaha.110.600775

Lindgren, A. E., Kurki, M. I., Riihinen, A., Koivisto, T., Ronkainen, A., Rinne, J., et al. (2014). Hypertension predisposes to the formation of saccular intracranial aneurysms in 467 unruptured and 1053 ruptured patients in Eastern Finland. *Ann. Med.* 46, 169–176. doi: 10.3109/07853890.2014.883168

Liu, Q., Jiang, P., Wu, J., Li, M., Gao, B., Zhang, Y., et al. (2019). Intracranial aneurysm rupture score may correlate to the risk of rebleeding before treatment of ruptured intracranial aneurysms. *Neurol. Sci.* 40, 1683–1693. doi: 10.1007/s10072-019-03916-1

Lu, Q., Meng, Q., Qi, M., Li, F., and Liu, B. (2019). Shear-Sensitive lncRNA AF131217.1 Inhibits Inflammation in HUVECs via Regulation of KLF4. *Hypertension* 73, e25–e34.

Meng, H., Tutino, V. M., Xiang, J., and Siddiqui, A. (2014). High WSS or low WSS? Complex interactions of hemodynamics with intracranial aneurysm initiation, growth, and rupture: toward a unifying hypothesis. *AJNR Am. J. Neuroradiol.* 35, 1254–1262. doi: 10.3174/ajnr.a3558

Meng, H., Xiang, J., and Liaw, N. (2012). The Role of Hemodynamics in Intracranial Aneurysm Initiation. *Int. Rev. Thromb.* 7, 40–57.

Metaxa, E., Tremmel, M., Natarajan, S. K., Xiang, J., Paluch, R. A., Mandelbaum, M., et al. (2010). Characterization of critical hemodynamics contributing to aneurysmal remodeling at the basilar terminus in a rabbit model. *Stroke* 41, 1774–1782. doi: 10.1161/strokeaha.110.585992

Qiu, T., Jin, G., Xing, H., and Lu, H. (2017). Association between hemodynamics, morphology, and rupture risk of intracranial aneurysms: a computational fluid modeling study. *Neurol. Sci.* 38, 1009–1018. doi: 10.1007/s10072-017-2904-y

Rosenørn, J., Eskesen, V., Schmidt, K., and Rønde, F. (1987). The risk of rebleeding from ruptured intracranial aneurysms. *J. Neurosurg.* 67, 329–332. doi: 10.3171/jns.1987.67.3.0329

Skodvin, T. O., Johnsen, L. H., Gjertsen, O., Isaksen, J. G., and Sorteberg, A. (2017). Cerebral Aneurysm Morphology Before and After Rupture: Nationwide Case Series of 29 Aneurysms. *Stroke* 48, 880–886. doi: 10.1161/strokeaha.116.015288

Starke, R. M., Connolly, E. S. Jr., and Participants in the International Multi-Disciplinary Consensus Conference on the Critical Care Management of Subarachnoid hemorrhage. (2011). . Rebleeding after aneurysmal subarachnoid hemorrhage. *Neurocrit. Care* 15, 241–246.

Tada, Y., Wada, K., Shimada, K., Makino, H., Liang, E. I., Murakami, S., et al. (2014). Roles of hypertension in the rupture of intracranial aneurysms. *Stroke* 45, 579–586. doi: 10.1161/strokeaha.113.003072

Tegeler, C. H., Crutchfield, K., Katsnelson, M., Kim, J., Tang, R., Passmore Griffin, L., et al. (2013). Transcranial Doppler velocities in a large, healthy population. *J. Neuroimag.* 23, 466–472. doi: 10.1111/j.1552-6569.2012.00711.x

Tian, Z., Zhang, Y., Jing, L., Liu, J., Zhang, Y., and Yang, X. (2016). Rupture Risk Assessment for Mirror Aneurysms with Different Outcomes in the Same Patient. *Front. Neurol.* 7:219. doi: 10.3389/fneur.2016.00219

Tulamo, R., Frösen, J., Hernesniemi, J., and Niemelä, M. (2018). Inflammatory changes in the aneurysm wall: a review. *J. Neurointervent. Surg.* 10, i58–i67.

Xiang, J., Natarajan, S. K., Tremmel, M., Ma, D., Mocco, J., Hopkins, L. N., et al. (2011). Hemodynamic-Morphologic Discriminants for Intracranial Aneurysm Rupture. *Stroke* 42:144. doi: 10.1161/strokeaha.110.592923

Xiang, J., Siddiqui, A. H., and Meng, H. (2014). The effect of inlet waveforms on computational hemodynamics of patient-specific intracranial aneurysms. *J. Biomech.* 47, 3882–3890. doi: 10.1016/j.jbiomech.2014.09.034

Xiang, J., Varble, N., Davies, J. M., Rai, A. T., Kono, K., Sugiyama, S. I., et al. (2017). Initial Clinical Experience with AView-A Clinical Computational Platform for Intracranial Aneurysm Morphology, Hemodynamics, and Treatment Management. *World Neurosurg.* 108, 534–542. doi: 10.1016/j.wneu.2017.09.030

Yang, Y., Liu, Q., Jiang, P., Yang, J., Li, M., Chen, S., et al. (2021). Multidimensional predicting model of intracranial aneurysm stability with backpropagation neural network: a preliminary study. *Neurol. Sci.* [Preprint].

Zhang, C., Zhou, T., Chen, Z., Yan, M., Li, B., Lv, H., et al. (2020). Coupling of Integrin alpha5 to Annexin A2 by Flow Drives Endothelial Activation. *Circ. Res.* 127, 1074–1090. doi: 10.1161/circresaha.120.316857

**Conflict of Interest:** The authors declare that the research was conducted in the absence of any commercial or financial relationships that could be construed as a potential conflict of interest.

The reviewer XY declared a shared affiliation, with no collaboration with the authors to the handling editor at the time of the review.

**Publisher's Note:** All claims expressed in this article are solely those of the authors and do not necessarily represent those of their affiliated organizations, or those of the publisher, the editors and the reviewers. Any product that may be evaluated in this article, or claim that may be made by its manufacturer, is not guaranteed or endorsed by the publisher.

frontiers in Aging Neuroscience

ORIGINAL RESEARCH
published: 13 September 2021
doi: 10.3389/fnagi.2021.707732

# Risk of Post-stroke Epilepsy Following Stroke-Associated Acute Symptomatic Seizures

*Ru Lin[1†], Yaoyao Yu[1†], Yi Wang[2], Emma Foster[3], Patrick Kwan[3], Mengqi Lin[1], Niange Xia[4], Huiqin Xu[4], Chenglong Xie[4], Yunjun Yang[1*] and Xinshi Wang[4,5*]*

*[1] Department of Radiology, The First Affiliated Hospital of Wenzhou Medical University, Wenzhou, China, [2] School of Public Health and Management, Wenzhou Medical University, Wenzhou, China, [3] Department of Neuroscience, The Central Clinical School, Monash University, Melbourne, VIC, Australia, [4] Department of Neurology, The First Affiliated Hospital of Wenzhou Medical University, Wenzhou, China, [5] Key Laboratory of Alzheimer's Disease of Zhejiang Province, Institute of Aging, Wenzhou Medical University, Wenzhou, China*

**Objective:** Post-stroke epilepsy (PSE) is associated with increased morbidity and mortality. Stroke-associated acute symptomatic seizures are an important risk factor: 20.8–34.3% of these patients will go on to develop PSE. Identifying these "high risk" individuals may result in earlier PSE diagnosis, treatment, and avoidance of seizure-related morbidity. This study was to identify predictors of PSE development in patients with stroke-associated acute symptomatic seizures.

**Participants and Methods:** This was a retrospective cohort study of 167 patients with stroke-associated acute symptomatic seizures admitted to the Neurology Department of a tertiary Hospital of China, from 1 May 2006 to 30 January 2020. Both those with primary ischemic stroke and intracerebral hemorrhage were included in the study. Patient demographics, medical history, stroke-associated, and seizure-related variables were evaluated with univariable analysis and multivariable Cox regression analysis. PSE was defined as unprovoked seizures occurring > 7 days post-stroke. Data points were extracted from medical records and supplemented by tele-interview.

**Results:** Of the 167 patients with stroke-associated acute symptomatic seizures, 49 (29.3%) developed PSE. NIHSS score > 14 [hazard ratio (HR) 2.98, 95% CI 1.57–5.67], longer interval from stroke to acute symptomatic seizures (days 4–7 post-stroke) (HR 2.51, 95% CI 1.37–4.59) and multiple acute symptomatic seizures (HR 5.08, 95% CI 2.58–9.99) were independently associated with PSE development. This association remained in the sub-analysis within the ischemic stroke cohort. In the sub-analysis of the hemorrhagic stroke cohort, multilobar involvement (HR 4.80, 95% CI 1.49–15.39) was also independently associated with development of PSE. Further, we developed a nomogram to predict individual risk of developing PSE following stroke-associated acute symptomatic seizures. The nomogram showed a C-index of 0.73.

OPEN ACCESS

***Edited by:***
*Shuo Wang,*
*Capital Medical University, China*

***Reviewed by:***
*Garrett Smith,*
*University of Florida, United States*
*Candice Delcourt,*
*University of New South Wales, Australia*

***Correspondence:**
*Yunjun Yang*
*yyjunjim@163.com*
*Xinshi Wang*
*wang_xinshi@163.com*

*[†] These authors have contributed equally to this work*

***Received:*** *10 May 2021*
***Accepted:*** *25 August 2021*
***Published:*** *13 September 2021*

***Citation:***
*Lin R, Yu Y, Wang Y, Foster E, Kwan P, Lin M, Xia N, Xu H, Xie C, Yang Y and Wang X (2021) Risk of Post-stroke Epilepsy Following Stroke-Associated Acute Symptomatic Seizures. Front. Aging Neurosci. 13:707732. doi: 10.3389/fnagi.2021.707732*

**Conclusion:** More severe neurofunctional deficits (NIHSS score > 14), longer interval from stroke to acute symptomatic seizures (days 4–7 post-stroke), and multiple acute symptomatic seizures were independently associated with development of PSE in patients with stroke-associated acute symptomatic seizures. This knowledge may increase clinical vigilance for development of PSE, facilitating rapid diagnosis and treatment initiation, and subsequently reduce seizure-related morbidity.

**Keywords: ischemic stroke, intracranial hemorrhage, symptomatic seizure, post-stroke epilepsy, predictors**

## INTRODUCTION

Stroke is the leading cause of epilepsy in the elderly, accounting for 30–50% of all-cause epilepsy in this group (Ruggles et al., 2001; Verellen and Cavazos, 2011; Zhao et al., 2018). Post-stroke seizures have been observed in 3.3–13.7% of patients with ischemic stroke (Lancman et al., 1993; Burn et al., 1997; Lamy et al., 2003; Guo et al., 2015; Koome et al., 2016; Chen et al., 2017, 2018; Stefanidou et al., 2017; Merkler et al., 2018; Naylor et al., 2018; Brondani et al., 2019) and 12.1–25% of patients with hemorrhagic stroke (Faught et al., 1989; Lancman et al., 1993; Burn et al., 1997; Madžar et al., 2014; Biffi et al., 2016; Claessens et al., 2017; Lahti et al., 2017; Merkler et al., 2018). The International League Against Epilepsy (ILAE) classifies seizures that occur within 7 days of strokes as acute symptomatic seizures (Beghi et al., 2010). These are thought to be provoked by acute disruption of brain integrity, dysfunction of metabolic homeostasis, and transient depolarizations of neurons (Camilo and Goldstein, 2004). Conversely, seizures occurring more than 7 days after strokes are defined as post-stroke epilepsy (PSE) since the risk of recurrent unprovoked seizures over the subsequent 10-year period is 71.5% (Hesdorffer et al., 2009) and thus fulfills ILAE criteria for epilepsy, i.e., post-stroke epilepsy (PSE) (Fisher et al., 2014). They are thought to be the long-term sequela of progressive structural changes secondary to the stroke, including neuronal loss, subsequent gliosis, and reorganization of neuronal networks (Sun et al., 2001, 2002; Camilo and Goldstein, 2004).

Previous studies have shown that stroke-associated acute symptomatic seizures do not significantly influence functional outcomes (De Herdt et al., 2011). In contrast, PSE can hamper post-stroke recovery and contribute to neurological deterioration (Kwan, 2010; Arntz et al., 2013b; Biffi et al., 2016). It is therefore important to identify those at increased risk of developing PSE. Several studies have identified stroke-associated acute symptomatic seizures as an important risk factor: 20.8–34.3% of these patients will go on to develop PSE (Roivainen et al., 2013; Haapaniemi et al., 2014; Lahti et al., 2017; Galovic et al., 2018), and these patients are also at increased risk of developing drug-resistant epilepsy (de Greef et al., 2015). However, most studies investigating risk factors associated with development of PSE were focusing on the entire cohort of patients with stroke, such as the SeLECT (Galovic et al., 2018) and CAVE score (Haapaniemi et al., 2014). Only a few studies focused on this higher-risk subgroup with acute symptomatic seizures that necessitate earlier initiation of anti-seizure medications. Glasgow Coma Scale (GCS) score $\leq$ 8 at presentation, larger hemorrhage volume, and larger intraventricular hemorrhage volume have been identified as predictors of PSE for patients with intracranial hemorrhage-associated acute symptomatic seizures (Biffi et al., 2016). A National Institute of Health stroke scale (NIHSS) score > 4 and post-stroke status epilepticus lasting > 16 h have been associated with a greater risk of developing PSE in those with stroke-associated status epilepticus (Abraira et al., 2019).

There remains several important limitations and knowledge gaps in this field. Existing studies are limited by sample size, with fewer than 100 patients included in each study. The factors associated with PSE development in those with ischemic stroke-associated acute symptomatic seizures are yet to be determined. Moreover, variables associated with the characteristics of acute symptomatic seizures were not included in these studies and therefore their correlation with development of PSE is unknown.

We aimed to identify the factors associated with PSE development in patients who have experienced acute symptomatic seizures following ischemic or hemorrhagic stroke, and to incorporate this into a nomogram for use at the bedside or outpatient clinic to predict PSE.

## MATERIALS AND METHODS

### Subjects

This was a retrospective study of inpatients admitted to the Department of Neurology, the First Affiliated Hospital of Wenzhou Medical University, Wenzhou, China, from 1 May 2006 through 30 January 2020. The primary inclusion criterion was patients with a diagnosis of seizure, epilepsy, or status epilepticus, occurring within the initial 7-day period following a new-diagnosis stroke (i.e., patients with stroke-associated acute symptomatic seizures). Stroke types included primary ischemic stroke and primary intracranial hemorrhage as per ICD-10 codes. Exclusion criteria included: (1) patients without available computed tomography (CT) and/or magnetic resonance imaging (MRI); (2) patients with a prior diagnosis of epilepsy; (3) patients with secondary intracranial hemorrhage or venous infarction; (4) patients whose seizure might be attributed to other potential causes (brain tumor, intracranial vascular malformation, traumatic brain injury, etc.); and (5) patients who were lost to follow-up or died within 3 months of the stroke incident; (6) patients who reported ambiguous event occurring > 7 days post-stroke. This study was approved by the Ethics Committee of our hospital (No.2020-185). Verbal

informed consent was obtained from the subject or the subject's legally authorized representative through tele-interview.

## Recognition of Seizures and Patient Follow-Up

Acute symptomatic seizures were defined as seizures occurring within 7 days of a stroke as per the ILAE definition (Beghi et al., 2010). PSE was diagnosed in patients with unprovoked seizures occurring 7 days after a stroke in the context of stroke-associated epileptogenic substrate as noted on neuroimaging. Presence of PSE seizures was ascertained by consensus agreement from two epileptologists (XW and NX), with disagreements adjudicated by a senior epileptologist (HX). Patients that reported ambiguous seizure-like events were conservatively excluded from the analysis. Other information collected included use of anti-seizure medications (ASMs), development of stroke-associated neurological symptoms (e.g., hemiparesis), and death. These were extracted from medical records, and supplemented by tele-interview using a modified standardized questionnaire (**Table 1**; Keezer et al., 2014). All participants were followed up until seizure recurrence, occurrence of a further stroke, death, or end of the study period (May 30, 2020).

**TABLE 1 |** Post-stroke epilepsy screening questionnaire.

**Q1: Self-reported diagnosis**

a. Has ever been diagnosed by a doctor to have seizures/epilepsies/convulsions after discharge? [a]

b. How soon after discharge did you experience the first recurrent seizure? [b]

Only patients responded Q1a with "yes" were recorded as post-stroke epilepsy, if not, patients were asked by following questions.

**Q2: Symptom-based screening questions: a, b**

a. Have you ever had, or has anyone told you that you had any of the following symptom after discharge? [c]

i. A seizure, convulsive, fit or spell under any circumstances?

ii. Uncontrolled movement of part or all of your body such as twitching, jerking, shaking, or going limp?

iii. An unexplained change in your mental state or level or unawareness; or an episode of "spacing out" that you could not control?

iv. Shortly after waking up, either in the morning or after a nap, have you ever noticed uncontrollable jerking or clumsiness, such as dropping things or things suddenly "flying" from your hands?

v. Have you ever had repeated unusual spells?

b. How soon after discharge did the symptom happen? [b]

**Q3: Questions about Anti-seizure medications?**

a: Are you currently using any anti-seizure drug including "valproate," "levetiracetam," "carbamazepine," or "oxcarbazepine"?

b: If not, when did you stop the drug? [d]

a Acceptable answers to each of the questions include: "yes," "no," "possible," or "don't know."

b Only if the patient or caregiver can provide the approximate date or we can obtain it from the medical records, he/she were included in analysis.

c Patients were diagnosed with PSE only if they fulfill 1 + 2 + 3 or 1 + 4 of the following: 1. "yes" for Q2a-i or ii, 2. Provide an approximate date for Q2b, 3. "yes" for Q3a, 4. confirmed by medical records. If they respond "no" for any of the questions, they were recorded as non-PSE. Otherwise, they're excluded from analysis to ensure the best accuracy of diagnosis.

d An approximate year

*PSE, post-stroke epilepsy.*

## Variables

### Stroke-Associated Variables

Stroke was categorized into primary ischemic stroke and intracranial hemorrhage. Ischemic stroke was further classified according to the TOAST (Trial of Org 10172 in Acute Stroke Treatment) criteria, i.e., large-artery atherosclerosis, cardioembolism, small-vessel occlusion, stroke of other determined etiology, and stroke of undetermined etiology (Adams et al., 1993). Stroke severity at admission was recorded as per the NIHSS. Medical treatment of stroke was categorized as thrombolysis, lipid-lowering therapy, antiplatelet therapy, anticoagulation, as well as surgical interventions. Variables related to stroke localization included cortical involvement, multilobar involvement, deep region involvement, as well as ventricular extension of hematoma. Volumetric assessment of the lesion location was completed through three-dimensional reconstruction of the regions of interest and manual depiction of the lesion circumference in multiple successive layers (Zhang et al., 2020). Infectious complications that occurred during hospitalization, such as respiratory tract infections, were also recorded.

### Other Variables

Other variables collected included demographic information, i.e., sex; age at time of stroke; concomitant medical diseases, i.e., hypertension, diabetes, hyperlipidemia, and hyperuricemia; and lifestyle factors, i.e., current smoking and alcohol intake status.

### Seizure-Related Variables

Acute symptomatic seizure-related variables included time interval (days) from stroke to seizure; presence of multiple acute symptomatic seizures, defined as $\geq$ 2 seizures occurring over $\geq$ 24 h time period but within 7 days of the stroke; and presence of status epilepticus, as per the ILAE diagnostic criteria (Trinka et al., 2015). Only events with clear focal motor or focal to bilateral tonic-clonic semiology were included in the study. Given the retrospective nature of the study, potential non-motor seizure events were conservatively excluded to reduce the risk of erroneously including ambiguous, non-seizure events. Electroencephalogram (EEG) results within 1 week of acute symptomatic seizure onset were classified as either normal, non-specific abnormalities, and/or epileptiform discharges. ASM regimen at the time of most recent follow-up was recorded. The time interval (days) from the stroke to first unprovoked seizure was recorded.

## Statistical Analysis

The primary endpoint was time to first unprovoked seizure. Age and stroke lesion volume were analyzed both as continuous and categorical variables, specifically, age $<$ 65 years and lesion volume $>$ 10 ml, as these factors have previously been associated with intracranial hemorrhage-associated PSE (Haapaniemi et al., 2014). Other factors were analyzed as categorical variables. Cut-off points with the best sensitivity and specificity to predict PSE development were identified for the NIHSS score and the time interval from stroke to acute symptomatic seizure. Univariable

analysis were conducted using the Kaplan-Meier method with a log-rank test or univariable Cox regression. Variables with $p \leq 0.1$ in the univariable analysis were then selected into the multivariable Cox proportional hazard regression analysis using "survival" package with a forward stepwise method based on likelihood ratio, to establish the fitted model and calculate the hazard ratio (HR). Censored patients in the Kaplan-Meier analysis and Cox regression analysis included those who experienced a further stroke before experiencing their first unprovoked seizure; those who were lost to follow up; those who died due to non-seizure related causes; and those who did not experience unprovoked seizures within the study period. A nomogram based on the multivariable analysis of the total cohort was built using the "rms" package, and Harrell's C-index was measured to quantify the discrimination performance of the nomogram. Forest plot displaying the results of multivariable analysis was completed with the "forest" package. Two-tailed $p$-values $< 0.05$ were considered to be statistically significant. Statistical analysis was conducted with R software (version 4.0.3).

# RESULTS

A total of 331 patients met the primary inclusion criteria with a stroke and early seizures occurring within the initial 7-day period. Among them, 167 met all eligibility criteria for new-onset acute symptomatic seizure secondary to the index stroke and were retained for analyses (**Figure 1**).

## Characteristics of All Subjects With Stroke-Associated Acute Symptomatic Seizures

**Table 2** displays characteristics of the study cohort. The final study cohort comprised of 111 (66.5%, $n = 111/167$) patients with primary ischemic stroke and 56 (33.5%, $n = 56/167$) with primary intracranial hemorrhage. Approximately half of these patients (54.5%, $n = 91/167$) experienced bilateral tonic-clonic seizures and 66 (39.5%, $n = 66/167$) experienced focal motor seizures. The median time of acute symptomatic seizure onset was 0 days [interquartile range (IQR) 0–2] post-stroke. Only a small proportion of patients (16.8%, $n = 28/167$) experienced acute symptomatic seizures $> 3$ days post-stroke. Status epilepticus was recorded in 44 patients (26.3%, $n = 44/167$). Multiple acute symptomatic seizures occurred in 21 patients (12.6%, $n = 21/167$). Only 38.3% ($n = 64/167$) of patients underwent EEG recording during their acute inpatient hospitalization. Of these, 26 (40.6%) had epileptiform discharges, 35 (54.7%) had non-specific abnormalities, and 3 (4.7%) were normal. Most of the patients (80.2%, $n = 134/167$) received ASM therapy for their acute symptomatic seizures. Twenty-nine (59.2%) patients were still taking ASM therapy at the time they experienced their first PSE-related unprovoked seizure, and 23 (19.5%) patients were still on ASM therapy at the end of the study without having experienced an unprovoked seizure. The median follow-up time was 592 days (IQR 170–1512). PSE developed in 49 (29.3%) patients: 18 (32.1%, $n = 18/56$) of those with hemorrhagic stroke, and 31 (27.9%, $n = 31/111$) of those with ischemic stroke. The PSE incidence over time is displayed in **Figure 2**.

## Analysis of PSE Predictors in the Total Cohort

The results of univariable analyses are displayed in **Table 3**. NIHSS score $> 14$ at admission and longer interval from stroke to acute symptomatic seizures (days 4–7 post-stroke) were significantly more likely in those who went on to develop PSE compared to those who did not (32.7% vs. 12.7%, $p = 0.002$ and 32.7% vs. 10.2%, $p < 0.001$, respectively). Multiple acute symptomatic seizures were also significantly associated with subsequent development of PSE (26.5% vs. 6.8%, $p < 0.001$). There were no statistical differences for other variables between the PSE and non-PSE subgroups. In the Cox proportional hazard model, NIHSS score $> 14$ at admission (HR 2.98, 95% CI 1.57–5.67, $p = 0.001$), multiple acute symptomatic seizures (HR, 5.08; 95% CI, 2.58–9.99; $p < 0.001$), and longer interval from stroke to acute symptomatic seizures (days 4–7 post-stroke) (HR 2.51, 95% CI 1.37–4.59, $p = 0.003$) were associated with PSE following stroke-associated acute symptomatic seizure(s) **(Figure 3A)**.

## Analysis of PSE Predictors Within the Ischemic Stroke Cohort

A subgroup analysis was performed to evaluate predictors of PSE in those with ischemic stroke-associated acute symptomatic seizures. NIHSS score $> 14$ (29.0% vs. 12.5%, $p = 0.04$), multiple acute symptomatic seizures (22.6% vs. 8.8%, $p = 0.01$), and longer interval from stroke to acute symptomatic seizures (days 4–7 post-stroke) (35.5% vs. 10.0%, $p = 0.002$) were associated with development of PSE in the univariable analysis. Interestingly, cortical involvement of the stroke territory (77.4% vs. 93.8%, $p = 0.004$) was less common in patients that went on to develop PSE compared to those without PSE, and reached statistical significance in the univariable analysis (**Table 2**). In the subsequent Cox regression analysis, NIHSS score $> 14$ (HR 2.94, 95% CI 1.28–6.73, $p = 0.01$), acute symptomatic seizures occurring $> 3$ days post-stroke (HR 3.84, 95% CI 1.77–8.31, $p = 0.001$), and multiple acute symptomatic seizures (HR 5.13, 95% CI 2.01–13.09, $p = 0.001$) were associated with PSE development (**Figure 3A**).

## Analysis of PSE Predictors Within the Hemorrhagic Stroke Cohort

We also conducted sub-analyses for patients with hemorrhagic stroke-associated acute symptomatic seizures. Significant predictors included NIHSS scores $> 14$ (38.9% vs. 13.2%, $p = 0.02$), multiple acute symptomatic seizures (33.3% vs. 2.6%, $p < 0.001$), and stroke lesions with cortical involvement (94.4% vs. 65.8%, $p = 0.04$). In the Cox proportional hazard model, multiple acute symptomatic seizures (HR 14.60, 95% CI 4.24–50.25, $p < 0.001$), NIHSS score $> 14$ at admission (HR 3.17, 95% CI 1.10–9.11, $p = 0.03$) and multilobar involvement (HR 4.80, 95% CI 1.49–15.39, $p = 0.008$) were associated with PSE development following a hemorrhagic stroke-associated acute symptomatic seizure (**Figure 3A**).

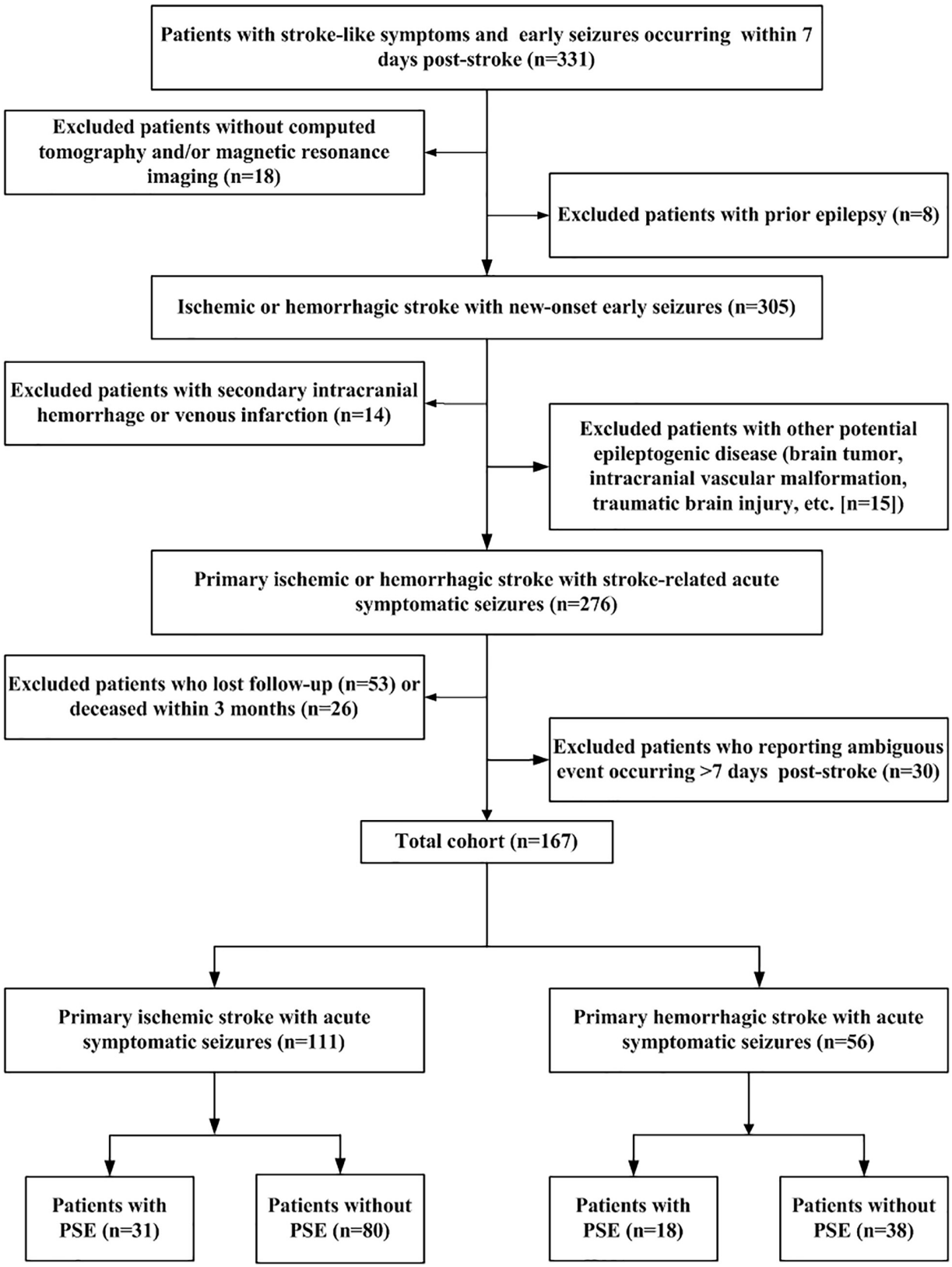


**FIGURE 1 |** Flow chart of patient recruitment. Flow-chart summarizing sequential application of inclusion/exclusion criteria leading to definition of final study cohort. PSE: post-stroke epilepsy.

**TABLE 2 |** Baseline characteristics of the total cohort.

| Variables | *n* = 167 |
|---|---|
| **Demographics** | |
| Male sex, No./total No. (%)<br>Female sex, n(%) | 114/167 (68.3) |
| Age at onset (years), mean (SD) | 64.4 (12.9) |
| **Medical history** | |
| Alcohol drinking, No./total No. (%) | 68/167 (40.7) |
| Smoking, No./total No. (%) | 73/167 (43.7) |
| Hypertension, No./total No. (%) | 121/167 (72.5) |
| Diabetes, No./total No. (%) | 38/167 (22.8) |
| Hyperlipidemia, No./total No. (%) | 12/167 (7.2) |
| Hyperuricemia, No./total No. (%) | 45/167 (26.9) |
| **Characteristics of stroke** | |
| Ischemic stroke, No./total No. (%) | 111/167 (66.5) |
| NIHSS score > 14, No./total No. (%) | 31/167 (18.6) |
| Location of the stroke, No./total No. (%)[a] | |
| Cortical involvement | 142/167 (85.0) |
| Multilobar involvement | 83/167 (49.7) |
| Deep region involvement | 61/167 (36.5) |
| Lesion volume (ml), median (IQR) | 9.0 (2.7–24.0) |
| Infectious complication, No./total No. (%) | 58/167 (34.7) |
| Follow-up duration (days), median (IQR) | 592 (170–1512) |
| **Characteristics of seizures** | |
| Seizure type, No./total No. (%) | |
| Bilateral tonic-clonic seizure | 91/167 (54.5) |
| Focal motor seizure | 66/167 (39.5) |
| Undetermined | 10/167 (6.0) |
| Stroke-to-acute symptomatic seizure interval (days), median (IQR) | 0 (0–2) |
| Stroke-to-acute symptomatic seizure interval > 3 days, No./total No. (%) | 28/167 (16.7) |
| Multiple acute symptomatic seizures, No./total No. (%) | 21/167 (12.6) |
| Status epilepticus, No./total No. (%) | 44/167 (26.3) |
| EEG, No./total No. (%) | |
| Normal | 3/167 (1.8) |
| Non-specific abnormality | 35/167 (21.0) |
| Epileptiform discharge | 26/167 (15.6) |
| Absent | 103/167 (61.7) |
| ASM treatment, No./total No. (%) | 134/167 (80.2) |
| PSE, No./total No. (%) | 49/167 (29.3) |

*Continuous variables with normal distribution were presented as mean [standard deviation (SD)]; non-normal variables were presented as median [interquartile range (IQR)]; quantitative variables were presented as number/total number (%).*
*NIHSS, National Institute of Health stroke scale; ASM, anti-seizure medication; EEG, electroencephalogram; PSE, post-stroke epilepsy.*
[a] *Some patients were counted in more than one group.*

## Development of a Clinical Prediction Nomogram

We built a nomogram based on the Cox proportional hazard model in the total cohort to predict an individual's risk of developing PSE following stroke-associated acute symptomatic seizures (**Figure 3B**). In the nomogram, an interval from stroke to acute symptomatic seizures > 3 days (days 4–7 post-stroke) equals 57.5 points, multiple acute symptomatic seizures equal 100 points, a NIHSS score > 14 equals 67.5 points. The corresponding risk of PSE was < 20%, approximately 27, 31, 47, 60, and > 80% for a patient with total points of 0, 57.5, 67.5, 100, 125 (57.5 + 67.5), and ≥ 160, respectively, during 1-year follow-up; and it was about 20, 35, 39, 58, 72, and ≥ 90% during 2-year follow-up. The C-index for the prediction nomogram was 0.73.

# DISCUSSION

This study revealed that people with stroke-associated acute symptomatic seizures are more likely to develop PSE if they have more severe neurofunctional deficits at time of stroke presentation; if their initial acute symptomatic seizure occurs between days 4 and 7 post-stroke; if the stroke involves multilobar and if patients experience multiple acute symptomatic seizures within the first week post-stroke. These factors have been incorporated into a nomogram to assist clinicians in calculating the risk of PSE development for individual patients, which in turn may assist with management decisions.

Our study found that seizures occurring between days 4 and 7 post-stroke were associated with a higher risk of developing PSE, compared to early seizures that occurred between days 0 and 3 post-stroke. This finding is consistent with previous studies which reported that acute symptomatic seizures mainly occurred within 3 days of stroke onset (Haapaniemi et al., 2014), and seizures that occurred later were associated with higher risk of long-term seizure recurrence (Sung and Chu, 1990; Bladin et al., 2000). These findings suggest that the definition of stroke-associated acute symptomatic seizures may be revised to those occurring within 3 days of the stroke onset, as opposed to the current definition of occurring within 7 days. The occurrence of multiple seizures within the first week following a stroke was a predictor for future PSE. Although these multiple early seizures all fell within the current definition of an "acute symptomatic seizure" timeframe, they may in fact represent the early stages of PSE. Supporting this, microarray analysis in a rat ischemic model has found that down-regulation of several ion channels and receptors begins as early as 1 day post-stroke (Lu et al., 2004).

Consistent with previous studies, our work found that stroke severity is strongly associated with development of PSE (Arntz et al., 2013a; Graham et al., 2013; Jungehulsing et al., 2013; Zhang et al., 2014). A previous study identified GCS score ≤ 8 at time of stroke admission was an important risk factor for development of PSE in those with intracranial hemorrhage-associated acute symptomatic seizures (Biffi et al., 2016). Although the GCS was not designed for this purpose, it may be interpreted as a surrogate marker for stroke severity. A previous study examined factors associated with development of PSE for patients with stroke-associated status epilepticus. An NIHSS cut score of > 4 at time of stroke admission was found to be a significant predictor of future development of PSE (Abraira et al., 2019). Our study found the significant NIHSS cut-score to be > 14, indicating more extensive neuronal damage was required to cross the PSE threshold for our patients. The lower NIHSS threshold for patients with status epilepticus may be due to the additional risk that status epilepticus carries in terms of developing PSE (Tomari et al., 2017).

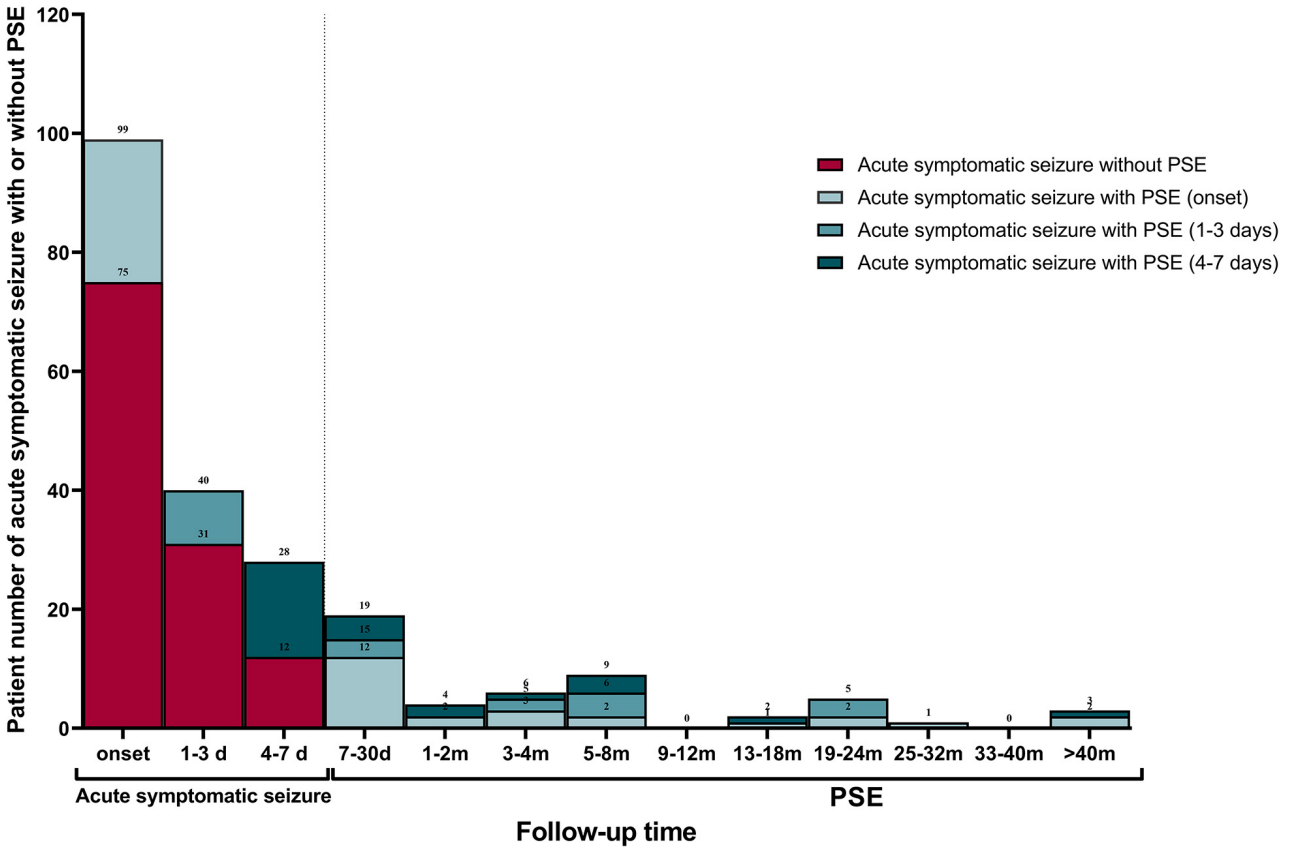


**FIGURE 2 |** Late recurrent seizure incidence over time. Frequency and distribution of patients with early seizures occurred within 7 days of index stroke and PSE occurred after 7 days of index stroke. PSE, post-stroke epilepsy.

Large stroke lesion volume has previously been associated with development of PSE, particularly in patients with hemorrhagic strokes (Bladin et al., 2000; Haapaniemi et al., 2014). However, this association was not found in our study. Instead, we found multilobar involvement to be an important predictor for the development of PSE. This finding has also been noted in other studies (Lancman et al., 1993; Beghi et al., 2011). Although large stroke volume and multilobar involvement represent similar measures, the latter may also be interpreted as a surrogate marker for more severe neurofunctional deficits. Supporting this, we found the lesion volume was significantly larger and NIHSS score was significantly higher in patients with multilobar involvement compared to those with single lobe involvement (**Table 4**).

There is conflicting evidence regarding the association between cortical involvement of stroke and risk of development of PSE. In the univariable analysis, those with hemorrhagic stroke-associated acute symptomatic seizures were more likely to develop PSE if there was cortical involvement compared to if there was not; this has also been reported previously (Haapaniemi et al., 2014; Biffi et al., 2016; Galovic et al., 2018). Conversely, cortical involvement was negatively associated with PSE development in those with ischemic stroke-associated acute symptomatic seizures; previous studies have reported similarly (Tomari et al., 2017; Abraira et al., 2019). Certainly, cortical involvement is a well-recognized risk factor for stroke-associated acute symptomatic seizures. The resultant cortical irritation may directly damage cortical neurons, causing increased neuronal excitability and leading to the onset of seizures in the acute stroke phase (Arboix et al., 1997; Roivainen et al., 2013). The negative association between cortical involvement and development of PSE is not necessarily indicative of a "protective" effect of cortical involvement. Rather, the development of acute symptomatic seizures in those without direct cortical irritation may be indicative of an increased predisposition to epileptic seizures. This may be genetic or lesional. For example, strokes within the deep brain matter may occur in individuals with small-vessel disease, which in turn is associated with development of epilepsy in the elderly (Pitkanen et al., 2016). Further research is needed to confirm this hypothesis.

Our study has important practical implications in terms of identifying those at higher risk for developing PSE following stroke-associated acute symptomatic seizures. This group may benefit from closer clinical follow-up, which may facilitate earlier PSE diagnosis and treatment initiation. This in turn may reduce the risk of future seizure-related morbidity and mortality. Our study reveals several important directions for future research. These include investigating the temporal association of

**TABLE 3 |** Univariable analysis of baseline characteristics associated with development of PSE.

| Variables | Total cohort | | | Ischemic stroke cohort | | | Hemorrhagic stroke cohort | | |
|---|---|---|---|---|---|---|---|---|---|
| | PSE ($n = 49$) | Non-PSE ($n = 118$) | *P*-value | PSE ($n = 31$) | Non-PSE ($n = 80$) | *P*-value | PSE ($n = 18$) | Non-PSE ($n = 38$) | *P*-value |
| **Demographics** | | | | | | | | | |
| Male sex, No./total No. (%) | 33/49 (67.3) | 81/118 (68.6) | 0.86 | 19/31 (61.3) | 55/80 (68.8) | 0.65 | 14/18 (77.8) | 26/38 (68.4) | 0.38 |
| Age at onset (years), mean (SD) | 64.5 (11.2) | 64.3 (13.6) | 0.50 | 67.8 (8.9) | 65.5 (12.1) | 0.34 | 59.8 (13.0) | 61.6 (16.2) | 0.91 |
| Age < 65 years, No./total No. (%) | 23/49 (46.9) | 59/118 (50.0) | 0.47 | 11/31 (35.5) | 37/80 (46.3) | 0.31 | 12/18 (66.7) | 22/38 (57.8) | 0.97 |
| **Medical history** | | | | | | | | | |
| Alcohol drinking, No./total No. (%) | 19/49 (38.8) | 49/118 (41.5) | 0.79 | 11/31 (35.5) | 30/80 (37.5) | 0.93 | 8/18 (44.4) | 19/38 (50.0) | 0.66 |
| Smoking, No./total No. (%) | 19/49 (38.8) | 54/118 (45.8) | 0.42 | 12/31 (38.7) | 37/80 (46.3) | 0.70 | 7/18 (38.9) | 17/38 (44.7) | 0.36 |
| Hypertension, No./total No. (%) | 37/49 (75.5) | 85/118 (72.0) | 0.56 | 20/31 (64.5) | 52/80 (65.0) | 0.86 | 17/18 (94.4) | 32/38 (84.2) | 0.18 |
| Diabetes, No./total No. (%) | 12/49 (24.5) | 26/118 (22.0) | 0.64 | 8/31 (25.8) | 20/80 (25.0) | 0.95 | 4/18 (22.2) | 6/38 (15.8) | 0.54 |
| Hyperlipidemia, No./total No. (%) | 4/49 (8.2) | 8/118 (6.8) | 0.60 | 2/31 (6.5) | 3/80 (3.8) | 0.31 | 2/18 (11.1) | 5/38 (13.2) | 0.90 |
| Hyperuricemia, No./total No. (%) | 12/49 (24.5) | 33/118 (28.0) | 0.88 | 8/31 (25.8) | 22/80 (27.5) | 0.98 | 4/18 (22.2) | 11/38 (28.9) | 0.77 |
| **Characteristics of seizures** | | | | | | | | | |
| Seizure type, No./total No. (%) | | | 0.43 | | | 0.94 | | | 0.10 |
| Bilateral tonic-clonic seizure | 26/49 (53.1) | 65/108 (60.2) | | 17/31 (54.8) | 41/75 (54.7) | | 9/18 (50.0) | 24/33 (72.7) | |
| Focal motor seizure | 23/49 (46.9) | 43/108 (39.8) | | 14/31 (45.2) | 34/75 (45.3) | | 9/18 (50.0) | 9/33 (23.3) | |
| Stroke-to-acute symptomatic seizure interval (days), median (IQR) | 0.0 (0.0–4.0) | 0.0 (0.0–2.0) | 0.01 | 0.0 (0.0–4.0) | 0.0 (0.0–1.0) | 0.03 | 2.0 (0.0–4.0) | 1.0 (0.0–2.0) | 0.23 |
| Stroke-to- acute symptomatic seizure interval > 3 days, No./total No. (%) | 16/49 (32.7) | 12/118 (10.2) | <0.001 | 11/31 (35.5) | 8/80 (10.0) | 0.002 | 5/18 (27.8) | 4/38 (10.5) | 0.08 |
| Multiple acute symptomatic seizures, No./total No. (%) | 13/49 (26.5) | 8/118 (6.8) | <0.001 | 7/31 (22.6) | 7/80 (8.8) | 0.01 | 6/18 (33.3) | 1/38 (2.6) | < 0.001 |
| Status epilepticus, No./total No. (%) | 16/49 (32.7) | 28/118 (23.7) | 0.36 | 10/31 (32.3) | 18/80 (22.5) | 0.50 | 6/18 (33.3) | 10/38 (26.3) | 0.59 |
| EEG, No./total No. (%) | | | 0.27 | | | 0.85 | | | 0.15 |
| Normal | 0/19 (0.0) | 3/45 (6.7) | | 0/12 (0.0) | 1/37 (2.7) | | 0/7 (0.0) | 2/8 (25.0) | |
| Non-specific abnormality | 9/19 (47.4) | 26/45 (57.8) | | 7/12 (58.3) | 23/37 (62.1) | | 2/7 (28.6) | 3/8 (37.5) | |
| Epileptiform discharge | 10/19 (52.6) | 16/45 (35.6) | | 5/12 (41.7) | 13/37 (35.1) | | 5/7 (71.4) | 3/8 (37.5) | |
| ASM treatment, No./total No. (%) | 41/49 (83.7) | 93/118 (78.8) | 0.44 | 28/31 (90.3) | 61/80 (76.3) | 0.09 | 13/18 (72.2) | 32/38 (84.2) | 0.23 |
| **Characteristics of stroke** | | | | | | | | | |
| NIHSS score > 14, No./total No. (%) | 16/49 (32.7) | 15/118 (12.7) | 0.002 | 9/31 (29.0) | 10/80 (12.5) | 0.04 | 7/18 (38.9) | 5/38 (13.2) | 0.02 |
| Infectious complication, No./total No. (%) | 19/49 (38.8) | 39/118 (33.1) | 0.39 | 12/31 (38.7) | 25/80 (31.3) | 0.52 | 7/18 (38.9) | 14/38 (36.8) | 0.66 |
| Lesion volume (ml), median (IQR) | 9.8 (2.3–28.6) | 9.0 (3.1–21.9) | 0.86 | 9.0 (1.1–21.6) | 7.6 (1.9–25.9) | 0.53 | 14.2 (5.0–42.5) | 13.4 (4.9–21.0) | 0.18 |
| Lesion volume > 10 ml, No./total No. (%) | 23/49 (46.9) | 51/118 (43.2) | 0.65 | 14/31 (45.2) | 30/80 (37.5) | 0.50 | 9/18 (50.0) | 18/38 (47.4) | 0.72 |
| Location of stroke, No./total No. (%)[a] | | | | | | | | | |
| Cortical involvement | 41/49 (83.7) | 101/118 (85.6) | 0.69 | 24/31 (77.4) | 75/80 (93.8) | 0.02 | 17/18 (94.4) | 25/38 (65.8) | 0.04 |
| Multilobar involvement | 27/49 (55.1) | 58/118 (49.2) | 0.35 | 20/31 (64.5) | 50/80 (62.5) | 0.61 | 7/18 (38.9) | 6/38 (15.8) | 0.08 |
| Deep region involvement | 16/49 (32.7) | 45/118 (38.1) | 0.64 | 12/31 (38.7) | 33/80 (41.3) | 0.89 | 2/18 (11.1) | 11/38 (28.9) | 0.65 |
| Extension into ventricle, No./total No. (%) | | | | | | | 3/18 (16.7) | 8/38 (23.7) | 0.85 |
| Surgical treatment, No./total No. (%) | | | | | | | 4/18 (22.2) | 5/38 (13.2) | 0.29 |
| TOAST classification, No./total No. (%) | | | | | | 0.33 | | | |
| Large-artery atherosclerosis | | | | 22/31 (71.0) | 43/80 (53.8) | | | | |
| Cardioembolism | | | | 2/31 (6.5) | 11/80 (13.8) | | | | |
| Small-vessel occlusion | | | | 3/31 (9.7) | 17/80 (21.3) | | | | |
| Stroke of other determined etiology | | | | 2/31 (6.5) | 5/80 (6.3) | | | | |
| Stroke of undetermined etiology | | | | 2/31 (6.5) | 4/80 (5.0) | | | | |

*(Continued)*

**TABLE 3 |** (Continued)

| Variables | Total cohort | | | Ischemic stroke cohort | | | Hemorrhagic stroke cohort | | |
|---|---|---|---|---|---|---|---|---|---|
| | PSE ($n = 49$) | Non-PSE ($n = 118$) | *P*-value | PSE ($n = 31$) | Non-PSE ($n = 80$) | *P*-value | PSE ($n = 18$) | Non-PSE ($n = 38$) | *P*-value |
| Thrombolysis, No./total No. (%) | | | | 1/31 (3.2) | 3/80 (3.8) | 1.00 | | | |
| Lipid-lowering therapy, No./total No. (%) | | | | 25/31 (80.6) | 68/80 (85.0) | 0.69 | | | |
| Thrombocytopenic therapy, No./total No. (%) | | | | 28/31 (90.3) | 60/80 (75.0) | 0.10 | | | |
| Anticoagulation, No./total No. (%) | | | | 8/31 (25.8) | 19/80 (23.8) | 0.80 | | | |
| **Follow-up duration (days), median (IQR)** | 74 (17–201) | 993 (496–2056) | | 55 (15–202) | 963 (504–1,669) | | 126 (30–242) | 1,155 (472–2,622) | |

*Continuous variables with normal distribution were presented as mean [standard deviation (SD)]; non-normal variables were presented as median [interquartile range (IQR)]; quantitative variables were presented as number/total number (%).*
*PSE, post-stroke epilepsy; NIHSS, National Institute of Health stroke scale; ASM, anti-seizure medication; EEG, electroencephalogram.*
[a] *Some patients were counted in more than one group.*

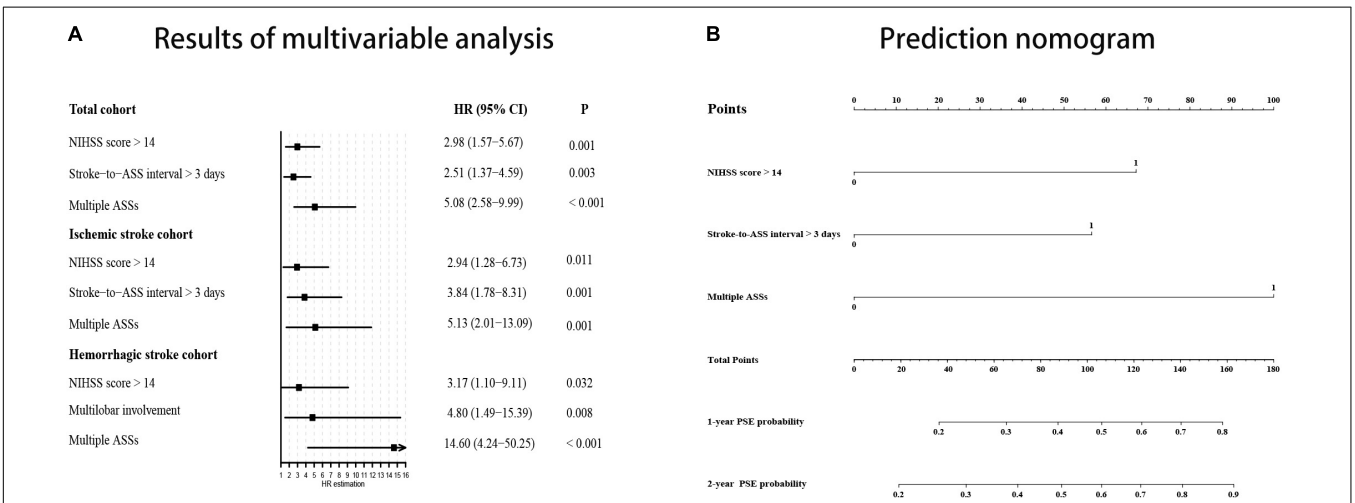


**FIGURE 3 |** PSE probability prediction using results of multivariable analysis. **(A)** Forest plot based on results of multivariable analysis. **(B)** Prediction nomogram on the basis of results multivariable analysis in the total cohort. NIHSS, National Institute of Health stroke scale; ASS, acute symptomatic seizure; PSE, post-stroke epilepsy; 95% CI, 95% confidence interval.

**TABLE 4 |** Comparing NHISS score and lesion volume between patients with and without multilobar involvement in hemorrhagic stroke cohort.

| | With multilobar involvement ($n = 16$) | Without multilobar involvement ($n = 40$) | *P*-value |
|---|---|---|---|
| NIHSS score, median (IQR) | 11 (6–17) | 4 (2–12) | 0.015 |
| Lesion volume (ml), median (IQR) | 18.9 (10.0–45.5) | 9.0 (3.9–21.4) | 0.023 |

*IQR, interquartile range; NIHSS, National Institute of Health stroke scale.*

stroke-associated acute symptomatic seizures and development of PSE by observing dynamic changes of critical molecules; exploring the shared pathophysiological mechanisms of neuronal damage and development of epileptic seizures induced by stroke; and eliciting the mechanisms underlying the predisposition for developing PSE. Further, our findings may be used to target high risk patients for recruitment in clinical trials that evaluate interventions to prevent PSE.

For example, based on the nomogram, for a patient whose seizures occur between days 4–7 post-stroke, if he/she has no other risk factors, the total points would be 57.5 and the risk of PSE is only 27% following the first year post-stroke and 34% following the second year; but if he/she has also a NIHSS score > 14, the total points would be 125 and the risk of PSE is about 60% following the first year post-stroke and 72% following the second year; if he/she experiences multiple seizures within 7 days post-stroke, he/she will get additional 100 points and thus the risk of PSE will be very high (>80%). Not only closer clinical follow-up should be conducted for these patients, but also prophylactic anti-seizure treatment might be necessary in view of the high PSE risk for the latter two conditions, especially the last one.

Our study has several limitations. As with all studies with a medical chart review component, identifying patients with acute symptomatic seizures relied on comprehensive medical documentation. Although it was felt that motor seizures could be correctly identified with reasonable confidence by both the treating clinician and the researchers who subsequently reviewed the medical chart, there was less certainty around the diagnosis for patients with subtle, non-motor events. As such, the latter events were excluded from the study. This focus on specificity rather than sensitivity resulted in a highly curated dataset, but potentially at the expense of under-reporting acute symptomatic seizure events. The follow-up diagnosis of PSE rested largely on patient and caregiver reports. PSE-seizures may present with non-motor semiology, and so may not be obvious to non-medically trained people. Therefore, it is possible that the true incidence of PSE was also under-reported.

In addition, a high proportion of males (68%) were included in our cohort as compared to other studies (Biffi et al., 2016; Abraira et al., 2019). As noted, an important difference between previous studies and our study is that we only included motor seizures. Therefore, a possible explanation is that women are more prone to non-motor seizures post-stroke. A hospital-based study has found that the female percentage of the patients with post-stroke non-convulsive status epilepticus (NCSE) was higher than that of the stroke patients without NCSE (50% vs. 35.9%) (Belcastro et al., 2014). Although the difference did not reach statistical significance, this might be due to the small sample size as there were only 32 patients with post-stroke NCSE (Belcastro et al., 2014). Further investigations were needed to verify the hypothesis. On the other hand, the male proportion is comparable to that of some large-sized stroke registry cohorts in China with 60–67.5% males (Wei et al., 2010; Zhang et al., 2021). This might be ascribed to the well-documented higher incidence of stroke in men than in women in all age classes (Reeves et al., 2008) and the higher male proportion in Chinese population.

## CONCLUSION

In summary, patients with an NIHSS score > 14, acute symptomatic seizures occurring > 3 days post-stroke, and multiple acute symptomatic seizures were at higher risk of developing PSE compared to patients with stroke-associated acute symptomatic seizures without these factors. In addition, multilobar involvement was also a predictor of PSE in patients with primary hemorrhagic stroke-associated acute symptomatic seizures.

## DATA AVAILABILITY STATEMENT

The raw data supporting the conclusions of this article will be made available by the authors, without undue reservation.

## ETHICS STATEMENT

The studies involving human participants were reviewed and approved by the Review of Ethics Committee in Clinical Research of the First Affiliated Hospital of Wenzhou Medical University. The ethics committee waived the requirement of written informed consent for participation.

## AUTHOR CONTRIBUTIONS

XW and YYa designed this study, obtained funding for this study, and supervised this study. ML and XW drafted this manuscript. XW, PK, EF, and YYa made critical revision of this manuscript for important intellectual content. ML, YYu, and YW conducted statistical analysis of this study. XW, HX, and YYa gave administrative, technical, or material supports. All authors collected the data.

## FUNDING

This work was supported by the National Natural Science Foundation of China (No. 82001363), the Health Foundation for Creative Talents in Zhejiang Province, China (No. 2016), and the Project Foundation for the College Young and Middle-Aged Academic Leader of Zhejiang Province, China (No. 2017).

## SUPPLEMENTARY MATERIAL

The Supplementary Material for this article can be found online at: https://www.frontiersin.org/articles/10.3389/fnagi.2021.707732/full#supplementary-material

## REFERENCES

Abraira, L., Toledo, M., Guzman, L., Sueiras, M., Quintana, M., Fonseca, E., et al. (2019). Long-term epilepsy after early post-stroke status epilepticus. *Seizure* 69, 193–197. doi: 10.1016/j.seizure.2019.04.022

Adams, H. P. Jr., Bendixen, B. H., Kappelle, L. J., Biller, J., Love, B. B., Gordon, D. L., et al. (1993). Classification of subtype of acute ischemic stroke. Definitions for use in a multicenter clinical trial. TOAST. Trial of Org 10172 in Acute Stroke Treatment. *Stroke* 24, 35–41. doi: 10.1161/01.str.24.1.35

Arboix, A., García-Eroles, L., Massons, J. B., Oliveres, M., and Comes, E. (1997). Predictive factors of early seizures after acute cerebrovascular disease. *Stroke* 28, 1590–1594. doi: 10.1161/01.str.28.8.1590

Arntz, R., Rutten-Jacobs, L., Maaijwee, N., Schoonderwaldt, H., Dorresteijn, L., van Dijk, E., et al. (2013a). Post-stroke epilepsy in young adults: a long-term follow-up study. *PLoS One* 8:e55498. doi: 10.1371/journal.pone.0055498

Arntz, R. M., Maaijwee, N. A., Rutten-Jacobs, L. C., Schoonderwaldt, H. C., Dorresteijn, L. D., van Dijk, E. J., et al. (2013b). Epilepsy after TIA or stroke in young patients impairs long-term functional outcome: the FUTURE Study. *Neurology* 81, 1907–1913. doi: 10.1212/01.wnl.0000436619.25532.f3

Beghi, E., Carpio, A., Forsgren, L., Hesdorffer, D., Malmgren, K., Sander, J., et al. (2010). Recommendation for a definition of acute symptomatic seizure. *Epilepsia* 51, 671–675. doi: 10.1111/j.1528-1167.2009.02285.x

Beghi, E., D'Alessandro, R., Beretta, S., Consoli, D., Crespi, V., Delaj, L., et al. (2011). Incidence and predictors of acute symptomatic seizures after stroke. *Neurology* 77, 1785–1793. doi: 10.1212/WNL.0b013e3182364878

Belcastro, V., Vidale, S., Gorgone, G., Pisani, L. R., Sironi, L., Arnaboldi, M., et al. (2014). Non-convulsive status epilepticus after ischemic stroke: a hospital-based stroke cohort study. *J. Neurol.* 261, 2136–2142. doi: 10.1007/s00415-014-7471-z

Biffi, A., Rattani, A., Anderson, C. D., Ayres, A. M., Gurol, E. M., Greenberg, S. M., et al. (2016). Delayed seizures after intracerebral haemorrhage. *Brain* 139(Pt 10), 2694–2705. doi: 10.1093/brain/aww199

Bladin, C. F., Alexandrov, A. V., Bellavance, A., Bornstein, N., Chambers, B., Coté, R., et al. (2000). Seizures after stroke: a prospective multicenter study. *Arch. Neurol.* 57, 1617–1622. doi: 10.1001/archneur.57.11.1617

Brondani, R., de Almeida, A. G., Cherubini, P. A., Secchi, T. L., de Oliveira, M. A., Martins, S. C. O., et al. (2019). Risk factors for epilepsy after thrombolysis for ischemic stroke: a cohort study. *Front. Neurol.* 10:1256. doi: 10.3389/fneur.2019.01256

Burn, J., Dennis, M., Bamford, J., Sandercock, P., Wade, D., and Warlow, C. (1997). Epileptic seizures after a first stroke: the Oxfordshire Community Stroke Project. *BMJ* 315, 1582–1587. doi: 10.1136/bmj.315.7122.1582

Camilo, O., and Goldstein, L. (2004). Seizures and epilepsy after ischemic stroke. *Stroke* 35, 1769–1775. doi: 10.1161/01.Str.0000130989.17100.96

Chen, Z., Churilov, L., Chen, Z., Naylor, J., Koome, M., Yan, B., et al. (2018). Association between implementation of a code stroke system and poststroke epilepsy. *Neurology* 90, e1126–e1133. doi: 10.1212/WNL.0000000000005212

Chen, Z., Churilov, L., Koome, M., Chen, Z., Naylor, J., Kwan, P., et al. (2017). Post-stroke seizures is associated with low alberta stroke program early CT score. *Cerebrovasc. Dis.* 43, 259–265. doi: 10.1159/000458449

Claessens, D., Bekelaar, K., Schreuder, F., de Greef, B., Vlooswijk, M., Staals, J., et al. (2017). Mortality after primary intracerebral hemorrhage in relation to post-stroke seizures. *J. Neurol.* 264, 1885–1891. doi: 10.1007/s00415-017-8573-1

de Greef, B. T., Schreuder, F. H., Vlooswijk, M. C., Schreuder, A. H., Rooyer, F. A., van Oostenbrugge, R. J., et al. (2015). Early seizures after intracerebral hemorrhage predict drug-resistant epilepsy. *J. Neurol.* 262, 541–546. doi: 10.1007/s00415-014-7592-4

De Herdt, V., Dumont, F., Hénon, H., Derambure, P., Vonck, K., Leys, D., et al. (2011). Early seizures in intracerebral hemorrhage: incidence, associated factors, and outcome. *Neurology* 77, 1794–1800. doi: 10.1212/WNL.0b013e31823648a6

Faught, E., Peters, D., Bartolucci, A., Moore, L., and Miller, P. (1989). Seizures after primary intracerebral hemorrhage. *Neurology* 39, 1089–1093. doi: 10.1212/wnl.39.8.1089

Fisher, R. S., Acevedo, C., Arzimanoglou, A., Bogacz, A., Cross, J. H., Elger, C. E., et al. (2014). ILAE official report: a practical clinical definition of epilepsy. *Epilepsia* 55, 475–482. doi: 10.1111/epi.12550

Galovic, M., Döhler, N., Erdélyi-Canavese, B., Felbecker, A., Siebel, P., Conrad, J., et al. (2018). Prediction of late seizures after ischaemic stroke with a novel prognostic model (the SeLECT score): a multivariable prediction model development and validation study. *Lancet Neurol.* 17, 143–152. doi: 10.1016/s1474-4422(17)30404-0

Graham, N. S., Crichton, S., Koutroumanidis, M., Wolfe, C. D., and Rudd, A. G. (2013). Incidence and associations of poststroke epilepsy: the prospective South London Stroke Register. *Stroke* 44, 605–611. doi: 10.1161/strokeaha.111.000220

Guo, J., Guo, J., Li, J., Zhou, M., Qin, F., Zhang, S., et al. (2015). Statin treatment reduces the risk of poststroke seizures. *Neurology* 85, 701–707. doi: 10.1212/WNL.0000000000001814

Haapaniemi, E., Strbian, D., Rossi, C., Putaala, J., Sipi, T., Mustanoja, S., et al. (2014). The CAVE score for predicting late seizures after intracerebral hemorrhage. *Stroke* 45, 1971–1976. doi: 10.1161/strokeaha.114.004686

Hesdorffer, D. C., Benn, E. K., Cascino, G. D., and Hauser, W. A. (2009). Is a first acute symptomatic seizure epilepsy? Mortality and risk for recurrent seizure. *Epilepsia* 50, 1102–1108. doi: 10.1111/j.1528-1167.2008.01945.x

Jungehulsing, G. J., Heuschmann, P. U., Holtkamp, M., Schwab, S., and Kolominsky-Rabas, P. L. (2013). Incidence and predictors of post-stroke epilepsy. *Acta Neurol. Scand.* 127, 427–430. doi: 10.1111/ane.12070

Keezer, M., Pelletier, A., Stechysin, B., Veilleux, M., Jetté, N., and Wolfson, C. (2014). The diagnostic test accuracy of a screening questionnaire and algorithm in the identification of adults with epilepsy. *Epilepsia* 55, 1763–1771. doi: 10.1111/epi.12805

Koome, M., Churilov, L., Chen, Z., Chen, Z., Naylor, J., Thevathasan, A., et al. (2016). Computed tomography perfusion as a diagnostic tool for seizures after ischemic stroke. *Neuroradiology* 58, 577–584. doi: 10.1007/s00234-016-1670-5

Kwan, J. (2010). Stroke: predicting the risk of poststroke epilepsy-why and how? *Nat. Rev. Neurol.* 6, 532–533. doi: 10.1038/nrneurol.2010.140

Lahti, A. M., Saloheimo, P., Huhtakangas, J., Salminen, H., Juvela, S., Bode, M. K., et al. (2017). Poststroke epilepsy in long-term survivors of primary intracerebral hemorrhage. *Neurology* 88, 2169–2175. doi: 10.1212/WNL.0000000000004009

Lamy, C., Domigo, V., Semah, F., Arquizan, C., Trystram, D., Coste, J., et al. (2003). Early and late seizures after cryptogenic ischemic stroke in young adults. *Neurology* 60, 400–404. doi: 10.1212/wnl.60.3.400

Lancman, M. E., Golimstok, A., Norscini, J., and Granillo, R. (1993). Risk factors for developing seizures after a stroke. *Epilepsia* 34, 141–143. doi: 10.1111/j.1528-1157.1993.tb02386.x

Lu, X. C., Williams, A. J., Yao, C., Berti, R., Hartings, J. A., Whipple, R., et al. (2004). Microarray analysis of acute and delayed gene expression profile in rats after focal ischemic brain injury and reperfusion. *J. Neurosci. Res.* 77, 843–857. doi: 10.1002/jnr.20218

Madžar, D., Kuramatsu, J., Gollwitzer, S., Lücking, H., Kloska, S., Hamer, H., et al. (2014). Seizures among long-term survivors of conservatively treated ICH patients: incidence, risk factors, and impact on functional outcome. *Neurocrit. Care* 21, 211–219. doi: 10.1007/s12028-014-9968-9

Merkler, A., Gialdini, G., Lerario, M., Parikh, N., Morris, N., Kummer, B., et al. (2018). Population-based assessment of the long-term risk of seizures in survivors of stroke. *Stroke* 49, 1319–1324. doi: 10.1161/strokeaha.117.020178

Naylor, J., Thevathasan, A., Churilov, L., Guo, R., Xiong, Y., Koome, M., et al. (2018). Association between different acute stroke therapies and development of post stroke seizures. *BMC Neurol.* 18:61. doi: 10.1186/s12883-018-1064-x

Pitkanen, A., Roivainen, R., and Lukasiuk, K. (2016). Development of epilepsy after ischaemic stroke. *Lancet Neurol.* 15, 185–197. doi: 10.1016/S1474-4422(15)00248-3

Reeves, M. J., Bushnell, C. D., Howard, G., Gargano, J. W., Duncan, P. W., Lynch, G., et al. (2008). Sex differences in stroke: epidemiology, clinical presentation, medical care, and outcomes. *Lancet Neurol.* 7, 915–926. doi: 10.1016/s1474-4422(08)70193-5

Roivainen, R., Haapaniemi, E., Putaala, J., Kaste, M., and Tatlisumak, T. (2013). Young adult ischaemic stroke related acute symptomatic and late seizures: risk factors. *Eur. J. Neurol.* 20, 1247–1255. doi: 10.1111/ene.12157

Ruggles, K. H., Haessly, S. M., and Berg, R. L. (2001). Prospective study of seizures in the elderly in the Marshfield Epidemiologic Study Area (MESA). *Epilepsia* 42, 1594–1599. doi: 10.1046/j.1528-1157.2001.35900.x

Stefanidou, M., Das, R. R., Beiser, A. S., Sundar, B., Kelly-Hayes, M., Kase, C. S., et al. (2017). Incidence of seizures following initial ischemic stroke in a community-based cohort: the Framingham Heart Study. *Seizure* 47, 105–110. doi: 10.1016/j.seizure.2017.03.009

Sun, D., Sombati, S., Blair, R., and DeLorenzo, R. (2002). Calcium-dependent epileptogenesis in an in vitro model of stroke-induced "epilepsy". *Epilepsia* 43, 1296–1305. doi: 10.1046/j.1528-1157.2002.09702.x

Sun, D., Sombati, S., and DeLorenzo, R. (2001). Glutamate injury-induced epileptogenesis in hippocampal neurons: an in vitro model of stroke-induced "epilepsy". *Stroke* 32, 2344–2350. doi: 10.1161/hs1001.097242

Sung, C. Y., and Chu, N. S. (1990). Epileptic seizures in thrombotic stroke. *J. Neurol.* 237, 166–170. doi: 10.1007/bf00314589

Tomari, S., Tanaka, T., Ihara, M., Matsuki, T., Fukuma, K., Matsubara, S., et al. (2017). Risk factors for post-stroke seizure recurrence after the first episode. *Seizure* 52, 22–26. doi: 10.1016/j.seizure.2017.09.007

Trinka, E., Cock, H., Hesdorffer, D., Rossetti, A., Scheffer, I., Shinnar, S., et al. (2015). A definition and classification of status epilepticus–Report of the ILAE Task Force on Classification of Status Epilepticus. *Epilepsia* 56, 1515–1523. doi: 10.1111/epi.13121

Verellen, R. M., and Cavazos, J. E. (2011). Pathophysiological considerations of seizures, epilepsy, and status epilepticus in the elderly. *Aging Dis.* 2, 278–285.

Wei, J. W., Heeley, E. L., Wang, J. G., Huang, Y., Wong, L. K., Li, Z., et al. (2010). Comparison of recovery patterns and prognostic indicators for ischemic and hemorrhagic stroke in China: the ChinaQUEST (QUality Evaluation of

Stroke Care and Treatment) Registry study. *Stroke* 41, 1877–1883. doi: 10.1161/strokeaha.110.586909

Zhang, C., Wang, X., Wang, Y., Zhang, J. G., Hu, W., Ge, M., et al. (2014). Risk factors for post-stroke seizures: a systematic review and meta-analysis. *Epilepsy Res.* 108, 1806–1816. doi: 10.1016/j.eplepsyres.2014.09.030

Zhang, J. F., Meng, X., Jing, J., Pan, Y., Wang, Y. L., Zhao, X. Q., et al. (2021). Serum calcium and long-term outcome after ischemic stroke: results from the China National stroke registry III. *Atherosclerosis* 325, 24–29. doi: 10.1016/j.atherosclerosis.2021.03.030

Zhang, M., Chen, J., Zhan, C., Liu, J., Chen, Q., Xia, T., et al. (2020). Blend sign is a strong predictor of the extent of early Hematoma expansion in spontaneous intracerebral hemorrhage. *Front. Neurol.* 11:334. doi: 10.3389/fneur.2020.00334

Zhao, Y., Li, X., Zhang, K., Tong, T., and Cui, R. (2018). The progress of epilepsy after stroke. *Curr. Neuropharmacol.* 16, 71–78. doi: 10.2174/1570159X15666170613083253

**Conflict of Interest:** The authors declare that the research was conducted in the absence of any commercial or financial relationships that could be construed as a potential conflict of interest.

**Publisher's Note:** All claims expressed in this article are solely those of the authors and do not necessarily represent those of their affiliated organizations, or those of the publisher, the editors and the reviewers. Any product that may be evaluated in this article, or claim that may be made by its manufacturer, is not guaranteed or endorsed by the publisher.

# Advantages of publishing in Frontiers

**OPEN ACCESS**
Articles are free to read for greatest visibility and readership

**FAST PUBLICATION**
Around 90 days from submission to decision

**HIGH QUALITY PEER-REVIEW**
Rigorous, collaborative, and constructive peer-review

**TRANSPARENT PEER-REVIEW**
Editors and reviewers acknowledged by name on published articles

**Frontiers**
Avenue du Tribunal-Fédéral 34
1005 Lausanne | Switzerland

**Visit us:** www.frontiersin.org
**Contact us:** frontiersin.org/about/contact

**REPRODUCIBILITY OF RESEARCH**
Support open data and methods to enhance research reproducibility

**DIGITAL PUBLISHING**
Articles designed for optimal readership across devices

**FOLLOW US**
@frontiersin

**IMPACT METRICS**
Advanced article metrics track visibility across digital media

**EXTENSIVE PROMOTION**
Marketing and promotion of impactful research

**LOOP RESEARCH NETWORK**
Our network increases your article's readership